DISPARATE PARTICULATE MATERIALS SUBJECTED TO PRINCIPAL STRESS ROTATION

by

Ali Dalili

A Thesis submitted to the University of London for the Degree of Doctor of Philosophy

Department of Civil and Environmental Engineering
University College London

1990

ABSTRACT

Many geotechnical engineering designs must accommodate the action of wind, waves and earthquakes. These loadings cause principal stress rotations on the foundation soil.

The experimental simulation of these in situ stress paths can only be achieved by using sophisticated laboratory test devices capable of controlling both magnitude and direction of principal stresses.

This research uses a new Directional Shear Cell with a modified shear sheet design that avoids hysteresis particularly under cyclic loading and allows tests to be carried out at constant mean stress level. Sample preparation techniques have been improved to provide fully saturated clay samples with minimum sample disturbance and a technique has been developed to measure pore water pressure accurately in the centre of the sample.

The experimental work investigates the stress-strain behaviour of dry Leighton Buzzard sand, damp coal and saturated kaolinite at low stress levels when subjected to continuous and cyclic rotation of principal stress directions under plane strain conditions.

The results of cyclic principal stress rotation tests on damp coal and saturated kaolinite show parallels with dry sand in that large strains occur at low applied stress ratios. Dilatancy is suppressed by continuous rotation of principal stress and no failure planes were observed. However, the underlying mechanism of deformation was different for partly saturated kaolin. The onset of flow in this material leads to the occurrence of discontinuities. These may be tension cracks as well as the more readily anticipated shear rupture layers.

Findings show that the principal stress rotation is the governing factor in initiating strain, and that cycling the stress level magnitude is secondary.

It has been found that for the samples that have been previously sheared under cyclic rotation of principal stress directions and subsequently tested under monotonic loading, large increases in stiffness, dilation rate and strength-brittleness were observed, i.e. loose sand can become as strong and stiff as dense sand.

It has been shown that soil strain can relate to two limiting stress-dilatancy relationships in slow shear flow in which volume change occurs, one attributed to energy dissipated through friction and the other through the dissipation of stored elastic energy.

to my lovely wife

NINA

and little son Danoob

ACKNOWLEDGEMENTS

I would like to express my deepest thanks and gratitude to Professor J.R.F. Arthur who supervised this work. His constant suggestions and continuous guidance were greatly appreciated. I am grateful to his kindness and generous understanding that he has shown me, and made this research possible. I am also extremely grateful to Dr T. Dunstan for his helpful interest and support throughout my work.

I would like to express my thanks to John Pulsford for his guidance in using of the DSC in the early stages. Numerous stimulating discussions with Drs R. Wong, O. Ogunbekun, Messrs. A. Zadekocheck and K. Kamhawi on the subject of soil mechanics and innovative experimental techniques are greatly appreciated.

Special thanks must go to John Ford, who was always willing to help, and Mr. F. Cutler; their invaluable advice and technical support and excellent workmanship in the fabrication of the apparatus. I am also glad to acknowledge Messrs D.W. Vale and L. Wade who were responsible for the design and maintenance of all the electronic instrumentation, and T. Walker and B. Vines for their company in many ways.

Sincere thanks are extended to Dr S. Bishop for his proof reading of the draft manuscript and my friends for their constant encouragement and support.

SERC partly funded the research and this is much appreciated.

Last, but by no means least I would like express my love and thanks to my parents for their moral encouragement throughout my life, with special thanks to my brother Parviz for his understanding and generosity.

TABLE OF CONTENTS

CHAPTER 1 INTRODUCTION AND RESEARCH CONTEXT

1.1 INTRODUCTION

1.2 OUTLINE OF THE THESIS

1.3 EXAMPLES OF SITUATIONS IN WHICH THE ROTATION OF PRINCIPAL STRESS DIRECTIONS ARE IMPORTANT

1.4 DEFORMATION MECHANISM OF FABRIC CHANGES IN PARTICULATE MATERIALS

1.5 LABORATORY SIMULATION OF STRESS PATHS INVOLVING ROTATION OF PRINCIPAL STRESS DIRECTIONS

1.5.1 Conventional axisymmetric triaxial testing

1.5.2 Plane strain biaxial testing

1.5.3 True triaxial testing

1.5.4 Direct shear testing

1.5.5 Simple shear testing

1.5.6 Hollow cylinder testing

1.5.7 Directional shear testing

FIGURES

1.1 INTRODUCTION

The effects of continuous rotation of principal stress directions on the shearing behaviour of soil are of important concern to engineers today.

The dependence of soil behaviour on stress path is widely recognised. Ideally, the prediction of the performance of soil, and soil supported structures should make use of the stress path approach (Lambe, 1967; Simons, 1972 and Lambe and Marr, 1979) which can realistically simulate in the laboratory the varied stress path conditions encountered in situ.

The existing stress path approach does not explicitly consider the effects of principal stress rotation and so there is serious doubt about the validity of calculating factors of safety. Of course this is not related to any limitation in the method but to limitation in equipment for simulating this particular feature of a stress path (Lambe and Marr, 1979). The experimental difficulties of achieving controlled rotation of principal stress directions, referred to by Bishop and Henkel (1962), have severely restricted investigations into the effects of principal stress rotation on the behaviour of soil, resulting a lack of knowledge in this area. A better understanding of the effects of anisotropy and continuous rotation of principal stress direction in relation to soil behaviour is highly desirable.

Rotation of principal stress direction is a common feature of stress paths associated with most field situations. There are several cases of cyclic loading environments in which the manner of load operation is associated with the continuous rotation of principal stress axes. These loads are either applied by forces of nature (eg. waves, winds, earthquakes) or in the course of engineering operations such as blasting, pile driving, vibrio-flotation, rotating machinery, railways, runways, etc..

The University College Directional Shear Cell (DSC) has been developed to study the role of anisotropy of soil and the effect of rotation of principal stress direction in both cohesionless; e.g. Arthur et al., 1977; Beckenstein, 1980; Arthur et al., 1981 and Wong, 1986) and cohesive soil (e.g. Germaine, 1982 and O'Neill, 1985). However, earlier versions of the DSC have been limited to maximum boundary shear stresses of 50 kPa and to a maximum cyclic principal stress direction rotation of 70°. Furthermore the mean stress level had to be changed in order to rotate the principal stress direction continuously.
In this research a new version of the DSC is developed and described to overcome

these limitations. An experimental investigation has been carried out using this newly developed Daisy Chain Directional Shear Cell (DCDSC) to study the stress-strain behaviour of a wide range of particulate materials such as dry sand, damp coal and saturated kaolinite under monotonic and continuous cyclic rotation of principal stress direction. A technique is developed to produce high quality fully saturated kaolinite samples that can be trimmed to cubical form with minimal disturbance and be tested undrained. A miniature pore water pressure probe has been designed and developed for insertion in the centre of the sample perpendicular to the plane of strain, this probe has 100% response within 5 seconds.

The main objective of this research was to provide a better understanding of behaviour of disparate particulate materials in terms of particle size, particle shape, mineralogy and saturation when sheared under generalized stress conditions involving principal stress rotation and to see how monotonic and cyclic behaviour of soil are linked.

1.2 OUTLINE OF THE THESIS

In Chapter 1 examples of situations in which rotation of principal stress directions are important are briefly reviewed. The mechanism of deformation of fabric in particulate materials is discussed to provide a context for interpreting results. Seven different types of laboratory apparatus (including the Directional Shear Cell) are briefly assessed and their limitations and capabilities to impose stress paths with rotation of principal stress directions.

Chapter 2 describes the design concept and underlying principle of the Daisy Chain Directional Shear Cell and the modifications carried out to improve the apparatus performance. Coverage includes methods of application and measurement of stresses in the device and determination of strains within the sample.

Chapter 3 outlines experimental techniques and procedures used for sample and equipment preparation of different particulate materials such as dry sand, damp coal, nearly and fully saturated kaolinite.

Chapter 4 presents and analyses the results of preliminary monotonic tests on both dense and loose Leighton Buzzard sand tested under different stress levels in the DCDSC. The results provide a thorough evaluation of the performance of the newly developed DCDSC and associated experimental techniques. This includes the effect

of boundary constraints on the drained strength and deformation behaviour of Leighton Buzzard sand.

Chapter 5 deals with a comprehensive experimental investigation of the drained behaviour of loose and dense Leighton Buzzard sand under continuous and cyclic rotation of principal stress direction. In these tests the mean stress level is held constant and continuous rotation of principal stress direction is introduced through cycling both the boundary shear stresses and the boundary normal stresses. These results are compared with those of earlier DSC tests in which the mean stress level had to be changed in order to provide a continuous rotation of principal stress directions. Data describing monotonic shear, imposed after cycling, are also presented and analyzed.

Chapter 6 reports on both the monotonic and cyclic shearing of damp coal.

Chapter 7 presents data on the constant volume shearing behaviour of nearly and fully saturated samples of kaolinite under monotonic and cyclic rotation of principal stress directions. It includes an account of the development of a technique to measure pore water pressure accurately in the centre of fully saturated samples.

Chapter 8 is an interpretation of experimental findings, and model development.

Chapter 9 is a summary of all experimental findings and some suggestions for further work.

1.3 EXAMPLES OF SITUATIONS IN WHICH THE ROTATION OF PRINCIPAL STRESS DIRECTIONS ARE IMPORTANT

Every foundation, embankment, cutting and retaining wall results in rotation of principal stress directions. In this thesis particular attention is given to the cyclic rotations imposed by fluctuating loading conditions.

There are several environmental examples of cyclic loading in which the mode of load application is associated with the continuous rotation of principal stress directions. A simple view of continuous rotation of principal stress directions under such a condition is illustrated in Figure 1.1. It shows the changes in principal stress direction induced in a seabed deposit by waves passing overhead (Henkel, 1970;

Ishihara and Towhata, 1983).

Figure 1.2 illustrates the state of stress that is imposed when waves propagate over a seabed. It can be seen that when the crest of a wave is positioned directly above the soil element, a positive vertical pressure increment will be applied, but when the trough is located above the element of soil, there will be a negative vertical pressure increment. Thus, a cycle of vertical stress occurs during the wave propagation through a distance of one wave length (Figure 1.2a). In the intermediate instant when the point of mean wave height comes right above the soil element, it will also be subjected to a horizontal shear stress (Figure 1.2b). The direction of this horizontal shear stress changes back and forth as the wave propagates. It should be noted that the cyclic variation of the vertical stress is out of phase with the cyclic changes in the horizontal shear stress; therefore, the soil element is subjected to continuous and cyclic rotation of principal stress during the cyclic alteration of these two components. This aspect of stress change can be more clearly observed in Figure 1.3.

Recently, construction of offshore structures such as gravity platforms has demanded a thorough understanding of the drained and undrained behaviour of sea-bed soil when subjected to cyclic loading induced by wave propagation. Offshore gravity platforms experience severe loading conditions during storms when the soil foundation is subjected to large cyclic forces. The behaviour of the foundations under cyclic loading may be separated into short-term and long-term conditions. Cyclic loading may generate pore water pressures in the soil, in the short term before significant drainage takes place, and the foundation can be considered as undrained. In the long-term drainage will occur and the pore water pressures generated by cyclic loading will dissipate (Andersen et al., 1976).

Hight (1983) has illustrated the stress path characteristics of the sea bed soil beneath a gravity structure when subjected to storm wave loading. It has been revealed that the element of soil undergoes cyclic changes in magnitude of shear stresses, as well as continuous rotation of principal stress directions. The amount of rotation depends on the location of the element of the soil relative to the platform footing (see Figure 1.4).

In its simplest form, the stress changes below a horizontal ground surface subjected to earthquake type loading are taken to be cyclic horizontal shear stresses. Under these conditions an element of soil undergoes bidirectional cyclic simple shear strains changes which involve continuous changes in the direction of principal stress

and the magnitude of the shear stress (Seed, 1976).

The shear stresses induced by traffic loads in the subgrade of road pavements or railways are also associated with the continuous rotation of principal stress directions. Here very high rates of rotations associated with traffic loading may make this a very difficult problem for instrumentation.

1.4 DEFORMATION MECHANISM OF FABRIC CHANGES IN PARTICULATE MATERIALS

In geotechnical engineering, the primary goal is to prevent failure of a soil structure. However, in many chemical engineering problems the initiation of flow in particulate materials is needed. For a thorough understanding of particulate behaviour both pre-failure and flow situations should be considered.

Terzaghi (1955) stated that "the mechanical properties of cohesionless sediments depend almost entirely on their relative density". Traditionally, most practising engineers continue to regard relative density as the main factor of importance in controlling the mechanical behaviour of particulate materials, and regard the friction angle, ϕ, as a property that depends primarily on the relative density.

However, relative density is dimensionless, only representing the average number of contacts per particle and, perhaps encouraging an idea that the particulate material could be isotropic in geometry and behaviour. Therefore, relative density is not expected to account fully for the behaviour of such materials.

Research has shown that the stress-strain relationships and strength of particulate materials are far too complex to be represented solely by the relative density of soil (Ladd et. al. 1977; Jamailokowski, 1985). Particulate material is a multiphase structure and consists of solid, liquid and gas phases; it is essential it be considered as an assemblage of individual particles interacting with the two other phases. In general the strength and deformation behaviour of particulate material will be dependent on the interrelationships between; (i) the type and direction of loading, (ii) particle size and shape, (iii) particle mineralogy, (iv) water content, (v) water pressure and (vi) spatial arrangement of the particles and the associated voids. Brewer (1964) defined as "fabric" the spatial arrangement of solid particles and associated voids. The discrete quantities, such as number and orientation of particle contacts, displacement of individual particles, and distribution of contact forces, are

fundamental parameters needed to describe the state of particulate materials.

Biarez and Wiendieck (1963) used an ellipse to describe the angular frequency of contacts of discs in two dimensions. Later Oda (1972a) developed an experimental approach to describe particle contacts in sand. He introduced quantitative measurements of the fabric in terms of the orientation of the contact normals (N_i), which are perpendicular to the tangent plane between two particles in contact. When the orthogonal reference axes X_1, X_2 and X_3 are selected the direction of N_i can be determined by the measurements of two angles α and ß (Figure 1.5). He determined angles α and ß using a microscope of two vertical and one horizontal thin section of about 400-500 contacts which were selected at random and introduced the function $E(\alpha, ß)$ to characterise the particle configuration. $E(\alpha, ß)$ represents the probability density of point contact and is a function of α and ß. Because the particles were deposited under gravitational force the fabric appeared isotropic in horizontal section and the density function $E(\alpha, ß)$ was independent of α. It was found that the three-dimensional distribution of contact normals had a high concentration close to the vertical direction.

Several investigators (Oda, 1972b; Mililis et al., 1975 and Mitchell et al., 1976) have shown that the method of sample preparation gives different stress-strain behaviours and cyclic liquefaction strengths for samples of the same sand at identical void ratio (Figures 1.6 and 1.7). Mogami (1965) also considered two boxes containing equal numbers of particles but with different particle distributions and stated that " it must be a matter of common sense that these two assemblage of sand grains do not behave in the same way even though they are of the same voids ratio". He suggested that the distribution of voids must be an additional factor in the discussion of mechanical properties of particulate materials.

The existence of anisotropic natural soils has been commonly accepted for a long time; Johannson (1963) reviewed situations in which the orientation of particles produced by deposition was clearly anisotropic.

By considering the concept of a material's fabric, it is reasonable that the pluviation method of sample preparation will result in samples having preferred contact orientations normal to the bedding plane. Accordingly, one can also appreciate how the direction of subsequently applied principal stress can result in different strength and deformation behaviour. Oda (1972a) examined the angular distribution of the contact normals for four sands prepared by pluviation. He showed that there is a

marked preferred orientation of the contact normals in the direction of deposition and the distribution of normals for a sand composed of rounded particles was found to be very similar to that of sand containing elongated flat shaped particles. Figure 1.8 illustrates the distribution of contact normals for four sands. It is clear that the number of contact normals in the vertical direction is larger than that in the horizontal. Oda concluded that, among the samples of the same voids ratio, the samples in which the contact normals has a concentration close to the vertical direction possess the most stable fabric. In other words contacts whose normals are parallel to the direction of axial compression are the most effective in supporting axial load.

Jenkins (1932) was probably the first to model strength anisotropy; Cassagrande and Carillo (1944) also modeled strength anisotropy in soils. Cassagrande and Carillo distinguished between inherent and induced anisotropy, and suggested that anisotropy may be present before the soil is strained or may be induced by the straining process. They defined "inherent anisotropy" as a physical characteristic inherent in the material and entirely independent of the applied stresses, and "induced anisotropy" was defined as a physical characteristic due exclusively to the strain associated with the applied stress.
Several investigators have studied experimentally the influence of inherent anisotropy on stress-strain and strength behaviour of laboratory prepared samples. Undrained strength anisotropy in naturally deposited clays has been investigated by Hansen and Gibson, (1949); Aas, (1965); Lo, (1965); Ward and Marsland and Samuels, (1965) and Bishop, (1966).

Phillips and May (1967) in a specially designed shear box studied the inherent anisotropy of Leighton Buzzard sand in various pouring directions. They observed that the maximum stress ratio was 24% higher for the dense samples which were poured through the side or end, than for those which were poured from the top of the box at an identical voids ratio. Dunstan (1971) also used the same shear box for testing several wide gradings of Ham river sand and observed a corresponding directional difference in shear strength. However the work of these researchers was limited by the shortcomings of the shear box testing apparatus. Arthur and Menzeis (1972) developed a new triaxial cell to investigate inherent anisotropy of granular materials under a wider range of loading conditions and indeed made a valuable contribution to understanding the inherent anisotropy in soils. Their triaxial apparatus with flexible boundaries was able to accommodate a cubical sample and enabled the principal stresses to be applied to the sample in any direction relative to the plane of

deposition. The sample was prepared in a specially designed tilting former. They found that inherent anisotropy influenced prefailure stress-strain relationships and peak strength (Figure 1.9).

Arthur and Assadi (1977) studied the shear strength of materials under plane strain conditions with and without pre-existing rupture layers. Their results indicated that the tests on samples with pre-existing rupture layers showed consistent strength variation which were related to inherent anisotropy and rupture layer orientation.

Effects of fabric anisotropy on the monotonic and cyclic deformation behaviour of naturally deposited sand have been studied by Miura and Toki (1984). They cut vertical and horizontal triaxial samples after in-situ freezing (Figure 1.10). Although these authors were aware that a truly undisturbed sand sample cannot be obtained by any sophisticated sampling method because of the release of the in-situ stress system and possible mechanical disturbance during sampling, they referred to these as undisturbed samples. The fabric characteristics were examined by taking micrographs of vertical and horizontal sections through the central region of triaxial samples. The orientation of 250 particles in each section were measured. It was observed that the particles had stronger preferred orientations in the direction of deposition. The existence of such fabric characteristics of granular material prepared by pluviation of gravel and sand through air has also been reported by Dunstan (1968) and Arthur and Dunstan (1969). Hadjieuthymiou (1979) investigated inherent anisotropy in gravel using X ray tomography. Figure 1.11 illustrates a tomograph of a gravel sample, the preferred orientations of particles can clearly be seen.

Mura and Toki (1984) observed that the stress-strain dilatancy characteristics of the samples whose axial direction was selected to be vertical in the field were less compressible and more dilatant than those with the axial direction perpendicular to it. These findings were similar to Menzies (1972) in that the strength and stiffness was greatest in the vertical direction. They also cyclically loaded triaxial samples and found that for samples cycled vertically strains and induced pore water pressure were small compared with those which were cycled in the horizontal direction, signifying inherent anisotropy of the sample.

The above results help highlight the significance of the orientation of interparticle contact normals. In the following paragraphs the significance of anisotropy of particle contacts and contact forces will be discussed.

Coker and Filon (1931) at UCL were the first to develop photo-elastic methods to study stress patterns in engineering components. In an attempt to study the transmission of stresses at the grain scale and the structure of particulate material, Dantu (1957) and Wakabayashi (1957) carried out a series of tests on assemblies of optically sensitive glass particles. When an external load was applied to the mass, a stress state was produced within the particles that were in contact which was visual in polarized light. They discovered that when such a stressed mass, enclosed between parallel glass plates was viewed in a dark field of circularly polarized light, fine light stripes appeared and formed a network, with one family of lines more pronounced than the other. They observed that the predominant stripe directions coincided with the principal stress directions.

The importance of anisotropic particle contact distribution was quantified by Biarez and Wiendieck (1963) and Wiendieck (1967). They used assemblies of irregular shape disks which were packed in a Biaxial Tester and demonstrated that contacts could be completely rearranged by strain. Jump rotations of 90° in the major principal stress direction were applied to samples with continuous measurements of distribution of contact normals. Figure 1.12 illustrates the changes of distribution of contact normals induced by this deformation. It can be seen there was a gain in contact normals in the direction of major principal stress and a loss in the minor principal stress direction.

Observations of fabric changes on real soil were also measured (Oda, 1972b) but only by solidifying the sample at some stage of loading which limits the measurements to one per sample and therefore makes the study of fabric changes during loading more difficult.

Oda and Konishi (1974) also used photoelastic discs in a simple shear device and showed that the normal contact planes tend to rotate during the increase of shear forces towards the major principal stress. The changes in frequency distribution of contact normals for such a series of dense and loose samples are shown in Figure 1.13. Similar results have been also reported by Matsuoka (1974) who showed that the contact normals tend to orientate towards the major principal strain axis during simple shear deformation.

Numerical experiments in computer simulations of granular assemblies have also confirmed independently the above behaviour of particulate materials (e.g. Cundall, 1971; Cundall and Strack, 1979 and 1983). Numerical analysis of particulate

assemblies is a relatively new concept that can be used to a great advantage in understanding particulate behaviour. However numerical modelling, like any other modelling, has its advantages and disadvantages. The advantages of numerical modelling are that the test can be stopped at any stage of loading and uniquely detected "measurements" taken, any time history of loading can be applied, the same sample can be repeatedly tested under various conditions, and any fabric parameter can be computed at any stage of loading. Difficulties still prevail when deciding what material properties and boundary conditions are to be used in the analyses. Commonly only two dimensional models are used, thus limiting simulation of particulate material, the numerical model then becomes a computer version of the laboratory "pin model". A more realistic view of soil, requires extensions in numerical analysis to three dimensional assemblies and particles of irregular shape.

The numerical method developed by Cundall and Strack (1979) has the ability to simulate granular material on an individual grain basis. Grains of sands are represented in the model by discs with different physical properties and can freely interact with each other. Cundall and Strack (1983) suggested that granular materials are made up of two phases, A and B. Phase A, being made up of stiff columns, behaves like a pin-joined structure that dissipates no energy and imposes no local deformation pattern on phase B particles. Phase B, however acts like a truly plastic material that dissipates energy at many contact points and serves as a restraint on phase A particles. As the shearing of the material proceeds the strain is increased and certain changes take place in the material's structure. The phase A columns become progressively more kinked and therefore less able to support their current load or any further increase. Load is then transferred to new columns that develop nearby as increasing deformation in the major principal stress direction leads to formation of new contacts with contact normals better aligned with the major principal stress direction. When the steady state condition is reached during continuous deformation, new columns are created at the same rate as old columns collapse and vanish, hence the total number of contacts remains more or less the same and the particles alternate between phase A and B. Figures 1.14a and 1.14b illustrate force columns at the initial isotropic state of stress and subsequent state of high deviatoric stress. Inhomogeneity is apparent after the deviatoric stress is applied and reveals that force directions could be of fundamental importance to the nature of the stress - strain deformation behaviour of particulate material.

In these investigations, attention has been concentrated on the distribution of contact normals; and shows that with shear the evolution of fabric is closely related to the

variation of the distribution of the contact normals. With strain the distribution gradually changes to produce a greater concentration of contact normals along the orientation parallel to the direction of major principal stress.

Oda, Nemat-Nasser and Konishi (1985) continued their investigation into the stress-induced anisotropy of granular media and suggested that as the granular material consists of solid particles and voids, then at least three sources of anisotropy (the distribution of contact normals, the shape of the particles and the shape of voids) must be taken into account. In this connection, they conducted two series of biaxial compression tests on two dimensional assemblies of photoelastic rods and studied the effect of anisotropy on the behaviour of particulate material. They showed that in the early stages of deformation (Figures 1.15a and 1.15b) voids are small with no special shape. As deformation proceeded, voids connected with each other and formed elongated voids with the longest dimension growing parallel to the direction of the major principal stress (Figures 1.15 c and 1.15.d). They suggested that the gradual concentration of contact normals is due to column-like load paths parallel to the major principal stress direction and that the voids shapes grow parallel to this direction between the columns. They proposed that elongated voids of this kind (Figure 1.16) can collapse under an additional lateral force, or the reduction of axial force. Such collapse of the elongated voids during load reversal may be a contributing factor in producing large volumetric strain changes in drained conditions or large changes in excess pore water pressure if the sample is saturated and undrained.

Arthur et al. (1986) studied changes in angular frequency of particle contacts using Koender's theoretical model (1984) and compared the results with that of sand tested under plane strain with a similar stress path. The heterogeneous deformation model of Koenders considers particles of granular assemblies as elastic with interparticle friction; similar to that of Cundall and Strack (1979). The key elements of the model are the changeable distribution of particle contact points and the angular distribution of forces across the contacts. These properties of the particulate assembly enable a global incremental stress-strain relationship to be set up. Each increment of stress and strain induces a certain degree of inhomogeneity and the distributions of contact normals and contact forces must be updated before another incremental load can be applied. This allows the feature of induced anisotropy to be modelled. Figures 1.17 and 1.18 illustrate the results of Koenders' biaxial computer experiments on random diameter circular discs, compared with the data from dense samples tested in the plane of strain in the Directional Shear Cell. Although the strain magnitudes in the

two classes of experiment were very different, there was a complete similarity in the form of the relationships. A notable feature of the predicted progression of anisotropy in contact normals, a→b→c→d in Figure 1.17a, is that it tends to be linked to strain rather than stress; the increase in the major axis of the ellipse is the same between b→c and c→d yet the increase in stress ratio c→d is much smaller. However, it should be noticed that at the same time contacts in the minor principal stress direction are reducing thus contributing to instability.

The above studies reveal the existence of structural anisotropy which evolves in order to increase the ability of the fabric to withstand the increasing shear stress which accompanies the increase in shear strain. When a specimen of a particulate material is loaded, normal and tangential contact forces develop between neighbouring particles. Particle instability is usually due to variation in normal forces at particle contacts and only to a secondary extent to the shear forces at the same contacts (Cundall, 1972; Rothenburg and Buthurst, 1989). The subsequent rearrangement of particles evolve a new fabric through formation of new contact points. As the sample is increasingly loaded, the process of sliding and rolling and rearranging of the particles continues until no increase in anisotropy is possible. This stage is conventionally referred to as failure and depending on the test conditions; i.e. initial packing, strain history and loading conditions, the sample either deforms continually under constant load or rupture planes develop within the sample.

The question as to whether sliding or rolling dominates the deformation mechanism of particulate material has been a subject of considerable debate. The continuous change of the initial fabric with increasing deformation has been attributed to frictional sliding of particles relative to one another, and it has been assumed that sliding is the major component, with particle rolling being small; Newland and Allely (1957); Rowe (1962); Horne (1965, 1969); Matsuoka (1973); Oda (1974); Murayama (1977); Nemat-Nasser and Tobita (1981). This assumption must hold partially, since higher inter particle friction produces higher shear strength. However, studies have revealed that particle rolling does take place during shear deformation and it is considered by some researchers to be the dominant mechanism (Roscoe and Schofield, 1964; Skinner, 1969; Oda et al., 1983). In a series of experiments on glass particles in a shear box Skinner (1969) observed that the angle of interparticle friction for dry glass ballotini was as low as ϕ_μ = 2°-7° but rose to ϕ_μ = 27°- 43° when flooded with distilled water. Nevertheless, both dry and flooded assemblies resulted in almost the same shear strength. Skinner concluded that if sliding of the particles was to be the predominant feature in the low friction case, then when

interparticle friction was raised, more particles must roll rather than slide in order to keep the energy balance the same.

Oda (1972b) also suggested a similar mechanism of fabric changes during compressional deformation of sand. Oda, Konishi and Nemat Nasser (1982), went a stage further using assemblies of oval cross-sectional rods, in an effort to evaluate the effects of interparticle friction, particle shape, and initial fabric on the overall strength of particulate materials. They monitored the variation in fabric and particle rolling and sliding by taking photoelastic pictures at different stages of deformation. Based on this, they concluded that : i)- particle rolling appears to be the major microscopic deformation mechanism, especially when interparticle friction is large, ii)- there are comparatively few contacts at which relative sliding is dominant, and this seems to be true even when the assembly reaches the overall failure state; this observation however, is in contradiction to the common assumption that particle sliding is the major microscopic deformation mode. iii)- as the deformation proceeds up to the peak stress, new contacts are continuously formed in a manner that contact normals tend to concentrate more in the direction parallel to major principal stress direction. This concentration seems to be closely related to the formation of column-like load paths which carry the increasing axial load under constant lateral forces. After the peak stress, such a column-like microstructure deteriorates and considerable rearrangement of load paths takes place, leading to a less homogeneous microstructure in the critical state. Figures 1.19 a and 1.19 b illustrate these two stages of deformation.

During cyclic loading of a particulate soil, the fabric continuously changes; these changes in microscopic scale are magnified compared with monotonic loading, for example, for a loose soil, there will be large compressive volume change in dry soil and liquefaction in saturated soils. The nature of the internal mechanisms during cyclic loading is largely unknown and there is little information on the fabric changes during cyclic loading conditions where continuous effects of principal stress rotations are involved.

Youd (1977) made a descriptive study of fabric changes during cyclic loading. Figure 1.20 illustrates a set of eight particles he used to explain the prestraining effects on the liquefaction potential of sand.

Oner (1984), used a numerical model to study fabric changes during cyclic loading. Cyclic loading was applied as in the simple shear test and the fabric changes were

depicted by using the method employed by Oda and Konishi (1974). In this method the frequency distribution of normals to the active contact planes were plotted in a rosette format. Figure 1.21 demonstrates the change in fabric relative to the loading history and major principal stress direction. The shear strain amplitude used in this analysis was 2%. Rotation of the contact normals to resist the major principal stress is apparent in the Figure. This phenomenon was very similar to the effects observed by photoelastic discs tested by several investigators under monotonic loading described earlier.

Overwhelming evidence of fabric anisotropy of natural soil suggests that realistic simulation of in-situ loading of any type requires laboratory devices capable of controlling both the magnitude and direction of principal stresses, particularly for stress paths under fluctuating loading conditions.

1.5 LABORATORY SIMULATION OF STRESS PATHS INVOLVING ROTATION OF PRINCIPAL STRESS DIRECTIONS

The laboratory simulation of cyclic loading investigating rotation of principal stress directions has, to a major extent, relied upon modifications to current laboratory equipment. Only recently more advanced laboratory equipment has been developed to investigate this more thoroughly. This part of the introductory Chapter gives a brief review of laboratory testing equipment capable of applying cyclic rotation of principal stress directions.

1.5.1 Conventional axisymmetric triaxial testing

The triaxial cell (Figure 1.22) is the most common laboratory shear device. In many versions a cylindrical sample of soil (often with a height:diameter ratio of 2:1) is sealed in a rubber membrane, placed under a state of hydrostatic stress and axially loaded through rigid platens to causing shear stresses in the sample. The membrane is usually sealed to end platens and lateral expansion of the sample over these platens is restricted by friction unless special precautions are taken (e.g. Rowe, 1962; Rowe and Barden, 1964, Bishop and Green, 1965; Norris, 1981). The rubber membrane acts as a flexible membrane and as a seal to separate pore water pressures and total stresses. The sample is assumed to remain a right cylinder during deformation with horizontal and vertical sides principal planes of stress.

The cyclic triaxial apparatus was devised by Seed and Lee (1966) and was the first

device capable of monitoring the cyclic behaviour of soil. Since then numerous investigators (e.g Lee and Seed 1967, Finn et al. 1971, Vaid and Chern 1983, etc.) have used the cyclic triaxial apparatus to study the cyclic behaviour of soil either with or without an initial static shear stress.

This apparatus can be used to investigate the response of soil to two types of cyclic loading.

1- The apparatus is used in triaxial compression in which the deviatoric stress is increased and then decreased continuously. Under this condition there is no change in the direction of the major principal stress but stress and strain increment directions may shift by 90° .

2- The apparatus is modified such that a cycle involving triaxial compression and triaxial extension is achieved. Here, tensile loading must be applied to the ram during part of the cycle and a discontinuous jump rotation of principal stress direction is achieved but is limited to a 90° jump only.

A thorough investigation of the effects of continuous rotation of principal stress direction can not be achieved; only rotation of the major principal stress in a sudden jump through 90° from vertical to horizontal or vice versa is possible. Furthermore, this 90° rotation changes the stress system from triaxial compression ($b= (\sigma_2-\sigma_3)/(\sigma_1-\sigma_3) =0$) to triaxial extension (b = 1) and it is also impossible to separate this effect from that due to the inherent anisotropy of the sand during deposition.

In the early cyclic loading investigations using the triaxial apparatus, the interest centred mainly on relating the resistance to liquefaction to the number of cycles of loading. Typical results of such a test are reported by Seed and Lee (1966), and are illustrated in Figure 1.23. They used the apparatus applying stress path 2 (triaxial compression and extension cycles). Such tests do not usually produce much information on stress-strain behaviour of particulate materials under cyclic loading, only the number of cycles to produce liquefaction under particular cyclic stress conditions. These may be useful as an index test. The number of cycles to failure is not a good parameter for giving a feel for the behaviour of the soil, as it is difficult to distinguish between a steady build-up of deformation and a sudden loss of strength (Figure 1.24). Only few attempts have been made to examine soil response within a loading cycle (Vaid and Chern, 1983). However, such an examination is essential for any fundamental understanding of the process, which could lead to pore water pressure generation and strain development with eventual liquefaction under cyclic loading conditions.

Indirectly other investigators (Castro, 1969; and Luong, 1979, 1980) have also shown the effects of jump rotation on liquefaction behaviour.

1.5.2 Plane strain biaxial testing

In many field situations (e.g. under long embankments) the loading conditions are such that a condition of zero lateral strain is maintained. The plane strain apparatus was developed in order to simulate such events in the laboratory in a more realistic way. A pair of opposite faces of the biaxial apparatus are prevented from moving whilst stresses are applied on the other four faces of a prismatic sample (Figure 1.25). To minimise friction in the direction parallel to the restrained surfaces lubricated rubber membranes are sandwiched between the sample face and the rigid boundaries. Thus the term plane strain can be considered a misnomer, in that it is impossible to maintain perfect plane strain.

There are a selection of plane strain devices available, some with all flexible boundaries, others all rigid boundaries and yet others with a mixture of flexible and rigid boundaries. The relative merits of the various types of boundary have been examined by Arthur (1987). One penalty in keeping zero intermediate principal strain during shear is generally an uncontrollable variation in the intermediate principal stress. However, the use of flexible boundaries in some biaxial testers (e.g. Davoudzadeh, 1982; Wong, 1986; Ogunbekun, 1988) have not only provided uniform boundary loading but also enabled a small degree of control of the intermediate principal stress. Davoudzadeh (1982) carried out tests with different values of b on the same Leighton Buzzard sand using a flexible boundary true triaxial cell and reported that b values between 0.3 and 0.4 gave the approximate condition of plane strain compression.

The biaxial device is subject to similar limitations as the conventional axisymmetric triaxial test. There can be only a jump rotation of principal stress of 90° and the direction of major principal stress cannot be rotated in a continuous manner. However, there is a major advantage over the triaxial apparatus in that the sample is subjected to plane strain condition throughout the rotation jump, the triaxial apparatus changes from triaxial compression to triaxial extension condition; i.e. (b= 0, to b= 1).

Arthur, Chua, and Dunstan, (1977) have shown the effects of a 90° jump rotation on a sample that was initially isotropic in the plane of strain and then was subject first to a loading in one direction and subsequently subject to loading after a 90° jump

rotation. It can be interpreted that the soil structure is significantly changed during first loading and becomes anisotropic so that on second loading this soil first behaves like a loose soil. This gives a potential for high pore water pressure build up and limited liquefaction in saturated soils.

1.5.3 True triaxial testing

In true triaxial Apparatuses (TTA) the magnitudes of three principal stresses may be controlled independently and the test is usually carried out on cubical samples (Figure 1.26). Very many versions of the true triaxial devices have been constructed. Sture and Desai (1979) divide them into three basic categories depending on the applied boundary conditions and discussed in detail their relative advantages and disadvantages.

The first category are displacement controlled devices with rigid boundaries, such as the Cambridge true triaxial apparatus (Hambly, 1969; Pearce, 1971). This consists of six rigid platens which are linked together around a cubical specimen so that they slide over each other to produce strains along all three orthogonal axes. Each face of the sample is completely covered by a platen and there are no gaps between the adjacent platens. The apparatus is capable of accommodating strains of up to 30% independently along each axis of the sample. Stresses are measured by load cells and strains are measured by means of displacement transducers. The problem of platen friction is reduced by enclosing the sample in a membrane which can be thoroughly greased on the outside. This apparatus was designed to test samples of clay.

The second category contains stress controlled devices with flexible boundaries (Ko and Scott, 1967; Sture and Desai, 1979; Davoudzadeh, 1982). Problems associated with cubical samples having rigid boundaries particularly when testing sand resulted in the development of devices stressed with six flexible boundaries. Flexible boundaries ensures that uniform stresses are applied over each face of the sample. The sample is free to deform and develop a rupture layer along the weakest plane. Radiography can be used to measure strains internally (e.g Davoudzadeh, 1982).

The third category consists of those devices using mixed rigid and flexible boundaries which apply known displacements in some directions and known stresses in others (Shibata and Karube, 1965; Green, 1971; and Lade, 1978). Generally in this case the axial load is applied by rigid platens, the minor principal stress by a

cell pressure and intermediate principal stress is applied independently by either rubber bags or rigid platens. The relative benefits and drawbacks of the various types of rigid and flexible boundary loading systems on cubical samples have been described by Arthur (1987).

In a true triaxial apparatus the entire principal stress space of an isotropic material can be examined. However, limitations exist as with the biaxial and triaxial apparatuses when investigating anisotropic materials.
In these devices the principal stress directions are fixed, and it follows that changes in the principal stress directions are again restricted to jump rotations through 90°. Therefore the TTA offers little improvement in controlling the rotation of the principal stress direction over the axisymmetric triaxial and plane strain apparatuses. However, there are major advantages over the other two in that the effect of the entire range of b values can be investigated during jump rotations.

1.5.4 Direct shear testing

The direct shear apparatus (DSA) was the earliest used laboratory device for measuring plane strain strength parameters of granular soil (Figure 1.27). The DSA and variations of this apparatus have been used for over a century with the first one being reported by Collin in 1846 (Skempton, 1947). Numerous changes have been made to the original design and many laboratories currently use a version designed by Bishop in 1946.

In a DSA a sample usually 60mm square in plan and about 25 mm thick is encased in a horizontally split box, occasionally larger samples are used in special shear boxes to examine coarse-grained soils. The sample is loaded vertically between rough top and bottom platens after which a shearing force is applied to move the top half of the box relative to the bottom half.

In the DSA the sample is first deposited through the top of the apparatus. At the start of a test the major principal stress acts in the vertical direction with the intermediate and minor principal stresses equal and act on the sides of the box. As the shearing proceeds the major and minor principal stresses rotate and the unknown intermediate principal stress can change in magnitude but not direction. This rotation is unavoidable, is unknown and cannot be controlled.

The application of shear force causes the soil to shear along the horizontal bedding

planes between the two halves of the box and may result in considerable stress concentration at the front and rear edges. The overall restriction of no linear incremental strain in the soil along the central plane has been reviewed by Assadi (1975); Scarpelli and Wood (1982); Dayer (1985) and Palmira (1987). Any measurements of strength anisotropy of sand in the shear box requires further apparatus development where sand can be deposited in different directions (e.g, Mahmood, and Mitchell, 1974; Dunstan, 1972).

The kinematic constraint that forces the failure plane to occur in a particular direction also introduces unknown conditions, such as uncertainty as to the principal stress directions within a sample. However, it can be interpreted if correlated with other apparatuses. This type of behaviour is often considered to be similar to that of simple shear (Roscoe, 1970; Stroud, 1971 and Jewell and Wroth, 1987).

1.5.5 Simple shear testing

Many cyclic loading situations in the field, e.g. seismic loading, make the simple shear principle a suitable way of reproducing cyclic deformation of an element of soil, particularly below level ground.

The concept for a one-dimensional consolidated simple shear test was first proposed by Kjellman (1951). Hvorslev and Kaufman (1952) described the apparatus and pointed out some advantages and disadvantages of simple shear testing of soils. Later Roscoe (1953) described the Cambridge simple shear apparatus (Figure 1.28b).

An alternative configuration was proposed by Bjerrum and Landva (1966) for testing Norwegian quick clays. The Swedish Geotechnical Institute (SGI) and Norwegian Geotechnical Institute (NGI) adaptations used non-rigid vertical boundaries and circular cross-sections (Figure 1.28b). The SGI type used stacked rings to confine the specimen and the NGI type used a wire-wound membrane. In the NGI apparatus a cylindrical sample 80 mm in diameter and 20 mm high, is confined in a reinforced rubber membrane fitted with a cap and base; the sample is allowed to undergo vertical deformations and horizontal displacements with no changes in diameter. The shearing of the sample is produced by holding the top cap in place and moving the base horizontally.

As in the DSA the SSA causes an unavoidable continuous rotation of principal stress

directions during non-cyclic loading. This rotation is unavoidable and uncontrollable. However, the advantage over the DSA is that state of stress can be defined from load cell measurements on the boundaries. Although rotations of 40° in the principal stress directions have been reported Roscoe, Basset and Cole stated that only a mere 10° of the principal stress rotation occurs during plastic straining. At an early stage, they showed non-coincidence between the principal axes of stress and strain increment during shear with the principal axis of stress lagging behind the principal axis of incremental strain. At failure, the principal axis of stress closely aligns with the principal axis of strain increment as larger plastic strains develops.

In spite of these limitations which seriously reduces the ability of the simple shear apparatus to investigate the effects of anisotropy and continuous rotation of principal stress rotation, it is extremely useful to simulate many cyclic loading situations in the field.

The first series of cyclic simple shear tests were conducted by Peacock and Seed (1968) using a Cambridge type device producing the first laboratory data on the behaviour of saturated sands showing that cyclic loading caused liquefaction. Many others have shown similar results. Finn, Pickering and Bransby (1971) in consultation with Roscoe developed an improved version of the Roscoe apparatus which resulted in more uniform deformation fields.

1.5.6 Hollow cylinder testing

The hollow cylinder apparatus (HCA) was developed to investigate basic soil behaviour. It has the distinct advantage of applying three independent principal stresses together with the ability to rotate principal stress directions over all ranges of b values. Rotation of principal stress is achieved by applying torsional shear to the upper surface of the sample together with control of the internal and external pressure and the axial load.

This apparatus represents the first device having the ability to fully rotate the principal stress directions through 360° in a continuous manner. This device can be used in a fundamental investigation of anisotropy and principal stress rotation in sands and clays (Ishihara and Towhata, 1983; Symes et al., 1984) and offers essential advantages over the simple shear and the true triaxial apparatuses in investigating soil behaviour under fluctuating types of load.

Figure 1.29a is a diagrammatic view of the hollow cylinder apparatus P_i , P_o , M_T and W can be varied independently. The average stresses on an element of soil (Figure 1.29.b) can be found from the external loads using the following equations:

$$\text{Average vertical stress: } \sigma_z = W/\pi(r_o^2-r_i^2) + (p_o\, r_o^2 - p_i\, r_i^2)/(r_o^2-r_i^2) \quad (1.1)$$

$$\text{Average radial stress: } \sigma_r = (p_o\, r_o + p_i\, r_i)/(r_o + r_i) \quad (1.2)$$

$$\text{Average circumfrencial stress } \sigma_\theta = (p_o\, r_o - p_i\, r_i)/(r_o - r_i) \quad (1.3)$$

$$\text{Average shear stress } \tau_{z\theta} = 3M_T/2\pi(r_o^3 - r_i^3) \quad (1.4)$$

where the symbols r_i and r_o denote the current inner and outer radii of the sample. The magnitude of three principal stresses, σ_1, σ_2 and σ_3 and the orientation of σ_1 and σ_3 can be determined from these average stresses. This is shown in a Mohr circle representation in Figure 1.29d. The magnitude of the three principal stresses are:

$$\sigma_1 = \sigma_z + \sigma_\theta/2 + \sqrt{\{(\sigma_z - \sigma_\theta/2)^2 + \tau_{z\theta}^2\}} \quad (1.5)$$

$$\sigma_2 = \sigma_r \quad (1.6)$$

$$\sigma_3 = \sigma_z + \sigma_\theta/2 - \sqrt{\{(\sigma_z - \sigma_\theta/2)^2 + \tau_{z\theta}^2\}} \quad (1.7)$$

The direction of major principal stress (Figure 1.29c) can be calculated as:

$$\alpha = 1/2 \times \tan^{-1} (2\tau_{z\theta}/\sigma_z-\sigma_\theta)$$

By controlling these average stresses the soil element can be subject to principal stress rotation, both in a fixed and a continuous manner, and changes can be made to the magnitude of intermediate principal stress relative to the major and minor principal stresses. It should be noted that in this device, principal stress rotation is restricted to two dimensions, i.e (z, θ) plane. The radial stress remains an intermediate principal stress.

Non-uniformity of stresses across the wall of the HCA are inevitably subjected to different internal and external pressure. A reason given in favour of having different internal and external pressure is that this allows one to control the b values. Non-uniformities are kept to a reasonable minimum by careful selection of geometry (Hight et al., 1982).

Advantages and disadvantages of the hollow cylinder apparatus against other laboratory testing devices have been fully described by Saada and Townsend (1981). Some of the main limitations are explained below:

(i) uniform stresses are unattainable, (good approximation can be achieved by forming a sample which is suitably tall, has a large radius and a thin wall).

(ii) undisturbed samples of natural soils are incompatible with a thin long cylinder.

(ii) fixing at cylinder ends combined with the thin wall imply limitations on sample deformation.

(iv) soil is always close to cylinder surfaces where surface effects exist.

(v) accurate strain measurement is difficult.

(iv) does not perform well at large strains.

Ishihara and Momenzadeh (1986) used the HCA to compare the effects of continuous cyclic loading of sand compared with jump rotation of principal stress direction. Figure 1.30. shows that greater volumetric strain is achieved when the major principal stress direction is continuously rotated.

Shibuya (1985), used the Imperial College HCA to conduct a series of cyclically loaded undrained tests on Ham River sand in which the principal stress direction was rotated continuously. He compared his findings with monotonic undrained tests by Symes (1983). Symes proposed an undrained state boundary surface related to the anisotropic structure of the soil during deposition (Figure 1.31). It can be seen that the undrained strength reduces as the major principal stress direction changes from being in line with the deposition direction. This surface can be reduced to two dimensions as shown in Figure 1.32, AO being a test in line with the deposition direction and A4 being one at 40° to the deposition direction.

Figures 1.32 and 1.33 illustrate the effects of undrained cyclic rotation of principal stress directions and the tendency to liquefaction due to directional changes of major principal stress related to different directional undrained monotonic stress paths. Note that in Figure 1.32 the angle of rotation measured 24.5° compared with the monotonic undrained path A2 at 20° to the pouring direction.

1.5.7 Directional Shear Cell

The Directional Shear Cell (DSC) (Figure 1.34) was designed and developed at University College London by Arthur et al., (1977). This apparatus is a flexible boundary plane strain device capable of applying uniformly distributed normal and shear stresses independently to four faces of a cubical sample constrained between two platens. The normal stress is applied through air filled rubber bags and the shear stress through stretching shear sheets. It aims to control magnitudes and directions of the principal stresses in the plane of shearing to simulate stress

conditions that may occur under fluctuating loading conditions. This device is explained in detail in Chapter 2.

The applied normal and shear stresses can be increased or decreased in nearly any combination while deformations of the sample are continuously measured. Early versions of the DSC have been used extensively to study the effects of inherent and induced anisotropy on the stress-strain behaviour of granular materials (e.g. Arthur et al., 1977, 1981; Rodriguez del Camino and Dunstan, 1981). The DSC has also been used to study the effects of continuous and cyclic rotation of principal stress directions on the stress-strain behaviour of Leighton Buzzard sand (Arthur et al., 1977; Wong, 1986). In all these versions the sample was 100 mm x 100 mm x 100 mm and strains were measured either by radiography or photography.

An alternative version of the DSC was developed at the University of Colorado, which, in its present configuration receives 178 mm cubical specimens. Here the normal and shear stresses are provided by a system of flexible cushions, shear pads and strips. These stresses are applied by pneumatically operated actuators and flexible cushions (Figure 1.35). The normal pressure bags are relatively thin cushions that are confined by wedge shaped rotatable cups in the rear, and at the front face by the shear pad and strip assemblies as well as the sample. The flexible strips, pads, and cushions are made of silicone rubber (Dow Corning-E-RTV and J-RTV) and fabricated by means of pressure moulding processes (Sture, et al., 1985).

The state of plane strain in the Colorado DSC is achieved by means of two rectangular, oversize, stiff, transparent and lubricated Lexan plates, that are connected by four axial rods. Although these boundaries are lubricated, stress concentration may develop. This problem is solved in the University College DSC in which a water-filled pressure bag produces the intermediate principal stress. The pressure in the bag can be monitored and controlled and tests with different b values can be conducted.

The DSC apparatus offers many advantages compared with the aforementioned devices and is free from theoretical criticisms (Symes, 1983). Some of the advantages that the DSC offers may be listed as:
i)-Homogeneous stress controlled boundaries, σ_2 can also be monitored or controlled,
ii)-Near uniform boundary stresses are applied through flexible boundaries,
iii)- The direction of the major and minor principal stresses can be varied in a totally controlled manner thus allowing for much more realistic stress paths to be imposed,

iv)- Internal measurements of strain, strain increment and strain distribution by radiography provide an accurate and clear picture of sample deformation during shear,
v)- Self checking apparatus through the use of monotonic tests on samples initially isotropic in the plane of strain by applying the major principal stress at different constant angles from 0°-90°,
vi)- A practical sample shape for testing undrained samples of natural soils coupled with a design concept which is not closely linked to sample size,
vii)- A good potential for automated testing controlled by micro-processor.

However, there are some limitations on the earlier version of the DSC; the maximum boundary shear stresses that can be applied to the four faces of the sample is 50 kPa restricting the apparatus to low stress levels. Also the stretching components of the shear sheets are confined between the normal stress bag and face of the sample, this gives a hysteresis during loading and unloading the shear sheets. The only way to provide a continuous rotation of principal stress direction in a cyclic stress path is to change the mean stress level and keep the boundary shear stresses constant. In this stress path the effects of stress level variation and that of principal stress directions are combined and can not be separated. One of the aims of the present research has been to reduce these limitations through design and construction of new shear sheets. As the sample deforms and changes shape there is a necessity in the device to adjust the boundary normal pressure bags and align the boundary shear sheets which involves operational difficulties.

In its present form it is not a displacement controlled device; it would therefore be impossible, for example, to imitate the strain path developed in the SSA which may closely follow certain ground cyclic loading conditions. Here the no-extension direction is fixed.

Nevertheless, these disadvantages are small sacrifices to pay when compared to the advantage of being able to rotate the directions of principal stresses; thus the Directional Shear Cell is an excellent instrument for investigating soil behaviour under complex loading situations (Sture et al., 1987).

The effects of principal stress direction on the behaviour of sand has been studied at UCL by Arthur et al. (1977, 1979, 1981 and 1985) using the Directional Shear Cell. Discussion of their findings will be included in later chapters as a comparative tool for this work.

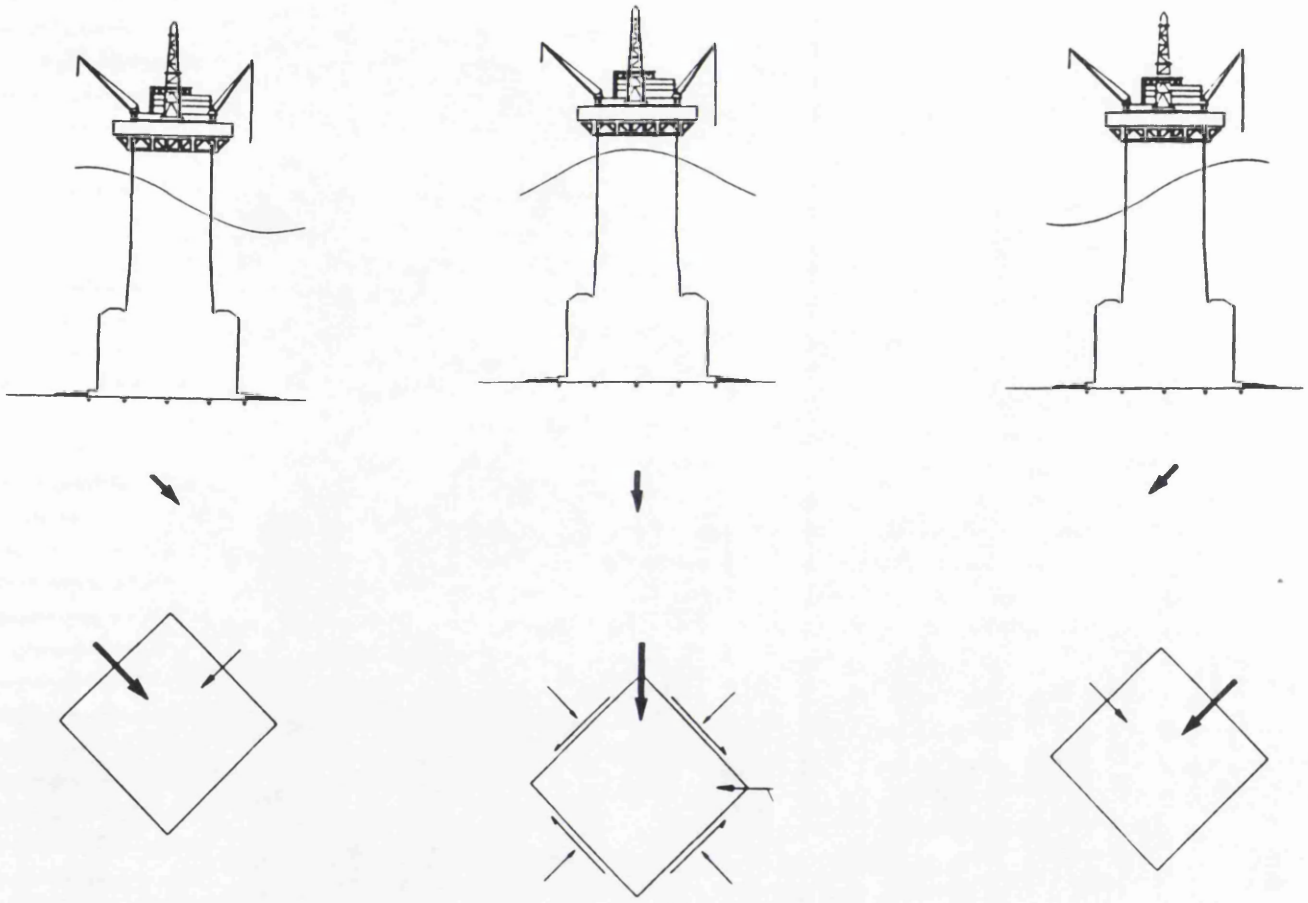

Fig. 1.1 A simple view of continuous rotation of principal stress directions under a gravity platform.

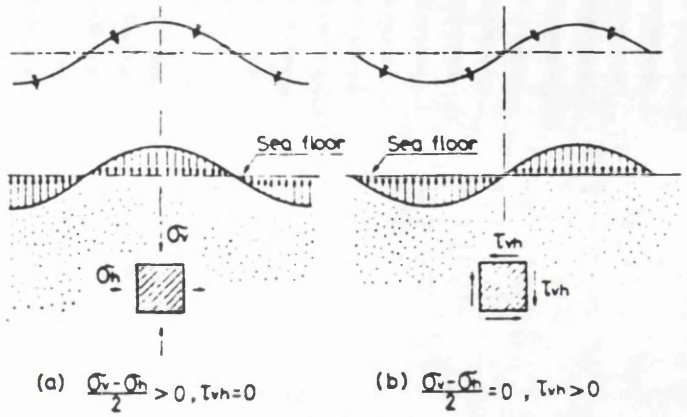

Fig. 1.2 Semi-infinite elastic medium subjected to harmonic loading on the surface (after Ishihara and Yamazaki, 1983)

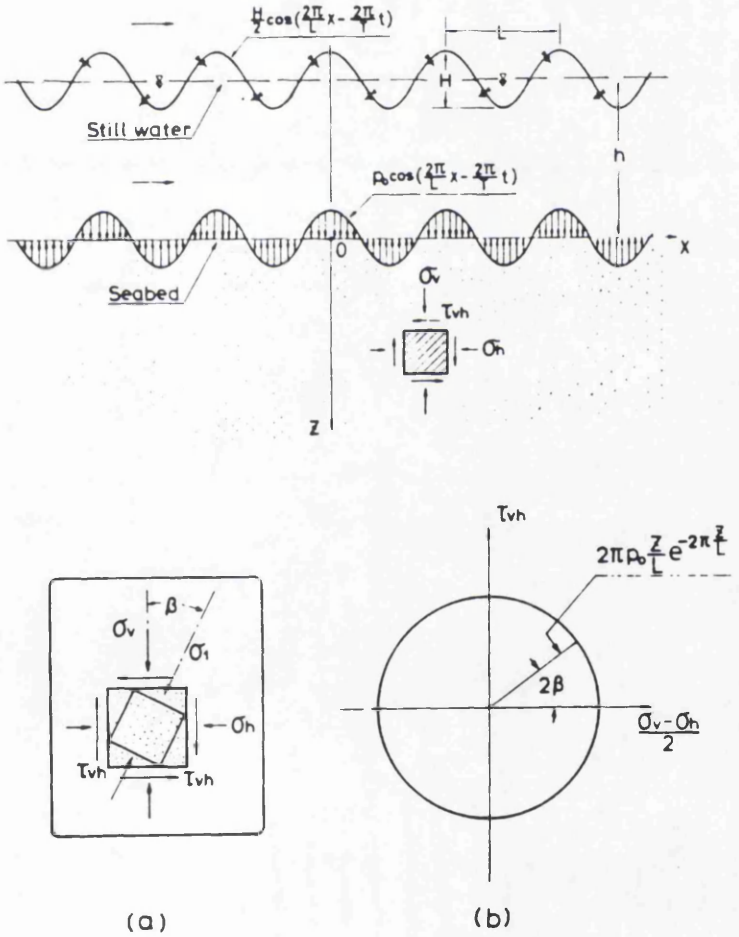

Fig. 1.3 Changes in state of stress due to propagation of water waves over the sea floor (after Ishihara and Yamazaki, 1983)

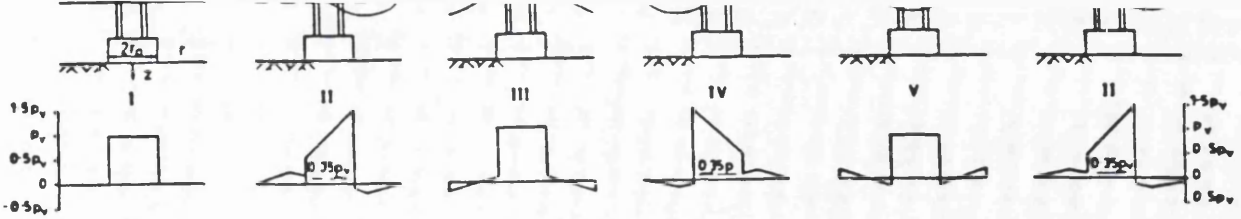

Loading Sequence and Assumed Sea-Bed Pressures

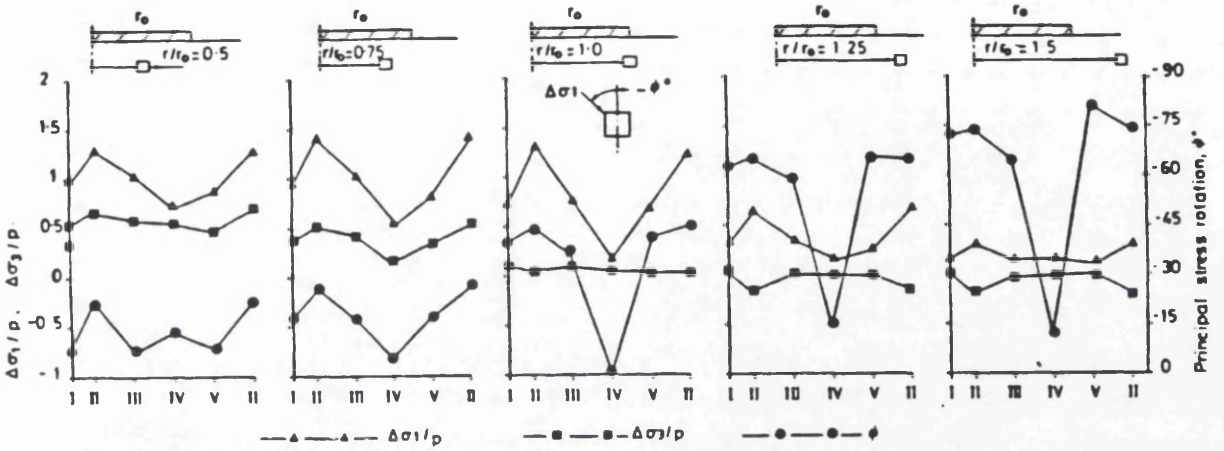

Cyclic Changes in Principal Stress Increments and Orientation at 0·25r_o Depth

Sequence of stress changes at depth of 0.25r_o in foundation to typical gravity structure.

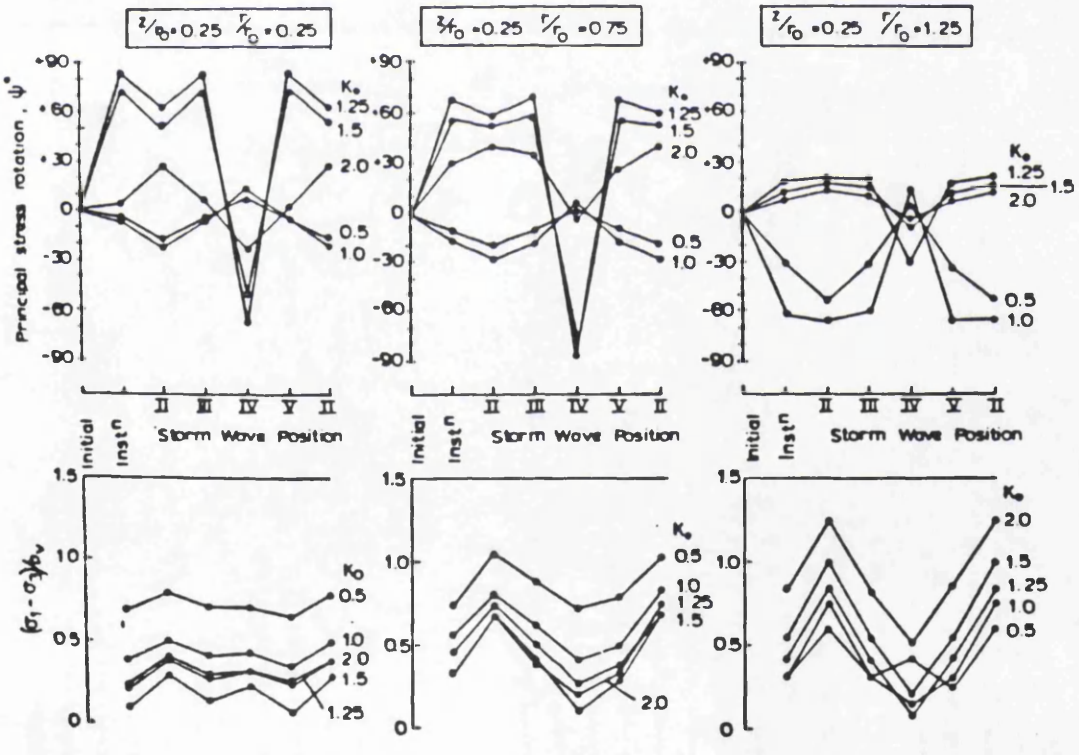

Principal stress rotations and changes in $(\sigma_1 - \sigma_3)$ accompanying wave loading on gravity platform.

Fig. 1.4 The stress path characteristics of the sea bed soil beneath the gravity structure when subjected to continuous and cyclic rotation of principal stress directions (after Hight, 1983)

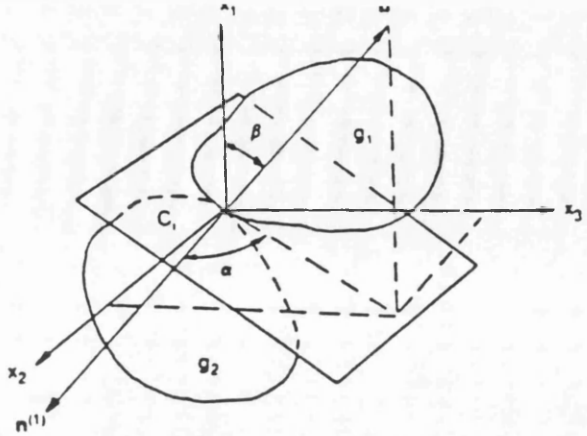

Fig. 1.5 Angles α and ß defining contact normals (after Oda, 1972a)

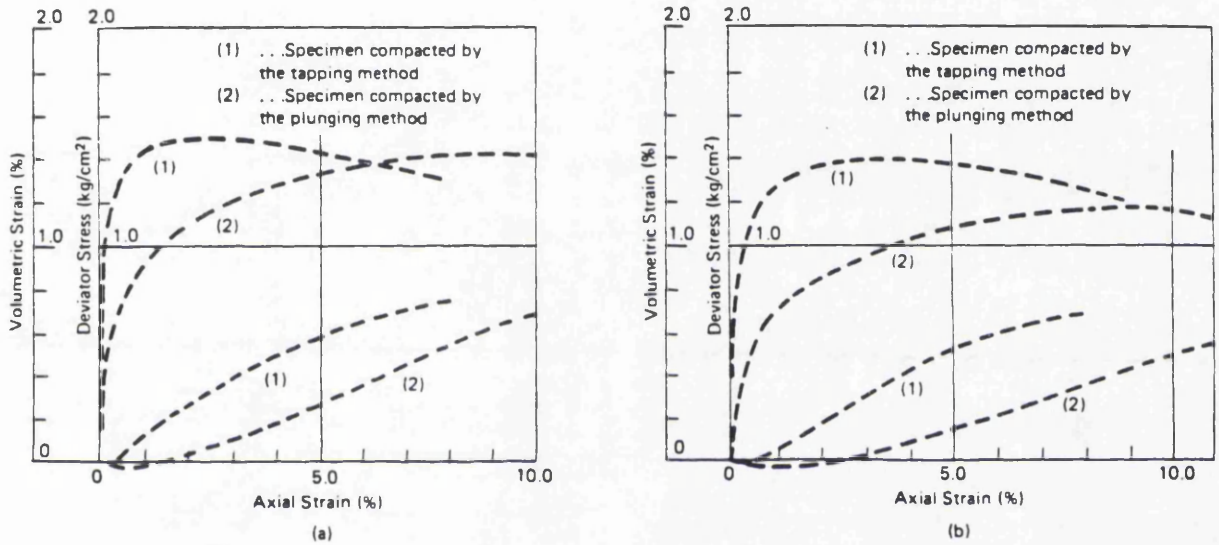

Fig. 1.6 Effects of sample preparation on stress-strain and volumetric strain curves for two samples of sand with identical void ratio.(after Oda, 1972)

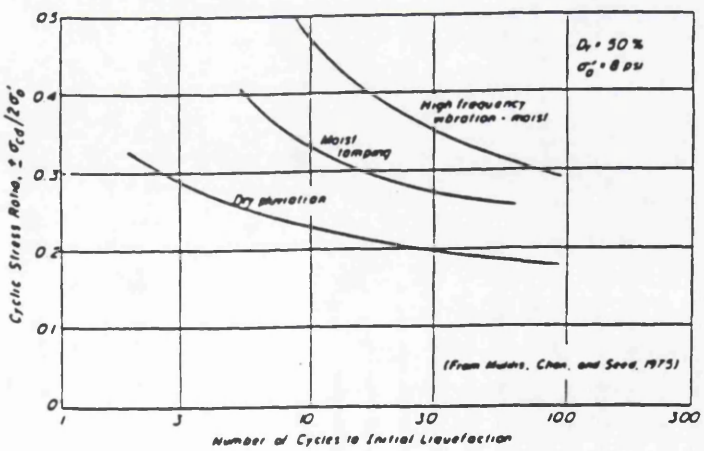

Fig. 1.7 Effects of sample preparation on Liquefaction Behaviour (after Mulilis, Chan and Seed, 1975)

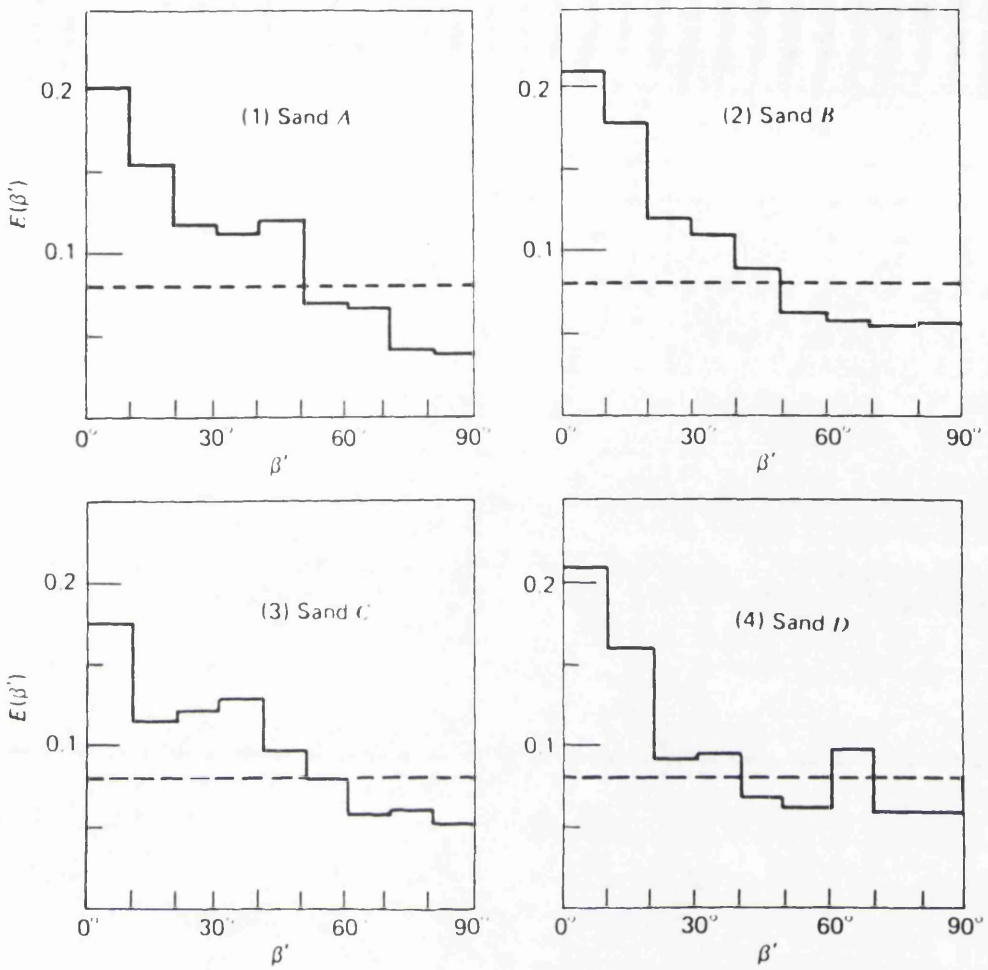

Fig. 1.8 **Distribution of interparticle contact normals for four different sands (after Oda, 1972b)**

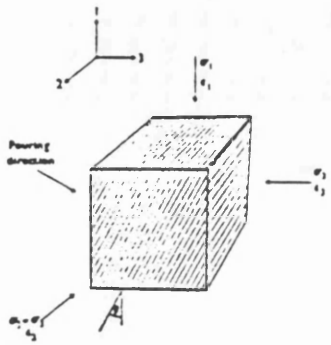

Fig. 19 (above). Reference directions

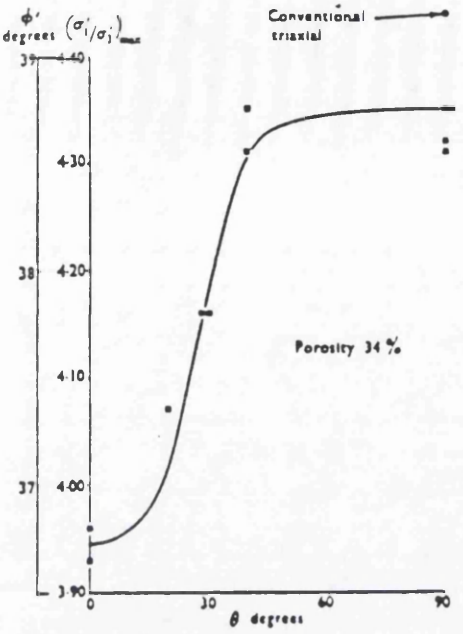

(right). Variation in drained strength with angle of tilt

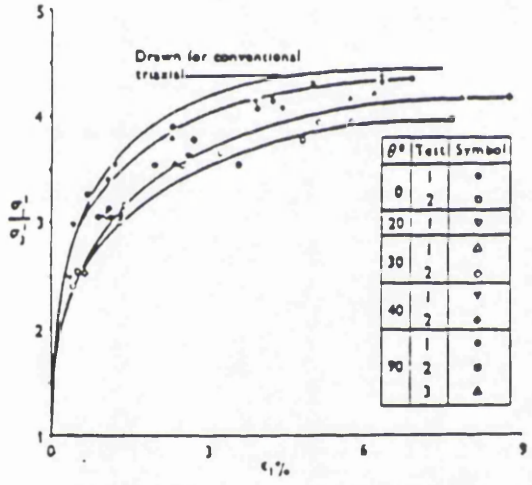

Stress ratios–major principal axial strain

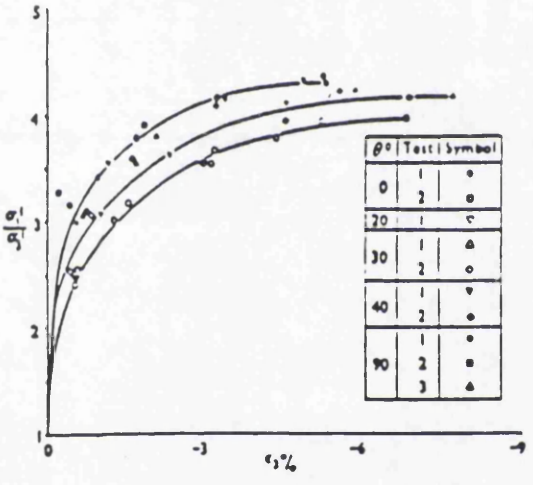

Stress ratios–minor principal lateral strain

Fig. 1.9 Effects of inherent anisotropy on strength and stress-strain behaviour of Leighton Buzzard sand tested in triaxial compression (after Arthur and Menzies, 1972)

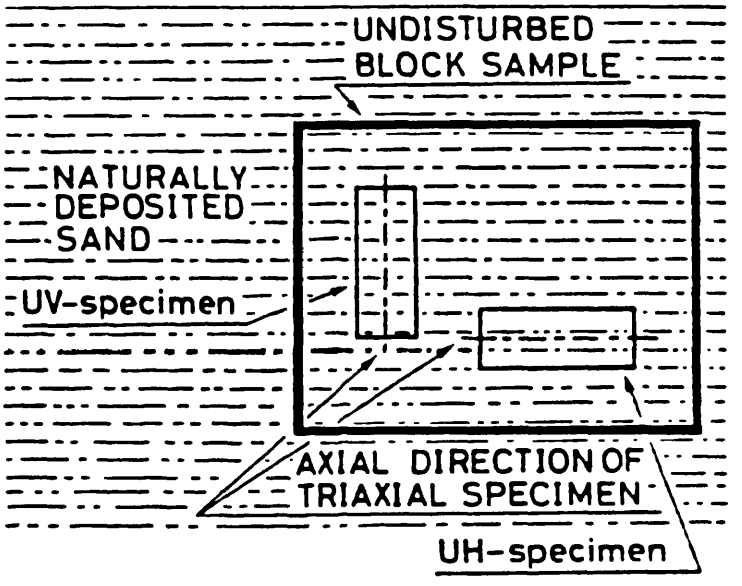

Fig. 1.10 **Method for preparing undisturbed vertical and horizontal samples from an undisturbed block (after Miura and Toki, 1984)**

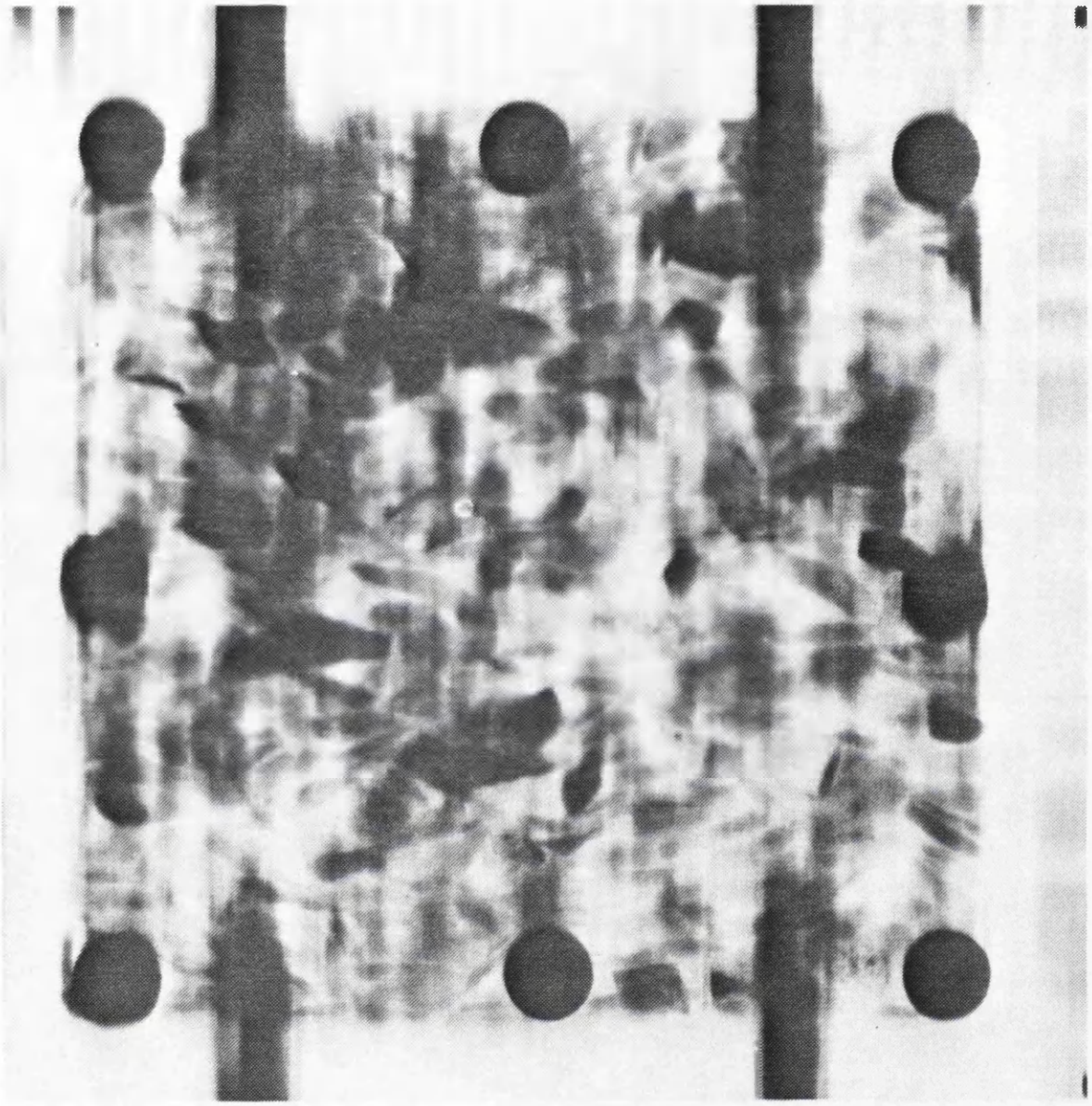

Fig. 1.11 A tomograph of a gravel sample illustrating the preferred orientations of particles (after the Hatjiethimiou, 1979)

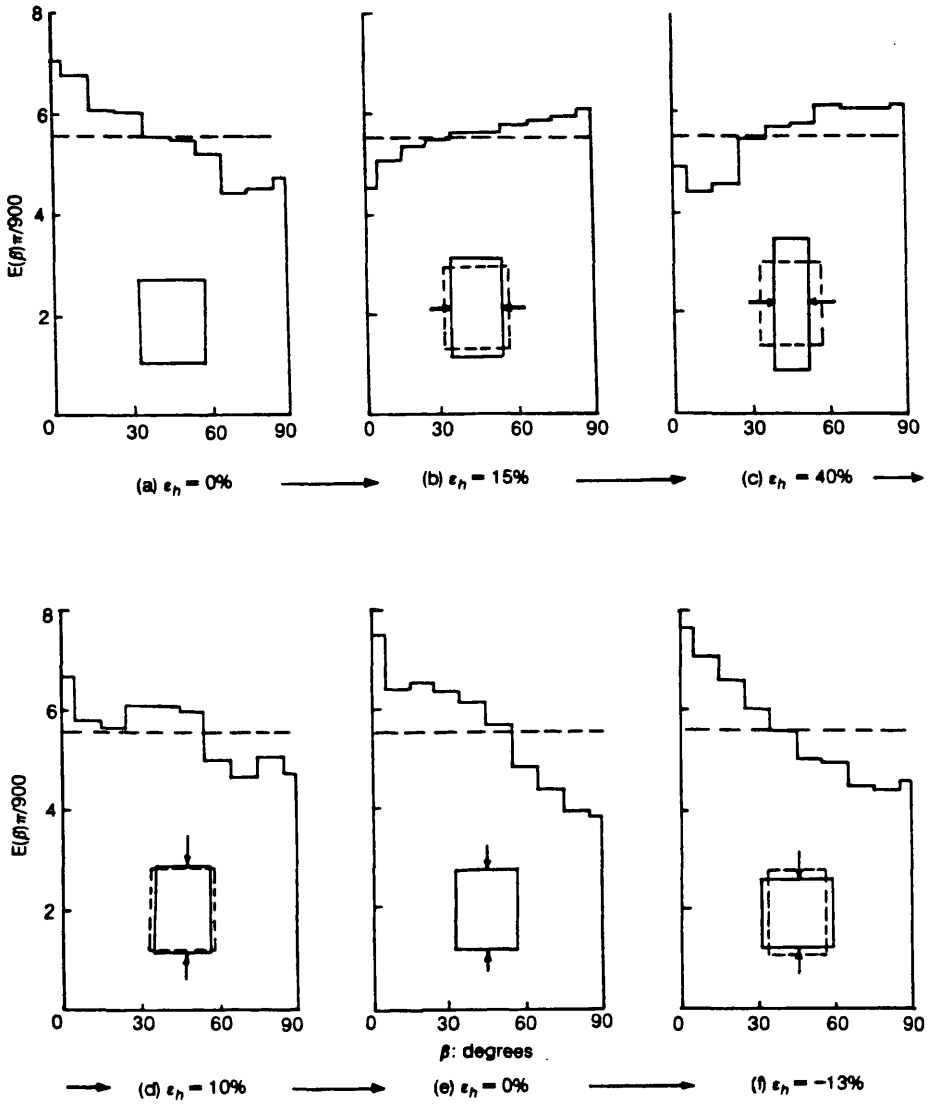

Fig. 1.12 Changes of fabric during biaxial compression test (modified from Biarez and Wiendieck, 1963; Wiendieck, 1967);(a) initial anisotropy of fabric; (b) and (c) sample is compressed laterally; (d) and (f) sample is compressed vertically; dashed line indicates the isotropic distribution (after Oda et al., 1980)

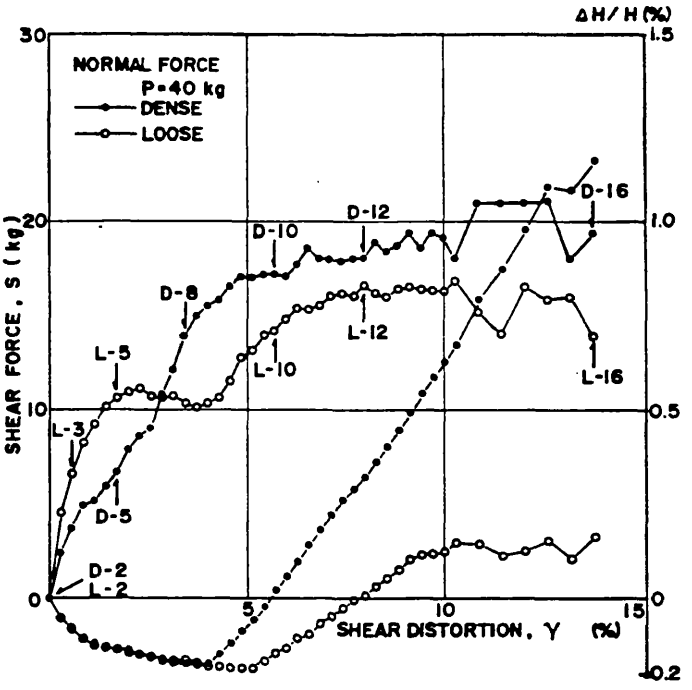

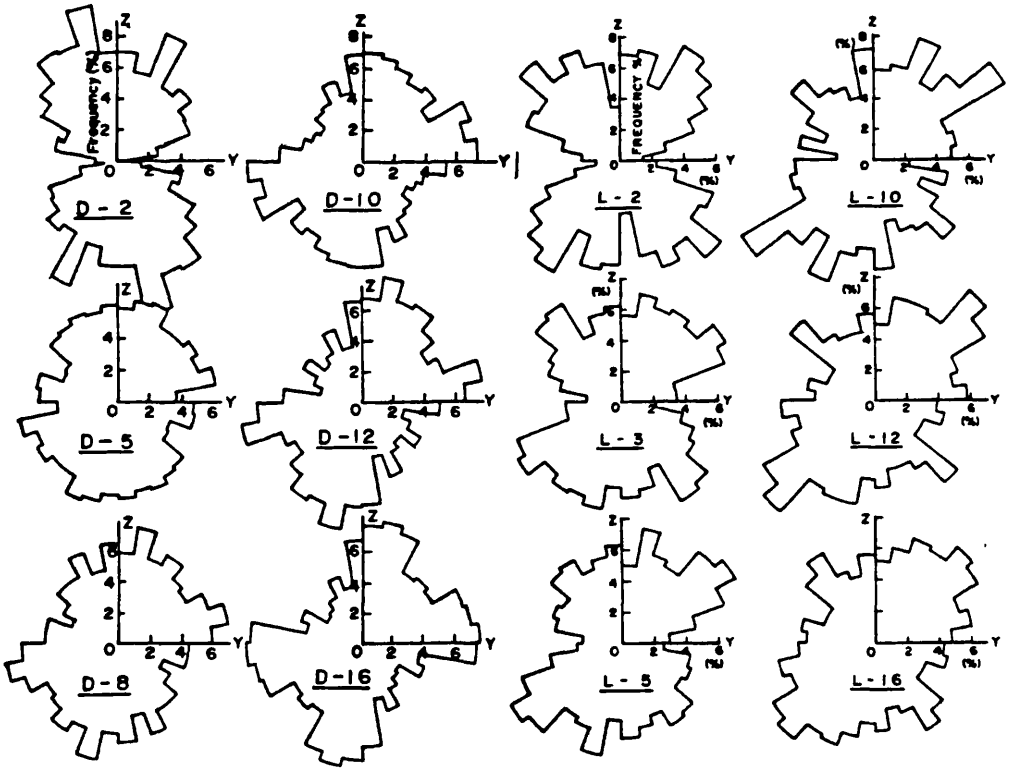

Fig. 1.13 Changes of fabric during two-dimensional simple shearing (Oda and Konishi, 1974)

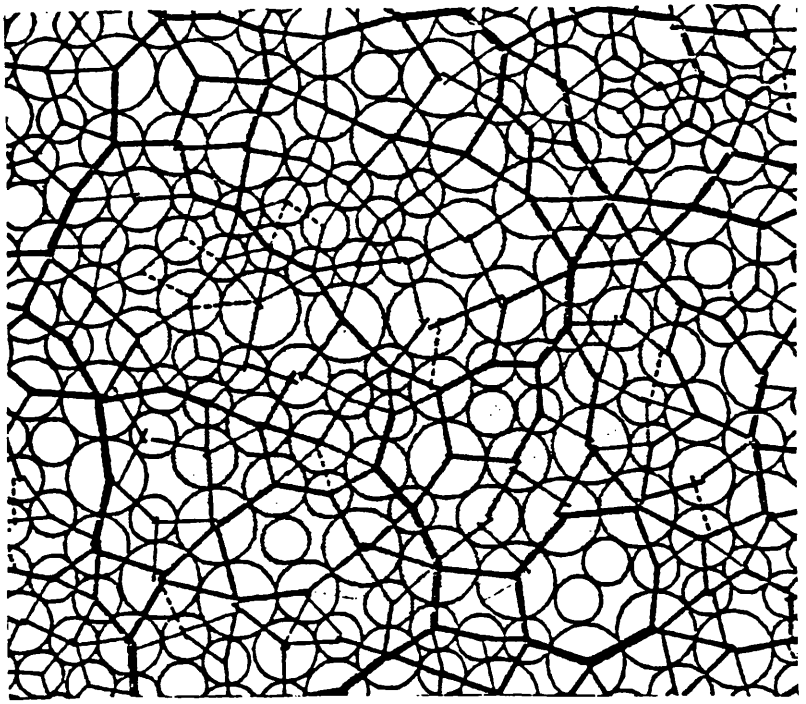

a) Starting state (isotropic stress)

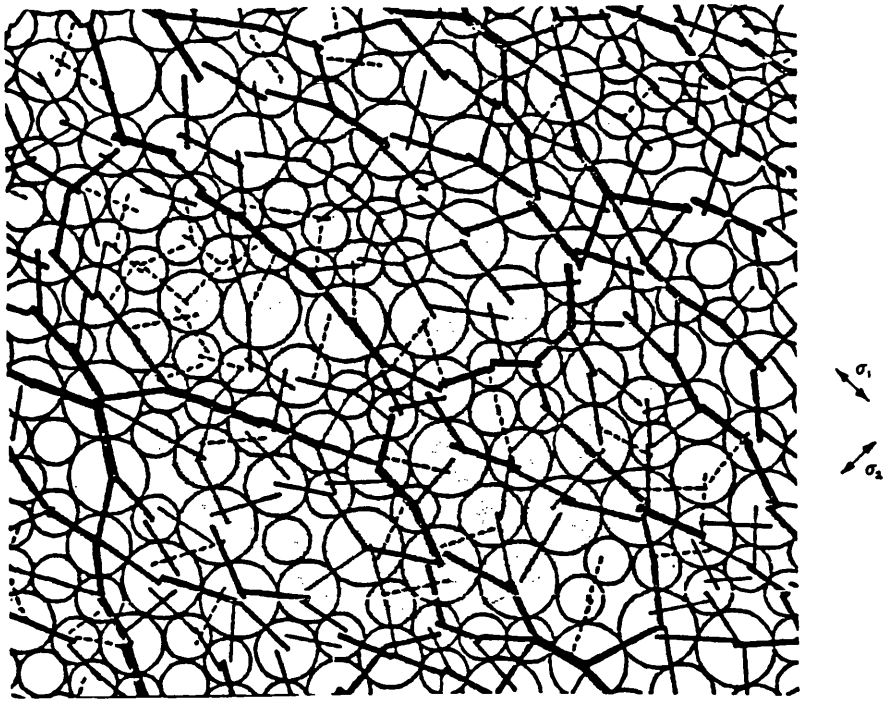

b) High deviatoric stress

Fig. 1.14 **Changes of column loads during shear (a) Column load at the initial isotropic state of stress and (b) column loads at high deviatoric stress (after Cundall, 1980)**

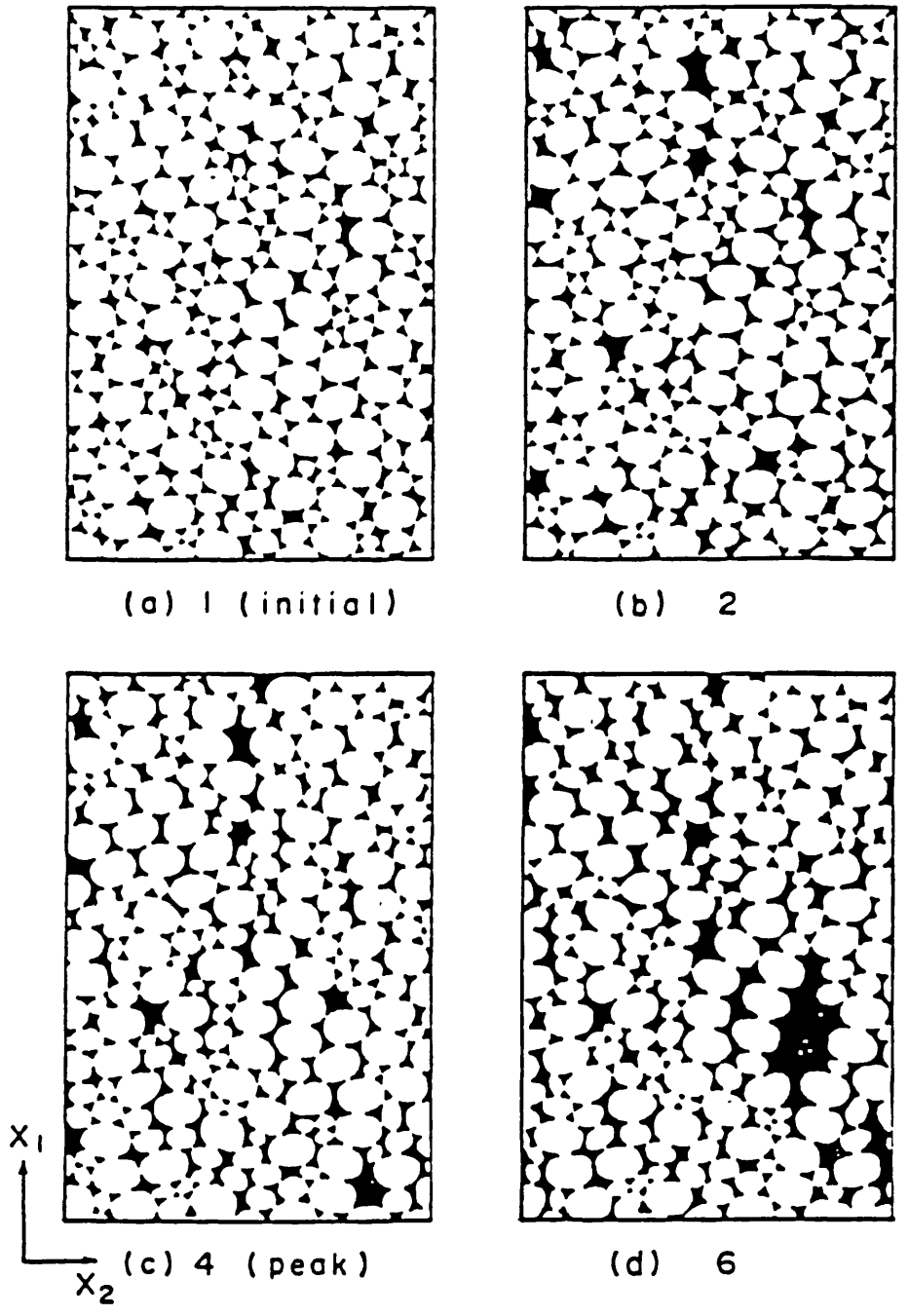

Fig. 1.15 Successive changes of void shape during axial compression for two dimensional Oval rods (after Oda, Nemat-Nasser and Konishi, 1985)

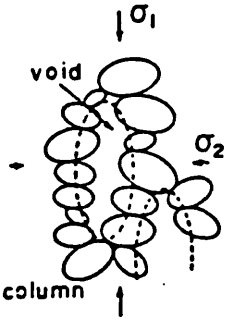

Fig. 1.16 Mechanism of void elongation parallel to the direction of major principal stress direction (after Oda, Nemat Nasser, and Konishi, 1985)

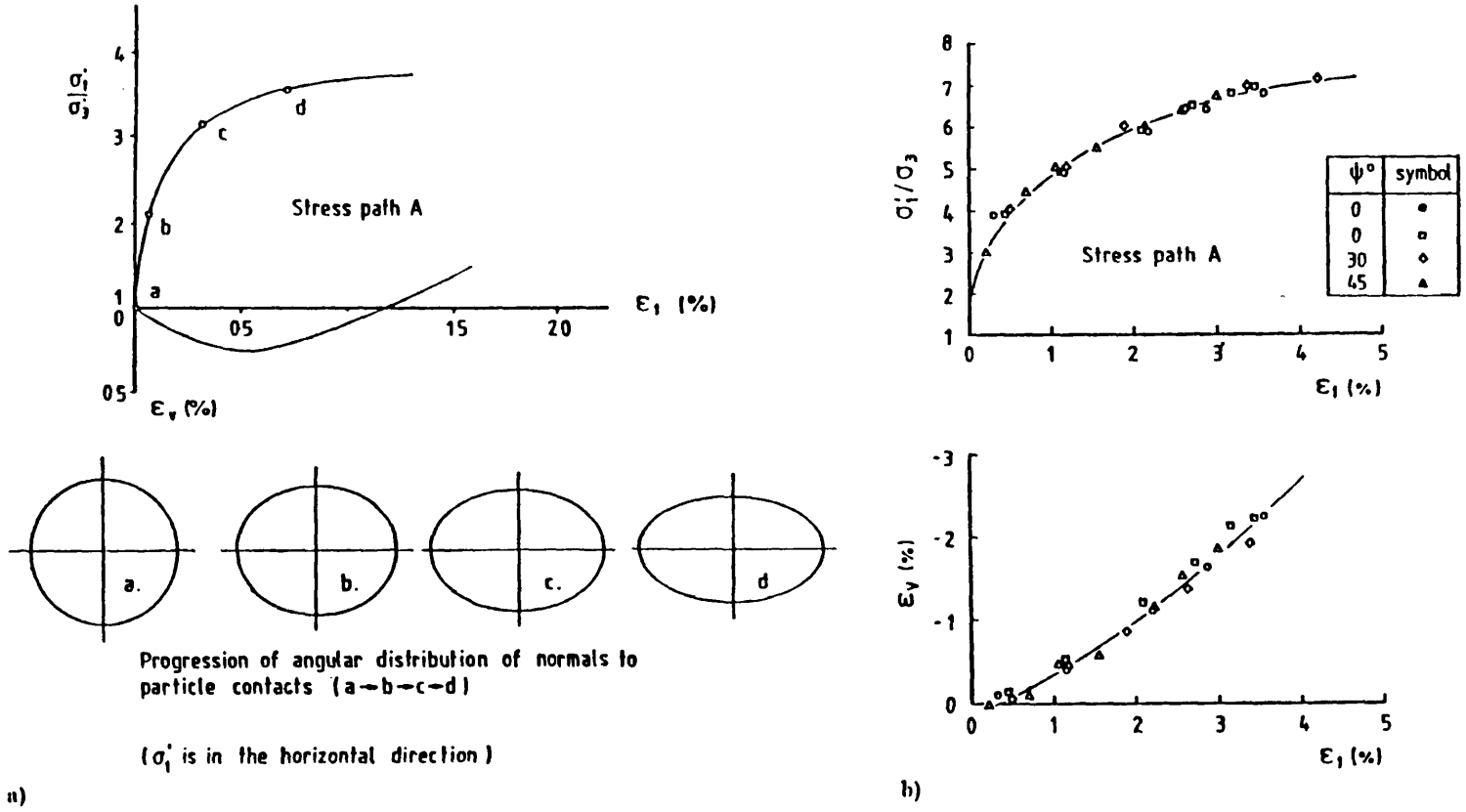

Fig. 1.17 **Comparison of stress-strain behaviour of dense sand in a theoretical model (a) with experimental data (b) in a monotonic type of loading (after Arthur, Koenders, and Wong, 1986)**

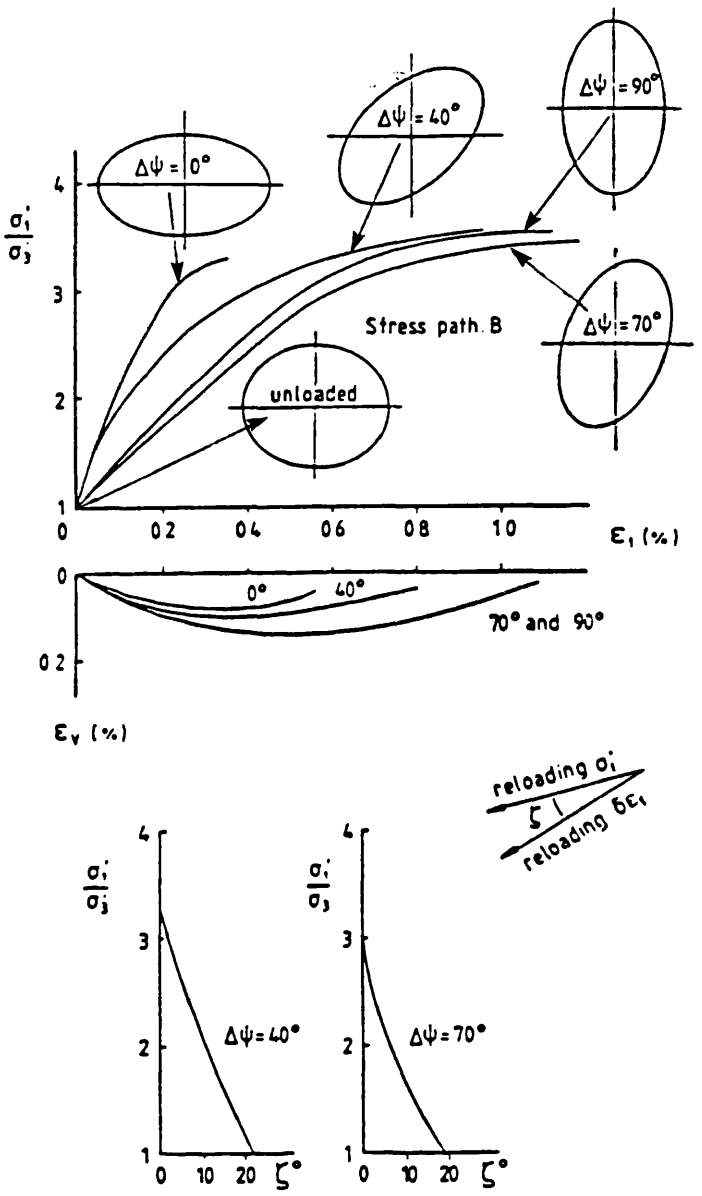

Fig. 1.18 **Comparison of model prediction and dense sand data for reloading (after Arthur, Koenders, and Wong, 1986)**

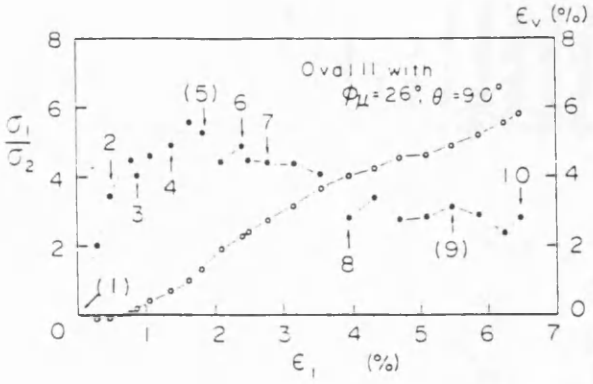

(a)

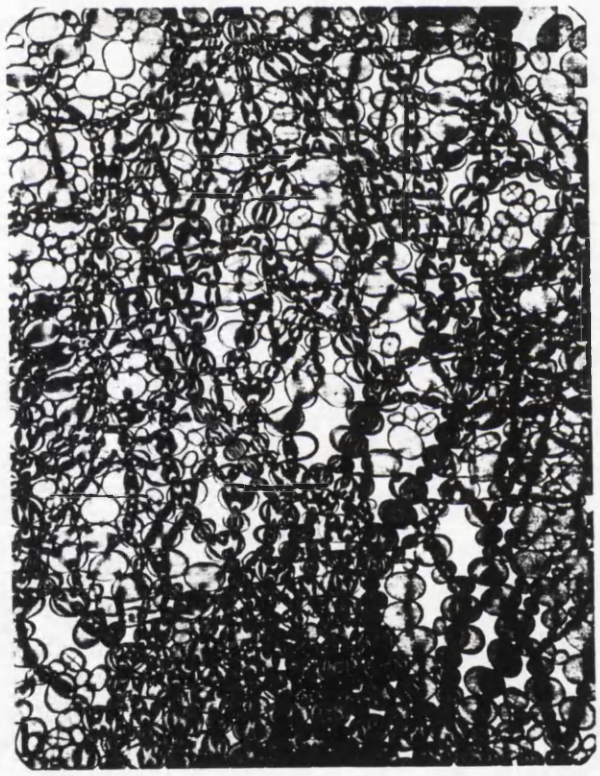

(b)

Fig. 1.19 Formation and collapse of column-like load paths at peak and residual stress state (after Oda et al. 1982)

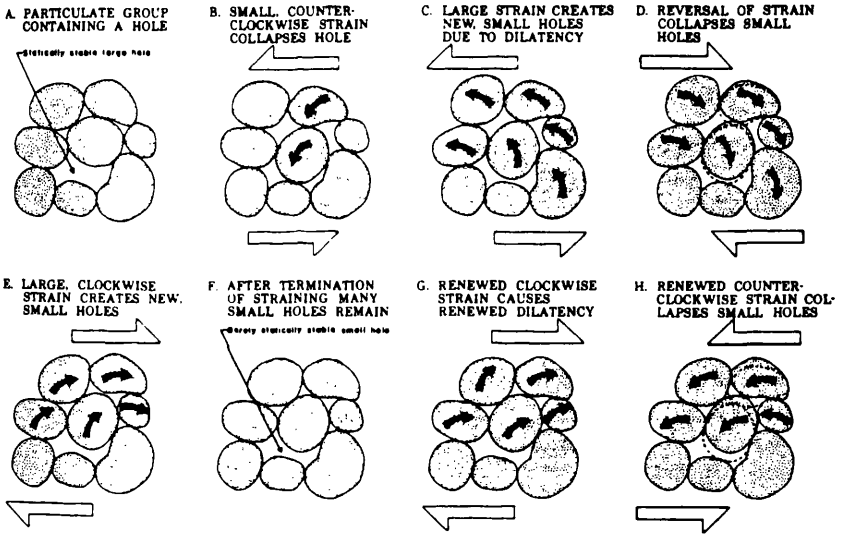

Fig. 1.20 **Descriptive study of fabric changes during cyclic loading (after Youd, 1977)**

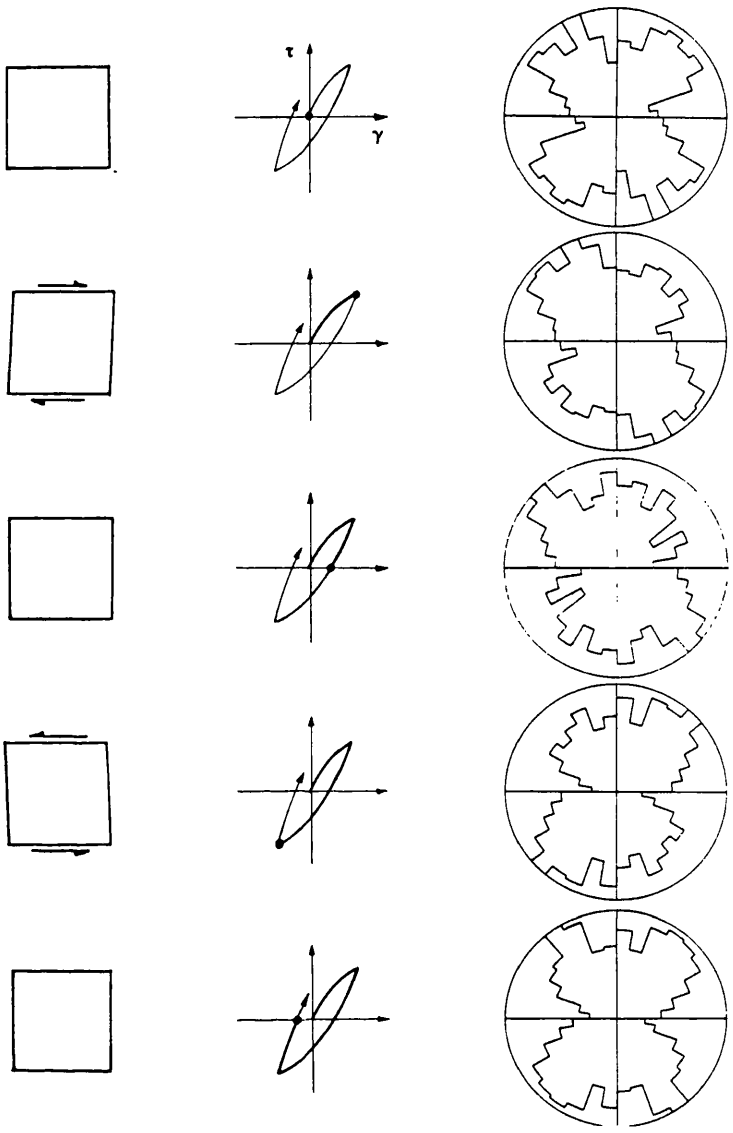

Fig. 1.21 Fabric changes during a simple shear cyclic loading of a "numerical sample" (after Oner, 1984)

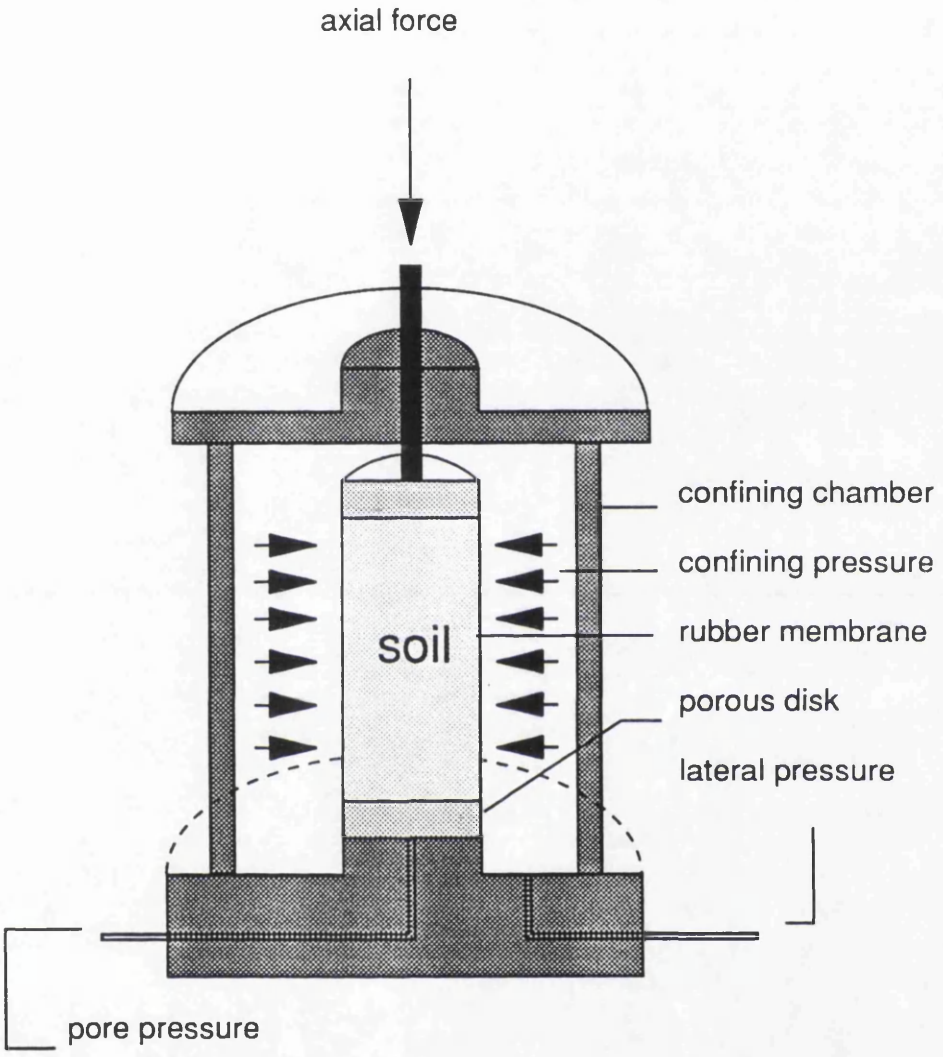

Fig. 1.22 A schematic view of the conventional triaxial apparatus

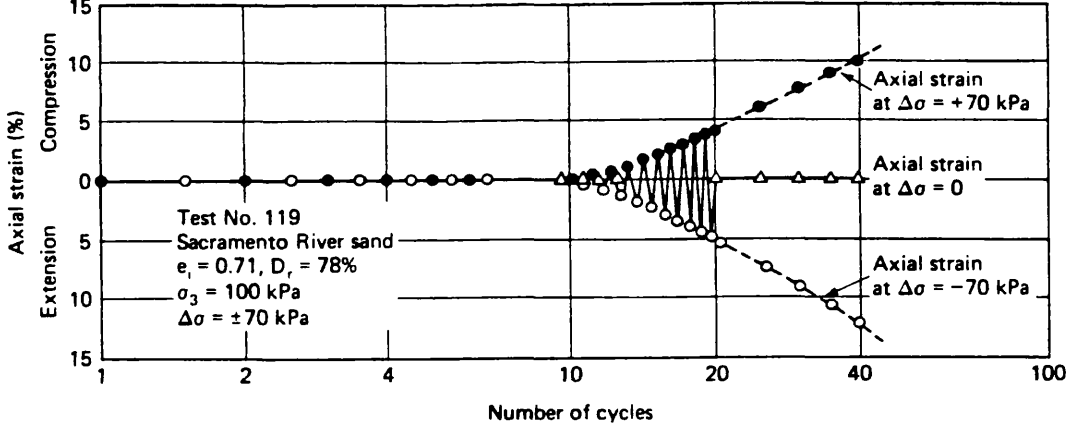

(a) Axial strain vs. number of cycles

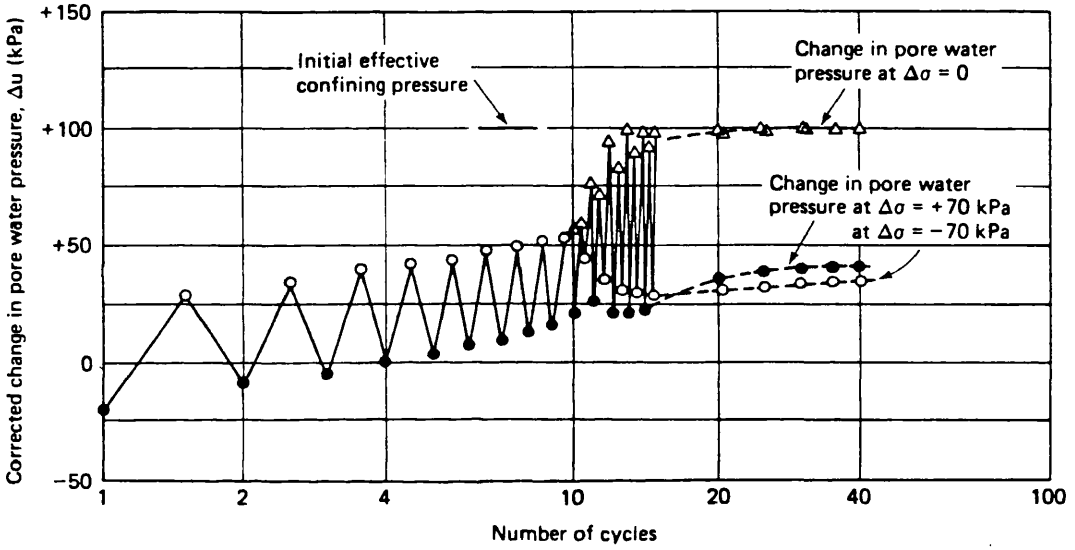

(b) Corrected change in pore water pressure vs. number of cycles

Fig. 1.23 **Results of a typical cyclic triaxial test on dense sand (after seed and Lee, 1966)**

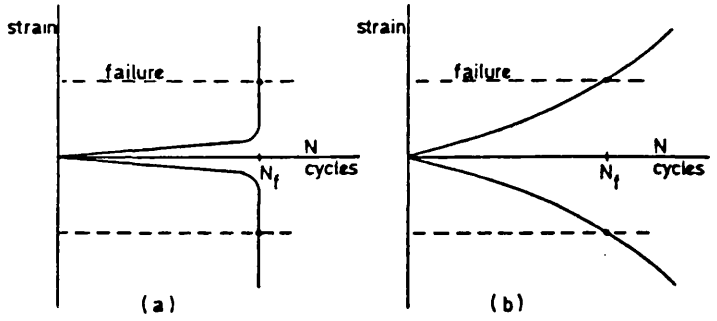

Fig. 1.24 **The limitation of number of cycles to failure as a material parameter.(a) and (b) illustrates plots of strain against number of cycles for cyclic stress controlled tests. Each test reaches the cyclic strain failure criterion at the same number of cycles, but the characters of the response are quite different (after Wood, 1980)**

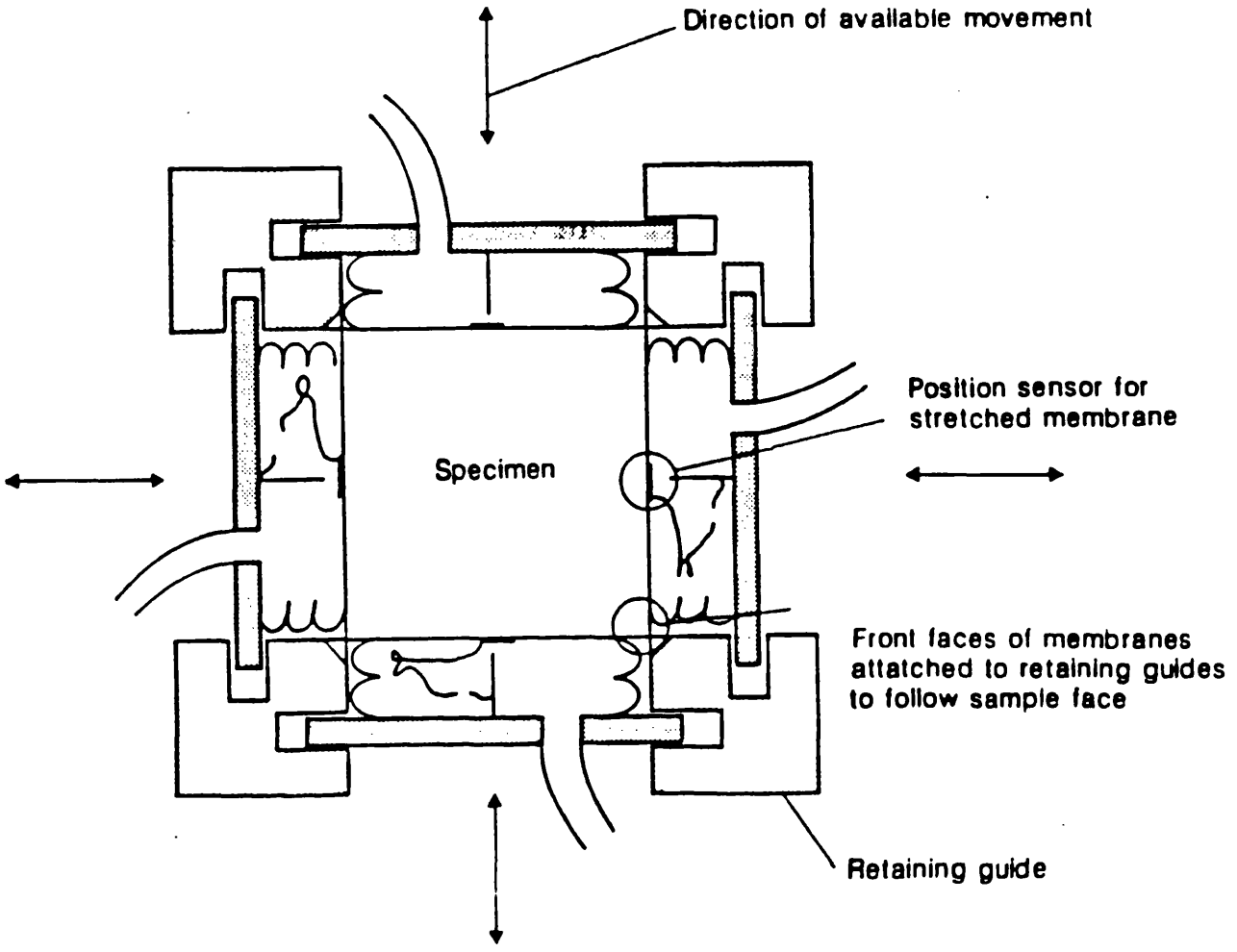

Fig. 1.25 Flexible boundary Biaxial Tester apparatus (after Arthur et al., 1985)

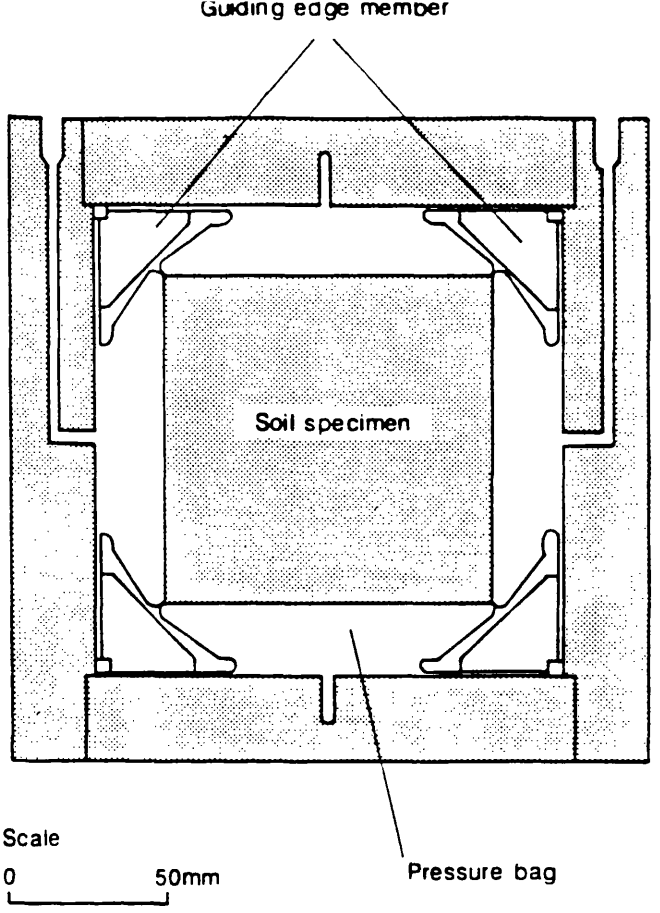

Fig. 1.26 **Cross section of Flexible boundary True Triaxial Apparatus (after Davoudzadeh, 1982)**

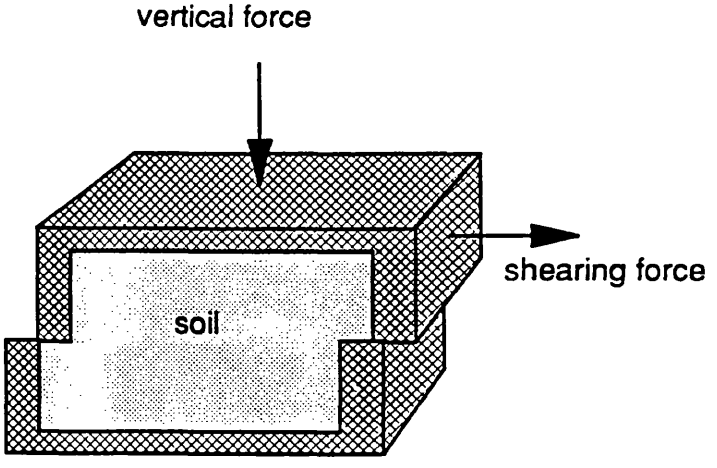

Fig. 1.27 **Principle of the Direct Shear Apparatus**

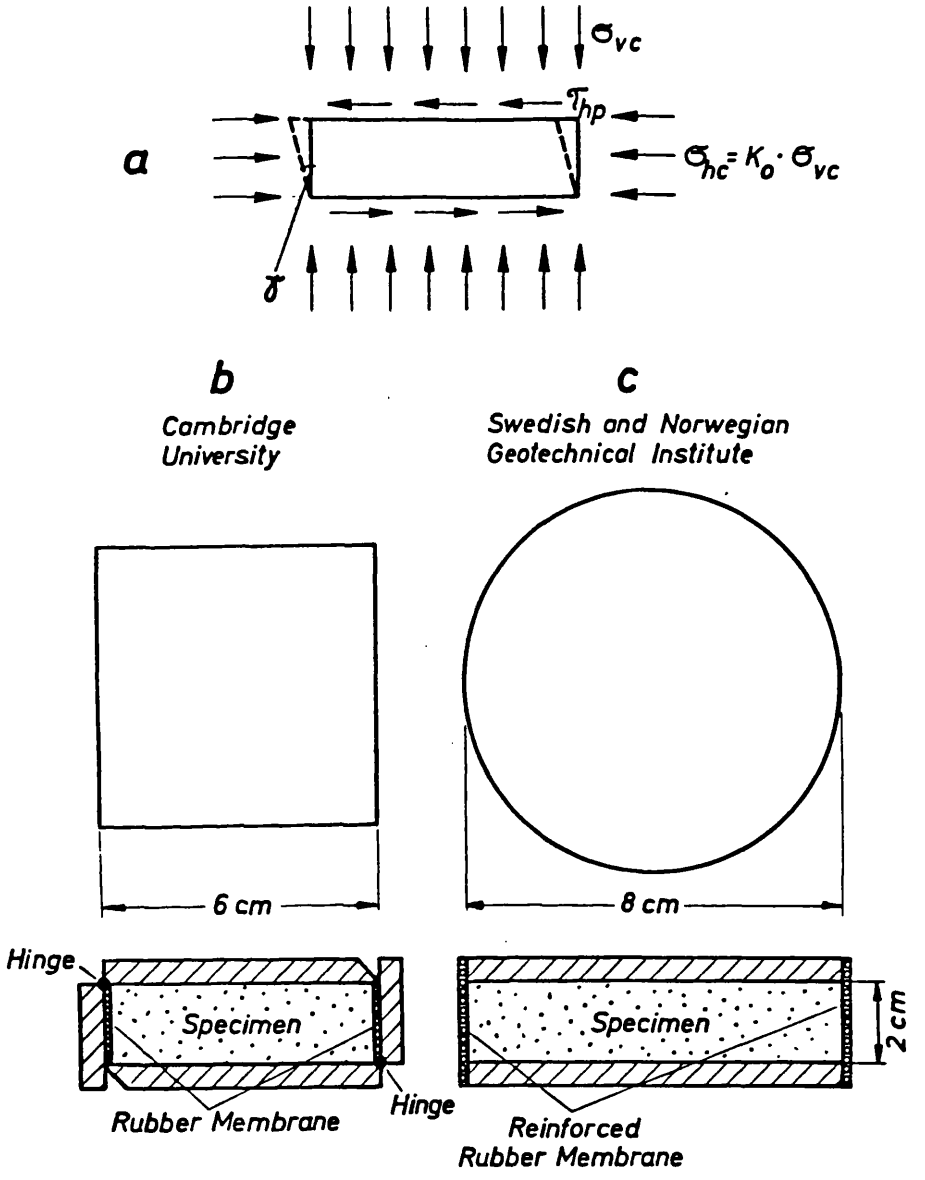

Fig. 1.28 (a) Stress condition in a Simple Shear Apparatus, (b) schematic view of the Cambridge simple Shear, (Roscoe, 1953) and (c) schematic view of the norwegian Geotechnical Institute (Bjerrum and Landva, 1966)

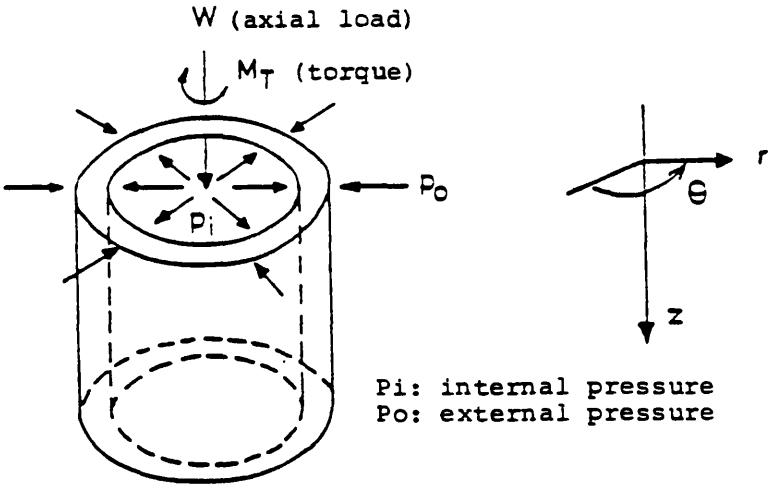

(a) Hollow cylinder sample under axial load, W, torque, M_T, internal pressure, p_i, external pressure, p_o

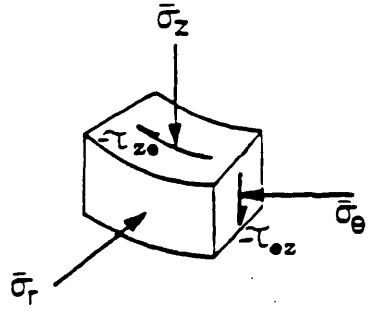

(b) Stresses on an element in the wall of a hollow cylinder sample

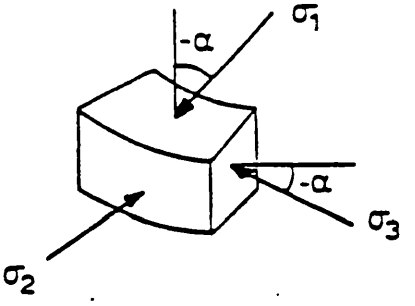

(c) Principal stresses on an element in the wall

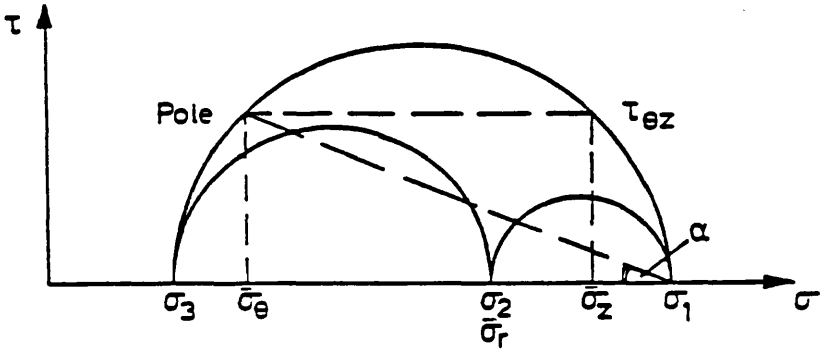

(d) Mohr circle representation of stress in the wall

Fig. 1.29 Idealized stress conditions in a hollow cylindrical element

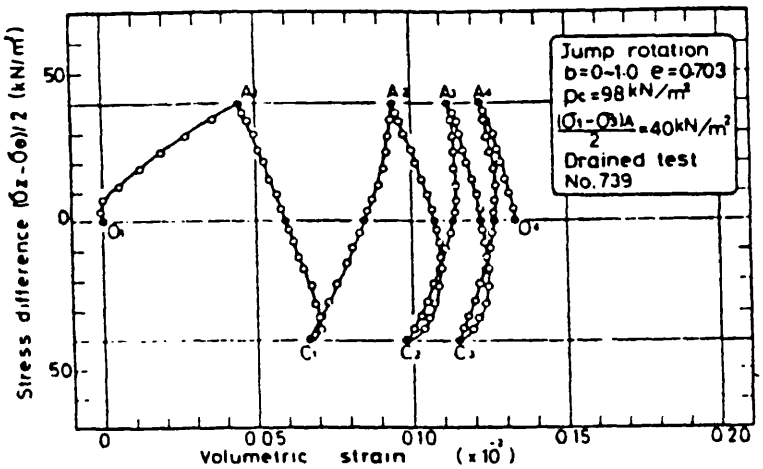

Volumetric strain in the test with changing b-value with jump rotation of P.S. directions

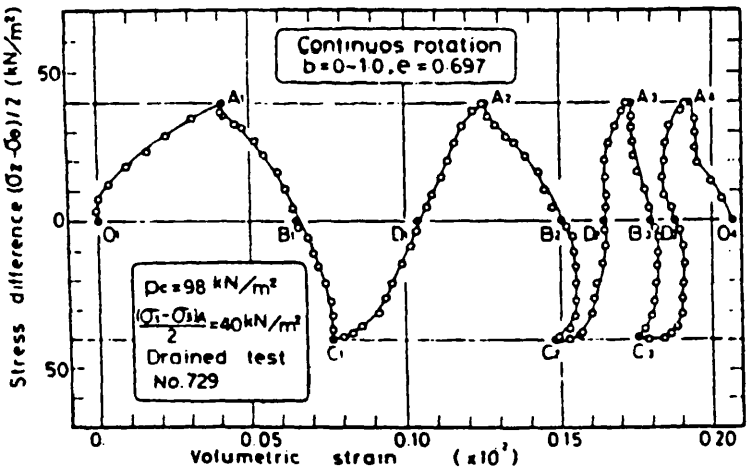

Volumetric strain in the test with b = 0.5 with continuous rotation of P.S. directions

Fig. 1.30 **Greater volumetric strain due to the continuous rotation of major principal stress direction. (after Ishihara and Momenzadeh, 1986)**

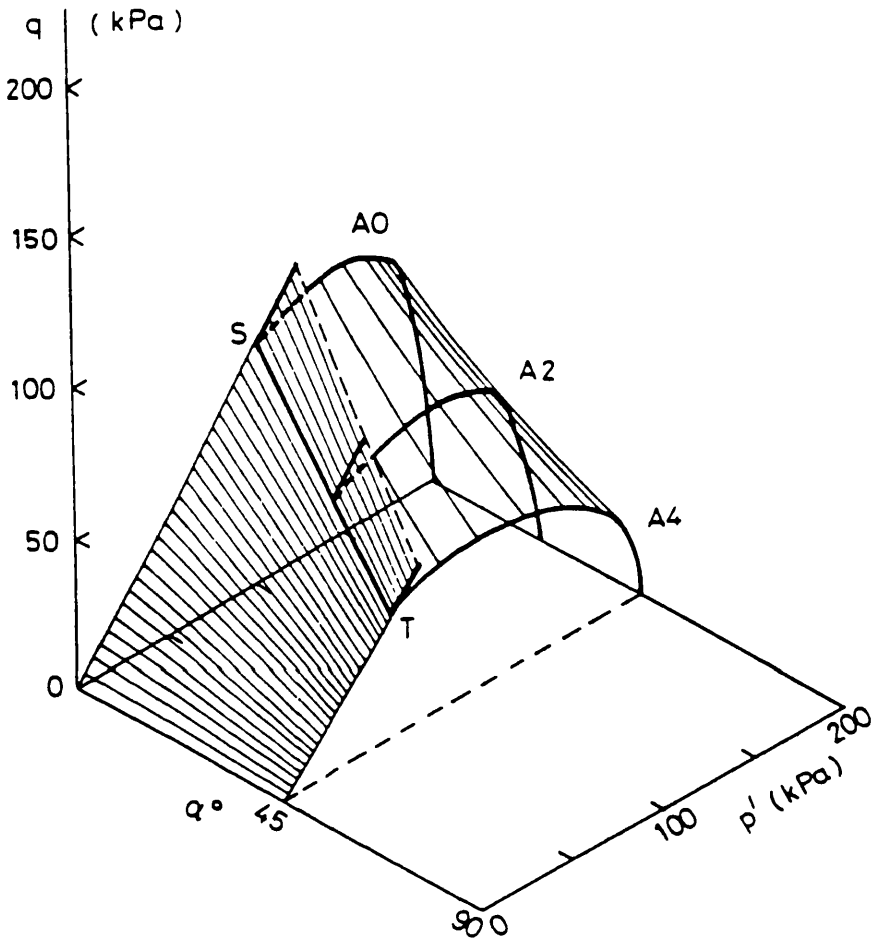

Fig. 1.31 **The complete State Boundary Surface for Undrained Tests (after Symes, 1983)**

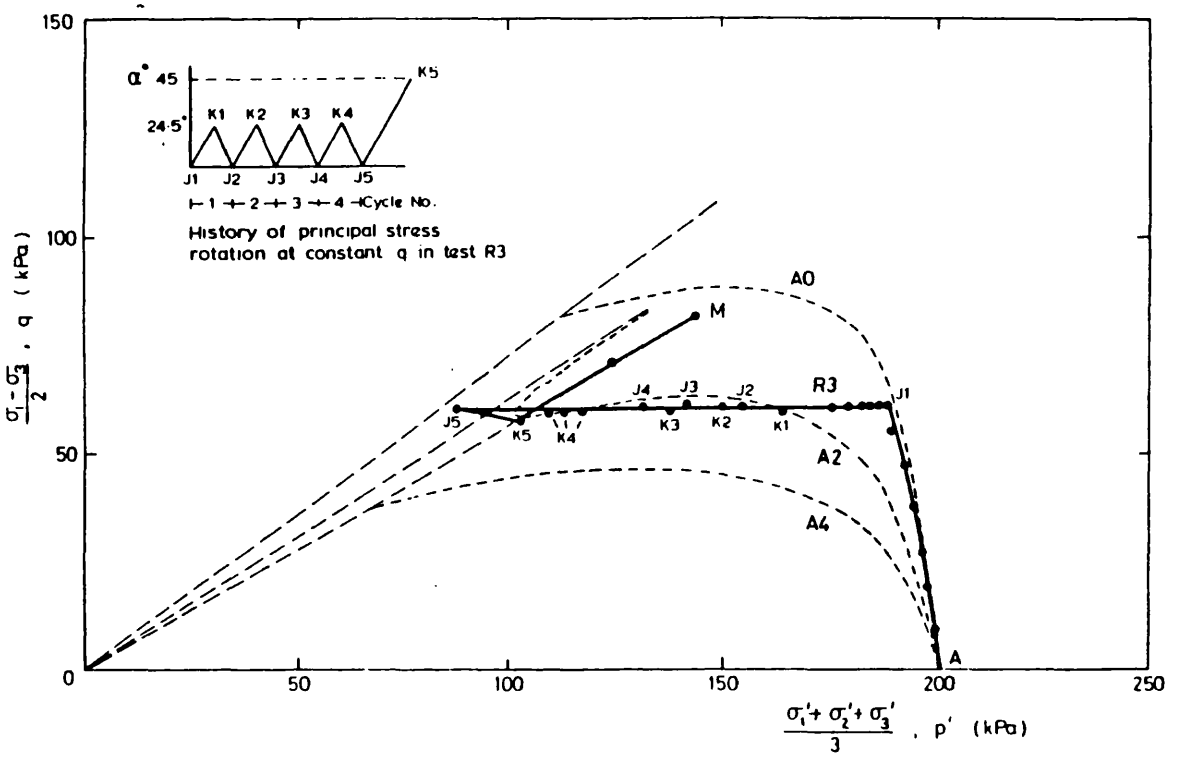

Fig. 1.32 Two dimensional view of State boundary Surface and the effective stress path for a rotational test, R3. (after Symes, 1983)

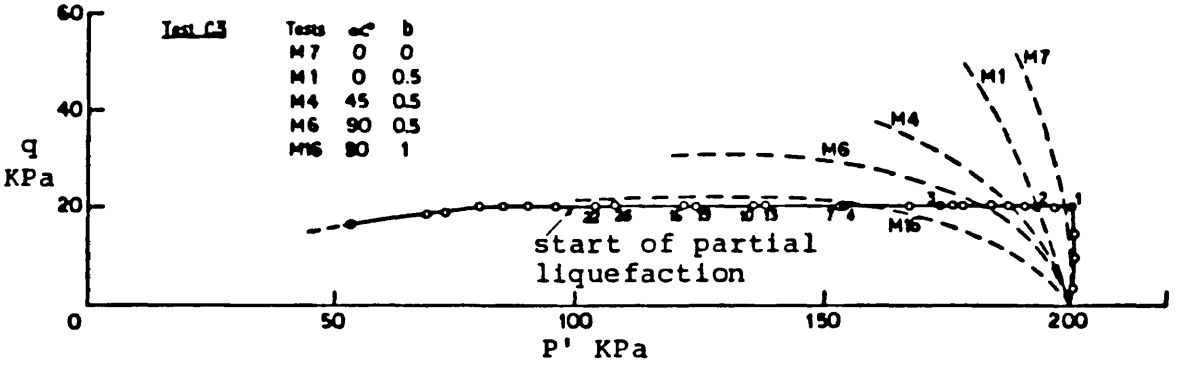

Fig. 1.33 Effects of undrained cyclic rotation of principal stress directions and the tendency to liquefaction due to directional changes of major principal stress

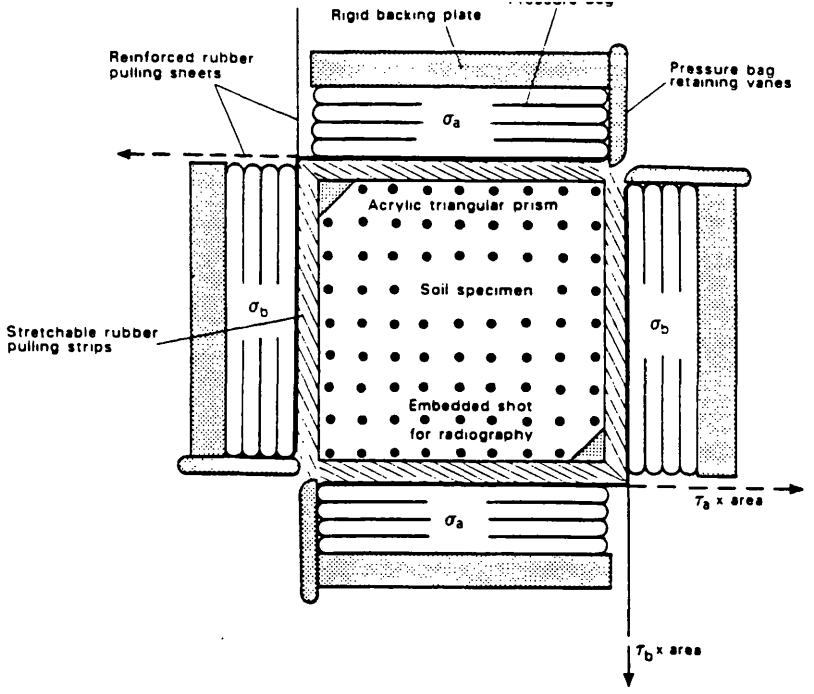

Fig. 1.34 **Schematic view of the Directional Shear Cell (after Arthur et al., 1977)**

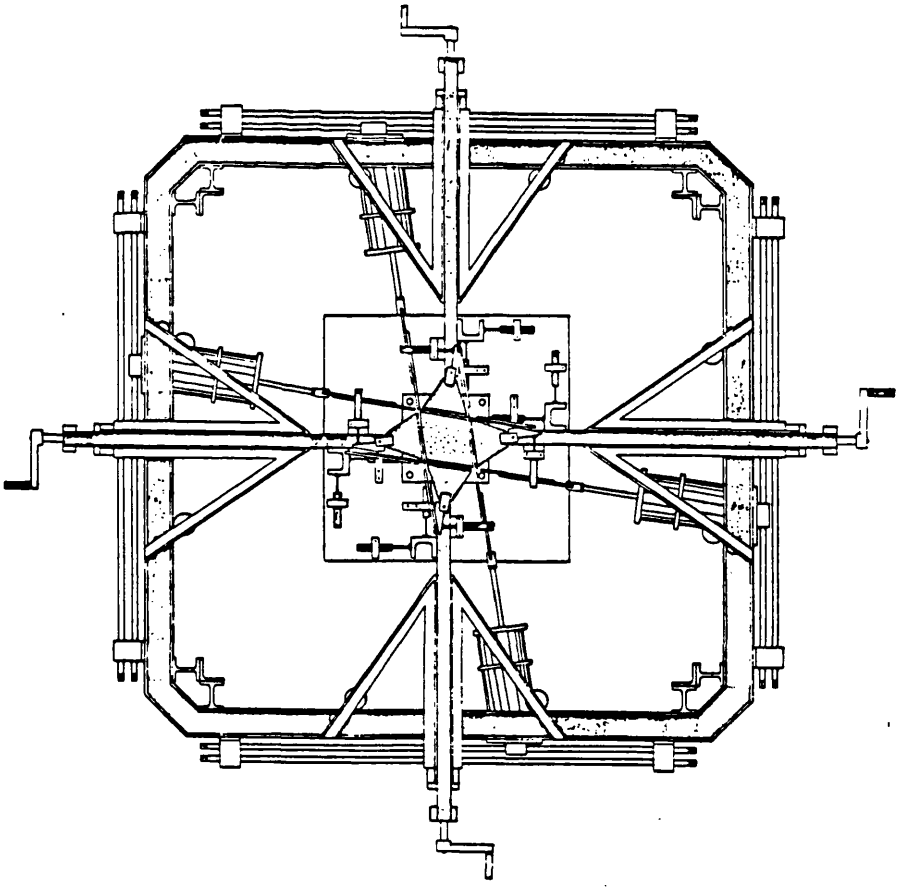

Fig. 1.35 **A schematic view of the Colorado Directional shear Cell (after Sture, et al., 1985)**

CHAPTER 2 DEVELOPMENT OF THE DAISY CHAIN DIRECTIONAL SHEAR CELL

2.1 INTRODUCTION

2.2 REVIEW OF PREVIOUS VERSIONS OF THE DIRECTIONAL SHEAR CELL

2.3 DESCRIPTION OF THE DAISY CHAIN DIRECTIONAL SHEAR CELL

2.3.1 Normal pressure system

2.3.1.1 Normal pressure bags

2.3.1.2 Adjustable backing plates

2.3.1.3 Semi-rigid thin retaining vanes

2.3.2 Shear stress system

2.3.2.1 Low stress shear sheets

2.3.2.2 Daisy Chain shear sheets

2.3.2.3 Actuating cylinders

2.3.2.4 Shear sheets aligning system

2.3.3 Plane strain system

2.4 STRESS CONTROL AND MEASURING SYSTEM

2.5 DEFORMATION MEASURING SYSTEM

FIGURES

TABLES

2.1 INTRODUCTION

The Daisy Chain Directional Shear Cell (DCDSC) is a flexible boundary stress-controlled apparatus that aims to impose uniform normal and shear stresses to the four faces of a cubical sample. The major principal stress direction can be controlled by varying the normal and shear stress components acting on the four faces of the sample. The sample is constrained on two faces so that deformation is essentially plane strain. The intermediate principal stress can be either monitored or controlled by the aid of a water-filled pressure bag that forms part of the bottom plane strain face. The basic features of the apparatus showing the location of normal pressure bags and daisy chain shear sheets are illustrated in Figure 2.1 .

This device has the capability of shearing undisturbed soil samples at stress levels normally encountered in engineering practice. The newly developed shearing sheets provide a higher load capability compared to earlier versions of the Directional Shear Cell, and also avoid hysteresis effects while cycling boundary shear stresses. The perfection and thorough evaluation of the operating mechanism of these shear sheets formed an integral part of development of the Daisy Chain DSC. An isometric view of a part of the Daisy Chain DSC is shown in Figure 2.2 .

This chapter presents the design concept and the underlying principle of the Daisy Chain Directional Shear Cell. First, it briefly reviews the earlier versions of the Low Stress Directional Shear Cell and then goes on to describe the Daisy Chain DSC which was used in the current study. Part of this research programme involved the development of the apparatus, consequently a section of this chapter is devoted to the description and development of the major components that make up the Daisy Chain DSC. The methods of application and measurement of stresses in the device are presented. Finally methods of determining the strains occurring in the sample are described.

2.2 REVIEW OF PREVIOUS VERSIONS OF DIRECTIONAL SHEAR CELL

The original Directional Shear Cell (DSC), described by Arthur et al. (1977), was designed to investigate the response of dense sands to changes in principal stress direction under plane strain conditions.

This first apparatus was a flexible boundary plane strain device which had the

unique capability of controlling the major principal stress direction by varying the normal and shear stresses acting on the four faces of the sample constrained between two rigid end platens. Figure 1.34 shows a cross section of this original DSC in the plane of strain. The cubical sample is enclosed in a thin rubber membrane (with sand glued on four internal surfaces) which is brought into complete adhering contact with the inner side of a thin rubber sheet known as a shear sleeve on four external surfaces. The shear sleeve is glued on its outer surface to a series of lubricated stretching rubber strips with an unstretched free length of 25 mm arranged almost parallel with the sample side and attached at their other ends to inextensible reinforced rubber pulling sheets. The pulling sheets apply the shear load which is transformed into uniform surface shear forces on the sample face by the evenly distributed and freely stretching rubber strips. The outer surfaces of the pulling sheets are lubricated so that these sheets can slide over the surfaces of the normal pressure bags which act on the sample faces through intervening rubber. These normal pressure bags were supported by acrylic backing plates screwed to the top and bottom plane strain sides. The shear and normal stresses were both produced from systems using water pressure. Any potential instability of the normal pressure bags was discouraged by retaining vanes attached to the sides of the backing plates. The three variables σ_a, σ_b, τ_a and τ_b may be varied to allow any change in principal stress directions up to a maximum change of 90°.

It was mentioned previously that this shearing cell was designed for tests on dense sands in which strains would be expected to be relatively small. Therefore the initial design was deliberately kept simple to focus on perfecting the novel shearing sheets which controlled changes in the principal stress direction. Loose samples which show large prefailure strain were never tested in this apparatus leaving many questions associated with this particular type of material unanswered.

When using the original DSC with fixed backing plates and testing loose sand Rodriguez (1977) experienced difficulties that can be seen in Figure 2.3a. In his loose tests the sample faces did not remain parallel to the backing plates and the normal pressure bags no longer remained rectangular, expanding in region (B) and contracting in (A). Also in region (B) the adjacent normal pressure bags touched each other resulting in stress concentrations in this area. In region (A) it could be seen that an area near the intersection of the shear sheets might not be covered by the normal pressure bags.

In order to overcome these problems, Rodriguez introduced a concept of adjustable

backing plates and an aligning shear sheet system which has since been incorporated in the later versions of the DSC. Large deformation of loose samples in which the backing plates are adjusted and the position of the shearing cylinders changed to conform to the changing shape of the sample are illustrated in Figures 2.3.b and 2.4.

Arthur et al. (1981) presented extensive data for drained shear tests performed at the Massachusetts Institute of Technology (MIT) using the DSC on both dense and loose Leighton Buzzard sand samples. Work covered the role of inherent and induced anisotropy. Germaine (1982) using Rodriguez's apparatus extended the work and the apparatus to investigate the anisotropic response of undrained soft clay soils (with pore water pressure measurements) that had previously been K_o consolidated.

Wong and Arthur (1985a) in an extensive series of drained tests on dense sand using the DSC explored the effects of rotating principal stress directions in a cyclic manner in sand. The version of the DSC used by Wong and Arthur in their investigation was modified to incorporate a flexible water-filled pressure bag enabling the intermediate principal stress to be monitored or imposed during a test. They also improved the performance of the DSC by installing a computer and its peripherals to control the application of cyclic stresses. This system also enabled rapid storage and manipulation of data.

However, all of these versions have two serious and inherent limitations. First, the DSC could only be used with the boundary shear stresses not higher than 50 kPa. Thus all of the previous experimental work using the DSC has been restricted to a low stress level in geotechnical engineering terms. The second problem was the hysteresis response of the shear sheets when subjected to the cyclic loading. The major advantage of the DSC over other testing equipment is attributed to the stretching component of the shear sheets which apply a uniform shear stress to the face of the sample while under normal pressure. The stretched components cannot easily recover when unloaded in cyclic loading tests and are held to some degree by the normal pressure bags. Although this limitation could be overcome by varying the mean normal stress levels during the continuous rotation tests while keeping the shear stresses constant (Figure 2.5), the rotation of principal stress directions is then inevitably linked to a change in mean normal stress level. Also it limited the angle of cyclic rotation to a maximum of 70°.

2.3 DESCRIPTION OF THE DAISY CHAIN DIRECTIONAL SHEAR CELL

The next version of the DSC was modified to provide a capability for higher stress levels and to avoid hysteresis of the shear sheets particularly in the cyclic tests when imposing cyclic variations of the boundary shear stresses. The new Directional Shear Cell is in many ways similar to the earlier DSC with the main difference appearing in the shear sheet system which was designed by Arthur and likened to a daisy chain.

The Daisy Chain Directional Shear Cell is a flexible boundary stress controlled apparatus and aims to apply uniform normal and shear stresses to opposing sample faces normal to the plane of strain. Figure 2.1 illustrates the basic features of the apparatus. The major principal stress direction can be controlled by varying the normal stress (σ) and shear stress (τ) acting on four faces of a 100 mm cubical sample constrained between the plane strain sides, while the intermediate principal stress could be either controlled or monitored during the test. The method used to apply normal and shear stresses is illustrated in Figure 2.6.

The soil specimen in its rubber membrane is in direct contact with the shear sheet inner rubber sleeve and, when degreased, the rubber membrane and inner rubber sleeve adhere together completely as the normal stress is applied across the pair. Fourteen non-stretchable rubberized pulling strips made of sail cloth (PE 70) are attached to the outer surface of each face of the shear sleeve. These strips are glued to fourteen stretchable pulling elements well away from the area of normal pressure operation (Figure 2.7). A combination of shear sleeve, non-stretchable strips and stretchable elements make up the Daisy Chain shear sheets. Fourteen single elements of these sheets are attached to a pressurized piston by an aluminum clamp. The shear force is transferrmed uniformly through these shear sheets and then evenly onto the sample by virtue of the stretchable elements. A layer of sand glued onto the inner surface of the specimen membrane is used in the final shear stress transfer into the specimen. The non-stretchable strips are thoroughly lubricated to prevent any shedding of load through adhesion along these strips, and ensures shear load will be evenly distributed to the shear sleeve even though normal stress is transferred across the strips from the normal pressure bags. The stress range in these shear sheets can be increased because each Daisy Chain shear sheet incorporates a succession of stretching elements of increasing stiffness along the Daisy Chain which come into play one after the other as stress level rise. When each element has stretched 25 mm, the strong cloth in parallel with it takes any further

increase in load. A further advantage of the new shear sheets is the elimination of hysteresis in the shear sheets while imposing cyclic variations in shear stress. Figure 2.8 shows a photograph of the DCDSC. Figure 2.2 illustrates an isometric view of the DCDSC with its associated parts identified.

Major components and functions of the DCDSC

The proper operation of the DCDSC requires the alignment of the surface of a deforming sample with the stressing system to be maintained. It is also necessary to maintain the shear stresses parallel to the faces of the sample and follow the changing shape of the sample with the normal pressure bags. Furthermore it is necessary to ensure that the normal pressure bags fully cover the sample sides at all stages of the test, particularly when large deformation is attained.

2.3.1 Normal pressure system

The normal pressure system is illustrated in expanded form in Figure 2.9 and in component form in Figure 2.10. It consists essentially of two separate parts (a) a set of flexible concertina pressure bags locked to a backing plate, and (b) a separate plate fixed to the plane strain sides but able to move sideways. It is also used to align the pressure bag plate parallel to the face of the sample at any stages of the test. Each component of the system will now be described.

2.3.1.1 Normal pressure bags

Normal stresses are applied to the four vertical faces of the sample by means of concertina type reinforced rubber bags, Figure 2.11. Each of these pressure bags consists of three separate bags glued together with evo-stik adhesive.

In the previous version of the DSC, used by Wong (1986), four separate bags were glued together to make a normal pressure bag. However, while conducting the preliminary tests (described in Chapter 4) with the DCDSC, the author noted that, the greater the number of bags used, the greater the likelihood of instability of the normal pressure bags, particularly at higher pressures. As the backing plates were adjustable, it was found that only three segments were required to achieve a uniform stress distribution on the sample face during a test.

The separate segments were manufactured by dipping a mould into latex and

allowing it to cure, a practice which is commonly used at UCL (Menzies and Phillips, 1972). These segments were reinforced with an open weave polyester material. The reinforcement of normal pressure bags is essential to prevent any local blow out. Figure 2.12 illustrates the process of reinforcement for one segment. Prior to assembling the individual bags, holes must be cut in the bag faces, so that there is an uninterrupted channel between the bags for air pressure to flow. The three reinforced segments were glued together with evo-stik, a contact adhesive which was spread on each surface to be glued. The alignment of individual bags before contact is very important. The communication hole in each reinforced rubber bag is cut in such a way that a reinforced cross-piece remains in the centre of the hole. This cross-piece increases the lateral stiffness of the bag and provides additional lateral support and stability to the pressure bag which is necessary at high working pressure. The rear of the outermost segment has a 50 mm diameter hole where the membrane forms a 18 mm deep neck and then opens up into a 86 mm diameter flange, Figure 2.12e. This type of normal pressure bag has been tested satisfactory to withstand over 300 kPa. The procedure of making pressure bags was described in detail by Bekenstein (1980) and Germaine (1982).

2.3.1.2 Adjustable Backing Plates

Front backing plate

The normal pressure bag is fixed to the front backing plate. The front backing plate, Part (a), as illustrated in Figure 2.10 is of aluminum alloy having dimensions of 100 x 100 x 15 mm with a 60 mm diameter central hole. Each normal pressure bag rests against the inner side of the backing plate and is fixed through its flange by a round clamping plate. An 'o' ring is placed on the inner side of the clamping plate to provide a seal between the flange of the pressure bag and the clamping plate.

A reinforced polyethylene tube of 12 mm bore diameter was connected through an "Instantair" coupling to the clamping plate in order to provide air pressure to the normal pressure bags. This "Instantair" coupling provides an easy means of decoupling the normal pressure bag when necessary. A Bell and Howell pressure transducer of 0-300 kPa capacity was also connected to the clamping plate to record the normal pressures in the bags.

Rear backing plate

The rear backing plate supports the front backing plate at three points. The rear backing plate Part (b), illustrated in Figure 2.10, is of aluminum alloy having dimensions of 98 x 106 x 25 mm. A central hole of 46 x 62 mm provides access for the pressure transducer and the pressure supply tube. It is connected to top and

bottom plane strain sides through four location pins and is free to move sideways but can be locked in position by four wing nuts when necessary.

The forward, backward and rotational movements of the front plates are achieved with the aid of three adjusting screws that pass through the rear backing plate. Two of these screws locate on counter bores on the front plate and the third just makes contact with the back of the front backing plate Part (a).

The test is run with a pre-determined distance of 20mm being maintained between the front of the normal pressure bag and front backing plate. This matching displacement is achieved with the aid of a precise grating on a transparent acetate film which is fixed to the top plane strain plate (Figure 2.13). This enables the operator to achieve the incremental sample deformation through adjustments at the rear backing plates. The rotational adjustment is the most commonly used in Directional Shear testing because of the wide variety of rotational tests; this is achieved through the three adjusting screws. Figure 2.14 illustrates an extreme setting of this type of adjustment at the end of a largely deformed sample.

2.3.1.3 Semi-rigid thin retaining vanes

Side support is also needed for the normal pressure bags. Despite decreasing the lateral expansion of the normal pressure bags by incorporating the reinforced cross-pieces, there tends to be an unwanted lateral expansion of the bag, especially at high stress levels. If not restricted this lateral expansion could easily misalign the shear sheets. Also, locking the adjustable backing plates does not provide total lateral stability for the bags during testing, because, when the sample strains and before realignment of the backing plates, unequal lateral forces can develop in the bags which can cause a sudden lateral movement of the bag. In order to provide stability, retaining vanes were screwed onto the sides of the front part backing plates, Figure 2.7.

Thickness and rigidity of the previous retaining vanes can create two other problems. Due to the thin nature of the Daisy Chain shear sheets there is only a small space between the normal pressure bag and the face of the sample compared to that of the conventional DSC. In the earlier DSC apparatuses the stretching component and non stretching pulling sheets occupied this space, the total thickness being about 8 mm. Employing the conventional retaining vanes of 4 mm thickness might be appropriate for the conventional DSC but could cause non-alignment of the shear

sheets in the DCDSC (Figure 2.15). This could result in a local unloading of the normal stresses near the edge of the sample, possibly producing a higher stress ratio and causing a greater local strain. The second problem was due to the rigidity of the thick vanes that could prevent the bag from following the sample deformation particularly at higher working pressures as illustrated in Figure 2.16. These problems were resolved by introducing semi-rigid retaining vanes made of high tensile spring steel, with thicknesses of 1mm. These thin vanes solved the thickness problem but were flexible enough to expand as the normal pressure increased. Different stiffness vanes could be used at different normal stresses.

2.3.2 Shear stress system

The unique feature of the Directional Shear Cell apparatus is the shear sheets. These sheets apply a uniform shear stress to the four faces of the sample while allowing uniform normal stresses to be transmitted through these sheets from the normal pressure bags.

The low pressure shear sheets subdivide the shear force into 120 small forces, (Figure 2.17). These forces are applied to different areas across the sample faces and are then transformed into shear stress through redistribution in the rubber sleeve, the sample membrane and the soil specimen itself.

Section 2.2 highlighted the two serious limitations of the earlier versions of DSC that were attributed to the design of the shear sheets. In the new design limitation on stress level has been improved by a factor of three, and shear sheet hysteresis in cyclic loading is mainly resolved. The author used both the low and high stress shear sheets in his research so for completeness both types will be described here.

2.3.2.1 Low stress shear sheets

The manufacture of low stress type of sheets has been described by Arthur et al. (1977), Bekenstein (1980), Rodriguez del Camino and Dunstan (1981) and Germaine (1982). These shear sheets consist of three main components: the inner rubber sleeve; the non-reinforced stretching strips; and the outer reinforced pulling sheets. Figure 2.18 illustrates an overall view of these sheets, each of these components serving a special function.

The thin inner rubber shear sleeve (0.6mm thickness) has the same dimensions as the sides of the sample. They surround its four faces and adhere to the membrane

when under normal pressure and consequently help in distributing the shear stresses. The shear stress is transferred across this boundary through the bonding achieved under normal stress after treating both rubber surfaces with trichloroethylene and then acetone prior to each test.

The non-reinforced stretching strips transmit the shearing forces from the pulling sheets to the shear sleeve. These strips have a free length of 25mm and thickness of 1.00 ± 0.05mm, and are glued to the non-reinforced inner shear sleeve at one end and the outer reinforced pulling sheet at the other. There are 120 pulling strips per side, arranged in 8 rows. These rows are in turn separated by 8 additional rows of strips. The function of the latter rows is to present a uniform surface for the normal pressure bags as well as keeping the pulling strips properly aligned. The pulling strips are connected at 6.5mm intervals and are 6.5mm wide. The thickness of these strips governs the shear capacity of the shear sheets. All strips are coated thoroughly with a special silicone lubricant (Arthur and Dalili, 1979). Lubrication is essential to prevent shedding of load through adhesion along these strips as appreciable normal stress is transmitted across the strips from the normal pressure bags. The large flexibility of these pulling strips, elastic at strains in excess of 300%, provides a reasonably uniform distribution of shear stress along each strip, thus minimizing the effect of non-uniform shear stress along the sample boundary.

The third component is the outer inextensible, reinforced, rubber pulling sheet which transmits the force from the pressurized cylinder to the individual rubber strips. Only 8 of the 16 rows of strips located at each face of the sample actually carry the shear load, primarily because the strips of the adjacent side must interleave in order to be attached to the shear pistons. The remaining strips only fill the gaps to allow the normal stresses to be transmitted evenly to the soil sample. The back end of each of these strips is extended 85 mm beyond the edge of the sample. This part, referred to as a tail, fills the gap created by the stretching of the strips in response to the applied shear force. The gap could also enable the normal pressure bag to apply an additional shear force to the surface of the sample.

2.3.2.2 Daisy Chain shear sheets

The Daisy Chain Shear Sheets shown in Figures 2.2 and 2.7, consist of fourteen single elements, each of these elements apply shear stress approximately to 1/15 of the sample face. No shear is applied to the reinforced edge of the sample. Figure 2.19 show a single element of these sheets. These shear sheets consist of three

main components namely the inner shear sleeve, the non stretching component and the stretching component.

1 - The Shear sleeve

The inner shear sleeve is a sheet of non-reinforced latex rubber and has the dimension of 98 x 89 x 0.6 mm. The inner surface of the shear sleeve which makes contact with the sample membrane has to be kept grease free and finally roughened with acetone to ensure a perfect bond to the outer side of the sample membrane which received similar treatment. Tricholorethylene is an effective degreasing agent but great care must be taken to not inhale the vapour.

The outer surface of the flexible shear sleeve is glued to 14 reinforced loaded areas of 98 mm x 6 mm with approximately 1 mm gaps between each reinforced area. These gaps provide the stretchability for the shear sleeve, so that the boundary of the sample can strain (Figure 2.19). However, these non-stretched regions could provide a restraint to boundary strain. Proving tests in Chapter 4 will show that this had little effect.

2 - The non-stretching component

The non-stretching component of the shear system transmits uniform shear forces to the shear sleeve from the loading system through 14 rubberized non-stretching strips. These strips are of a special sailcloth-type material (PE 70 made in Switzerland). The strips are constructed by placing the material on a clean glass sheet and held in place with tape. Latex is worked into the fabric with the excess latex being scraped off. The rubberized fabric is left in contact with air to cure, and is cut to the required shape with a soldering iron (approximately 25 watts). The soldering iron eliminates fraying of the edges of the cloth by melting the threads as it cuts. A few tension tests on the rubberized sail cloth with 25 mm overlap joint glued with evo-stick indicated that a single strip could withstand up to 35 kg load. Fourteen of these strips are glued at one end to the outer side of shear sleeve and to the stretching component at other end. All strips are lubricated thoroughly with a special silicone grease (Arthur and Dalili, 1979). Lubrication is conducted up to the region where strips interweave with the adjacent set at the sample edges. Lubrication ensures an even distribution of load to the shear sleeve, even though appreciable normal stress is transmitted across these strips by normal pressure bags. The total thickness of the non-stretching components at the sample face after lubrication does not exceed 3 mm which allows the normal stress to be applied close to the sample. Regular inspection is essential to ensure adequate lubrication exists to prevent

shedding of load through adhesion along these strips.

3 - The stretching elements

In the new design of the DSC the stretching elements have been moved away from the sample face and arranged as a daisy chain. The Daisy Chain elements are clamped and attached to a pressurized piston as shown in Figure 2.2. To prevent any unwanted slippage of the single sheets at the clamped edges, thin pieces of spring steel with dimensions of 98 mmx 50 mm x .1 mm are sandwiched between the pulling sheets and then securely clamped.

Figure 2.19 illustrates each stretching element which consists of overlength reinforced fabric glued across rubber sheets. There are four stations with overlength loops where there is a stretchable rubber sheet. The maximum increased length of each stretchable station is 25 mm, and the length of reinforced fabric is 50 mm. The stretchable rubber used for these elements is SriLankan rubber which has a Kaolin filler to prevent deterioration in the light. All sheets have a uniform thickness of 1 mm ± 0.05 .

In order to provide uniform shear to the sample over a large stress range the stretchable rubber at each station is given a different stiffness. The first station has the weakest rubber and when fully stretched the reinforced fabric prevents any further stretch but still allows stretch of the second station which has stronger rubber in the loop. This process is followed through four stations with the rubber being thicker and therefore getting stronger at each station. Figure 2.20 shows a stage at which the first station is fully stretched. Through this process shear forces are transmitted uniformly to the shear sleeve, via non-stretching strips, and consequently the faces of the soil sample. This system allows shear stresses to be increased to 180 kPa satisfactorily. In the set of shear sheets used in this investigation the first station was made of natural rubber, and the others of Kaolin filled rubber which is less sensitive to light. In the second set of DCDSC shear sheets, the natural rubber was replaced by kaolin filled rubber for all stations.

2.3.2.3 Actuating Cylinders

The shear force was applied to the end clamp of the Daisy Chain Shear sheets by means of a metal yoke, attached to the piston (Figure 2.2). The piston was cased in a duralumin cylinder with an internal length of 282 mm and a diameter of 100 mm (Figure 2.21) .

The piston was pressurised by passing air into the cylinder. A Bellofram Rolling Diaphragm which is a woven terylene fabric membrane impregnated with a sealant of synthetic rubber is clamped to the cylinder and the piston. The Bellofram is responsive to extremely small pressure changes, so that response is detected at 0.2 kPa.

The rolling action of the bellofram is shown in Figure 2.21. As the diaphragm and piston are in the axial direction, due to the applied pressure, the diaphragm will roll off the piston sidewall and on to the cylinder sidewall, with a smooth and continuous almost frictionless motion.

2.3.2.4 Shear sheets aligning system

In order to achieve a uniform shear and normal force distribution in directional shear testing it is necessary that shear stresses be applied parallel to the faces of the sample at all stages of the test. This alignment is especially critical at the sample corners where the contact between the normal pressure bag and specimen can be lost if the shear sheets become misaligned. In the conventional DSC the realignment is accomplished by rotating the hydraulic pistons along the circular frame as the sample change shape as shown at the bottom of Figure 2.4.

In the DCDSC the shearing cylinders are fixed on the supporting frame of the apparatus, Figure 2.2 and the alignment is maintained through a manual carriage system. A photograph of the carriage and the guide roller assembly is shown in Figure (2.22). The alignment of the shear sheets was carried out incrementally through these rollers as the sample was changing shape. A long ruler was used to ensure that the face of the sample was parallel to the shear sheets at all stages of the test. The ruler was placed parallel to inked lines of the grid on top of the sample membrane and by rotating the spindle of the guide roller, the shear sheets were aligned parallel to the face of the sample. This alignment was carried out for all four faces of the sample. The roller system consists of two guide rollers fixed on a carriage plate, and the shear sheets pass between these rollers. The carriage plate is connected to a spindle which provides the movement to align the pulling sheets. The contact surfaces of the shear sheets and rollers were lubricated to prevent friction resulting from differential movements of each sheet.

Precise alignment of the pulling sheets is essential in the DCDSC, since the non stretching component is very thin compared with the original DSC and pulling is

performed very close to the surfaces of the sample. Any divergence from correct alignment will cause problems. The shear stresses may not be distributed uniformly through the sample faces, and under-alignment may cause restraint of the sample, whereas over-alignment could cause lifting off of the normal pressure bags and consequently premature failure at the corner of the sample may occur. Figure 2.23 illustrates the maximum deformation a sand sample can achieve in the apparatus.

2.3.3 Plane strain system

The problems associated with apparatuses incorporating rigid plane strain boundaries include the effect of friction developing between the rigid platens and the surfaces of the sample.

In the earlier designs of the DSC (Arthur et al., 1977; Rodriguez del Camino and Dunstan, 1981) both the top and bottom platens were rigid. The problem of platen friction was reduced by introducing lubricants between the platens and the sample surfaces. Although the rigid planes aim to create plane strain, the amount of the grease spread over the sample surfaces and the plane strain sides will allow for some strain in the intermediate principal strain direction and cause differences in the shear strain build up during shearing. This was reported by Arthur et al. (1981), who showed that smaller strains in both dense and loose samples of Leighton Buzzard sand were observed when tested at the Massachusetts Institute of Technology than similar tests conducted at UCL. This difference was attributed to variations in the build up of the magnitude of the intermediate principal stress during shear caused by differences in the thickness of lubricating grease applied to the top and bottom plane strain sides. The authors suggested that a closer control over this variable should reduce scatter in test results, and a means for measuring the intermediate principal stress should be developed. The influence of intermediate principal stress on the stress-strain behaviour of soils has also been widely recognised (e.g. Lade and Duncan, 1973; Davoudzadeh, 1982; Wong and Arthur, 1985a).

Wong and Arthur (1986) resolved the problem by modifying the existing rigid boundary DSC to a partially flexible plane strain boundary device in which the upper plane strain end is rigid while the lower one was replaced by a flexible rubber bag filled with de-aired water. The intermediate principal stress could then be either monitored or imposed during the test through this flexible boundary. The authors observed that strain in the intermediate principal stress direction for most of the cyclic tests was limited to $\varepsilon_2<0.7\%$ when $\varepsilon_1=15\%$.

Although Marachi et al. (1981) reported that a small amount of strain in the intermediate principal stress direction could be tolerated, because the measured stress-strain behaviour is practically unaffected by the small amount of intermediate principal strain, it was considered better to be able to measure the acting intermediate principal stress. The DCDSC apparatus uses the same type of plane strain boundaries as described by Wong (1986). The top rigid plane strain boundary used in all sand and coal tests consisted of a square duralumin plate 250 x 250 x 20 mm with a thick glass plate of 150 x 150 x 10 mm set into the duraluminum. The glass plate was of sufficient size to allow the sample, the shear sheets, the normal pressure bags, the front backing plates and the retaining vanes to be clearly seen even when large deformation was attained. However, when testing re-sedimented Kaolinite a different top platen was used to provide a bore passage for insertion of a miniature transducer to the sample for pore water pressure measurements. This will be described later in Chapter 7.

The bottom flexible boundary plane strain sides (Figure 2.24) is made of an aluminum alloy plate 250 x 250 x 20 mm and is fixed to the main base by four fixing clamps. A circular central depression 10 mm deep and 140 mm diameter was made in the plate and a water filled reinforced rubber pressure bag of the same size and shape as the circular depression was attached to the plate using an aluminum alloy ring and a rubber 'o' ring seal. Water pressure in the pressure bag could be controlled or measured via a small bore passage connected to a pressure supply system and transducer through the side of the platen. The dimensions of the circular water filled pressure bag was chosen so that it covered as much as possible of the sample face during all deformation stages of the sample. Interaction between the normal pressure bags and the intermediate principal stress was kept to a minimum through choice of dimension of the σ_2 bag. Although the design of this flexible boundary was to enable monitoring and provide a uniform distribution of intermediate principal stress during plane strain shear, the apparatus was mainly used to conduct tests in which the intermediate principal stress could be controlled to maintain the ratio $b= (\sigma_2 - \sigma_3)/(\sigma_1 - \sigma_3)$ constant throughout a test.

Sample movement parallel to the plane strain surfaces is assisted by an effective grease. The most common method was two layers of rubber membranes of 0.25 mm thickness coated with a suitable silicone grease. The lubricant used in this investigation was Dow Corning Molykote silicon grease with the addition of 20% fine polytetrafluoroethylene powder. Tests have shown that this is the best combination for the stress range of the DSC (Arthur and Dalili, 1979).

The plane strain sides are linked together through four vertical steel rods fixed to the bottom platen. The top plate was placed onto location nuts on the four upright rods and then locked in the correct position by screw wing nuts to achieve the upper and lower platens parallel.

2.4 STRESS CONTROL AND MEASURING SYSTEM

The DCDSC is a stress controlled apparatus where uniform boundary stresses are maintained by applying loads through a flexible loading system. Figure 2.6 illustrates the method used to apply normal and shear stresses to the four vertical faces of the 100 mm cubical soil sample. In addition, the intermediate principal stress may be controlled by a de-aired water filled pressure bag. All these components are under independent manual control with a combination of pressure regulators and valves and pressure transducers. A schematic representation of the pressure control panel is illustrated in Figure 2.25.

Compressed air was supplied to this panel from a general laboratory compressor via a pressure reservoir which has the capacity of providing a constant pressure of 1400 kPa. Five Fairchild Model 10 precision flow regulators, mounted on the control panel, were used to regulate the pressure supply to the normal pressure bags, shear pistons and water-filled σ_2 pressure bag. The layout of the pressure control panel was based on the assumption that the opposite sides of the sample remain parallel during testing, and therefore can be loaded using the same regulator. This resulted in the application of equal stress to opposite faces of the sample and in consequence, also ensured equilibrium of the sample.

The DCDSC was mainly designed to investigate the influence of cyclic rotation of principal stress directions on the behaviour of particulate materials. As this was to be achieved through cycling the boundary normal and shear stresses, only ball valves and connecting pipes of inner diameter not less than 13 mm were used in the control panel. These large diameter pressure pipes and connectors significantly reduced any delays in flow.

The air pressure in the system was monitored by Bell & Howell transducers. Transducers measuring normal stresses (range 0-300 kPa) were screwed to the circular plate of the backing plate of normal pressure bags (Figure 2.9). Normal stresses applied to the surfaces of the soil sample were assumed equal to the internal air pressure in the boundary normal pressure bag. Thus the pressure

transducer located at the back of the normal pressure bag provided direct monitoring of the normal stress applied to a sample. Transducers used to record shear stresses (range 0-700 kPa) were screwed onto the actuating cylinders. The applied shear stresses were not measured directly but were related to the shear stress by the ratio of the area of the sample face to the effective area of the shear cylinder. This will be discussed in detail in Chapter 4. The output from each of these pressure transducers was recorded on a digital voltmeter. Alternatively, a permanent record could be obtained using a multichannel chart recorder.

Pressure control system for cyclic loading

Cyclic Directional Shear testing of soil was first conducted by Arthur et al. (1979). They used a system of mercury pots on rotating arms that provided the required stresses for the cyclic rotation of principal stresses. This set up, together with a fixed value of applied boundary shear stress, made it possible to apply a continuous cyclic rotation of principal stress directions while maintaining a nearly constant principal stress ratio. This was superseded when Wong (1986) introduced a computer controlled pressure system into the DSC testing facilities.

The computer peripherals used in the author's automation consisted of a Sharp (MZ-80 1/0-1) desktop computer system, analogue to digital converter box and a stepper motor box. These boxes accommodated all the required interface cards for stepping motor control to the pressure regulators and data acquisition. The computer and these boxes were linked together using a general purpose input/output interface. These computer prepherals enabled a variety of pre-determined stress paths to be performed. With the efficiency of these automatic controls and data acquisition, the boundary stresses applied to a sample tested in the DCDSC could be checked, recorded and subsequently and rapidly updated.

The computer controlled pressure regulator was linked through a small gear box to a d.c. stepper motor. The stepper motors were driven through an input signal from the computer and could be pulsed in any direction, and by any number of pulses up to a maximum of 700 steps in a single command. One pulse of the stepper motor was approximately equal to 0.4 kPa. The calibration of each stepper motor consisted of pulsing the regulator by a known number of steps and registering the pressure difference, the change in pressure produced by a single step could then be deduced.

The motorized regulators, which were linked to Fairchild 1:1 volume booster relays to

increase the bleeding capacity of the pressure system, were placed on two pressure panel boards. The layout of the two air pressure panel boards are identical and are used to supply regulated air pressure independently to the two pairs of normal pressure bags and shear sheet actuating pistons required for cyclic loading tests. Small manual adjustment to the shear stresses were sometimes required to compensate for the changes in the angle between the adjacent sample faces as the sample underwent deformation. Operation of the motorized regulators, either by computer or manually, was achieved via the motor control box (Figure 2.26). For setting up the sample in the apparatus, regulators can be operated manually from the motor control box; this procedure will be described in Chapter 5.

A computer control programme calculated the conditions of continuous and cyclic principal stress rotations to be performed on the sample. It calculated all necessary changes in the boundary stresses during one cycle. The changes in stresses were then converted to the equivalent steps for the stepper motors which operated the pressure regulators. Actual applied boundary stresses acting on the four faces of the sample were measured through transducers, and read back to the computer. The boundary stresses could be updated at the beginning of any cycle to correct for sample shear deformation. This enabled the computer to be used both as a controller to the stepper motors and also a data logger.

2.5 DEFORMATION MEASURING SYSTEM

Radiography was used to record the deformation of a sample when sheared. This technique involves placing a grid of markers (usually tungsten spheres) on a plane within the sample and recording their positions during sample deformation by successive radiographs. This method is a major improvement over boundary displacement measuring techniques in that it is independent of strains that may be associated with local boundary displacements. Examples of non-uniform distribution of strains within the different areas of the sample are discussed in detail in Chapter 4.

The use of radiography techniques for strain measurements in soil media was largely developed at Cambridge (Roscoe et al., 1963b) and it is now commonly used at UCL. A detailed description of strain determinations from the displacements of these markers has been given by Wong and Arthur (1985b) and Wong (1986). The fundamental assumptions in deriving strains from the marker displacements were stated by Roscoe et al. (1963b), namely:

(i) There are no discontinuities of strain passing through the area defined by the adjacent markers. Consequently, strain in the area can be determined from the displacement of the markers at the boundary of the area.
(ii) There is no relative movement between the sample material and the marker.
(iii) The marker lies in, and remains in a single plane to which the calculated strains apply.

This method does not rely on the assumptions of coaxiality, and is essential when evaluating the effects of principal stress rotation. It also precludes the assumption of uniformity of strain in the entire sample. The versatility of this method permits the calculation of strains in local areas of the sample, and enables a description of strain distributions within a deforming sample, a property which is vital in evaluating apparatus performance. The contribution of this method in developing the DCDSC will be discussed in detail in Chapter 4.

To use the radiographic technique in the DCDSC, a 7 x 7 grid pattern of tungsten balls of 2.5 mm diameter was usually placed on the central plane of the sample. For the loose samples, preparation dictated placing the grid on a plane strain face.

At different stages of the shearing process, the grid pattern was exposed to X-rays discharged from a head located centrally above the shearing cell. The radiographic images were recorded on Kodak Industrex MX film, the grain size of which provided adequate definition for the purpose of the present research. During the exposure of an X-ray film, it was assumed that the sample strain was zero.

A good definition of the images of the tungsten spheres on radiographs was necessary for accurate measurements of the coordinates of the images. The definition of an image results from the sharpness or visible clarity of its boundaries. The perfect sphericity and high density of the tungsten carbide spheres helped to ensure well defined images of markers on the radiographs. The major feature that controls image definition on the radiograph is the size of the focal spot of the X-ray tube. A Large focal spot increases the penumbra around the images and makes it extremely difficult to measure the precise position of the images; this effect is illustrated in Figure 2.27. Arthur (1977) reported that a focal spot of 0.4mm provides adequate geometric sharpness on the radiographs.

The X-ray system was a 150 kV X-ray tube (Thermax 0.6 mm focal spot). This system was operated at fixed energy setting of 150 kV and 6 mA for 4 minutes, a

combination found to be suitable for penetrating 100 mm thick soil samples. The quality of the image definitions on the radiographs can be also improved by increasing either the distance between the focal spot and the tungsten sphere or decreasing the distance between the X-ray film and the marker grid. To avoid computing fictitious strains, it was essential to maintain a constant distance between the X-ray source and the plane of markers for the duration of the test. The best distance between the X-ray head and the film was found to be 750 mm for this set up. The X-ray film was parallel to the plane of markers.

To minimise errors due to repositioning of X-ray film, the aluminum frame which supported the DCDSC also held the film cassette perpendicular to the X-ray radiation direction close to the bottom plane strain platen. This arrangement permitted the repositioning of a film cassette in exactly the same location after each exposure. Only one film cassette was used throughout any one experiment to eliminate any possible errors involved with a different cassette. This cassette had to be marked on one side and be positioned under the sample allowing with the same side facing upwards.

When X-rays strike the sample and apparatus, radiation will be scattered and will effect the image of the tungsten spheres and subsequently the accuracy of measurements. To reduce this problem a lead shield was used to absorb some of the scattered radiation.

The exposed radiographs were developed and fixed in a constant temperature bath of approximately 20°C soon after the exposure had been completed. Developing was carried out by dipping the film in a tank filled with the Kodak X-ray developer for 4 minutes. The film was then quickly rinsed in a water bath and dipped for a further 4 minutes in a fixer and placed in a bath of running water to be washed for at least twenty minutes prior to drying. The developer and the fixer were changed at regular intervals.

Once the films were dry, they were scanned, a process during which the coordinates of the tungsten spheres were registered and filed in a computer. The accuracy of the measurement of these coordinates was, as already explained, dependent upon the whole process including the scanning accuracy. The scanning of radiographs for this research used an optical monocomparator (National Panasonic, model W51E), an electronic digitising display unit (MDR2a, Scientific and Surveying Instruments) and a computer system (Sharp ZX80K). Through this system the marker locations were

digitised and recorded from successive radiographs with reference to a fixed X-Y co-ordinate system. The radiograph alignment and the scanning procedure is explained in detail by Wong (1986).

The computer, using these co-ordinates, calculates the magnitude and the direction of strain; with both total and incremental strain being calculated. The total strain indicates the strain between the first radiograph, taken while the sample is under isotropic stress, and any other radiograph of the deformed sample. The incremental strains are those between two consecutive radiographs. The strain calculation is based on the triangular elements originally proposed by Burland (1967) using the method described by James (1973). This method assumes that each sub area, described by markers undergoes uniform deformation. The strain analysis divides each area surrounded by four images of tungsten spheres into four triangles. The average strain from the four triangles is taken to represent the strain at the centre of each square element. The programme is repeated for each area surrounded by four markers and thus gives the strain distribution for the entire sample. The results are printed for each area. Averages for selected zones of the sample, defined in Figure 2.28. These zones were chosen to check the uniformity of strain within the sample. The strains in area (1) are representative of the strains of 65% of the whole sample and contain all the tungsten sphere images i.e. 7 x 7 images or the average strain of 6 x 6 positions. Area (2) contains 4 x 4 positions and represents 25% and area (3) contains 2 x 2 position and represents 6% of the total area strains.

It should be noted that the error in the strain calculation does not only depend on obtaining well defined images but more importantly on determining the marker positions on radiographs. The accuracy of positioning the target cursor of the monochromator is very important. It should be emphasised that the patience and diligence of the operator can be more important than the limits set by the equipment. With the above set up, the position of an image could be determined within $\pm$ 5 μm. The possible error limits in the above scanning system has been evaluated by Wong (1986) using a 7 x 7 grid of tungsten spheres positioned at 12 mm intervals. A repeated scanning of the same radiograph, that should ideally produce a strain calculation of zero, produced a mean linear strain, of 0.007% with a standard deviation of 0.08%. In this research to ensure the accuracy of measurements the first and the last radiographs were scanned twice and, if the computed strains between these radiographs were not within the above limits, the whole scanning process was repeated. Table 2.1 illustrates these mean values of strains that were add by scanning one radiograph twice and comparing it with another radiograph.

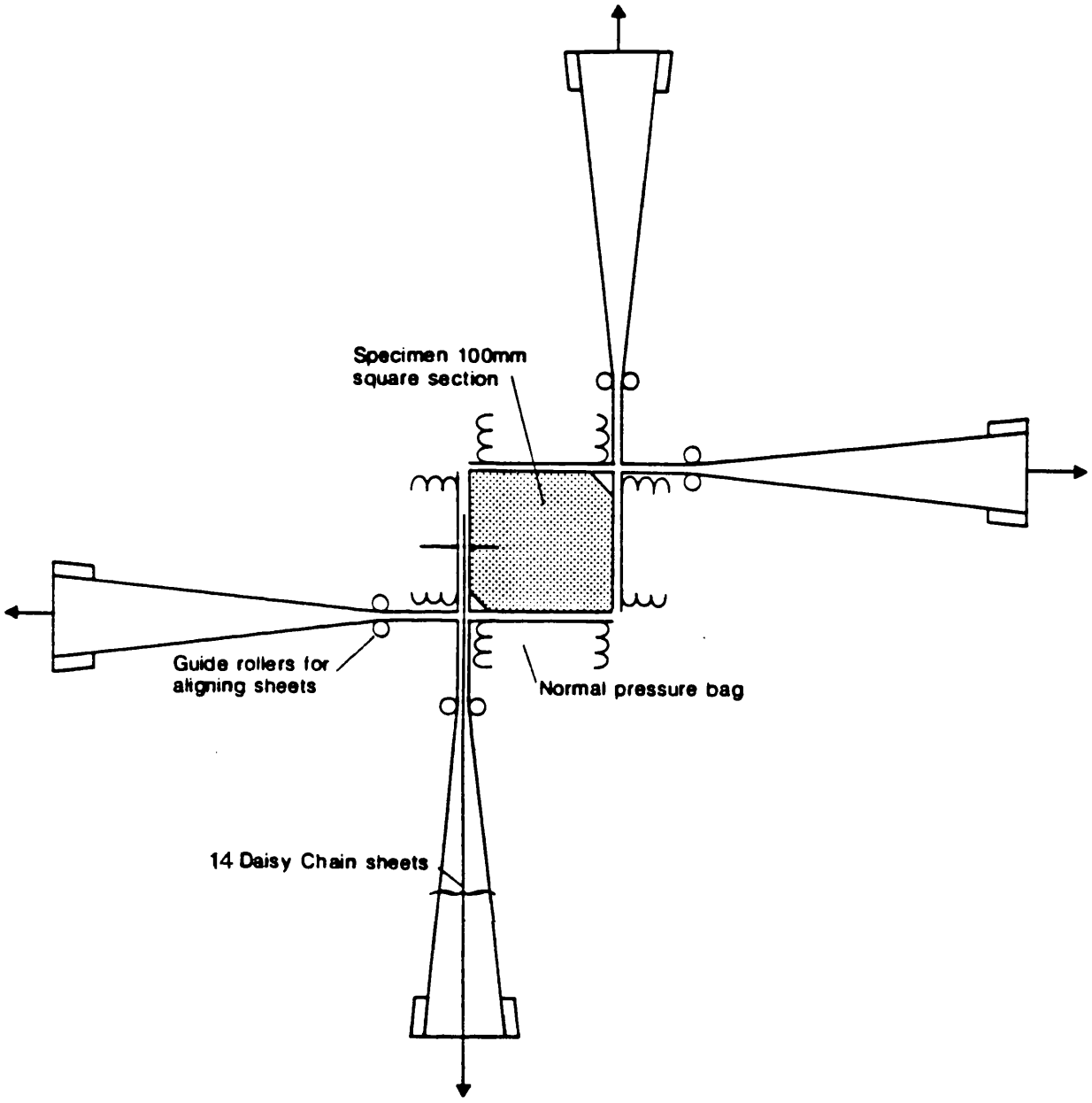

Fig. 2.1 The basic features of the apparatus showing the location of normal pressure bags and daisy chain shear sheets

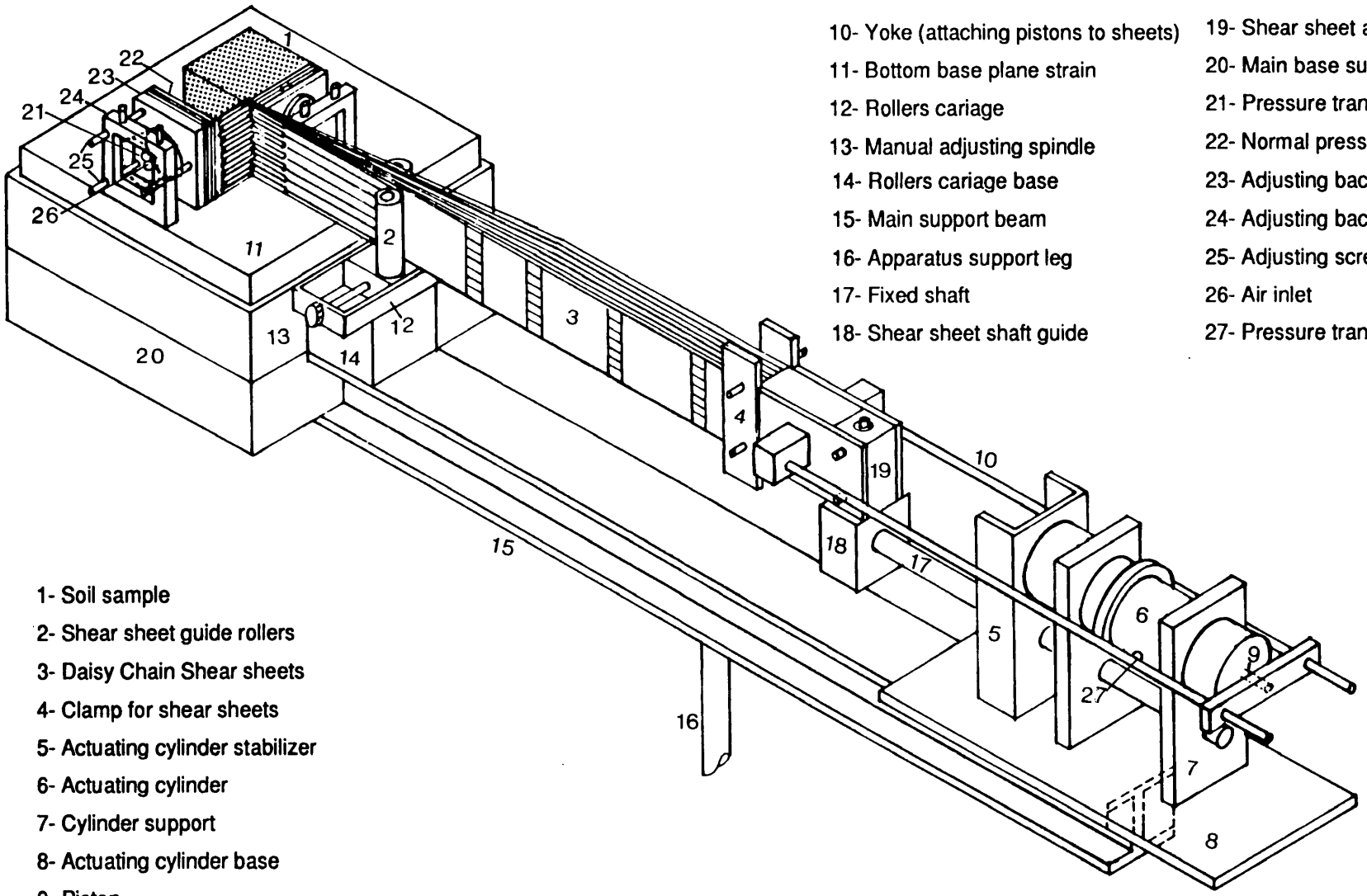

1- Soil sample
2- Shear sheet guide rollers
3- Daisy Chain Shear sheets
4- Clamp for shear sheets
5- Actuating cylinder stabilizer
6- Actuating cylinder
7- Cylinder support
8- Actuating cylinder base
9- Piston
10- Yoke (attaching pistons to sheets)
11- Bottom base plane strain
12- Rollers cariage
13- Manual adjusting spindle
14- Rollers cariage base
15- Main support beam
16- Apparatus support leg
17- Fixed shaft
18- Shear sheet shaft guide
19- Shear sheet alignment hinge
20- Main base support
21- Pressure transducer
22- Normal pressure bag
23- Adjusting backing plate (a)
24- Adjusting backing plate (b)
25- Adjusting screws
26- Air inlet
27- Pressure transducer

Fig. 2.2 Isometric view of a part of the Daisy Chain DSC

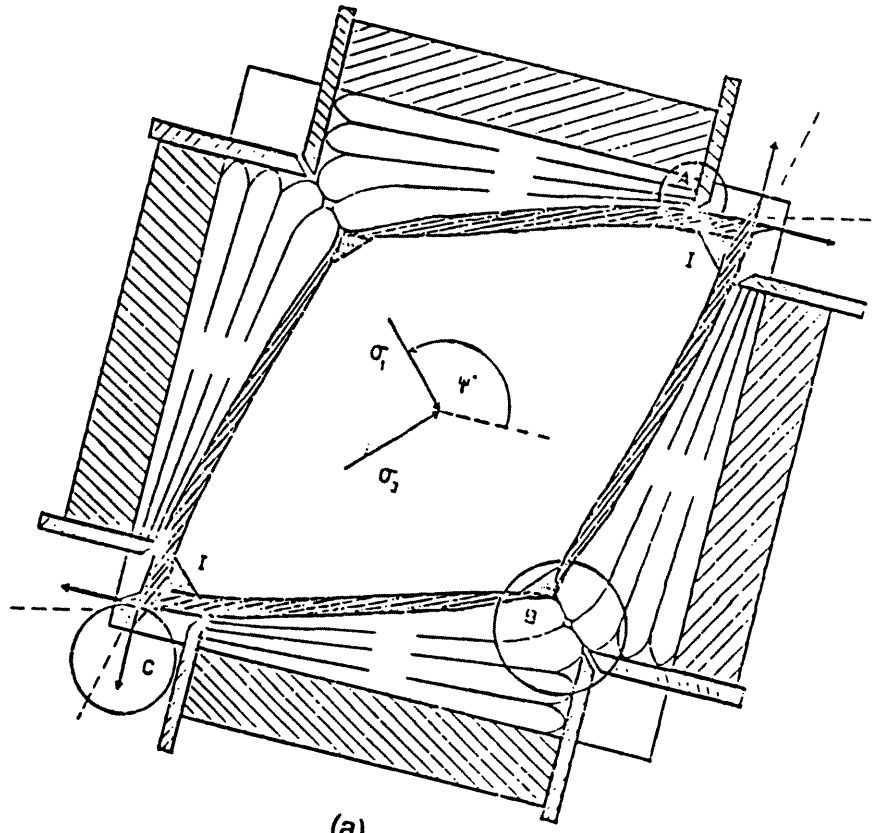

(a)

Problems encountered when testing loose sand $\psi = 45°$
(at very large strains)

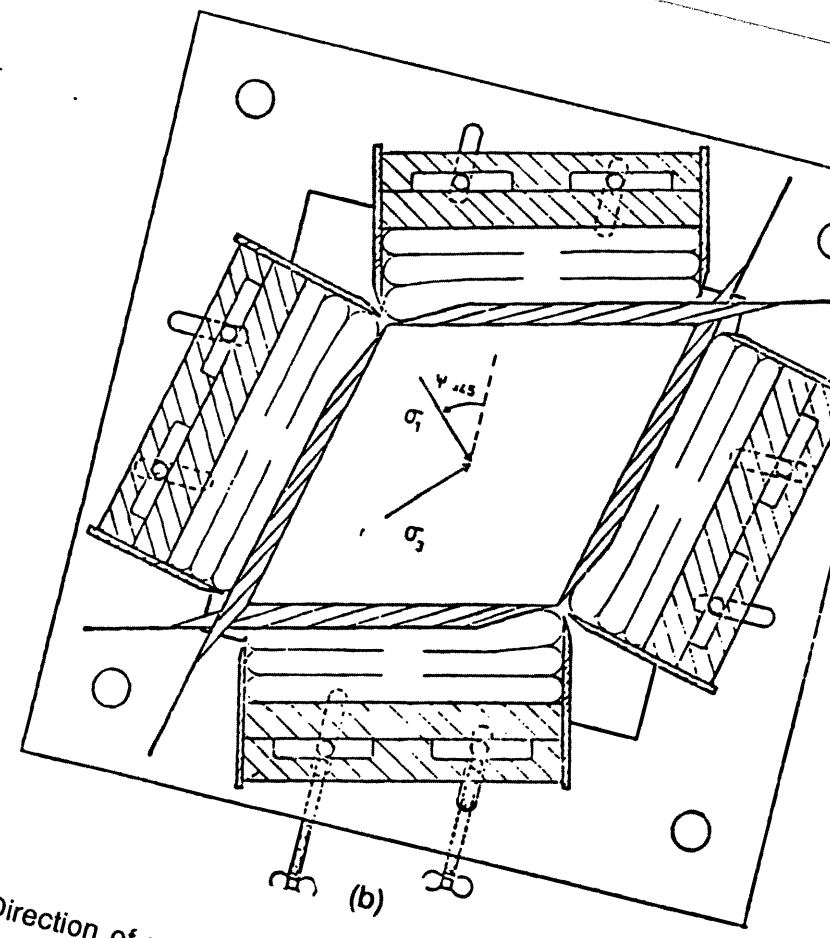

(b)

Direction of normal and shear stresses at failure $\psi = 45°$

Fig. 2.3 **(a) Fixed backing plates in the original DSC (b) adjustable backing plates in the modified DSC (after Rodriguez, 1977)**

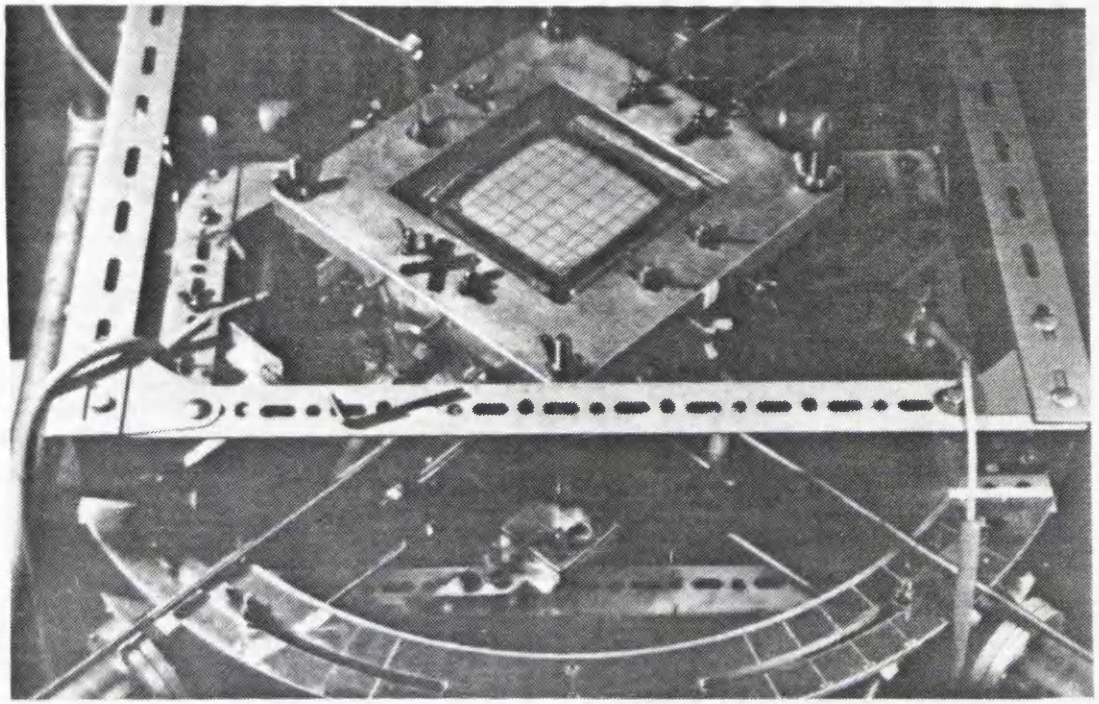

(a)

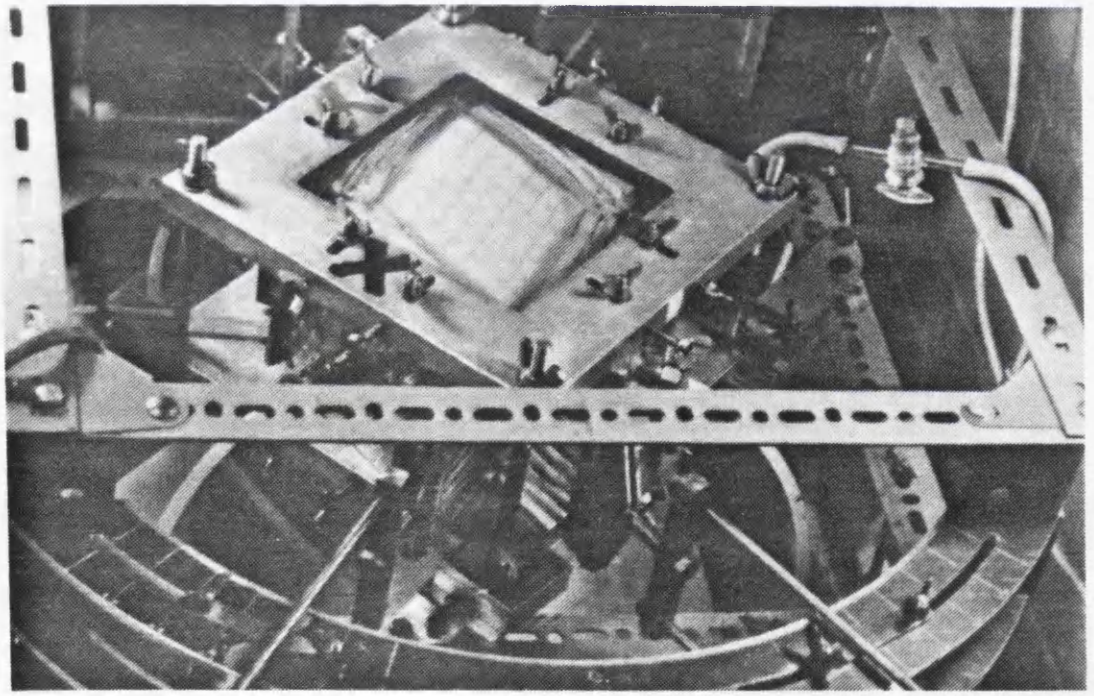

(b)

Fig. 2.4 (a) Location of shear pistons prior to sample deformation and (b) position of pistons after the sample changed shape (after Rodriguez, 1977)

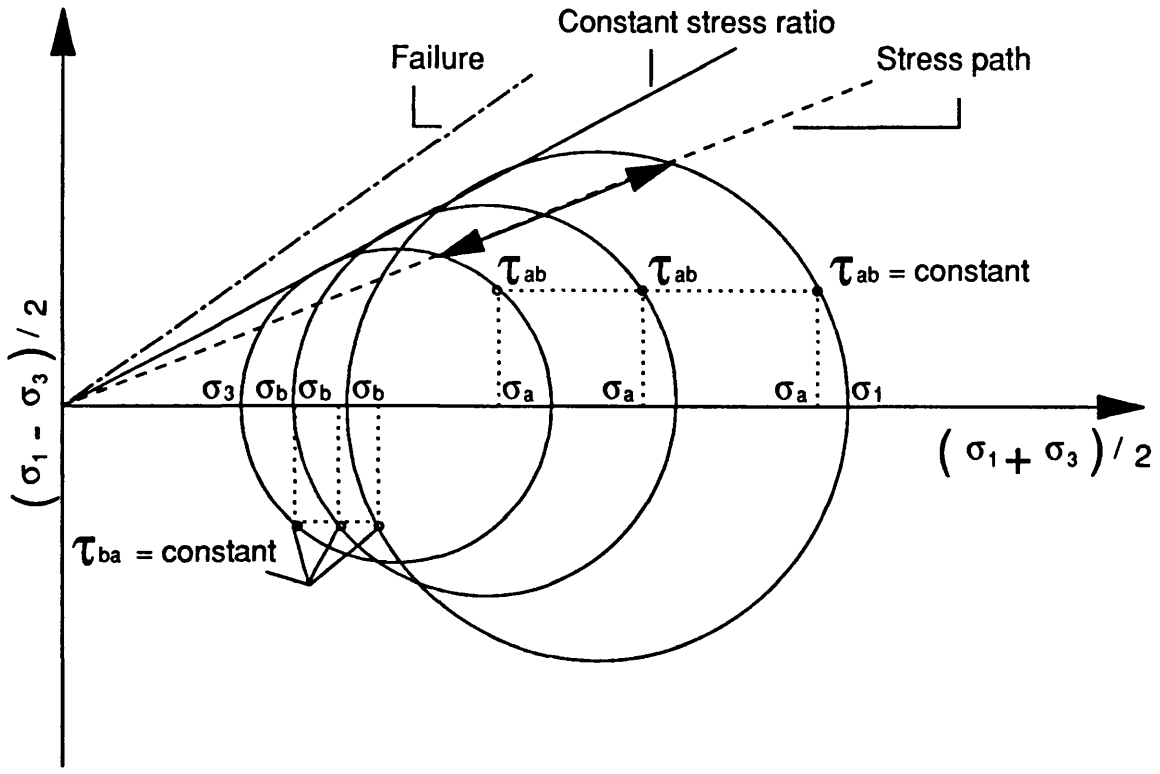

Fig. 2.5 **Stress path of a typical continuous rotation test in the earlier version of the DSC in which the mean stress level varies during the cyclic process (after Wong, 1986)**

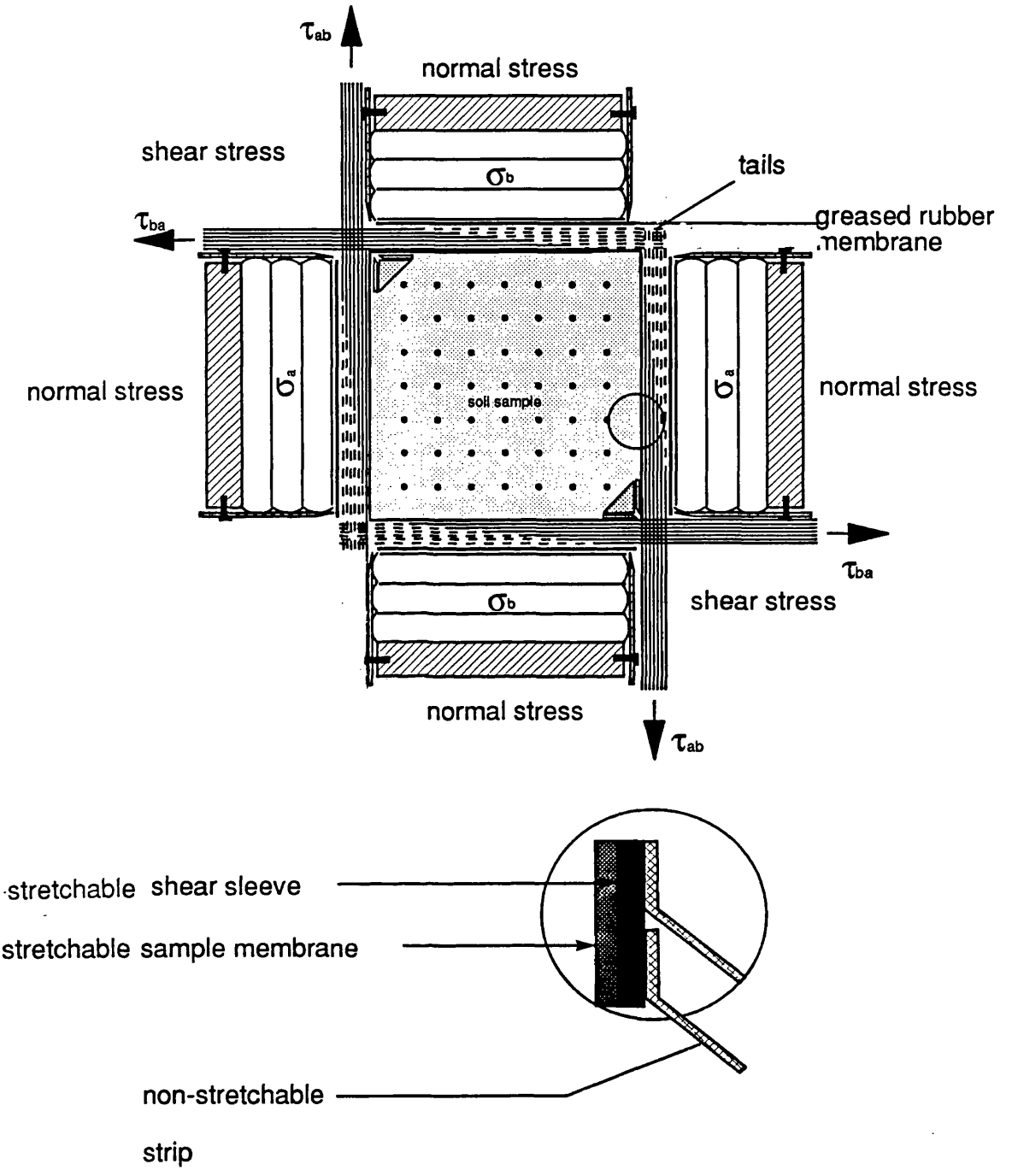

Fig. 2.6 **The method used to apply normal and shear stresses in the Daisy Chain Directional Shear Cell**

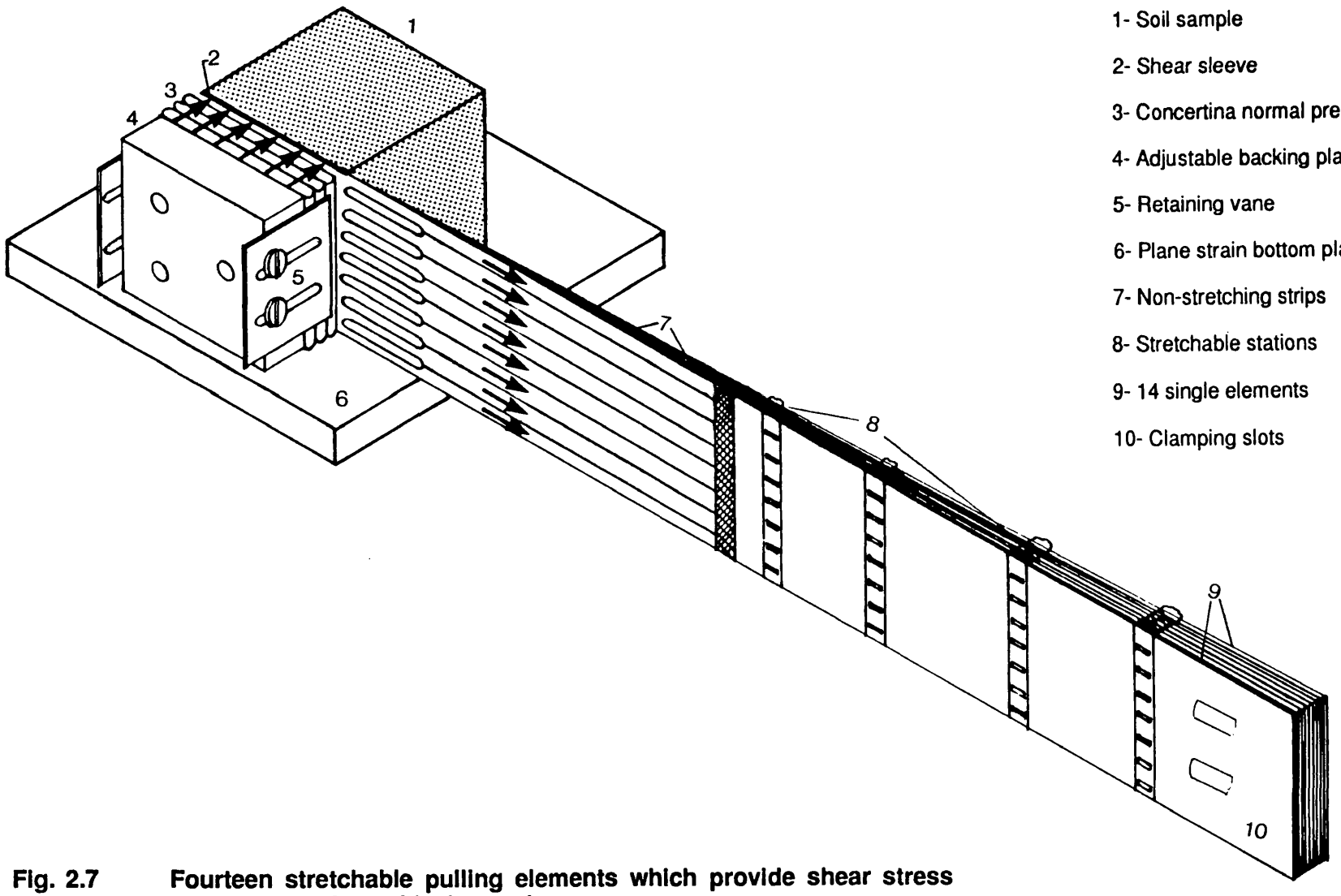

1- Soil sample

2- Shear sleeve

3- Concertina normal pressure bags

4- Adjustable backing plate

5- Retaining vane

6- Plane strain bottom plate

7- Non-stretching strips

8- Stretchable stations

9- 14 single elements

10- Clamping slots

Fig. 2.7 **Fourteen stretchable pulling elements which provide shear stress on the face of a cubical sample**

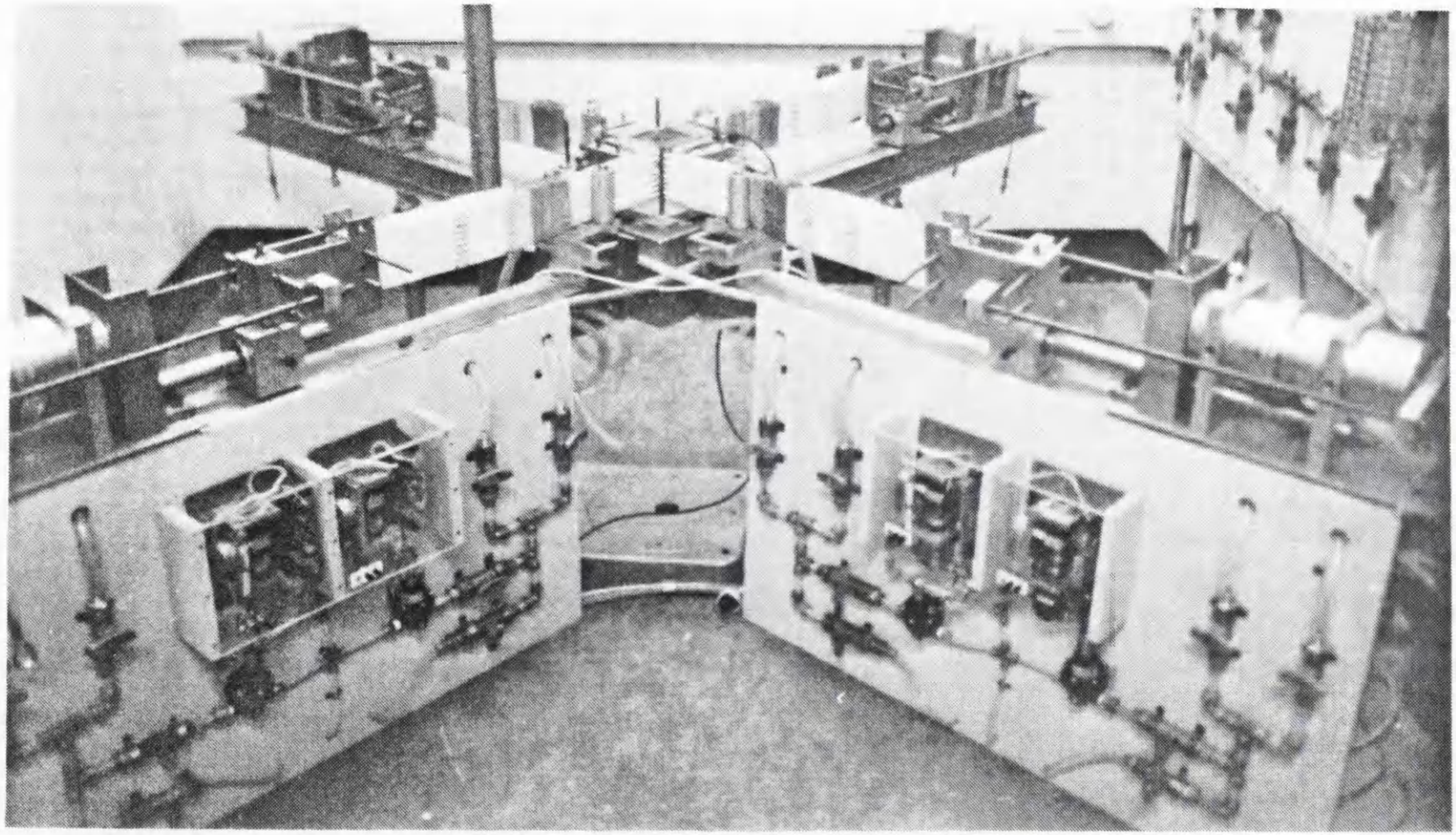

Fig. 2.8 An over all view of the Daisy Chain Directional Shear Cell

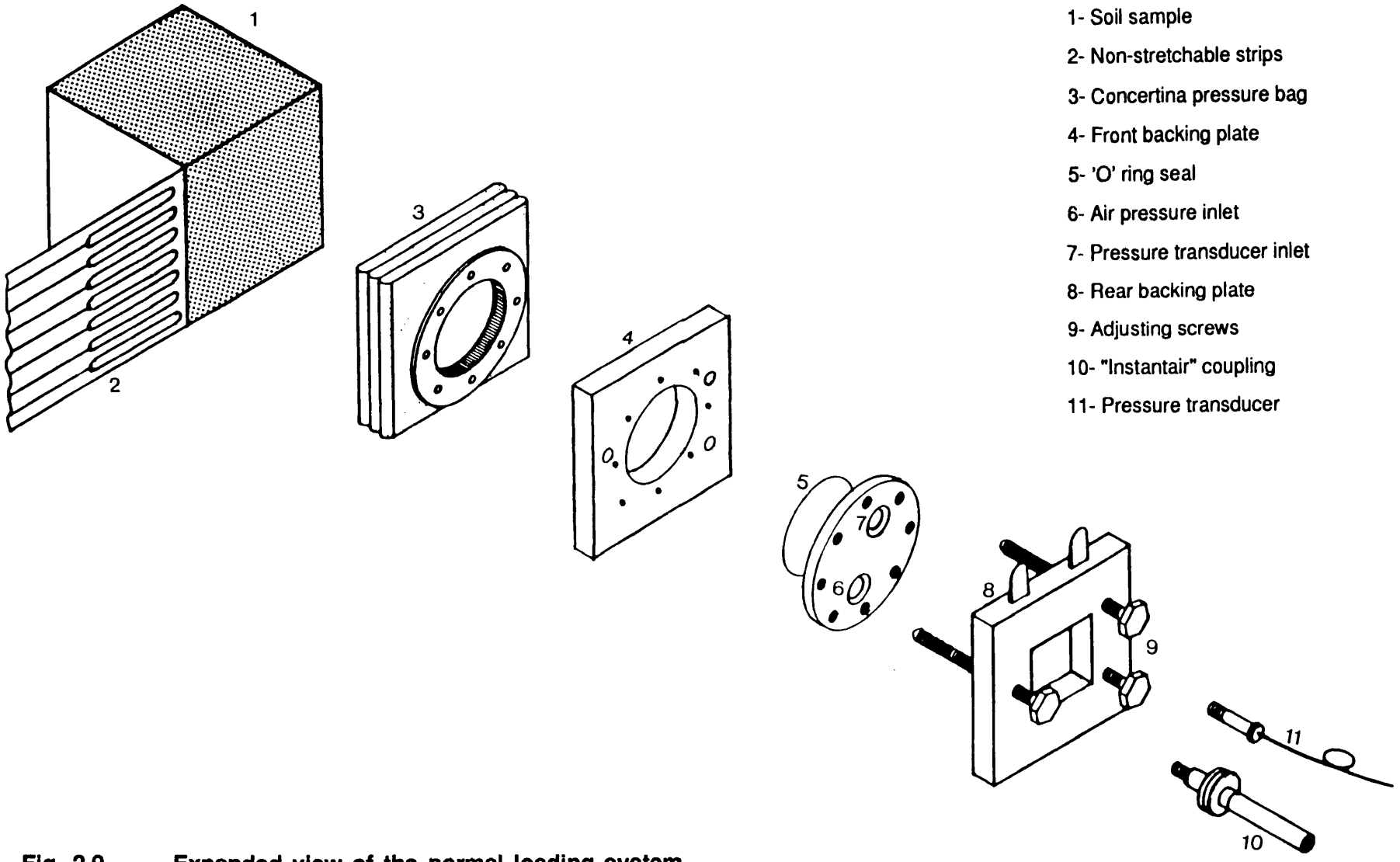

1- Soil sample
2- Non-stretchable strips
3- Concertina pressure bag
4- Front backing plate
5- 'O' ring seal
6- Air pressure inlet
7- Pressure transducer inlet
8- Rear backing plate
9- Adjusting screws
10- "Instantair" coupling
11- Pressure transducer

Fig. 2.9 Expanded view of the normal loading system

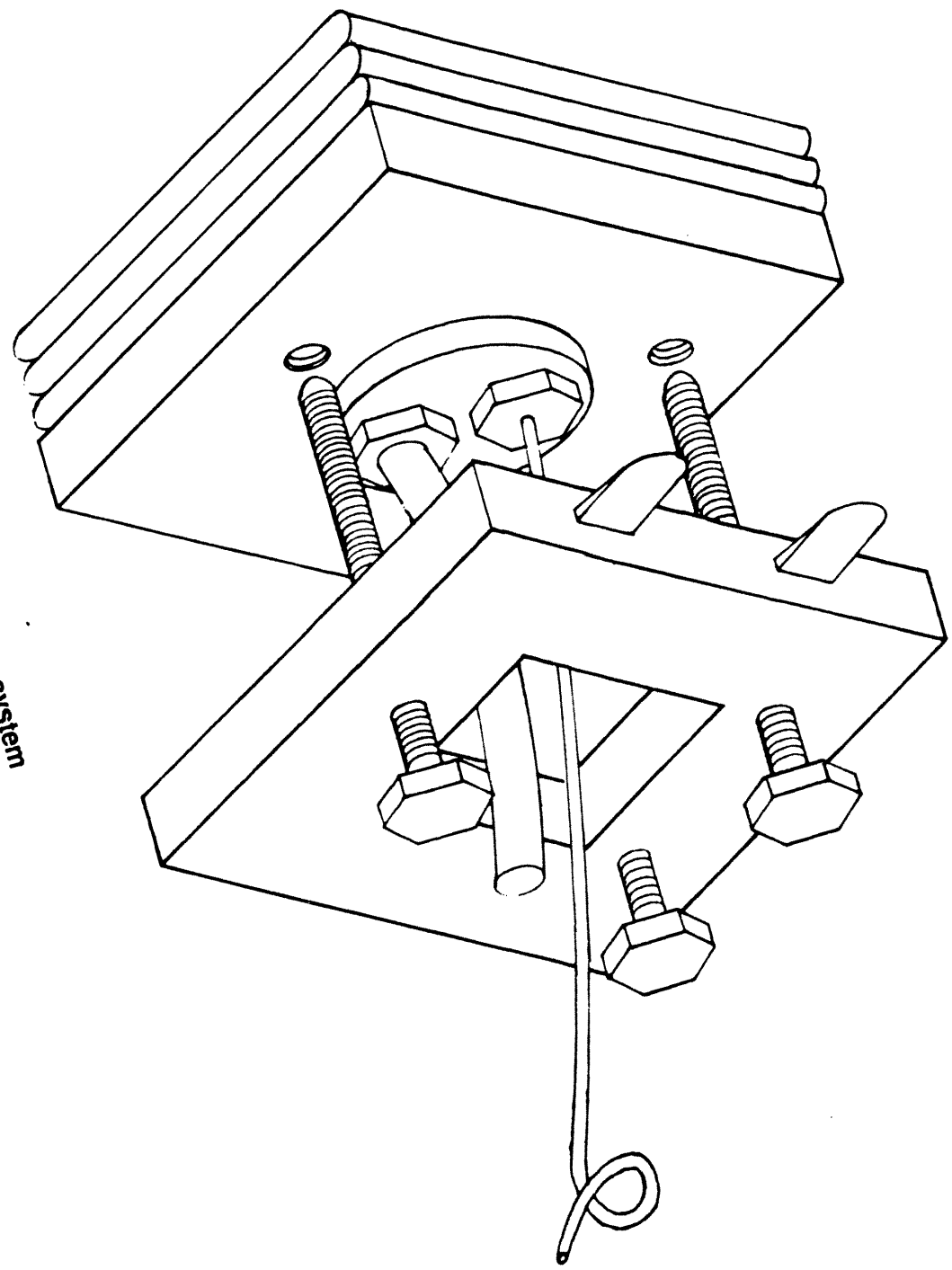

Fig. 2.10 Assembled parts of the normal loading system

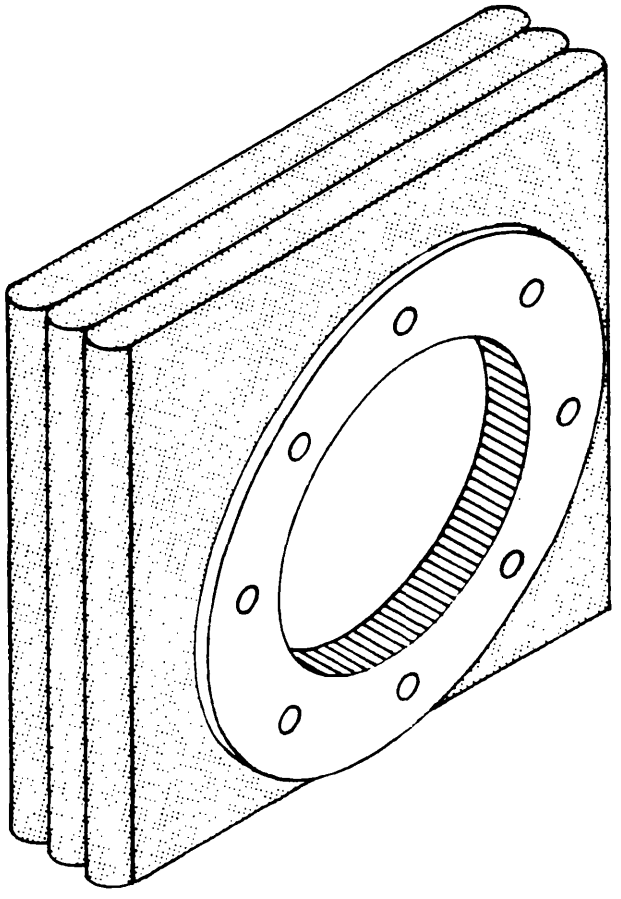

Fig. 2.11 Concertina type re-inforced normal pressure bag

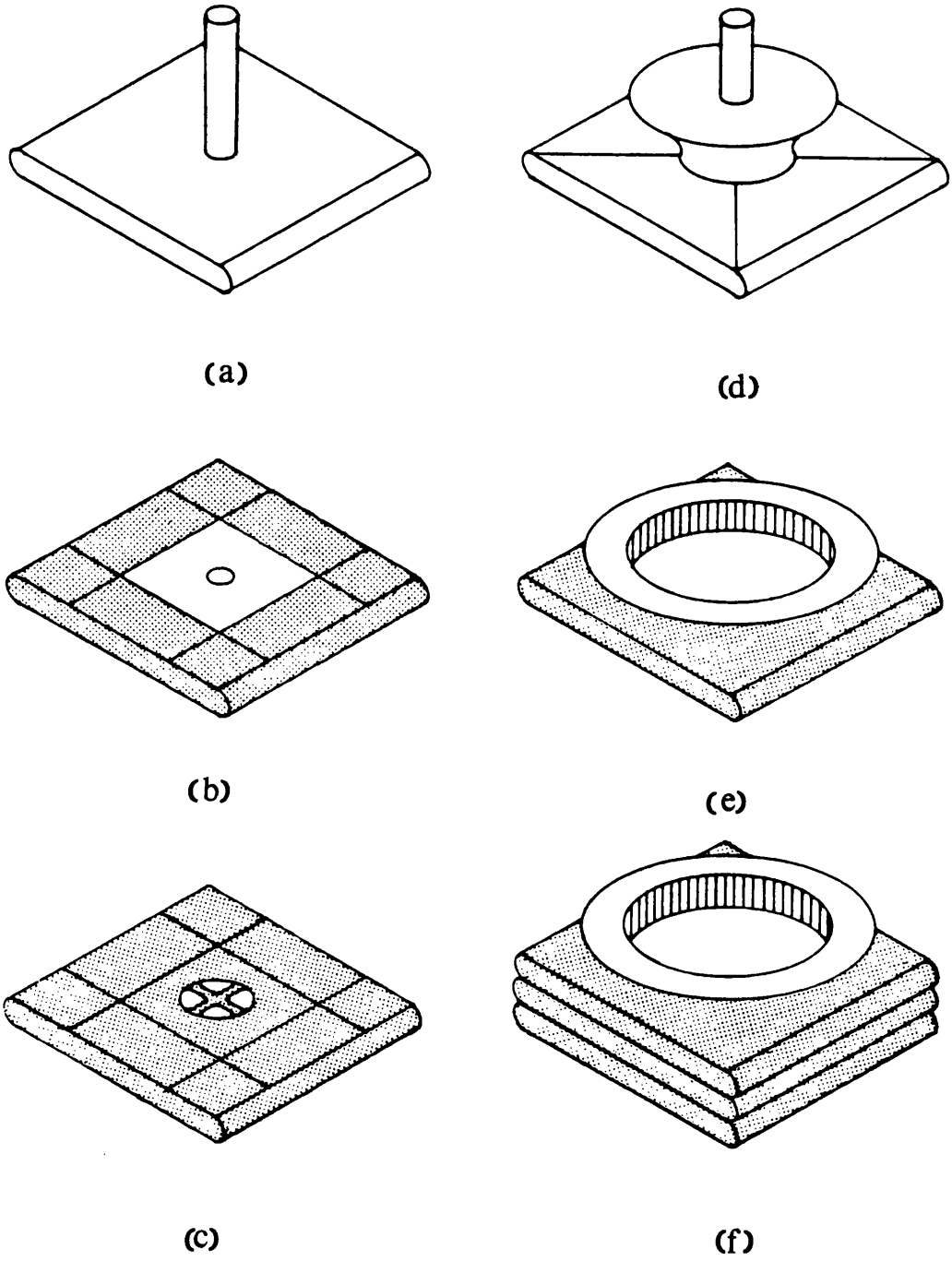

Fig. 2.12 Assembly of concertina shape normal pressure bag

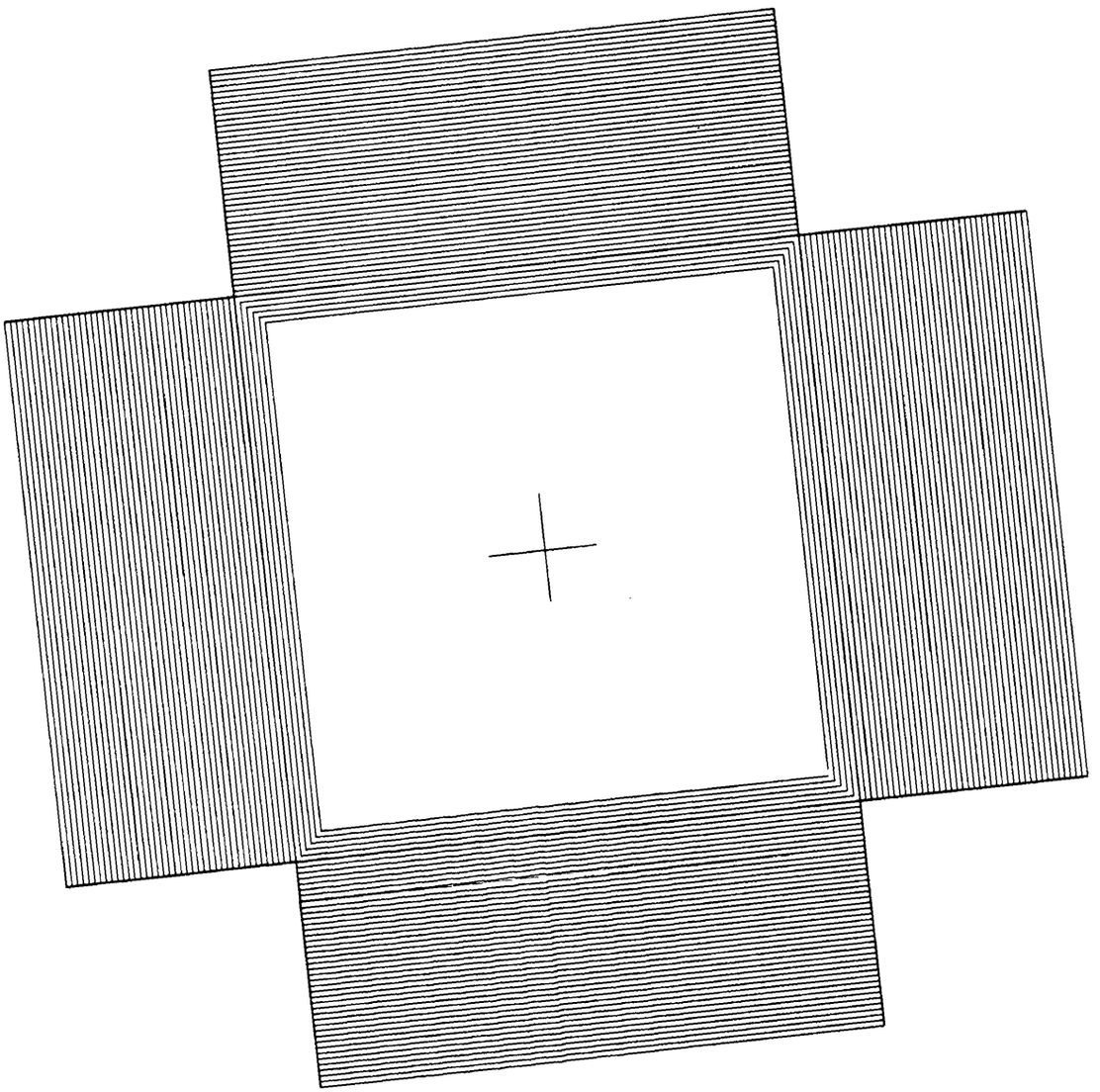

Fig. 2.13 A precise grating on an acetate transparent film

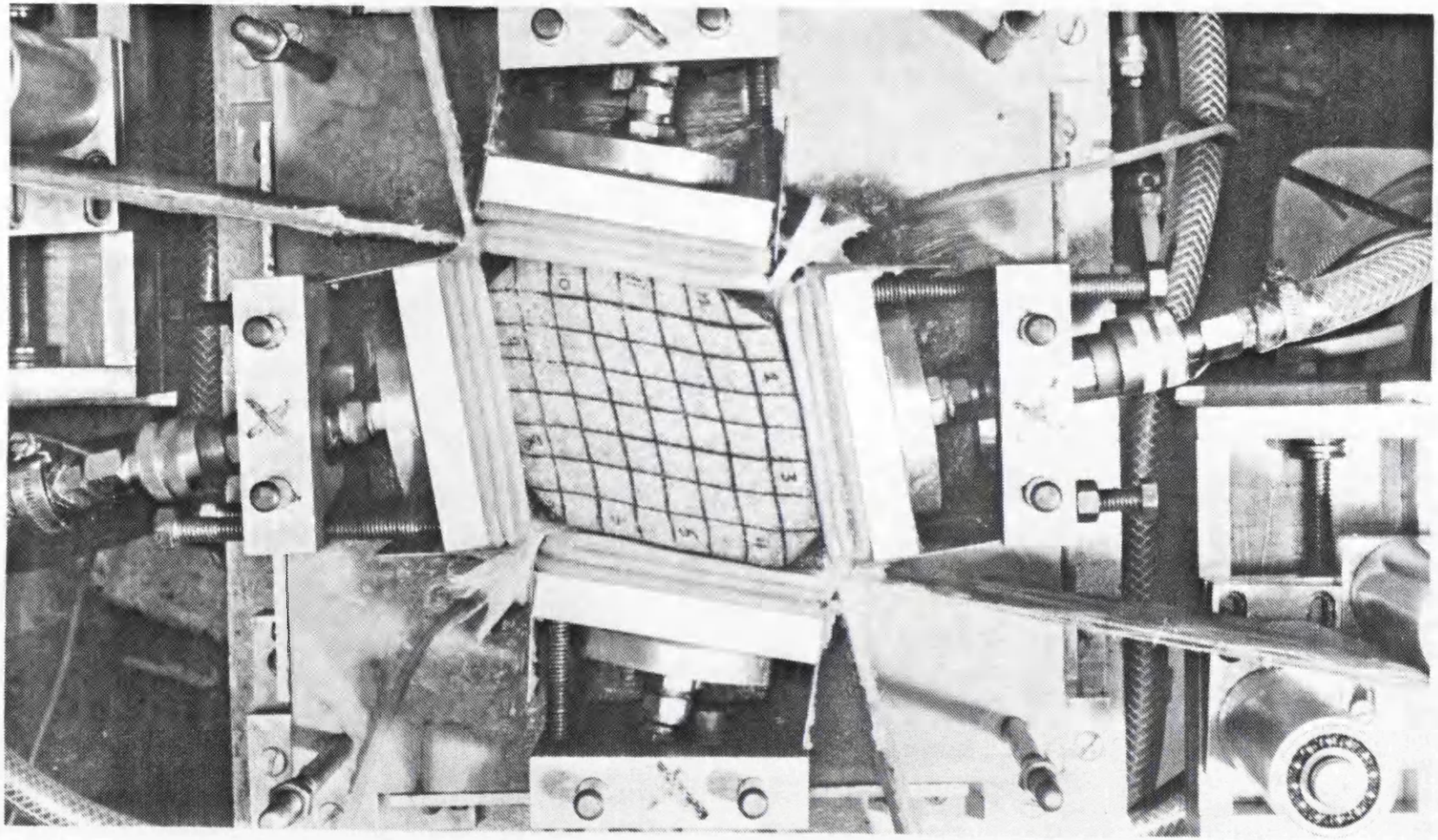

Fig. 2.14 **Positions of adjusted backing plates at the end of a largely deformed dense Leighton Buzzard sand sample (ψ = 45°)**

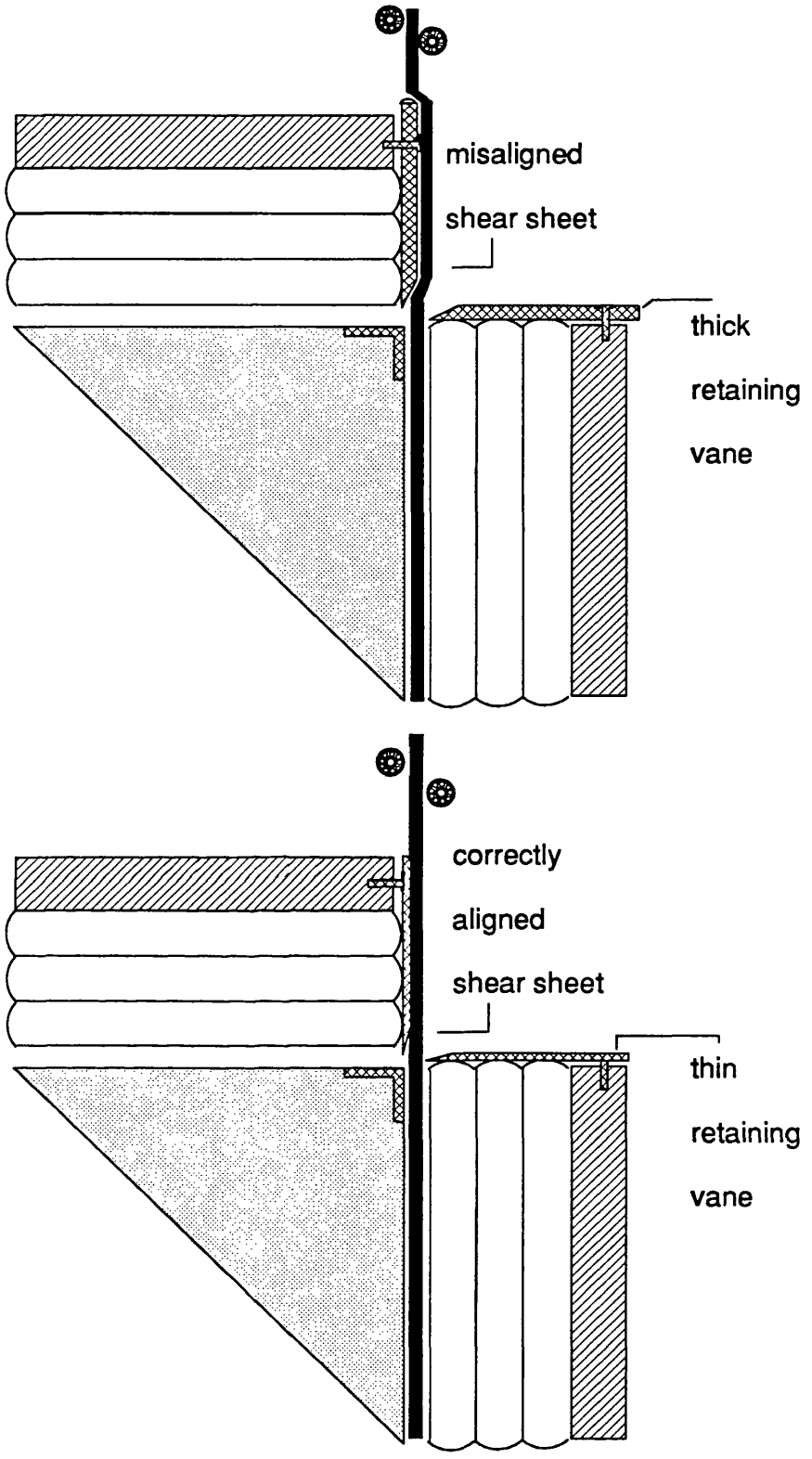

Fig. 2.15 (a) Mis-alignment of shear sheets created by using thick retaining vanes and (b) correct alignment by using thin retaining vanes

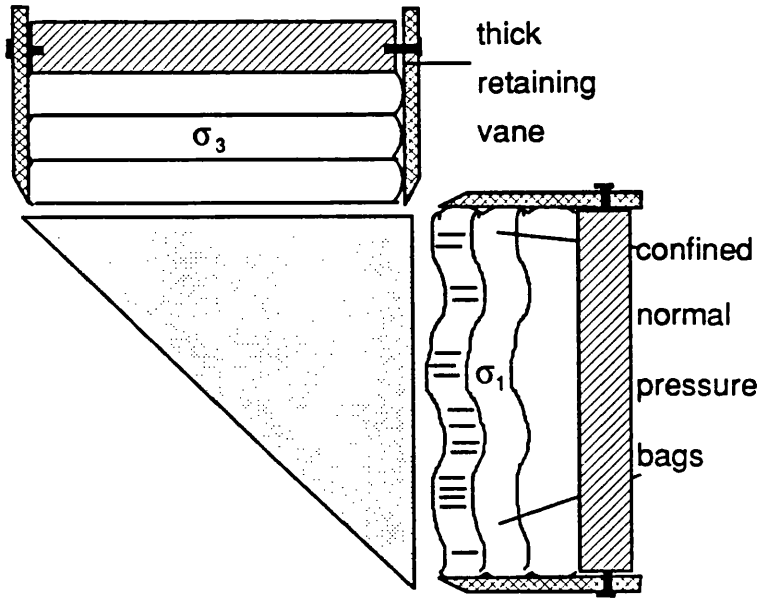

(a)

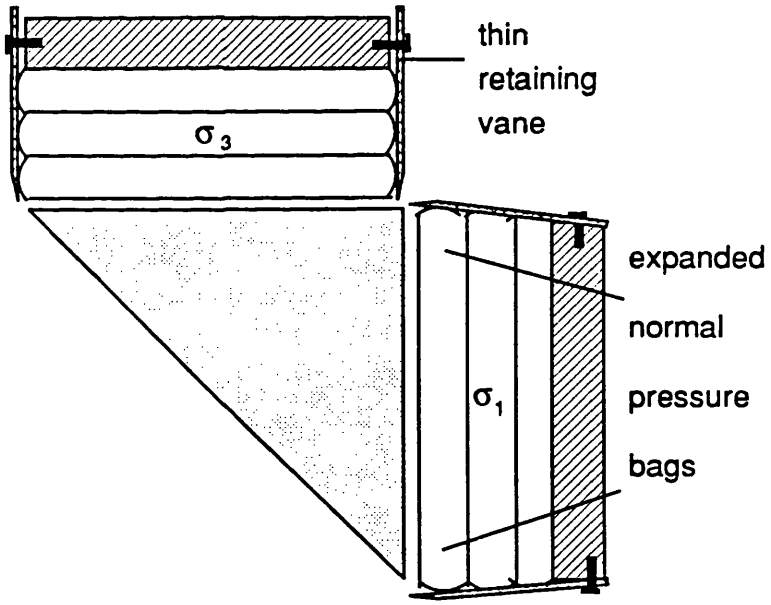

(b)

Fig. 2.16 **(a) Confinement of normal pressure bag due to the rigidity of the thick vanes (b) Thin vanes provided the normal pressure bag to follow the sample deformation**

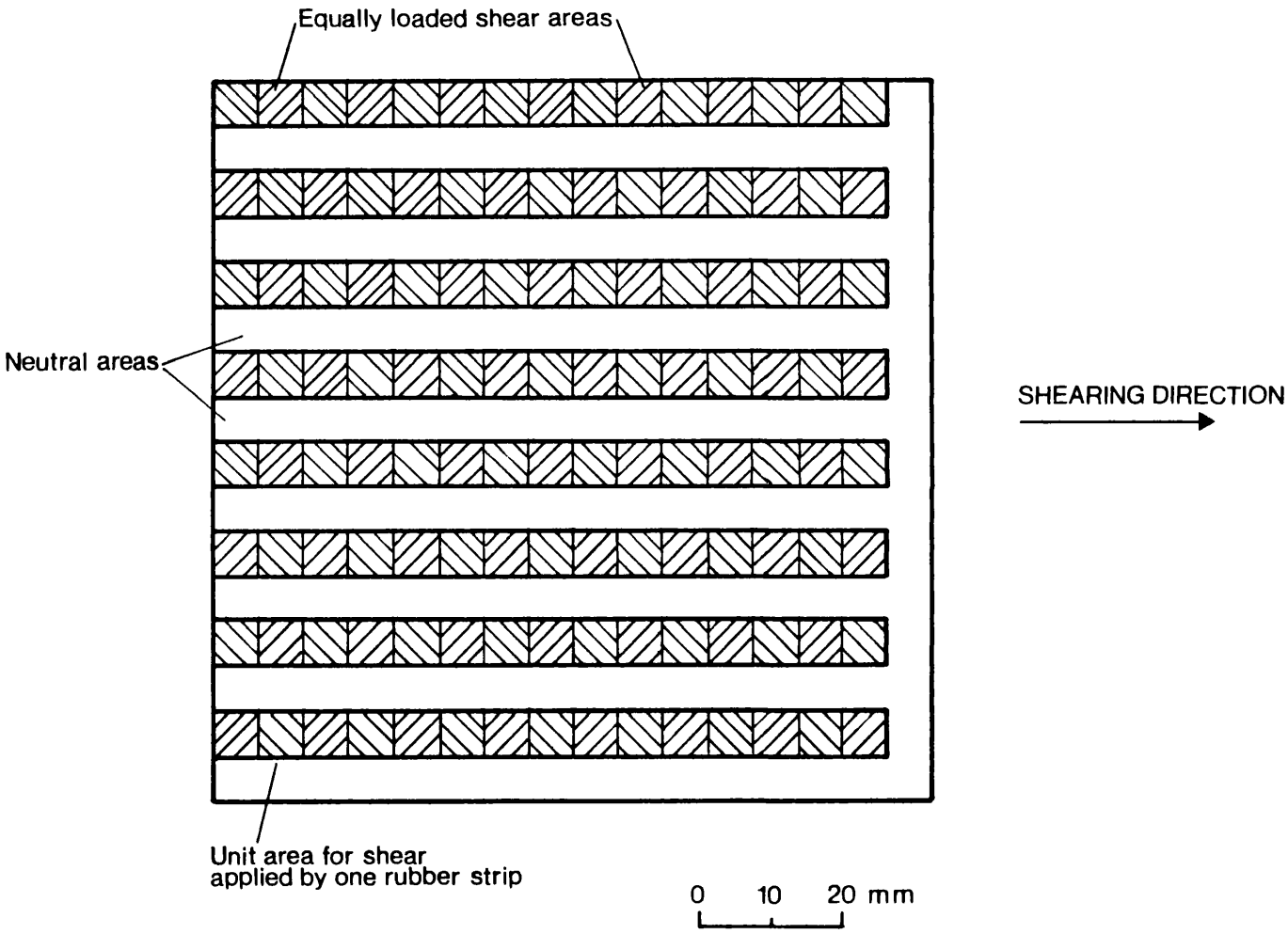

Fig. 2.17 **Areas over which shear was applied to the outer surface of shear sleeve in the earlier version of DSC**

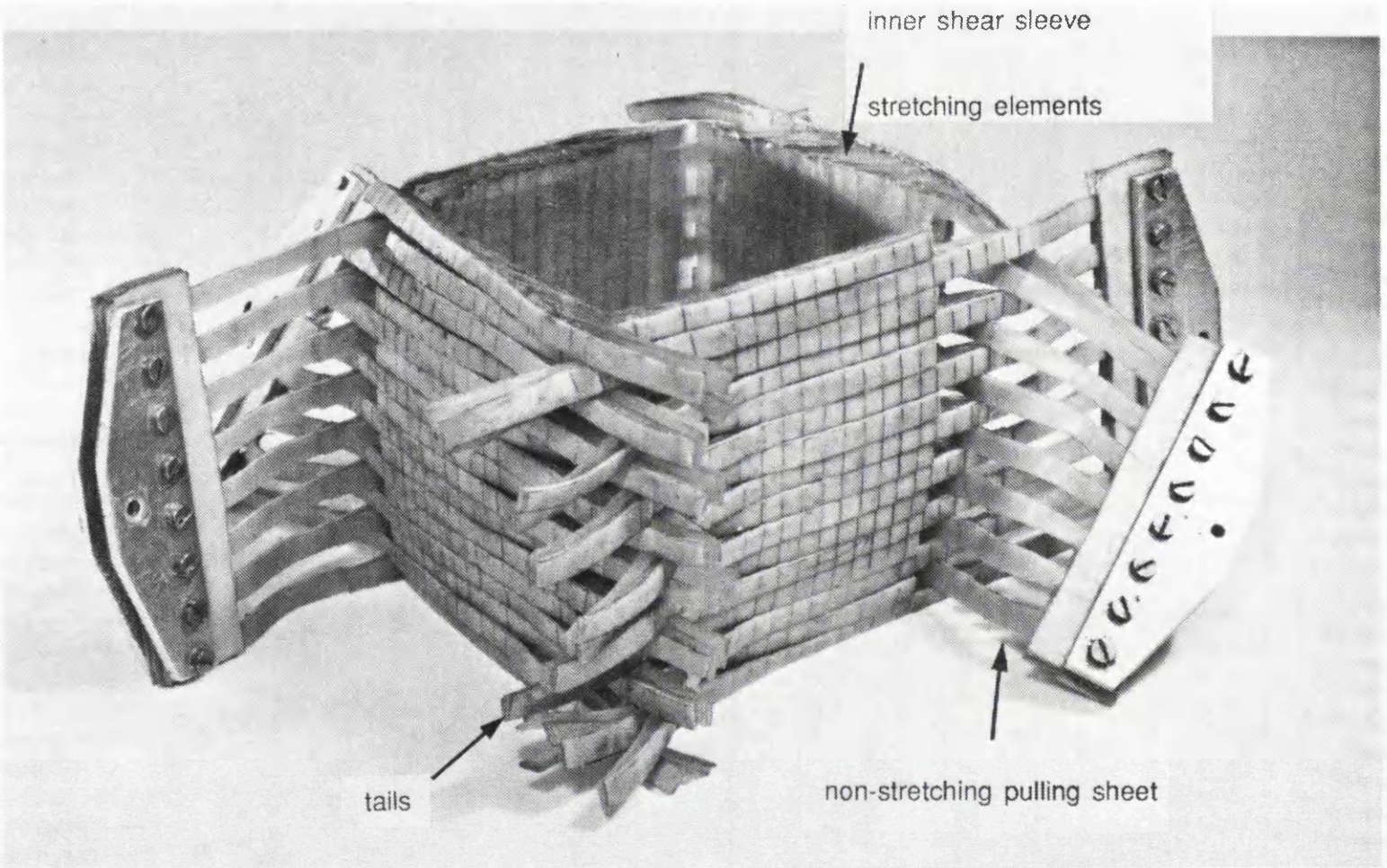

Fig. 2.18 An overview of original (low stress) shear sheets

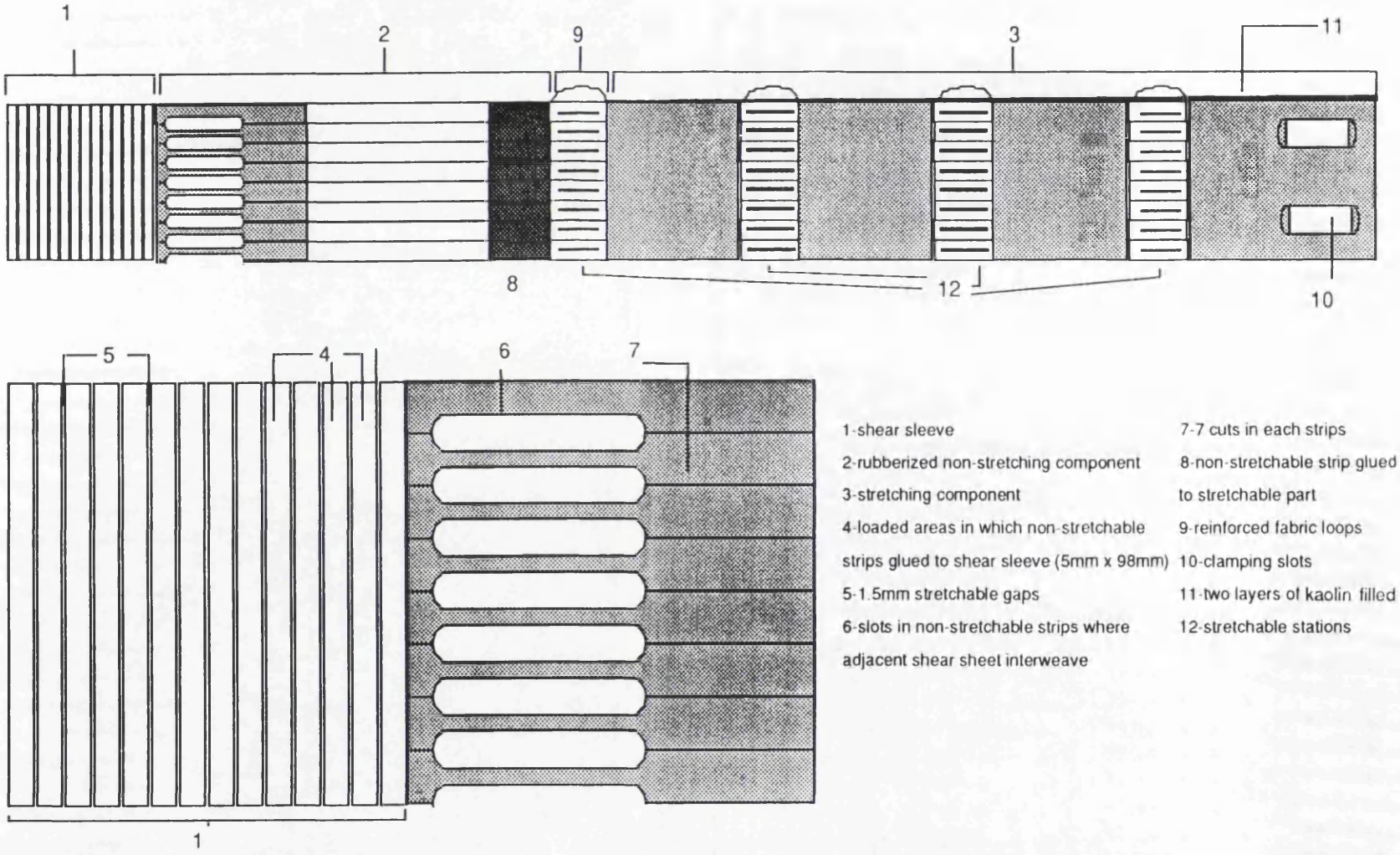

Fig. 2.19 **Description of a single element of the Daisy Chain shear sheets**

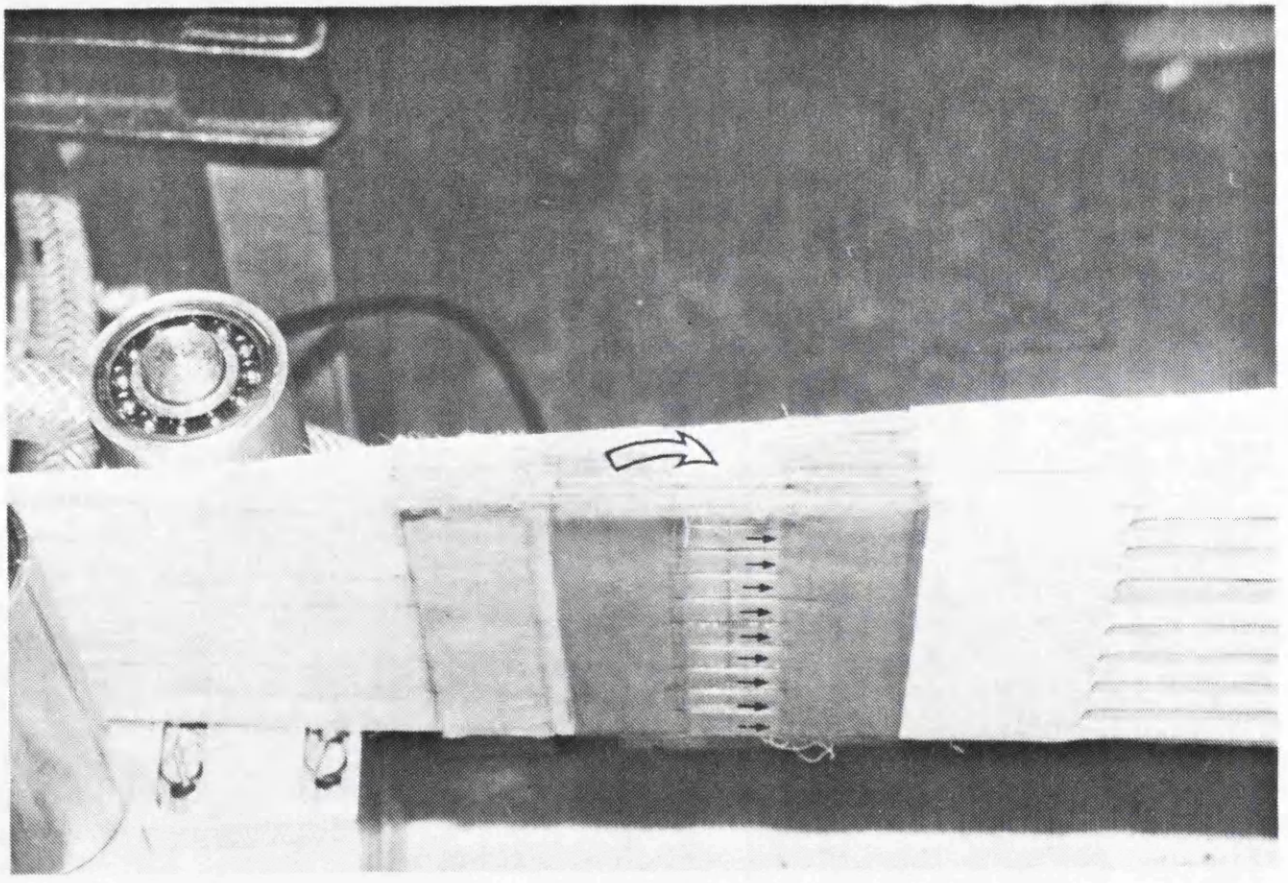

Fig. 2.20 **The first stretching component of the 14 single elements of shear sheet fully stretched**

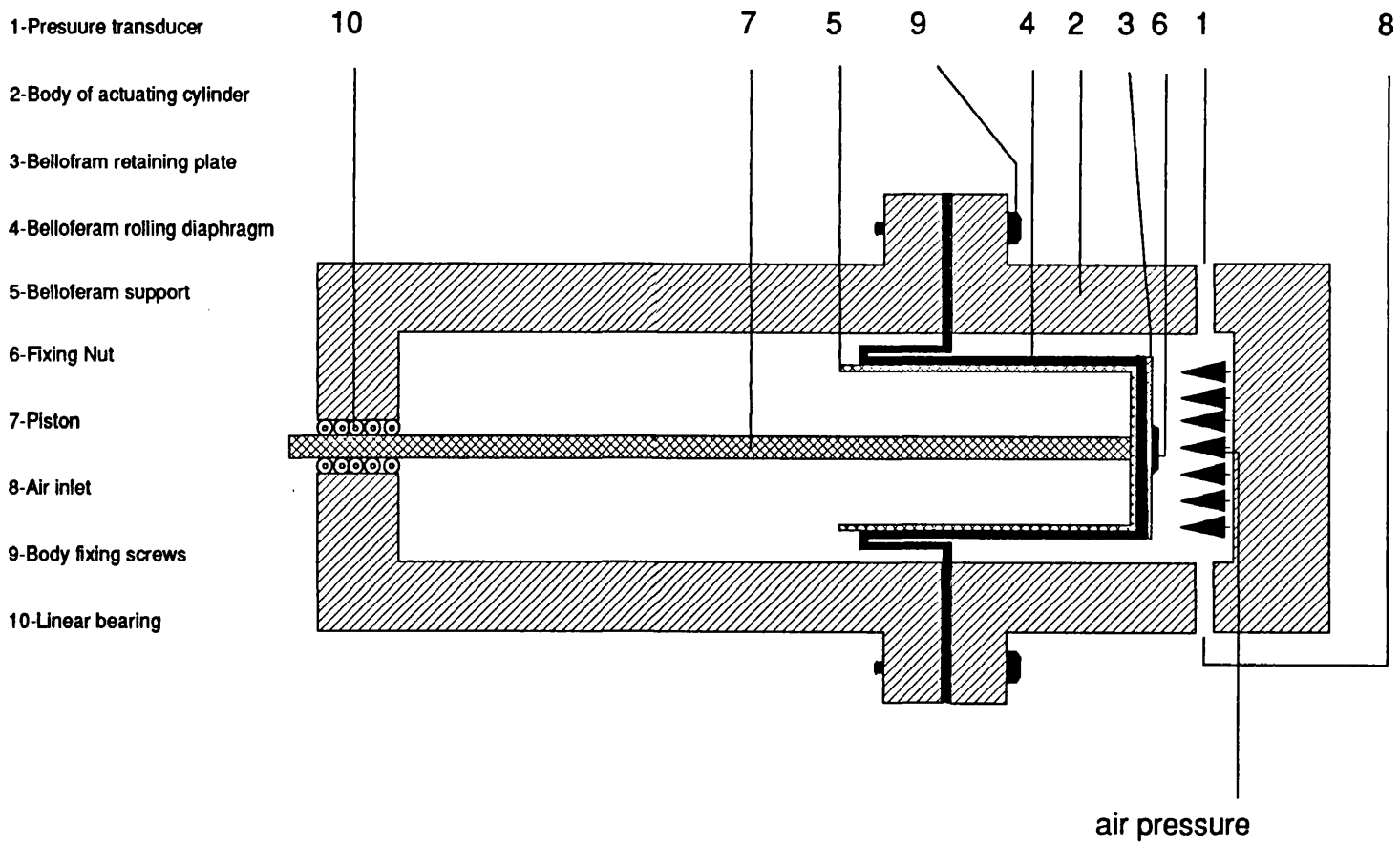

Fig. 2.21 A plan view of the actuating shear cylinder

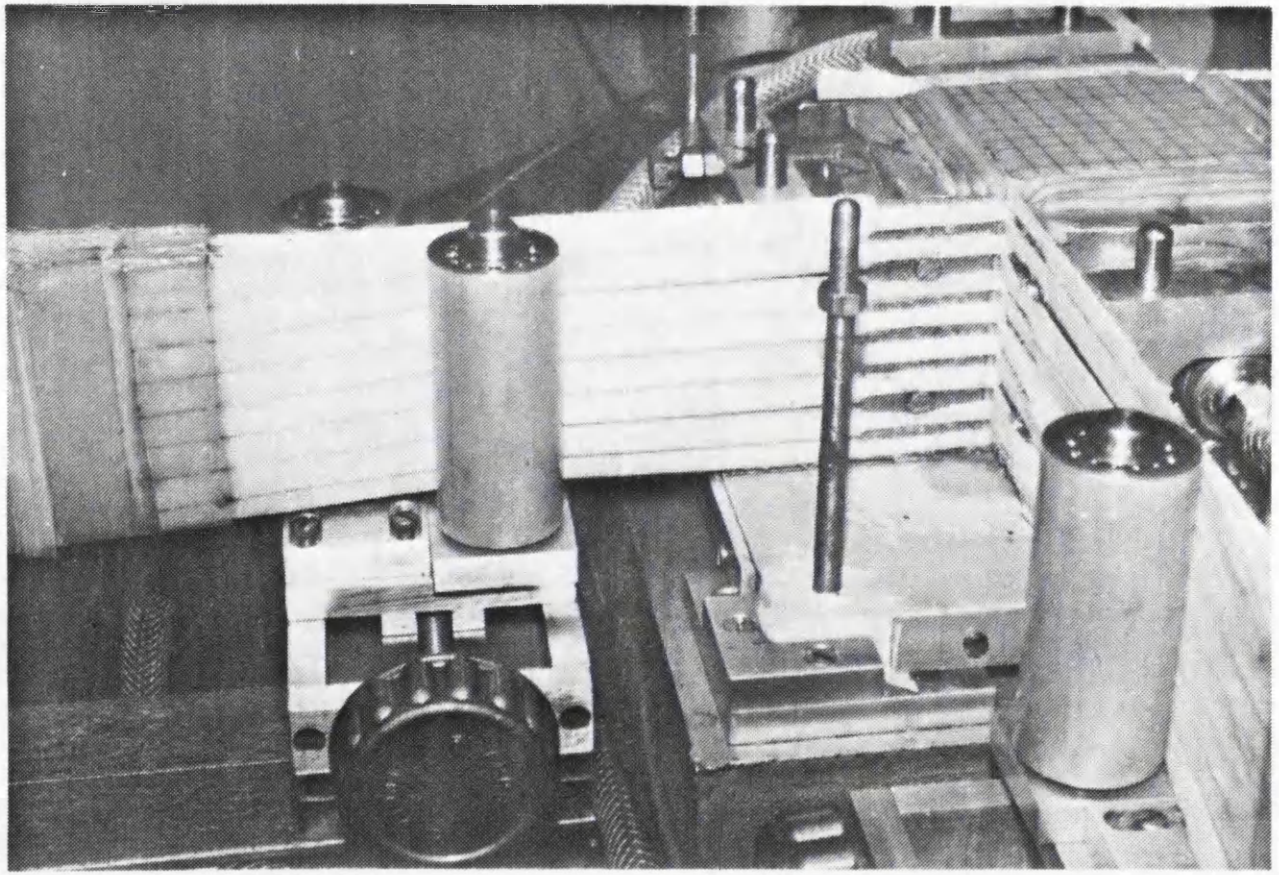

Fig. 2.22 Shear sheets aligning system

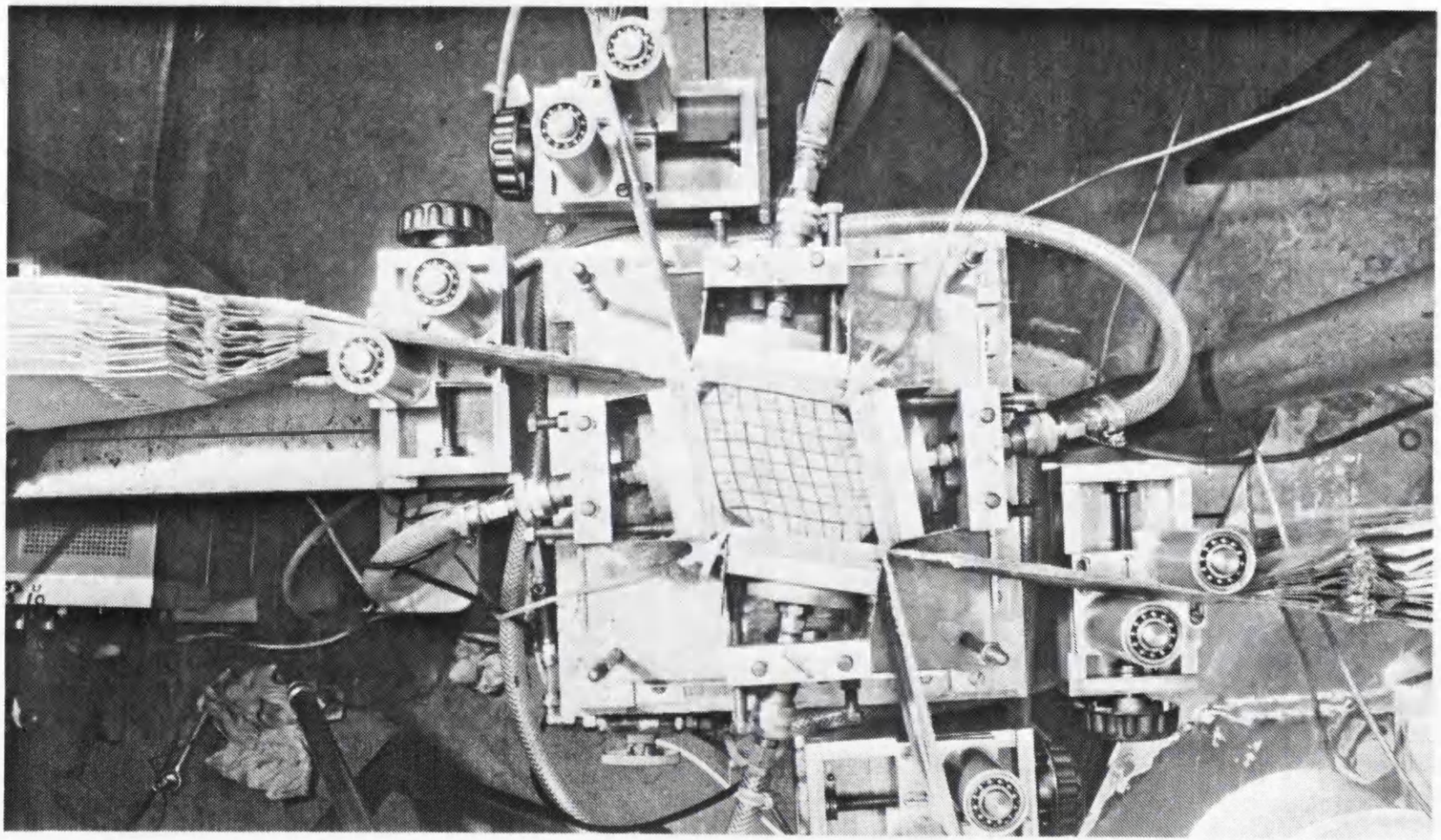

Fig. 2.23 **Positions of the shear sheets at the end of a largely deformed sample (ψ = 45°)**

1- Steel rods to maintain plane strain condition

2- Top and bottom plane strain sides

3- Adjustable backing plates

4- Normal pressure bags

5- Adjusting screws

6- Waterfilled σ_2 pressure bag

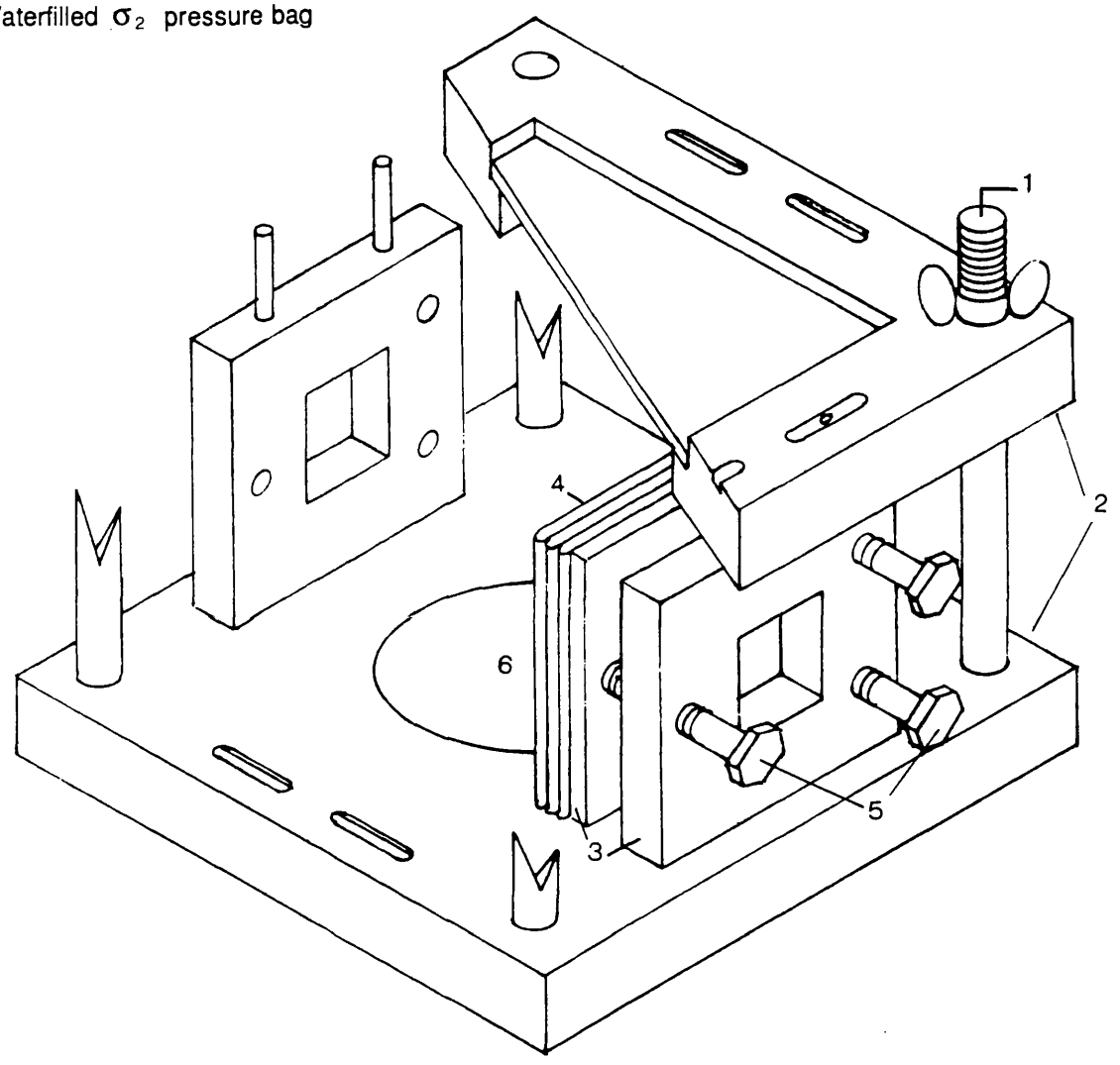

Fig. 2.24 Isometric view of part assembled cell

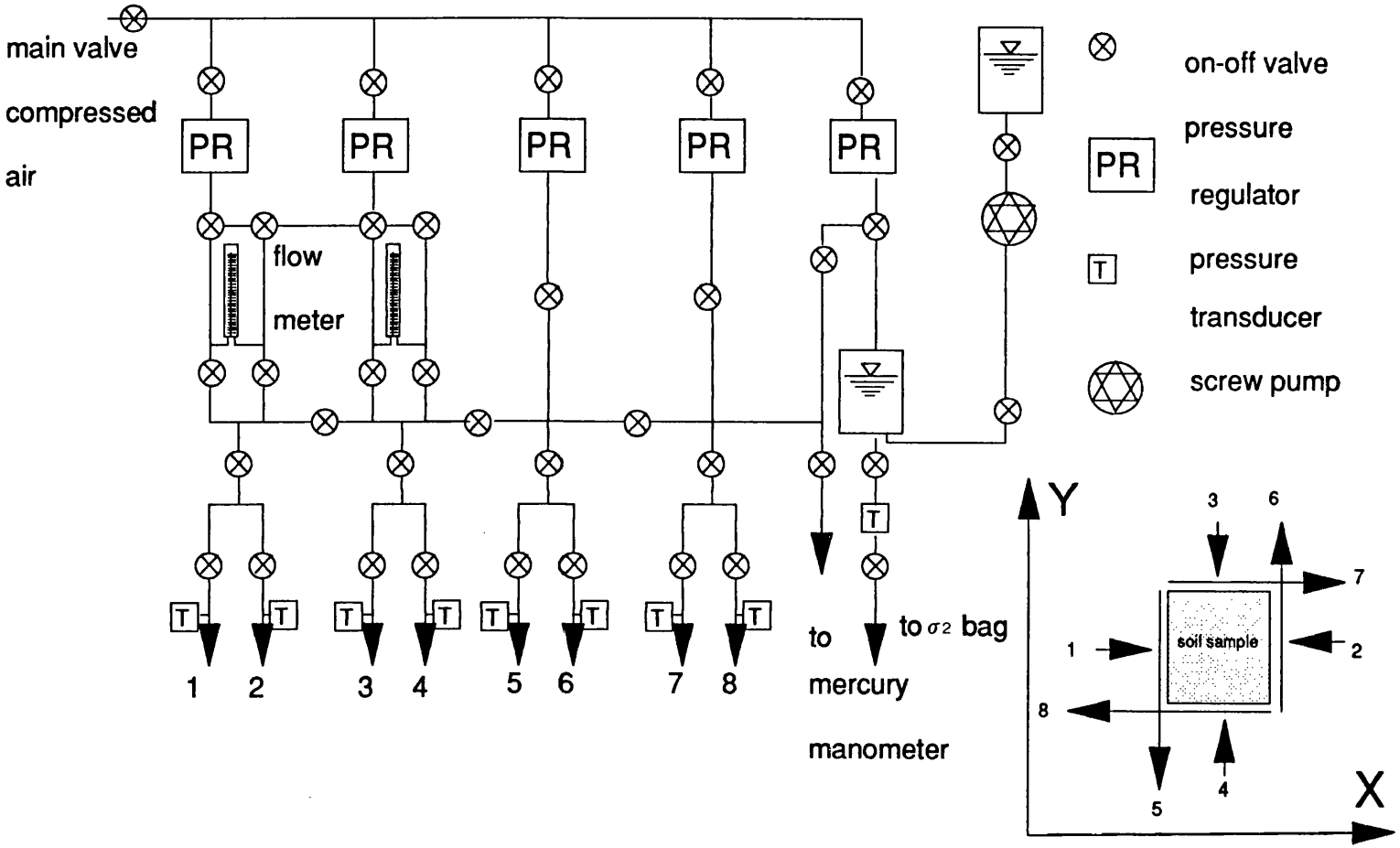

Fig. 2.25 Schematic representation of the pressure control panel

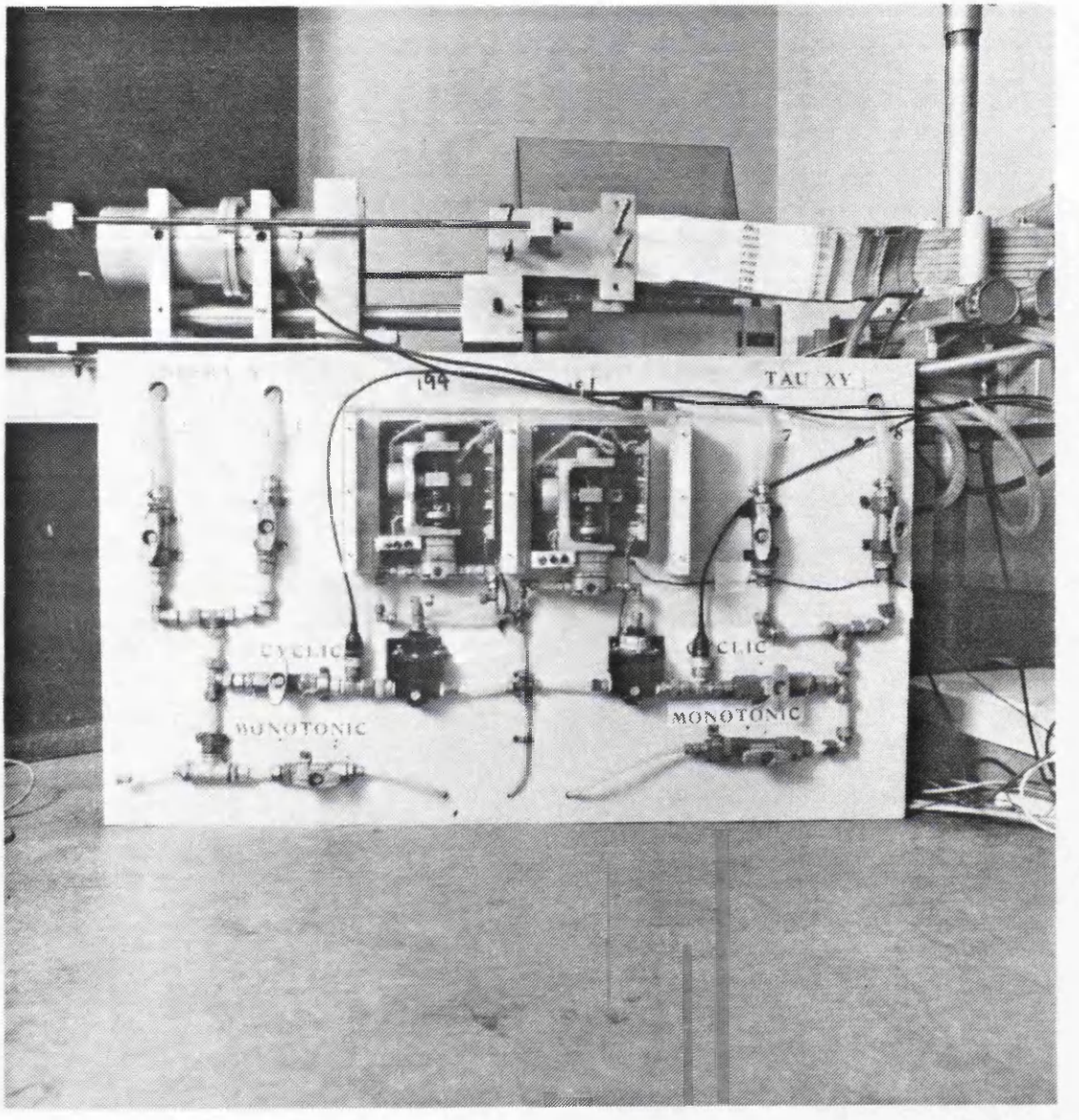

Fig. 2.26 Automated air regulators control boxes mounted on the control board

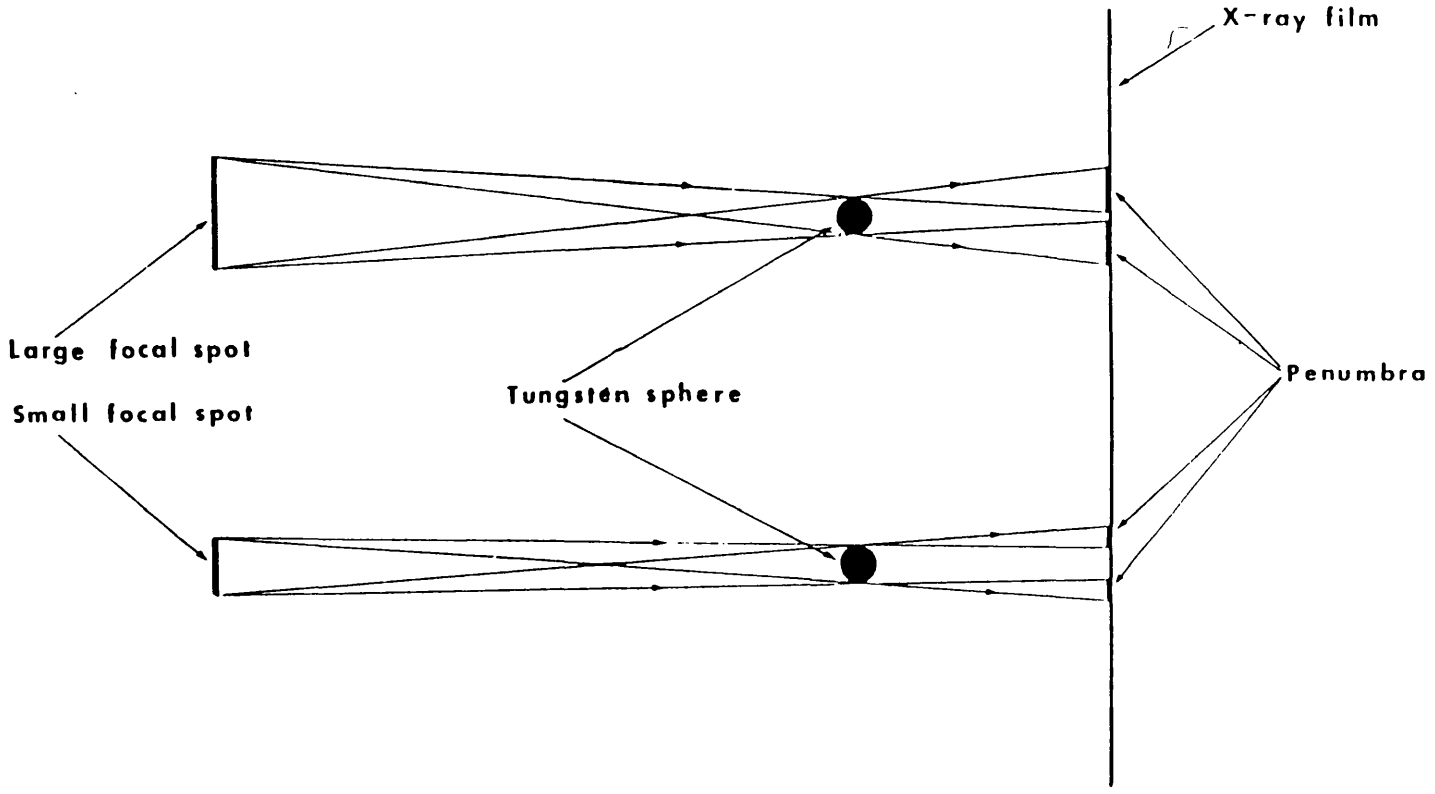

Fig. 2.27 The effect of focal spot size on image boundaries

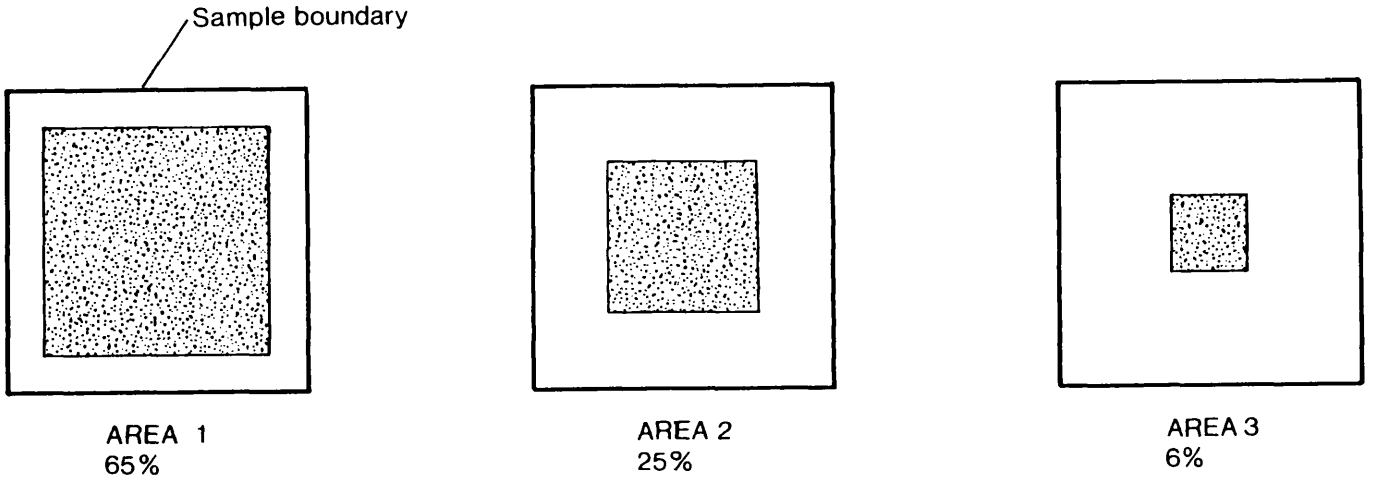

Fig. 2.28 **Definition of zones used for strain analysis**

F. No.	ε_x %	ε_y %	ε_{yx} %	ε_1 %	ε_3 %	ε_v %	γ %	ξ degree	ν degree	$\varepsilon_1/\varepsilon_3$
5	0.33	1.18	2.44	3.23	-1.72	1.51	4.96	49.94	-17.73	-1.88
5*	0.32	1.18	2.44	3.22	-1.72	1.50	4.95	49.95	-17.64	-1.87

5* = No.5 re-scanned

Table 2.1 An example of accuracy of measurements in radiographs

CHAPTER 3 SAMPLE PREPARATION AND SETTING UP PROCEDURES

3.1 INTRODUCTION

3.2 PREPARATION OF SAND SAMPLES AND SETTING UP PROCEDURE

3.2.1 Sample membrane and preparation box

3.2.2 Dense sample preparation

3.2.3 Loose sample preparation

3.2.4 Equipment preparation procedure

3.2.5 Setting up sand samples in the DCDSC

3.3 PREPARATION OF DAMP COAL SAMPLES AND SETTING UP PROCEDURE

3.3.1 Loose sample preparation

3.4 PREPARATION OF KAOLINITE SAMPLES AND SETTING UP PROCEDURES

3.4.1 Background

3.4.2 Remoulded Kaolinite sample preparation

3.4.2.1 Moulding cubical sample

3.4.2.2 Sample membrane and stretching box

3.4.2.3 Setting up remoulded Kaolinite samples in the Directional Shear Cell

3.4.3 Consolidated samples using Rowe's cell

3.4.4 Consolidated samples using a modified oedometer

3.4.4.1 Mixing and de-airing procedure

3.4.4.2 Consolidation procedure

3.4.4.3 Extracting and trimming procedure

3.4.4.4 Sample membrane and stretching box

3.4.4.5 Special porous corners

3.4.4.6 Placing the sample in a rubber membrane

3.4.4.7 Setting up pre-consolidated Kaolinite samples in the DCDSC

FIGURES

3.1 INTRODUCTION

This chapter describes the methods used for preparing cubical samples of different particulate materials and the setting up procedure prior testing in the DCDSC. A wide range of materials from dry sand to damp coal and saturated kaolinite were studied to evaluate their strength and deformation behaviour of these materials when subjected to continuous and cyclic rotation of principal stress directions.

3.2 PREPARATION OF SAND SAMPLES AND SETTING UP PROCEDURE

All experiments carried out on sand samples used dry Silver Leighton Buzzard sand with grain sizes between 0.60mm and 0.85mm and a specific gravity of 2.65. This subrounded sand was chosen because its properties have been closely defined in previous test programmes performed at UCL (Wong, 1986) and other research laboratories in various parts of the world; Figure 3.1 shows a micrograph of the material.

The aim of any sample preparation procedure is to provide an initially homogeneous sample with minimum disturbance. A typical method of preparing homogeneous samples of sand is by pluviation; i.e. deposition of sand grains by raining through air from a fixed height above the top level of the sand. Raining dry sand at slow rates yielded dense samples with voids ratio of 0.52 ± 0.01 and rapid mass raining gave loose samples with voids ratio of 0.72 ± 0.02. All samples were prepared with deposition direction right angles to the subsequent plane of strain, thus eliminating the influence of inherent anisotropy due to deposition from all the tests. Cubical samples of sand were enclosed in thin rubber membranes that were made in the laboratory. The following sections describe the different stages that one must follow in order to provide a successfully prepared sample of granular material for testing in the DCDSC.

3.2.1 Sample membrane preparation

Thin non-reinforced rubber membranes were used to seal and enclose the sand samples. These membranes provide a good contact between the sand sample and the shear sheets if the rubber surfaces are very clean and when a sufficient normal load is applied. The general procedures for preparing rubber membranes has been outlined by Menzies and Philips (1972) and Ogunbekun (1988), but will be explained

briefly here for completeness.

The manufacture of a thin rubber membrane begins with the thorough cleaning the aluminum former (Figure 3.2a) with scouring powder and a sponge. The former was rinsed with hot water until complete wettability was achieved. Special attention was paid to the edges and the corners. The former was allowed to dry in air and further cleaned with acetone and cotton wool. Throughout the cleaning process the former was held by the handle and no direct contact was made with the surface of the former; touch usually deters a uniform coating of coagulant forming over the former. The former was 7% oversize to allow for sample shrinkage after removal from the former.

The coagulant is a solution of hydrated Calcium Nitrate crystals ($Ca(NO_3)_2.4H_2O$) dissolved in Methanol (CH_3OH). The strength of the coagulant is an important factor in determining final thickness of the membrane; weight proportions of 40% Calcium Nitrate (analar):60% Methanol (analar) were used. The Calcium Nitrate was slowly poured into the Methanol and continuously stirred until all the Calcium Nitrate was dissolved, a process which took several hours. The clean former was dipped into the coagulant and then removed and the excess coagulant was allowed to drain off from one corner of the former back into the container. A check was made to ensure the former was thoroughly covered by the shiny coat of coagulant. If any parts of the surfaces were detected to be uncovered the former was recleaned and the dipping process repeated. Next the former was placed in an oven at 60°C for about 30 minutes during which time fine crystals of Calcium Nitrate formed a continuous film on the surface of the former, a state which was easily recognised by a matt surface over the former. After removal from the oven it was allowed to cool in a dry atmosphere.

Prior to immersing the former, the surface of the latex was skimmed to remove all bubbles, particles etc.. When the former was cool enough to be handled, it was slowly immersed into a liquid latex (Figure 3.2b) (Dunlop, A330 rubber latex) for approximately 15 seconds. The former was dipped at an angle such that the corner entered the latex first to prevent air bubbles being trapped on the former surface; then, when it was completely submerged it was rotated steadily through 180° before being lifted out slowly at a similar angle to that of entry. The excess latex was allowed to drain off while the former was again gently rotated to avoid any preferential build up of latex at any part of the former. The latex should form a smooth and uniform coating on the former. The thickness of the rubber membrane,

apart from the coagulant strength and the strength of the liquid rubber, is also dependent on the time of immersion. By varying the period of immersion, membranes of different thicknesses could be made. The above procedure resulted in thin membranes of about 0.25mm thickness. Any small defects, particularly at the corners and edges, were patched at this stage, using a glass rod dipped in latex, but this was avoided as far as possible. A careful preparation procedure provided a satisfactory membrane. This was allowed to dry in air for about 30 minutes before it was fully immersed in water, for at least four hours, to leach out any excess coagulant. This latter process makes the rubber membrane more elastic and waterproof and requires a continuous flow of water.

Once the leaching process was completed, the sample membrane was placed in an oven at 60°C for about six hours to be cured. After cooling, the top surface of the membrane was cleaned by acetone and a ball point pen was used to draw a regular grid onto one face. Talcum powder was dusted on the surface of the membrane to enable easy removal of the membrane from the former. A surgical blade was used to cut the membrane at the enlarged base of the former from the centre to the corners. The membrane was then carefully peeled off from the former avoiding any contact to prevent sticking; also finger contact was kept to a minimum to prevent contaminating the surface of the former. The membrane was again dusted with talcum powder to prevent formation of wrinkles and was then either ready for immediate use, or could be stored in a cool dark place.

Membrane positioning in the sample preparation box

The sample membrane was placed into a cubical sample preparation box (Figure 3.3) of 100 x 100 x 100 mm after a few drops of water had been applied to the outer side of the membrane to ensure adhesion to the box. This procedure also ensured the formation of a good cubical sample especially along the edges and a small soft haired brush was used to smooth out wrinkles. The overhangs of the sample membrane were laid over the sides of the box and held with a rubber band.

After carefully adjusting and fitting the sample membrane in the preparation box, sample preparation began by gluing two aluminum strips (Figure 3.4b) close to each of two opposite edges of the membrane using Evo-stik, 9162 made by Evode Ltd., United Kingdom. It has been found that these strengthened edges prevent progressive failure at the corners where the shear sheets emerge, yet deform to follow the change in shape of the sample. Prior to gluing, internal faces of the

sample membrane as well as the entire body of the aluminum strips were cleaned with acetone. Evo-stik was spread on one side of the strips, and on the inside surface of the membrane where the strips were to be stuck. The glue was left for a while until it appeared transparent. The strips were then carefully laid down on to predetermined positions of the membrane as illustrated in Figure 3.4b. If one of the strips were not laid in a correct position, it could not be peeled off and be relaid, the whole process then had to be repeated from the beginning to produce another sample membrane.

After placing the aluminium strips on the membrane a toothed coating of sand particles, similar to those to be used for making up the sample, was required to be stuck to the inside surfaces of the membrane to aid transmission of shear stresses to the sample. One face of the membrane was coated at a time. The preparation box was positioned so that the surface which was going to be worked on was horizontal. Evo-stik adhesive was then spread generously on the face as illustrated in Figure 3.4c. Particles were spread evenly over the face using a small scoop and flattened with a metal ruler while tamping and pushing the grains into the adhesive. Sand teeth on the inside of the membrane were formed by pushing the edge of the ruler into the levelled sand at predetermined intervals; a marker was used to determine the position of the grooves. The grooves between the teeth should correspond to the position of the vertical non-reinforced strips in the shear sleeve when these strips are later brought into contact. The excess sand particles were poured off before the process on the next side was repeated. The space between aluminum strips was filled with a sand and Evo-stik matrix while the box was placed on a wedge shaped base (Figure 3.4d). The glued sand boundaries and corners were allowed to dry for at least twelve hours.

3.2.2 Dense sample preparation

When preparing the sand sample, a deflecting shield was placed on the top of the preparation box (Figure 3.5a) and deposition by pluviation commenced. The use of a deflector during the deposition was aimed to prevent sand grains from bouncing back into the sample resulting in differential packing around the edges of the sample.

The rate of deposition in air predominantly governs the density of the sample; the height of deposition has a further but less significant influence. Thus both variables should be kept constant during deposition. Furthermore a horizontal sand surface should also be maintained to encourage homogeneity and uniform density.

Sand particles were deposited by gently shaking a sand filled container held at constant at 250 mm above the top level of the sample. A spiral motion was described with the sand filled container in order to produce an approximately level surface of sand at all times. When the preparation box was half full, a 95 mm x 95 mm acrylic template with regular spaced holes was gently lowered and rested on the sand surface. The acrylic marker enabled positioning a grid of 2.5 mm diameter tungsten balls. The tungsten balls where spaced at 12 mm centres. The template was then carefully lifted without disturbing the tungsten balls, Figure 3.5b. Deposition of the sand was then continued until the sand surface was slightly above the top of the preparation box. To provide a level sand surface with the preparation box (Figure 3.5c), the excess sand was removed by suction using a commercial vacuum cleaner through a 3 mm diameter nozzle. The nozzle was fixed to an acrylic spacer which was supported on the deflecting shield and thus could be positioned at any distance from the surface of the sand.

The deflection shield was removed and any particles still remaining on the membrane that covers the top horizontal rim of the preparation box were brushed off. Then the exposed flap of the sample membrane was cleaned with acetone and coated with Evo-stik adhesive. A separate thin rubber membrane of approximately 150 x 150 mm, which has been prepared in a similar method as the sample membrane but on a flat former, was also cleaned and coated with Evo-stik. In addition, two vacuum line assemblies were prepared. These lines consisted of polyethylene tubing (4 mm external diameter, Wykeham Farrance WF11320), of which of one end of 20 mm was sheathed in a thin rubber sheath made earlier, and connected using a "push fit" thick rubber tubing at the other end. The rubber sheath was also cleaned and coated with Evo-stik and the thick rubber tubing incorporated a glass stopcock. The end of the tubing was stuffed with a very small roll of polyester material to prevent sand particles from blocking the vacuum lines. While one tube was used to apply negative pressure to the sample, the other tube line was used to monitor the negative pressure in the sample through a mercury manometer. After the glue became transparent, these tubes were laid at the two diagonally opposite corners where there were no aluminium strips. The tubes were then carefully pushed into 5 mm diameter grooves at these corners of the perspex box. Care was taken that only the section of the thin tubes that contained the polyester material extended into the sample particles. Then the other ends of the polyethylene tubing was rested on supports to avoid disturbance of the sample and the membrane. The thin rubber sheet was then carefully placed over the levelled sample surface and sealed to the sample membrane at the edges by pressing the

two bonding surfaces, especially around the vacuum assembly lines, to ensure a good seal.

At this stage a negative pressure was applied to the sample by opening the glass tap to provide a rigid block; this was necessary to enable the removal of the sample from the preparation box and the positioning in the apparatus. The applied vacuum was less than the normal stress to be applied in the test because changes in sample stiffness could have been induced. Prior to the removal of the sample from the preparation box inspection was made through a manometer to ensure there was no leakage in the membrane. It should be noted that any minute holes which result from the improper membrane preparation or any subsequent accidental damage would make it difficult to maintain vacuum to the sample. The excess rubber on the sealed edges of the sample was trimmed off, so that only approximately a 6 mm lip of rubber remained. The preparation box, made up of five separate sides, was unscrewed to remove the sample without disturbance before placing in the DCDSC. Sometimes the moisture between the external faces of the rubber membrane and internal faces of the preparation box had dried so that the rubber membrane adhered to the sides of the box. This made the removal of the sample difficult without disturbing it and, then water soaked cotton wool was placed on the gaps between the sample faces and the sides of the box such that the water could percolate into the gaps to dampen the dried off areas; the sample could then easily be removed from the preparation box.

3.2.3 Loose sample preparation

The preparation of loose samples was identical to that of dense samples, prior to the point where deposition of sand began. The loose samples were prepared by instantly releasing a large quantity of sand from a fixed height of 750 mm above the preparation box. This technique has been reported to produce uniform Leighton Buzzard sand samples having voids ratios of 0.73 ± 0.02, (Rodriguez, (1977); Bekenstein, (1980); and Wong (1986). This method of deposition however makes it difficult to maintain the position of the tungsten balls in the middle plane of the sample on subsequent deposition. Lord (1968) attempted to place the lead shot in loose sand by dropping them through a number of glass tubes inserted in the sample. Bransby (1968) believed that the removal of the glass tubes may disturb the loose sample and considered a method in which the lead shot could be supported by a fine tensile wire, of 0.01 mm diameter, before pouring the sand. When pouring was completed an electrical current was passed through the wire to vaporise it.

However, this method was time consuming and expensive. Rodriguez, (1977) also aimed to place an array of lead shot in a central plane. The preparation box was partially filled by allowing the sand to fall from a suitable height and then levelled using a suction technique. An array of lead shot was then placed at the middle plane and the other half of the box was subsequently filled by using the same method as before. However, radiographs indicated that the lead shot were disturbed from their original positions by the sand falling on them. Rodriguez adopted an alternative procedure, that measured strain only on the top plane of samples poured through air after he observed that strain in the middle and top planes of the same sample were identical in water prepared samples which gave the same voids ratios. He then used photographs of a grid of lines drawn on the membrane.

Although photography is a straight forward and simple procedure, it requires good resolution of the top of the sample. However, in order to minimize the friction between the sample and the top plane strain platen, a generous amount of grease is needed which is sandwiched between two thin rubber sheets, each slightly larger than the sample face; but this in turn decreases the possible photographic resolution. Bekenstein (1980) omitted these two rubber sheets on the loose samples "to ensure high quality photographs of the inked lines". However, she reported some scatter on loose stress-strain curves, also the overall strains in her tests were lower than Rodriguez (1977) who used a thicker layer of grease.

In order to overcome the friction problem and minimize the end restraint as well as describing an identical lubricating procedure throughout the current research for dense and loose sand, the author employed the radiographic technique. The tungsten balls were stuck to the bottom of the sample membrane using Evo-stik adhesive. The grid drawn on the rubber membrane helped in positioning the tungsten balls. Once the glue was dry, the preparation box was ready to be filled. It should be noted that the position of tungsten grid on the boundary of the sample provided a sharp resolution when that side of the sample was placed on the σ_2 bag. This made for an easier scanning during the strain measurement process. These preparations are illustrated in Figure 3.6 (a-d).

Deposition procedure started by placing the deflector shield in position on the top of the preparation box, the box was then placed beneath a sand filled container which has a sliding door that provides for sudden deposition of sand in one action. The container was filled with enough sand to enable the preparation box to be filled in one deposition action (Figure 3.6e). The sliding door was then opened to release the

sand as illustrated in Figure 3.6f. Obviously this method of deposition implied that both the preparation box and the deflector shield were filled and removal of sand was necessary. However, loose samples are more subject to disturbance than dense samples and thus must be handled very carefully, especially during removal of the excess sand by suction. Consequently, removal of the surplus sand was achieved in a gradual process in which the extra sand was extracted in layers via suction from a vacuum cleaner until a final flat surface that was level with the top of the preparation box was obtained (Figure 3.6g).

Sealing the sample followed the dense sample procedure (Figure 3.6h) and a negative pressure of 10-15 kPa was applied to enable the removal of the sample from the preparation box. The sample was typically left for a few hours under vacuum until the glued parts were firmly set. The sample was connected all the time to a mercury monometer to ensure there was no leakage. Figure 3.3i illustrates a complete loose sample ready to be placed in the DCDSC. Then the sample was placed into the DCDSC with the side containing the tungsten balls placed against the σ_2 bag. The preparation procedure eliminates any effects of inherent anisotropy in the plane of strain.

3.2.4 Equipment preparation procedures

Preparation of the DCDSC to test a sample involved an extremely tedious and time consuming procedure, but it was essential if it was to function properly. The shear stress system, the normal pressure system, the plane strain system and the electronics all required careful attention.

To function properly, the pistons, the guiding shaft, and the rollers (Figure 2.2) had to be efficiently lubricated before each test to ensure there was no friction. The lubricant used for this purpose was a low viscosity hydraulic fluid (Mobil DTE light) which was anti-corrosive and sulphur free. This would not damage the belloferams and the pulling sheets if they were contaminated while the rollers were lubricated.

The shear sheets only worked correctly when they well lubricated in some parts and entirely grease free in others. The rubberized non-stretching strips of the shear sheets which transmit shear forces to the shear sleeve from the loading system had to be well lubricated between the normal pressure bags and the sample. Lubrication ensured each rubber strip performed independently of its neighbours, thereby ensuring an even distribution of load to the shear sleeve, even though appreciable

normal stress was transmitted across these strips by the normal pressure bags. In addition to these strips the tails were also thoroughly lubricated. Regular inspection was made between tests to ensure adequate lubrication existed and additional grease was applied to these rubber strips to compensate for the grease lost during a test. The lubricant used was Dow Corning Molykote silicone grease with the addition of 20% fine polytetrafluorelthylene powder. The inner surface of the shear sheet which makes contact with the sample membrane had to be kept grease free. The inner shear sleeve was cleaned with trichloroethylene and finally roughened with acetone to ensure a perfect bond to the outer side of the sample just prior to being placed around the sample. To protect the treated shear sleeves from grease contamination, the shear sleeves were always wrapped with clean paper towels after use.

Each of the four shearing sheets and their yokes were located in a position on the arms of the main frame such that the shear sheets could freely be placed around the sample without imposing any forces to the shear sleeve.

The normal pressure was provided through concertina flexible bags. Prior to testing, all exposed parts of each normal pressure bag were coated with a thin film of grease. To minimize friction between the shear sheets and the normal pressure bags, two thin well lubricated rubber sheets (100 x 100 mm) were smoothed over the front face of each pressure bag. Thus between the normal pressure bag and the shear sheets there exists three layers of grease and two sheets of rubber. The thickness of the grease layers was important, as thick layers of grease could endanger the stability of the normal pressure bags particularly at large deformation. Before each test, the old grease was removed and a freshly prepared silicone grease with PTFE filler was replaced. Any air bubbles trapped between the lubricated thin rubber sheets and the pressure bags were worked out. Then the thin spring steel retaining vanes were screwed to the backing plates. The bags were then set aside close to the apparatus.

The bottom plane strain platen shown in Figure 3.7a consisted of a flexible reinforced pressure bag through which σ_2 could either be monitored or controlled. This bag was inflated to the same level as the base platen and then was isolated to keep the pressure bag at constant volume. An even layer of lubricating grease was applied to the surface and then covered with two sheets of thin rubber (150x 150mm) which already had been coated with the same grease. The air bubbles which were trapped when placing these sheets over the intermediate pressure bag

were carefully worked out. Then another even layer of grease was spread over the top of the rubber sheet.

Finally checks were made on the power supply, digital voltmeter, pressure transducers, stepping motors and chart recorders. Particular care was taken in obtaining the appropriate zero readings and calibration constants of transducers and these devices were connected to a continuous power source. If the power was cut off after finishing a test it was necessary to calibrate the pressure transducers again.

3.2.5 Setting up sand sample in the DCDSC

After a sand sample had been removed from the preparation box it was placed on a clean glass plate with the inked grid facing up while the sample was kept under vacuum. At this stage measurements of the initial height of the sample were recorded at 16 points prior to testing. This was to check on strain in the direction of intermediate principal stress. A more efficient method of determining strain in this direction is to place a layer of tungsten balls in the vertical direction orthogonal to the existing plane of shot. By taking radiographs in the vertical direction measurement of strain in the σ_2 direction can be determined. This latter method was not used throughout this research.

As it was necessary for the sample membrane to adhere to the inner side of the shear sleeve, all sides were thoroughly cleaned with trichloroethylene and then roughened with acetone to ensure grease free surfaces. It was found that this procedure produced extremely good traction with the shear sheets.

The sample face that was going to rest on the σ_2 bag, was coated with grease and positioned centrally onto the well lubricated σ_2 pressure bag (Figure 3.7b). A small amount of grease was then smeared on to those external faces of the sample where the sample membrane is reinforced along two edges. Arthur et al. (1977) observed that the DSC generally fails to apply stress right to the edge of the sample from which the shear sheets emerge and an incorrect edge stresses can easily induce progressive extensive failure at the corners. Greasing this area of the sample membrane was an additional precaution to ensure no shear was applied in this region.

After the sample was in place, each shear sheet was matched to the edges of the sample and pushed firmly onto the sample sides. This procedure was repeated for

all four sides of the sample (Figure 3.7c). Finally the tails, that had already been greased were located in the correct position.

Precise centralization of the sample was necessary to obtain correct alignment of the sample and the shear sheets. This was achieved by placing the top platen above the sample. There was a grating on an acetate transparent film which was fixed to the top plane strain platen and this was compared with the inked lines on the four edges of the sample.

The four normal pressure bags which had already been greased were set around the sample. To achieve virtually the correct normal stresses the concertina bags were kept within ± 5 mm of optimum thickness and the bag edges were evenly spaced on either side of the sample (Figure 3.7d). This positioning of the normal pressure bags was obtained by adjusting the nuts in the backing plates. The location of backing plates was loosely fixed by locking the wing nut screws to the bottom platen.

Since the adjustment of the normal pressure bags might have dislocated the sample from the central position, the top plate was located on the apparatus and, by using the acetate sheet once again, a check of position could be made.

At this stage The shear sheets were aligned with the sample faces and guiding rollers were located in the correct position. The alignment was gained with the aid of a ruler which was placed parallel to the edge of the sample. For correct shear stresses, the shear pulling sheets must continually be aligned with the sample faces throughout the test.

Once sample centralization had been ensured and the shear sheets were aligned, the top platen was prepared and placed on the top of the sample. To prepare the top platen the acetate transparent film was first carefully cleaned and then evenly spread with a coating of the transparent grease as already described. This was then covered with two thin rubber sheets already coated with the same grease. Air bubbles trapped beneath these sheets were worked out and another even layer of grease was spread over the top of these rubber sheets.

The top platen was then located on four steel rods and allowed to rest freely on top of the sample, and four wing nuts were then loosely screwed on the rods. Finally the top platen was made parallel by repeatedly measuring the distance between each of the four corners with a parallel gauge, and then carefully adjusting the internal

locking nuts and the external wing nuts. Any slight error in sample position was corrected at this stage of the setting up procedure. Once the top platen was locked the sample was kept in a plane strain condition. Finally a pressure of 14 kPa was applied to the four normal pressure bags and the intermediate principal stress bag simultaneously.

3.3 PREPARATION OF DAMP COAL SAMPLES AND SETTING UP PROCEDURES

To further understand the effects induced by cyclic rotation of principal stress direction on a different type of particulate material, a few tests were conducted on damp coal (7% moisture content). The coal was obtained by courtesy of Dr Matchett of Teeside Polytechnic and was the same coal as used by him in a joint research project with British Steel. The moisture content used in the present research was chosen on his advice. Figures 3.8a and 3.8b illustrate a particle size and particle shape distribution of the coal tested herein.

3.3.1 Loose sample preparation

In an attempt to obtain a loose sample of coal, the same conventional method of sample preparation for loose sand was initially followed. Since the coal was provided in its natural grading and consisted of particles much larger than could be tested in the DCDSC, it had previously been sieved and particles greater than 2400 μm were not used. The average moisture content of the coal was 4.04% on supply, and 3.66% after being sieved. Extra water was added to the coal to achieve a moisture content of 7%.

The sample membrane was prepared in the same manner as described earlier and placed in a preparation box with the deflector shield on the top. Sample preparation follows that for loose sand (Figure 3.6). However, due to the damp nature of the material, a number of particles stuck together and formed groups which resulted in nonuniform packing, especially around the edges of the sample. Despite repetition of this procedure and several variations, obtaining a uniform sample was not possible.

A method similar to that introduced by Arthur et al. (1985) and Ogunbekun (1988), for preparation of cohesive bulk solid samples to be tested in the Biaxial Tester apparatus was adopted. The method involved allowing a sample to be prepared by compressing layers of the test material with a plunger. This method of sample

preparation ensured the formation of a relatively uniform sample. The use of the plunger also ensured a degree of control over the initial state of the sample but a degree of layered anisotropy was introduced perpendicular to this direction.

A rubber membrane was prepared in a similar way to that for sand samples. It was turned inside out and slipped over a cubical hollow brass former. A thick layer of Evo-stik was spread on the inner face of the rubber membrane and using a small scoop, an adequate amount of dry coal, was spread on the glue and the coal particles were pushed into the glue. The same process was applied to the other three sides and the glue allowed to dry for at least 30 minutes. This process is illustrated in Figure 3.9.

The membrane was then placed in a slightly over sized box and after being secured by two rubber bands, a vacuum was applied to stretch the membrane back to come into contact with the box faces.

Pouring commenced by shovelling a sufficient amount of coal into the box to fill it to a depth of about 15mm in a loose state. Using a small ruler the damp coal was very gently flattened and a plunger of 100 x 100 x 100mm with a central seating was subsequently lowered and very carefully placed on the coal. The coal was loaded via a hanger equivalent to 14kPa pressure positioned on the central seating of the plunger; extreme care was taken to prevent any impact. Figure 3.10 illustrates a schematic view of the device used to compress the coal. The filling at 15 mm intervals and loading was continued until the sample was half full, a grid of tungsten spheres was then placed as shown in Figure 3.11, and filling and loading continued until the sample membrane was entirely filled.

At this stage the vacuum behind the stretching membrane was released and two vacuum line assemblies were set in place, the sample membrane was then sealed and subsequently a vacuum of approximately 10kPa was applied to the prepared coal sample.

Once the sample was removed from the box, two very thin strips made of stainless steel were glued flush to each of two diagonal edges of the sample, as illustrated in Figure 3.12. These strips ensured the stability needed where the shear sheets interleave and prevented local non-uniform strain development.

After measuring the height of the sample prior to testing in at least 16 places with

Vernier Callipers, the coal sample was placed in the DCDSC and an identical setting up procedure to that of sand was followed.

3.4 PREPARATION OF KAOLINITE SAMPLES AND SETTING UP PROCEDURES

3.4.1 Background

Cyclic tests involving nearly saturated and fully saturated kaolinite, used three different types of sample preparation. In all clay tests Speswhite kaolin, with a liquid limit of 63% and plastic index of 30% was used as a comparison with the previous work by Wong and Arthur (1987). A micrograph of the material used is illustrated in Figure 3.13.

The first series of samples were prepared using a method described by Wong, Arthur and Dunstan (1987) in their investigation into the effects of induced anisotropy on wet remoulded kaolinite and bentonite. In this method the aim of the preparation technique was to eliminate all effects of inherent anisotropy. This was achieved by mixing the dry Speswhite kaolinite powder with specific proportions of water and then forming the kaolinite into 100 mm cubical block samples with no directional bias. These samples were not prepared from a slurry and no special techniques were used to ensure saturation, consequently the samples contained 10% of air voids. This acceptance of air voids saved much time and was thought to have no effect on an examination of directional properties; moreover it was considered that it might be a realistic complication of the material in some cases. The resulting kaolinite mix was sufficiently stiff to withstand the subsequent handling when being placed in the DSC.

In an attempt to provide fully saturated samples to be tested in DCDSC so that the pore water pressure could be measured in the middle of the sample, the second series of kaolinite samples were prepared using a consolidation cell which was developed by Rowe. The samples consolidated in this cell were prepared from a slurry of 100% moisture content. The slurry was prepared by mixing dry kaolinite powder in a laboratory mixer with de-aired, distilled water. However the slurry used in the Rowe cell could not be de-aired satisfactorily during the mixing process under vacuum with the above moisture content. Adopting a higher moisture content would not produce enough material for a cubical sample of 100x 100 x 100mm to be used in the DCDSC if the existing Rowe cell of 250 mm diameter was to be employed.

Therefore a third means of preparation of fully saturated samples was investigated.

The author believed a slurry of moisture content as high as 300%-400% and a new de-airing technique was necessary to be able to obtain a high quality fully saturated sample. In order to fulfil these requirements new equipment for mixing and de-airing the kaolinite slurry were developed. Since the existing Rowe cell could not accommodate enough slurry of this kind, therefore, the third series of samples were prepared using a conventional 1-D laboratory consolidation procedure developed by Terzaghi, et al.(1930). In this device load is applied to the kaolinite sample through the top platen by means of a hanger, a lever arm and dead weight. In the following sub-sections these procedures are described fully.

3.4.2 Remoulded Kaolinite sample preparation

Sample preparation was begun by mixing of 1.5 Kg of dry Speswhite Kaolinite with 750cc of de-aired, distilled water in a laboratory mixer under vacuum to gain a 50% moisture content. Regularly during the mixing process, the vacuum was released and the mixer switched off. Any unmixed Kaolinite which was left on the edges was pushed into the middle of mixer. This action was repeated several times during the mixing process which took about two hours. Once a relatively satisfactory mixture was obtained the paste was placed in a container and covered with a sheet of Cling-film to prevent any moisture loss.

3.4.2.1 Moulding the cubical sample

The paste was moulded by hand, into a 100 x 100 x 50 mm deep perspex box to form half of the final sample. Moulding commenced from the corners towards the centre and care was taken to minimise the amount of trapped air. The bottom and internal faces of the box were lined with water soaked blotting paper to prevent the kaolinite from sticking to the sides of the perspex box. The preparation box used for forming the paste is illustrated in Figure 3.14. Once the box was full the top surface was levelled with a sharp edged ruler and perspex box was then dismantled by unscrewing its different sides. The prepared half of the kaolinite sample was placed on a wet base and subsequently wrapped with cling-film to prevent loss of moisture whilst the other half was prepared in a similar method. This type of sample preparation allowed for the placement of a grid of Tungsten balls on the middle plane. In some cases in this research the author placed a grid of lead dust on the middle plane utilising an appropriate template. The aim was to capture the initiation

of the rupture planes by the aid of radiography during shearing. Once the grid had been placed, one half of the sample was carefully picked up and placed very gently on top of the other half. This formed the 100 x 100 x 100 mm cubical kaolinite sample.

If shear stresses were to be applied to the sample an additional treatment was necessary. This required placing two rigid aluminium angles on opposite edges of the sample where the shear sheets interleaved. To locate these aluminium pieces an exact amount of kaolinite equal to that of their volume was removed by using a surgical blade and then the angles were pressed into place.

At this stage all faces of the sample were again covered with water soaked blotting paper and wrapped with cling-film. The sample was then ready for placing in a rubber membrane.

3.4.2.2 Sample membrane preparation and stretching box

The sample membrane provides the interface between the kaolinite and either the normal pressure bags or the shear sheets depending upon the test to be performed. The membrane preparation procedure for remoulded kaolinite samples was identical to that for sand up to the end of curing, but the former to be used was different. As the sample preparation procedure required a sample membrane which was open at two ends, two thin duraluminuim plates were screwed to both ends of the cube (Figure 3.15). This former provided the rubber membrane that could be slipped over the kaolinite sample.

As the square edges and corners of the kaolinite samples could easily be damaged and it was necessary to stretch the membrane sufficiently in order to slip it over the sample while maintaining the proper prismatic form. Here an oversized brass box that could apply a vacuum to the membrane was employed (Figure 3.16a). The overhanging part of the membrane was laid over the sides of the box and fixed using rubber bands (Figure 3.16b).

To stretch the sample membrane, a slight vacuum was necessary to expand the membrane, this was applied through a laboratory vacuum line centred at one side of the box. A filter covered the vacuum port in order to prevent a concentrated vacuum from puncturing the membrane. The expanded membrane was then ready to be placed over the kaolinite sample.

The internal faces of the membrane then were cleaned with acetone and coated with a uniform thin layer of Evo-stik using a spatula. Next a very thin layer of fine uniform sand was sprinkled onto the adhesive on the four inner faces of the rubber membrane (Figure 3.16b). This coating of glued sand was found to be necessary to prevent slippage between the rubber/soil interface, thereby enabling shear stresses to be transmitted to the sample during shear as illustrated in Figure 3.16b.

3.4.2.3 Setting up remoulded Kaolinite samples in the Directional Shear Cell

As these were the first DSC tests on wet clay to be carried out by the author, and because the DCDSC was in the development stage for testing clay; it was appropriate to start with the low stress DSC used by Wong (1986). The main difference between the two is in the structure of pulling sheets. This has been fully described in Chapter 2.

The equipment preparation procedure for remoulded kaolinite samples was the same as for the sand samples even though a different version of the DSC was going to be used.

After preparing the DSC to accept a kaolinite sample, the cling-film enclosing the sample was gently removed and the pieces of blotting paper were carefully peeled off the sides of the sample. Then the expanded sample membrane was slowly slipped over the sample whilst still stretched under vacuum in the box. Care was taken so that the edges and corners of the cube were not disturbed. The vacuum was then gradually released and the box was removed. Care was exercised to minimise the amount of trapped air between the membrane and the sample. As with the inner surface of the shear sleeve, the sides of the sample membrane were thoroughly cleaned with trichloroethylene and then roughened with acetone.

Once thoroughly cleaned, the shear sheets were placed loosely around the sample with the aluminium edges next to the interleaving pulling sheets. A small amount of grease was then applied to external surfaces of the sample membrane which were attached internal aluminium strips. This was an additional precaution to ensure no shear was applied to this area. The shear sheets were then arranged by matching the edges of the sample and pushed carefully onto the sample sides ensuring no grease was introduced between the two contact surfaces. Finally the tail of the shear sheets were properly arranged and the pulling surfaces smoothed.

Then the sample was gently lifted and positioned centrally onto the σ_2 bag on the bottom platen and the acetate grid on the plane strain face was used to finally align the sample in the DSC.

3.4.3 Consolidated samples using Rowe's cell

In an attempt to provide fully saturated samples where measuring pore water pressure the second series of kaolinite samples were prepared using a Rowe cell. Figure 3.17 illustrates a Rowe cell full assembled. The samples consolidated in this cell were prepared from a slurry of 100% moisture content. The slurry was prepared identical to the slurry prepared for the remoulded samples by mixing the dry kaolinite powder in a laboratory mixer with de-aired, distilled water. To prepare the equipment a cintered bronze disc and a plastic porous plate were first de-aired in boiling water. After de-airing a filter paper was placed on top of the cintered disc and positioned onto the bottom of the cell. The walls of the cell were cleaned thoroughly and the slurry was carefully poured into the cell. Care was exercised to minimise trapped air. The saturated plastic porous plate was then placed on the top of the slurry. Distilled water was poured onto the porous plate and the rubber jack was lowered slowly into position and the cell cover was clamped in position. Pressure was applied to the rubber jack from an air/water cylinder. The expelled pore water escaped through both top and bottom drains. The spindle that was fastened to the rubber jack followed the movement of the jack. A dial gauge that was mounted on top of the of the spindle recorded the settlements of material during the consolidation. Readings of settlement were then taken at suitable intervals of time. When the required consolidation stress was attained the unloading of the consolidated sample commenced within appropriate intervals while the top and bottom drain valves were opened. This resulted in a moisture content of approximately 50% and OCR of 7.5.

Once swelling was completed the top cap was unscrewed and removed. Using a screw type jack the sample was carefully extruded from the cell. The kaolinite cake was placed on a flat surface, and the top porous disc removed. Then by using a taut wire, the kaolinite cake was cut on vertical planes to the required size. Figure 3.18 illustrates the sequence in which the cake was cut.

After cutting the cake, the same process was carried out as for the remoulded kaolinite in terms of encasing the sample in a rubber membrane and setting up in the shearing device.

3.4.4 Consolidated sample using a modified oedometer

In an attempt to prepare fully saturated samples and be able to measure pore water pressure accurately, de-airing was imperative, especially as the DSC cannot provide a back pressure to push any trapped air into solution. Once a satisfactory de-aired slurry was obtained, the slurry was consolidated one-dimensionally under an axial stress of 150kPa for more than a week. The consolidation stress was chosen in an attempt to gain samples of about 50% moisture content and OCR= 7.5 (see Figure 3.19), in order to compare the results with previous preparation techniques. Cylindrical specimens of 155 mm diameter and nearly 40mm tall were achieved from three consolidation cells which were put together, trimmed and encased in a rubber membrane to provide a cubical sample suitable for testing in the DCDSC. The preparation of fully saturated specimens used the following procedures:

3.4.4.1 Mixing and de-airing procedures

The mixing and de-airing process played a significant role in obtaining completely saturated kaolinite samples. Figure 3.20a shows the equipment that was used to mix and de-air the kaolinite.

This mixing and de-airing process consisted of three different stages; mixing under vacuum, spraying under vacuum and shaking under vacuum.

For the first stage 1000 g of Speswhite kaolinite was mixed with 3000 cc of de-aired, distilled water under vacuum in a PVC cylindrical chamber (Figure 3.20a). The chamber was 500 mm high and 160 mm in diameter. A 13 mm thick PVC plate formed the top platen of the chamber to which the mixing motor and two vacuum lines were attached. The central hole of the top plate was fitted with a rotary vacuum bearing (Figure 3.20b). Stirring of the slurry under vacuum was continued for about two hours.

At the second stage the stirring action was stopped and the vacuum was released from the PVC cylinder chamber. The slurry was then gently evacuated through a plastic pipe by opening an outlet valve and sprayed under vacuum of 80 kPa into a thick glass container of 10 litres capacity through a nozzle as illustrated in Figure 3.20c. Great care must be taken when using vacuum especially if the container is made of glass to prevent breakage. As an additional precaution a metal mesh was placed around the container under vacuum. The purpose of using a glass container

was to ensure that there were no air bubbles left in the slurry, this could easily be checked through visual inspection. Once the PVC cylinder was fully evacuated the same process was repeated until the required volume of slurry (approx.10 litres) was attained. The slurry was then left under vacuum for several hours; even so, when the container was shaken by hand a visual inspection revealed some air bubbles still trapped in the kaolinite.

The third stage was commenced by placing the container on a shaking table while the slurry was kept under full vacuum. To place the glass container on the shaking table a metal frame was clamped to the table and then lined with soft pieces of sponge. The container was then placed into these sponges while the whole frame was covered with a safety metal mesh as shown in Figure 3.20d. Vibration accelerated the de-airing process and after four hours of shaking, a satisfactory de-aired sample was obtained in which no air bubbles could be detected.

3.4.4.2 Consolidation procedure

To consolidate the kaolinite slurry conventional oedometers were modified to accommodate the larger consolidation cells. To obtain a cubical sample of 100 x 100 x 100 mm for the DCDSC at least three larger sized cells were necessary. Figures 3.21a and 3.21b shows the arrangement of the modified oedometers.

Once the slurry was fully de-aired the glass container was dismantled from the shaking table and laid horizontally on a soft base and rolled back and forth gently till the slurry was thoroughly mixed and of a uniform thickness. This was conducted while the slurry was under vacuum but with the valve to the vacuum pump closed. The next step was to release the vacuum gently and pour the slurry into the consolidation cells.

The principal features of the consolidation cell illustrated in Figure 3.22, consist essentially of:
The cell body, for accommodating the sample which is made of PVC tubes of 170 mm external diameter and 200 mm height. The internal diameter of these tubes were machined to the required diameter of 155 mm. This was sufficient to permit trimming the edges of the sample that might have been disturbed during the extracting process. The inner surface of the cell was then lined with 0.1 mm thickness PTFE lining. The PTFE lining provided a very smooth surface and minimized friction between the wall clay and the loading cap.

The loading cap, is made of PVC of 153 mm diameter and 10mm thickness. The diameter of loading cap was about 2 mm smaller than the inside diameter of the consolidation cell. The height of the loading cap was increased to 35 mm by gluing a 25mm high, thin PVC tube on the top to prevent the cap plunging into the slurry if the sample should tilt. The force was applied to the sample centrally via a steel ball seated to the centre of thecap.

The base plate, was also of PVC and was formed from a tube of 175 mm internal diameter and 100 mm height. A porous plate of 4mm thickness was cut to about the same size as the internal diameter of the base plate. A groove of 1mm deep was cut into the porous plate for accommodating the cell body. A 6.4 mm tube was fixed close to the top of the plate to drain the extra water into a container.

To prepare the consolidation cell, the porous plate was de-aired by immersing in boiling water for 10 minutes. It was then withdrawn from the water and immersed into the de-aired water in the base plate. A filter paper exactly the size of the porous plate was soaked in de-aired water and placed gently on the porous plate. Any air trapped between the filter paper and the porous plate was carefully worked out and the cell body was placed into the grooves already cut in the porous plate. The cell was now ready to be filled with the kaolinite slurry.

Slurry was slowly siphoned from the glass container into the consolidation cell through 6.4mm plastic pipe. Care was taken to minimise the amount of air trapped by pouring. Equal amounts of slurry were placed in three consolidation cells and the depth of the slurry was measured at four points from the top of the cell. The consolidation cells were then left for 24 hours to consolidate under self weight.

Once the self weight consolidated kaolinite was strong enough to carry the weight of the loading cap, a wet filter paper was placed on the inner surface of the loading cap. The loading cap was then gently lowered and placed on the top in contact with the kaolinite specimen and left for at least two hours. Finally the consolidation cell was placed centrally in position on the rigid base of the lever-arm loading device. The loading yoke assembly were placed carefully in position in order to enable the vertical force to be applied axially in suitable increments to the kaolinite sample. The counter balanced loading beam was then adjusted to a level position and a small load applied.

As the moisture content of consolidating samples was as high as 300%, measuring

the height of the sample or the depth of the consolidation cell using the conventional dial gauges of 25 mm travel was not feasible, at least for the initial increments. Consequently, rulers with an accuracy of 0.5 mm were initially employed and 25 mm travel dial gauges to an accuracy of 0.01 mm were used.

The loading sequence commenced in the form of 1/2kg, 1kg, 2kg, 4kg, etc and these were sufficiently low to prevent the kaolinite being squeezed out. One dimensional consolidation up to 150 kPa and unloading to 14 kPa provided clay samples of approximately 50% moisture content and OCR = 10.7.

3.4.4.3 Extracting and Trimming procedure

The extracting procedure started by removing the consolidation cell from the frame and taking it to a humid room to extrude the sample from the consolidation cell. Humidity was supplied through a humidifier and was measured by a humidometer. Care was taken to keep the room at 100% humidity.

To extrude the sample out of the cell the water was drained from the top and bottom plates and the whole cell was turned upside down and placed on a flat surface. The bottom plate was rotated gently in order to release the porous plate from the base plate and then slowly lifted up. Then the porous plate was carefully removed and the filter paper was peeled off from the sample. The sample then was pushed out of the cell (Figure 3.23).

The kaolinite cake resulting from each consolidation cell was 155 mm diameter and about 40 mm tall. To obtain a cubical block of 100 x 100 x 100 mm from these cakes with minimum disturbance required developing of a special trimming device which is shown in Figure 3.24.

A fixed duralumin base plate 300mm square accommodates two vertical silver steel columns of 16mm diameter and 180mm high. A rotating base of 155mm diameter made of PVC is located in the centre of the rigid base. A stretched trimming piano wire is attached, to two sliding guide blocks, which have PTFE bushes and could slide vertically along the guide columns. The tension of the wire could be controlled with the aid of two adjusting screws. The sliding system is supported by means of a steel tie bar as illustrated in Figure 3.24. The diameter of the rotating base is identical to the internal diameter of the consolidation cell. Four slots are cut into the rotating base in order to provide clearance for the cutting wire. The slots cover a

100mm square area which is centrally located within the circular rotating base. Prior to use, a thick filter paper was cut to the size of the square soaked in water, and accurately positioned on the square.

After the kaolinite cake was extruded from the cell it was turned upside down and gently placed on the trimmer base while the central seating part was used as a handle. By applying a tilting action the seating was separated from the kaolinite cake and the top filter paper was peeled off. Care was exercised to prevent any slippage of the square blotting paper at the bottom of the cake which could obstruct the movement of the trimming wire into the slots (Figure 25a).

In order to cut the first slice of the sample the rotating base was set so that a slot and the trimming wire were in line; then the wire was gently drawn down with the aid of the steel frame support. The cut clay was bent away using a fork to prevent the cut piece sticking back to the main slice (Figure 3.25b). After the piece was cut it was used for moisture content determination. It was essential to cut only one side of the cake at this stage, in order to leave a maximum curved edge which would help in a precise alignment of the next slice when it was placed exactly on the top of the previous slice. The next stage was to place a grid of lead shot on the cake using a template. The template was lifted up gently and using a steel ruler lead shot were pushed very carefully into the sample, see Figure 3.25c.

The extruding process was repeated for the second slice of the kaolinite and the cake was placed on the top of the first slice on the rotating base. This is shown in Figure 3.25d. Cutting was repeated for the second slice and the spare piece weighted and labled for moisture content measurement. The same process was repeated for the third slice. At this stage three slices of consolidated kaolinite were placed on top of one another and one edge was totally cut. Trimming the other three edges was achieved by rotating the base and aligning the slots with the wire using markings on the rotating plate and the fixed plate as illustrated in Figure 3.25e. As each face was exposed a wet filter paper was placed on the face. The block was then transferred gently to a second plate (Figure 3.25f) and rotated through 90° as shown in Figure 3.25g, and the top face subsequently trimmed. The trimming process was carried out such that the final product was a 100 x 100 x 100mm cube and properly aligned. The cube was then transferred again to the first rotating base to sit on its natural bottom face where the positioned grid would be perpendicular to the X-ray beam.

3.4.4.4 Sample membrane and Preparation box

When the saturated Kaolinite sample of final dimension of 100 x 100 x 100 mm (Figure 3.25h) was formed it was sealed in a rubber membrane.

Since the pore water pressure was to be measured centrally in these samples, a special type of membrane was required to provide a central passage to allow the pore water pressure measuring probe to be inserted into the sample. The former for making the required membrane is illustrated in Figure 3.26. The membrane preparation procedure was virtually the same as that for sand.
In order to place the sample into the membrane, it was necessary to stretch the sample membrane sufficiently and slip it over the sample while maintaining its proper cubical shape. Prior to placing the sample membrane into the oversized box, a brass needle guide of 5 mm external diameter and 1.5 mm internal diameter was pushed into the central rubber tube which was coated with a thin film of lubricant; this is illustrated in Figures 3.27a and 3.27b. The membrane was then turned over and slipped loosely over onto a brass hollow cube, and its internal faces were coated with a thin layer of fine sand. After the sand glued faces were dry the incased needle guide was inserted in the centre hole of the stretching box which was lined with a special porous material (Figure 3.28a). The overhanging part of the membrane was laid over the sides of the box and fixed using rubber bands. Vacuum was applied to five sides of the perspex cube and the porous paper provided an excellent uniform distribution of vacuum, and thereby, a uniform stretch of the rubber membrane (see Figure 3.28b). Since the internal dimensions of the perspex stretcher were 105 x 105 mm enough clearance was provided for the sample and the coated sand.

3.4.4.5 Special porous corners

It was previously mentioned that DSC testing requires the use of some kind of support at the two vertical edges of the sample where the shear sheets interweave, especially when the principal stresses are applied diagonally to the sample or cyclic tests are to be conducted. For clay a drainage passage was also necessary at different stages of the tests. Combining these two requirements resulted in a need to develop special porous edges which could fulfil both requirements.

Each porous edge consisted of a thin stainless steel angle 98 mm tall and 16mm wide which was lined with a 2mm thick porous lining. A copper tube of 2.5mm

external diameter was soldered to the junction of the angle at 2mm distance from the bottom end and push fit polythene tubing of 2.5 mm internal diameter connected the copper tube to a miniature plastic tap. To ensure a good seal and prevent any leakage, the copper and the polythene tubes were sheathed in a thin rubber tubing of 2.5mm diameter. Figure 3.29 illustrates an assembly of the drainage system.

3.4.4.6 Placing the sample in a rubber membrane

Once the membrane was stretched, the two diagonal edges of the membrane, through which the porous drainage tubing was to pass, were cleaned and coated with adhesive. Porous edges were immersed into boiling water to be de-aired. The immersion was such that the tubing and the miniature tap were exposed to air, thereby the tubing could be cleaned and coated with adhesive. When the glue was dry, the porous corners were positioned at the corner of the kaolinite by removing the correct amount of kaolinite using a surgical blade. After locating the porous corners the sample was ready to be encased in the expanded membrane. At this stage the sample was placed on a guiding device which is illustrated in Figure 3.30. This device consists of a square fixed plate with a central hole which accommodates both the rotating base and four vertical steel guiding columns of 3mm diameter. Two of the columns are higher than the height of the sample and the other two are as high as the sample. The sample is loaded centrally within the columns. To place the sample in the membrane the stretched membrane in the box was gently lowered onto the four guiding columns as illustrated in Figure 3.31a. When the box covered the sample properly the whole system was turned upside down Figure 3.31b. Next, the guiding device was lifted clear (Figure 3.31c) and the top edges of the sample membrane cleaned with acetone and coated with adhesive. If strain was to be measured on the boundary of the sample, another set of lead shot was placed (Figure 3.31d).

At this stage the vacuum to the rubber was released so that the sample membrane could stretch back onto the sample and a small positive pressure was applied from the box to faces of rubber membrane to provide a better adhesion between the kaolinite/rubber interface. To seal the sample a glued thin sheet of rubber, which was already prepared, was gently placed on the edges and pressed to ensure a good seal especially around the porous edge tubing passages and the excess rubber around the edges was trimmed off. Finally the stretching box was turned upside down and removed, the sample was then ready to be placed in the DCDSC (Figures 3.32).

3.4.4.7 Setting up pre-consolidated kaolinite samples in the DCDSC

Centralisation of any DCDSC sample was vital to achieving a good test, and as these samples had a different type of membrane a new technique was needed.

A thin metal plate with a centrally positioned 104 x 104 mm square opening was placed on the bottom plane strain platen and the opening was filled with a 1.5 mm thick rubber sheet of the same dimensions. Lubrication was applied to the horizontal surface of this plate that came in contact with the normal pressure system as illustrated in Figure 3.33a. The opening area was then covered with two thin rubber membranes of 115 x 115mm, each coated with grease.
The sample was carefully lifted up from its base and then, very gently, lowered onto the pre-marked central position on the σ_2 bag (Figure 3.33.b). To ensure that the sample was central, a half sheet of thin perspex with a precise grating acetate sheet attached to it, was used. Half of the plate which had two slots was lowered onto the plane strain columns and rested on the sample. If the needle guide was away from the central cut location, the sample was, very gently pushed to slide on the base, and then the second half of the plate was positioned as illustrated in Figures 3.33c and 3.33d. The centralising perspex plate was then removed.

It was essential to minimise air trapped between the membrane and the sample, therefore two small cuts were made employing a small pairs of scissors on the membrane where the porous corners were located, and air was carefully worked out. The cuts were then patched using a thin piece of rubber and adhesive.

Next, the faces of the sample were thoroughly cleaned with acetone and a small amount of grease smeared on the membrane where the shear sheets interweave to minimise shear being applied to these edges of the sample. The shear sheets were then set by matching the edge of the kaolinite sample and pressed gently to keep then in position as illustrated in Figure 3.33e; the shear sheet tails were properly arranged and the pulling surfaces smoothed.

The four normal pressure bags which had been greased were located in the correct positions then the normal pressure bag backing plates were locked to the bottom plane strain platen using four wing nut screws. The normal pressure bags were positioned so that the distance between the backing plate and the sample face was always 20mm. This position was obtained with the aid of three adjusting screws and kept constant throughout the shearing process.

Alignment of the shear sheets was carried out by moving the guiding roller spindles back or forth whilst a straight edge ruler was placed parallel to the inked line on the edge of the sample. The sample at this stage is illustrated in Figure 3.33f.

Since the pore water pressure probe needed to be guided and inserted into the centre of the sample without leakage, a needle guide had to be used. This had to be kept fixed in position while the top plane strain platen was lowered and this could be done only if a split platen was used. Figure 3.33g shows the split platen locked in position after first being lubricated in the usual manner.

Finally a thick perspex plate with a central passage for inserting the probe was gently lowered (Figure 3.33g) and slipped onto the four vertical uprights so that the perspex rested freely on the top of the split platen. The four wing nuts were then positioned on the uprights but not tightened. The horizontal position of the plate was ensured using a parallel gauge. A pore water pressure probe was then inserted into the sample through the needle guide and fixed, the process of assembly of the pore water pressure device will be fully discussed in Chapter 7. A completely assembled DCDSC prior to testing is shown in Figure 3.33h.

Any sample placed in the DCDSC in this manner was isotropically consolidated at 14 kPa for 24 hours to ensure that the proper contact was made with the inner fine sand coated surface of the rubber membrane which, subsequently transfers shear to the sample.

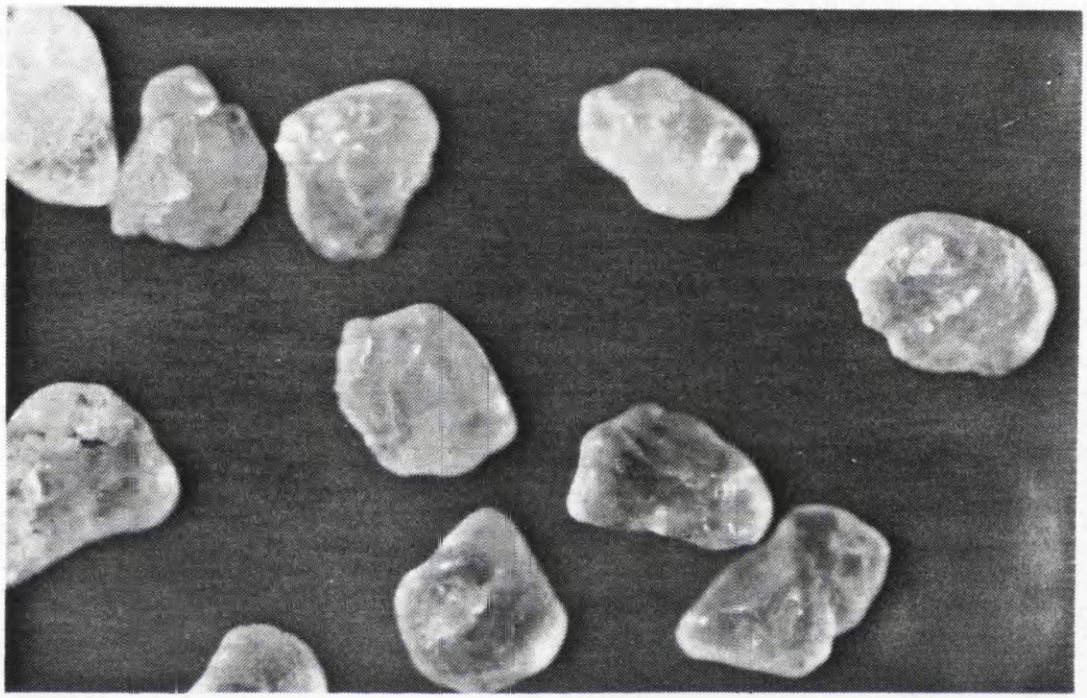

Fig. 3.1 A micrograph of Leighton Buzzard sand

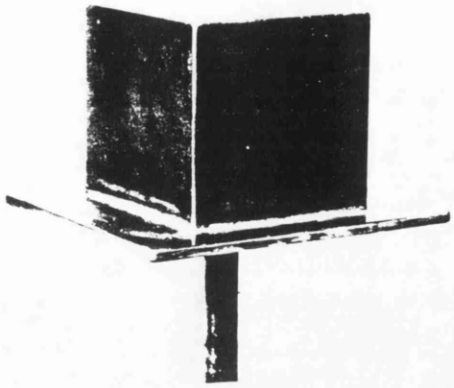

(a)

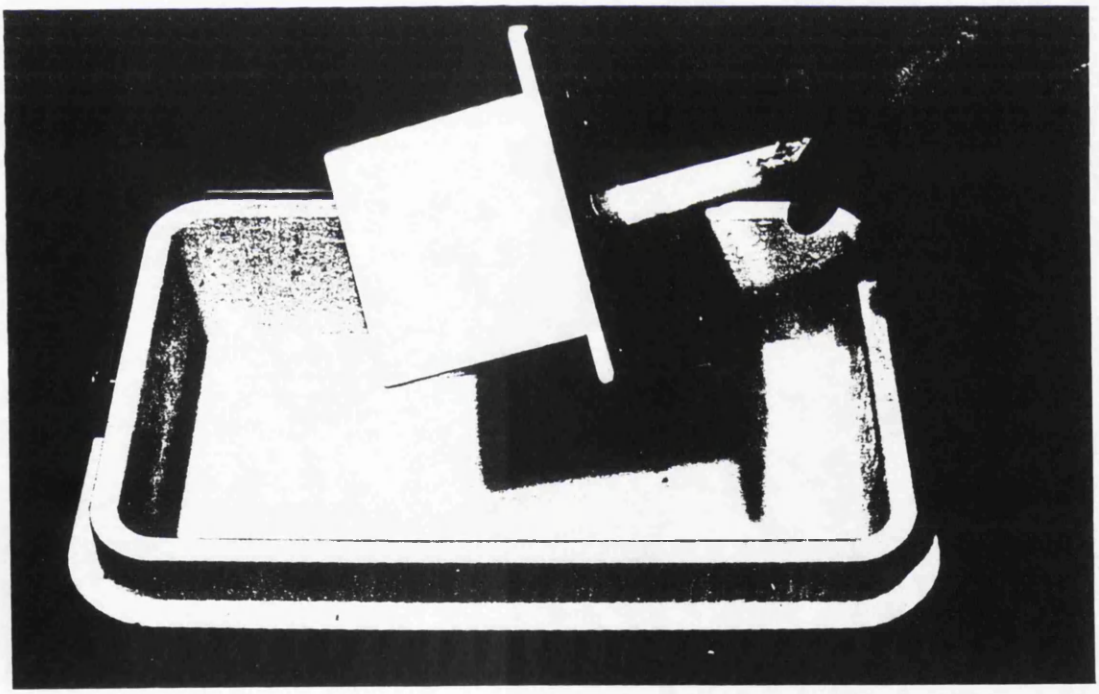

(b)

Fig. 3.2 Making rubber membrane; (a) former used for making the sand sample membrane and (b) former dipped into the latex

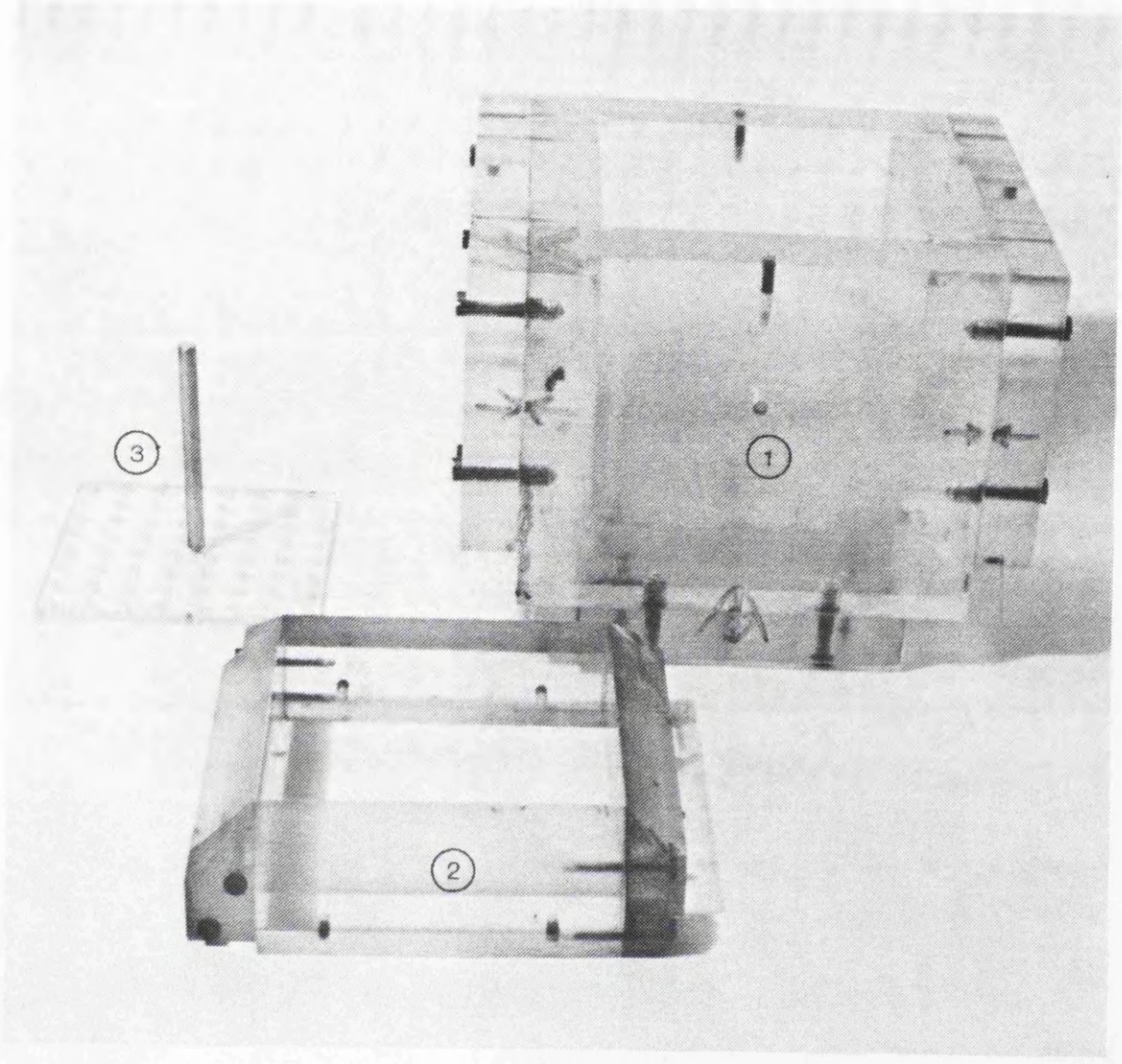

1- preparation box
2- deflection shield
3- acrylic template

Fig. 3.3 The preparation box used for sand samples

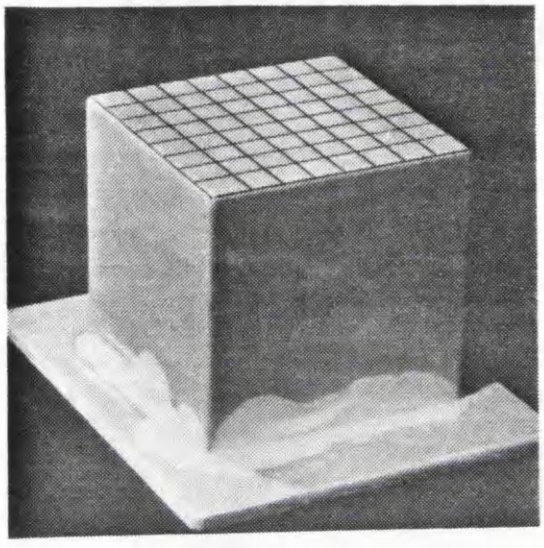

(a)

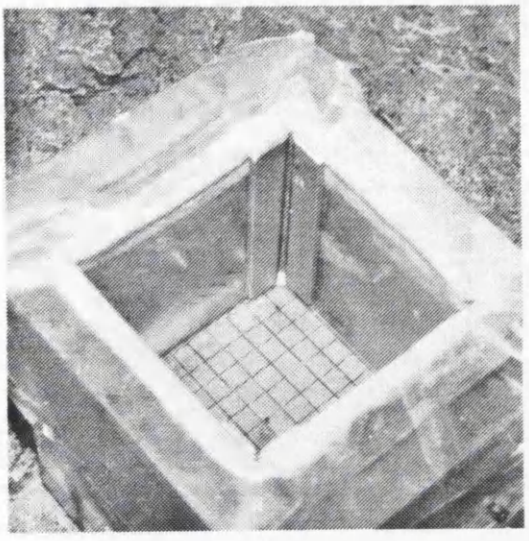

(b)

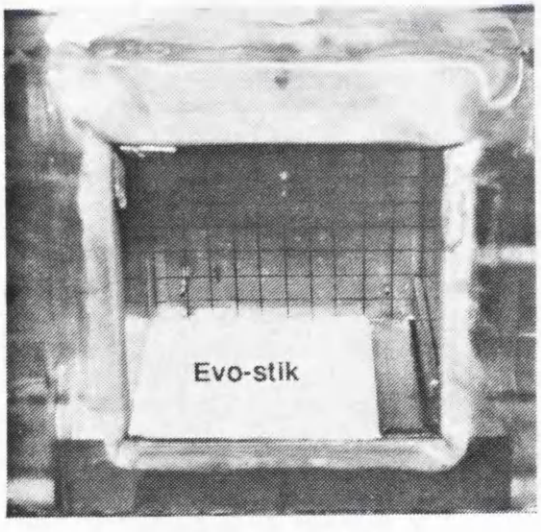

(c)

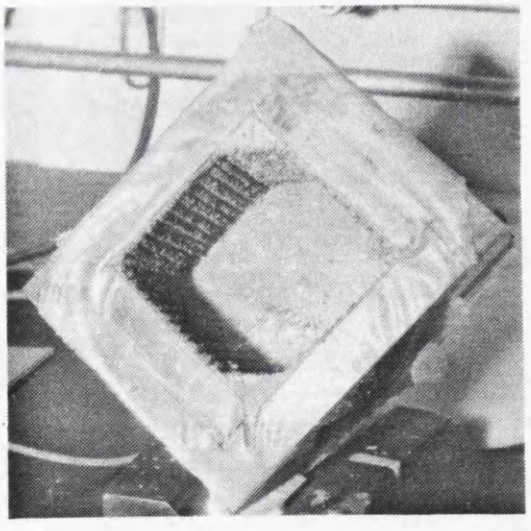

(d)

Fig. 3.4 Sand sample membrane preparation procedure; (a) grid drawn on top of the membrane, (b) sample membrane in the cubical preparation box and aluminium strips in position, (c) Evo-stik adhesive on one face of the rubber membrane and (d) filling the space between the two aluminium strips

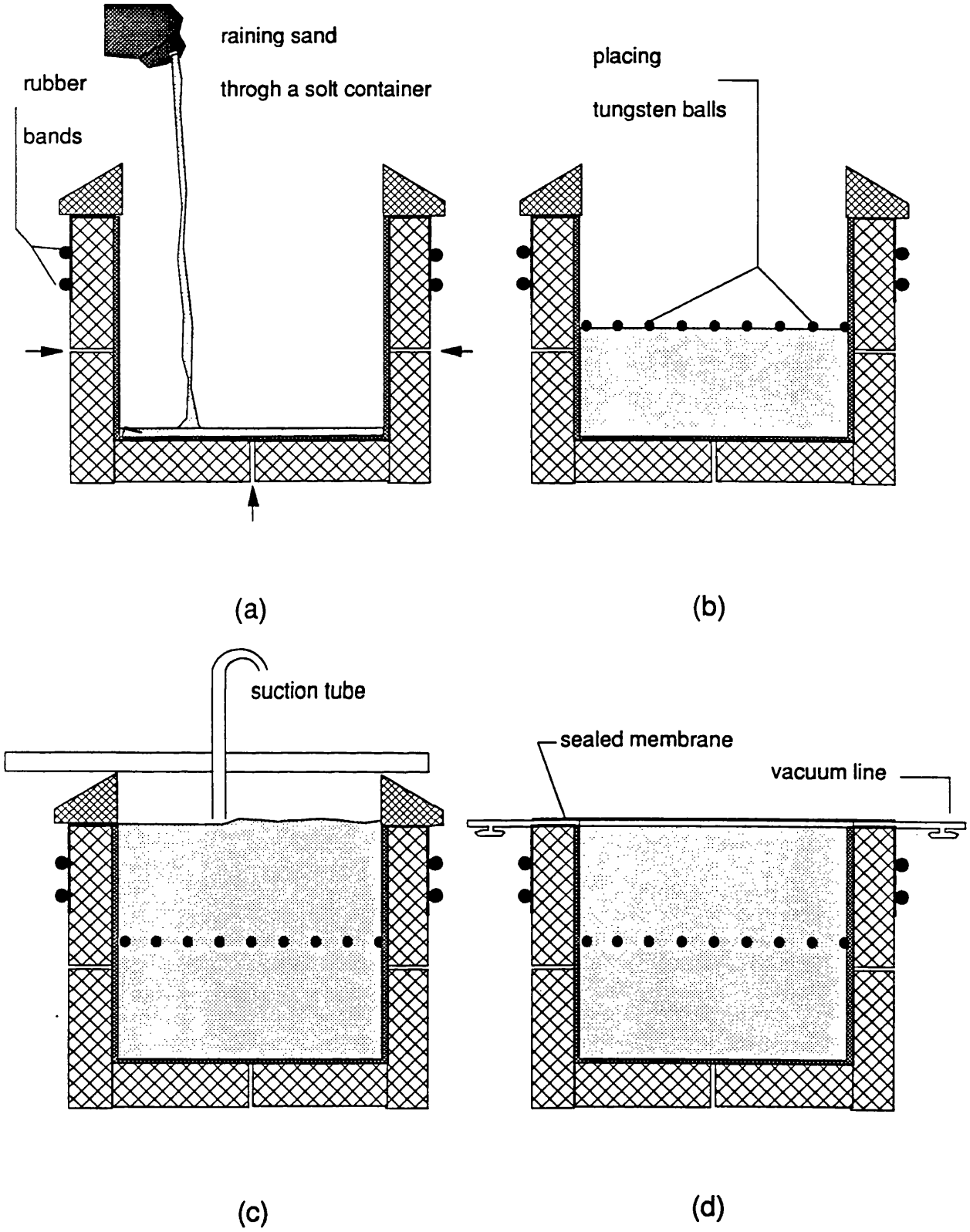

Fig. 3.5 **Dense sand sample preparation procedure; (a) deflecting shield placed on the top of the preparation box, (b) grid of tungsten spheres on middle plane of the sample, (c) levelled sand surface using suction, (d) sealed edges of a sample after trimming and (e) a completed sand sample**

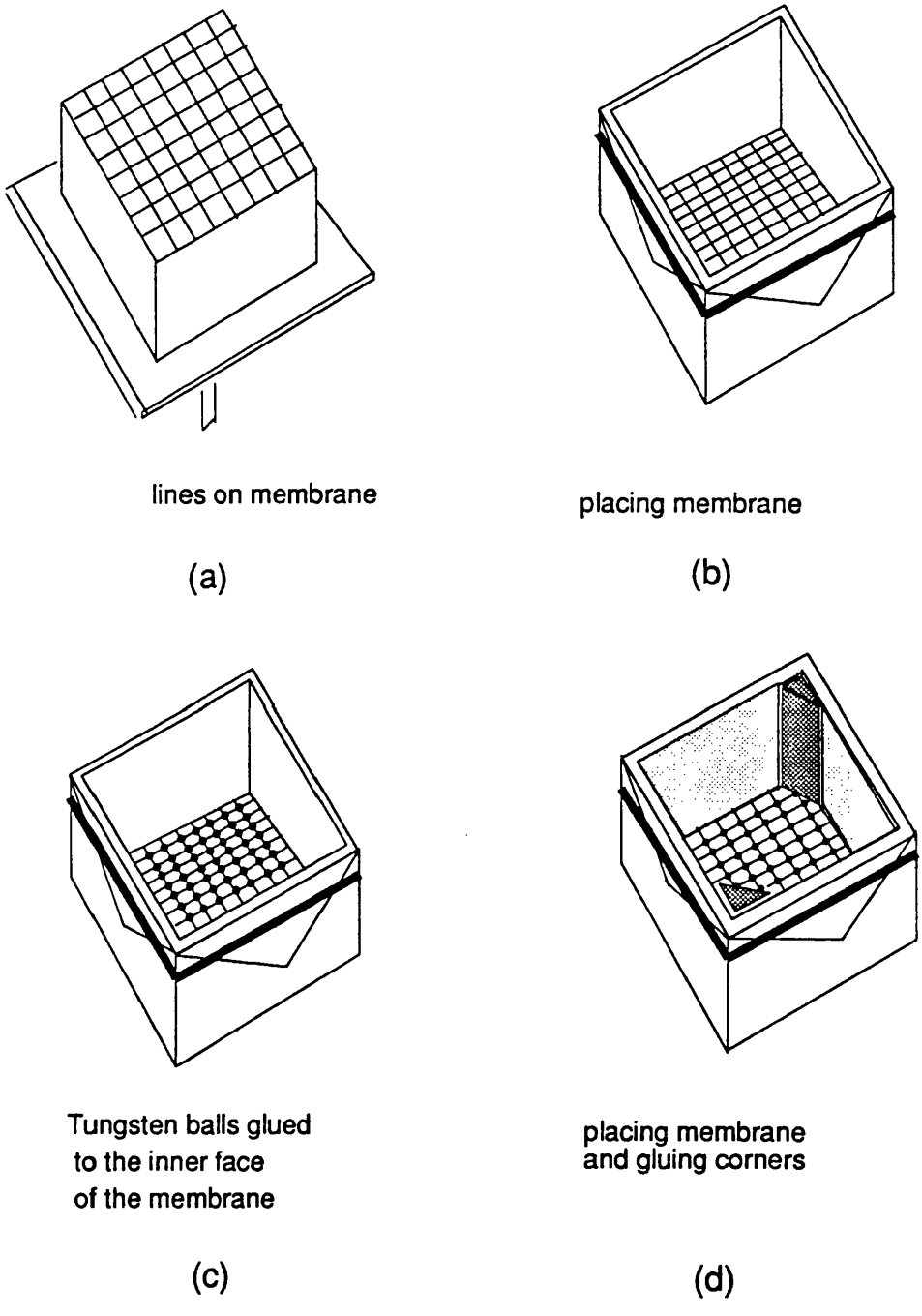

Fig. 3.6 **Loose sand sample preparation procedure**

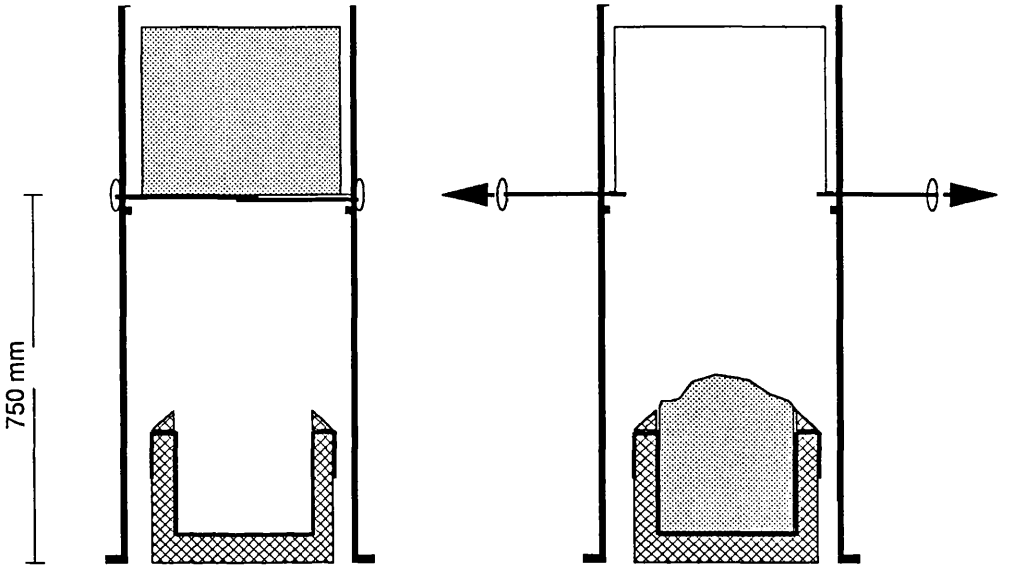

(e) (f)

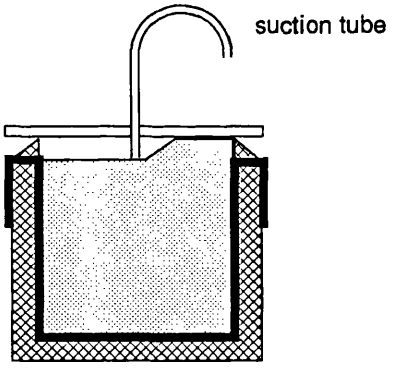

levelling sand through suction

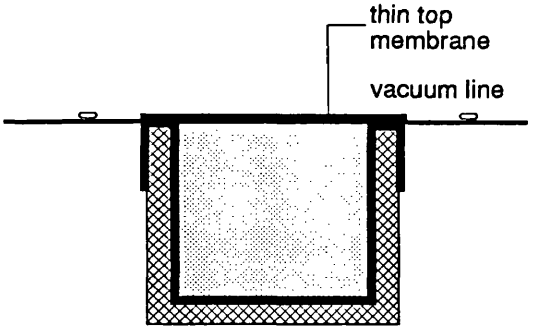

sealing the sample membrane

(g) (h)

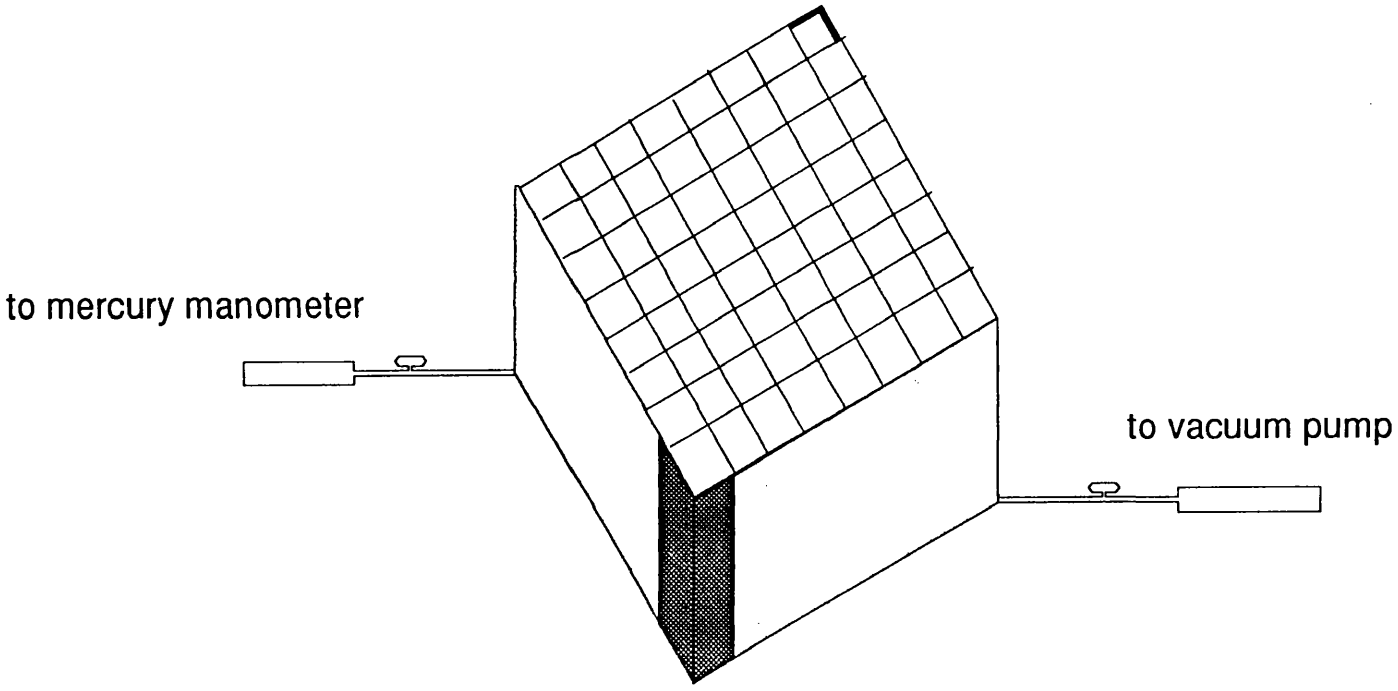

(e)

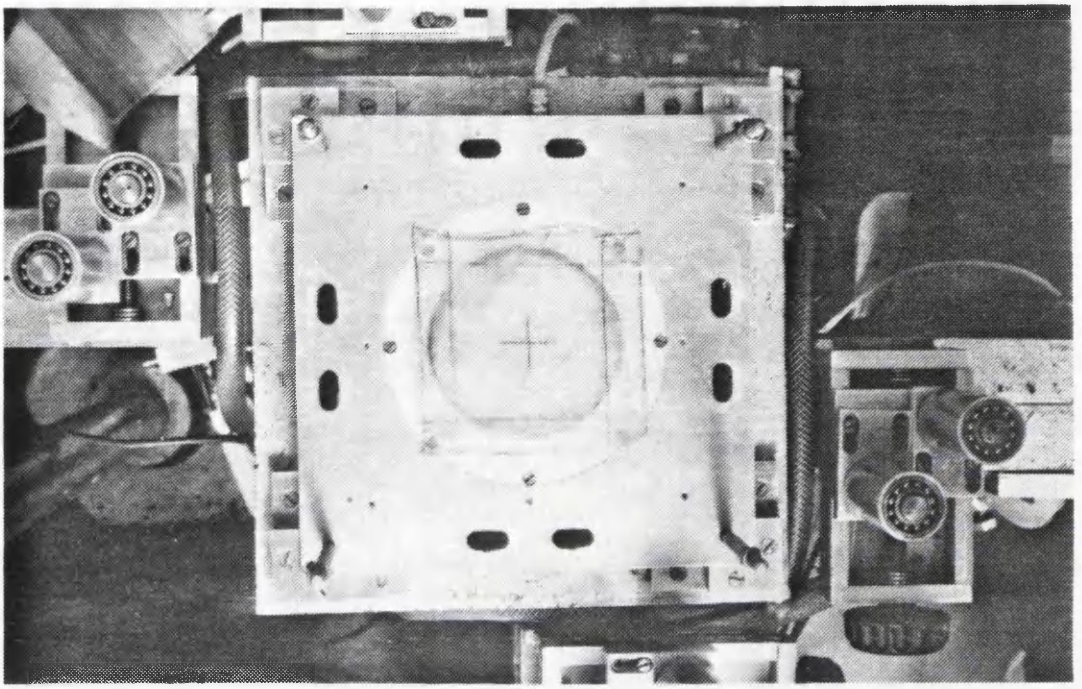

(a)

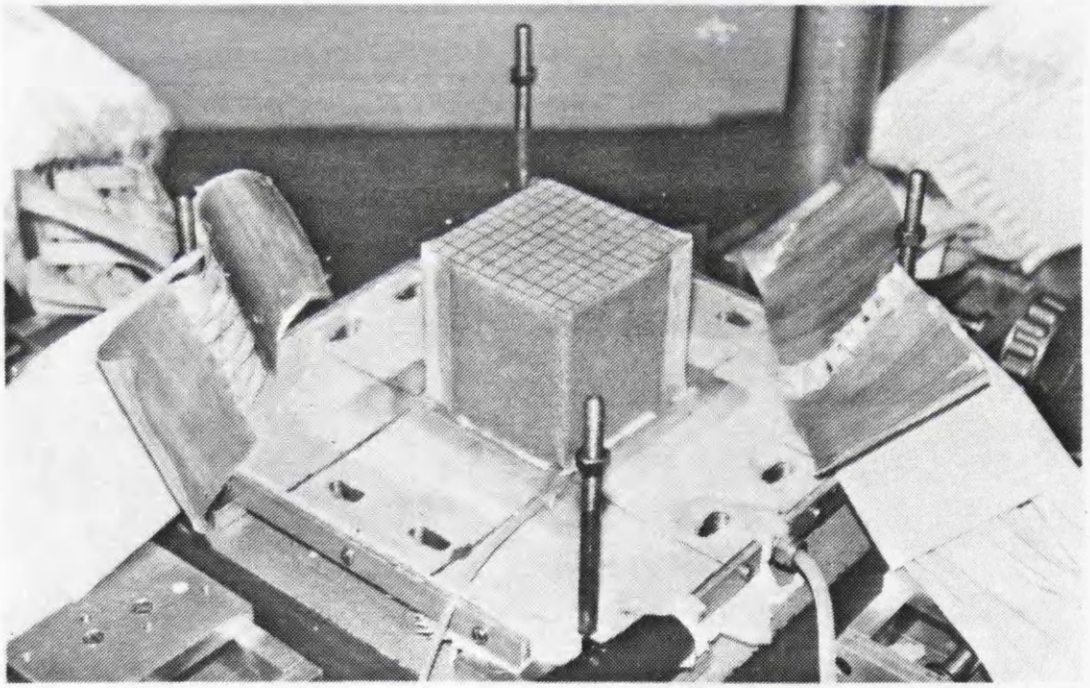

(b)

Fig. 3.7 Setting up sand samples in the DCDSC; (a) the bottom plane strain platen, (b) position of shear sheets prior to placing the sample onto the botttom plane strain side, (c) shear sheets positioned tight around the sample and (d) normal pressure bags positioned around the sample

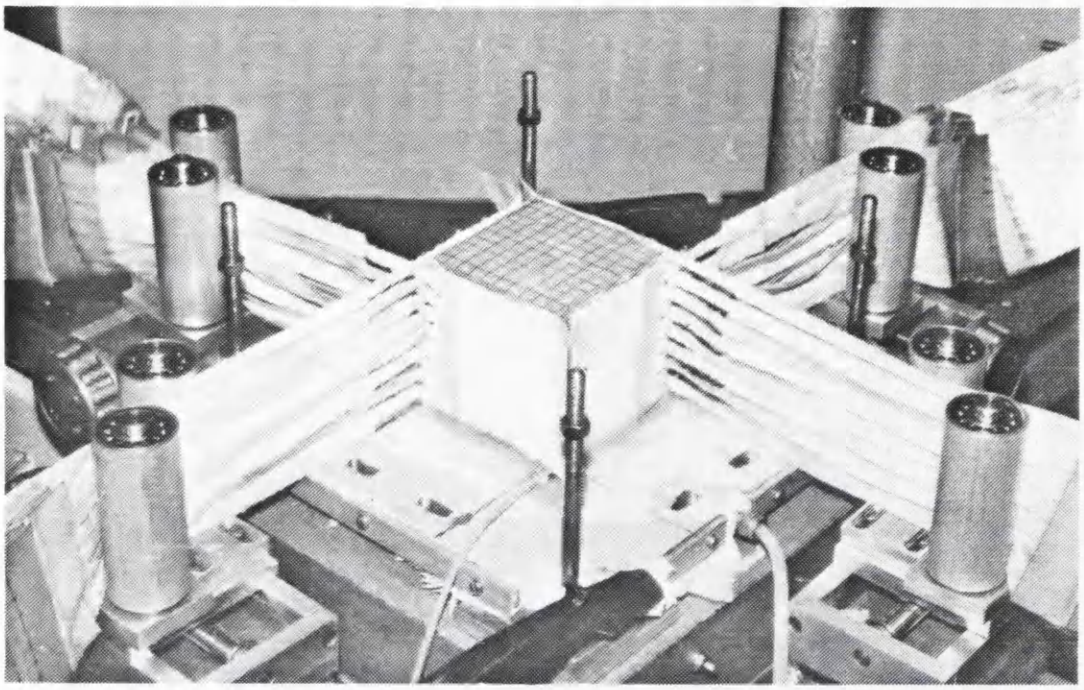

(c)

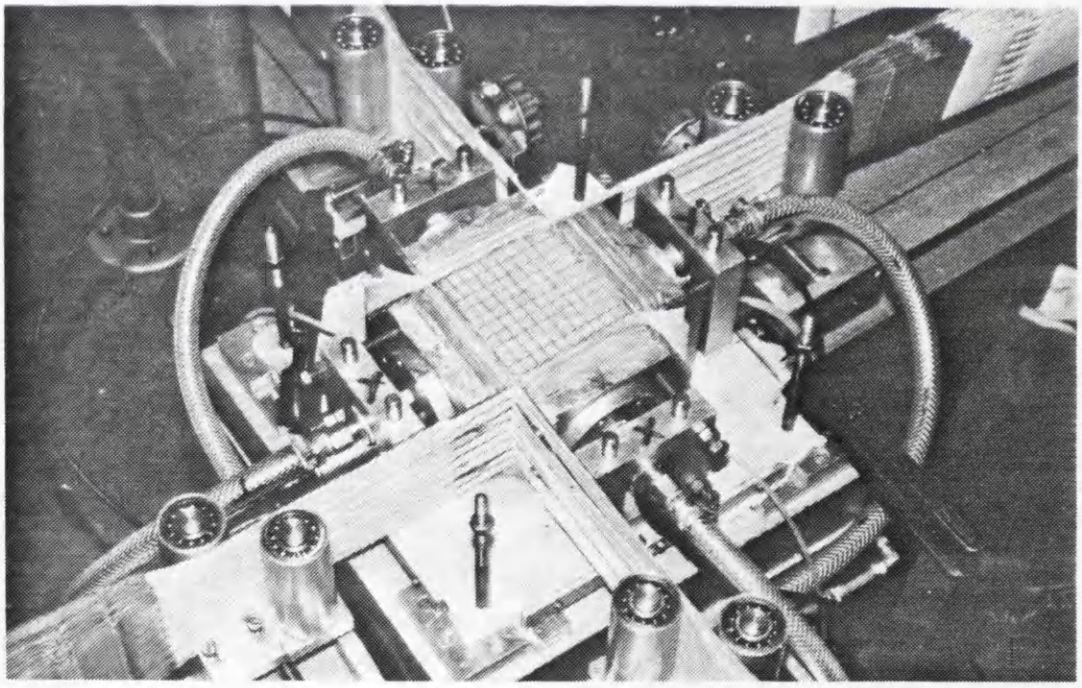

(d)

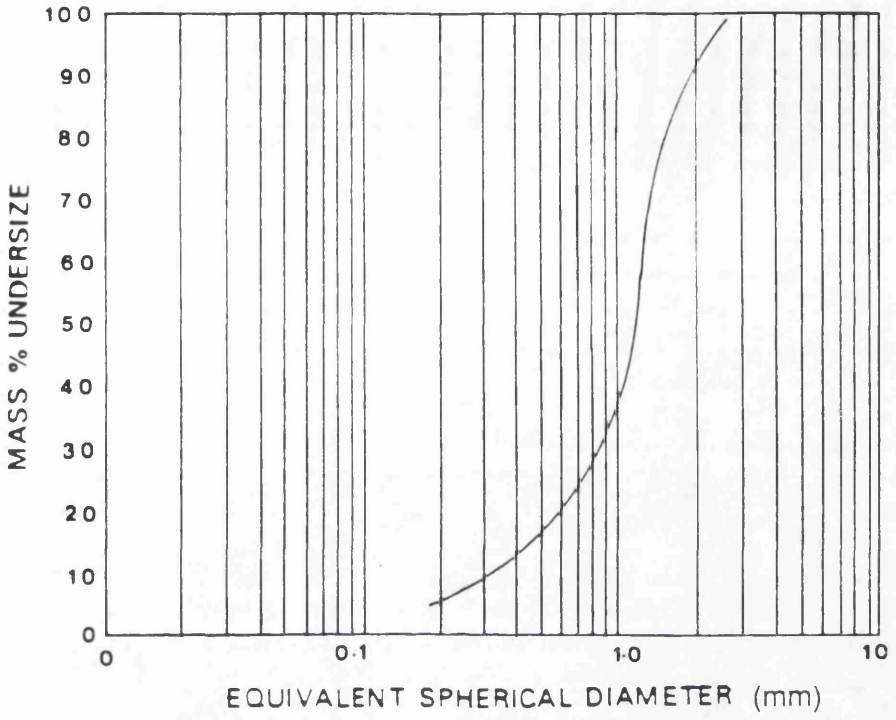

Fig. 3.8 Grain size distribution and micrograph of coal

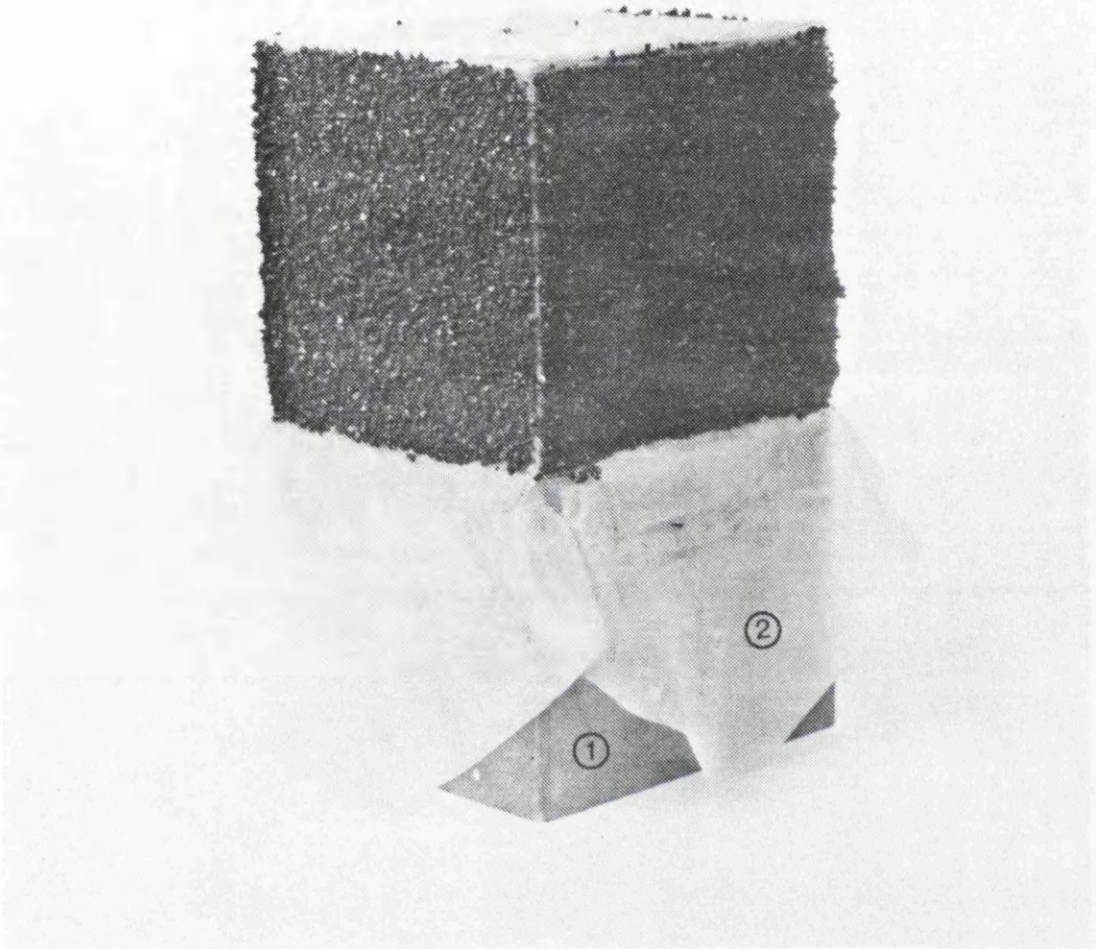

1- hollow brass former
2- rubber membrane

Fig. 3.9 Coal coated inner sides of rubber membrane

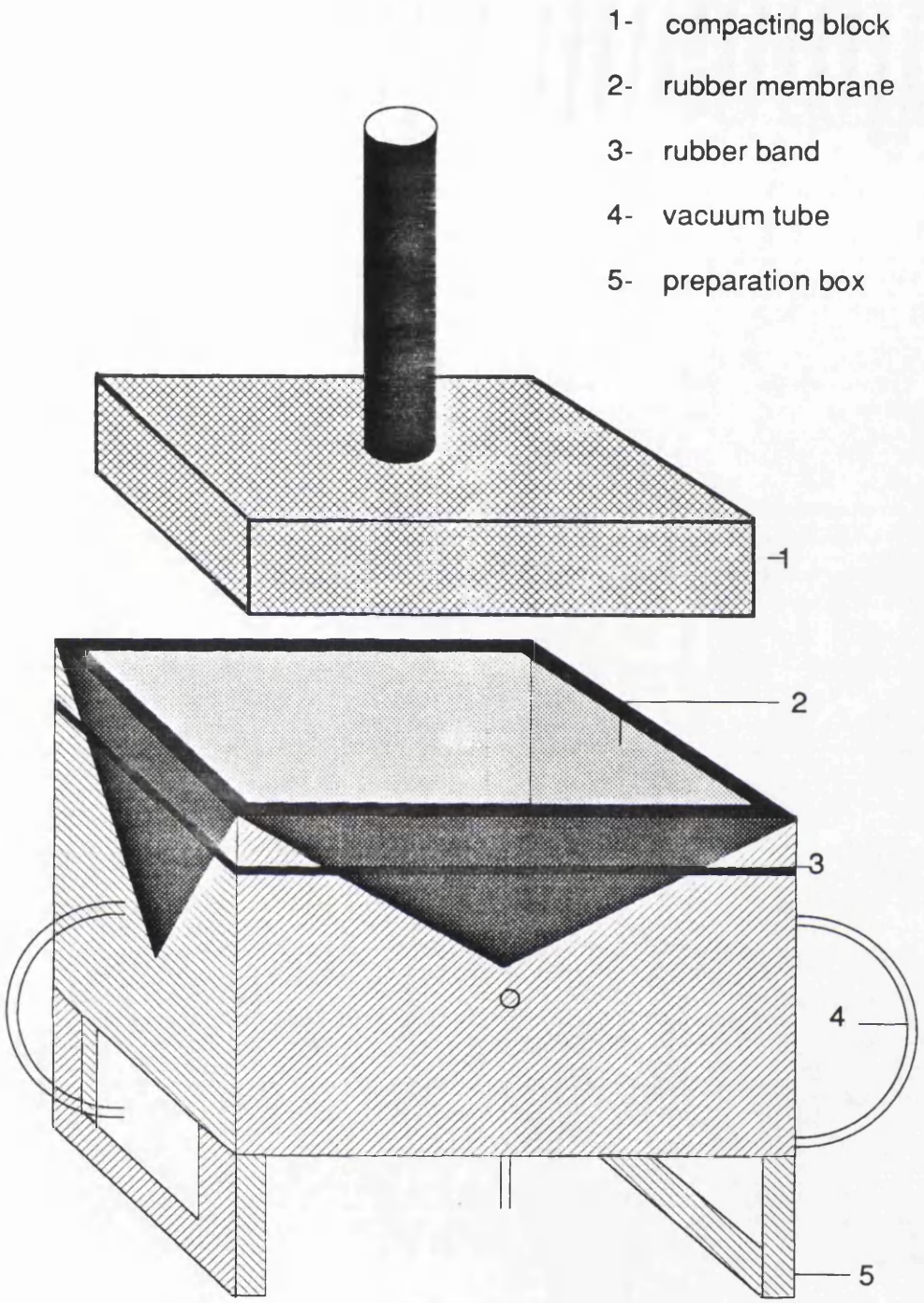

Fig. 3.10 **A schematic view of the loose coal sample preparation**

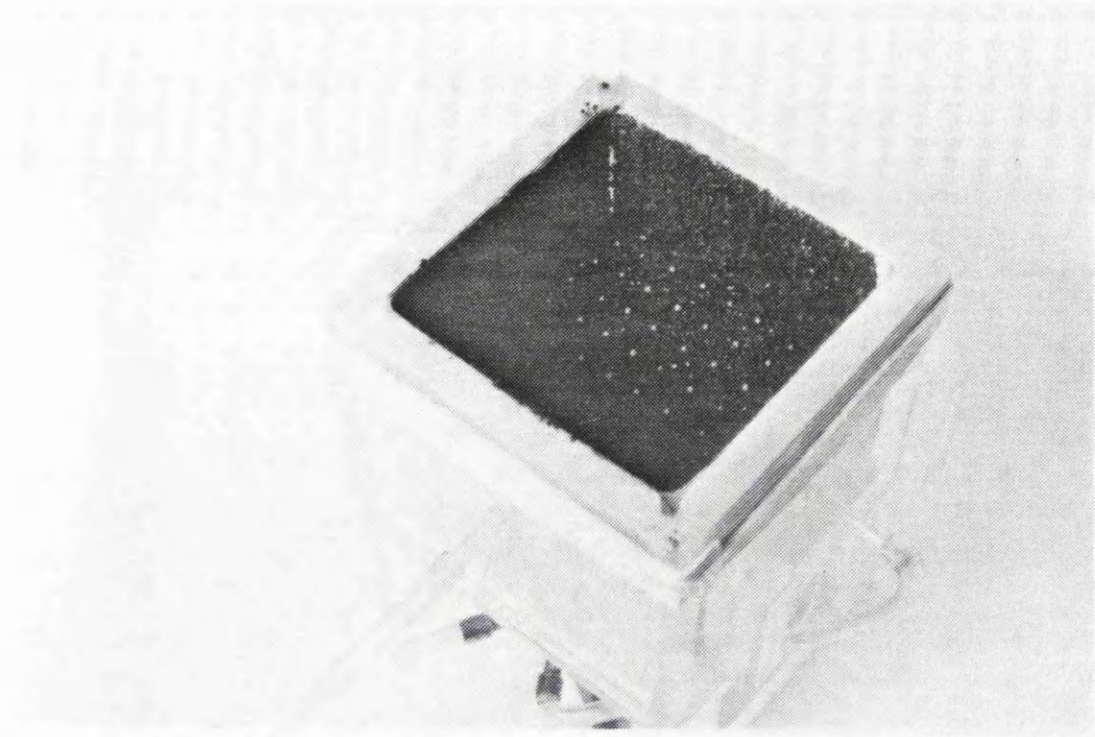

Fig. 3.11 Placing tungsten spheres on the middle plane

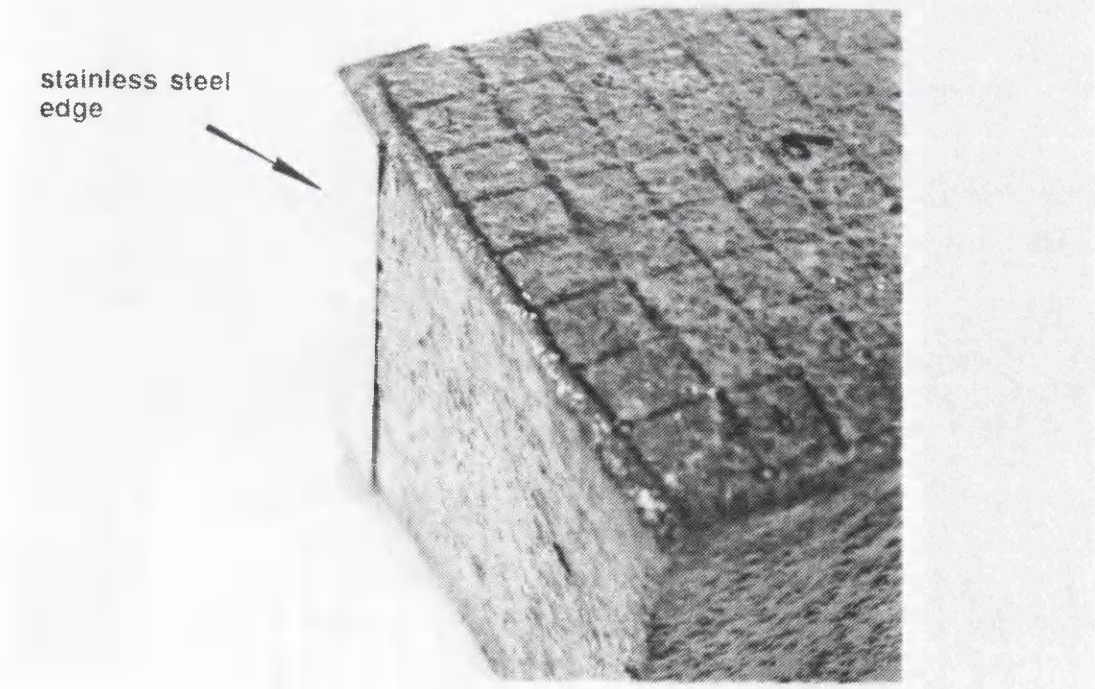

Fig. 3.12 Thin stainless steel diagonal edge in place

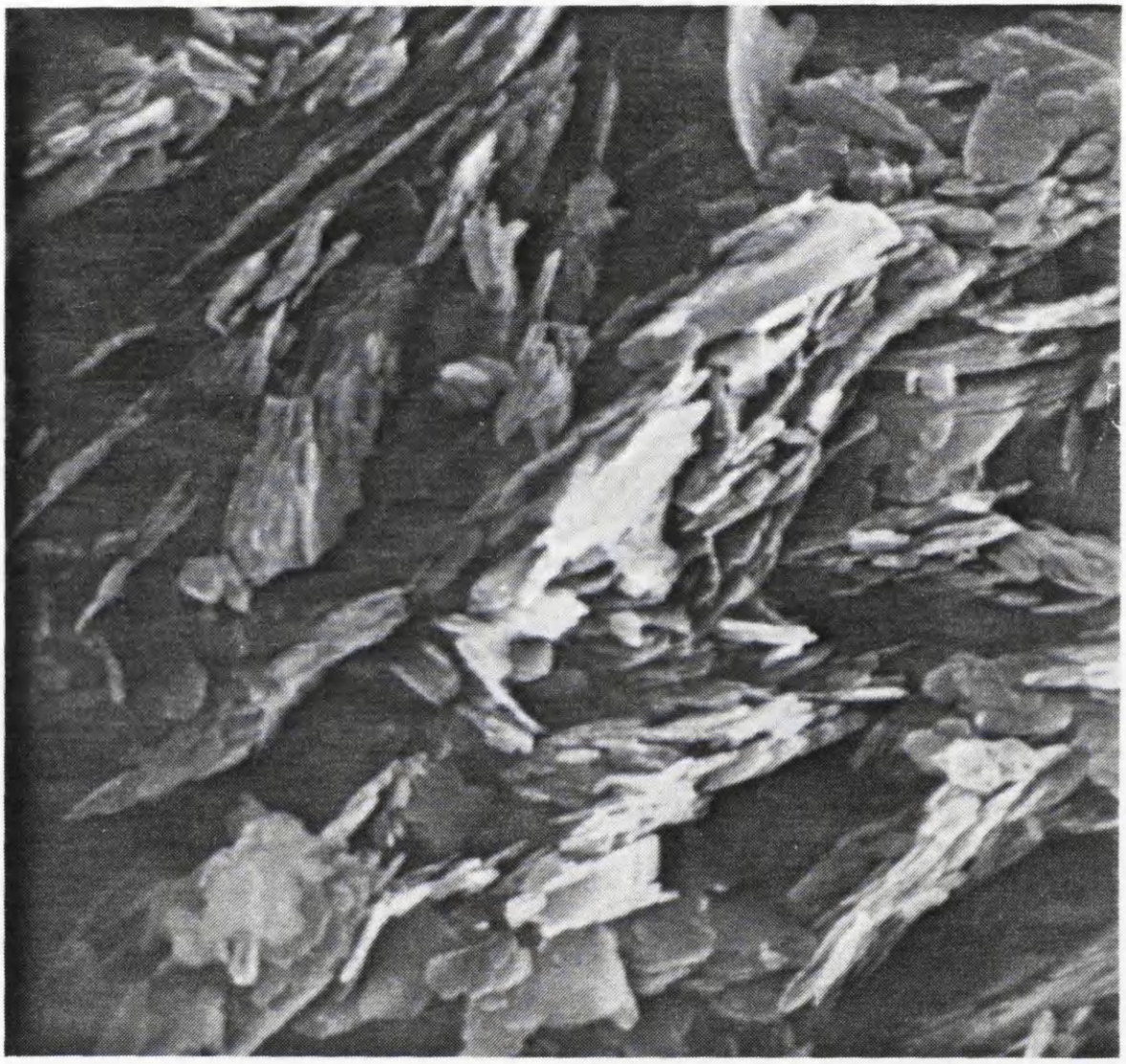

(courtesy of Dr Tovey, University of East Anglia)

Fig. 3.13 Grain shape distribution of kaolinite

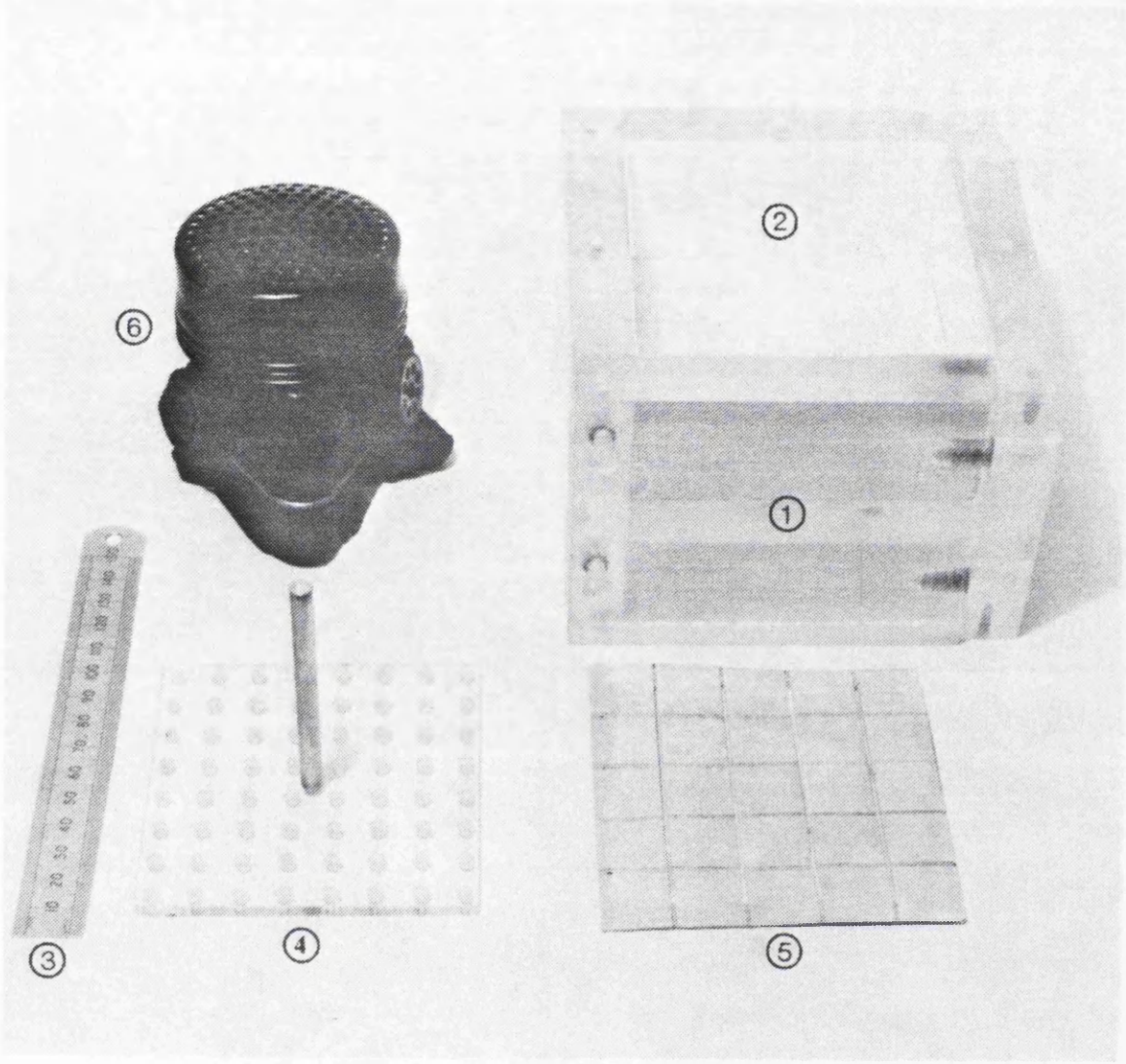

1- preparation box
2- filter paper
3- sharp edge ruler
4- tungsten ball markers
5- lead dust marker
6- safety mask

Fig. 3.14 Preparation box used to form kaolin into a cubical shape

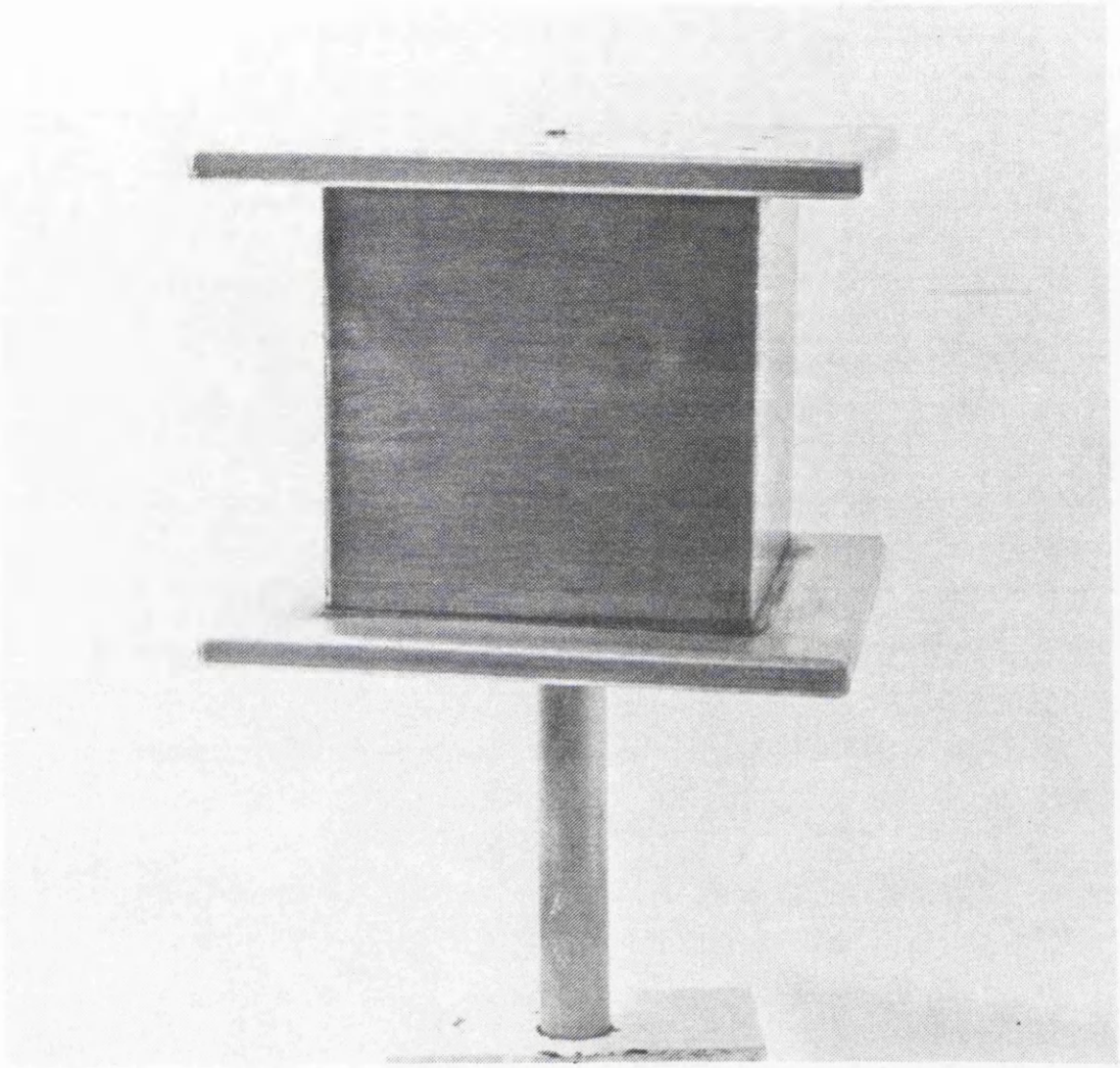

Fig. 3.15 Former used to make rubber membrane for remoulded kaolin samples

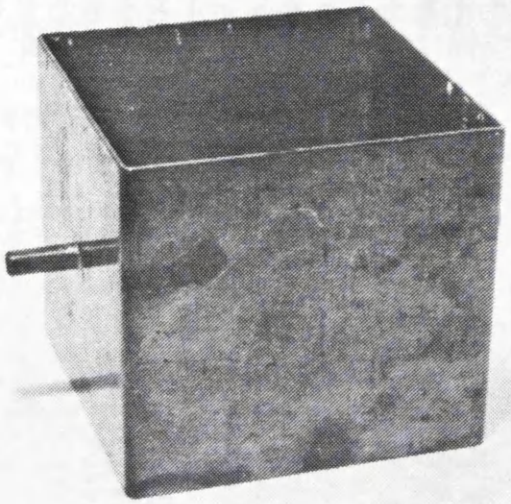

(a)

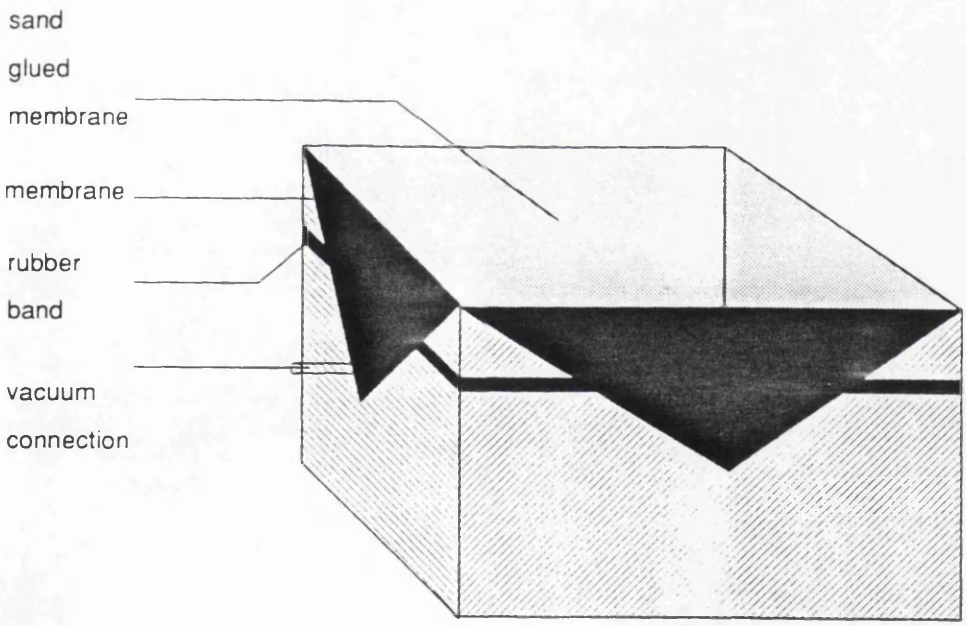

(b)

Fig. 3.16 (a) Stretching box used to expand the rubber membrane and (b) fine sand glued to the inner surface of the rubber membrane

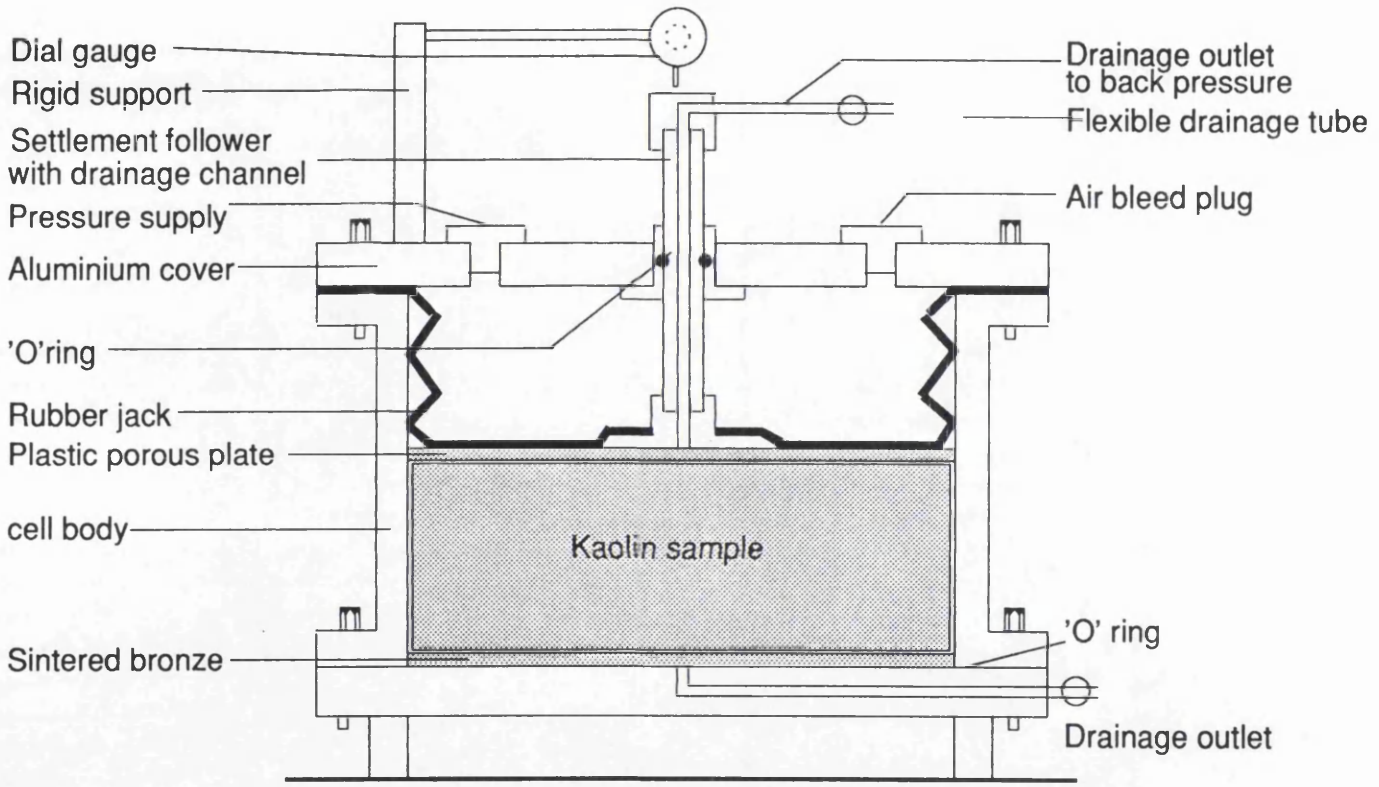

Fig. 3.17 Rowe cell in full assembly

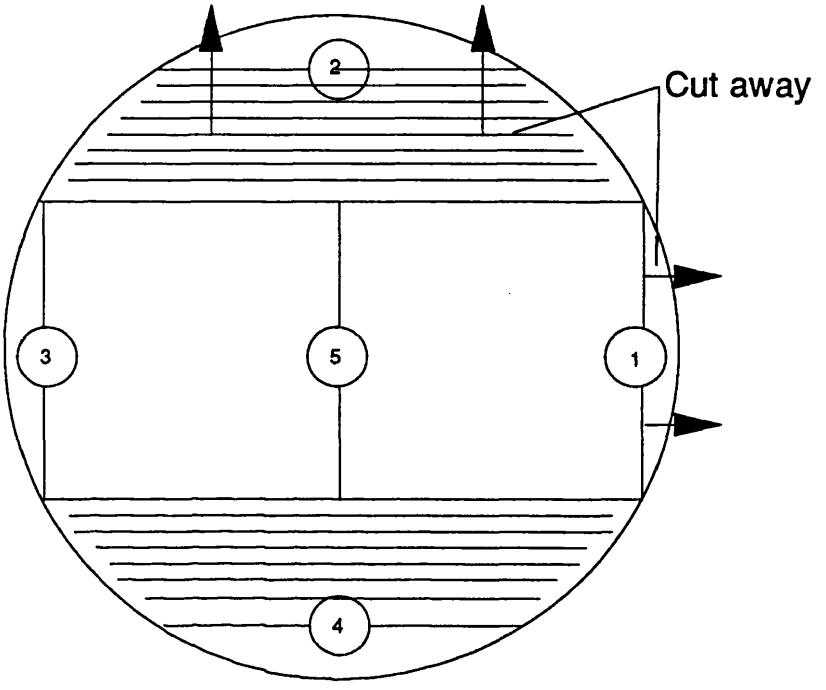

Fig. 3.18 The sequence in which the consolidated cake in the Rowe cell was cut

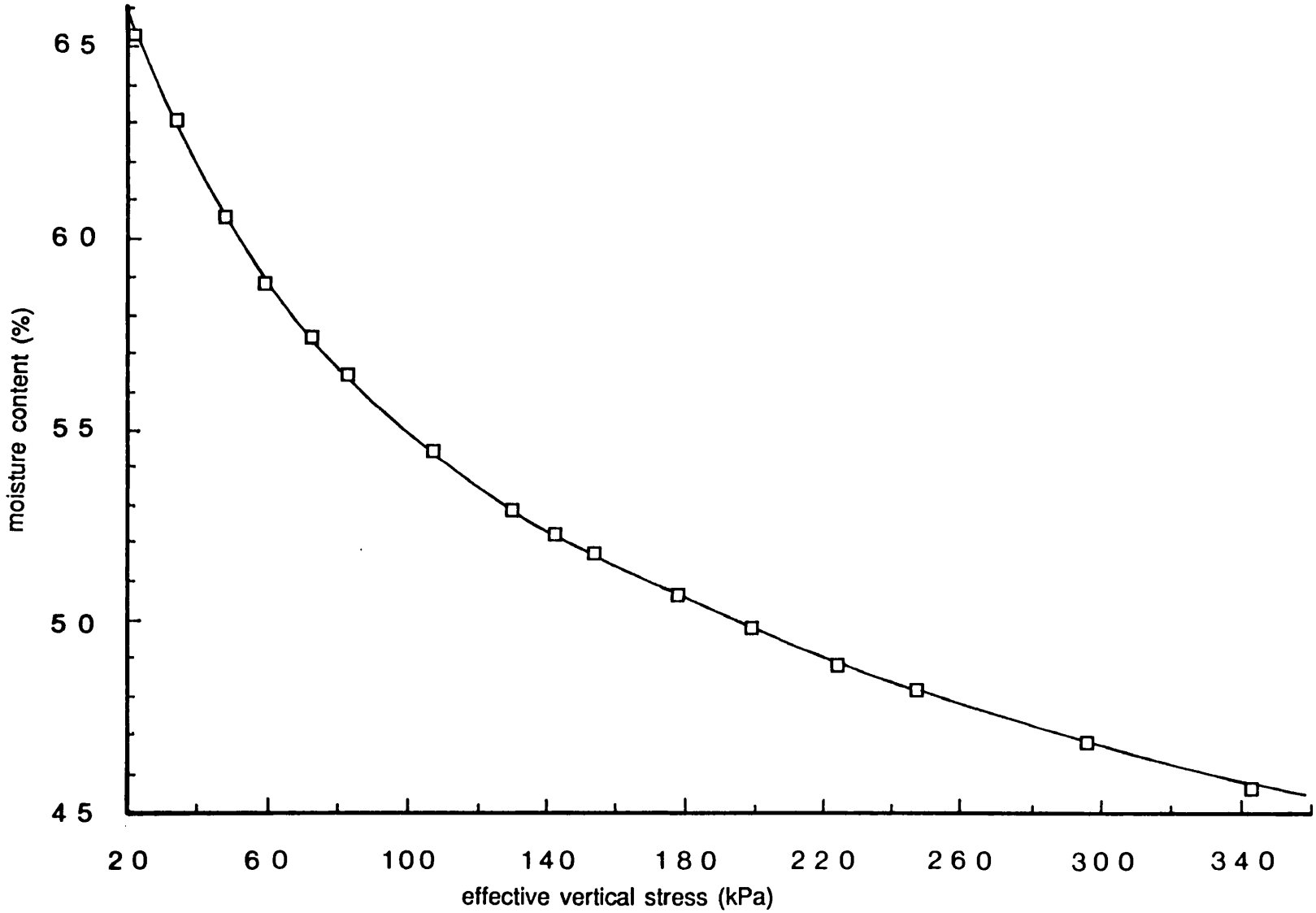

Fig. 3.19 **The consolidation stress versus moisture content for speswhite kaolin using conventional Oedometer**

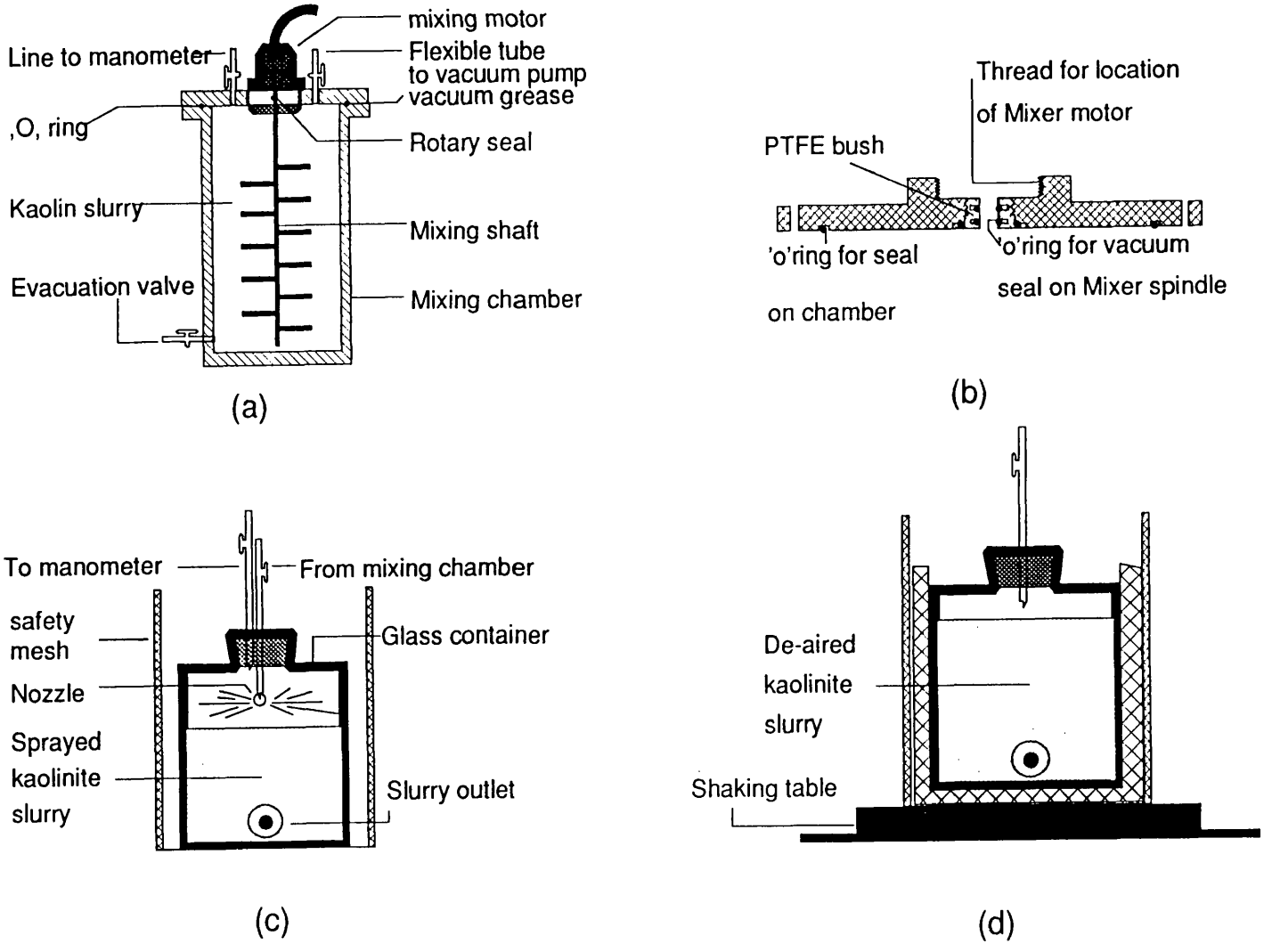

Fig. 3.20 **Mixing and de-airing procedure for speswhite kaolinite; (a) assembly of the equipment to be used to mix and de-air the slurry, (b) a schematic view of the rotary bearing used for vacuum sealing the centre shaft of the mixing chamber, (c) spraying the kaolin slurry into a thick glass container and (d) the glass container placed on the shaking table for de-airing**

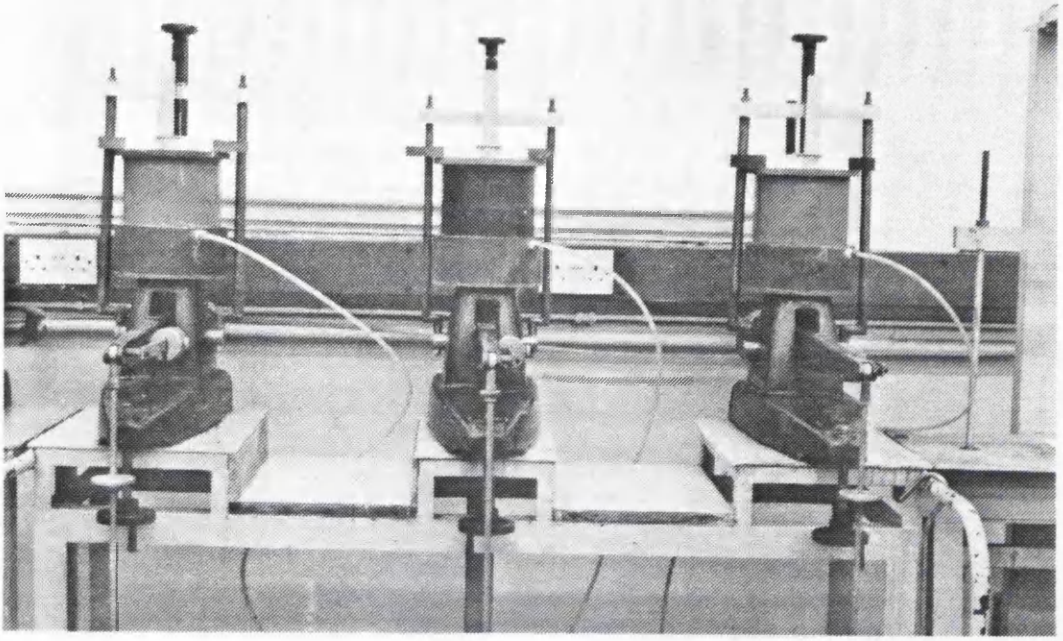

(a)

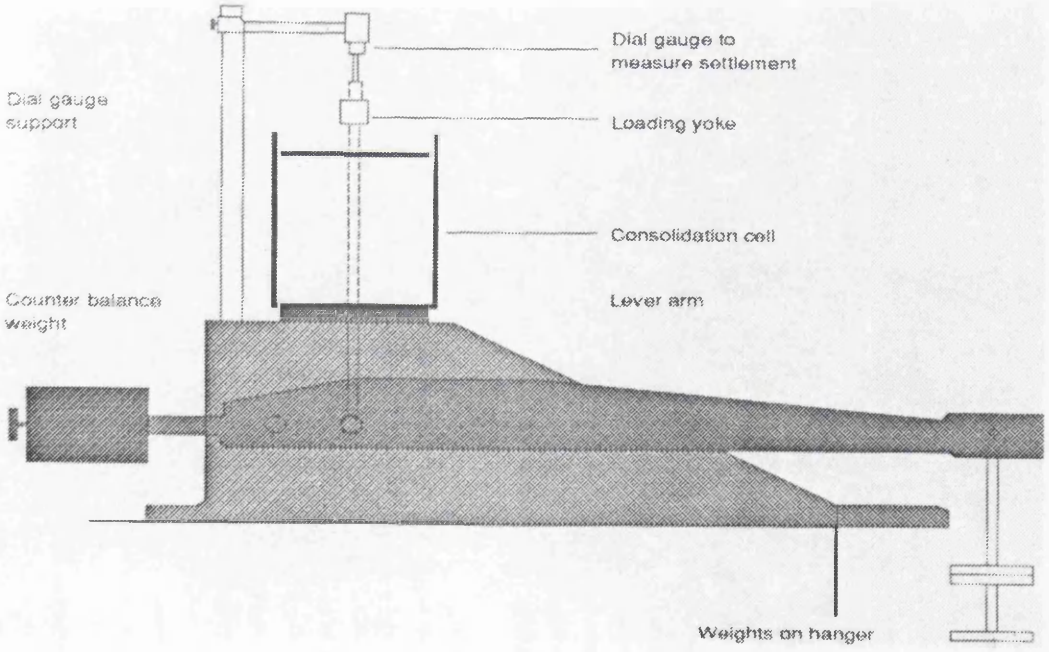

(b)

Fig. 3.21 (a) Arrangement of modified oedometers and (b) a schematic view of modified oedometer

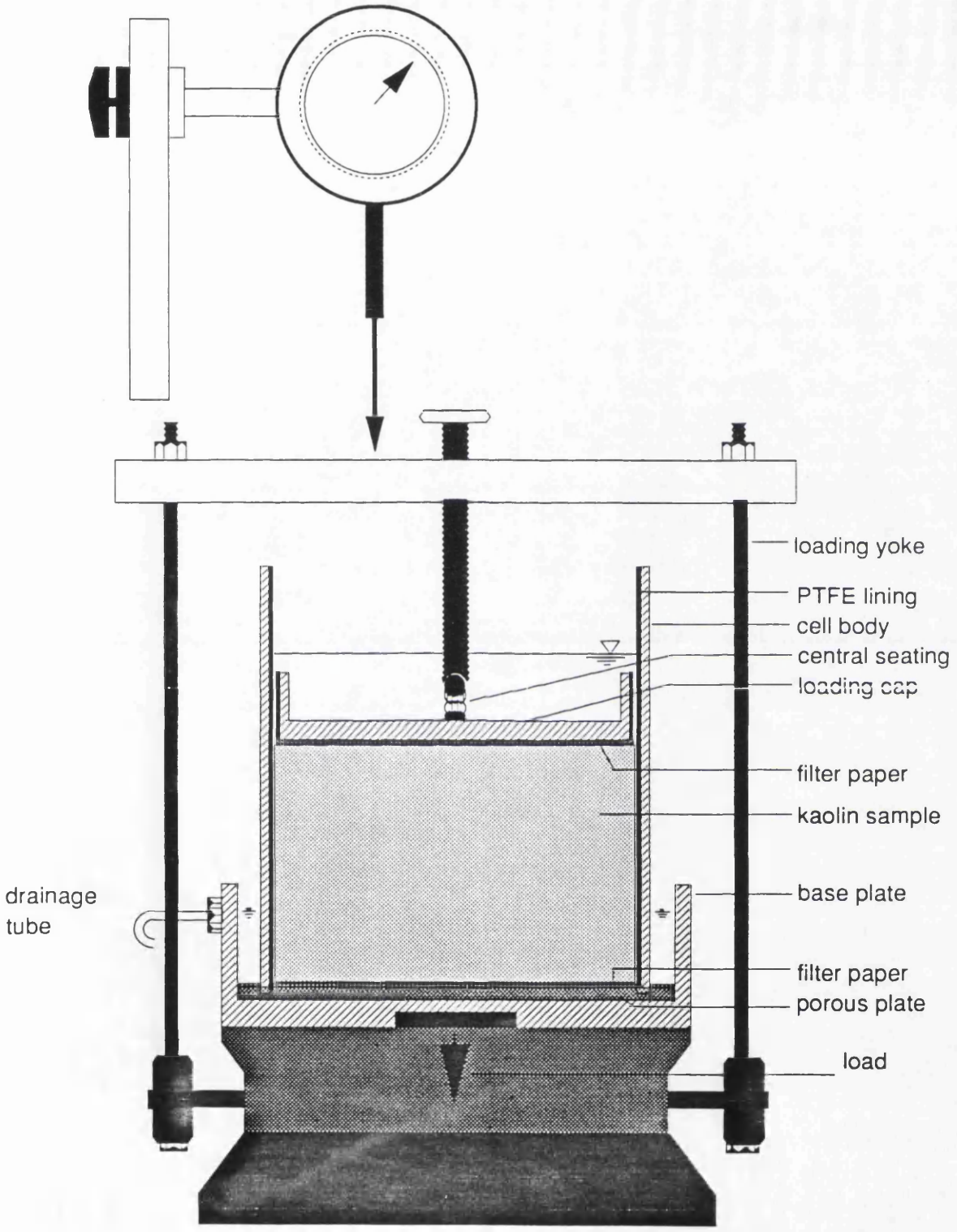

Fig. 3.22 The principal features of a consolidation cell

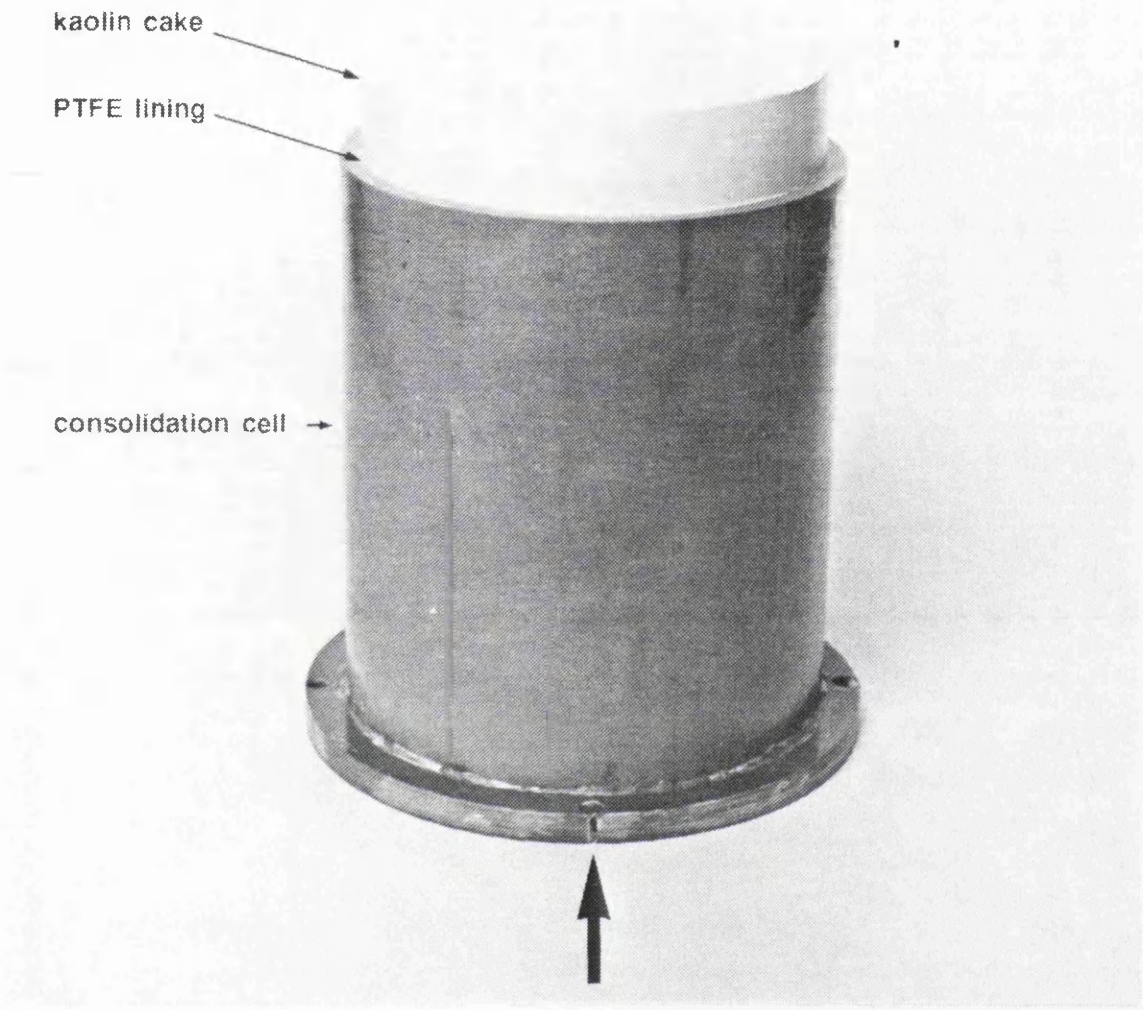

Fig. 3.23 Part of the sample pushed out of the cell

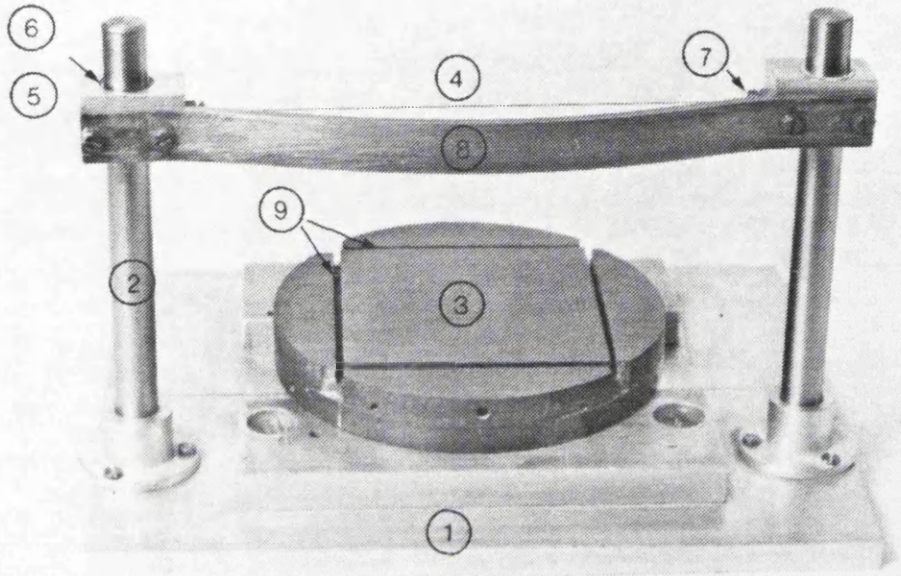

1- fixed duralumin base
2- silver steel column
3- rotating base
4- stretched trimming wire
5- sliding guide block
6- PTFE bush
7- adjusting screw
8- steel tie bar
9- slots

Fig. 3.24 The trimming device used for fully saturated samples

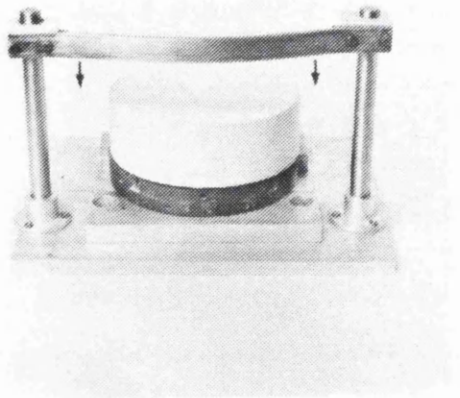

(a)

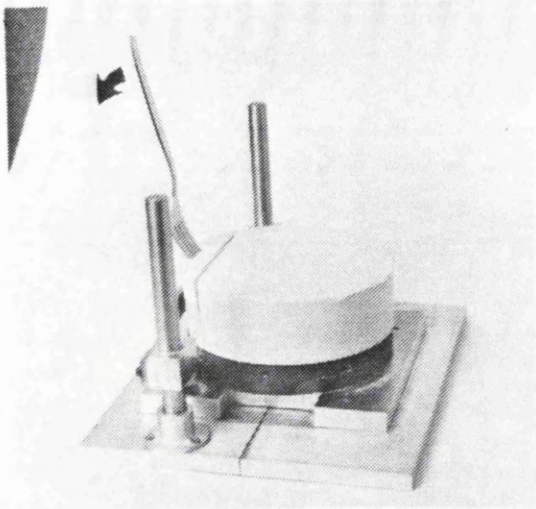

(b)

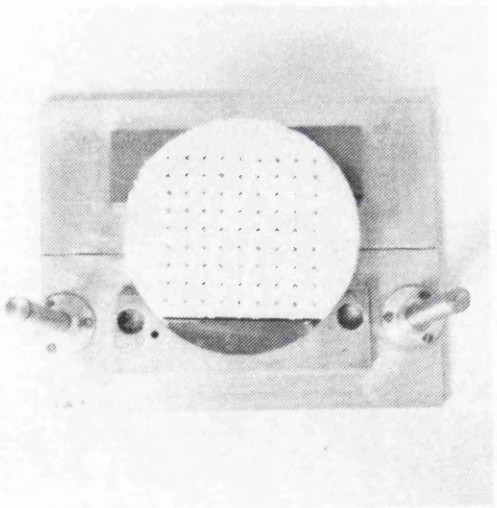

(c)

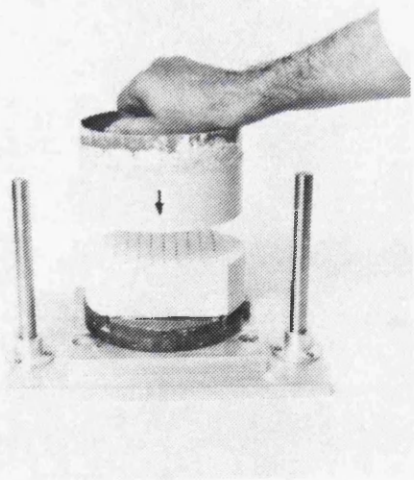

(d)

Fig. 3.25 Trimming procedure to provide a 100 x 100 x 100mm fully saturated kaolin sample; (a) the kaolin cake is placed on the trimming device, (b) method to prevent the cut slice from resticking, (c) lead shot placed onto the x-y plane, (d) positioning the second slice on the first cut, (e) four faces of the sample is cut, (f) second rotating base used to rotate the sample vertically, (g) placing the sample on the second rotating base and (h) a fully cut sample of kaolin

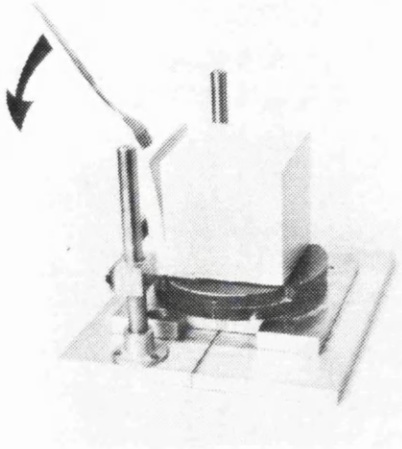

(e)

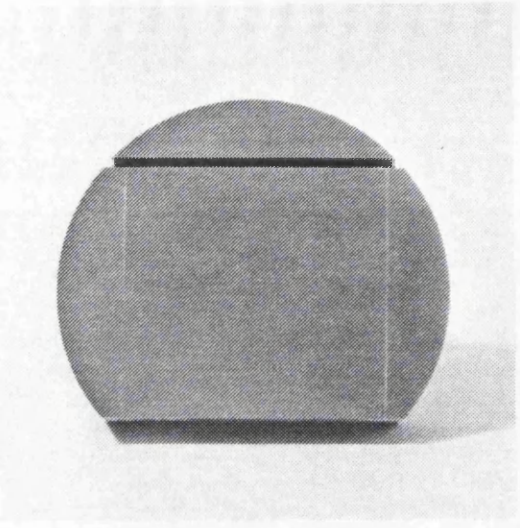

(f)

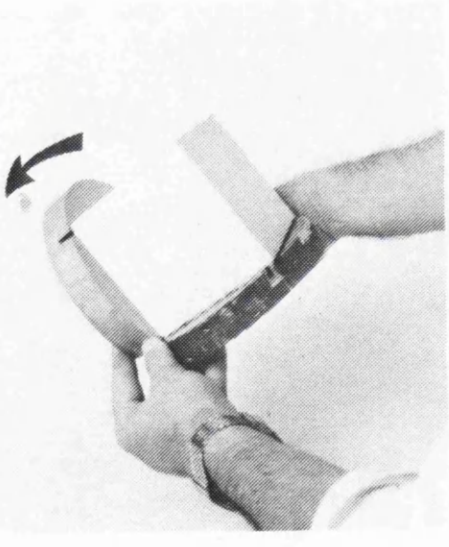

(g)

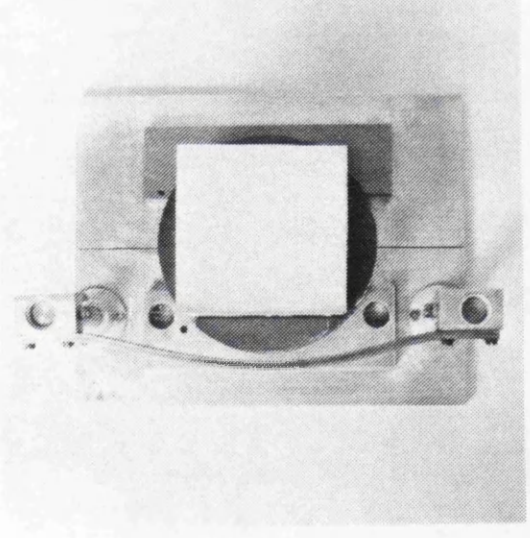

(h)

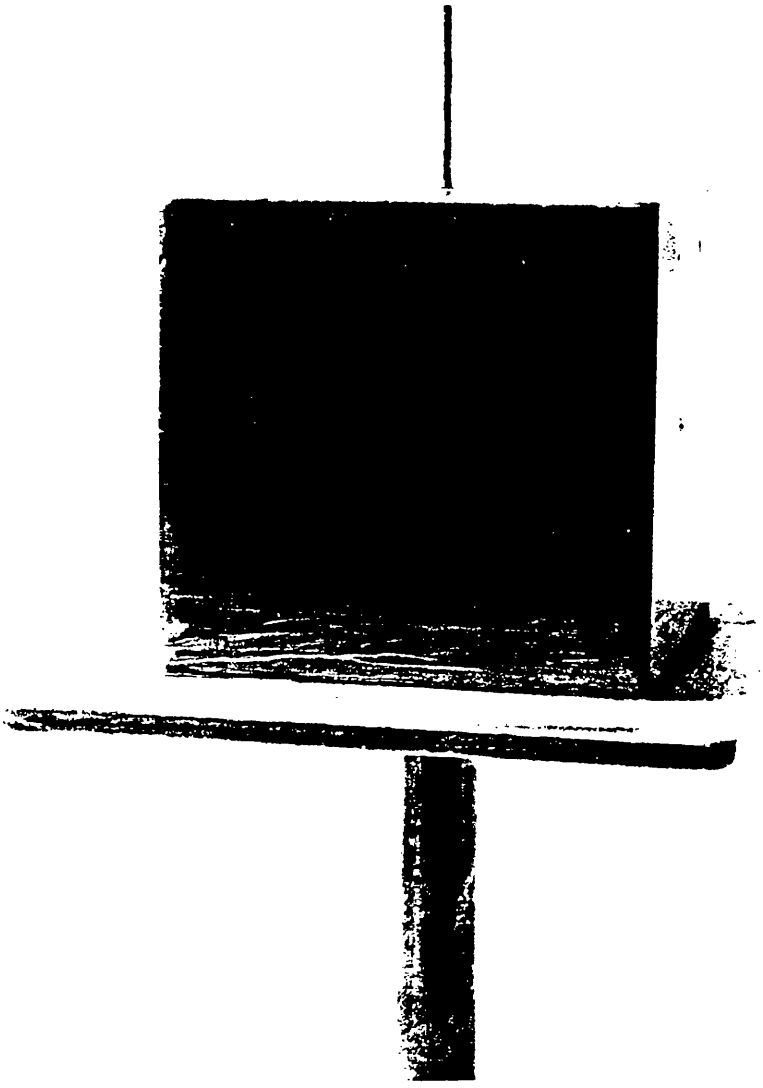

Fig. 3.26 Former for making rubber membrane used to conduct fully saturated samples

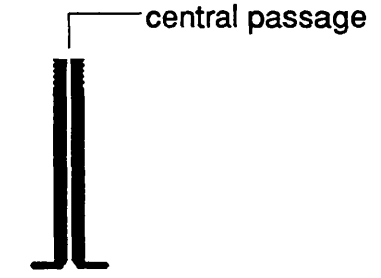

Brass needle guide

(a)

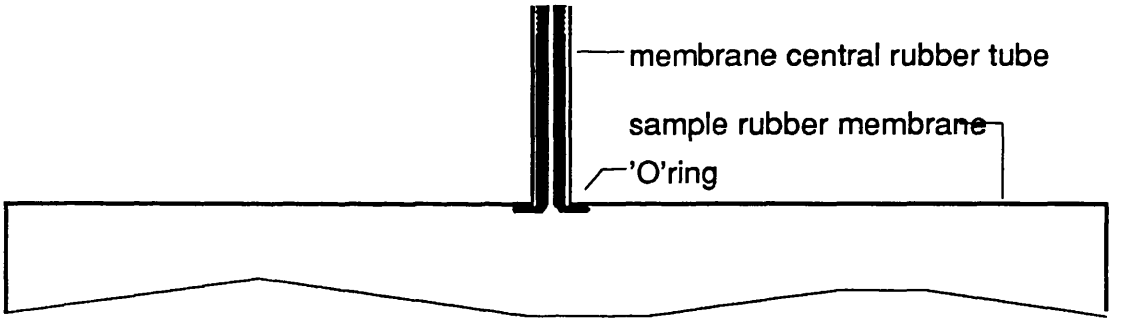

(b)

Fig. 3.27 **(a) Needle guide prior to being pushed into the tube located in the central part of membrane and (b) needle guide in place**

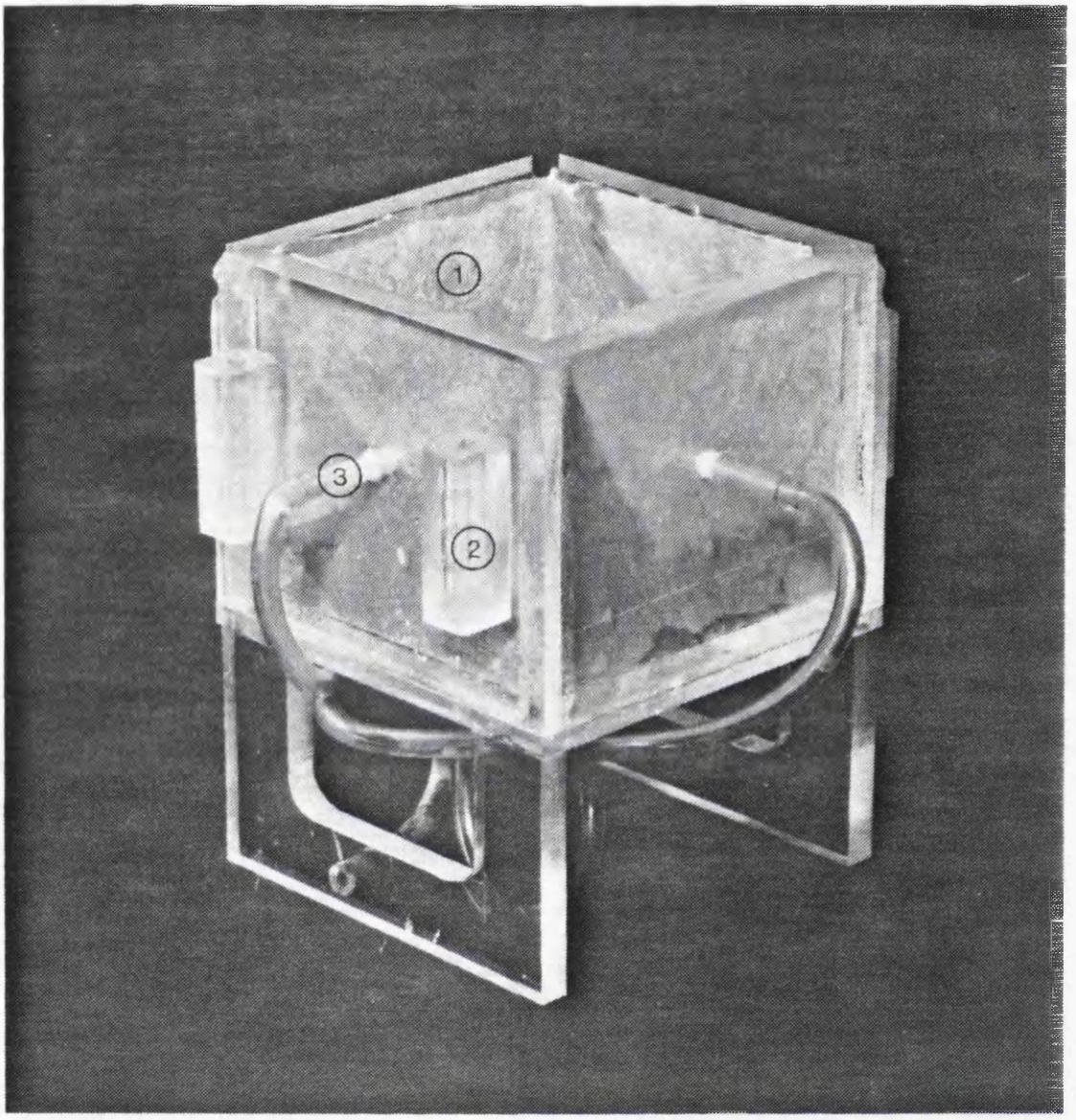

(a)

1- porous lining
2- guiding block
3- vacuum tube

Fig. 3.28 (a) Stretching box with porous material in place and (b) uniformly expanded membrane in the stretching box

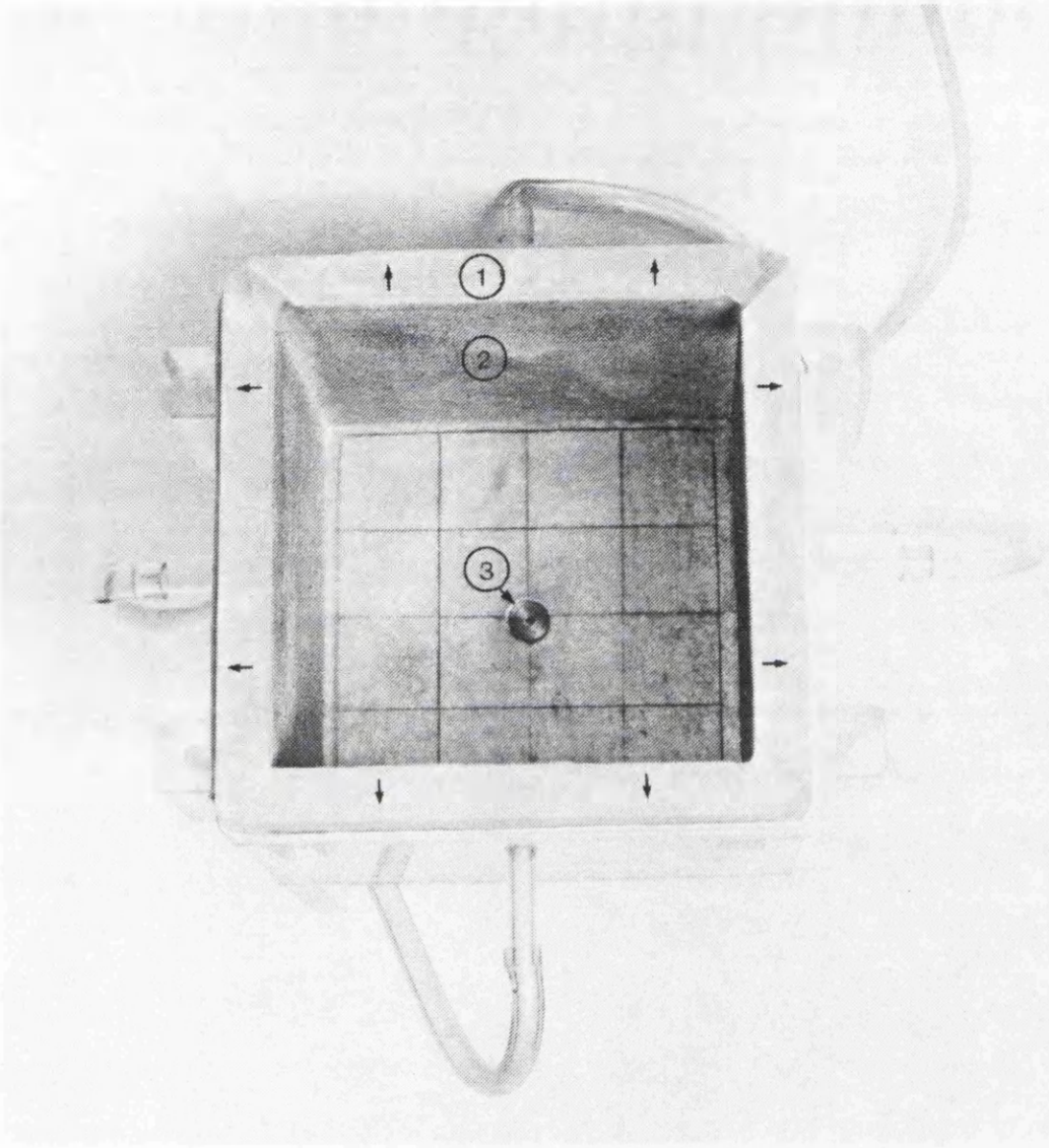

(b)

1- stretched membrane
2- fine sand coating
3- brass needle guide

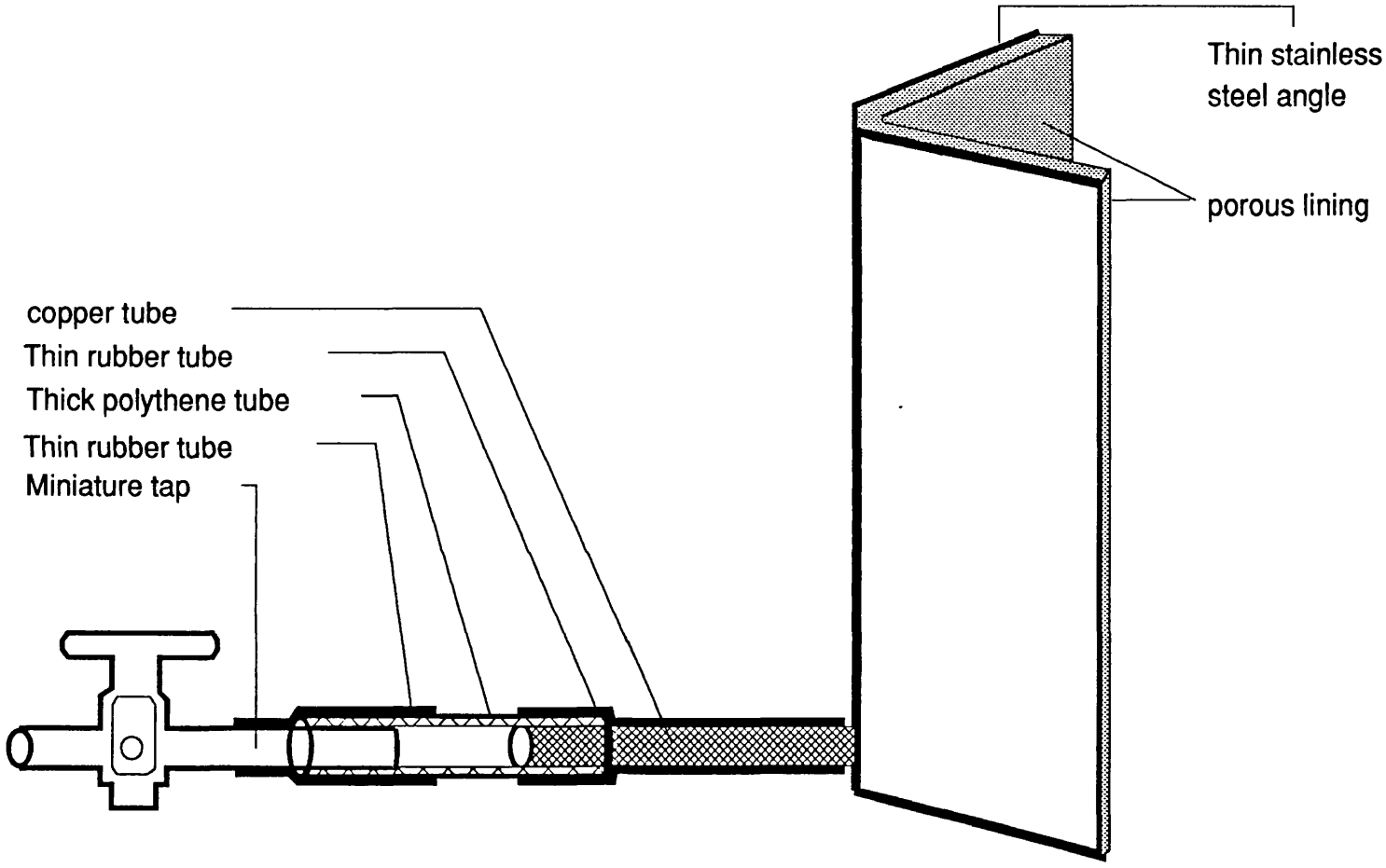

Fig. 3.29 Drainage system for fully saturated kaolinite samples

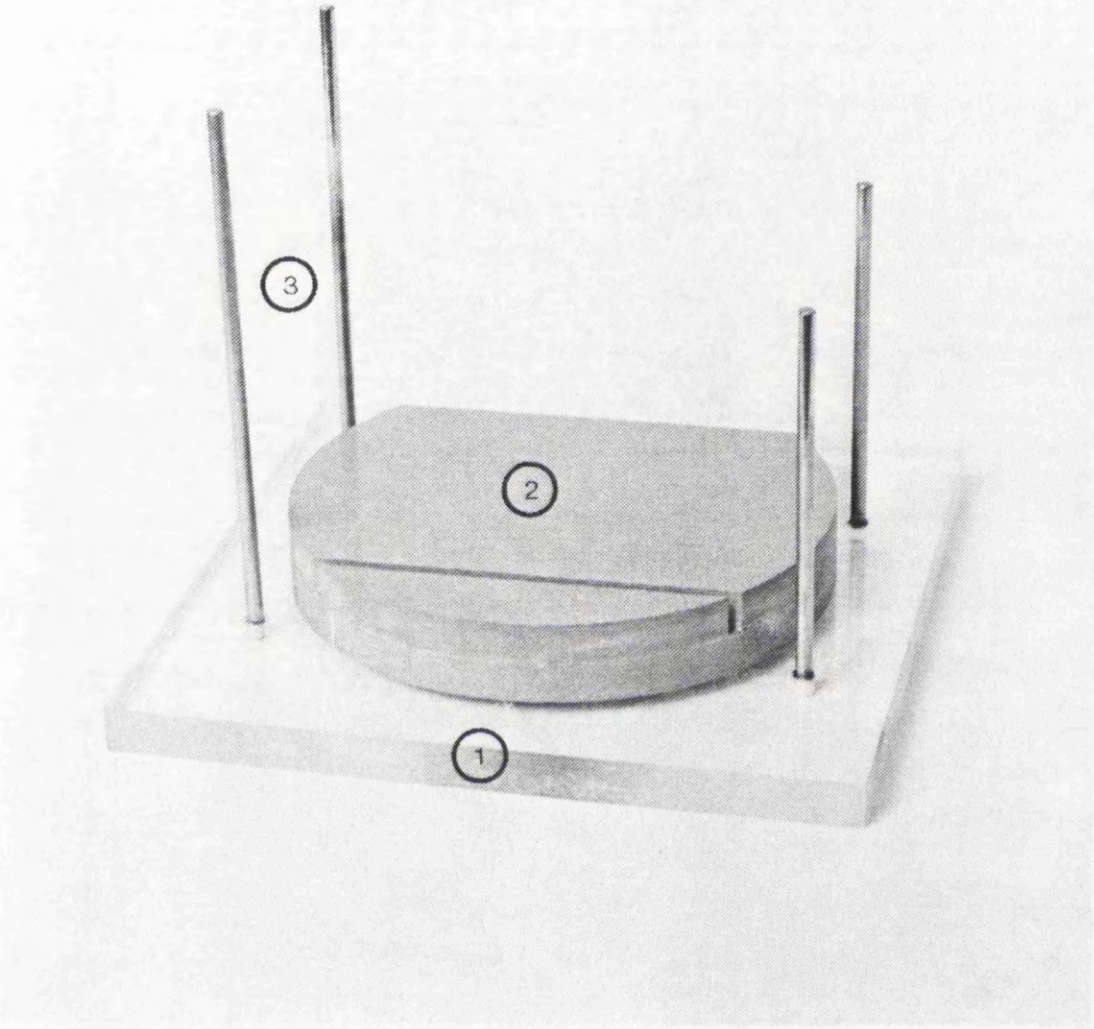

1- fixed plate
2- rotating base
3- steel guiding columns

Fig. 3.30 Stretching box guiding device

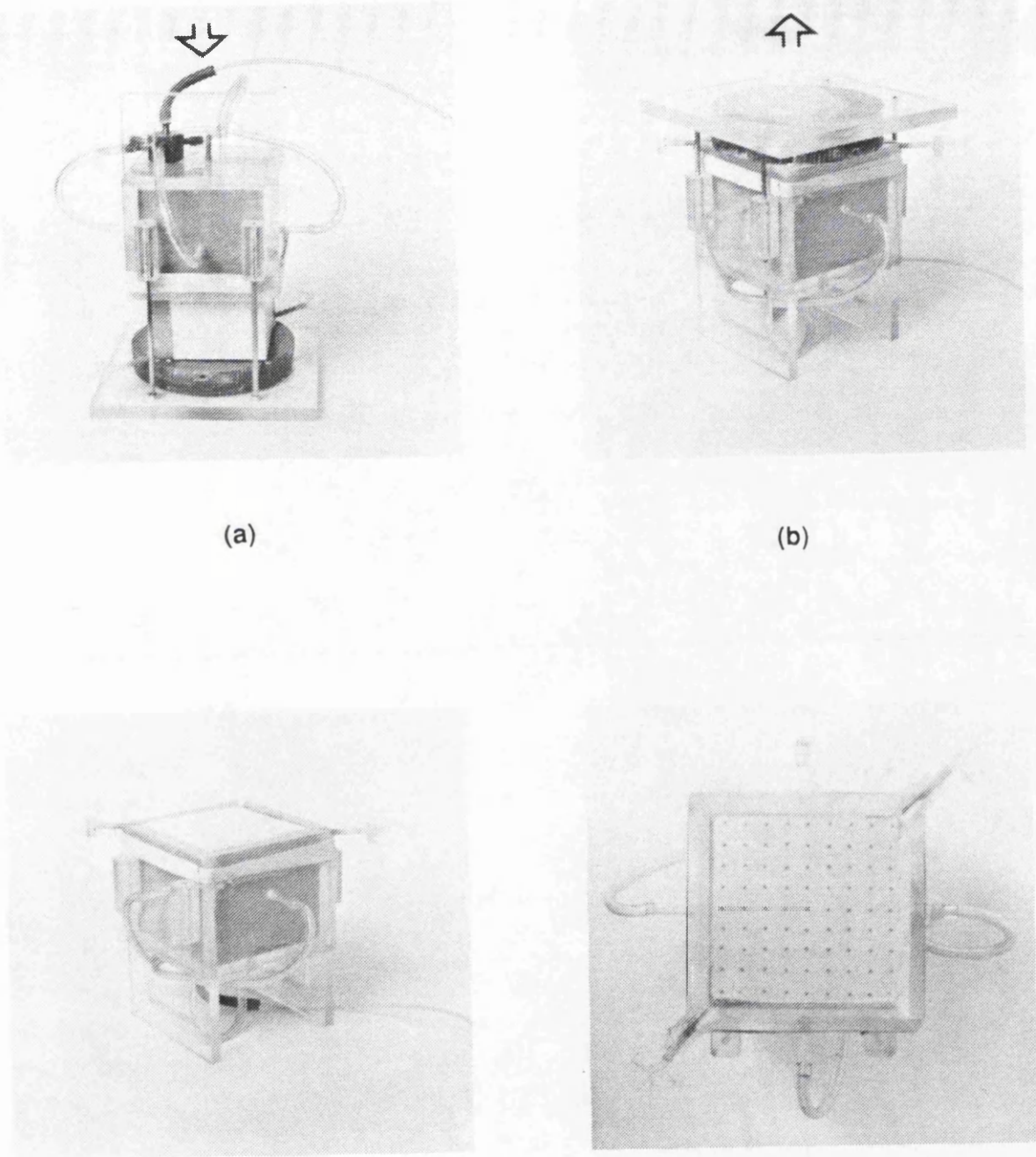

Fig. 3.31 Placing the sample into the rubber membrane and sealing procedure; (a) encasing the sample into the rubber membrane, (b) pulling the guiding device out, (c) coating the edges with adhesive and (d) sealing the fully saturated sample

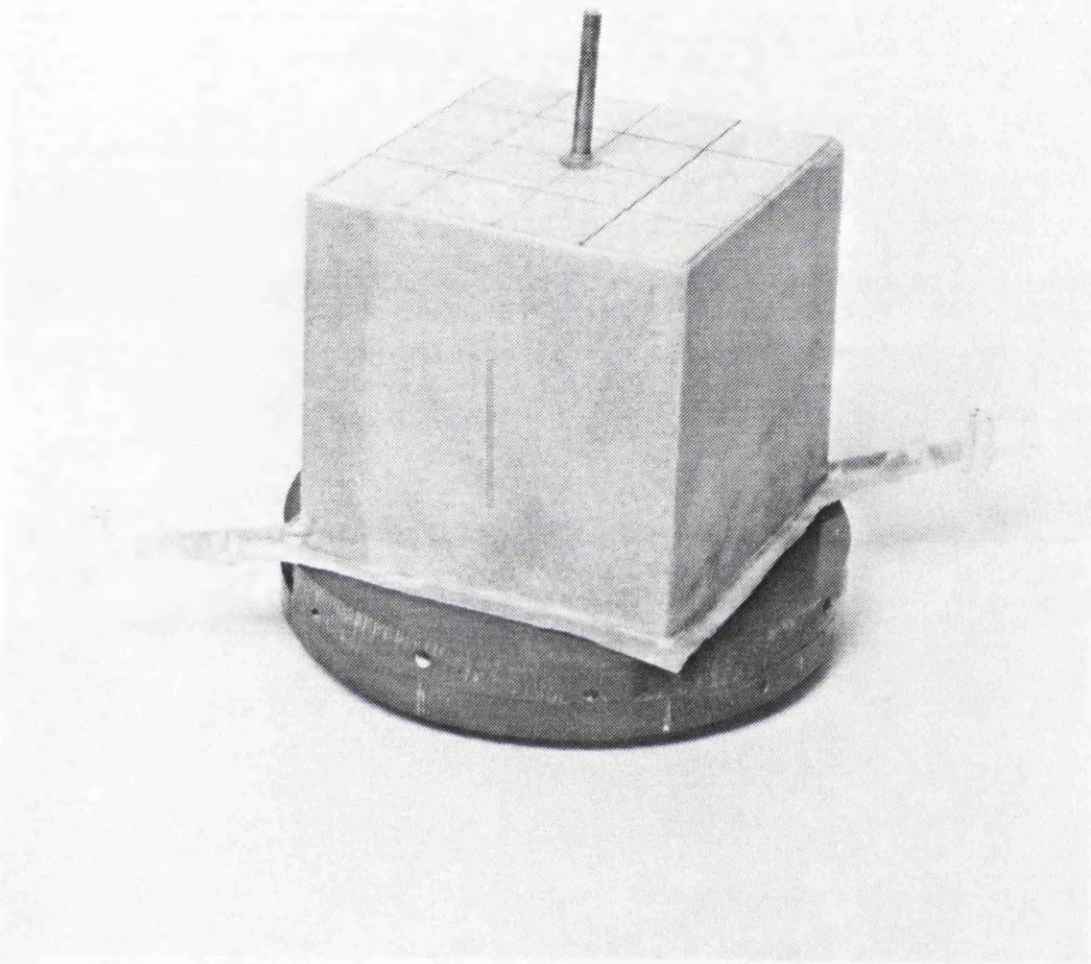

Fig. 3.32 A completed sample in rubber membrane

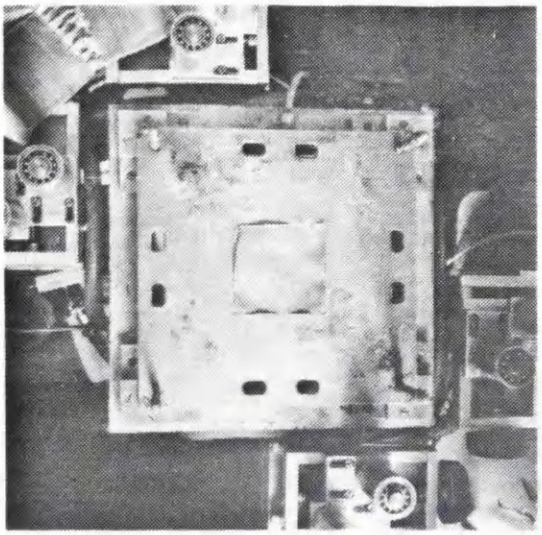

(a)

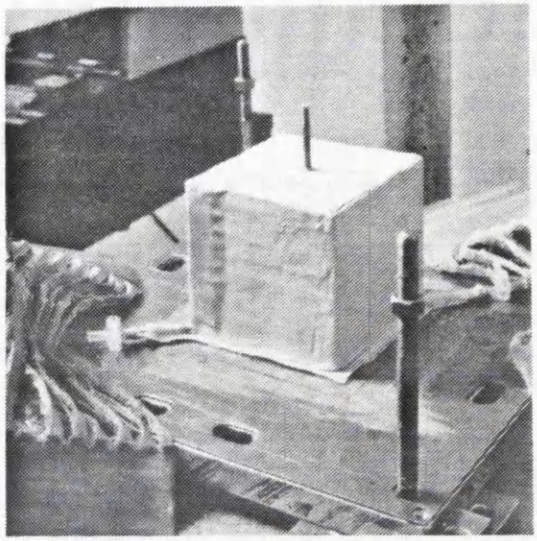

(b)

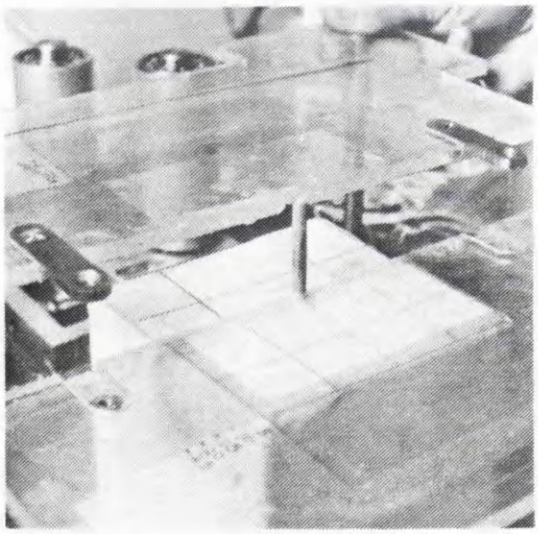

(c)

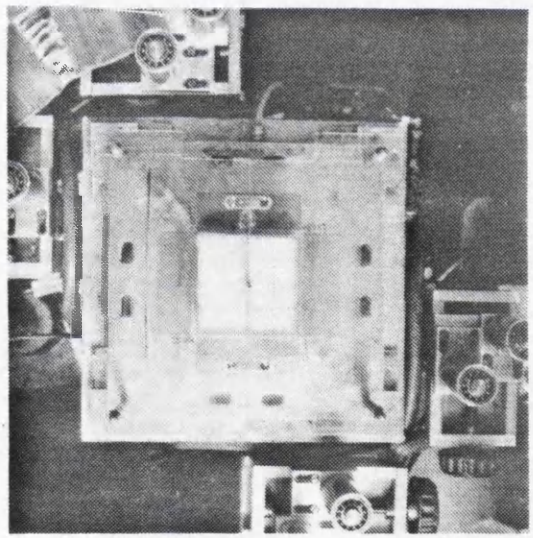

(d)

Fig. 3.33 Setting up procedure for fully saturated kaolin sample in the DCDSC; (a) bottom plane strain platen, (b) sample placed on the σ_2 bag, (c) and (d) centralising the sample using the split perspex plate, (e) placing the shear sheets around the sample, (f) normal pressure bags and shear sheets in place, (g) split platen locked in position and (h) complete set up with the centrally inserted probe in position

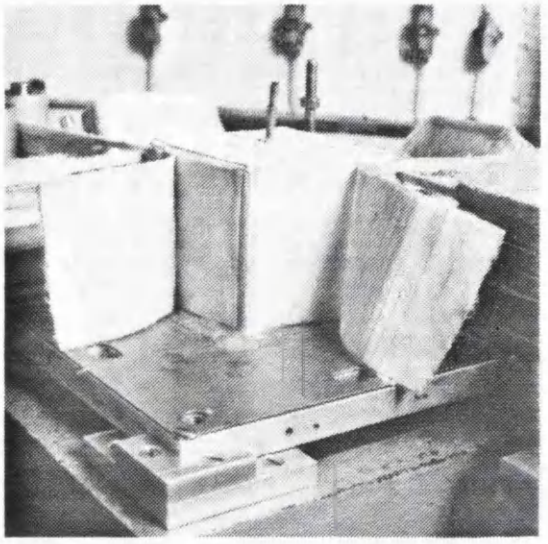

(e)

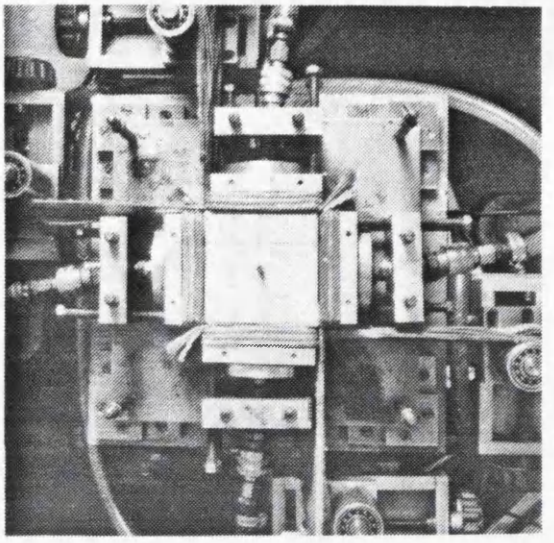

(f)

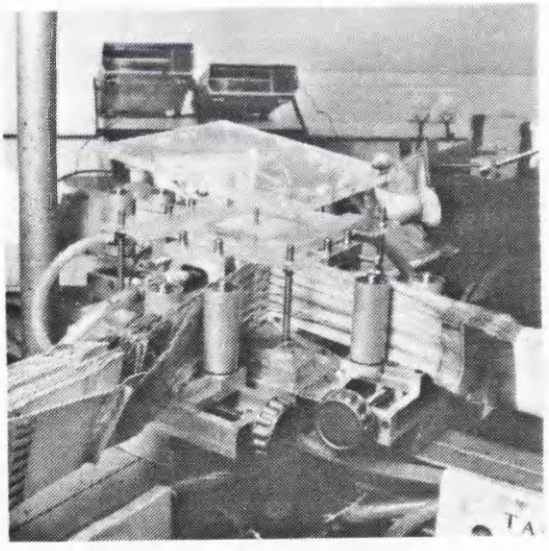

(g)

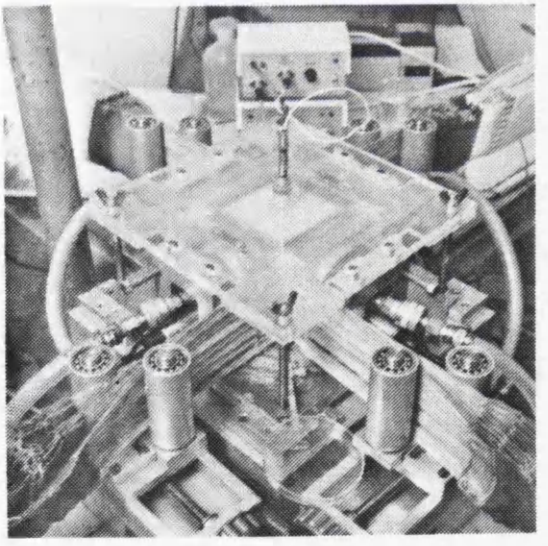

(h)

CHAPTER 4 PRELIMINARY TESTS AND VERIFICATION OF APPARATUS PERFORMANCE

4.1 INTRODUCTION

This chapter is divided into four sections. In this, the first section, a general outline is given of the calibration procedures for the transducers which were used in the normal, shear and the plane strain pressure systems. Calibration of the shear sheets was also needed to ensure that there was a linear relationship between the pressure in the shear cylinders and the shear stresses applied to the faces of the sample. The second section explains the general experimental procedures used for testing sands in the DCDSC. The third section outlines the test programme, and includes tests to evaluate the apparatus performance. In the fourth section two types of simple plane strain model tests are presented to provide independent verification of the apparatus and to establish the effects of stress level variation at very low stress levels.

The first phase of this research was to become familiar with the operation of the Directional Shear Cell and its supplementary equipment. This provided ideas on the modifications and developments required to improve the performance of the apparatus. These tests, made it possible to evaluate the overall performance of the newly developed Daisy Chain Directional Shear Cell regarding both the equipment and the experimental techniques. Also the tests were used to establish the basic stress-strain behaviour of dense (e=0.52) samples of Silver Leighton Buzzard sand at three different minor principal stress levels 14 kPa, 30 kPa and 60 kPa. The stress controlled nature of the DCDSC limited study of the shear behaviour up to peak strength. However, changes in lubrication conditions and thickness of the sample membrane on the plane strain boundaries also enabled the investigation of the boundary effects on the shear deformation behaviour of Leighton Buzzard sand.

4.2 MEASUREMENT OF BOUNDARY STRESSES

The stress controlled nature of the DCDSC required an accurate way of measuring the boundary stresses which were applied to the surfaces of the sample through shear sheets, normal pressure bags and a σ_2 bag. Electronic Bell and Howell transducers of appropriate ranges were employed to measure these stresses. All transducers were connected to a power supply and a calibration unit. Each channel in the unit was attached to a variable resistor and provided the necessary voltage required to energise the transducers. Each different transducer output was measured using a digital voltmeter (DVM). The transducers were initially calibrated using a mercury manometer.

4.2.1 Calibration of normal pressure system transducers

The normal stress applied to the surface of the sample in the DCDSC was assumed equal to the internal air pressure in the normal pressure bags. Therefore the pressure transducers located at the normal pressure backing plates would provide a direct monitoring of the normal stresses applied to the sample.

Calibrations of the normal pressure system transducers were carried out on a dense sand sample after setting it up in the DCDSC. The sample was under vacuum throughout the calibration process so that it behaved as a rigid block. Transducers were connected to the power supply and calibration unit at least one hour prior to use to allows these to stabilise. Calibration commenced by setting the transducers readings to zero. Next by opening only one of the air regulators a pressure of up to 100 kPa (which could be monitored by a mercury manometer) was gently and simultaneously applied to all four normal pressure bags. The variable resistor for each channel then was adjusted to a convenient reading, say 10mV, on the digital voltmeter. The pressure then was decreased to 50 kPa and zero to check if there was any zero shift shown in the DVM reading. This process was repeated until a satisfactory reading with a maximum shift of 0.01 mV was obtained.

4.2.2 Calibration of σ_2 bag transducer

The plane strain boundaries consisted of a rigid plate on the top plane strain side and a water-filled flexible pressure bag on the bottom. The main purpose of using a water filled pressure bag was that it could operate at nearly constant volume and provide a facility to monitor the build up of intermediate principal stress during a plane strain test if required. In these types of tests, the bag was isolated so that the imposed pressure on the bag could be recorded. The calibration of the transducer for measuring the intermediate principal stress was identical to that the of the normal pressure bags, although the medium was water instead of air. It was easier to achieve a correct calibration by maintaining the air-water interface which was contained in a metal mesh framed acrylic cylinder at the same height as the σ_2 bag, thereby eliminating differences in elevation head.

4.2.3 Calibration of shear sheets

The shear stresses were applied to the faces of the sample through Daisy Chain shear sheets. These stresses could not be computed directly from the pressure

applied to the actuating cylinders due to the small frictional effects in the system. If there were no frictional losses, there would be a constant factor between them. This factor is the ratio of the area of the sample face to the loading area of the shear cylinder. Thus, there is a well defined ideal calibration to which the real calibration approximates. As lubrication kept frictional effects to a minimum the real calibration hardly changed with time but required an occasional check.

The general procedure to calibrate the shear sheets in DSC testing has been described in detail by Arthur et al. (1977), Rodriguez (1977), Beckenstien (1980), Germaine (1981) and Wong (1986). However, all DSC versions that they used were operated by a air/water interface pressure system. Since compressed air was used to pressurise the normal pressure bags in the DCDSC and no air/water interface was involved, a slightly different procedure was needed to calibrate the daisy chain shear sheets.

The procedure to calibrate the shear sheets was to pull an adjacent pair of shear sheets which were resisted by the pair of adjacent water filled normal pressure bags. The increase in the shear load will be registered by an increase in normal stress in the constant volume bags (Figure 4.1).

The first step was to fill two normal pressure bags with de-aired water adjacent to a pair of shear sheets which were going to be calibrated; Figure 4.1. The water-filled bags were to be used as constant volume sensors, therefore the volume of water in the normal pressure bags was important. Great care was taken to eliminate any air bubbles, and the bags were filled with a correct volume of water to ensure uniform distribution of stress over the sample face (Figure 4.2c). In the present research to achieve the correct volume of water, the normal pressure bag assembly was placed on its back under water, with no load applied to the concertina segments. Then the outlet was blocked. To assess the correct volume of water in the bag an improved method was introduced by Arthur et al. (1988) in which the correct volume of water was obtained through finding the correct effective area. They applied a dead load to the bag through a plate with the same dimensions as the bag face whilst the bag was positioned on its back. Knowing the dead load and measuring the imposed stress through a transducer the effective area could be calculated. This procedure was carried out with different volumes of water until the correct effective area was obtained.

Once the two normal pressure bags were filled, a dense sand sample was set up in

the DCDSC; the normal pressure bags and the shear sheets were placed around the sample while water in the σ_2 was set so that the sample just floated above the plane strain side. The shear sheets were positioned so that no restraint was imposed by the unstressed pair. To increase the stress equally and simultaneously in the other two pressure bags only one manual pressure regulator was used. The pressure was increased gently and set at an appropriate magnitude of, say 50kPa, while watching both the DVM reading and the elevation of the mercury in the manometer. The magnitude of this stress is immaterial within a limited range (Bekenstein, 1980). Figure 4.1 illustrates the experimental arrangement for the shear sheet calibration.

Next, the actuating cylinder transducers were calibrated by locking the pistons to the cylinder supports as illustrated in Figure 4.3. The calibration was carried out by initially setting these transducers to zero and subsequently pressure of 150 kPa was applied through a pressure regulator. The upper limit of the transducer resistor was adjusted to a convenient reading in mV and kept constant throughout the DSC testing.

The shear sheets adjacent to the isolated normal pressure bags were then loaded incrementally. The area of the shear sheet is taken equal to the normal pressure bag area so the increase in normal stress recorded in the isolated constant volume normal pressure bags was the shear stress transmitted to the sample through the adjacent face (Figure 4.1). With proper alignment of the normal pressure bag backing plate and the Daisy Chain shear sheets, the two adjacent normal pressure bags should record identical stress increments.

The calibration process continued with the incremental loading of shear sheets over a range of 2 to 100kPa. The entire procedure was repeated for the opposite pair of shear sheets. Figure 4.4 illustrates the actual experimental results in a loading and unloading cycle of the shear stresses. The difference between the experimental calibration and the theoretical idealisation was approximately 2 kPa at all levels of stress above 5 kPa (Figure 4.4). This difference in stress was thought to be caused by the accumulative frictional resistance along the surfaces of the shear sheets and normal pressure bags.

4.3 GENERAL PROCEDURES FOR DCDSC TESTING

Once a sand sample had been positioned in the DCDSC using the methods explained in Chapter 3, shearing the sample with the desired stress path was

commenced. The stress path and major principal stress direction in the monotonically loaded tests are illustrated in Figure 4.5. The shearing process was basically the same for both loose and dense samples and involved the application of an isotropic stress to the faces of the sample while it was under vacuum. The magnitude of this isotropic stress was equal to the value of the minor principal stress of the chosen stress path, i.e. 14 kPa or 30 kPa. Application of negative pore pressure to the sample during the initial setting up procedure was unavoidable, particularly for dry sand samples in order to be able to handle the sample without disturbance. In earlier DSC testing on Leighton Buzzard sand samples (Rodriguez del Camino, 1977; Bekenstein, 1980), the testing process was carried out by applying a high vacuum to the sample, while the boundary stress increments were set up, and subsequently the vacuum was released to allow sample deformation. This method of testing is easier and larger stress increments could be used without any detrimental effects, however, experiments by Wong (1986) suggested that the stress-strain behaviour of sand at low stress levels was somewhat affected by applying a high vacuum during testing. In the present research to eliminate this effect, all tests load increments were carried out under atmospheric pressure and with no negative back pressure.

Prior to releasing the vacuum a proper inspection was made to ensure that every aspect of setting up was correct before the sample was ready to be tested i.e. the sample was centred, the shear sheets were properly aligned, the yokes were in contact with the piston rods, the retaining vanes were in the right position, the correct regulators were in operation, the σ_2 tap was open, the chart recorder was in operation and the main compressor was on.

At this stage a radiograph of the sample was taken. The radiograph was then developed and fixed. Once the quality of the first radiograph was verified, the sample vacuum was released and was allowed to equilibrate with atmospheric pressure and the sample was free to deform. Then the second radiograph was taken at this stress ratio (R=1), and developed. This radiograph was the reference film from which the subsequently induced sample strains were computed. The test was started out by increasing the stress ratio, with small adjustments of the pressure regulators to apply corresponding values of normal and shear stresses to keep a constant minor principal stress and a fixed major principal stress direction. This was repeated and radiographs taken when necessary until the sample reached failure.

Ideally the normal and shear stresses should always be applied simultaneously to

the sample in order to maintain a constant major principal stress direction. The simultaneous application of the boundary components was impossible. Therefore stress components were increased in a sequential series of the smallest convenient increments by always starting with the normal stresses being increased before the shear stresses which the lowest normal stress followed by a higher one and then the lower shear stress, the higher shear stress, etc. The small size of these increments would ensure the minimum deviation from the intended stress path and major principal stress direction. Obviously, this "no vacuum" technique led to many mini-increments before the strain increment was big enough to warrant a radiograph.

As the sample strained with the boundary stress application, the sample changed shape and the boundary stresses no longer acted on orthogonal surfaces, in loose samples and in cases of cyclic loading, large deformations were involved. Thus, it was necessary to plan a stress path in terms of principal stresses and their directions so that a correction could be made increment by increment according to the current measurements of the deformed shape. The corrections are defined in Figure 4.6 and the boundary stresses could be computed from the following equations:

$$\sigma_a = 1/2\ \sigma_3\ [(R+1)+(R-1)\cos 2(\psi-\alpha)]$$
$$\sigma_b = 1/2\ \sigma_3\ [(R+1)+(R-1)\cos 2(\psi-\beta)]$$
$$\tau_a = 1/2\ \sigma_3\ (R-1)\sin 2(\psi-\alpha)$$
$$\tau_b = 1/2\ \sigma_3\ (R-1)\sin 2(\psi-\beta)$$

where the α and β were the angles of distortions which could be measured using a protractor through the glass window of the top platen between each radiograph.

It was mentioned in Chapter 2 that in order to be able to conduct a proper test using the DSC, the sample faces should remain parallel to the backing plates and the shear sheets at all stages of deformation. Thus, the adjustment of backing plates and alignment of shear sheets was carried out depending on the amount of deformation and the major principal stress direction. Ideally the adjustment of the backing plates and alignment of the shear sheets should be continuous as the test proceeds. This is possible only if the shear sheets and normal pressure bags are adjusted automatically. However, in the present research since the equipment was in its transitional form, from manual to automatic, these adjustments were carried out by hand, employing the adjusting screws and shear sheet guide rollers. Adjustment of backing plates and alignment of shear sheets was very important as even small

mis-adjustment and mis-alignment could lead to appreciable errors. The alignments were particularly important in tests where ψ=45° as the sample changed shape from a square to a rhombus.

As sudden failure was accompanied by a sudden large displacement, a rapid manual response was needed to avoid damage to the more delicate parts of the apparatus. First the sample was placed under vacuum and then the main air supply valve was switched off to allow all pressurized and stretched components to relax together.

4.4 EXPERIMENTAL PROGRAMME AND TEST PROCEDURE

The test programme performed using the DCDSC was divided into four main categories. In the first series which will be presented in Section 4.4.1, shear tests were performed on dense Leighton Buzzard sand at three different stress levels of minor principal stresses: 14 kPa, 30 kPa and 60 kPa. In these tests two different thicknesses of lubrication for the top and bottom plane strain sides were employed. The low stress level tests provided a reference for comparing the DCDSC with earlier versions and could be checked with previous published data (Arthur et al.,1977; 1979; 1980; and Wong 1986). The higher stress level tests provided more information on the shear deformation behaviour of Leighton Buzzard sand, as well as the difficulties experienced with high stress level DSC testing. The highest stress level tests were not successful as element tests, but nevertheless will be discussed briefly and suggestions for further improvement will be made.

The second series which will be presented in Section 4.4.2, involved shear testing in the DCDSC using special thick plane strain membranes on the plane strain faces.

In addition, Section 4.5 presents a series of simple model wall and slope stability tests performed on Leighton Buzzard sand with the aim of obtaining an independent verification of the possible angle of shearing resistance at low stress levels.

4.4.1 Monotonic shear tests with constant principal stress directions

The purpose of this series of tests was to become familiar with the equipment, check that the apparatus was working as expected and extend the information available on stress-strain-strength behaviour of the Leighton Buzzard sand at three different stress levels i.e. σ_3 14 kPa, 30 kPa and 60 kPa.

Equipment familiarization started by first running tests similar to those of a conventional plane strain apparatus, without applying boundary shear stresses. The next test was one in which the major principal stress direction was aligned with the sample diagonal. All samples were prepared by deposition in the direction of the intermediate principal stress, which eliminates inherent anisotropy, so these apparently isotropic samples should produce a unique stress-strain relationship accompanied by uniform strain distributions throughout the test. Deviations from this could be due to sample heterogeneity either within or between the test samples improper operational procedures, application of non-uniform boundary normal and shear stresses by the DCDSC, boundary restraints, or imprecise measurements of the applied stresses, and associated strains. Evaluation of the DCDSC therefore involves the comparison of stress-strain relationships from tests at various ψ angles, analysis of strain distributions within the samples, and the coincidence of the major principal stress and strain increment directions.

The tests followed a stress path similar to that described by Wong (1986) in which plane strain tests were carried out starting with b=0.0 and measured the value of σ_2 with increasing the stress ratio to b=0.3 near failure. Here σ_2 was changed to match that of Wong at the appropriate stress ratios.

Monotonic shearing involved a stress path in which the major principal stress direction was held constant and the magnitude increased until sample failure. It can be seen from Figure 4.5 that the plot of the stress path is simple but it does not give any information on the direction of the principal stresses.

Although the maximum boundary shear stress was improved in the Daisy Chain DSC to 180 kPa, the highest stress level tests were not successful because of the technical problems at the soil sample boundary interface. Four tests were carried out under high stress levels of σ_3= 60 kPa and all these tests failed prematurely. The failure occurred at the sample boundary interface which indicated the present method of gluing sand to the internal face of the rubber membrane was not adequate to provide enough traction for the transmission of shear load to the sample. To provide enough traction at this interface and prevent surface failure needs further investigation. An example of this type of failure is indicated in Figure 4.7. Therefore the testing programme at present research has been restricted to stress levels of σ_3=14 kPa and σ_3=30 kPa.

4.4.1.1 Stress and strain response

Figures 4.8 and 4.9 show the stress strain and deformation response of both dense and loose sand samples respectively tested at a minor principal stress of 14 kPa. In each of these Figures, the principal stress ratio is plotted against the major principal strain. For both types of samples, the stress-strain response rose steeply from the initial condition where R=1. As the strength of the sand was further mobilised by increasing the stress ratio, the rate of increase of deformation became progressively faster until failure was reached. Here for tests with ψ=0° no shear sheets were placed around the sample.

For dense samples, the formation of a rupture layer was deemed to be failure and tests were then terminated. This usually occurred at approximately 3.5% major principal strain and corresponded to a stress ratio of 6.8 ± 0.2. The actual stress ratio to cause rupture was not precise. At about a stress ratio of 6.8 under these loading conditions, a dense sand is near failure and a rupture layer can be triggered off by minute sample disturbances. When the adjustment of normal pressure bags, backing plates and the alignment of the shear sheets are conducted manually the operators judgment is essential. For instance, over adjustment of the backing plates can induce boundary disturbance and trigger the rupture layer at a lower stress ratio, whereas an under alignment of shear sheets results in a thrust back into the sample and delays the formation of failure planes. Nonetheless, the angle of shearing resistance, 48.5° (i.e. sin ϕ_f = (R-1)/(R+1)), associated with the stress ratio of R=7.0 is comparable with the angle of shearing resistance for Leighton Buzzard sand of similar void ratio in other devices tested under plane strain condition, e.g. 50.9° with the simple shear apparatus (SSA) (Stroud, 1971), 49° with the earlier version of DSC (Wong, 1986) and 48° with the Biaxial tester, (Ogunbekun, 1988) at a similar stress level of σ_3 = 14kPa.

It is interesting to note that the presence of unstressed shear sheets surrounding the specimen when ψ=0° tests were performed, delayed the formation of rupture layer and led to a higher value of principal stress ratio at failure (an increase equivalent to 2 degrees in ϕ_f) when σ_3=14 kPa. Figure 4.10 indicates the effect of restraint, partly due to shear sheets, on the stress-strain behaviour of dense Leighton Buzzard sand tested in this condition. However, stress-strain curves up to 2.5% are only slightly affected. Also, this did not effect the uniformity of strain distribution throughout the test. Figure 4.11 illustrates the strain distribution within the sample at stress ratios of R=7. Bekenstein (1980) and Wong (1986) also reported a similar effect using the

DSC on their sand samples with an increase equivalent to 1 degree in the angle of friction. This was probably due to the compressive stiffness of the unstressed shear sheets caused by the normal stresses behind them which could lead to a re-distribution of stresses throughout the sample and prevent the formation of rupture layers at the sample boundaries. This re-distribution of stress and delay of failure was not observed when a higher stress level, i.e. σ_3=30 kPa, was imposed. Therefore this did not impose a serious limitation on the DCDSC because the same principal stress ratio at failure could be obtained from tests with stressed shear sheets when $\psi>0°$ or without shear sheets for $\psi=0°$.

When testing loose samples no rupture planes were observed even though the major principal strain attained was more than 11% (Figure 4.9). For the loose sample, the test was terminated when a small increment of stress resulted in large deformation, and this state of stress was interpreted as failure. This failure occurred at a major principal strain of about 11%. The associated stress ratio of approximately 4.2, and the corresponding ϕ_f value of 38° is comparable to the value of 39.5° obtained by Stroud (1971) using the simple shear apparatus Rodriguez (1977) and Wong (1986), 39° with the Biaxial tester, (Ogunbekun, 1988) for sand of the same voids ratio and at the same stress level of σ_3 =14kPa. Figures 4.12 and 4.13 illustrate the comparison curves of stress-strain behaviour of both dense and loose samples tested in the DCDSC with those of Wong (1986) carried out in the DSC. Later (section 4.4) independent methods of testing will be used to show that whilst the dense shear strength is correctly measured the loose sample shear strength is influenced by boundary restraints.

Vague

4.4.1.2 Volumetric deformation behaviour

The volumetric behaviour of the dense and loose samples is also illustrated in Figures 4.8 and 4.9 respectively. In these figures, the minor principal strain is plotted against major principal strain. These figures show an initial contraction of the material followed by expansion as the sample deforms. This contraction is minute for dense samples in the early stages of deformation, and is below the limit of measurement. This phenomenon is understandable as the initial void ratio e_0 = 0.52 which is close to that of the minimum possible void ratio of e_{min} = 0.49. The possible maximum and minimum voids ratios of 0.79 and 0.49 were determined by Wong (1986) using methods recommended by Kolbuszewski (1948). The larger initial contraction in loose samples was due to the highly sensitive nature of the sand close to the maximum voids ratio (e_0=0.74). Obviously at this voids ratio there could be a minimum number of contact points between the particles that could be just

sufficient to maintain a stable structure. This structure would collapse and a new fabric would form which would be capable of resisting the new applied stress.

A relationship between the average major and minor principal strains can be represented by a single curve and the observed rate of volumetric expansion (dilation rate) just before failure could be compared to those obtained in other plane strain apparatuses for similar test conditions (Stroud, 1971; Arthur et al., 1977, Rodriguez, 1977, Wong, 1986, Ogunbekun, 1988). The average angle of dilation v_{13} is defined by the equation:

$$\sin v_{13} = - (\delta\varepsilon_1 + \delta\varepsilon_3)/(\delta\varepsilon_1 - \delta\varepsilon_3)$$

The average angle of dilation for the final stress increment, just before failure was 16.9° for dense sand. The incremental ratio $\delta\varepsilon_1$ / $\delta\varepsilon_3$ was calculated from the slope line drawn tangentially to the data points prior to failure. For comparison, Stroud (1971), using the data from the SSA, quoted an angle of dilation of 21.4° for dense Leighton Buzzard sand. Arthur et al. (1977), using data from the earliest version of the DSC, calculated an average angle of dilation of 15°. Wong (1986), using the earlier version of the DSC quoted a dilatancy angle of 16° with a range of 16° to 18°. More recently Ogunbekun (1988), calculated an average angle of dilation of 19.5° using the Biaxial Tester for the dense sample. Although there does not appear to be a wide scatter in the various quoted values for dilation rate in the different versions of DSC (15°-18°), there is a wide scatter (15°-21.4°) for sand samples with a similar initial voids ratio and similar failure stress ratio when other devices such as SSA and Biaxial tester are involved. However, it should be noted that the computed dilation rates are dependent on the strain measurements taken just prior to failure when the formation of rupture layers may have effects.

For loose samples, there again appears to be a scatter in the value of dilation angle at failure in the DCDSC and the Biaxial Tester, i.e. 11° for the Biaxial Tester and 5° for the DCDSC. Also the earlier tests on loose samples performed by Rodriguez (1977) gave a value of 8.2° at failure. Nonetheless, there is an excellent similarity in volumetric behaviour in the updated version of the DSC (Wong, 1986) and the DCDSC as illustrated in Figure 4.13. The differences in the Biaxial Tester value and the earlier versions of DSC could be attributed to the different method of measurements of strain in loose samples. In the DSC used by Rodriguez, sample strains were determined from displacement of markers positioned within the sample. In the DSC used by Wong and the DCDSC, strains were determined from the

surface grids and the markers glued to the inner side of the membrane respectively. A comparison of these tests are shown in Figure 4.13 in which it can be seen that the ε_1 versus ε_3 curves are similar at failure and measurements of v_{13} may be overemphasised.

4.4.1.3 Effects of variation in confining stress level

Figure 4.14 shows the stress-strain relationships of dense samples of Leighton Buzzard sand tested at a minor principal stresses of 30 kPa when sufficient lubricant on the top and bottom plane strain surfaces was used. The stress-strain relationship obtained at 14 kPa has also been included for comparison. The stress-deformation curves indicate a softer response and a lower failure strength of ϕ_f = 47.5° with increase in confining stress level. The curves also indicate that there is no difference in volumetric deformation behaviour when comparing the two different stress levels. Recent empirical data, with corrections for both frictional and membrane effects (Fukushima and Tatsuoka, 1984; Tatsuoka et al; 1986), tends to suggest that there is no appreciable variation in strength in deformation behaviour of granular material with increase in confining pressure up to 50 kPa. It would appear on this evidence that the observed changes in material behaviour with variation in stress level could mainly be due to membrane confining effects as, at this stress level, no appreciable particle damage would occur. The deformation of the sample in the ε_3 direction requires expansion of the sample membrane and also that of the lubricated membranes on the plane strain sides as particle penetration will tend to indent the sample membrane into the lubricating membrane (Tatsuoka and Haibara, 1985).

The stress ratio at failure could be corrected for possible effects of membrane confinement for tests carried out at σ_3= 14 kPa. It could be assumed that the sample membrane as well as the lubricated membrane inhibits the ability of the sample to strain in ε_3 direction, therefore inducing an extra δF_3 into the sample as it deforms. In other words, the horizontal forces induced in contact with the plane strain boundaries increase the minor principal stress by $\delta\sigma_3$. The value of increase in minor principal stress due to the membranes can be calculated using the theory of elasticity (after Tatsuoka et al., 1986):

$$\delta\sigma_3 = - 2t_m [2E_m (\varepsilon_1 + 2\varepsilon_3 + 2\varepsilon_0)/3 + (\sigma_2 - \sigma_3)]/L$$

where:

t_m = Thickness of sample membrane + the thickness of the first lubricated membrane (measured as .6mm),

E_m =1.4 x 10^3 KN/m2 (measured in the laboratory for the same membrane of similar thickness),

ε_1 = 3.33% and ε_3 = 6% (strain near failure of the dense samples),

ε_0 = 0 (initial horizontal strain in membrane),

L = 0.1 m (length of the sample),

σ_3 = 14 KN/m^2,

σ_2 = 39.06 (assuming b = 0.3)

Hence,

$$\delta\sigma_3 = - 2\ [0.6 \times 10^{-3}]\ \{2\ (1.4 \times 10^3)[0.0335 - (2 \times 0.06)]/3 + (39.06 - 14\ )\}/0.1$$

$$\delta\sigma_3 = 0.66\ KN/m^2$$

Measured stress ratio at failure = 7.0. To correct the stress ratio for extra $\delta\sigma_3$:

$$R_{corr.} = \sigma_1(\sigma_3 + \delta\sigma_3)$$

$$R_{corr.} = 6.65$$

The 5% reduction in stress ratio could be accounted for membrane confinement. In a similar condition, Ogunbekun (1988) using the Biaxial Tester apparatus reported a reduction of 4% in stress ratio at failure (ie. $R_{measured}$ = 6.8; while $R_{corrected}$= 6.56) for his conventional lubrication tests. However, a negligible extra $\delta\sigma_3$ of 0.12 kPa is thrown into the samples tested at higher stress level, i.e. σ_3 = 30 kPa, which failed at R_f = 6.6. The corrected stress ratio at failure for these tests was 6.57. These values appear to indicate that the effects of membrane confinement would be minimal at σ_3 = 30 kPa. Further independent verification procedures described in section 4.4 will show that the effects of rubber membranes are more complicated than this.

4.4.1.4 Effects of end lubrication

Most laboratory devices for shearing soil impose boundary conditions which lead to unwanted frictional restraint on sample surfaces. The most obvious example is the restraint of unlubricated end platens on conventional triaxial cell samples, but in plane strain tests sample surfaces normal to the direction of intermediate principal stress also provide frictional restraint. The problem is not limited to rigid boundaries; pressurised re-inforced rubber bags (flexible) also provide a suitable reaction for frictional restraint across these surfaces.

Lubrication with silicone grease separated from the soil samples by a thin rubber membrane has proved to be the solution to the problem of frictional restraint for a long time and has been recommended by Roscoe (1953) and Rowe and Barden

(1964). This lubrication method has been found to be the most effective amongst the lubrication techniques currently available.

The aim of lubrication is to achieve as low a coefficient of friction as possible and continued good performance through time and cyclic variation in stress. Of course lubrication has always been a problem in DSC testing (Arthur, 1985). Different lubrication procedures produce different results, e.g. Beckenstein (1980) observed a reduction in magnitude of strain in her DSC results compared with those of Arthur et al.(1977). Wong (1986), also reported a decrease of 25% in strain in his preliminary cyclic tests compared to those of Arthur et al. (1980) under identical cyclic conditions. Germaine (1980) proposed a method to control the thickness of grease and used a thickness of 0.6mm ±.02mm. Wong (1986) conducted a few lubrication tests and showed that the same thickness of grease layer should always be obtained when using an identical lubrication procedure. There can be however, a significant change in the thickness when a second operator is involved.

Figures 4.15 and 4.16 illustrate the comparison of the stress-deformation relationships and volumetric behaviour of dense samples of Leighton Buzzard sand tested using the DCDSC at a minor principal stresses of 14 kPa and 30 kPa when two different thicknesses of lubrication on the sample/plane strain boundary interface were employed. The stress-strain curves indicate a stiffer response and higher failure strength, i.e. R_f = 8.7 for samples tested at σ_3 = 14 kPa and R_f = 7.15 for the samples tested at σ_3 = 30 kPa when less lubrication is used. The increase in R_f was approximately 22% for the low stress levels and 8% for the higher stress level. This illustrates that adequate lubrication is crucial especially at low stress levels.

In the present research a different lubrication procedure was adopted by the author and was used throughout. In this method the role of the operator was minimized. A generous amount of PTFE powder filled silicon grease was spread on the top glass plate within a 0.5 mm thick metal window of 120mm x 120mm opening. The surface of the grease was levelled with a sharp edged ruler while care was taken to eliminate the entrapment of air bubbles. The window was lifted up and two layers of thin rubber sheet (0.25 ± 0.05mm thickness) were thoroughly coated with the same grease and placed carefully on the existing layer of grease. Any air bubbles trapped beneath these sheets were worked out with a finger in one direction and the metal window was placed on the second rubber membrane and the first step was repeated. The same procedure was carried out for the bottom plane strain side, however, as this side was a water-filled bag it was impossible to achieve the exact

thickness of grease. Once the sample was set up in the DCDSC an isotropic pressure of approximately 40 kPa (nearly half of the dense sample negative pressure) was applied to the samples. The sample was left for about 5 hours until the grid on the top of the membrane became visible and the excess amount of grease was squeezed out. This procedure was sufficient to create relatively repeatable and identical layers of grease at the two boundaries.

4.4.1.5 Distributions and scatter of strain measurements

The significance of measuring strain distribution within the sample is essential when Verifying any new and complex shear device performance. Radiography frequently shows that the samples with apparently uniform strains have in fact an unacceptable degree of non-uniformity. The uniformity of strain within a sample sheared in the DCDSC could be quantitatively evaluated by using strain data obtained within each of the 7 x 7 grid areas used for strain measurements. A uniform distribution of strain implies that the homogeneous sample has been subjected to uniform boundary stresses. Figure 4.17 illustrates the magnitudes and directions of major principal strains measured in a dense sample sheared to R=6.00 at ψ =0° and σ_3 = 30 kPa. Figure 4.18 also shows the strain distribution within a loose sand sample sheared to R=4 at ψ =45° and σ_3 = 14 kPa.

Comparisons with strain distribution data derived from similar types of marker grid set in the central third of sand samples tested in triaxial compression (with enlarged and well-lubricated end platens) show an equal range of coefficient of variation (Wong and Arthur, 1985b).

A better evaluation on the data scatter uses the coefficient of variation which is a well established measure and is defined as the standard deviation divided by the mean value. Figure 4.19 illustrates the coefficient of variation for three dense samples that were loaded monotonically under different principal stress directions at σ_3 = 30kPa. In this Figure the coefficient of variation corresponding to the system accuracy (based on 0.15% standard deviation) is shown by the hatched zone. The system accuracy is obtained by comparing two radiographs of the same grid with no intervening grid distortion (Wong and Arthur, 1985b). Thus the actual experimental data will plot above this zone. The coefficient of variation is dominated by the measurement uncertainty at major principal strain magnitudes less than 0.5 and only when the measured strain approaches 1% it is controlled by the sample behaviour. Figure 4.19 shows that the coefficient of variation with strain decreases from its initial

value to a minimum and then settles down as the strain proceeds. Then with larger deformation the coefficient of variation starts to rise again. This is an indication of increasing non-uniformity in the sample as it approaches failure and indicates that sample deformation is increasing. However, for the three different tests the coefficient of variation is very similar.

4.4.1.6 Directions of principal stress and strain increment

The main feature of the DCDSC is the capability to apply shear and normal stresses to four faces of the sample. This provided for principal stress directions to be changed. The direction of principal stresses could be computed using the following equation (see Figure 4.5)

$$\tan 2\psi = 2\tau_a/(\sigma_a-\sigma_b)$$

in which ψ is the angle that the major principal stress makes with the Y-axis. Whereas the principal stress in each DCDSC test was calculated from the applied boundary stresses, successive radiographs made it possible to determine the principal strain increments from the displacement of the markers. Figure 4.20 defines the axes of principal stress and strain increment. If there was a fixed direction of major principal stress, then there should be coincidence of axes of stress and strain increment for an initially isotropic material.

The deviation of axes of principal stress and strain increment can be used as an additional indication on the performance of the DCDSC. Coincidence of the axes reveals the correct combination of normal and shear stresses being applied to the sample faces in order to achieve the assumed major principal stress direction. The deviation between the major principal stress and strain increment directions is defined in Figure 4.20. The experimental data for monotonic tests on dense sand at 14 kPa (Figure 4.21) showed a deviation of ±2° in the directions of principal stresses and strain increments which was an improvement to that of Wong (1986) which reported ±5°. Also there was no difference for the tests in which the boundary shear stresses were involved compared to those when no shear stresses were applied. Tests at 30 kPa on dense sand show a little more deviation (Figure 4.22).

4.4.1.7 Problems encountered in DCDSC testing

Testing in the DCDSC involved two types of stresses: the normal stresses were applied to the four faces of the sample through concertina designed flexible bags

and the shear stresses were applied across a sand/rubber interface via a pair of daisy chain shear sheets. Also the intermediate principal stress was applied through a de-aired water filled reinforced pressure bag. Due to the flexibility of these boundaries, the normal stresses were assumed to be equal to the internal air pressure acting in the normal pressure bags. This assumption allowed the states of stress to be calculated from direct pressure readings without the complication of corrections provided the normal pressure bags covered the four faces of the sample properly. This required the pressure bags to remain rectangular and follow freely the sample deformation. Furthermore there must be no interference between adjacent pressure bags and the normal pressure backing plates have to be positioned in correct locations from the sample faces throughout the test.

The correct positions of normal pressure bags were very important in applying the correct normal stresses to the boundaries of the sample. The bags must be properly inflated because if the bags were too close to the sample face they could cause an undesirable stiffness to the boundaries. Having the normal pressure bags away from the sample faces could result in the bags punching into the central part of the sample and consequently creating non-uniform strains. Table 4.1 illustrates an example of strain distribution of two dense samples of Leighton Buzzard sand monotonically sheared in DCDSC at R=6 under a minor principal stress of 14 kPa with sufficient lubrication on the top and bottom plane strain surfaces. The normal pressure bags backing plates were positioned at 17mm and 22 mm in ε_1 and ε_3 directions respectively for both tests and were kept constant throughout the sample deformation. A consistent non-uniformity of strain distribution within the sample can be seen which is an indication of non-uniform distribution of boundary stresses. Major and minor principal strains decrease towards the centre of the sample. This problem was solved when the appropriate position for initial setting up of normal pressure bags were found to be 19 mm and 22 mm.

The manual incremental adjustment of the boundary normal stresses could be problematical, because it was subjective and chiefly involved the operator's judgment. It is interesting to note that over-adjustment of the boundary normal pressure bags provided a uniform distributed disturbance over the boundary of a loose sand sample and resulted in a uniform distribution of strain but a lower shear strength of $\phi_f = 32°$. This sample was prepared in an identical geometrical packing as other loose samples and was subjected to the same loading geometry. Figure 4.23 illustrates the stress strain curve and Figure 4.24 shows the strain distribution within the sample at R = 3. Although the sand was more contractive initially compared to the usual loose

test, the angle of dilation for the final stress increment just before failure was measured at 4.5° which was very close to that of 5° measured by Wong (1986). However, when one considers the boundary adjusting mechanism, it is clear that the adjustment action is likely to produce some destabilizing effects to the sand structure. The adjustment, though performed in minute increments, is a sequential action rather than a simultaneous one. The importance of stable contacts in the way a granular sample supports an externally applied load has been highlighted by photo elastic studies (e.g. Drescher and De Josselin de Jong, 1972; Oda and Conishi, 1974) and also by computer simulations of the deformation of granular materials subjected to applied loads (e.g. Cundall and Strack, 1983). Therefore, for the loose sample tested in this condition in the DCDSC one could suggest that, as the sample attains equilibrium under an applied load increment, a wave of instability is further introduced into the sample as the adjustment of the normal pressure system is performed. Since in a loose structure there could be a minimum number of contact points between the particles that could be just sufficient to maintain a stable structure, this instability leads to particles with less efficient distribution of contact forces and a softer stress-strain response than would normally be associated with a sample of such packing. A similar value of ϕ_f =32° was obtained for a loose sample tested in Biaxial Tester by Ogunbekun (1988) where the sample was tested in a natural plane strain condition and all boundaries of the sample were adjusted through an incremental adjusting mechanism without imposing any related loads on the sample.

The author believes that the position of normal pressure bags and even the number of normal pressure bag segments were only crucial because of the manual adjustment of the normal pressure system in DCDSC. Figure 4.17 shows substantial uniformity in distribution of strain within a dense sand sample monotonically sheared when a normal pressure system consisting only two segment pressure bags was employed. This indicated that as the operational skill improved the number of normal pressure bag segments could be reduced from four to two and possibly even one, if the pressure bag was correctly inflated and adjusted as the sample changed shape. However, as stated before, an ideal and precise adjustment of the boundary normal stresses and alignment of shear sheets could only be possible if carried out automatically.

The overlapping of adjacent normal pressure bags also could produce a reduction in the total applied stress along the sample. This could be minimised by applying a generous amount of grease in between the touching areas. The presence of

lubricated shear sheets also helps to eliminate the overlapping problem.

Effects of rigid corners and shear sheets mis-alignment

Incorrect edge stresses, in addition to the effects already described in relation with normal stresses, could easily induce progressive extensive failure at the corners especially when ψ=45°. In earlier versions of the DSC rigid corner prisms were employed to prevent instability in these corners. However, the problem using this type of corner in the DCDSC was that as the sample deformed and changed shape, the boundaries of the sample were locally restrained and could not change shape with the deforming sample in the two corners containing the rigid prisms, this resulted in a discontinuity along the boundaries (Figure 4.25). Also the pulling sheets alignment was distorted and the sheets were pushed away from the sample face resulting in a reduction of normal stresses in these areas. In the DCDSC since the non-stretching component is relatively thin (3mm), compared to the earlier versions of the DSC (8mm), the pulling is performed very close to the boundaries of the sample, and any deviation from the correct alignment could cause serious problems. In the earlier version pulling is performed rather away from the boundaries and a larger deformation at the corners is possible before interfering with the pulling sheets alignment.

In order to solve the problem one shear strip within 5mm of the edge and the rigid aluminum corner was removed and the deformable corners were replaced. To provide a failable corner the sample membrane was reinforced with fabric around the corner, and within the membrane two aluminum strips were glued to the orthogonal inside faces close to the corner (Figure 4.26a). The angle of these corners could now change with the distortion of the whole sample (Figure 4.26b); the aluminum strips were also needed to provide a small end restraint so that pre-failure non-uniform strains could not develop near the edges. Figure 4.27 illustrates a test in which the aluminum corners were removed and the sample membrane was reinforced only with a polyester fabric. In this case a small variation in load could produce large strain in the central plane of the deforming sample.

It was mentioned in Chapter 2 that lateral expansion of concertina type normal pressure bags could easily mis-align the pulling sheets. To solve this problem thin spring steel semi-rigid retaining vanes were used. A correct positioning of the retaining vanes were important throughout the shearing process; close positioning of the vanes could prevent the sample being strained. Figure 4.28 illustrates a correct

position of retaining vanes, this position should be kept constant throughout shear.

Effect of normal pressure bag on σ_2 bag

In the prototype DCDSC σ_2 bag was circular with an area of 215cm^2 and the area of the sample was 100cm^2. Therefore the sample occupied only about 50% of the area of the σ_2 bag. The area of σ_2 bag not in contact with the sample which was directly beneath the normal pressure bag and through this contact area the intermediate principal stress could be effected. Figure 4.29 illustrates a procedure in which this effect was observed. In this procedure a dummy sample was placed in the cell and an isotropic stress of 14 kPa was applied to the sample, the σ_2 bag was then isolated to keep the volume constant. The normal stresses were then incremented and σ_2 was found to be responding linearly to the change in pressure. The influence of the normal pressure on the σ_2 bag could invalidate the tests in which intermediate principal stress was monitored. This type of test could only be carried out where the normal stress did not interfere with the σ_2 pressure. In order to overcome this problem a smaller re-inforced σ_2 bag of 130 mm diameter was used and almost all tests were carried out in the mode in which the intermediate principal stress was controlled.

It can be concluded that to operate the DCDSC properly, provide element tests and to prevent any possible false stiff stress-strain response or premature failure the operator must patiently and carefully make sure that:

a) the sample is prepared in a uniform and homogeneous manner and the correct negative pressure is applied to the sample.

b) the sample faces are degreased properly and the sample is centrally positioned on a very slightly pressurized well lubricated σ_2 bag which is covered with two greased thin rubber sheets.

c) a small amount of grease is applied to the corners where the shear sheets interweave; the shear sheets are cleaned thoroughly and adhered properly to the sample faces; the shear sheets and their tails are lightly lubricated.

d) the normal pressure bags are adequately greased, covered with two lubricated thin rubber sheets cut to size, placed in a correct position from the sample face and their vanes are located correctly.

e) the top plane strain boundary is sufficiently lubricated and placed precisely horizontal on the sample and locked.

f) the shear sheets are properly aligned and the shear pistons, guiding shaft and rollers are lubricated sufficiently.

Testing procedures should be conducted gently and in a precise way i.e.-: the stresses are calculated for desired stress paths and applied in very small increments, normal stress should always be increased before the shear stresses; the shear sheets should be aligned and the normal pressure bags adjusted very carefully.

Radiographs should be taken whenever required, developed and the state of deformation be checked prior to application of next increment.

4.4.1.8 Verification of the apparatus performance

From the monotonic tests data presented in this section it could be observed that the DCDSC is capable of yielding apparently reliable stress-strain data on loose and dense sand samples.

Figures 4.8 and 4.14 illustrate the stress-strain curves and volumetric response of dense Leighton Buzzard samples sheared with different fixed orientation of major principal stress direction from ψ=0 to ψ=90° at two different stress levels. Although there are clear differences between stress-strain relationships at the two stress levels there are no significant variations with ψ.

The results show that good repeatability was achieved during the research not only with the operation of the DCDSC but also with sample preparation, strain measurements and operator control. The reproducibility is also confirmed where the data of two different types of DSC are compared, see Figure 4.12 for dense sand. Also Table 4.2 indicates a good agreement in angle of failure obtained using the DCDSC, and with other shear testing apparatuses at low stress levels.

Analysis of strain distributions throughout the samples which were obtained from internal measurements also provided a means of assessing the performance of the DCDSC. The strain data used in studying the material behaviour was obtained from the central 25% area of the sample and described as Area 2. Three examples of strain distributions for dense and loose samples at stress ratios close to failure are illustrated in Figures 4.11, 4.17 and 4.18. Figure 4.19 illustrates a comparison of the coefficient of variation in strain distribution for three samples tested at different fixed major principal stress directions of ψ =0°, ψ =30° and ψ =45°. This figure shows a good uniformity and comparability with results obtained by Wong and Arthur (1985b). These authors obtained coefficients of variation between 0.15 to 0.25 at major

principal strains of 3% for the dense samples tested in the DSC with major principal stress directions at ψ = 0°, 30° and 45°. This confirmed that samples exhibit the same coefficient of variation irrespective of imposed principal stress direction. A similar range of uniformity was also found on homogenously prepared sand samples tested in a large triaxial apparatus by Phillips (1972). Also coincidence of the axes of the major principal stress and strain increment are confirmed in Figures 4.21 and 4.22.

Results show that the DCDSC deforms the sand samples with a degree of uniformity comparable to other apparatuses.

4.4.2 Special plane strain membrane tests

A series of monotonic tests were performed to investigate the effects of boundary constraint on the stress-strain behaviour and shear strength of dense Leighton Buzzard sand.

Usually boundary friction on the plane strain boundary surfaces is effectively reduced by using layers of grease separated by thin layers of rubber (e.g. Arthur and Dalili, 1979; Tatsuoka and Hibara, 1985) or alternatively by stretching the plane strain boundaries independently of the sample (e.g Arthur et al. 1985 and Ogunbekun, 1988). Here thick membranes were used to constrain the sample on the plane strain boundaries. The constraint revealed an unrecognised aspect of particulate material behaviour. The particulate nature of granular materials leads to inhomogenieties in deformation; discontinuity is inevitable at the level of individual particles and higher levels involving groups of particles. For particulate materials, the continuum concept of stress is an idealization of contact forces distribution; these are usually far from uniformly distributed over existing contacts. The large and continually changing inhomogenieties in contact forces regularly observed in photo elastic disc experiments and in computer simulations of deforming granular materials support this assumption (e.g. Oda and Konishi, 1974; Cundall and Strack,1979). At the boundaries of samples used in element tests, the individual contact forces often appear to adjust to establish an approximation of continuous stress. These special plane strain membrane tests in the DCDSC have drawn attention to the effects of forces applied to individual particles at the boundaries.

Specially prepared thickened rubber membranes were incorporated on the plane strain sides of the sample membrane. Tests were carried out at σ_3=14 kPa and

ψ=90°, with no shear sheets around the sample which eliminated the possible boundary restraint induced by the presence of unstressed shear sheets. These tests were conducted using the conventional method of lubrication. One set of tungsten balls was placed close to the plane strain face and the other on the central plane to compare the strain distributions in both regions. The thick membranes were glued to the sample membrane using Evo-stick to ensure a proper bonding (Figure 4.30).

Figure 4.31 illustrates the stress-strain curve for three different tests, in which membranes with thicknesses of 1.6 mm, 2.10 mm and 3.60 mm were used on the plane strain surfaces. A stiffer response was observed and the samples failed at a higher stress ratio, i.e. R=9.4, although the volumetric deformation was not affected by the constraining mechanism. Also beyond a comparatively low limit, increasing the thickness of rubber had no effect on the stress-strain behaviour. Figure 4.32 shows the stress-strain curve and strain distribution within the sample. Comparison of strains measured in the central plane of strain with those measured close to the edge indicate rather good uniformity of strain in spite of boundary constraint, certainly as good as comparisons of end and central plane strains for tests giving the accepted values of ϕ carried out by Wong and Arthur (1985).

It is interesting to note that conducting a series of plane strain tests using a special plane strain apparatus (Ogunbekun, 1988) illustrated the large effects of the de-constraining mechanism on the stress-strain behaviour of Leighton Buzzard sand. The device he used has become known as the Biaxial Tester (BT) and has been fully described by Arthur et al. (1985) and Ogunbekun (1988). The Biaxial Tester is a flexible boundary plane strain apparatus capable of incrementally adjusting its boundaries to accommodate the sample boundaries deformation, the process is illustrated in Figure 4.33. The effect is to adjust the boundary strains to follow those on the central axes of the sample and apply the correct stresses to the whole of these boundaries. This is achieved without applying any net sample loading through the boundaries because the rubber membranes are stretched or released to their new dimensions by an external mechanism. Moreover as the surfaces of the sample and pressure membranes are degreased the normal pressure across them bond the two together so that the same external mechanism also changes the dimensions of the sample membrane. When desired, a similar process of unrestraining of the boundaries could be extended to the plane strain surfaces by rubber sheets in contact with the sample ends and stretched uniformly.

Figure 4.34 illustrates typical stress-strain curves for the Biaxial Tester in which the

top and bottom plane strain rubber sheets were stretched. In this figure, a comparison of strains measured in the central plane of strain with those measured in plane of strain near the plane strain surfaces are also demonstrated, indicating rather good uniformity of strain. This figure shows that the use of these plane strain sheets produces a considerable reduction in stiffness and shear strength. It should be noted that the results with the normal form of lubrication (three layers of silicone grease separated by two thin rubber membranes) correspond closely to that of DCDSC tests with normal lubricated ends. This indicates that the matching boundary strain on the faces applying σ_1 and σ_3 have a negligible effect compared to that of plane strain ends.

Figure 4.35 summarises results from the Biaxial Tester, the DCDSC with standard lubrication and thin plane strain membrane and those from the DCDSC with thickened rubber on the plane strain faces. In all cases the dilation rate was the same but there were significant differences in stress-strain behaviour. This illustrates the significant effects of restraints on the plane strain faces.

It can be summarised that tests conducted in the DCDSC and the Biaxial Tester were made on initially homogeneous samples in flexible boundary devices which applied uniform boundary stresses. The uniform distribution of strain within the samples established that all were true element tests in spite of the constraining and deconstraining effects in the plane strain boundaries. It can be concluded that the differences in boundary conditions produced rather uniform yet different contact force distributions within the sample which suppressed inhomogenieties in deformation to a quite surprising degree without altering the dilation rate. The most interesting feature of Figures 4.8, 4.31 and 4.34 is that they show that the volumetric strain at which rupture (frictional slip) intervened was the same for all tests regardless of the plane strain end conditions suggesting that geometric unlocking controls the initiation of frictional slip.

4.5 SIMPLE PLANE STRAIN MODEL TESTS

Two classical plane strain model experiments, failure of the active retaining wall and the tilting slope, were used to obtain an independent measurement of the shear strength of Leighton Buzzard sand at very low stress levels. These tests were used to evaluate the performance of the DCDSC and to establish that there was no appreciable variation in shear strength with stress level at very low stress levels.

In these tests the samples were prepared by raining at a slow rate for dense samples and rapid mass tipping from a scoop for loose samples. Surfaces were levelled by carefully controlled suction of grains using a vacuum pump.

4.5.1 The active retaining wall failure

Figure 4.36 illustrates the ideal active wall experiment. For dense sand, which was deposited slowly, it was possible to lay horizontal layers of dyed sand and define the rupture, but loose sand could only be achieved by dry rapid scoop tipping, so a long hypodermic needle was used to introduce ink lines, and the rupture layer could be detected from these lines.

The linear break out of the failure wedge on the sand surface indicated that there was no appreciable side friction. Glass was also used on the front face of the wall. All tests on loose and dense sands exhibited straight rupture layers from the toe of the wall to the surface. Although the final form of rupture layers looked similar, the process to reach these states were different. In dense sand the final rupture layer formed rapidly after small displacement, whereas in loose sand a fan of shear deformation gradually changed to a thin rupture layer.

The two boundaries of the rupture layers were recorded as coordinates and a regression analysis used to find the rupture layer orientations; Figures 4.37 and 4.38 illustrate this for dense sand. The averaged results are shown in Table 4.3 for both loose and dense conditions. This table shows results in two forms: uncorrected, and corrected for anisotropy. Phillips (1975) showed that correction for strength anisotropy is negligible for loose sand. For dense sand the correction for anisotropy is based on the plane strain data of Arthur and Assadi (1977) shown in Figure 4.39. For the active wall the direction of pouring was zero (δ=0°) and the value of ϕ could be reduced to an equivalent value for a sample deposited normal to the subsequent plane of strain by the measured value by the ratio 49.3/50.8. The correction factor here is 49.3/46 giving $\phi_{corrected}$ =47.9 x 49.3/46= 51.3°

4.5.2 Infinite slope stability model tests

In a wide range of tests carried out at UCL (Arthur et al. 1988 and Ogunbekun, 1988), horizontal beds of dense and loose sand were placed on horizontal trays of suitable dimensions and tilted until failure occurred (Figure 4.40). The angle in which slip occurred was interpreted as the angle of friction according to infinite slope

analysis.

These tests employed a method suggested by Habib (1986). Habib identified two different failure mechanisms in model tilting tests. When a mass of dry densely prepared bed of sand was tilted, a progressive "avalanche" type of failure occurred with a low angle. This type of failure was initiated by a small local slip which immediately back sapped and propagated laterally to produce complete failure. To deter this "avalanche" type of progressive failure the surface grains should be prevented from loosing equilibrium. To do this, the surface of sand was wetted by a fine spray of water before tilting, this made the surface layer cohesive and the local surface failure could not occur. Consequently failure occurred simultaneously throughout the dry sand beneath.

In the case of loose samples, sand did not show this local failure phenomenon because the surface was strengthened by the disturbance of the suction process used for levelling the surface after preparation. However, large mass strains at failure tended to blur the angle of failure. This problem was solved by using a long tray of 1500 mm and inserting a ramp of 30° at the end of the tray as illustrated in Figure 4.40. The ramp provided a ready made exit line for the rupture, previously sand compressed at the lower end prior to failure. The effects of side restraint were minimised by using very wide trays.

In the tilting tests it is not possible to define the direction of principal stresses. However, the results of tilting tests could be compared with that of the active wall test which has a secure interpretation. In the tilting tests, the rupture plane is parallel to the bedding plane, and aligns with the plane of maximum stress obliquity and, using this assumption, very reasonable agreement with the wall result is found for both the loose and dense sand. A similar form of correction could be used for the tilting slope data as was used in the active wall. In this case $\delta = 45 + \phi/2$. Taking ϕ, measured from the slopes gives $\phi = 47.9°$ and $\delta = 69°$. The correction factor here is 49.3/46 giving $\phi_{corrected} = 47.9 \times 49.3/46 = 51.1$.

It is commonly accepted that the rupture planes in these tests orientate themselves according to Coulomb's prediction at $(45° - \phi/2)$ to the major principal stress direction and the results could be interpreted on this basis. Results as measured and corrected for anisotropy using Arthur and Assadi's relationship (Figure 4.39) are given in Table 4.4 together with similarly corrected results for the wall test from Table 4.3. The strength data presented in these tables refer to ultra low stress levels

in the region of 0.5 kPa to 3.0 kPa. This extends the range over which negligible effects of stress level have been reported (Fukushima and Tatsuoka, 1984; Hettler, 1985; and Tatsuoka et al., 1986).

4.5.3 Discussion on the boundary effects at low stress level

Figure 4.35 presents the main stress-strain data for the central planes of strain of three types of tests under different boundary conditions. From the data there appears to be three groups of results with three different peak shear strengths depending on the level of restraint on the plane strain surfaces for the samples with the same initial packing; a low value, an intermediate value and an upper value, for samples with the same initial packing. The intermediate shear strength agrees well with the accepted value of ϕ measured by several other apparatuses at comparable stress levels (e.g. Stroud, 1971; Arthur and Assadi, 1977; Wong and Arthur, 1987; Jewell and Wroth, 1987; and Ogunbekun, 1988). The other two groups show that ϕ is either raised or lowered by about 5° with corresponding differences in pre-failure stiffness. It should also be noted from Figure 4.35 that none of the tests showed significant differences in dilation rate. All samples failed by the formation of rupture layers. This poses the question : which one is the real shear strength?, or which strength is applicable to which practical situations? Some discussion of these questions has been prepared in a paper by (Arthur, Dunstan, Dalili, Ogunbekun and Zadekochek, which is to be published. Here discussion is limited to the assessment of the DCDSC performance. The results of the slope stability tests in which the progressive surface failure was allowed to develop (ϕ_f=42.9°) presents an immediate example of the lower value of shear strength. The angle of failure defined by the slope of the linear envelope to the Mohr circles in the deconstrained condition was the low strength with ϕ_f=42° (Ogunbekun, 1988). The friction angle associated with the intermediate level of constraint was ϕ_f=48.5, which corresponds to the results of infinite slope stability tests in where the progressive failure was deterred by preventing surface failure ϕ_f=51.1°. The results of wall experiments gave ϕ_f=51°. This suggests that in many practical situations it is most likely that the intermediate value of shear strength (ϕ_f) would be the applicable parameter as there is unlikely to be any deconstraint. This lateral restraint is generated internally by the material itself as a result of the inherent inhomogenieties in deformation and contact force distribution. This brings the realisation that the long established belief of experimentalists that perfect lubrication and leading to zero friction on plane strain surfaces was the ideal for an element test may be incorrect. There remains the requirement to achieve the "correct" degree of restraint; the most obvious way to

check this is to carry out tests on samples with different widths in the intermediate principal stress direction.

The formation of rupture layers in samples with virtually identical dilation rates at quite different stress ratios suggests that the controlling condition is reaching maximum dilation in continuum strain. The different boundary conditions by which the extreme stiffness and strength results were obtained suggests that these may be true limits.

It is interesting to note that the effects of boundary constraint is more profound in the case of the loose sand samples. There appears to be two different values of shear strength for two different boundary conditions, Figure 4.41. A value of approximately ϕ_f=38° is obtained in DCDSC samples when normal lubrication is used on the plane strain boundaries and the boundaries are adjusted in the normal way that already has been explained in Chapter 4. This value of shear strength agrees well with the accepted value of ϕ' measured in other devices at similar stress levels (e.g. Stroud, 1971; Rodriguez, 1977; Arthur and Assadi, 1977; Wong, 1986; and Ogunbekun, 1988). However, this value is higher than those found for loose samples tested in the wall and tilting experiments, here ϕ_f= 30°. On the other hand when the boundaries of the samples were adjusted incrementally and more lubrication was used on all boundaries, a lower value of 32° was observed. Obtaining this lower shear strength could be attributed to the destabilising effects introduced by the boundary adjusting mechanism. The same value of 32° was observed by Ogunbekun (1988) in Leighton Buzzard sand of similar voids ratio in the Biaxial Tester where the samples were tested in a natural plane strain condition and all boundaries of the sample were adjusted through an incremental adjusting mechanism. This implies that the lower values obtained in the deconstraining conditions either in DCDSC or the Biaxial Tester could be the correct strength for the loose specimens as these are closer to the values obtained in the wall and tilting experiments.

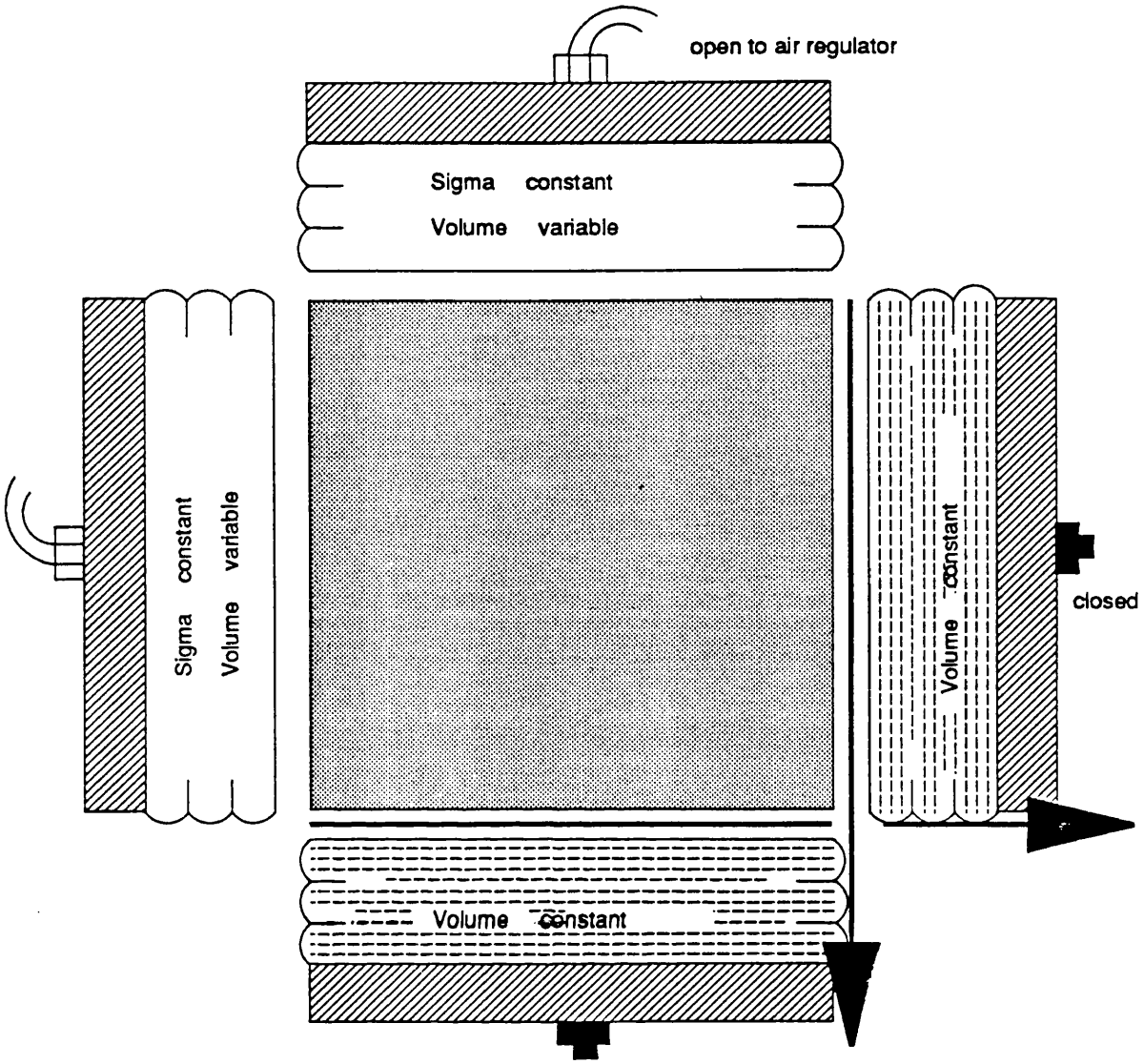

Fig. 4.1 The experimental arrangement for shear sheet calibration

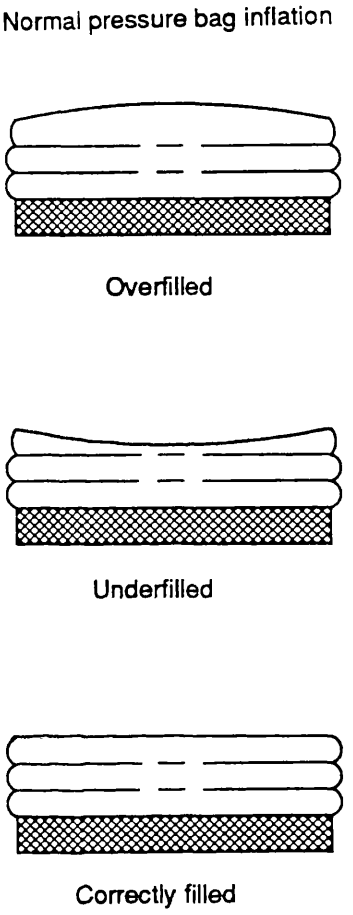

Fig. 4.2 The effects of different volumes of water in a normal pressure bag used to calibrate the shear sheets

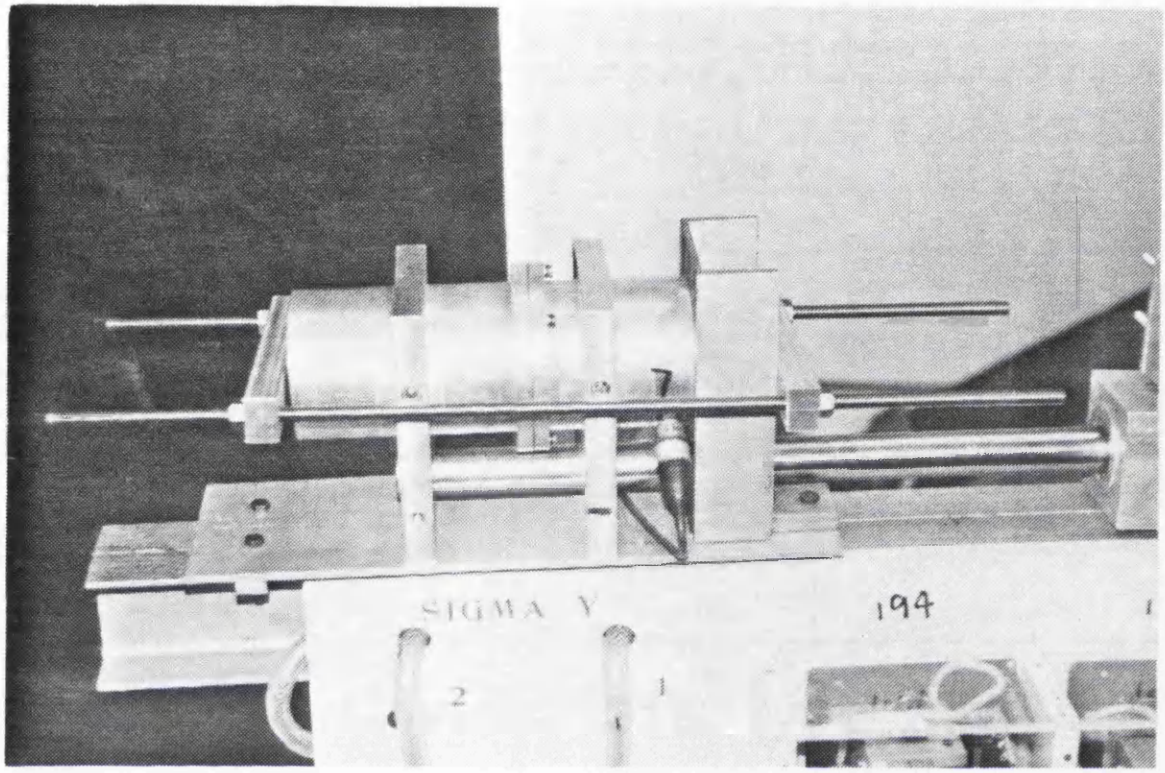

Fig. 4.3 The method used to calibrate the shear piston transducers

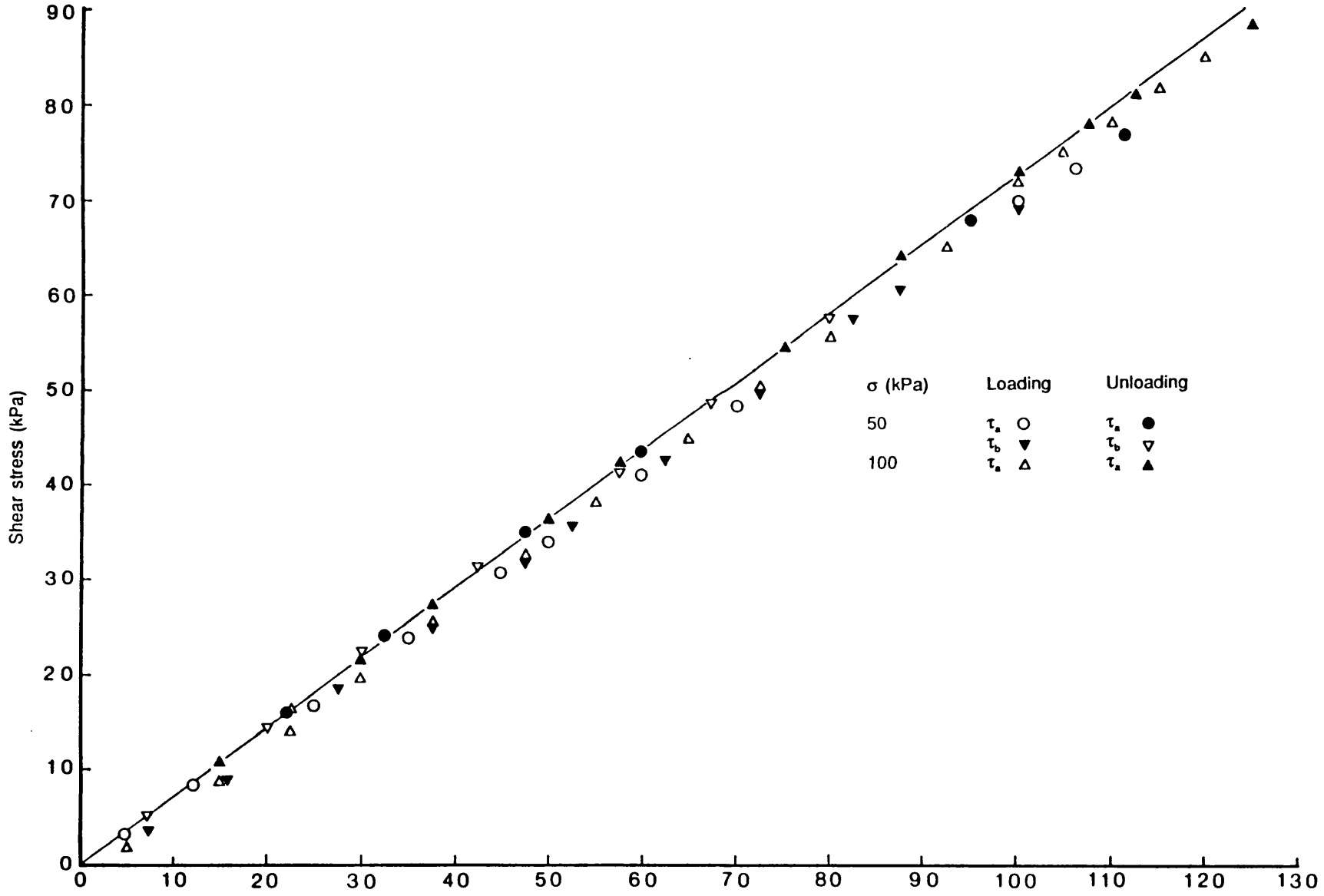

Fig. 4.4 The theoretical and experimental results of calibration of the shear sheets

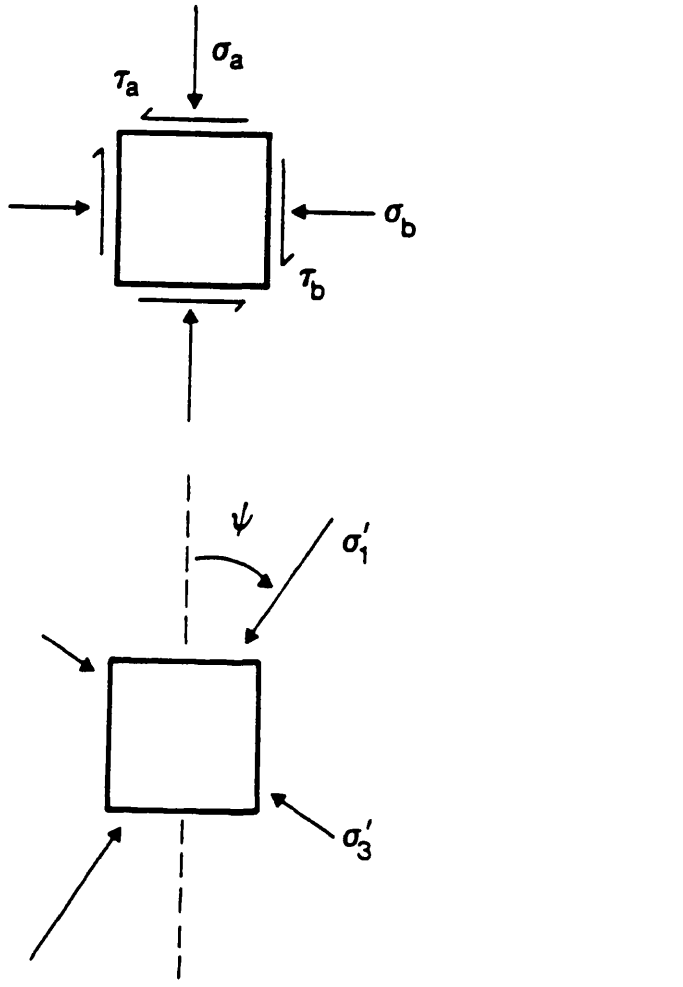

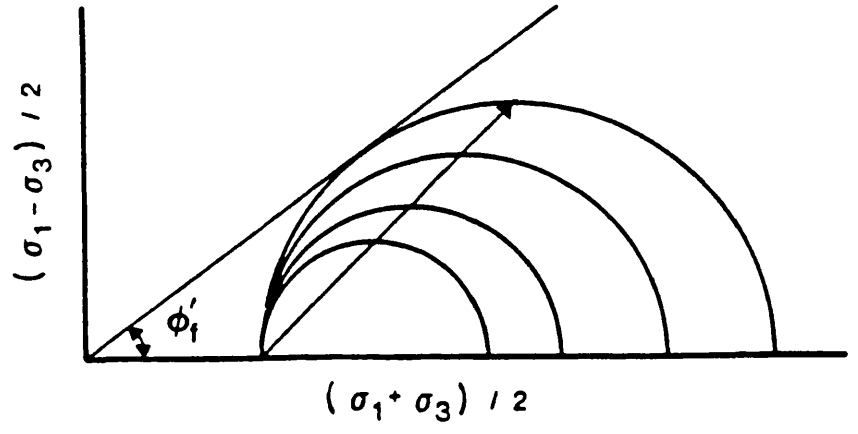

Fig. 4.5 The major principal stress direction and stress path in monotonic shear tests

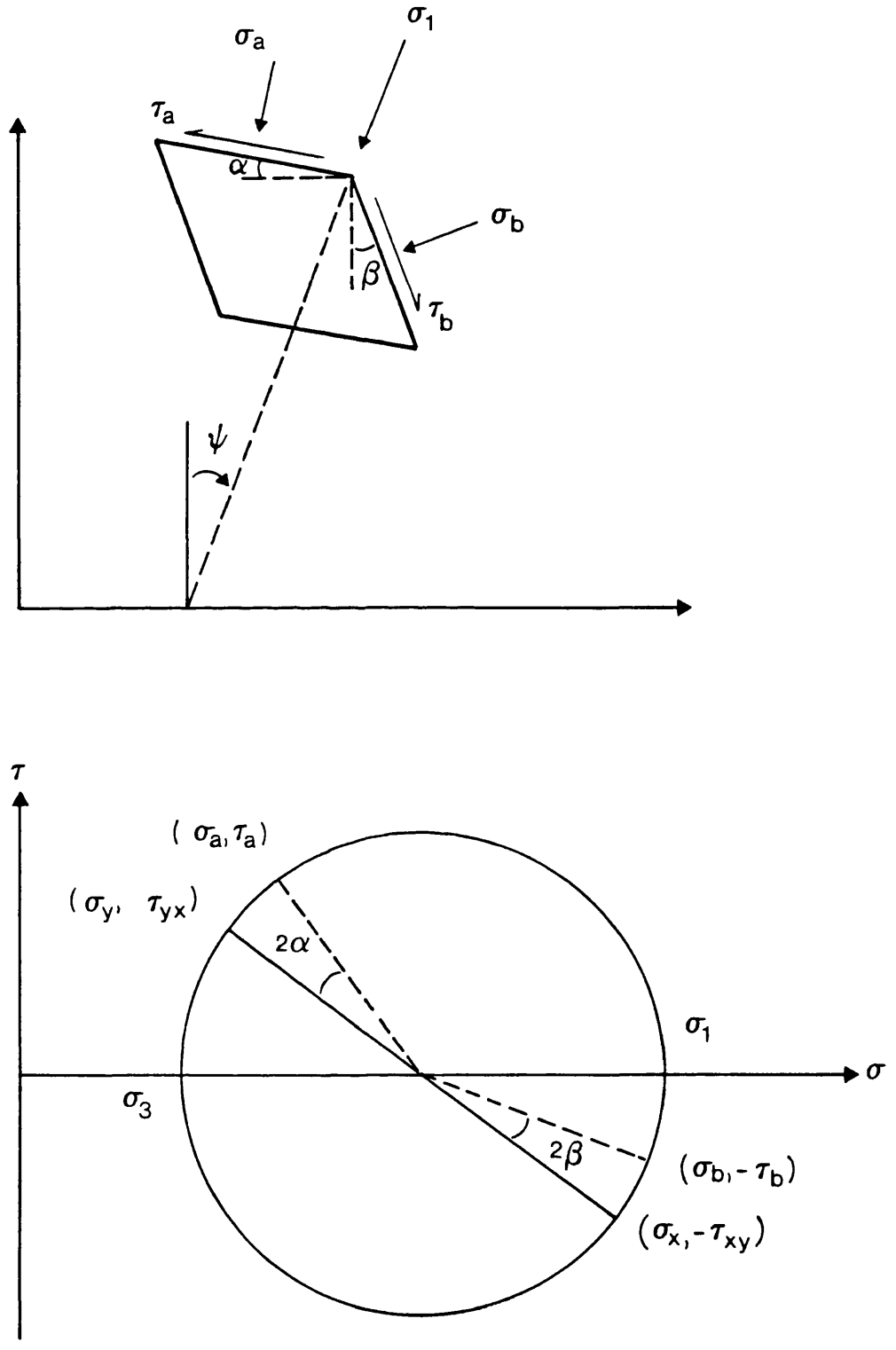

Fig. 4.6 Correction for angular distortion of a deformed sample during directional shear testing

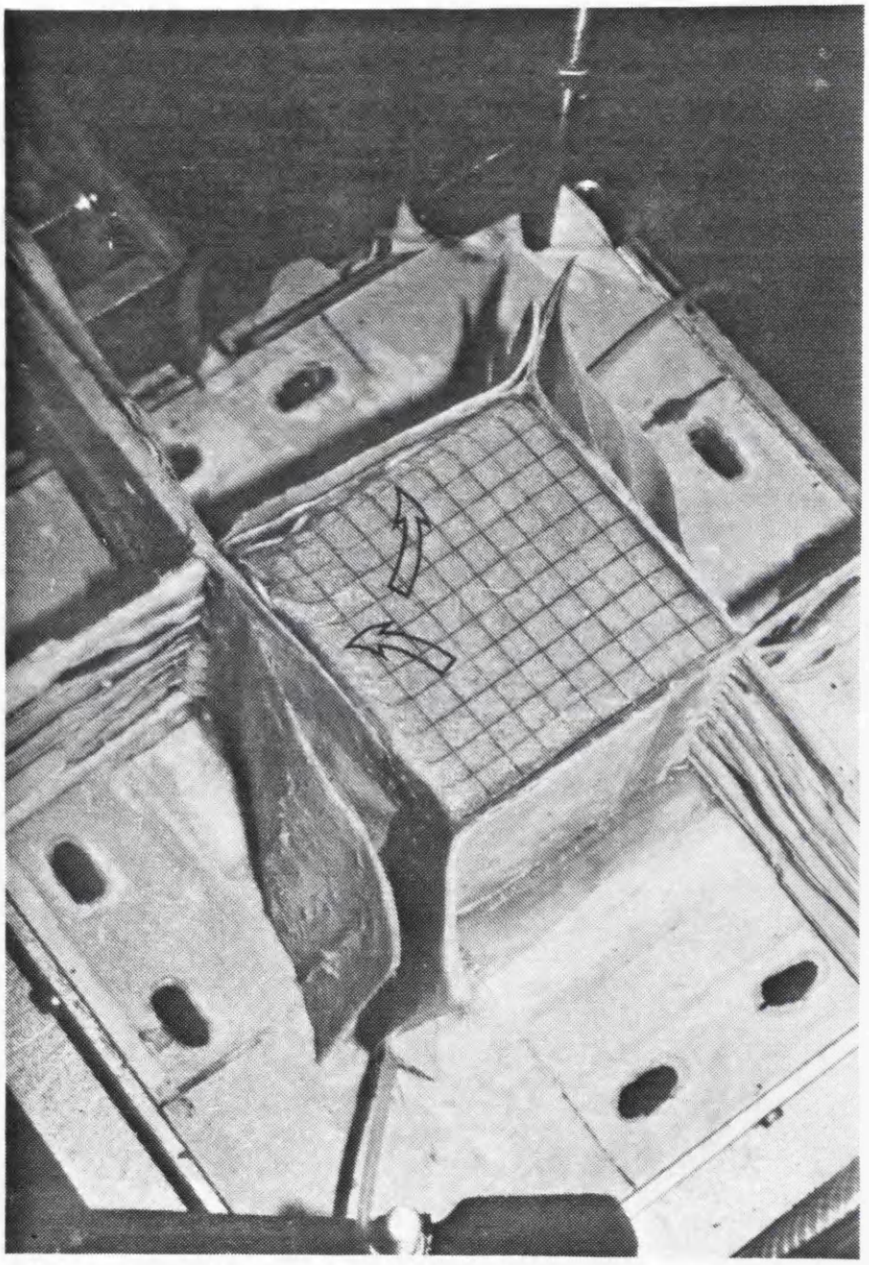

Fig. 4.7 surface failure in the boundaries of dense samples of Leighton Buzzard sand sheared monotonically at σ_3= 60 kPa.

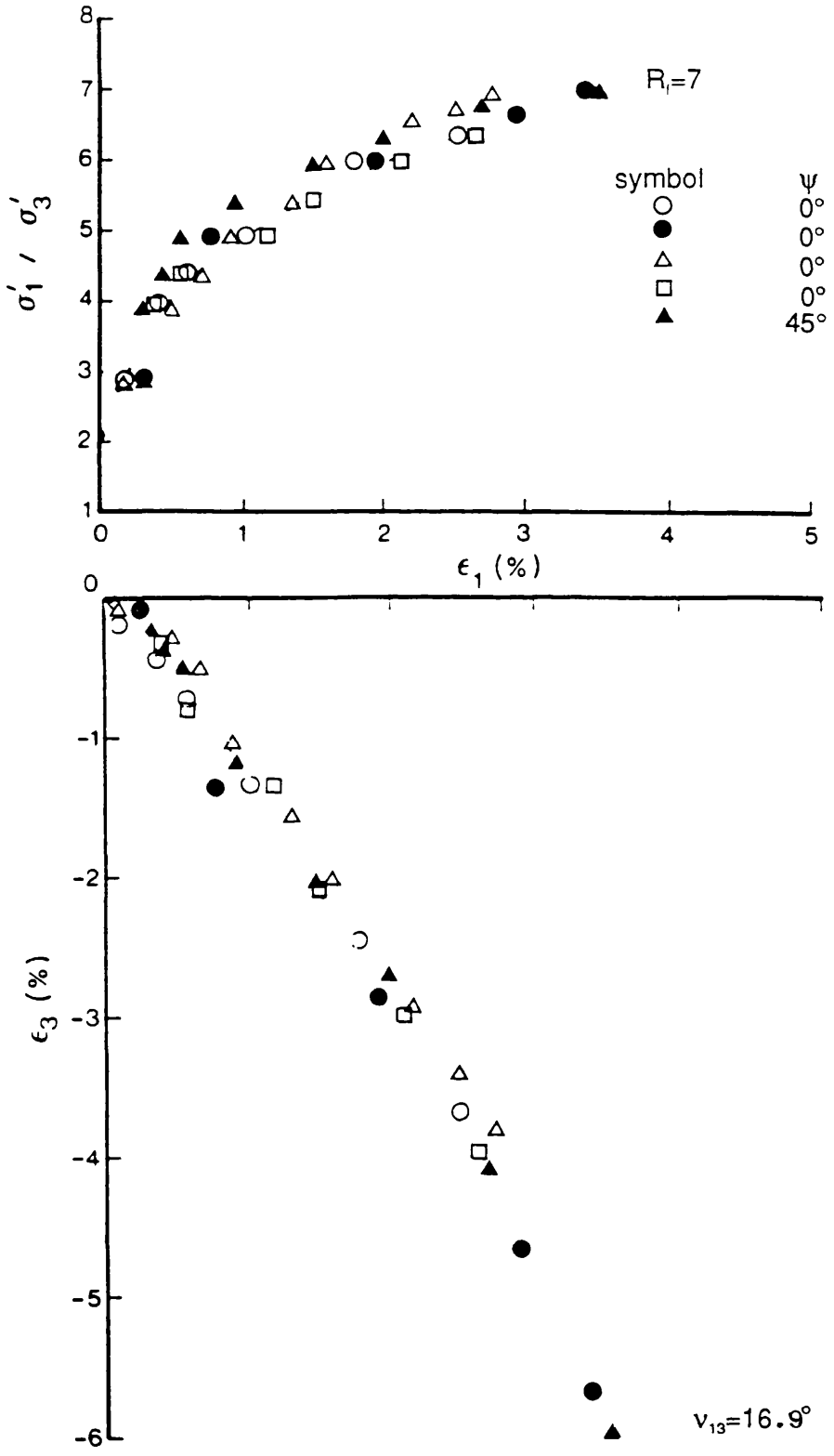

Fig. 4.8 Stress-strain and deformation response of dense samples of Leighton Buzzard sand monotonically sheared in the DCDSC with sufficient lubrication on plane strain surfaces at σ_3=14 kPa

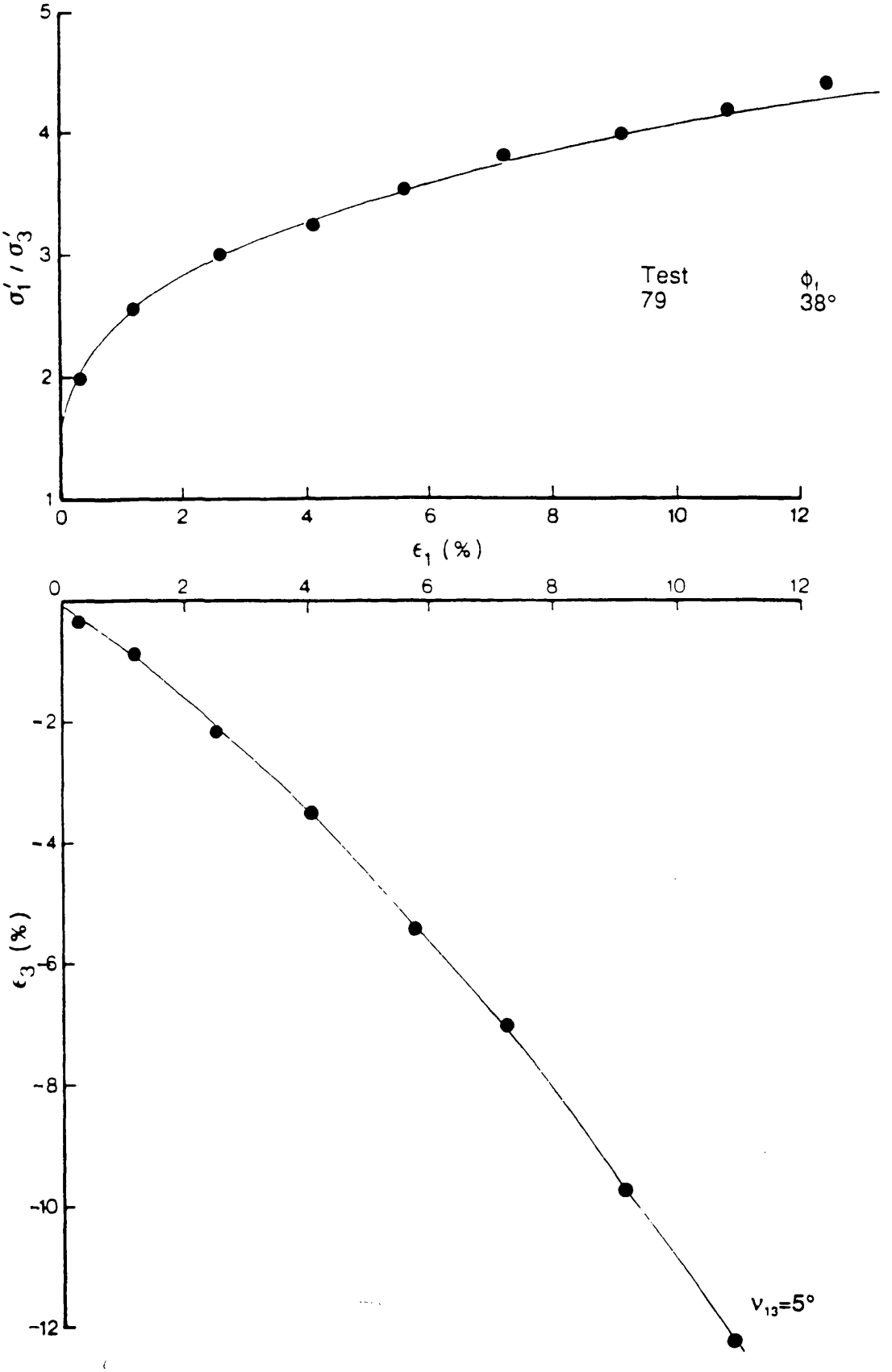

Fig .4.9 Stress-strain and deformation response of loose sample of Leighton Buzzard sand monotonically sheared in the DSC with sufficient lubrication on the plane strain surface at σ_3=14 kPa

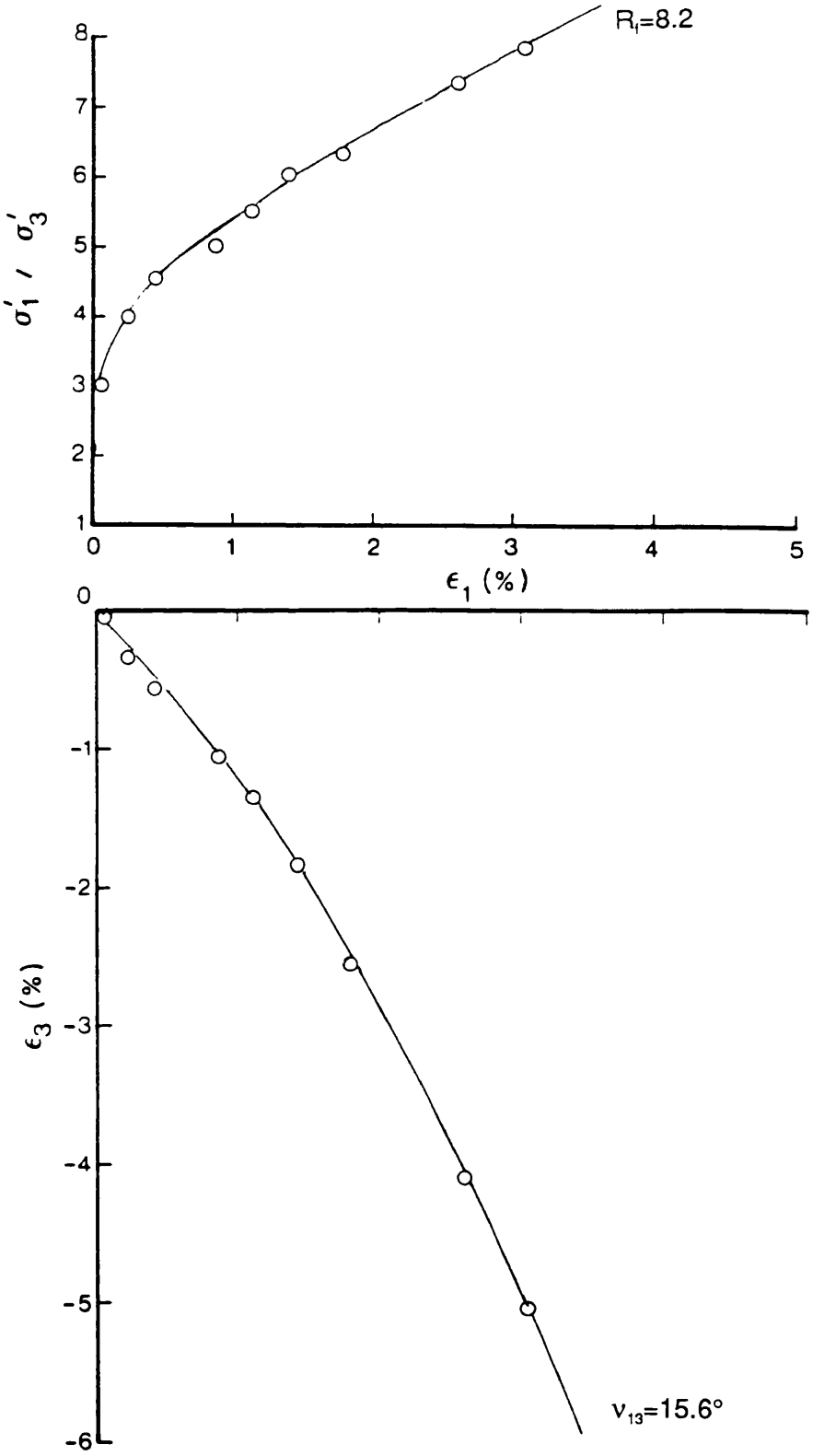

Fig. 4.10 Effects of unstressed shear sheets surrounding the sample on stress-strain behaviour of dense sand in the DCDSC at σ_3=14 kPa and ψ=90

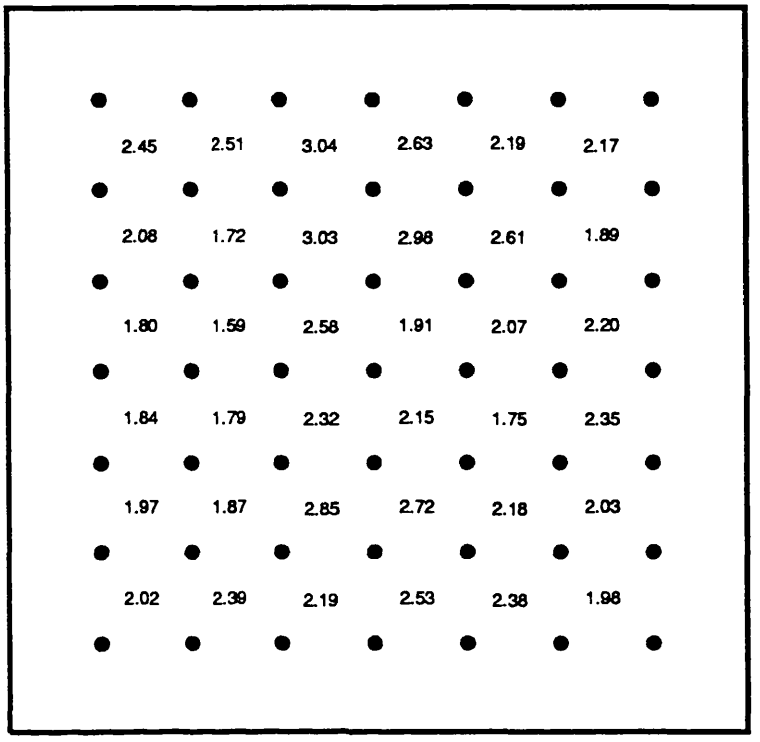

Major principal strain ε_1 (%)

Ave in Area (1): 2.24% with standard deviation : 0.39%
Ave in Area (2): 2.26% with standard deviation : 0.48%
Ave in Area (3): 2.26% with standard deviation : 0.28%

Principal Stress Ratio =7.0
Principal stress Direction =90°
Principal strain Direction =91.°

Fig. 4.11 Example of strain distribution within the dense sample of Leighton Buzzard sand sheared monotonically in the DCDSC which was confined with unstressed shear sheets at σ_3= 14 kPa

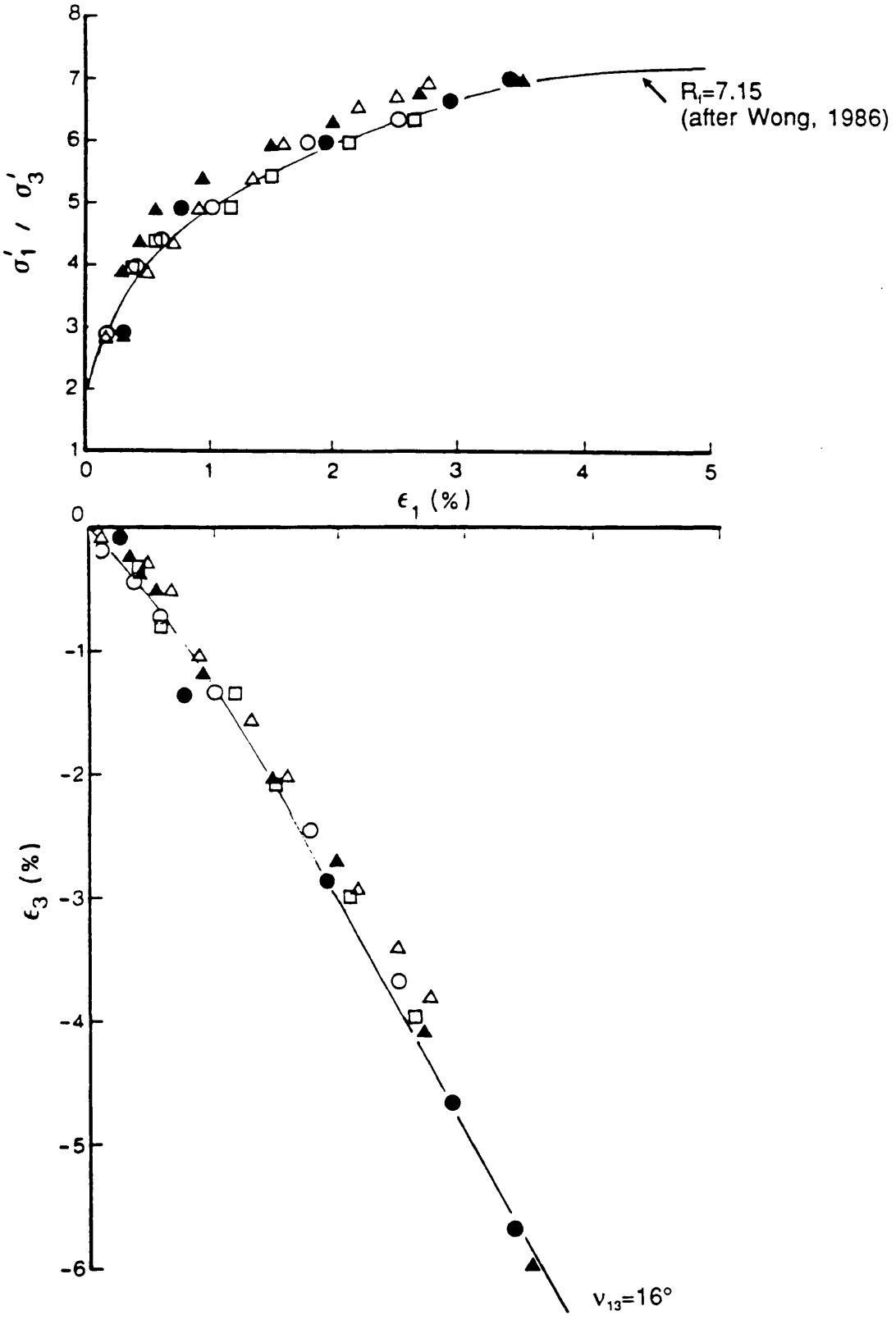

Fig. 4.12 Comparison of stress-strain deformation behaviour of dense sand samples monotonically loaded in the DCDSC and the earlier version of DSC at σ_3=14kPa

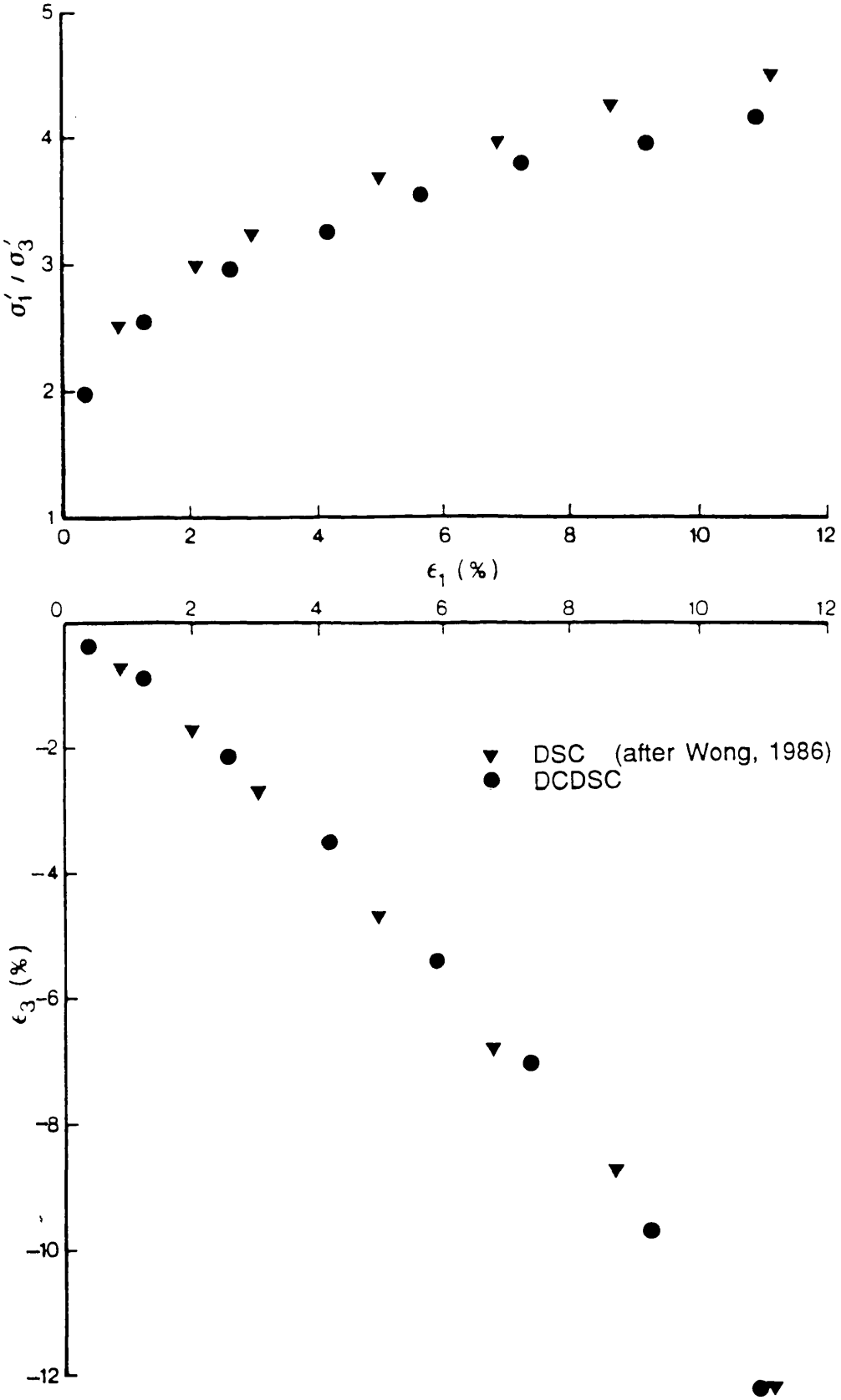

Fig. 4.13 Comparison of stress-strain deformation behaviour of loose sand samples monotonically loaded in the DCDSC and the earlier version of DSC at σ_3=14kPa

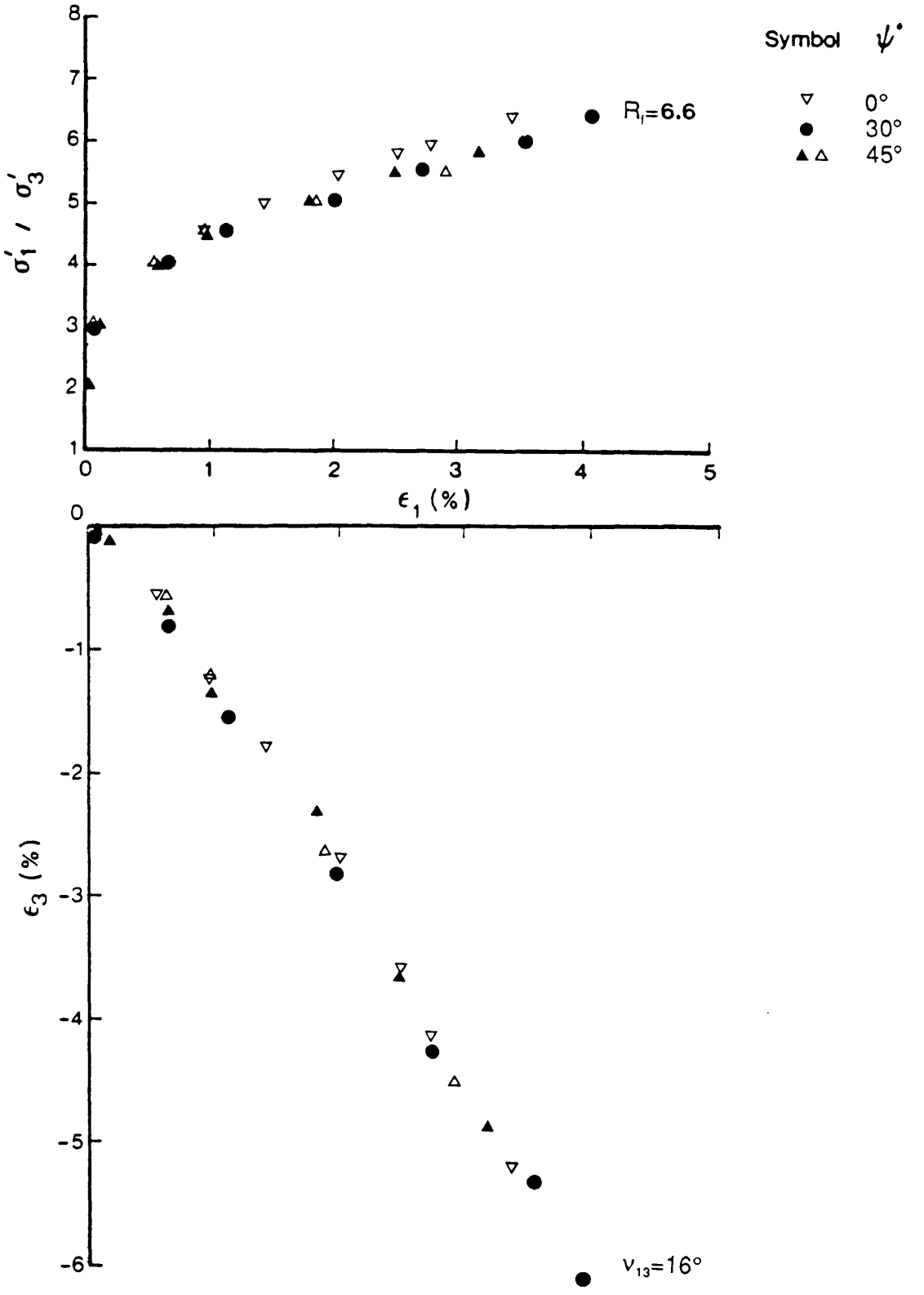

Fig. 4.14 Stress-strain and deformation response of dense sample of Leighton Buzzard sand monotonically in the DCDSC with sufficient lubrication on the plane strain surface at σ_3=30 kPa.

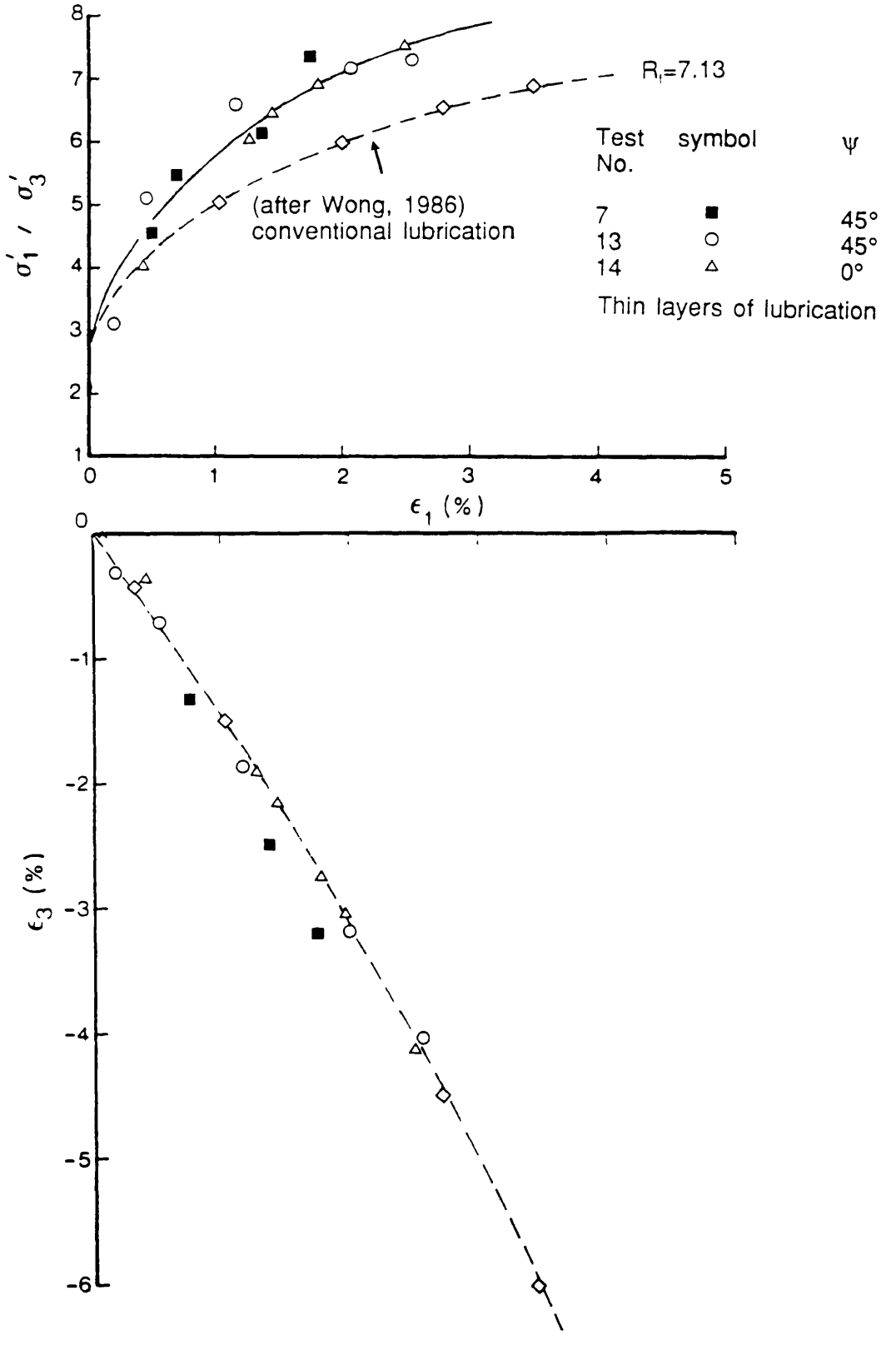

Fig. 4.15 **The effects of end lubrication on Stress-strain and deformation response of dense samples of Leighton Buzzard sand monotonically sheared in the DCDSC at σ_3=14 kPa**

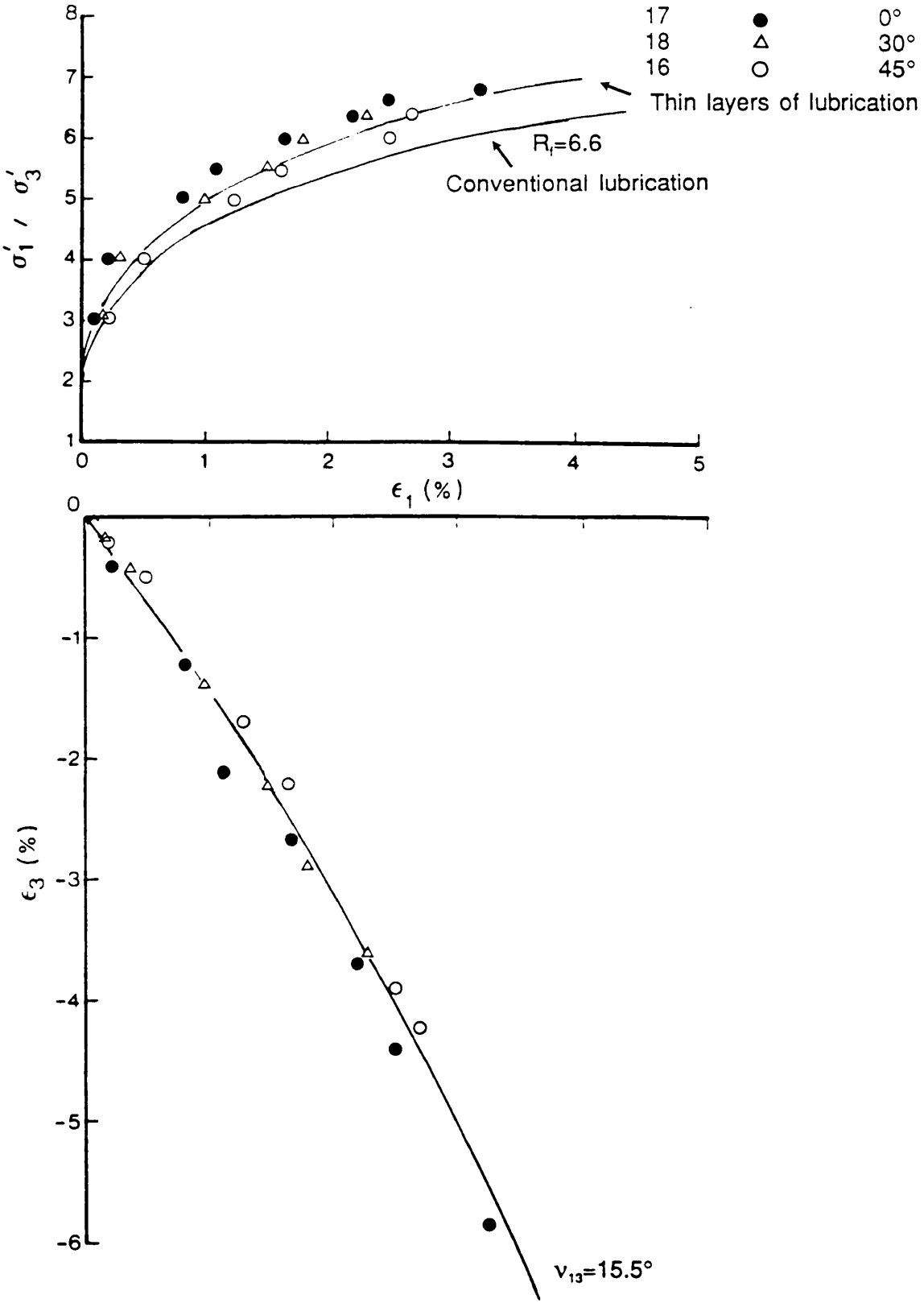

Fig. 4.16 The effects of end lubrication on Stress-strain and deformation response of dense samples of Leighton Buzzard sand monotonically sheared in the DCDSC at σ_3=30 kPa

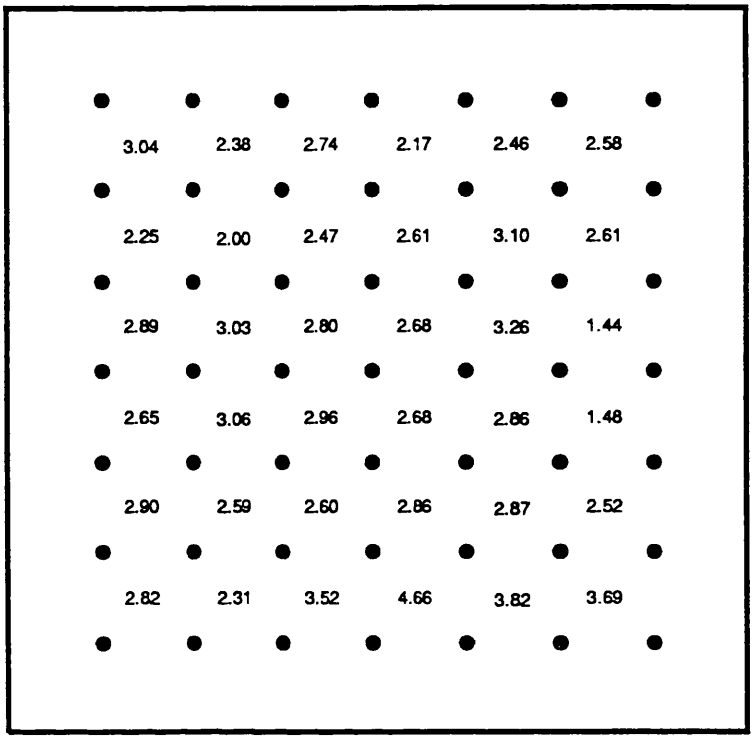

Major principal strain ε_1 (%)

Ave. in Area (1): 2.76% with standard deviation : 0.59%
Ave. in Area (2): 2.78% with standard deviation : 0.30%
Ave. in Area (3): 2.78% with standard deviation : 0.13%

Principal Stress Ratio =6.0
Principal stress Direction =90°
Principal strain Direction =91.5°

Fig. 4.17 **Example of strain distribution in dense samples of Leighton Buzzard sand sheared monotonically in the DCDSC at σ_3= 30kPa in plane strain condition**

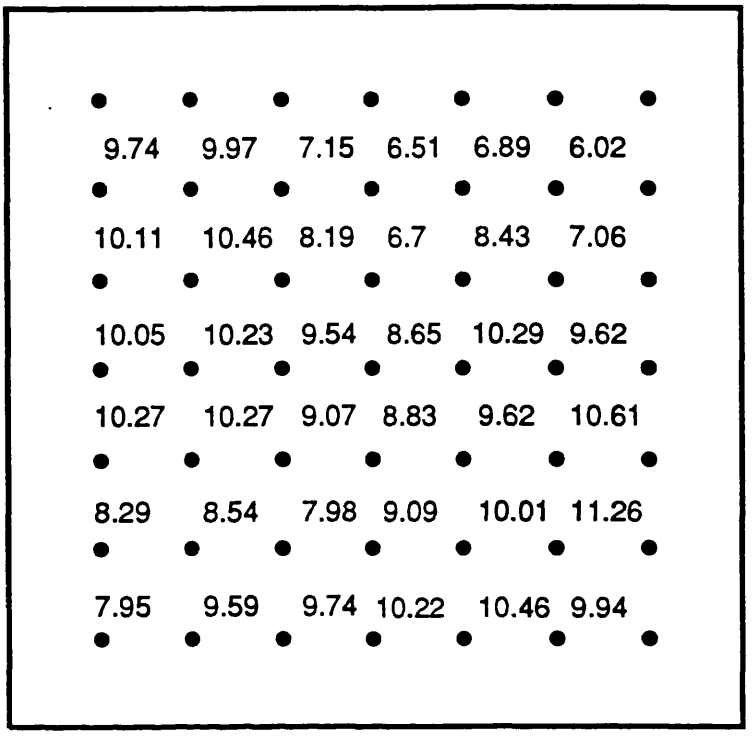

Major principal strain ε_1 (%)

Ave. in Area (1): 9.09% with standard deviation : 1.34%
Ave. in Area (2): 9.12% with standard deviation : 1.04%
Ave. in Area (3): 9.02% with standard deviation : 0.39%

Principal Stress Ratio =4.0
Principal stress Direction =45°
Principal strain Direction =45.73°

Fig. 4.18 **Example of strain distribution in loose samples of Leighton Buzzard sand sheared monotonically in the DCDSC at σ_3= 14kPa in plane strain condition**

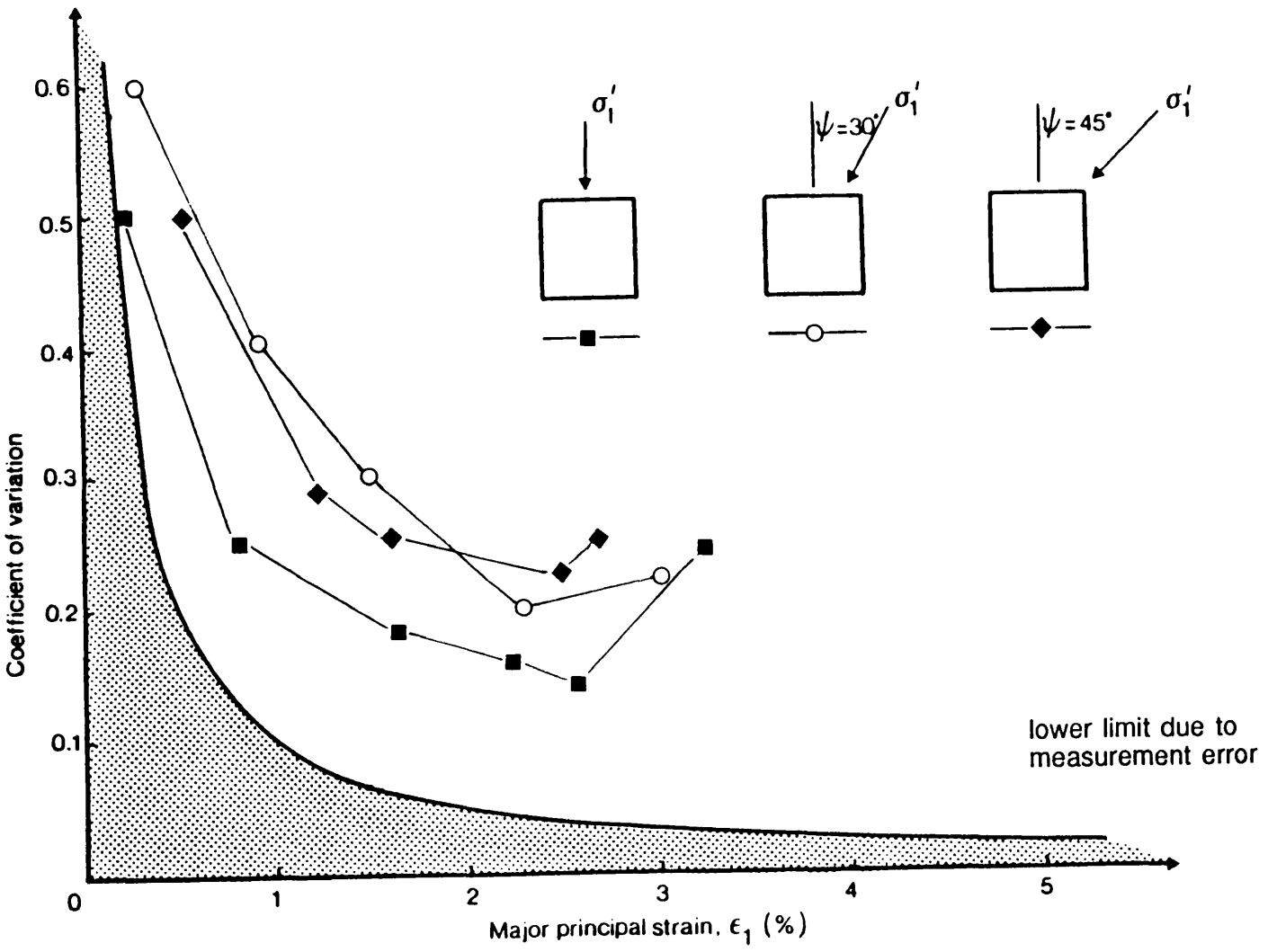

Fig. 4.19 Coefficients variation for three different monotonic tests with identical stress path

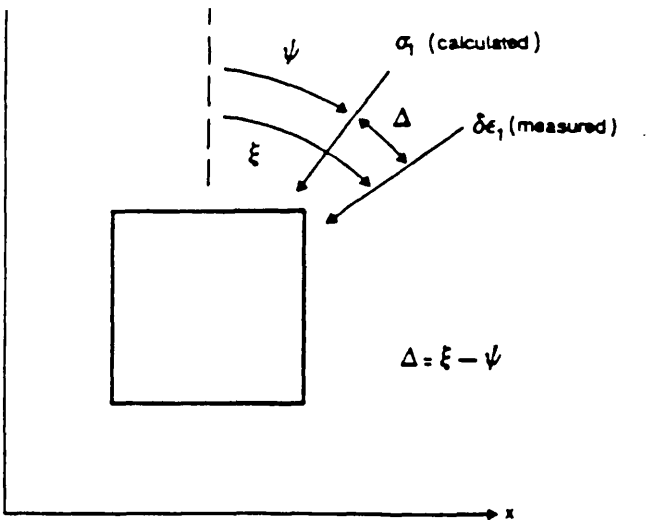

Fig. 4.20 Definition of axes of principal stress and strain increment

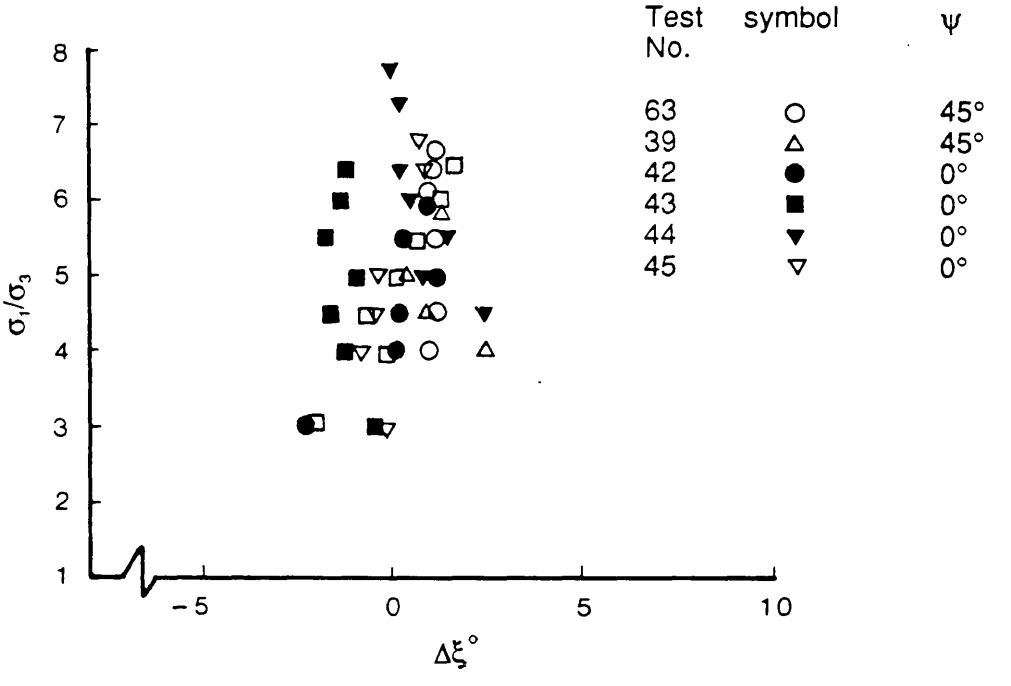

Fig. 4.21 Deviation between axes of principal stress and strain increment with principal stress ratio in dense samples of Leighton Buzzard sand monotonically loaded in the DCDSC at σ_3=14 kPa

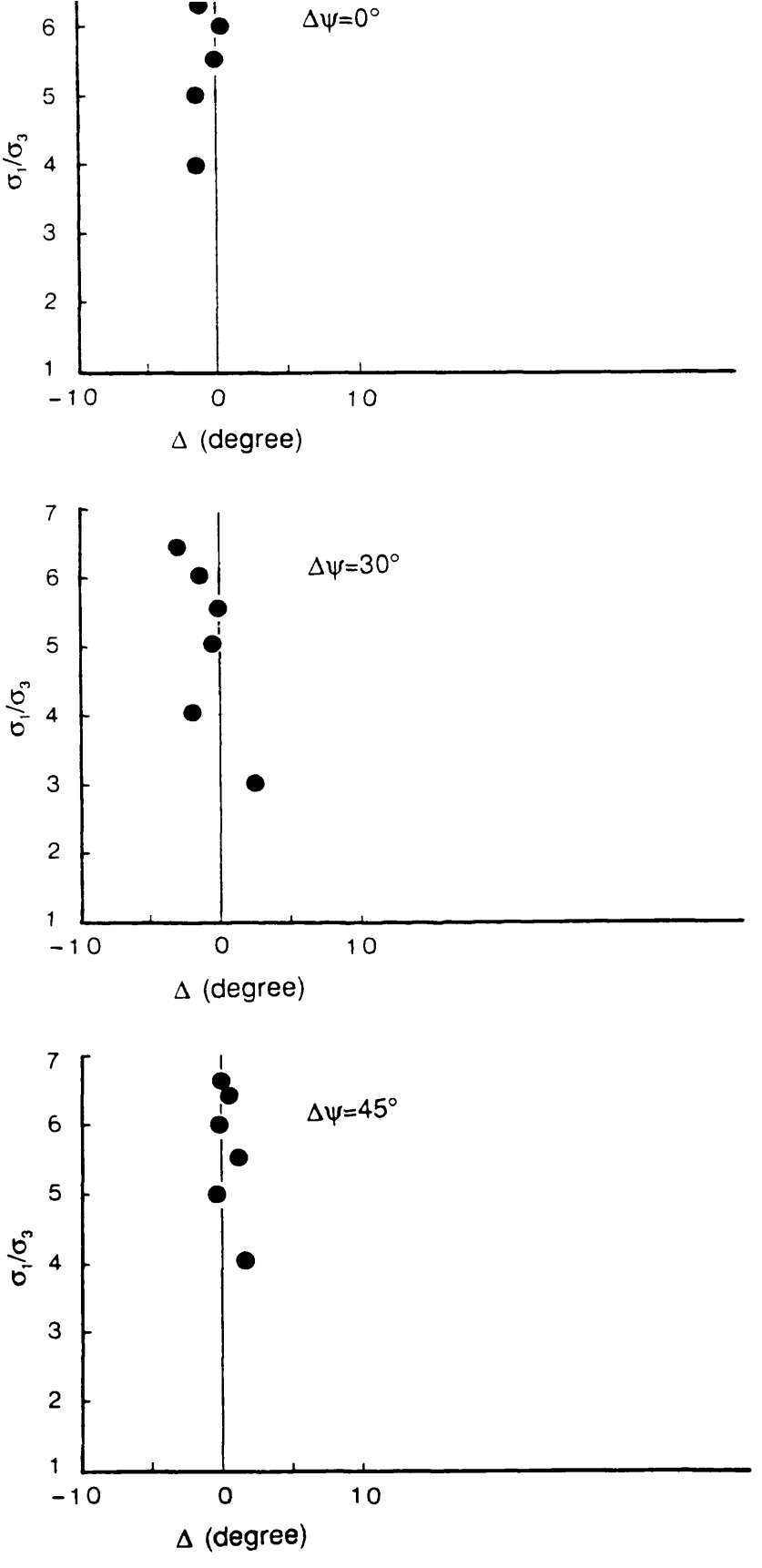

Fig. 4.22 Deviation between axes of principal stress and strain increment with principal stress ratio in dense samples of Leighton Buzzard sand monotonically loaded in the DSC at σ_3=30 kPa

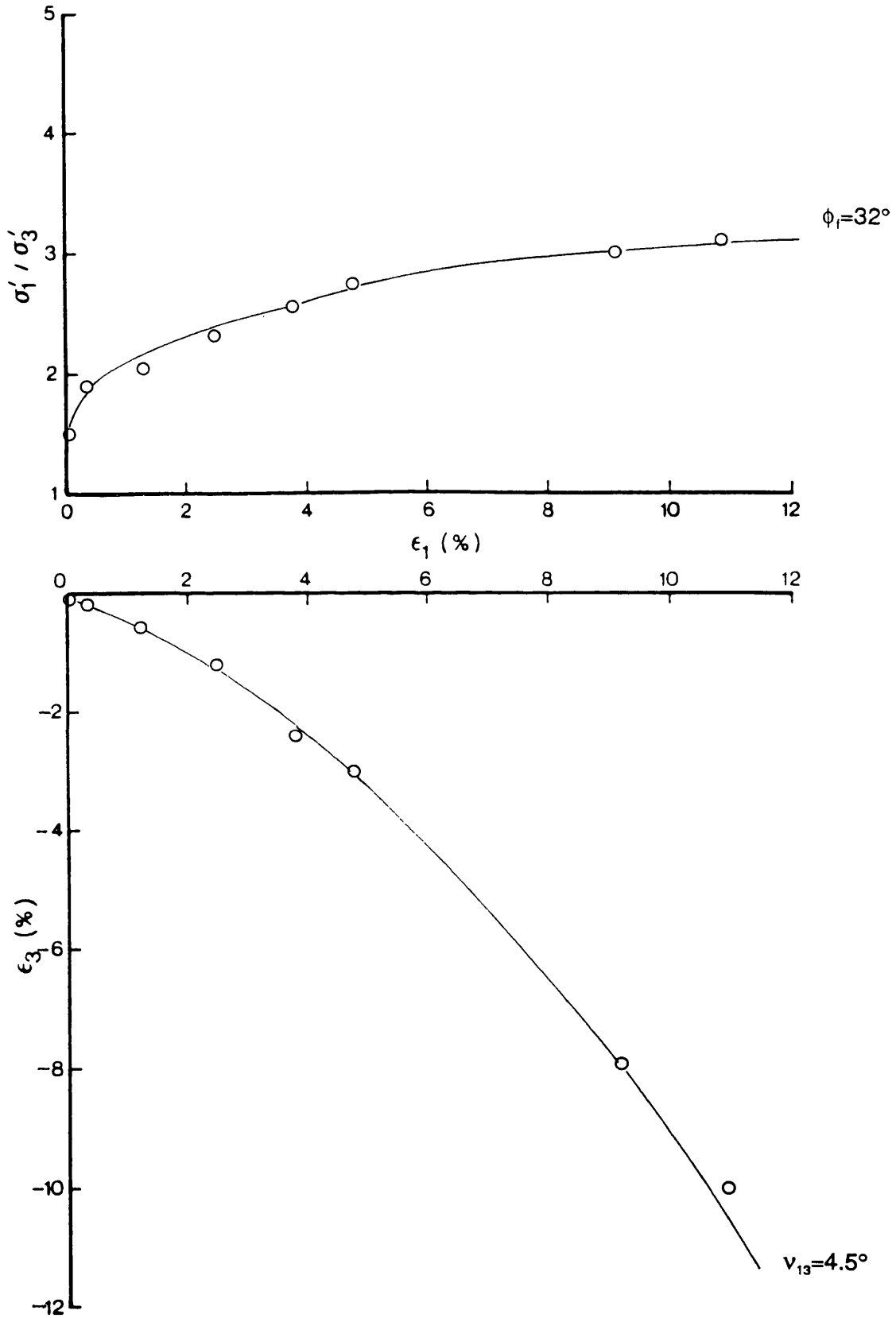

Fig. 4.23 The effects of boundary adjustment on Stress-strain and deformation response of loose samples of Leighton Buzzard sand monotonically sheared in the DCDSC at σ_3=14 kPa

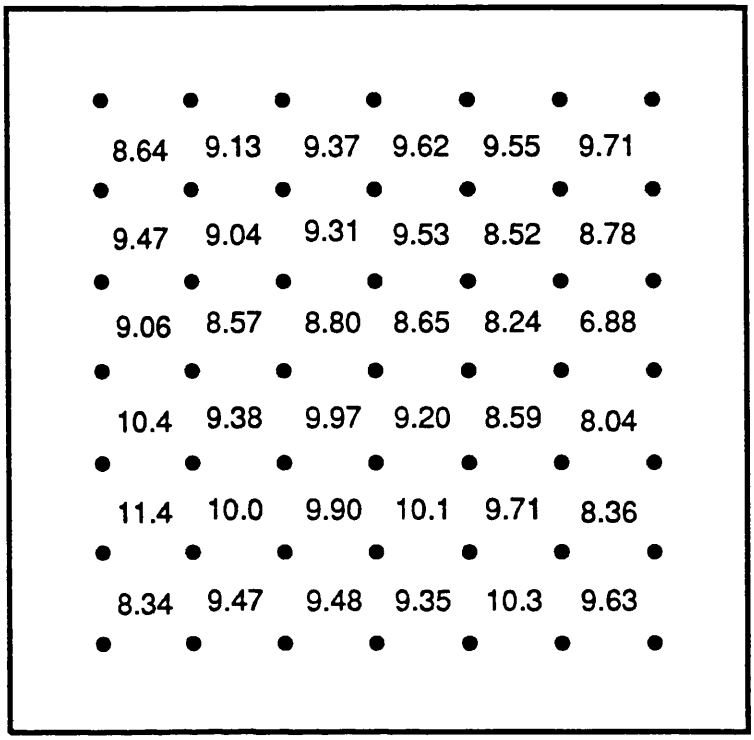

Major principal strain ε_1 (%)

Ave. in Area (1): 9.24% with standard deviation : 0.82%
Ave. in Area (2): 9.22% with standard deviation : 0.62%
Ave. in Area (3): 9.16% with standard deviation : 0.59%

Principal Stress Ratio =3.0
Principal stress Direction =45°
Principal strain Direction =45.54°

Fig. 4.24 **Strain distribution within a loose Leighton Buzzard sand monotonically tested in DCDSC at σ_3=14 subjected to incremental boundary adjustment**

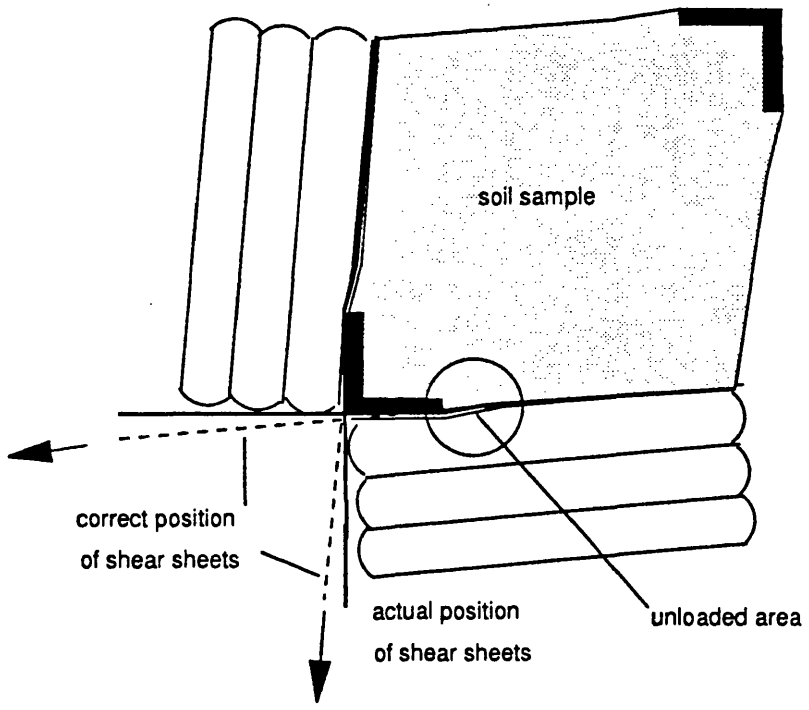

Fig. 4.25 **Deviation from correct alignment of shear sheets when the rigid aluminum corners were employed**

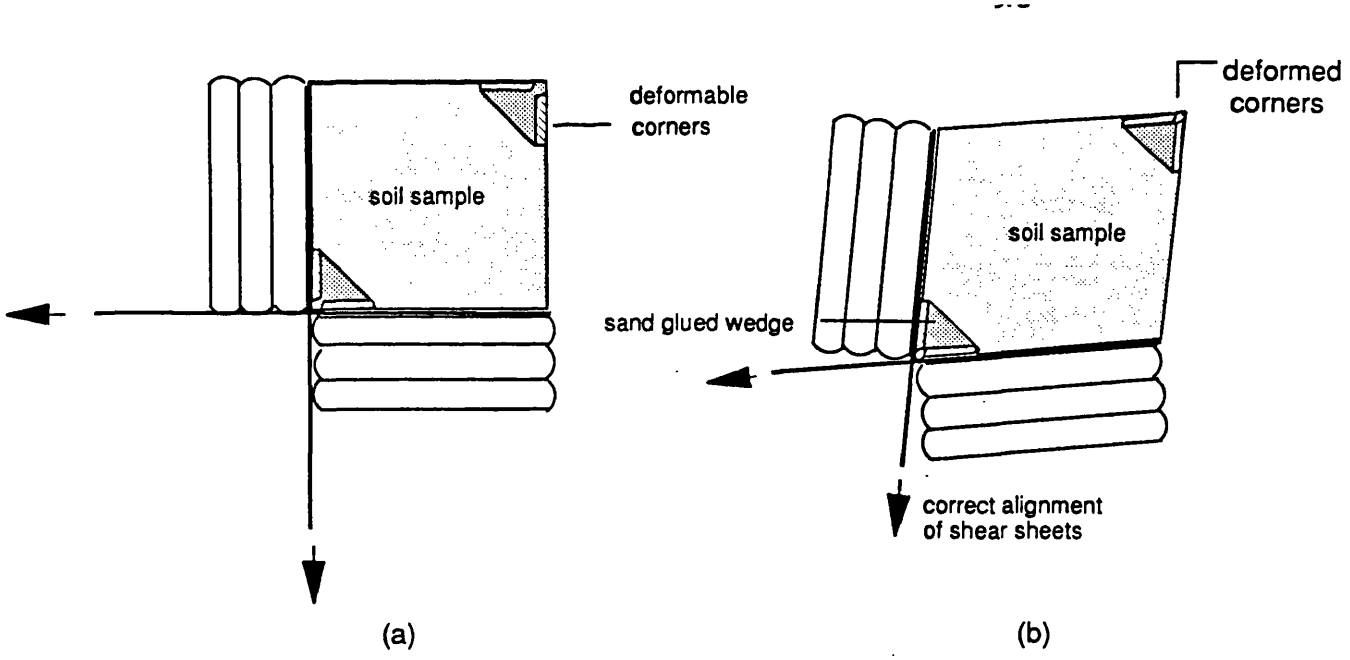

Fig. 4.26 **The deformable corner used to follow the deformation of the sample changing shape**

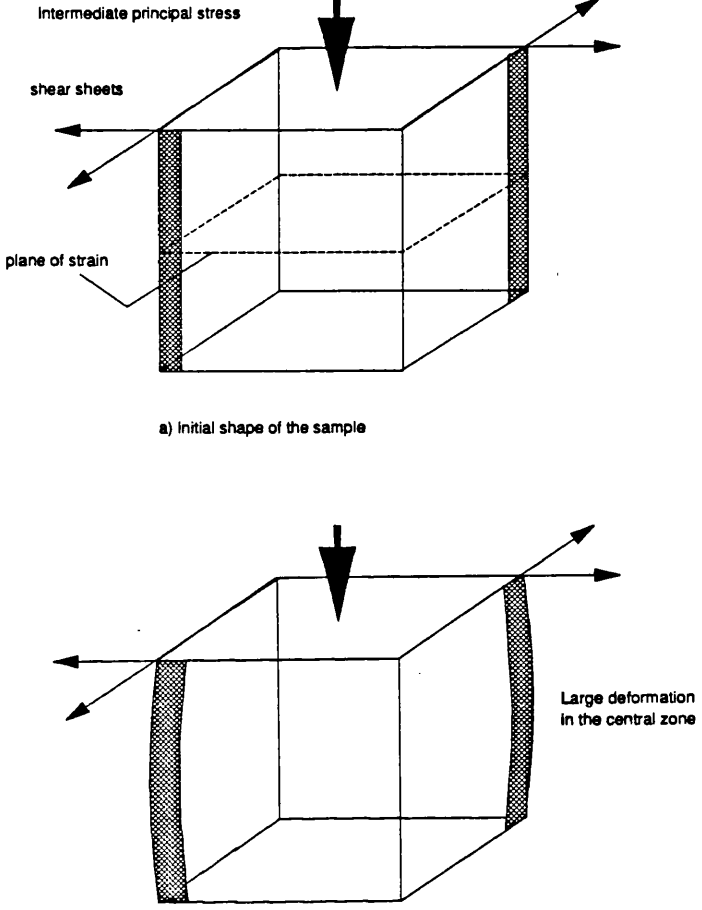

Fig. 4.27 **Bulging effect and non-uniform distribution of strain within the sample where the pulling sheets emerge when only reinforcement material was employed**

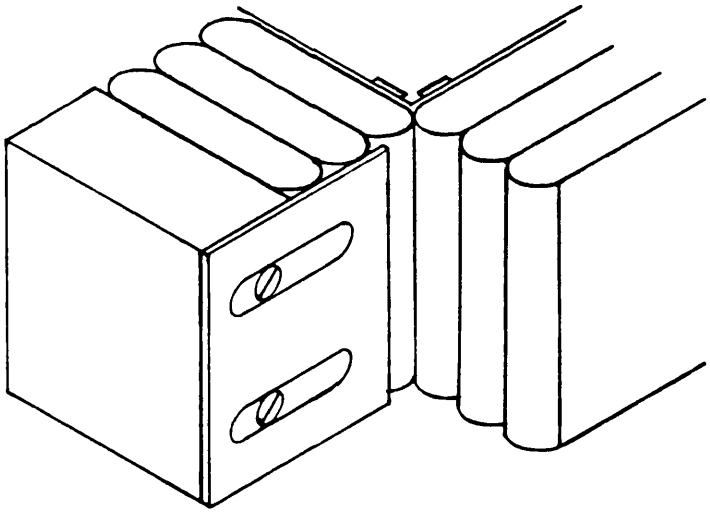

Fig. 4.28 **The correct position of retaining vane**

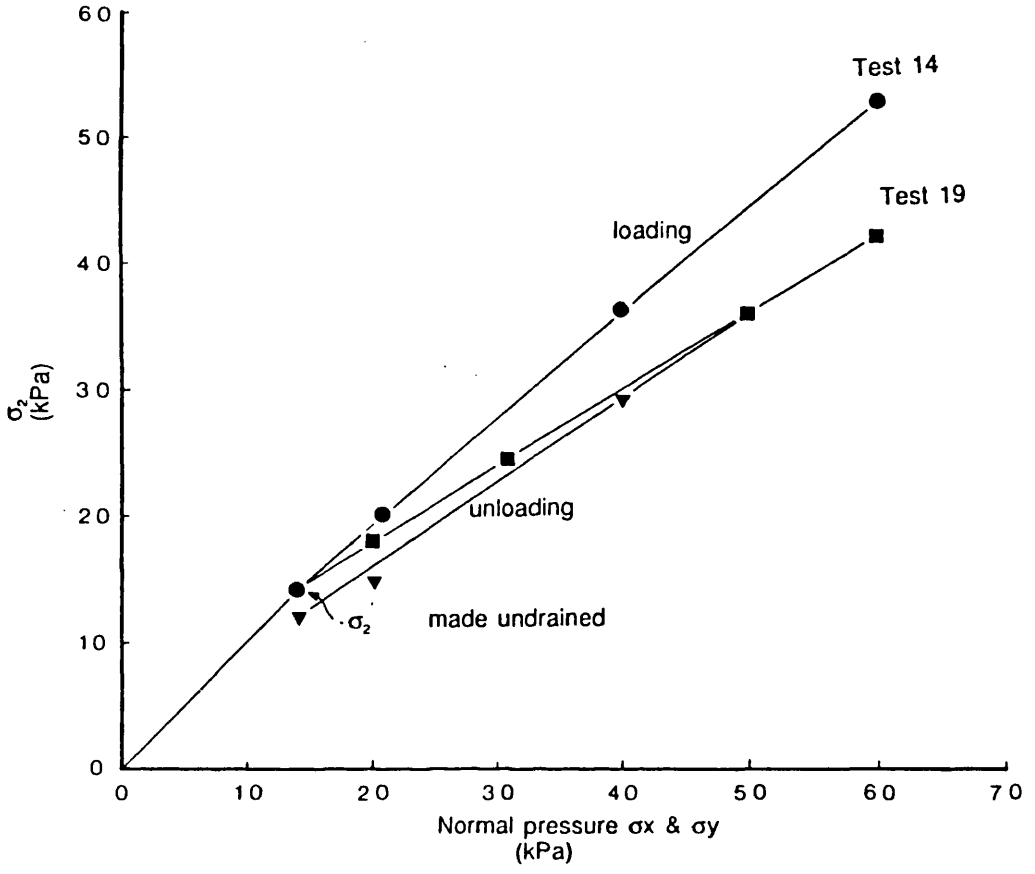

Fig. 4.29 Effect of normal pressure bags on the magnitude of σ_2

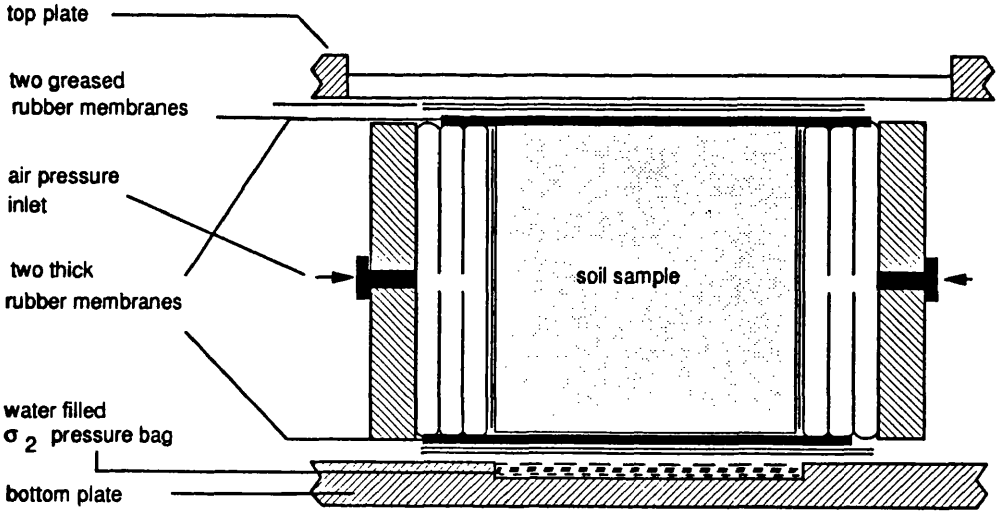

Fig. 4.30 Method used to place a thick membrane on the top and bottom plane strain surfaces

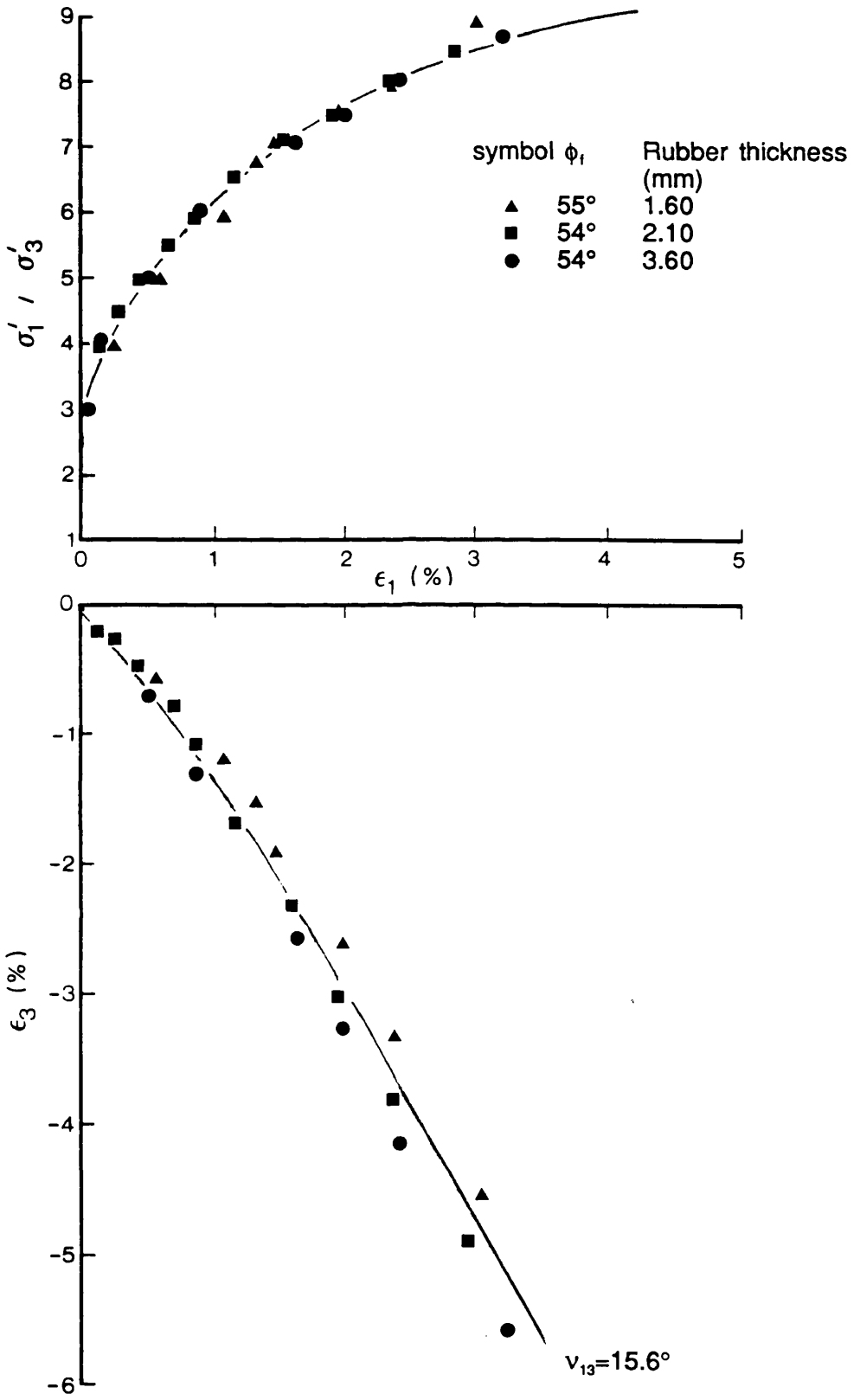

Fig. 4.31 Stress-strain behaviour of dense samples tested in DCDSC using specially thickened membranes on the plane strain surfaces

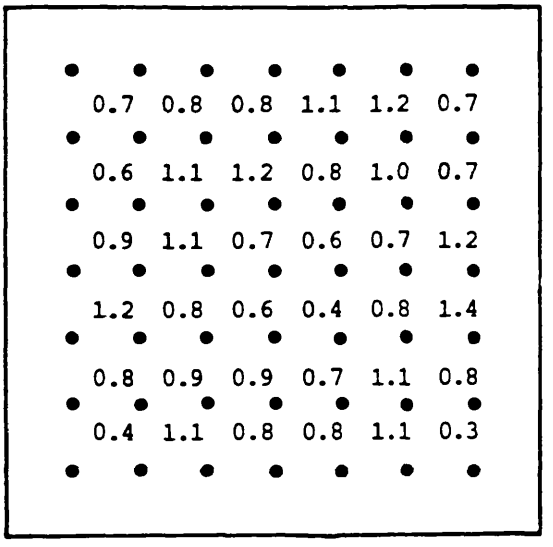

Distribution on plane A-A
of Major Principal Strain at R = 6.0
Ave. in Area 1 = 0.87 % (S.D. = 0.28 %)
Ave. in Area 2 = 0.85 % (S.D. = 0.24 %)
Ave. in Area 3 = 0.59 % (S.D. = 0.15 %)

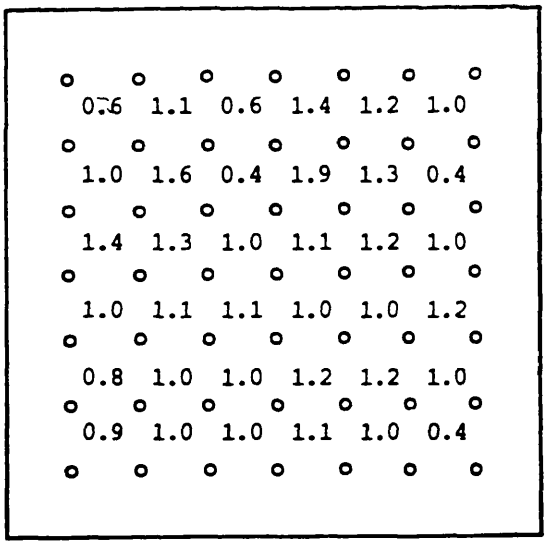

Distribution on plane B-B
of Major Principal Strain at R = 6.0
Ave. in Area 1 = 1.03 % (S.D. = 0.37 %)
Ave. in Area 2 = 1.17 % (S.D. = 0.33 %)
Ave. in Area 3 = 1.04 % (S.D. = 0.09 %)

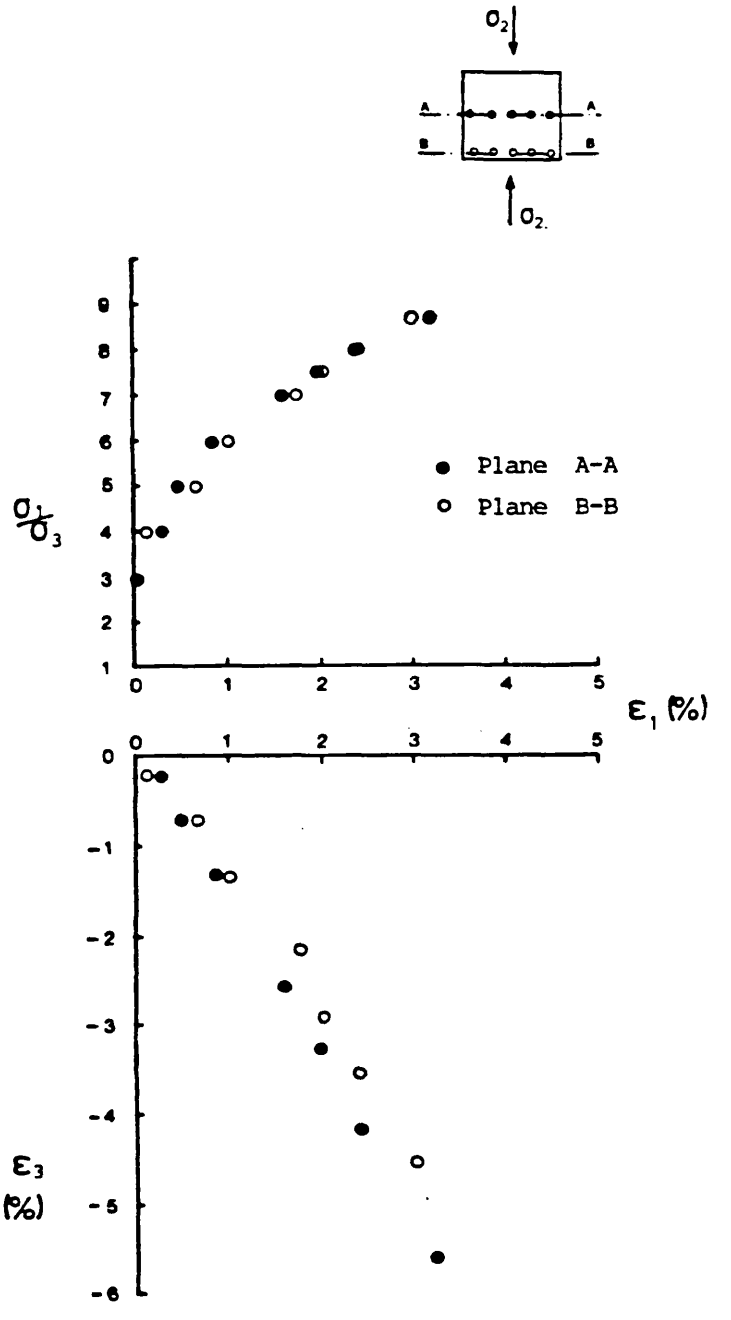

Fig. 4.32 Comparison of strain distribution and stress-strain response on the middle plane and near the edge plane of a dense sample sheared in the DCDSC using the special thick plane strain membrane

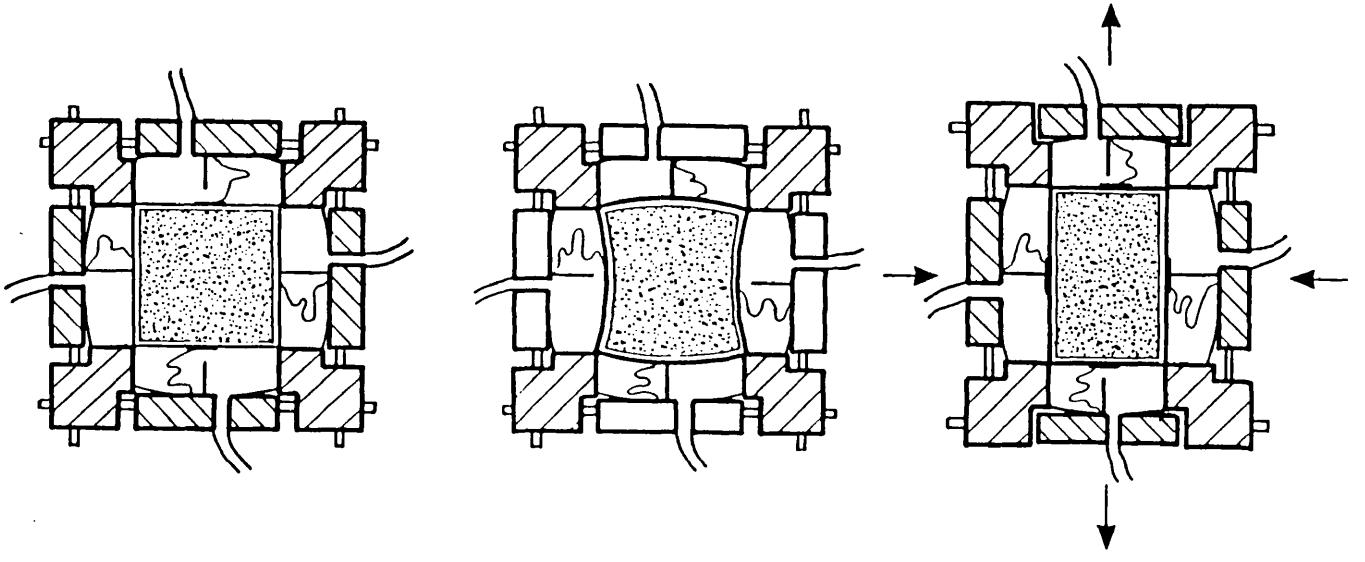

a) Sample before shearing

b) Sample deformation after a 'Small' stress increment

c) Apparatus & sample after boundary adjustment

Fig. 4.33 **Principal of matching displacement in Biaxial Tester Apparatus (after Ogunbekun, 1988)**

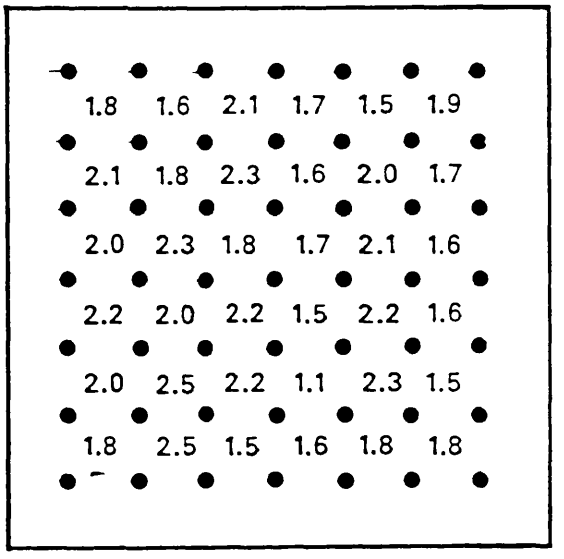

Distribution on plane A–A
of Major Principal Strain at R = 4.9

Ave. in area 1 = 1.90 % (S.D. = 0.32 %)
Ave. in area 2 = 1.98 % (S.D. = 0.36 %)
Ave. in area 3 = 1.82 % (S.D. = 0.31 %)

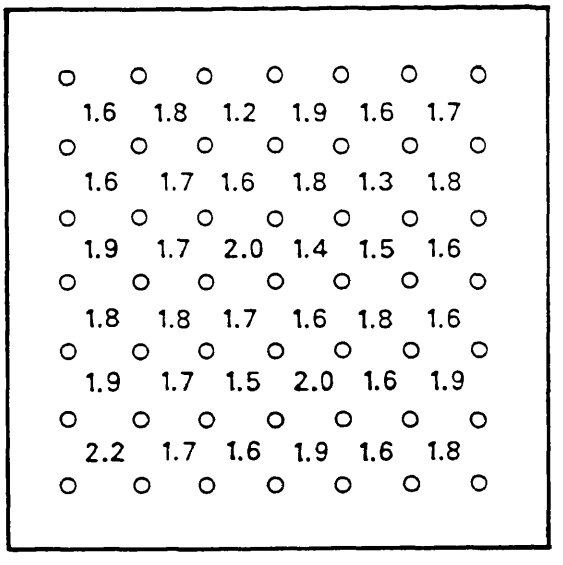

Distribution on plane B–B
of Major Principal Strain at R = 4.9

Ave. in area 1 = 1.76 % (S.D. = 0.27 %)
Ave. in area 2 = 1.72 % (S.D. = 0.19 %)
Ave. in area 3 = 1.69 % (S.D. = 0.23 %)

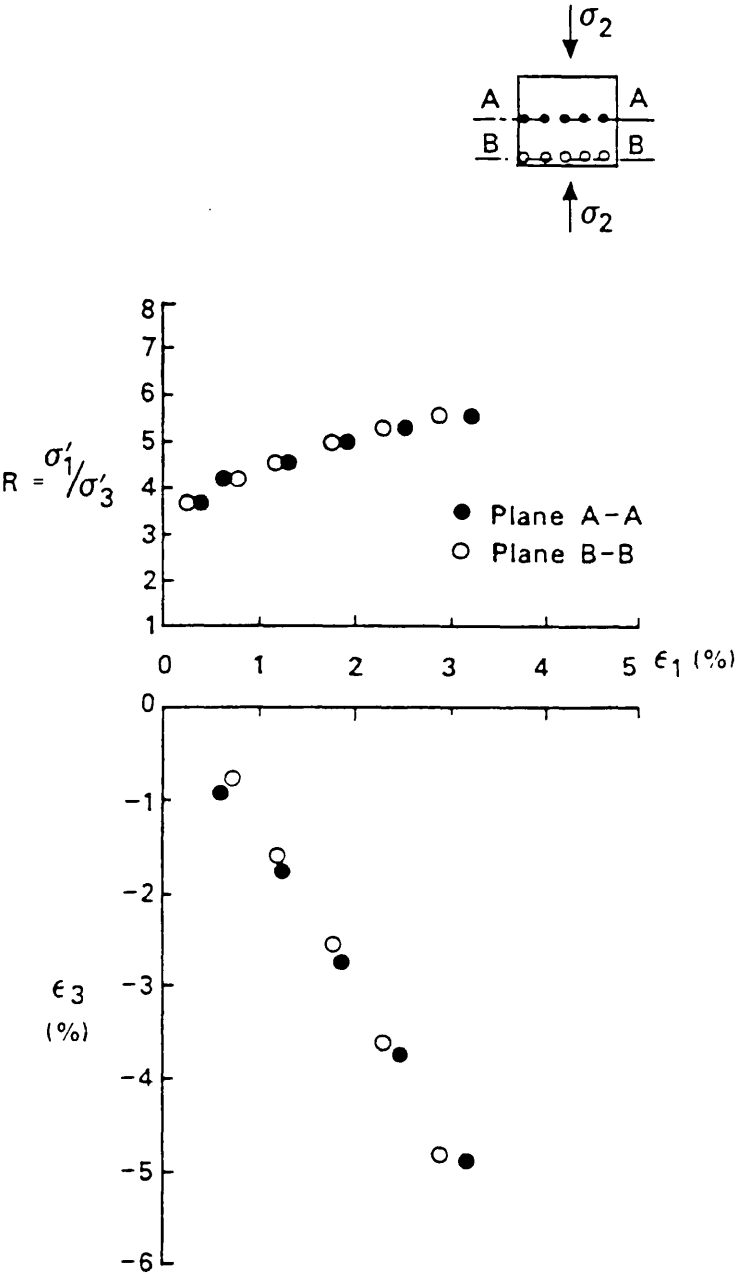

Fig. 4.34 Stress-strain behaviour of dense sand sample sheared monotonically in the Biaxial Tester when the top and bottom plane strain rubber sheets were stretched (after Ogunbekun, 1988)

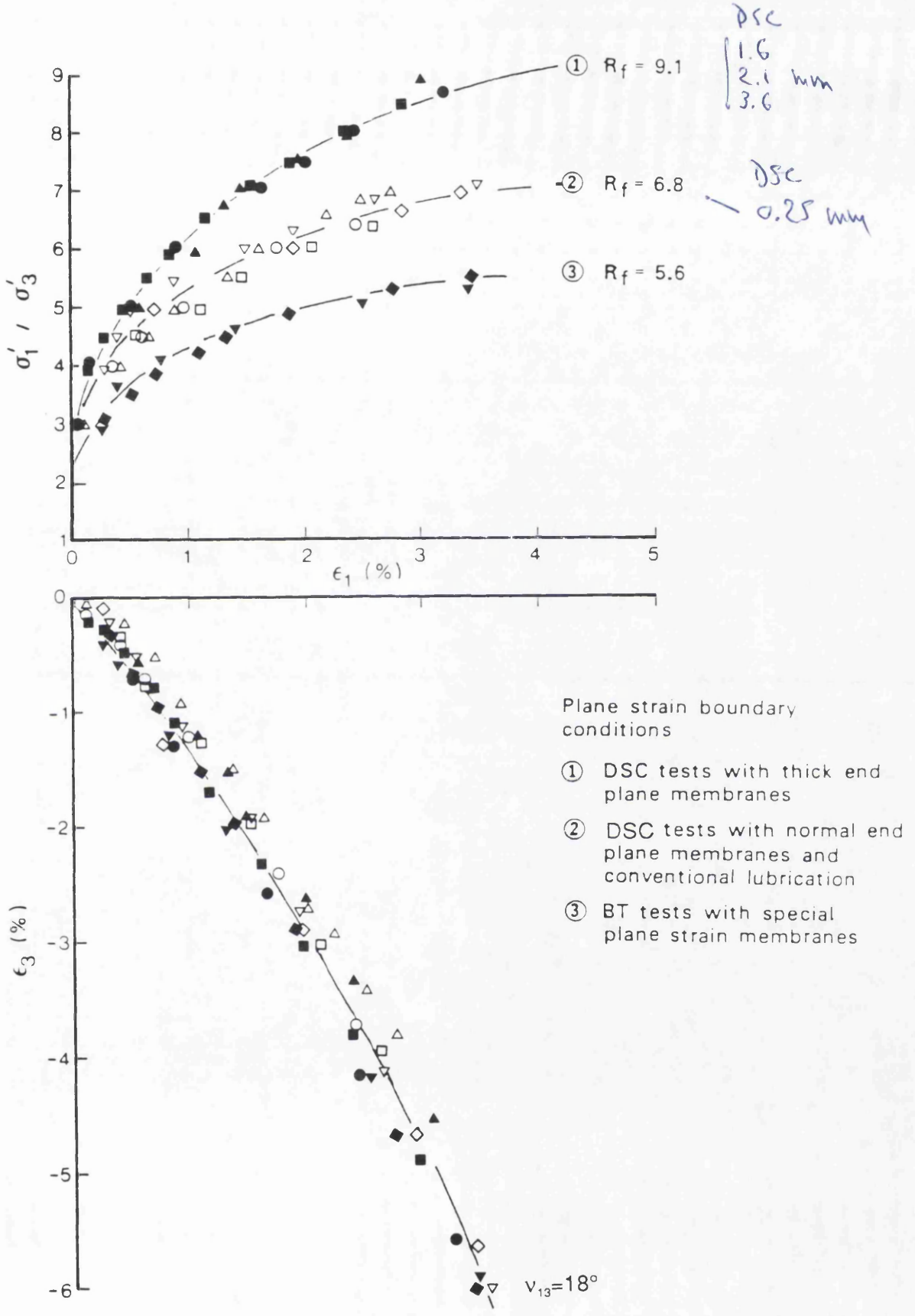

Fig. 4.35 Stress -strain and deformation response of dense samples of Leighton Buzzard sand monotonically sheared with three different levels of plane strain end constraint

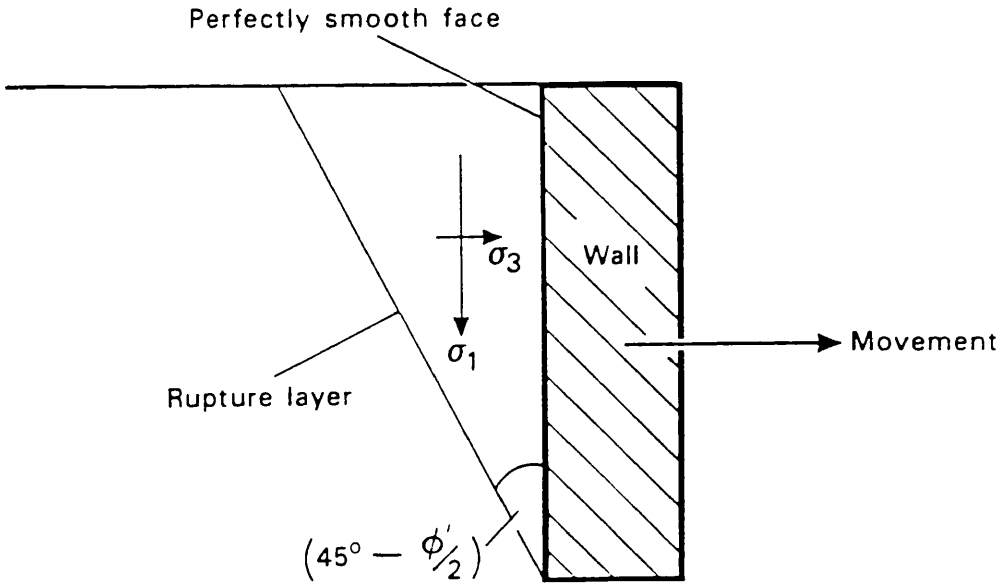

Fig. 4.36 Schematic view of retaining wall experiment

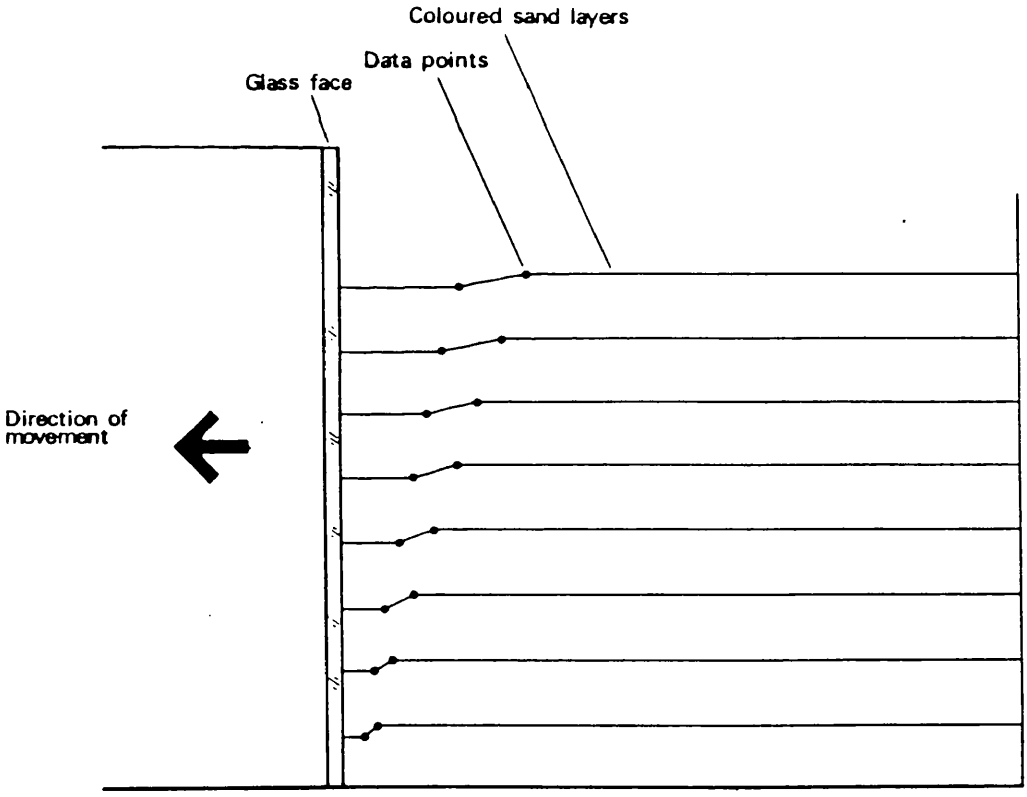

Fig. 4.37 The method used to record the boundaries of the rupture layers in the wall experiment

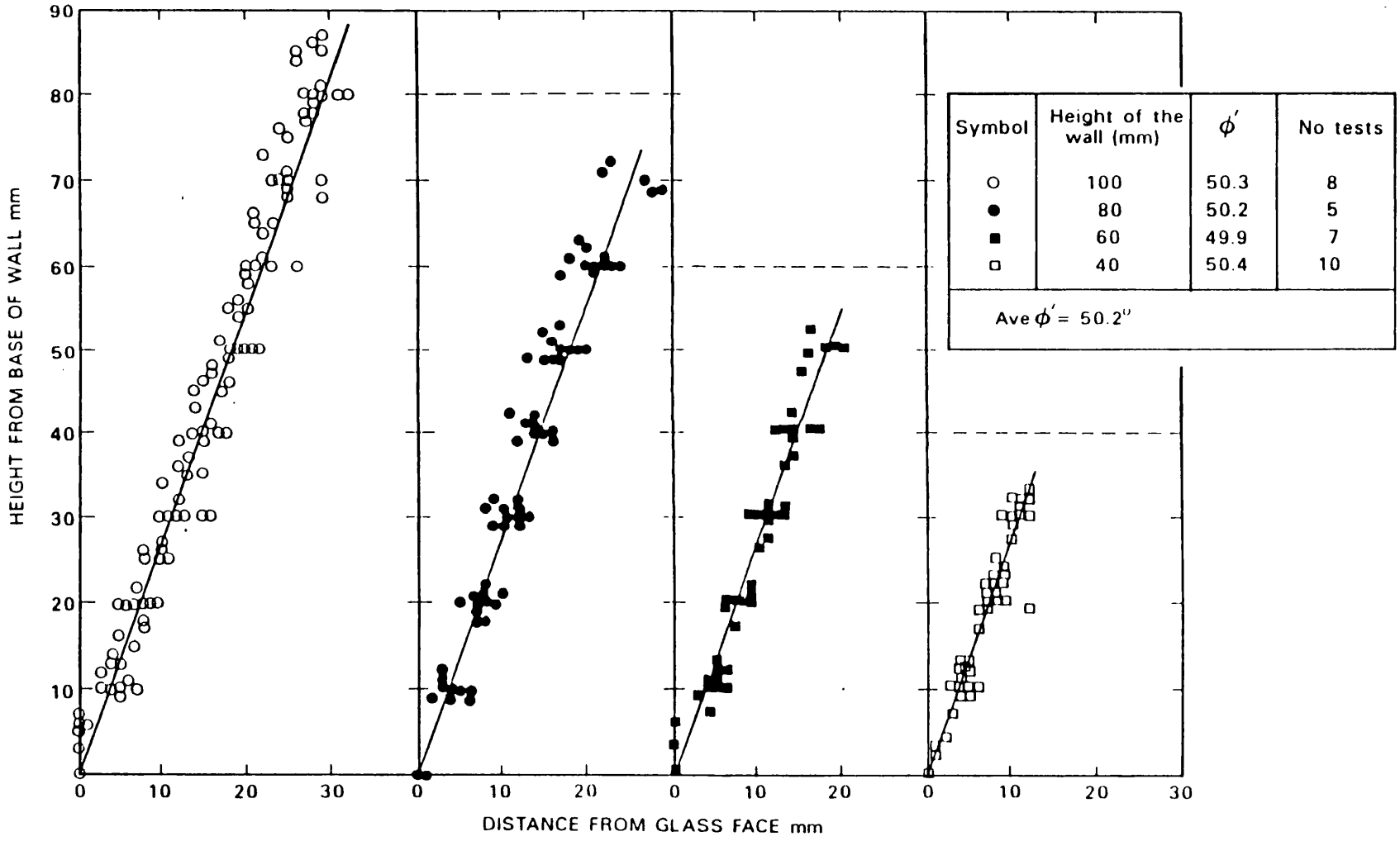

Fig. 4.38 Experimental data for dense samples tested using the retaining wall equipment

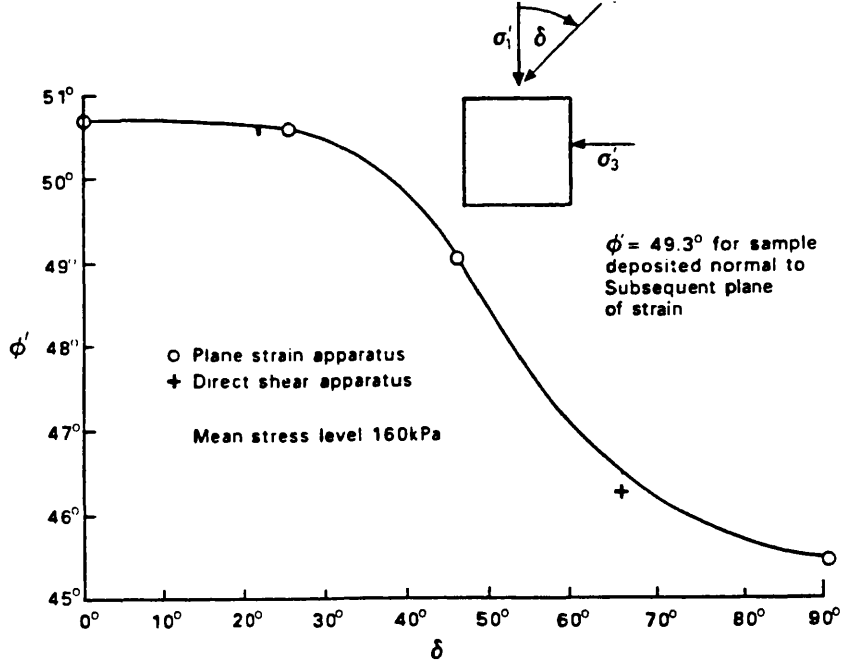

Fig. 4.39 **Plane strain strength-anisotropy relationship for Leighton Buzzard sand (after Arthur and Assadi,1977)**

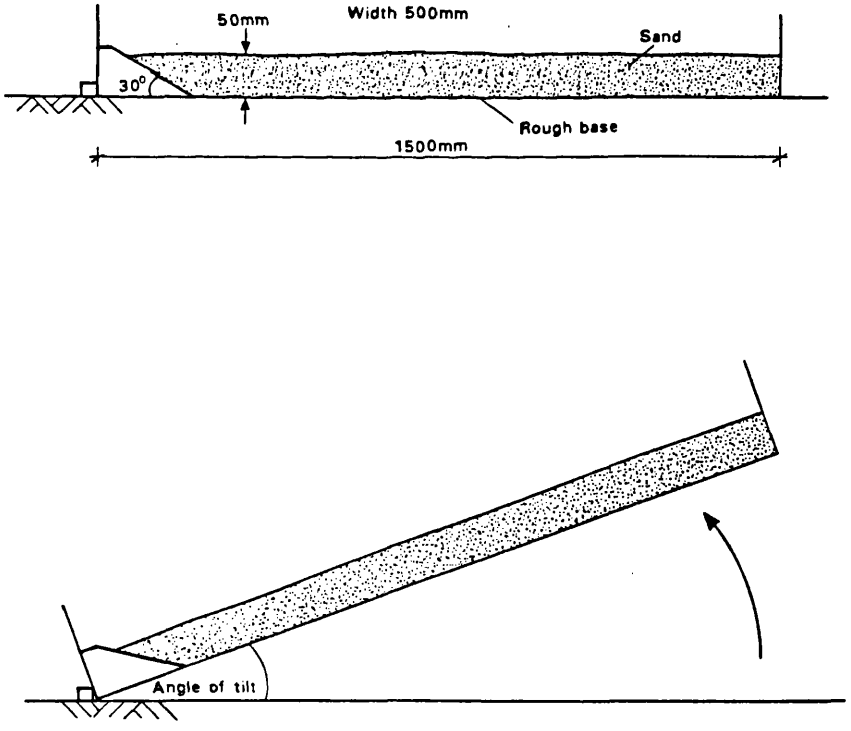

Fig. 4.40 **Schematic view of tilting experiment**

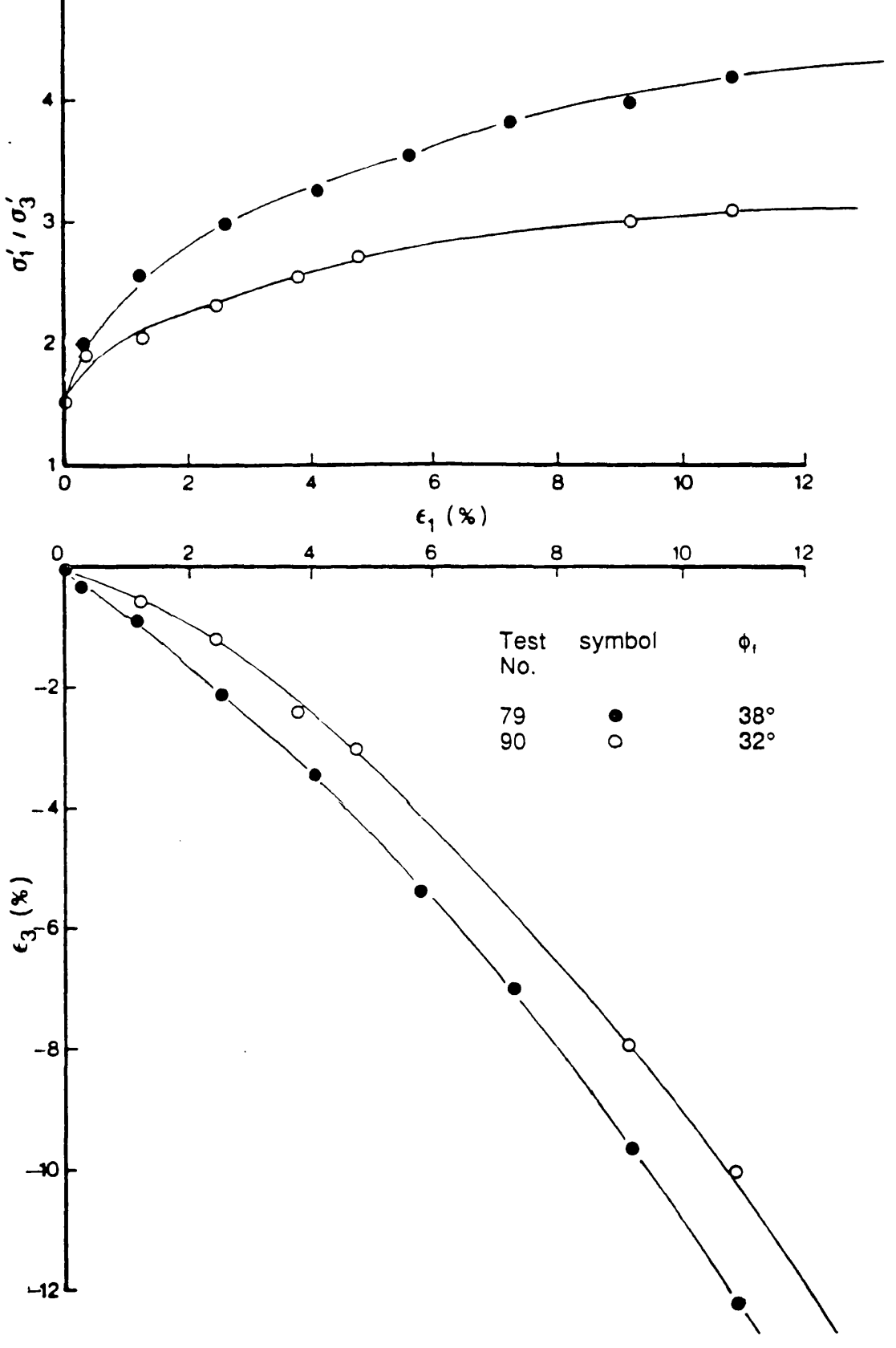

Fig. 4.41 Stress -strain and deformation response of loose samples of Leighton Buzzard sand monotonically sheared with two different levels of boundary constraint

Test Number	stress ratio	Area	ε_1 (%)	Coeff. of Var.	ε_3 (%)	γ (%)	Coeff. of Var.
47 dense L.B.S.	(6)	(1)	2.32	0.22	-3.43	5.76	0.27
		(2)	2.08	0.26	-2.99	5.07	0.32
		(3)	1.43	0.22	-1.90	3.33	0.09
45 dense L.B.S.	(6)	(1)	2.38	0.24	-3.40	5.79	0.29
		(2)	2.13	0.26	-2.95	5.08	0.33
		(3)	1.41	0.15	-1.73	3.14	0.09

Table 4.1 Examples of non-uniform distribution of strain within two samples due to non-uniform transmission of stresses through the flexible boundaries.

Different P.S. apparatuses	$b=\frac{\sigma_2-\sigma_3}{\sigma_1-\sigma_3}$	dense L B	Loose L B
CONVENTIONAL PLANE STRAIN APPARATUS (ASSADI, 1975)	N.P.S.	49.3°	—
BIAXIAL TESTER (MODE-2) (OGUNBEKUN, 1988)	N.P.S.	49.0°	39.0°
DIRECTIONAL SHEAR CELL (WONG, 1986)	0.3	49.0°	40°
DCDSC (NORMAL LUBRICATION)	0.0-0.3	48.5°	38°

Table 4.2 Comparison of shear strength for Leighton Buzzard samples tested in different apparatuses

VOIDS RATIO	NUMBER OF TESTS	WALL HEIGHT mm	AVERAGE UNCORRECTED Ø'	AVERAGE Ø' CORRECTED FOR ANISOTROPY
0.73 ± 0.03	10	50	29.7°	29.7° } 29.2°
	10	100	28.7°	28.7° }
0.52 ± 0.02	10	40	50.4°	48.9°
	7	60	49.9°	48.4° } 48.7°
	6	80	50.2°	48.7° }
	8	100	50.3°	48.8°

Table 4.3 Active wall experiment for Leighton Buzzard sand

VOIDS RATIO	SURFACE CONDITION	NUMBER OF TESTS	RANGE OF TILT ANGLE DURING FAILURE	AVERAGE UNCORRECTED Ø'	AVERAGE Ø' CORRECTED FOR ANISOTROPY
0.73 ± 0.05	Dry	5	31° - 34.5°	31.9°	31.9° (29.2°)*
0.52 ± 0.02	Dry	6	39.5° - 41.2°	40.3°	42.9°
	Damp surface	4	46.9° - 48.5°	47.9°	51.1° (48.7°)*

*Corresponding corrected ø' from active wall experiments

Table 4.4 Tilting experiments for Leighton Buzzard sand

CHAPTER 5 DRAINED SHEARING BEHAVIOUR OF LEIGHTON BUZZARD SAND UNDER CONTINUOUS AND CYCLIC ROTATION OF PRINCIPAL STRESS DIRECTIONS

5.1 INTRODUCTION

The work presented in this chapter is the description of a series of cyclic and subsequent monotonic tests which were performed on both dense and loose Leighton Buzzard sand samples. The monotonic stress-strain behaviour of this sand has been reported in Chapter 4.

In an extensive study Arthur and Wong (1986) illustrated the behaviour of Leighton Buzzard sand when subjected to continuous and cyclic principal stress rotation. However, all their experiments were carried out at a low stress level of σ_3 = 14 kPa due to the limitation of boundary shear stresses in the early DSC apparatus. Furthermore, all the tests were conducted with a variation of the mean normal stress level during the cyclic loading. Thus the effects of stress level fluctuation could not be separated from principal stress rotations. This stress path was imposed because of the hysteresis response of the shear sheets when subjected to the cyclic loading (Chapter 2). Their study excluded cyclic tests in which principal stress direction rotations where larger than 70°. The stress path for these tests is illustrated in Figure 2.6. Arthur and Wong indicated that there was an effect on the behaviour of Leighton Buzzard sand due to the fluctuation of mean stress levels, particularly in the early cycles, even if the major principal stress directions were not rotated during cyclic loading. The effect of cyclic variation in stress level is illustrated in Figure 5.1.

As an improvement to the early work, the development of the Daisy Chain shear sheets provided the facility to conduct cyclic tests in which the principal stress directions could be continuously rotated by introducing cyclic boundary shear stresses without changing the mean stress level ($(\sigma_1 + \sigma_3)/2$ held constant). Hence the effects of stress level variation could be separated from that of the principal stress rotation. Figure 5.2 illustrates a typical continuous rotation test at constant mean stress level. Design of the new shear sheets also made it possible to conduct tests under higher stress level, and angles of rotation up to 90°.

5.2 CALIBRATION OF COMPUTER CONTROLLED PRESSURE REGULATORS

It was mentioned in Chapter 2 that in a cyclic test the boundary stresses were applied to the sample through computer controlled pressure regulators. These pressure regulators linked a stepper motor to a precision regulator. It was necessary to calibrate the step changes in the stepper motor to the corresponding output pressure from the regulator.

The calibration was performed by placing a dummy sample in the cell and calibrating the pressure regulators individually. A computer programme was used which gave specific amount of step changes in the stepper motor and recorded the corresponding response of stress changes using the pressure transducers and the chart recorder. The control also incorporated step changes in the form of a sinusoidal wave to account for any irregular changes in pressure which might occur during a cyclic test. The relationship between the step input to the stepper motor and the pressure output from the regulator could be obtained by comparing the input and output waveform.

Pressure measurements were made at the sample boundaries to get a true reading of applied normal stress in a similar manner as described in chapter 3. The regulators were linked to Fairchild 1:1 volume booster relays to increase the bleeding capacity. Also, equal length of polythene pressure pipe were used to connect computerized pressure regulators and the normal pressure bags to ensure no unequal transient pressures.

An output pressure of approximately 0.4 kPa was obtained for every single step in the stepper motor. This calibration value remained constant with time and only needed to be measured if different pressure boosters were going to be used.

5.3 EXPERIMENTAL PROGRAMME AND TEST PROCEDURE

The initial aim of this research was to operate a series of cyclic tests at a minor principal stress of 14 kPa, to make a direct comparison with the results of Wong (1986) and to identify if there was any differences in the behaviour of Leighton Buzzard sand when subjected to continuous and cyclic rotation of the principal stress direction under the two different stress paths. The pressure range of the computer controlled stepping motors through which the cyclic loading was to be applied, was 14-420 kPa. Hence a precise application of load could not be achieved at this lower limit. Therefore the first series of cyclic tests were conducted at a higher stress level, of 30 kPa, and are presented in section 5.3.2.

After improvements were made to the cyclic system by employing 4-1 reduction boosters (which will be described later), a reliable application of load at the lower limit was attained, and the second series of cyclic tests were conducted at 14 kPa. These tests could then be compared with those of Wong (1986). The improvement of the pressure controllers also made it possible for the experimental observation of

the effects of principal stress rotations on Leighton Buzzard sand to be extended to very low mobilised angles of friction. This gave the opportunity for tests to be carried out at high amplitudes of rotation and very low mobilized stress ratios. The results of this series are presented in section 5.3.3.

It is already known that during monotonic loading the interparticle contact normals tend to align themselves in a direction which is parallel to the direction of the major principal stress (Weindieck, 1967; Oda, 1972b; Arthur et al., 1977; Arthur et al., 1981; and Wong, 1986). The alignment of the interparticle contacts becomes more subtle when the principal stress directions are changed continuously (Youd, 1977). Based on the experimental observations made by Cundall et al. (1982) and Wong (1986), it can be suggested that the mean direction of principal stress rotation is the preferred orientation of interparticle contacts. This interpretation was further investigated by a series of monotonic tests conducted after cyclic rotation tests for both dense and loose sand and are described in section 5.3.4.

5.3.1 Procedure for continuous rotation tests through cycling the boundary shear stresses

The continuous rotation of principal stress directions at constant major principal stress and mobilised angle of friction was achieved by cyclic simultaneous variation of the boundary normal and shear stresses (σ_a, σ_b and τ_a, τ_b). Oscillations of σ_a, σ_b, τ_a and τ_b between points A,B,C and D are illustrated in Figure 5.2. This rotation followed a backward and forward sequence to complete one cycle. As both the boundary normal and the shear stresses could be cycled in the DCDSC, no mean stress level variation was involved and the size of the Mohr's circle was constant throughout the test. Figure 5.3 illustrates the different stages in a typical continuous rotation test. It should be noted that each cycle of principal stress rotation started and finished at the ψ=45° (Figure 5.3a and 5.3e).

The variation of principal stress direction with time was chosen to be a sinusoidal waveform and illustrated in Figure 5.4. Figure 5.5 shows typical waveforms required by the normal and shear stresses. The actual waveforms for the normal and shear stresses, were controlled and monitored by a computer programme linked to four motorised pressure regulators. Figure 5.6 is an example of a chart recorder plot of actual sinusoidal waveforms produced in a typical cyclic test.

The procedures for conducting cyclic rotation tests were the same for testing both

dense and loose sand samples and could be divided conveniently into two separate parts. The first part of the test, was a manually controlled monotonic shear test at ψ =45°. This was to achieve the required mobilised angle of friction from which the cyclic part could start. The procedure for this part was similar to the constant principal stress direction tests that have already been described in Chapter 4. The second was the computer controlled cyclic part in which the principal stresses were rotated through combined cyclic variation of the boundary normal and shear stresses at the mobilised angle of friction while the mean stress level was held constant (Figure 5.3).

Once the required mobilized angle of friction was attained in the monotonic part of the test, a radiograph was taken and the deformation of the sample at this stage was recorded as the strains developed at cycle number zero.

To commence the second part of the tests the sample was placed under vacuum to prevent any sample disturbance during the computer control set up.

Operation of the motorised regulators was achieved via motor control boxes fixed next to each of the stepper motors (Figure 2.26). There were four motor control boxes for each of the four motorised regulators enabling the regulators to be operated independently using either the manual or the automatic mode. To set up the process, the motorised regulators were operated manually from the motor control boxes. The auto/manual switch was set on manual. In this mode there were two direction buttons which, when pressed, could either increase or decrease the pressure. Prior to the application of primary pressure, the main pressure supply to the motorised regulators had to be closed. The regulators were manually operated to the lowest limit; the main pressure supply to the regulators was then opened and, using the "increase" button, the required pressures were regulated through the motorised valves which were read by four pressure transducers mounted after the stepper motor outlet. At this stage the "cyclic valves" were opened and all "monotonic valves" were closed except the one for the intermediate principal stress which was kept constant throughout the cyclic process. When the application of correct initial stresses was ensured the auto/manual switch was put on automatic.

Through a computer programme, changes in normal and shear stresses required in each continuous rotation test were pre-calculated once the magnitude of the principal stress rotation and the mobilised angle of friction were inputted to the computer. Before releasing the vacuum from the sample and commencing the actual cycle, a

trial cycle was conducted to ensure the stepper motors were operating properly. The vacuum was then released and the cyclic phase started by specifying the number of cycles and the rotation angle. When the required number of cycles was completed the deformation was halted, and a radiograph was taken to provide a permanent record of strain. This process was repeated until a large deformation of the sample was obtained or until the desired number of cycles was reached.

All cyclic tests were conducted at periods of greater than 60 seconds. This enabled the author sufficient time to re-align the shear sheets and adjust the normal pressure backing plates as the sample changed shape. It should be noted that in the case of a stress level of σ_3 =30 kPa, the semi-rigid retaining vanes also had to be adjusted. The effects of a variation in the cyclic period on the strength of particulate materials have been reported by several investigators (Peacock and Seed, 1968; Lee and Focht, 1975; and Wong, 1986). All these authors reported no significant effects of cyclic frequency on the cyclic strength or the number of cycles to achieve failure. Wong (1986) conducted a series of cyclic tests on dense Leighton Buzzard sand samples using the DSC. All tests were carried out at a constant mobilised angle of friction of ϕ_m= 42° whilst the principal stresses were rotated through 55° under different cyclic periods. He observed that cyclic periods of greater than 20 seconds did not influence the rate of strain accumulation provided that there was a good lubrication at the plane strain sides, but reduced rates of strain accumulation per cycle were recorded using cycles with shorter periods. This was thought to be an effect of the lubricating grease viscosity.

The number of cycles between radiographs was arbitrarily chosen. More stops for radiography were necessary during the initial stage of most cyclic tests as the rate of deformation was less predictable. The cumulative strain distributions could then be calculated using these radiographs. It was assumed that the stress-strain behaviour was not affected by the pause for radiography.

A correction for angular distortion was also made within the cyclic test whenever required. This was achieved by inputting the angle of distortion (α) as defined in Figure 4.6 and the new normal and shear stresses required by the motorised pressure regulators were then recalculated.

At the end of a cyclic test the sample was placed under vacuum. In order to eliminate the effects of intermediate principal stress all cyclic tests were performed at a constant value of b= 0.3.

5.3.2 Continuous rotation tests on dense sand at σ_3=30 kPa

The first series of cyclic tests were carried out on dense sand samples at σ_3=30 kPa. The main objective of these tests was to make checks on the completely new design of the Daisy Chain shear sheets in which the stretching component would be loaded, unloaded and then reloaded during the cyclic process. It would also be possible to compare the experimental results with previous published data (Arthur et al., 1980; and Wong and Arthur, 1986), as well as investigate the effects of cyclic rotation of principal stress directions when the boundary shear stresses were cycled.

Figure 5.7 illustrates the results of several cyclic rotation tests carried out using the DCDSC at σ_3 =30 kPa with different angles of rotations and different mobilised angles of shearing resistances. From this Figure an unending accumulation of shear strain was attained when the material was loaded cyclically under a sufficient mobilised angle of friction. The same trend has been observed by other investigators (e.g. Arthur et al., 1980; and Wong, 1986). A lower accumulation of strain was observed when lower mobilised angles were involved. The effects of cyclic amplitude and the effects of the magnitude of the mobilised angles of friction are clearly shown in Figures 5.8 and 5.9 respectively. The results of five tests are illustrated in Figure 5.8. In the monotonic stage of all tests the mobilised shearing resistance was raised to 42° as 4% of shear strain accumulated. In the cyclic tests the amplitude of rotation was increased but the mobilised the angle of shearing resistance was held constant at ϕ_m=42°, for all tests. At a glance these curves indicate that there was a tremendous variation in the development of permanent shear strains with different cyclic amplitudes. The tests with larger angles of rotation accumulated strain at a higher rate as the number of cycles increased.

Figure 5.9 illustrates the effects of mobilised angle of shearing resistance when the rotation angle was held constant at 40°. The magnitude of accumulated strains recorded in these tests was higher than in the tests carried out by Wong (1986), as well as those which were conducted in the present research at a lower stress level of σ_3 =14 kPa, which will be discussed later. It may be that the effect of membrane confinement was reduced at this higher stress level. The dense sand sample could then more easily deform with less artificial boundary restraint being imposed by the sample membrane on the sample.

The tests described above were carried out when a liberal amount of lubrication was applied to the plane strain boundaries. Figure 5.10 shows the effects of insufficient

lubrication on the boundaries for the continuous cyclic tests. Comparison of Figures 5.10 and 5.8 show that the rate of strain accumulation was reduced substantially due to the effect of end restraint.

The accumulation of strain due to the continuous cyclic rotation of principal stresses was also accompanied by accumulation of the volumetric strains. Figure 5.11 indicates different dilatancy for four of the tests. Volumetric behaviours are presented using the relationship between major and minor principal strains. The angle of dilation for each test was derived from the slope of the plot. A quite linear relationship could be observed for all tests which indicated all samples were dilating at a constant rate of dilation, cycle after cycle. This Figure also illustrates an increase in rate of dilation as the mobilised angle of friction was increased. This behaviour was also found to be independent of the amplitude of rotation.

Figures 5.12 and 5.13 illustrate the uniformity of distribution of strain within these samples. These Figures once again provide valuable information to verify the performance of the apparatus for large deformations. Figure 5.14 shows the coefficient of variation for these tests. It can be seen that the uniformity of strain within the cyclic process is higher than in the monotonic tests indicating a homogeneous media. Figures 5.15 and 5.16 show a dense sample after accumulating up to 50% shear strain during a cyclic loading. This amount of deformation is approximately five times greater than the shear strain that an initially dense sample would gain at failure under monotonic loading. Also even with such large deformations no failure planes were observed in these cyclic tests.

5.3.3 Continuous rotation tests on dense and loose sand samples at σ_3=14 kPa.

After incorporating 4-1 reduction volume boosters (Fairchild Model 20), the performance of the pressurised regulators at low stress levels were improved to a satisfactory level and there was every confidence in the motorised regulators to conduct cyclic tests at a stress level of σ_3 =14 kPa. Figure 5.17 illustrates a typical experimental chart recorder plot of both the boundary normal and shear stresses during 50 cycles in a 90° rotation test. This Figure shows the precise and uniform application of cyclic waveforms through the motorised regulators after the reducing boosters were incorporated. The required values for maximum and minimum boundary stresses are compared with the actual ones. It is clearly seen that a minimum shear stress of 0.7 kPa was achieved instead of zero but this could be

tolerated at this stress level.

As mentioned earlier these tests were carried out with the aim of providing a direct comparison with those of Wong (1986), to identify the effects of principal stress rotation when the boundary shear stresses were cycled and the mean stress level was held constant, and to extend the experimental observations of Arthur and Wong (1986) for the lowest mobilised ϕ and highest angle of rotation θ= 90° for both dense and loose sand samples.

Figure 5.18 illustrates the results of four dense samples which were subjected to the same amplitude of cyclic principal stress rotations. In each of these tests a constant mobilised ϕ was set up whilst the principal stress directions were rotated continuously. There was a very distinct response for tests 85a and 86a which only differed by two degrees in the mobilised angle of friction. These results suggest the possible existence of a threshold for the mobilised shear strength of the sand at a particular amplitude of cyclic principal stress rotation above which large strains might tend to develop with increasing number of cycles. In the same Figure, test 80a was cycled up to 1000 cycles but only 1.79% shear strain was achieved at the end of the cyclic process.

Figure 5.19 again shows linear relationship in the dilation rate which implies a constant dilation rate after several cycles. There was an increase in the dilation rate as the mobilised angle of friction was increased. An example of uniform distribution of strain for these samples is illustrated in Figure 5.20.

The results indicating the development of shear strain in loose samples of Leighton Buzzard sand when subjected to cyclic rotation of principal stress direction is demonstrated in Figure 5.21. The possible threshold for the lowest mobilised angle of friction, ϕ_m =15°, at which loose sand samples tend to gain large strain is identified. Also the lowest limit at which the material would not gain appreciable strain even after 2000 cycles is established. The low stress ratio tests were all cycled with large angles of rotation.

The volumetric behaviour for loose cyclic rotation tests was quite different from those of dense samples and were not linear. Figure 5.22 illustrates the volumetric behaviour of loose samples when subjected to cyclic rotation of principal stress direction. It can be seen that the material was extremely contractive in the initial cycles particularly in the rotation tests at low mobilised angles of friction. This low

dilatancy rate did not continue, but the rate increased after some strain was attained. This larger dilatancy rate was associated with reduced strain and eventually the sample stabilised.

The volume change behaviour of these continuous rotation tests is illustrated in Figure 5.23. The volume change of a loose monotonic test is also included for comparison. A significant contraction can be observed, particularly in the first few cycles of the tests when compared with the monotonic one and is directly attributed to rotation of principal stress directions.

Figure 5.24 illustrates the comparison of two continuous rotation tests carried out, one in the DSC and the other in the DCDSC with identical mobilised angles of friction and angle of rotation. The only differences in these two tests were the imposed stress paths. Although, as illustrated in Figure 5.1, there may be an effect due to the stress level variation in the initial cycles of the continuous cyclic tests, these two tests showed very good repeatability. Thus it appears that the influence of continuous rotation of principal stress direction on the stress-strain behaviour of particulate material is dominant and the stress level variation is secondary. This also is a means of comparison of the two apparatuses.

The presented data demonstrates the effects of continuous and cyclic rotation of principal stress direction on the Leighton Buzzard sand. It was stated that there were no failure planes in the continuous rotation samples while failure planes have occurred in all jump rotation tests previously reported (e.g. Arthur et al., 1980; and Wong, 1986; and special cyclic tests with no rotation of principal stress directions by Wong, 1986) as well as all the monotonic tests. However, two samples failed after gaining an enormous amount of strain. This was thought to be due to the boundary disturbance when adjusting the normal pressure backing plates. Absence of failure planes even in large deformation of 50% shear strain in continuous rotation tests could be attributed to the uniformity of contact distribution of particles that is gained through cyclic rotation of the principal stress direction.

It was mentioned earlier that the principal stresses were rotated continuously in a sinusoidal waveform. It is interesting to note that although the principal stresses rotate continuously during a cycle, the principal stress increment directions rotate discontinuously through 90°. Figure 5.25 illustrates this for a typical cycle. It is seen that although there was only one pattern for principal stress increment direction, i.e. 90°, the variation in principal stress directions was arbitrary and could be selected

between 0° and 90°.

Wong and Arthur (1986) in an investigation using a high quality photographic camera, studied the principal strain increment direction variation through typical continuous cycles for both loose and dense Leighton Buzzard sand samples. Figure 5.26 shows their results with three different amplitudes of principal stress rotation. These authors showed that the phase differences were effectively independent of the angle of rotation and the voids ratio; the lowest amplitude (θ=30°) still resulted in a nearly 90° rotation of principal strain increment, following the data of the other larger amplitude cycles (θ=55°, θ=70°). They indicated that within a cycle the principal strain increment direction is controlled by the stress increment direction rather than the stress.

5.3.4 Post cyclic monotonic tests

Induced anisotropy is defined as anisotropy caused by strain under applied stresses. One of the methods to study the effects of induced anisotropy in a soil sample is to load the initially isotropic sample to a pre-determined stress ratio; return the stress state to the isotropic condition; impose a jump rotation of a fixed amount of the major principal stress on the sample; then finally examine the strain response of the reloaded sample. This method has been employed by several investigators (e.g. Arthur et al., 1977; Arthur et al., 1980; Wong and Arthur, 1985; and Wong, 1986). These authors extensively studied the effects of induced anisotropy on Leighton Buzzard sand, and observed several important results from their experiments. They found that the stiffness obtained on reloading the sample at a different direction was significantly altered but the ultimate failure strength of the material was not significantly affected by the induced anisotropy in drained conditions.

These results have important implications from the "engineering" as well as the research points of view. Most soils in field conditions have, at some stage in their history, been loaded and subsequently unloaded. This is frequently apparent in areas of high seismic activity and where wind and wave action occurs. The results of such events, in the light of the above experiments, would have effected the stress-strain behaviour, but not the strength.

Most previous work was restricted to the study of induced anisotropy caused by a monotonic type of loading. In the present research the author has covered a range of dense and loose samples which have initially been loaded under continuous and

cyclic rotation of principal stresses and then subsequently loaded monotonically. The results of such tests will give an insight into the fabric changes which take place within the samples that have already been affected by the continuous and cyclic rotation of principal stress directions.

5.3.4.1 Procedures for monotonic post cyclic tests

To consider anisotropy tests samples were initially cyclically loaded as previously described. At the end of the cyclic process, the deformed sample was placed under vacuum and the cyclic loading valves closed whilst the monotonic valves were opened. The vacuum was released and the sample was monotonically unloaded. The unloading process was carried out in very small increments and in each small increment the boundary shear stresses were first reduced, then the reduction of the normal stresses and the intermediate principal stress followed until an isotropic state of stress was reached. At this stage a radiograph was taken and developed that was to represent the initial state for the subsequent loading. The sample was then monotonically loaded and radiographs taken at different stress ratios as required. Adjustment of the backing plates and the alignment of the shear sheets was conducted depending on the state of sample deformation. All tests were conducted with the major principal stress direction acting at ψ =45° ,$\delta\psi$= 0°; the mean direction of the previous major principal stress rotations. The stress path for these tests is defined in Figure 5.27.

5.3.4.2 Test results for dense samples

Figure 5.28 shows the subsequent stress-strain response of constant direction monotonic tests carried out on initially dense sand samples which had already been subjected to continuous and cyclic rotation of principal stress directions (Figures 5.18 and 5.21). The volumetric behaviour of these tests is also illustrated in this Figure. As the major principal stress direction coincided with the mean direction of the previous cyclic rotation, a pronounced stiff behaviour was observed in the stress-strain curves.

The degree of induced anisotropy was controlled by the magnitude of strain that was accumulated in the previous cyclic loading. From this Figure it can be seen that the test in which the final accumulated shear strain was only 1.7% (in spite of being cycled up to 1000 cycles), produced an initially stiffer stress-strain curve but failed at the same stress ratio as simple monotonic tests of similar voids ratio i.e. R= 7. The

corresponding volumetric curve for this test was hardly affected and differed little from that of the normal simple monotonic test although the angle of dilation at failure increased by two degrees. However, the tests 84b and 86b in which the previous accumulated strains were 9.19% and 17.25% were much stiffer in their stress-strain behaviour. These tests did not strain more than 0.5% in the subsequent loading and failed at a sudden brittle type of failure. Lower stress ratio's of 6.4 and 6.0 at failure were observed for these tests. Nevertheless, these values for stress ratio at failure were not precise and could not be relied upon as the material at this stage of deformation was in a highly unstable state and any small changes in the boundary stresses could have triggered the rupture planes off. This could be observed from a high dilation rates for these samples. The angles of dilation at failure were increased from 16°, for a simple monotonic sample, to as much as 28° where the initially dense sample was continuously cycled under rotation of principal stress direction.

It was also noted that in these tests the angle of failure plane with the major principal stress direction was reduced from 30°±2° (Arthur et al., 1977) in the simple monotonic tests to 21°±2° which is generally considered as Coulomb failure. A summary of results of these post cyclic monotonic tests and their previous cyclic loading are shown in Table 5.1.

5.3.4.3 Test results for loose samples

Figure 5.29 illustrates the effects of induced anisotropy on loose samples. The stress-strain curve and volume change for simple monotonic loose test is also plotted for comparison. Here again the influence of cyclic rotation of principal stress direction on the stress-strain behaviour and volumetric behaviour of initially loose samples are clearly demonstrated. The deformation in these samples also depended on the previous strain accumulated during the cyclic process. There was a stiffer stress-strain deformation response as the previous accumulated strains increased. The initially loose samples behaved as dense samples although the final voids ratios for these tests did not decrease substantially at the end of the cyclic rotation tests. For example, maximum decrease in the voids ratio for the test that sustained 21.94% shear strain was only 0.05, i.e. from e_0 =0.74 to e_f=0.69, but the stress ratio at failure increased to R=6.1 (ϕ_f =46°). This interesting phenomenon in loose samples which had been subjected to continuous rotation of principal stress direction and gained substantial strength without being significantly densified is important in the assessment of the behaviour of particulate materials.

It is interesting to note that although the loose samples in the simple monotonic tests were strained up to 14%, no failure planes were observed in these tests. All loose samples which underwent a continuous cyclic rotation path produced failure planes when subjected to subsequent monotonic loading even though they were not strained more than 8%. The observed failure planes occurred at angles of 30°±2° with the major principal stress direction.

The volumetric behaviour of these tests also illustrates that the dilation rates increased from a loose behaviour to a dense as the previous cyclic accumulated strains were increased. Angles of dilation at failure increased from 5° in the simple monotonic test to 14.5°. A summary of these tests along with the previous cyclic tests illustrated in Table 5.2.

It can be concluded that cyclic rotation of principal stress did not only effect the initial part of the stress-deformation behaviour of both dense and loose sand samples but also affected the entire structure of the material. In the dense samples, a substantial increase in the dilation rate was observed. Changes in the failure plane angles from 45-1/4 ($\phi+\upsilon$) proposed by Arthur et al. (1977) to 45-ϕ/2 i.e Coulomb failure with brittle failure was observed. In the loose samples, the pre-failure stiffness and ultimate strength were significantly increased and failure planes were observed in all tests although the initial voids ratio did not change significantly.

These results suggest that there was a gain in contact normals aligned with the mean major principal stress direction during the cyclic loading process. The behaviour of material under subsequent loading were thought to be related to the super homogeneous structures which had been created during the cyclic loading with perhaps some increase in contacts of all alignments.

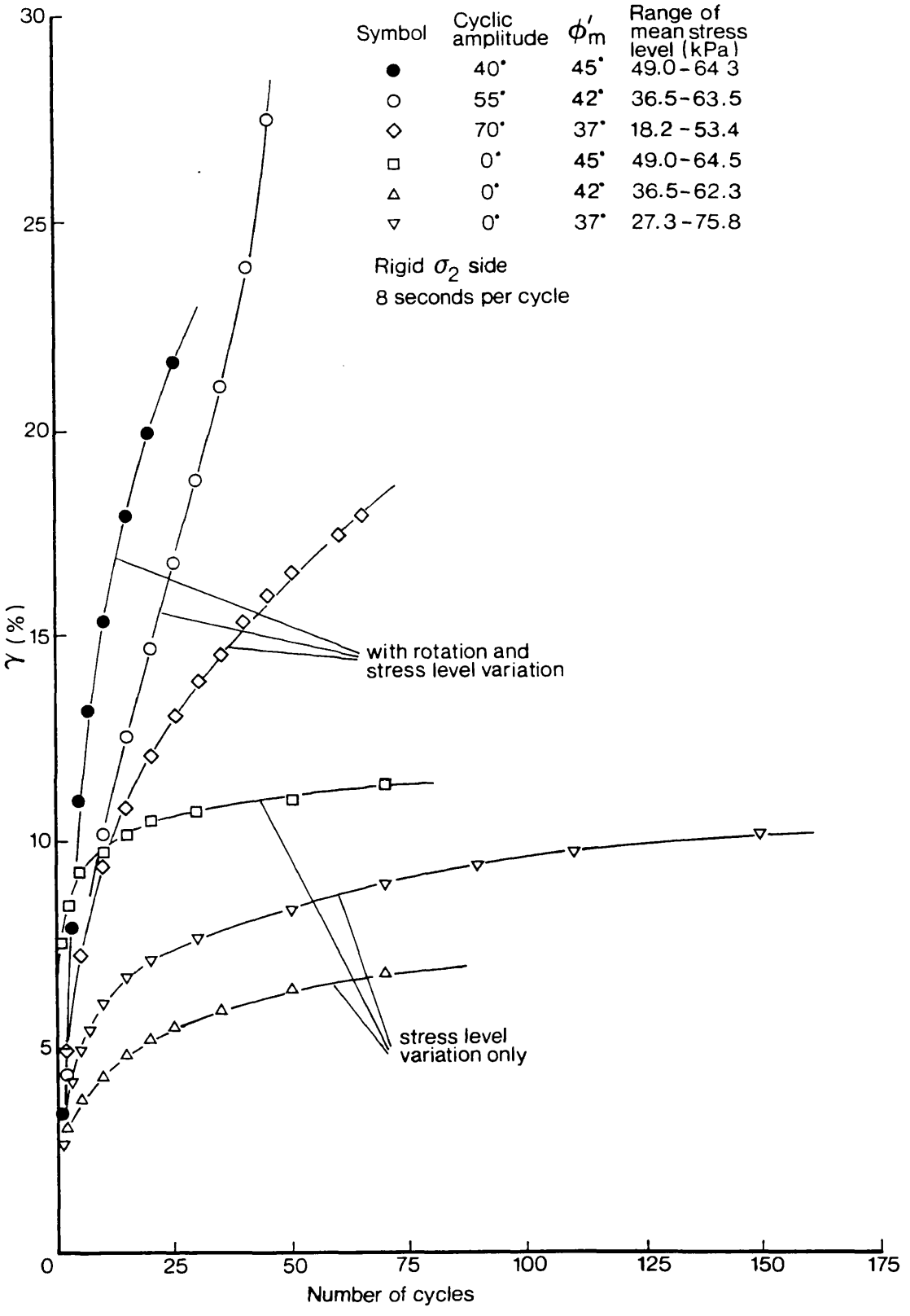

Fig. 5.1 **The effects of fluctuation in mean stress separated from cyclic rotation of principal stress direction (after Wong, 1986)**

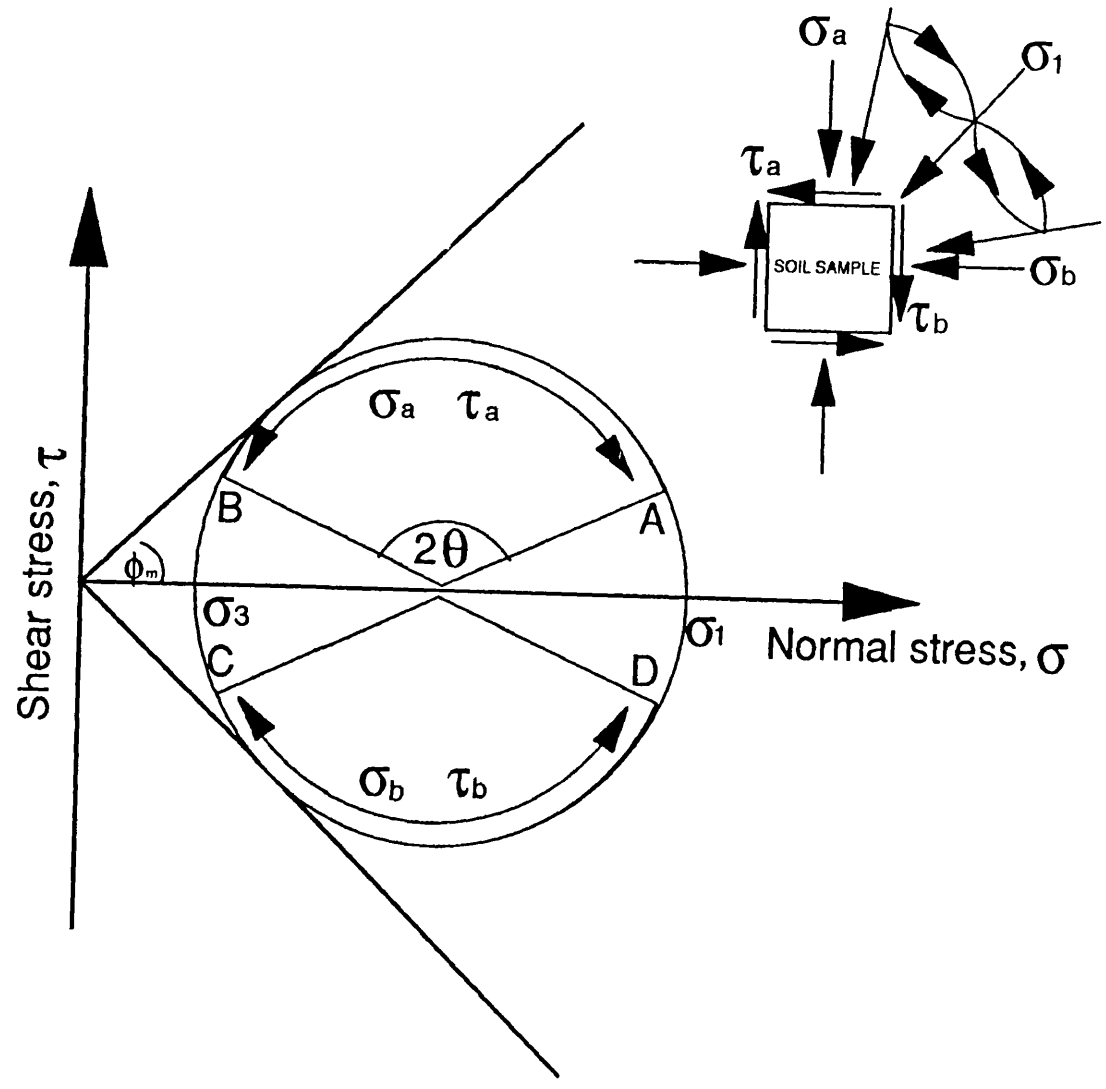

Fig. 5.2 **Rotation of principal stress direction during a typical continuous rotation test**

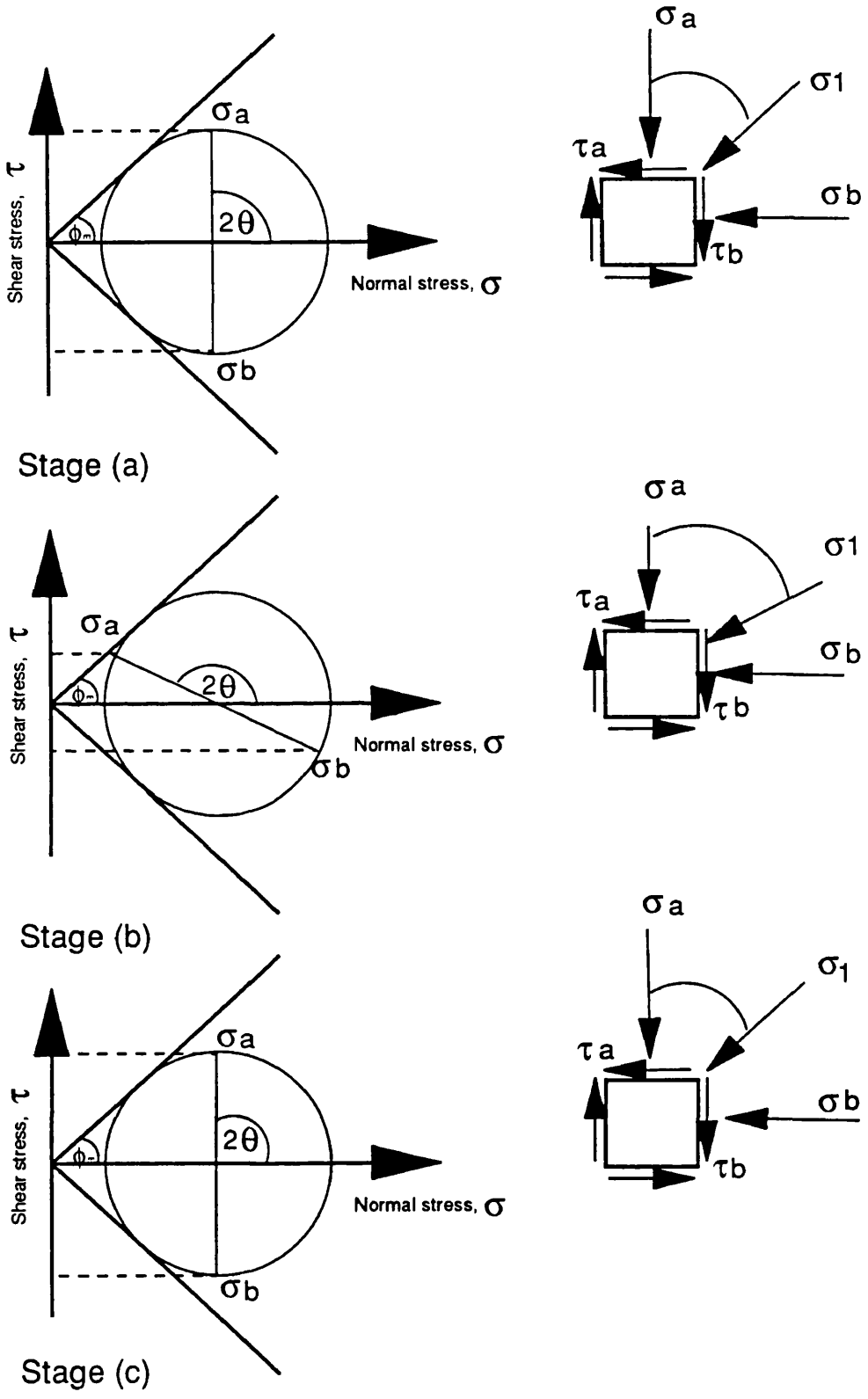

Fig. 5.3 **Different stages during a typical continuous rotation test when $(\sigma_1 + \sigma_3)/2$ is constant**

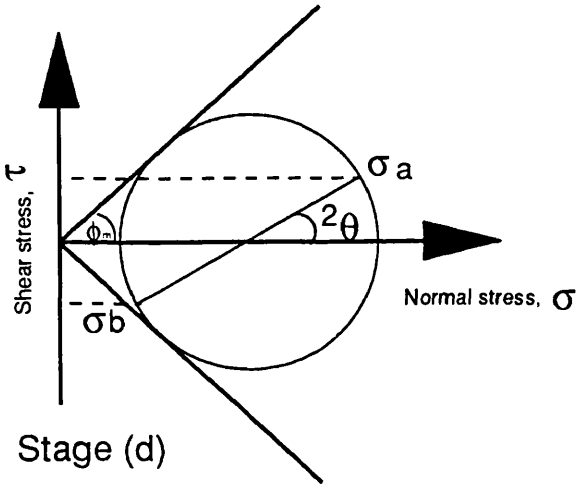

Stage (d)

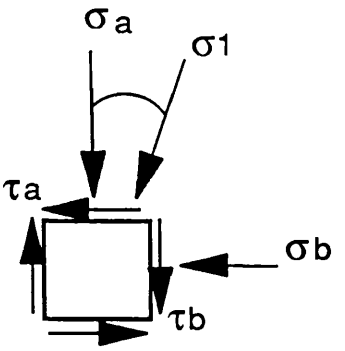

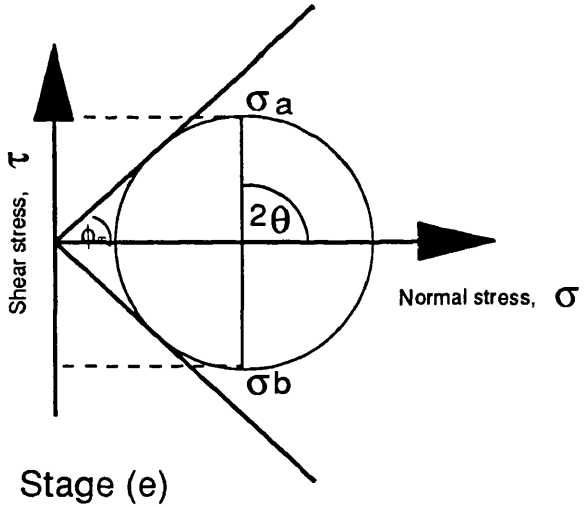

Stage (e)

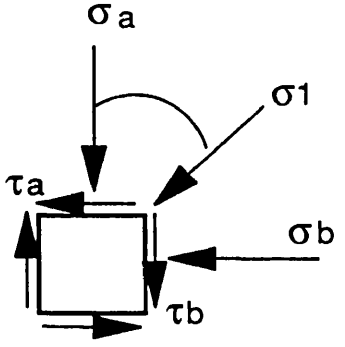

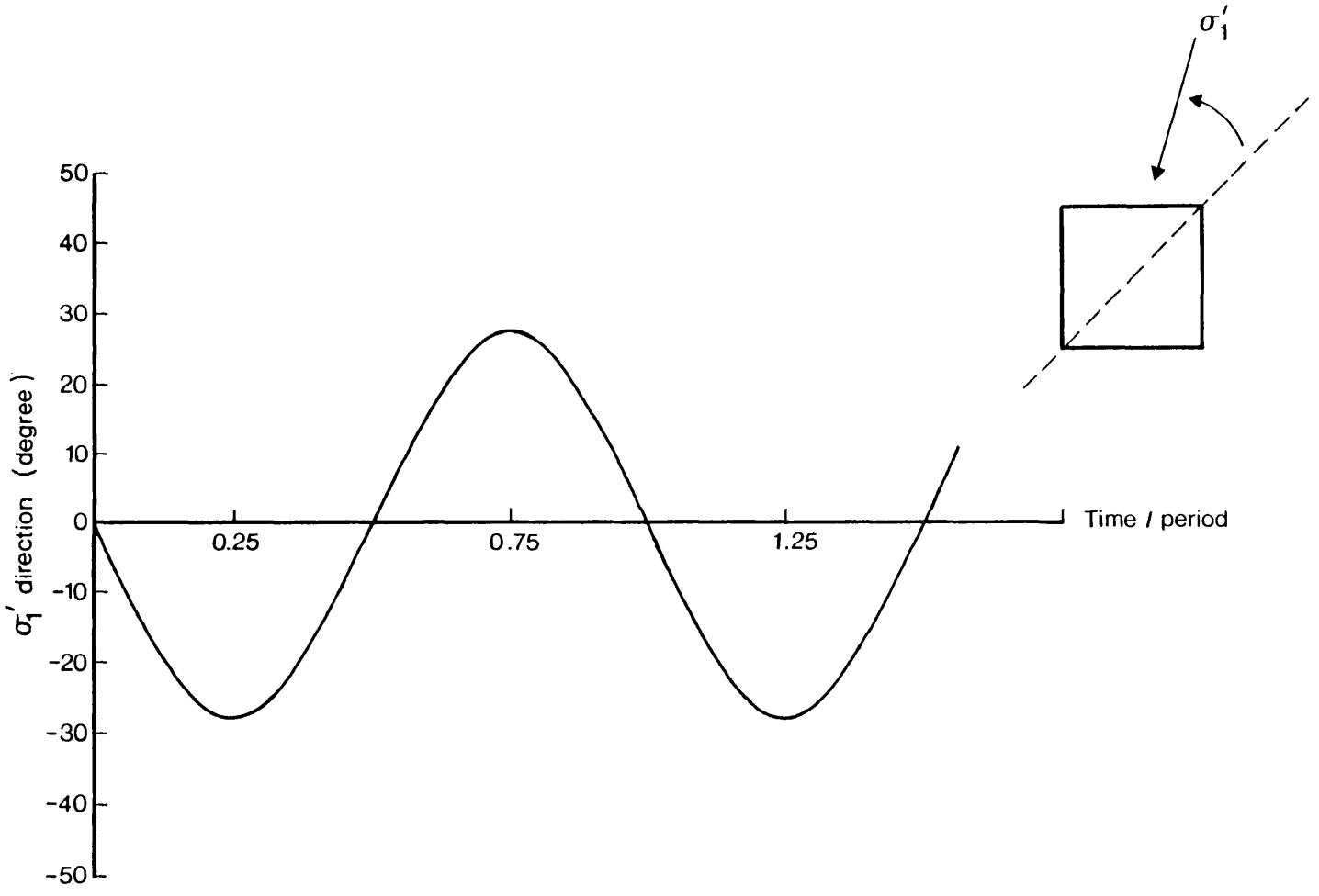

Fig. 5.4 **The sinusoidal variation of major principal stress direction in continuous rotation tests with time**

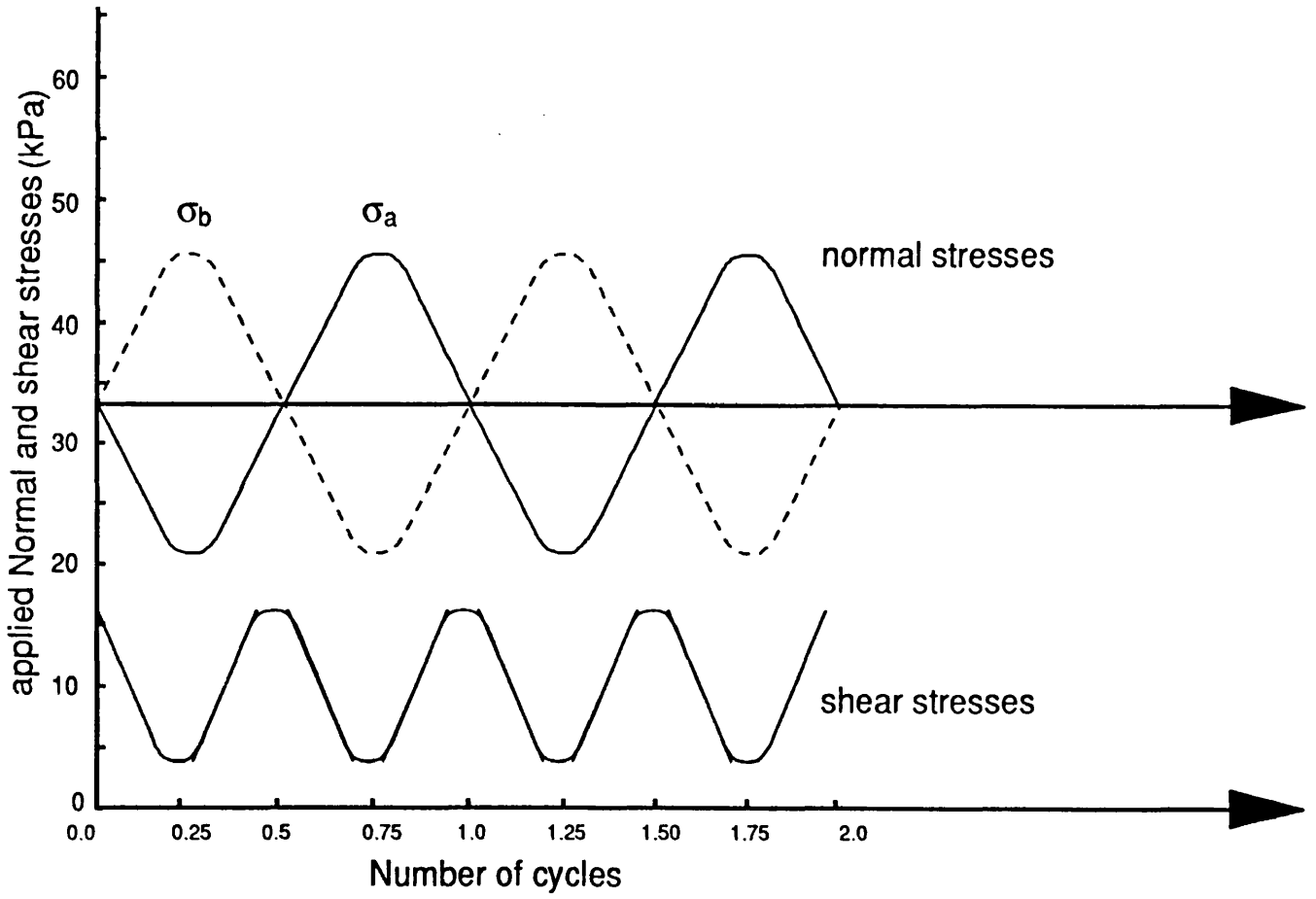

Fig. 5.5 **Normal and shear stress waveforms for the required stress path in a continuous rotation test**

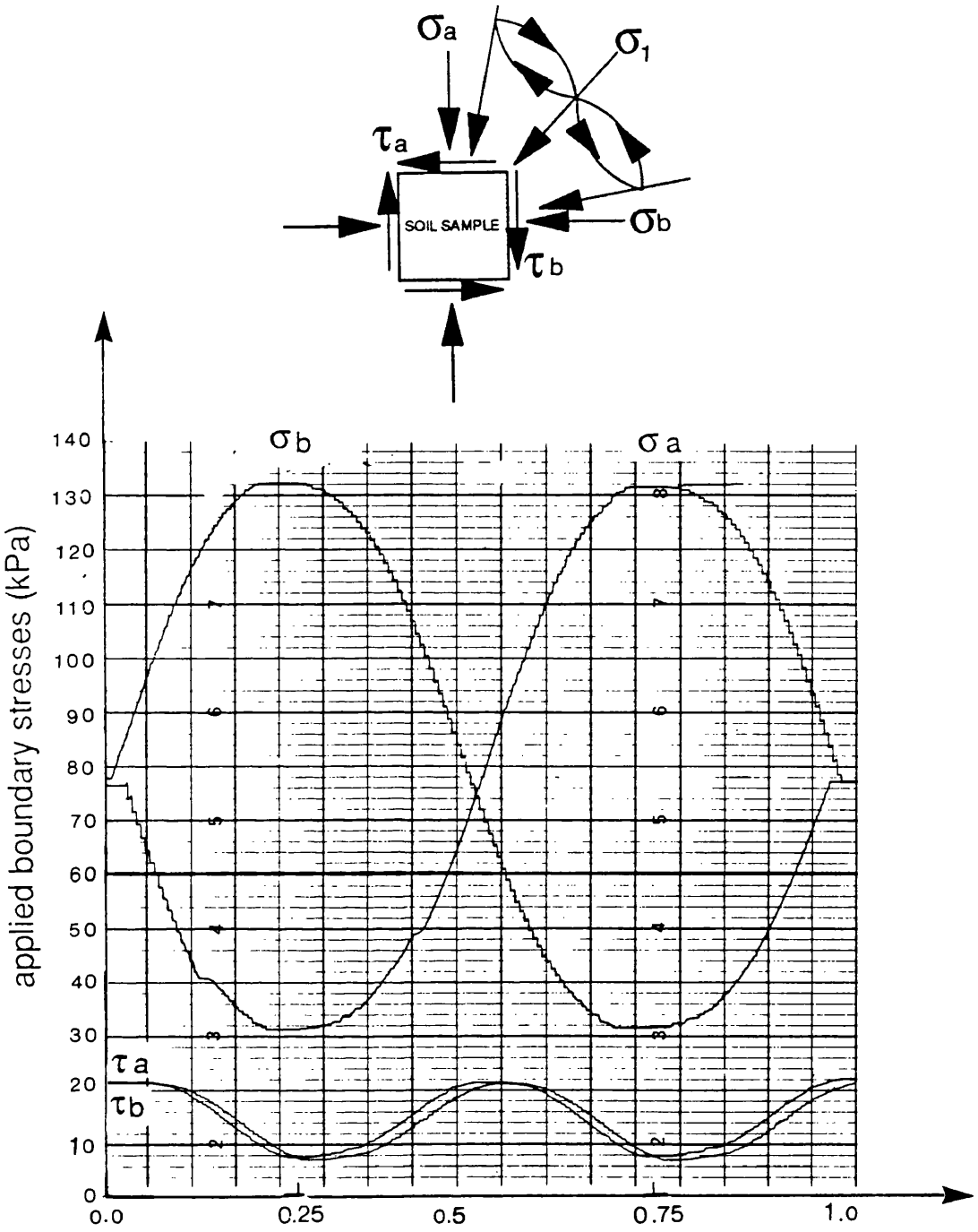

Fig. 5.6 Experimental boundary normal and shear stresses obtained during a cycle of continuous rotation test

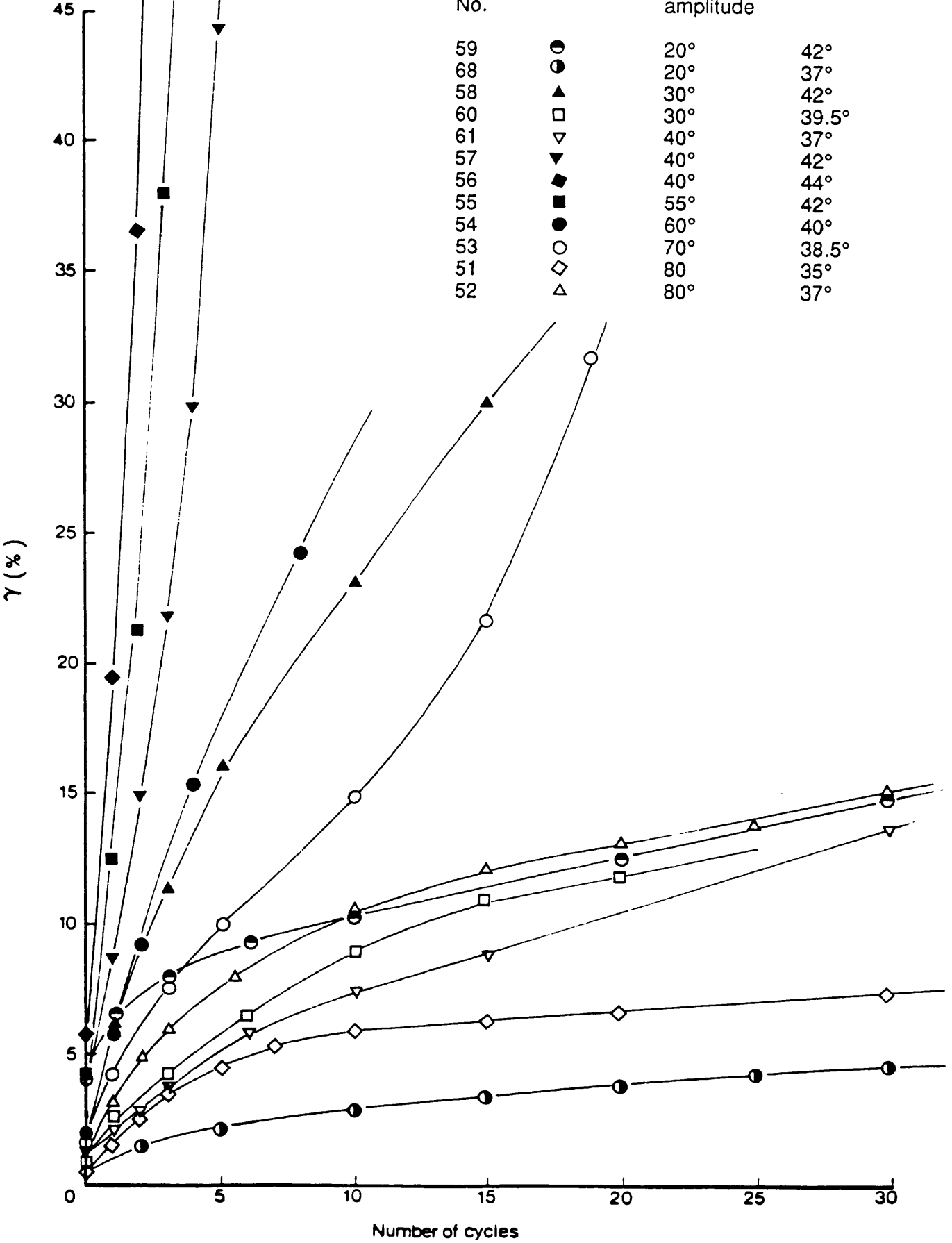

Fig. 5.7 The development of shear strain in dense samples of Leighton Buzzard sand during continuous and cyclic rotation of principal stress directions tested in DCDSC at σ_3 = 30 kPa

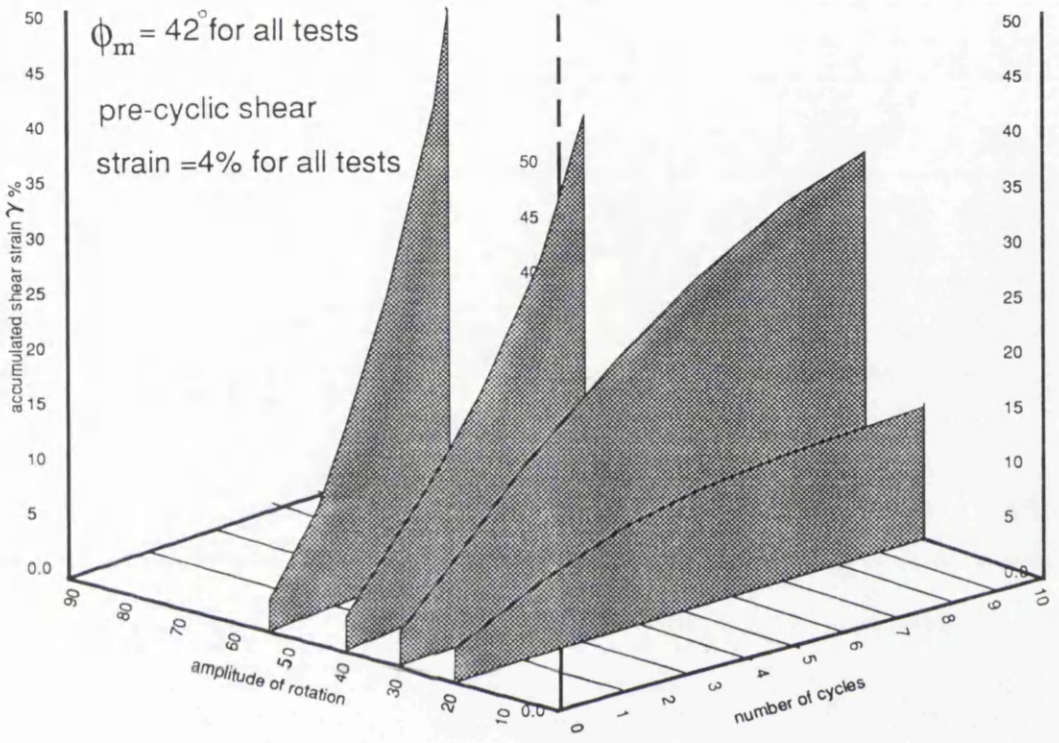

Fig. 5.8 Effects of cyclic amplitude on the behaviour of dense Leighton Buzzard sand samples tested with continuous and cyclic rotation of principal stress direction in DCDSC at σ_3 =30 kPa

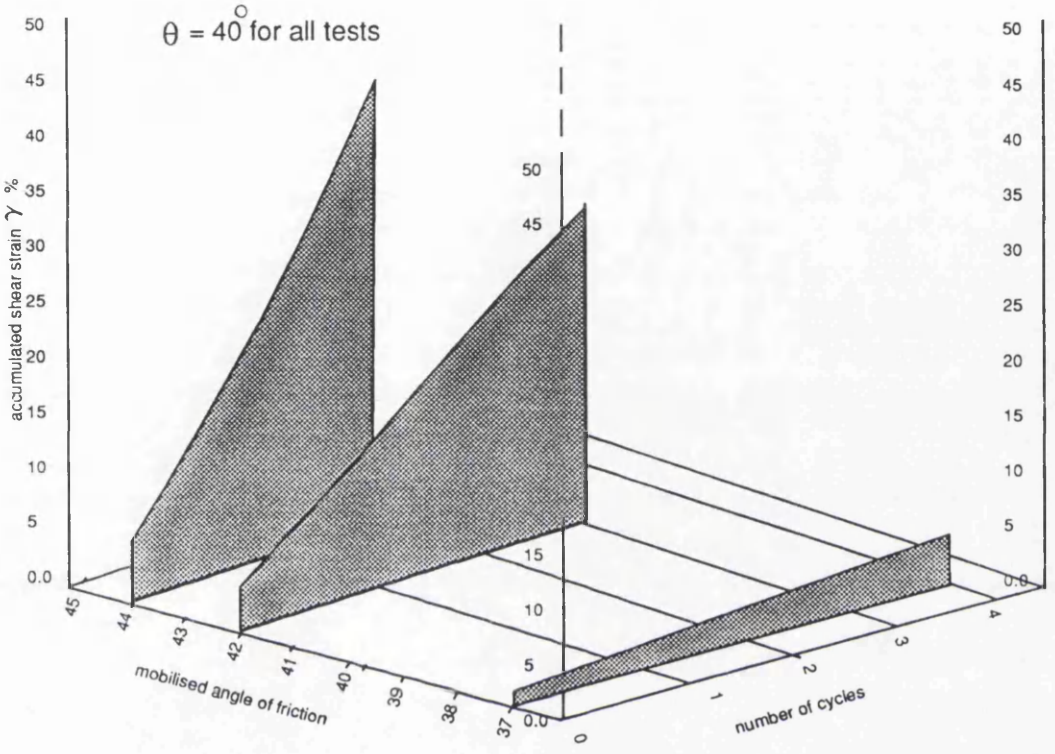

Fig. 5.9 Effects of the magnitude of mobilised angle of friction on the dense samples of Leighton Buzzard sand tested with continuous rotation of principal stress directions in the DCDSC at σ_3 =30kPa

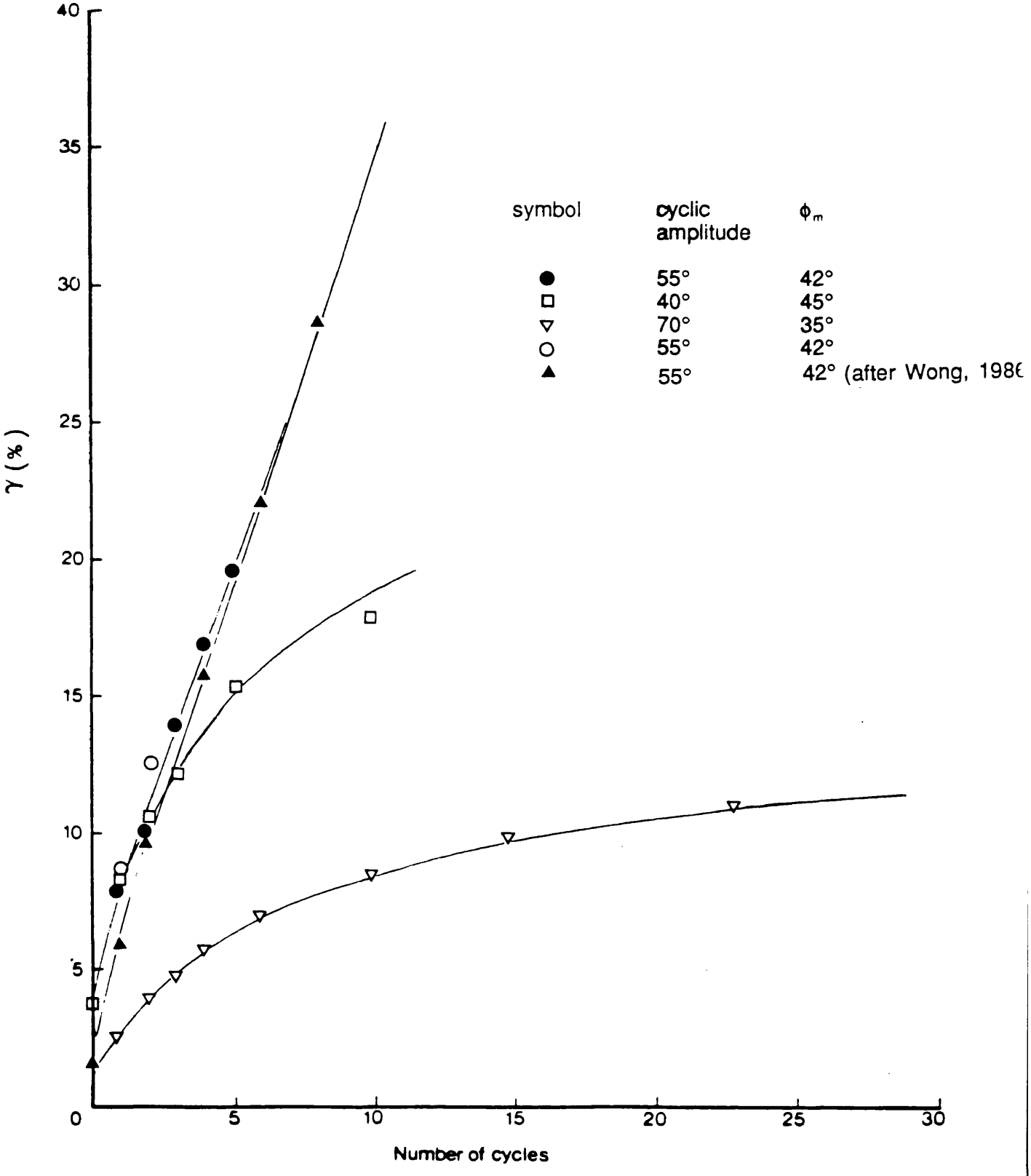

Fig. 5.10 The effects of in-sufficient lubricating boundaries on the continuous cyclic tests

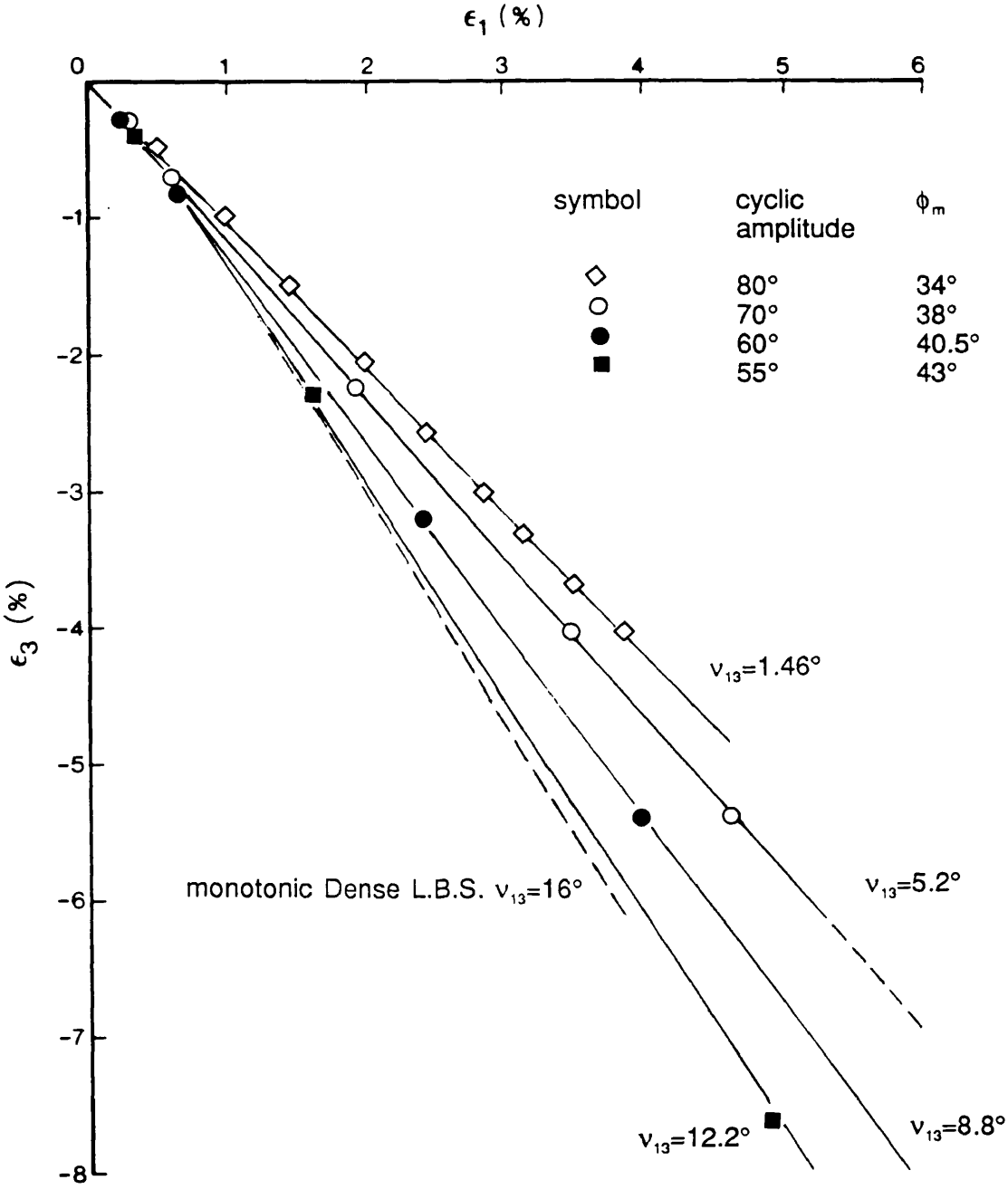

Fig. 5.11 Variations in the angle of dilation with amplitude of principal stress rotation and mobilised angle of friction on dense Leighton Buzzard sand samples tested in the DCDSC at σ_3 = 30 kPa

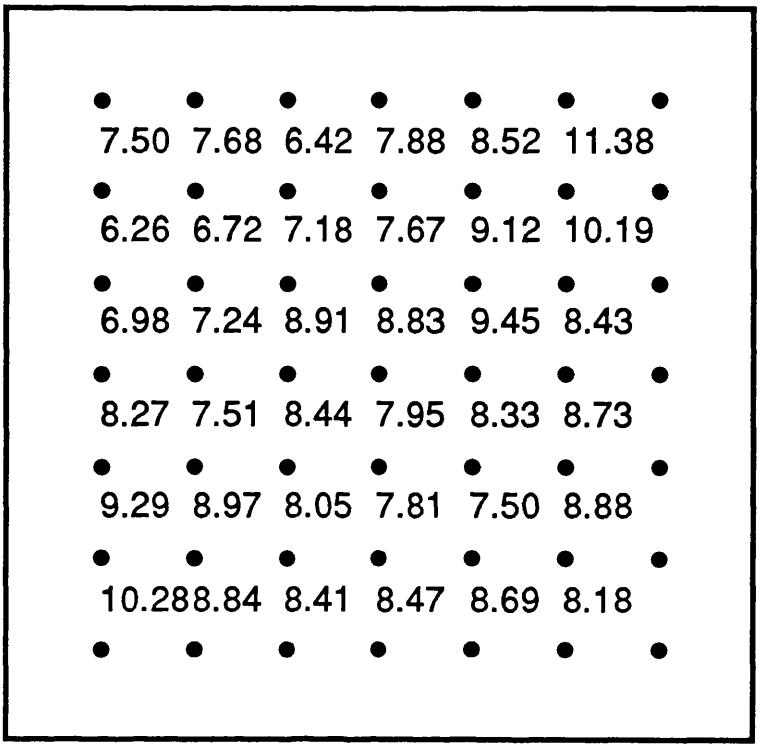

Major principal strain ε_1 (%)

Ave. in Area (1): 8.30 % with standard deviation : 1.07 %
Ave. in Area (2): 8.10 % with standard deviation : 0.79 %
Ave. in Area (3): 8.53 % with standard deviation : 0.18 %

Fig. 5.12 Typical strain distribution of a dense sample in a continuous rotation test at σ_3 =30 kPa

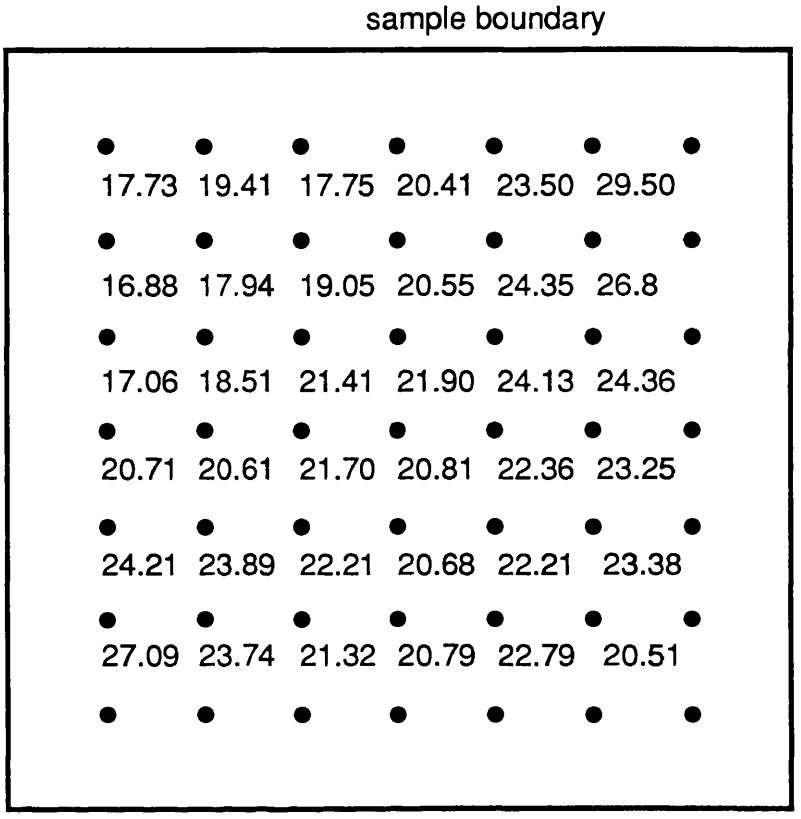

Shear strain (%)

Ave. in Area (1): 21.77 % with standard deviation : 2.85 %
Ave. in Area (2): 21.39 % with standard deviation : 1.88 %
Ave. in Area (3): 21.45 % with standard deviation : 0.48 %

Principal stress ratio =5
Principal stress direction =45°
after 2 cycles

Fig. 5.13 Strain distribution after large accumulated strain in a continuous rotation test

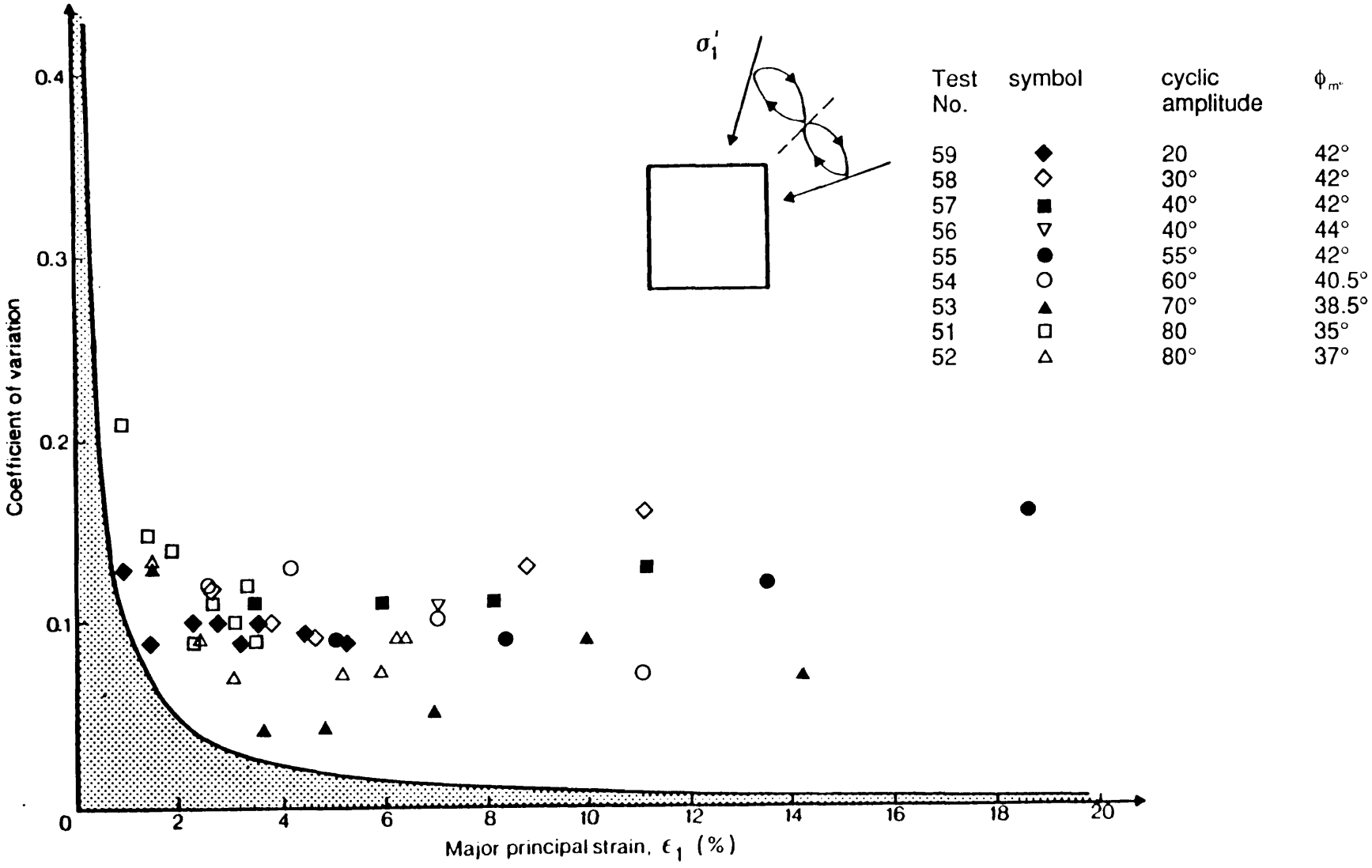

Fig. 5.14 Coefficient of variation for dense samples during continuous and cyclic rotation tests at σ_3 =30 kPa

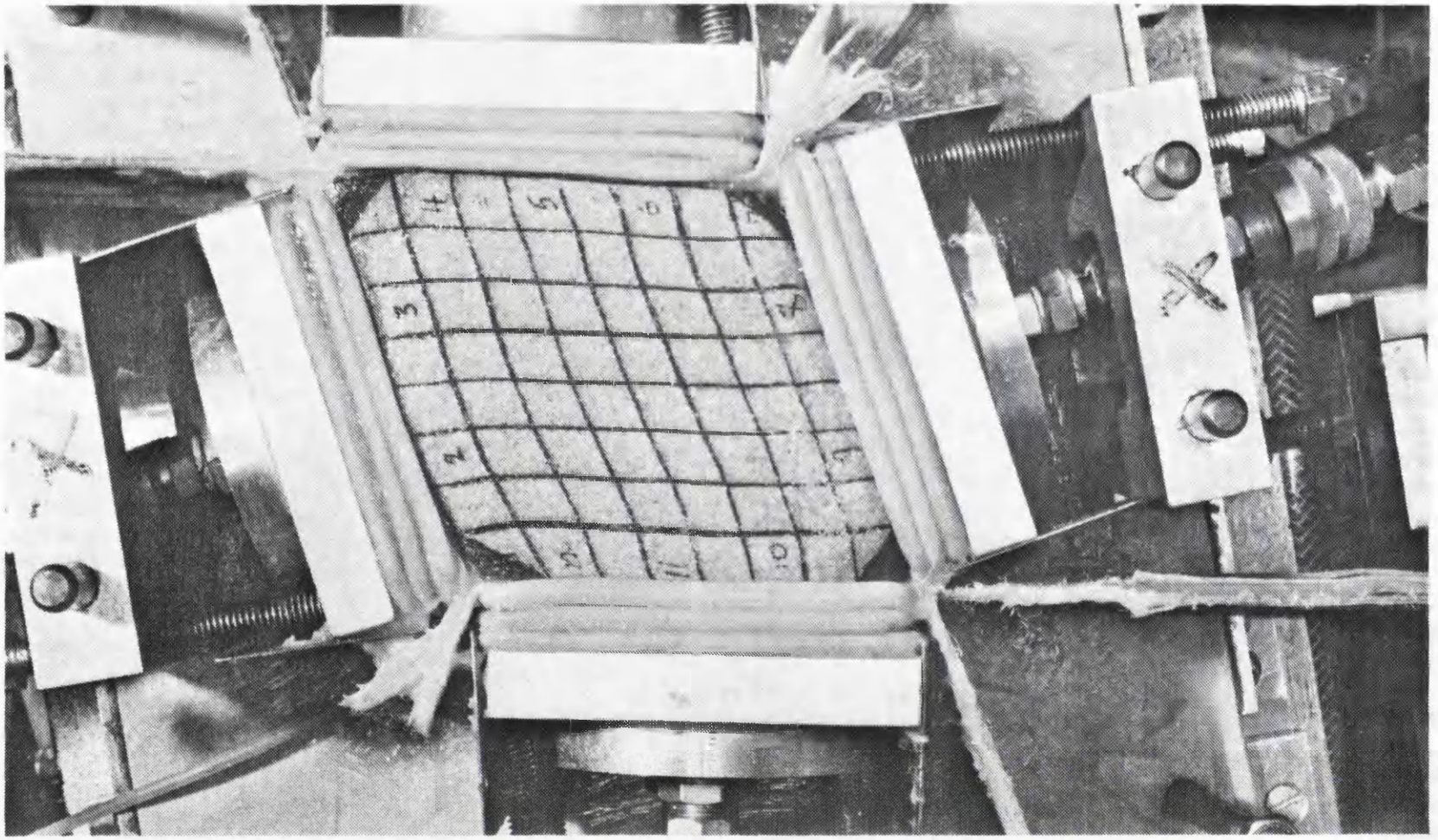

Fig. 5.15 A dense sample after an accumulation of up to 50% shear strain tested under continuous cyclic rotation of the principal stress direction in the DCDSC

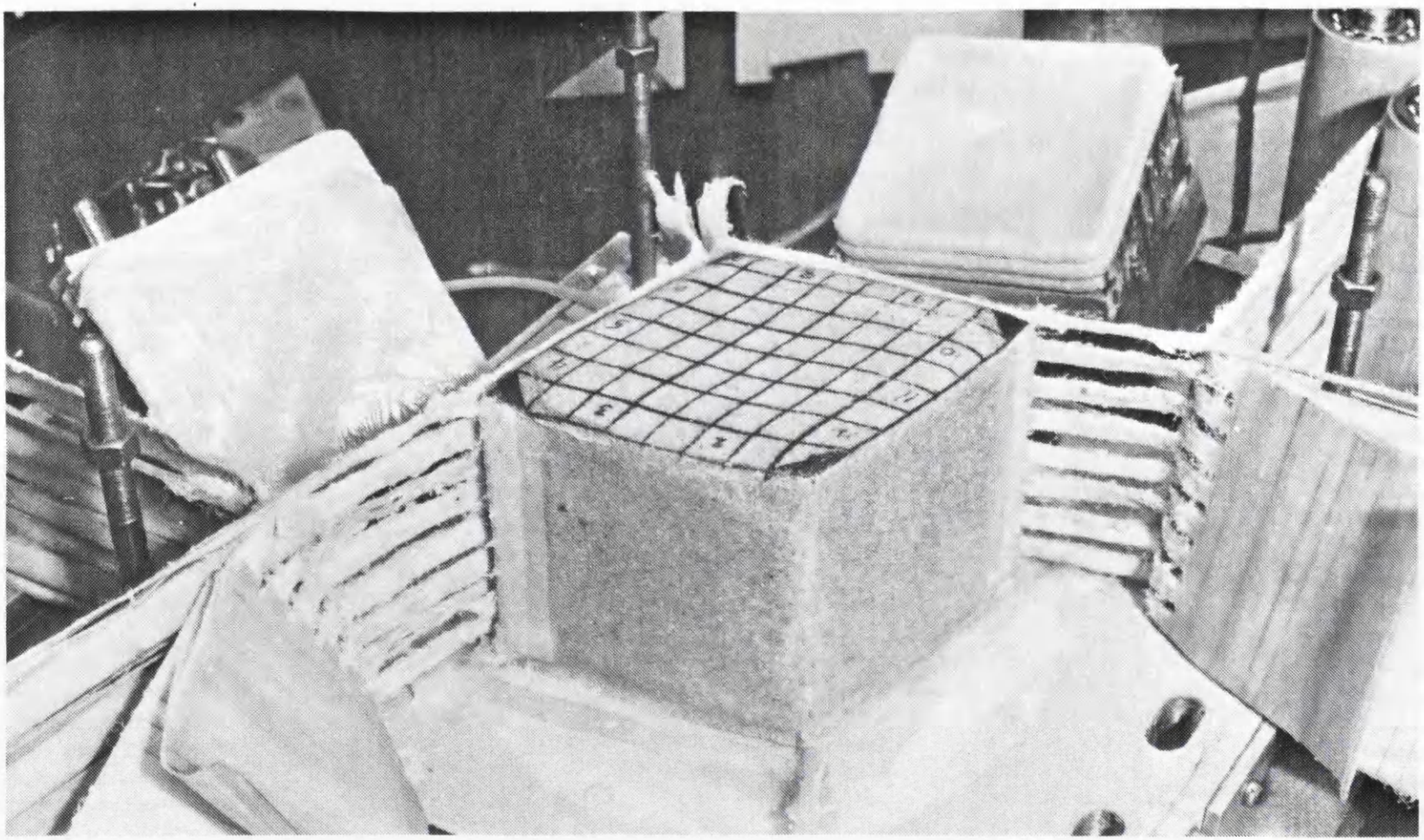

Fig. 5.16 **Dismantled sample of dense Leighton Buzzard sand after an accumulation of up to 50% shear strain tested under continuous cyclic rotation of principal stress direction in the DCDSC**

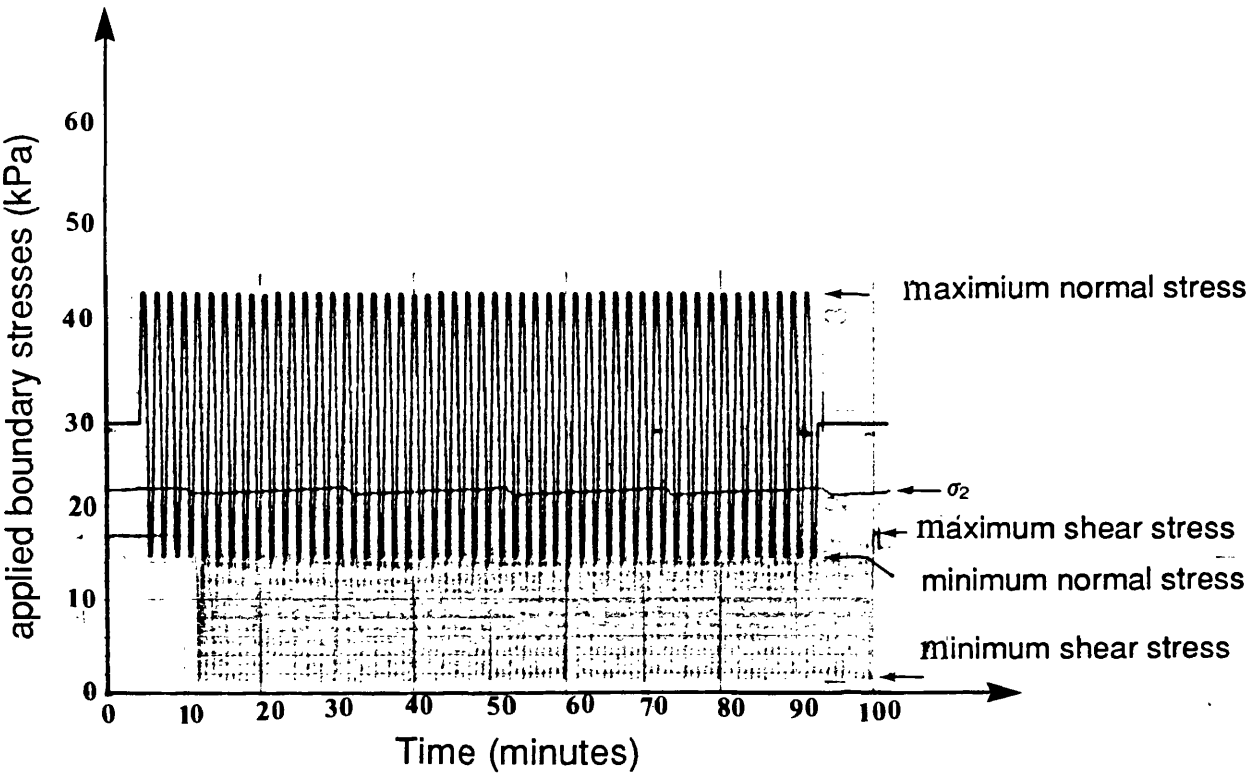

Fig. 5.17 A typical experimental chart recorder plot of both the boundary normal and shear stresses during 50 cycles in a 90° rotation test

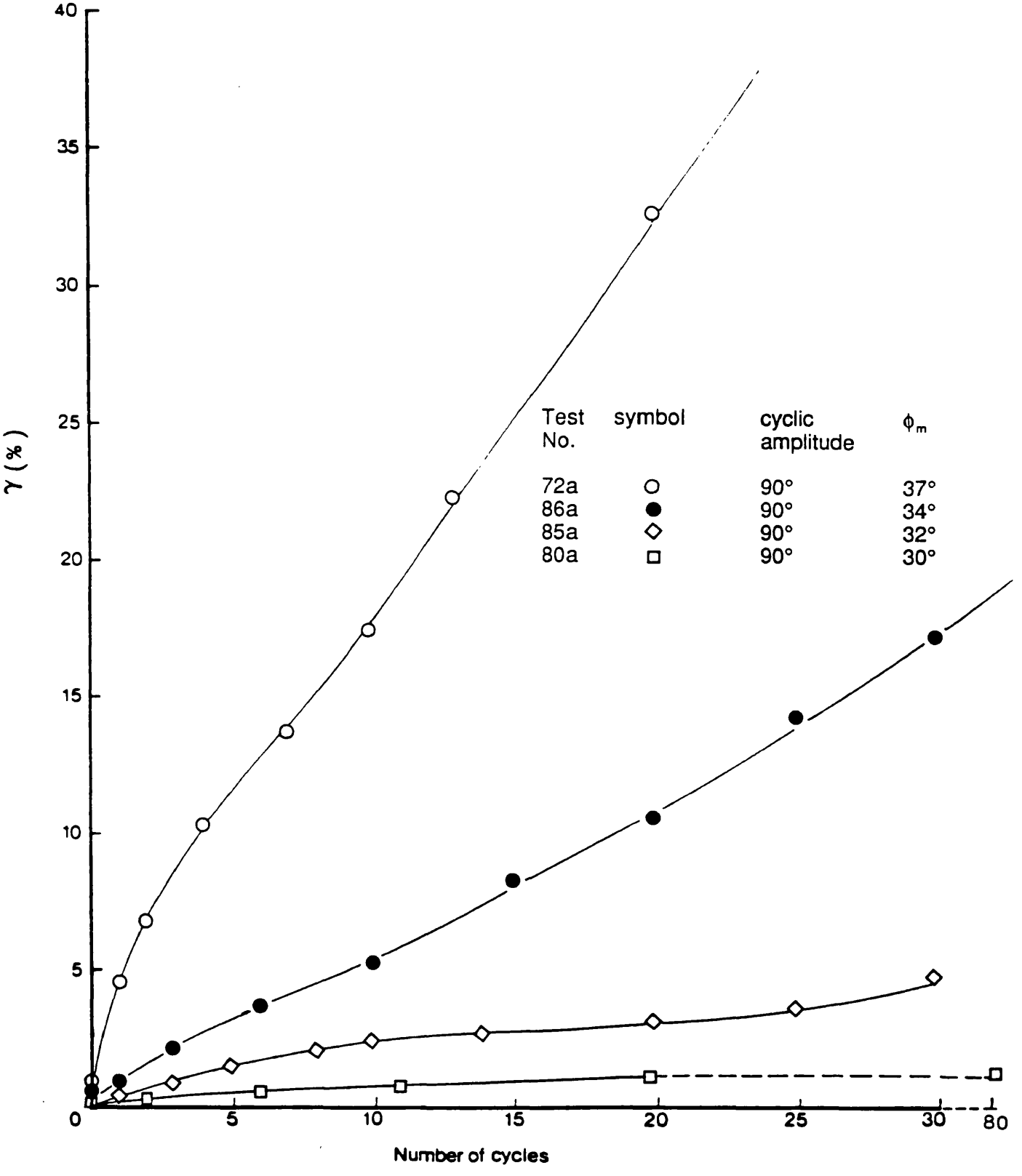

Fig. 5.18 **Development of accumulated shear strain for four dense samples subjected to the same amplitude of cyclic principal stress rotations tested in DCDSC at σ_3 =14 kPa**

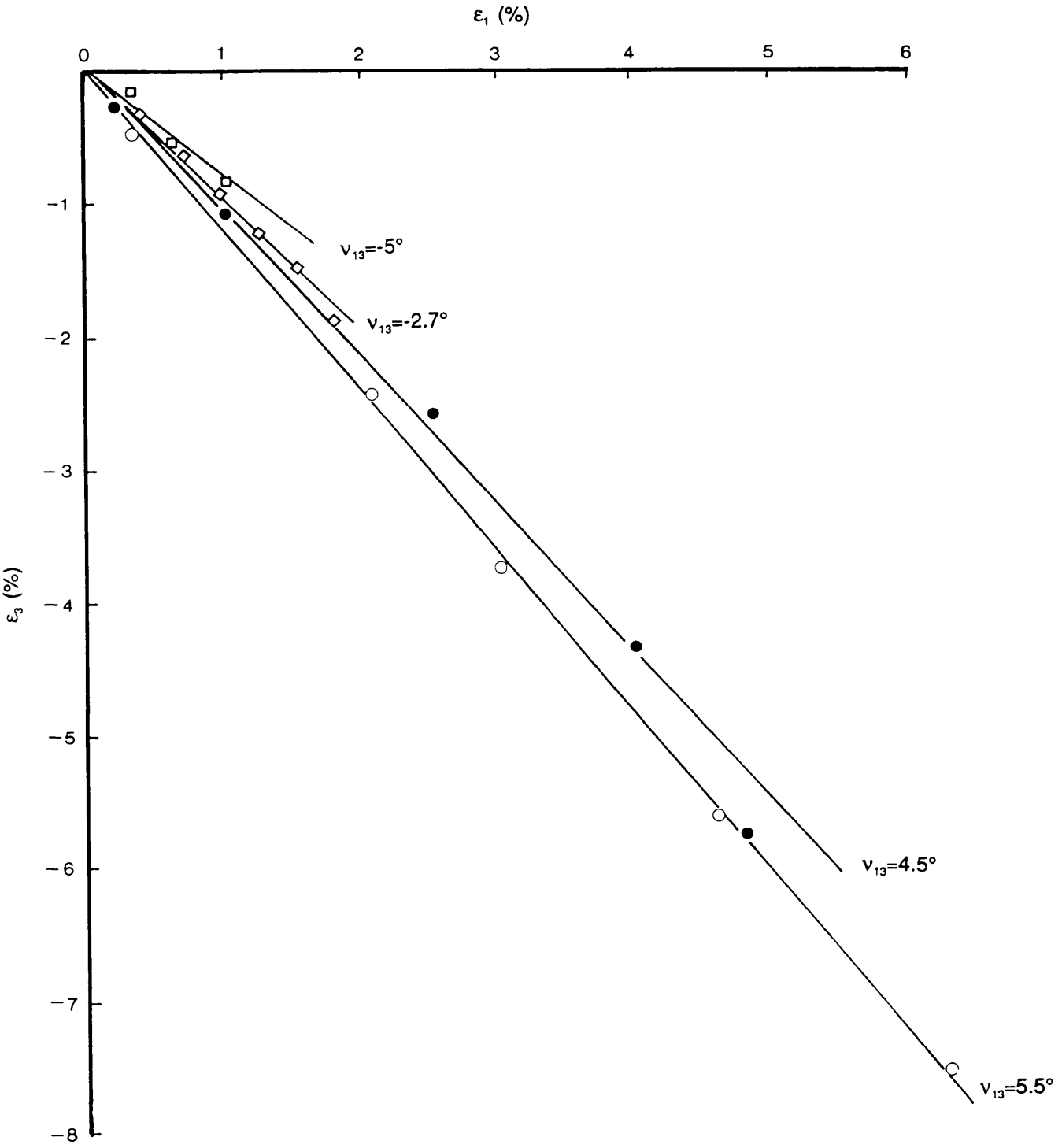

Fig. 5.19 **Variations in the angle of dilation with amplitude of principal stress rotation and mobilised angle of friction on dense Leighton Buzzard sand samples tested in the DCDSC at σ_3 = 14 kPa**

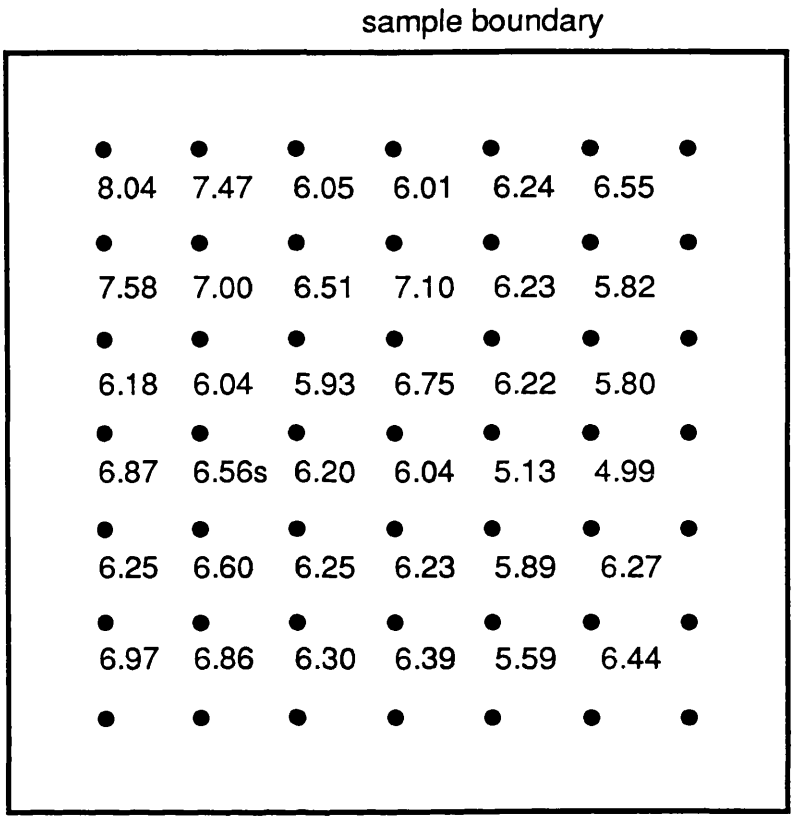

Major principal strain ε_1 (%)

Ave. in Area (1): 6.37 % with standard deviation : 0.62 %
Ave. in Area (2): 6.29 % with standard deviation : 0.48 %
Ave. in Area (3): 6.23 % with standard deviation : 0.36 %

Principal stress ratio =4
Principal stress direction =45°
after 7 cycles

Fig. 5.20 An example of uniform distribution of strain within a sample tested under continuous cyclic rotation of principal stress direction at σ_3 = 14kPa

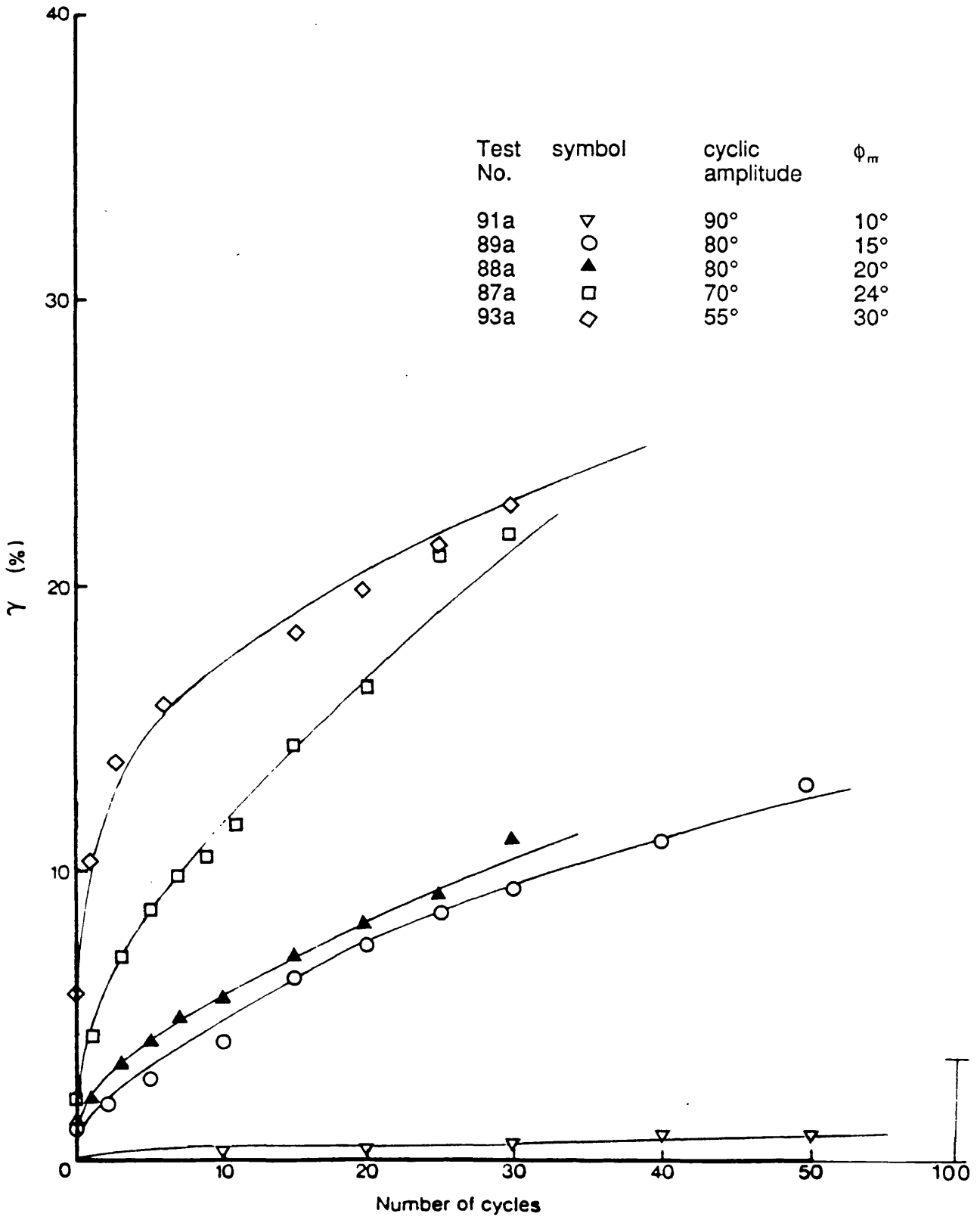

Fig. 5.21 The results of development of shear strain in loose samples of Leighton Buzzard sand when subjected to cyclic rotation of principal stress direction

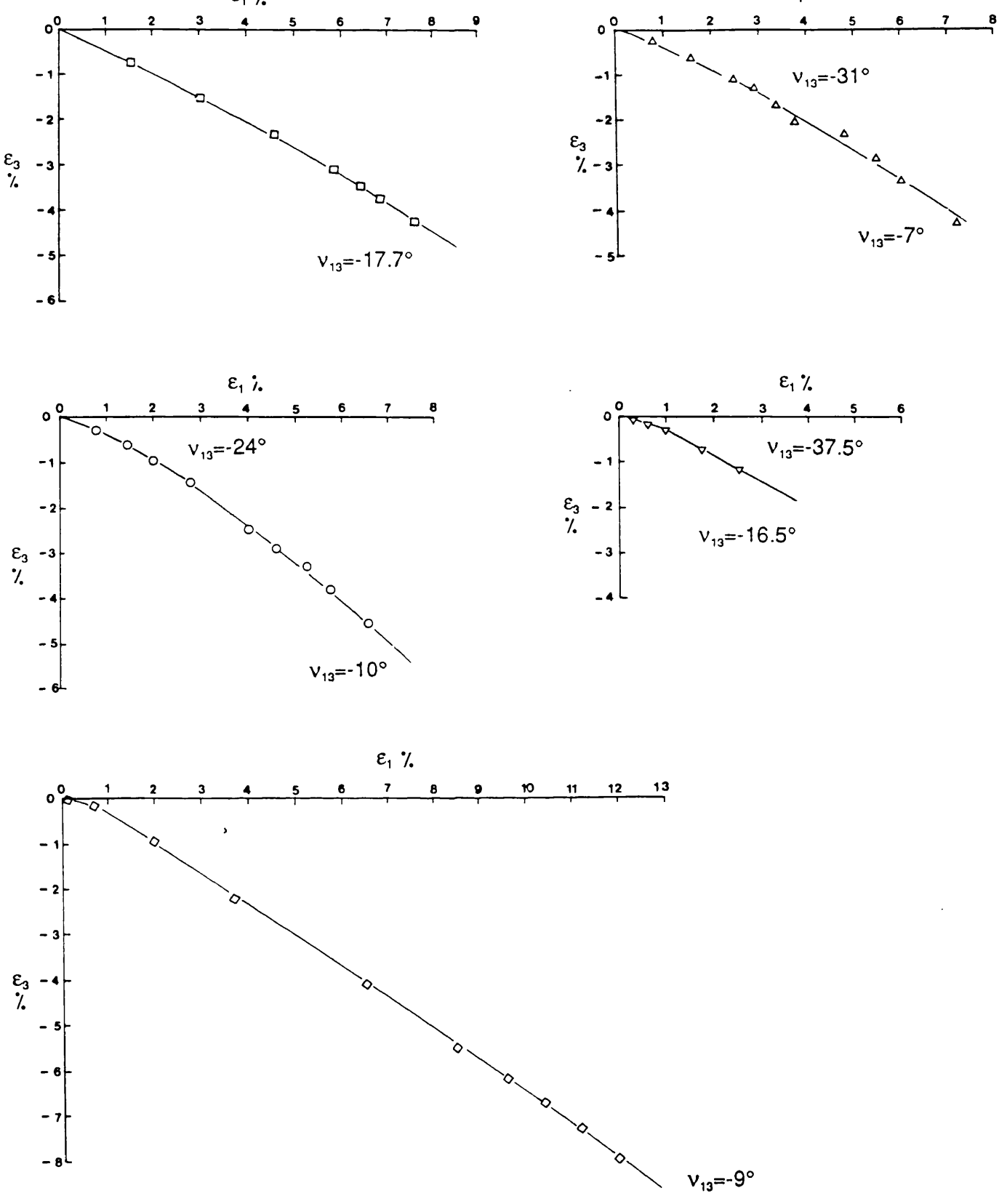

Fig. 5.22 Variations in the angle of dilation with amplitude of principal stress rotation and mobilised angle of friction on loose Leighton Buzzard sand samples tested in the DCDSC at σ_3 = 14 kPa

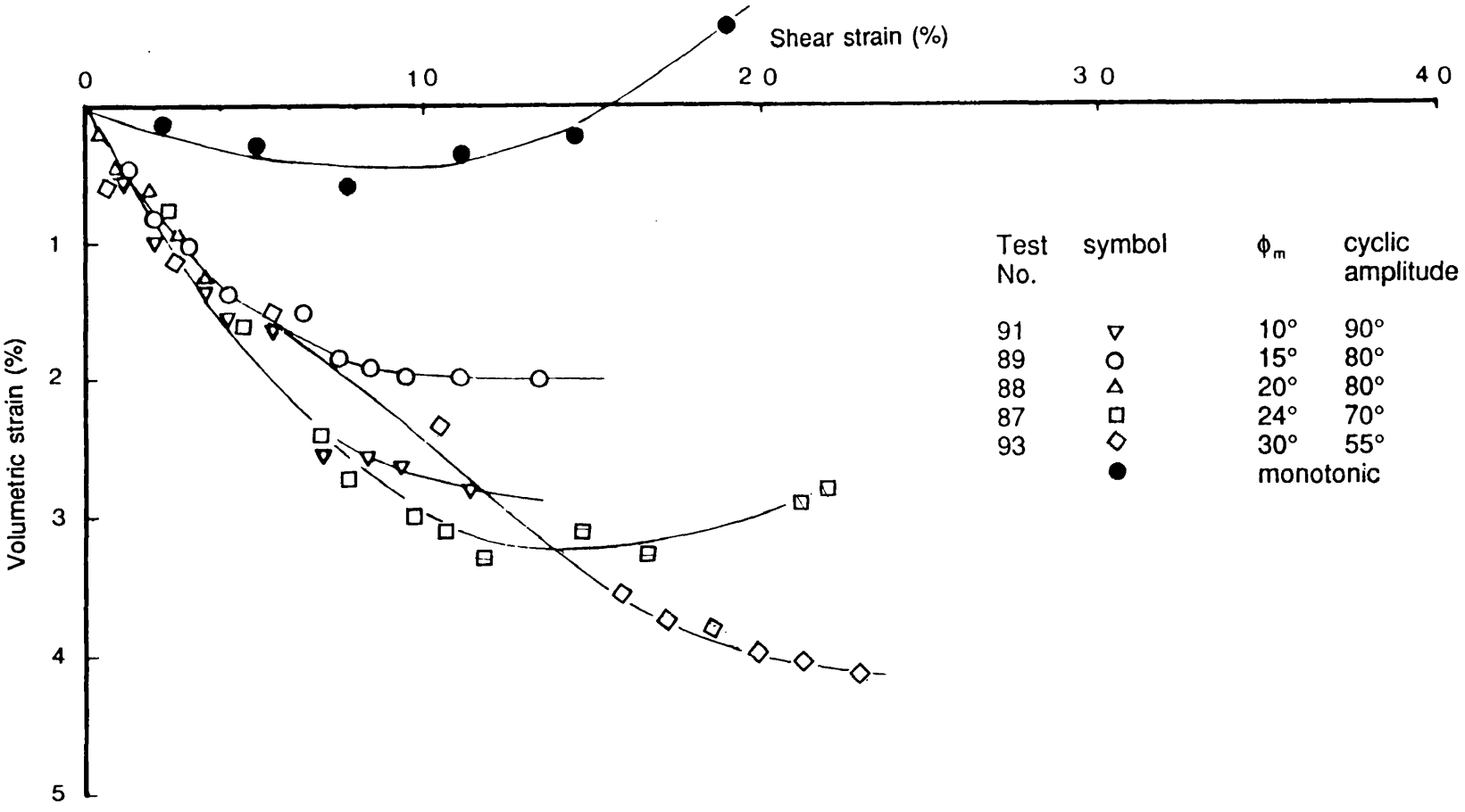

Fig. 5.23 Volumetric behaviour of loose samples of Leighton Buzzard sand tested under continuous and cyclic rotation of principal stress direction in the DCDSC at σ_3 =14kPa

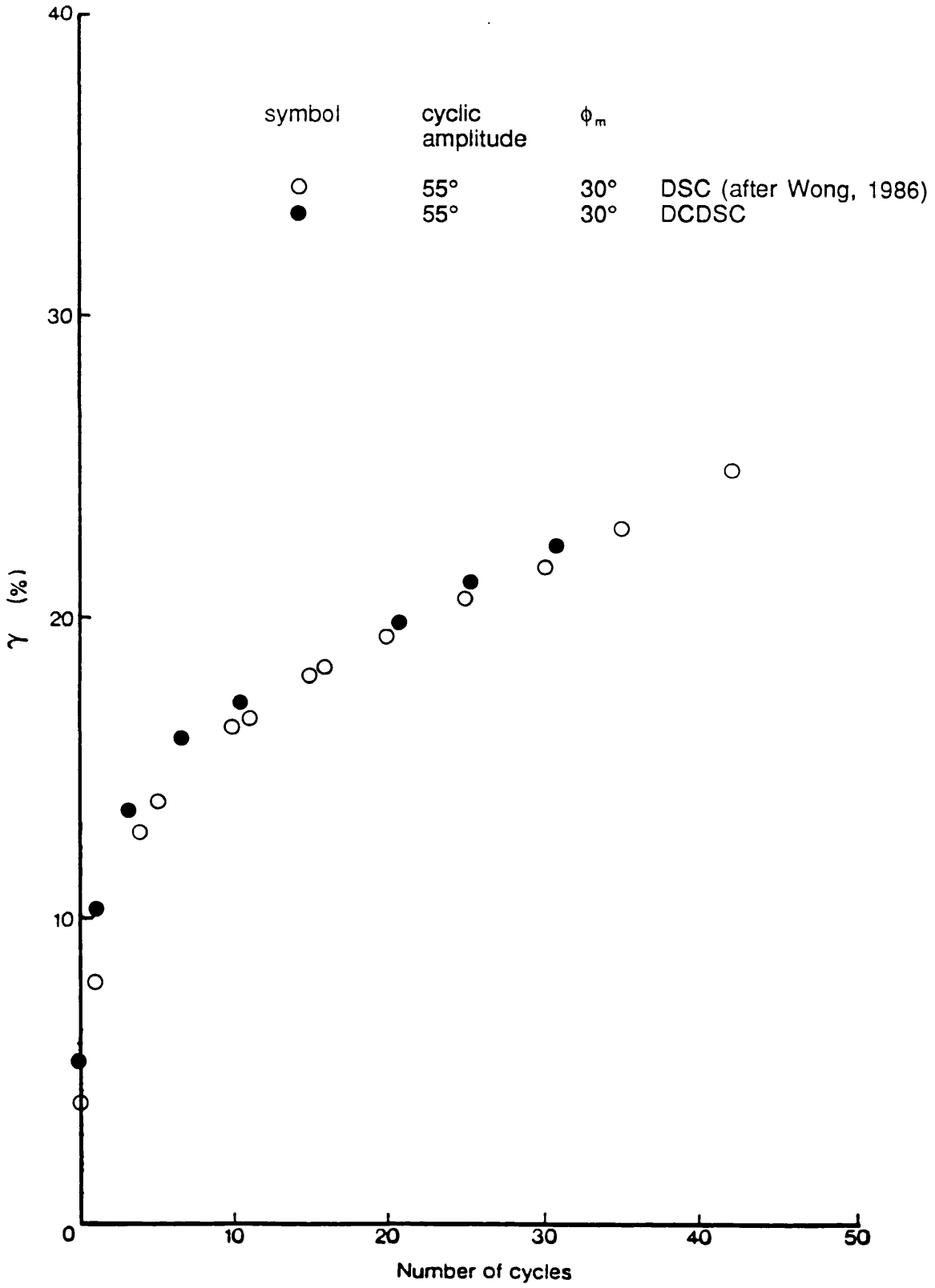

Fig. 5.24 **A comparison of two continuous rotation tests carried out in the DSC and DCDSC with an identical mobilised angle of friction and angle of rotation but with different cyclic stress paths**

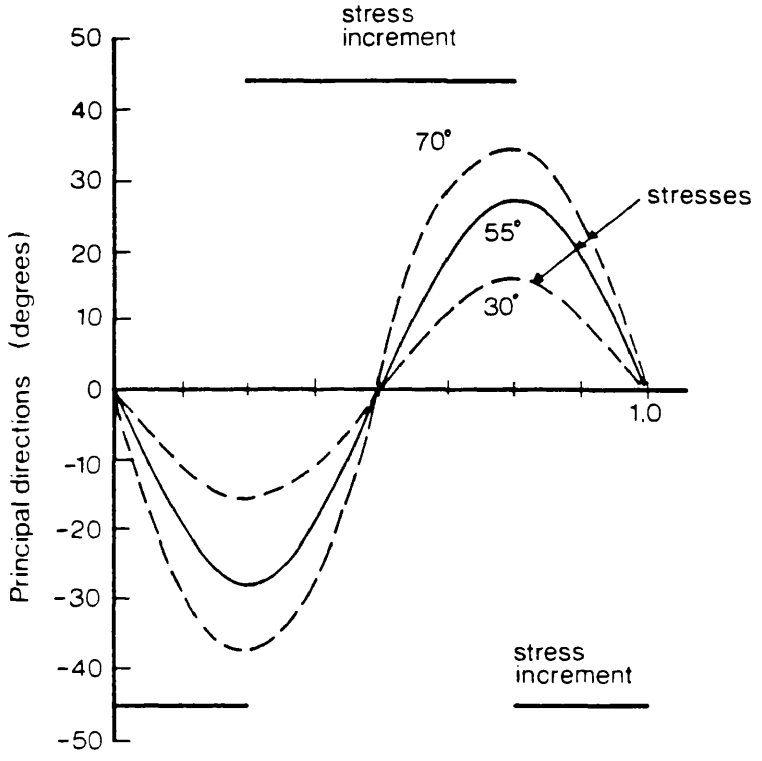

5.25 Directional variation within a typical cycle of continuous rotation tests. (stress and stress increment direction)

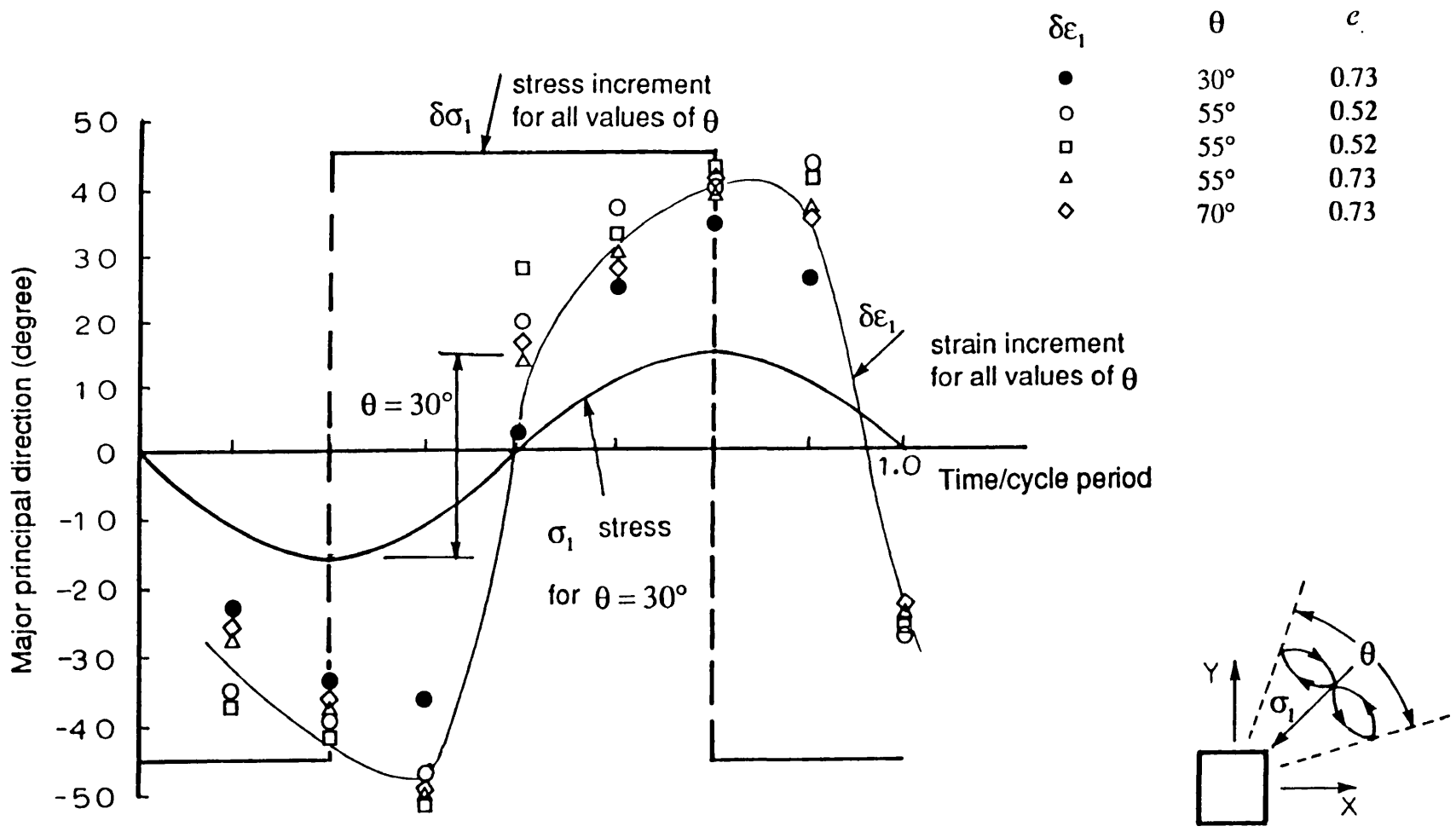

Fig. 5.26 **Stress increment direction within typical cycles of continuous rotation tests on dense and loose samples tested in DSC (after Wong, 1986)**

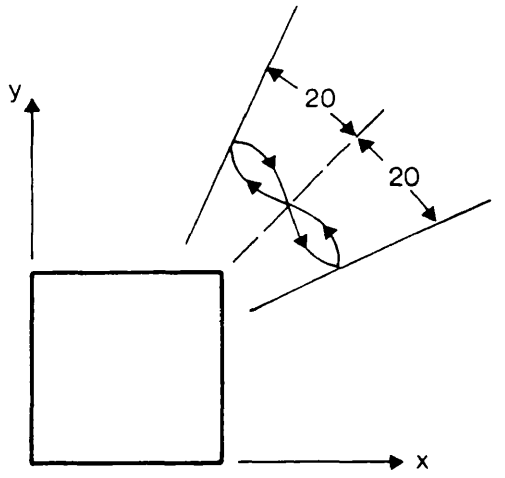

a) Cyclic stress path with $\phi'_m = 37°$

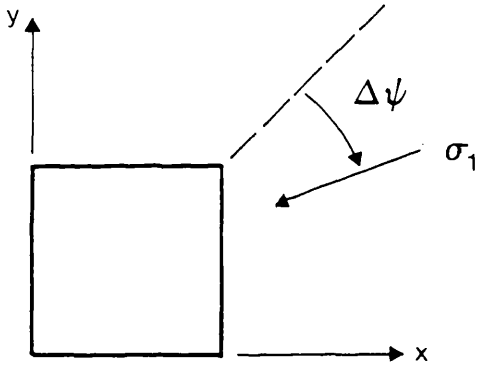

b) Monotonic shear tests after cyclic principal stress rotations

Fig. 5.27 **Stress path for monotonic shear after continuous and cyclic rotation of principal stress directions**

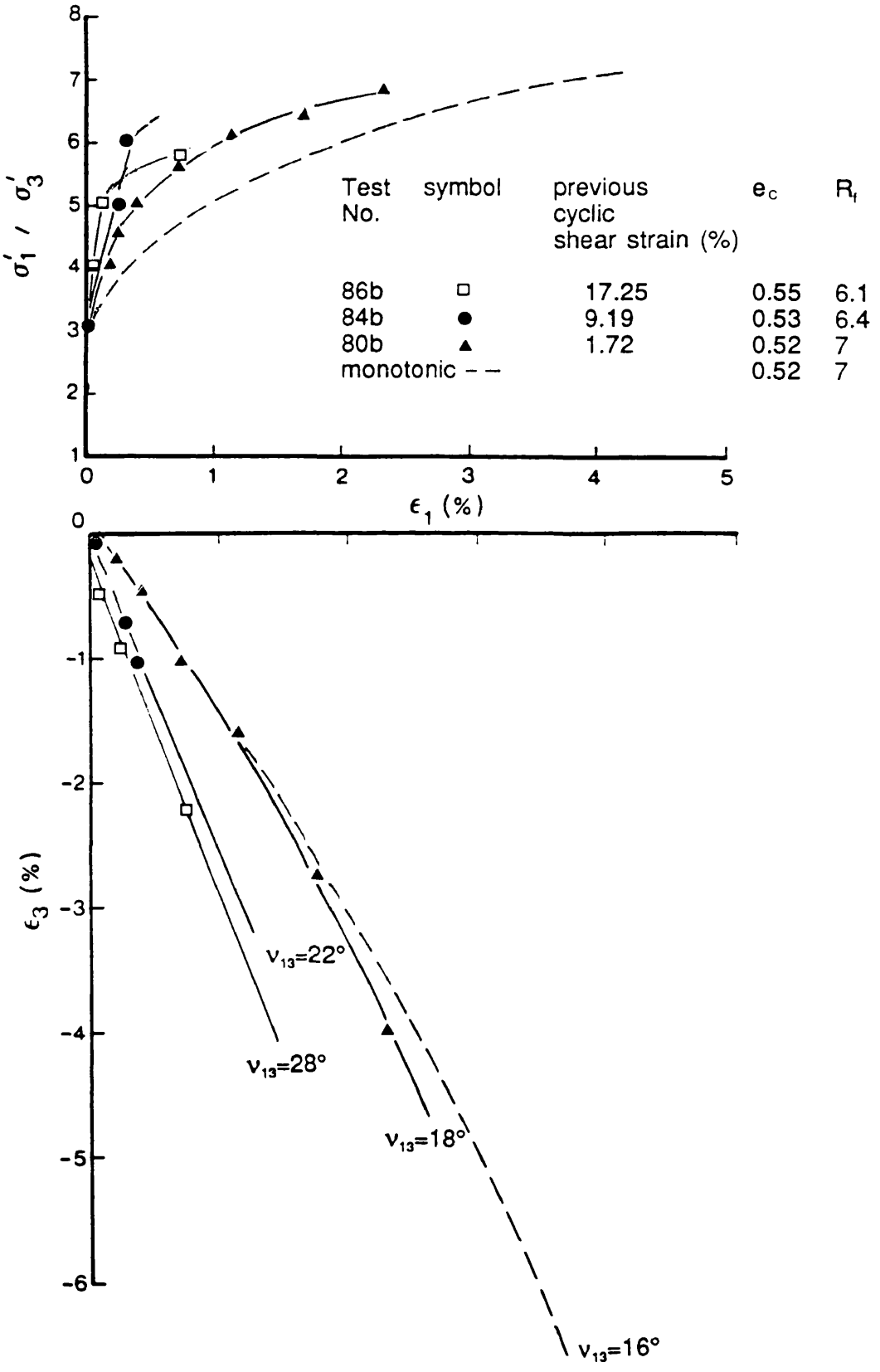

Fig. 5.28 **Stress-strain response from subsequent monotonic shear tests after continuous and cyclic rotation of principal stress directions on dense Leighton Buzzard sand samples tested in DCDSC**

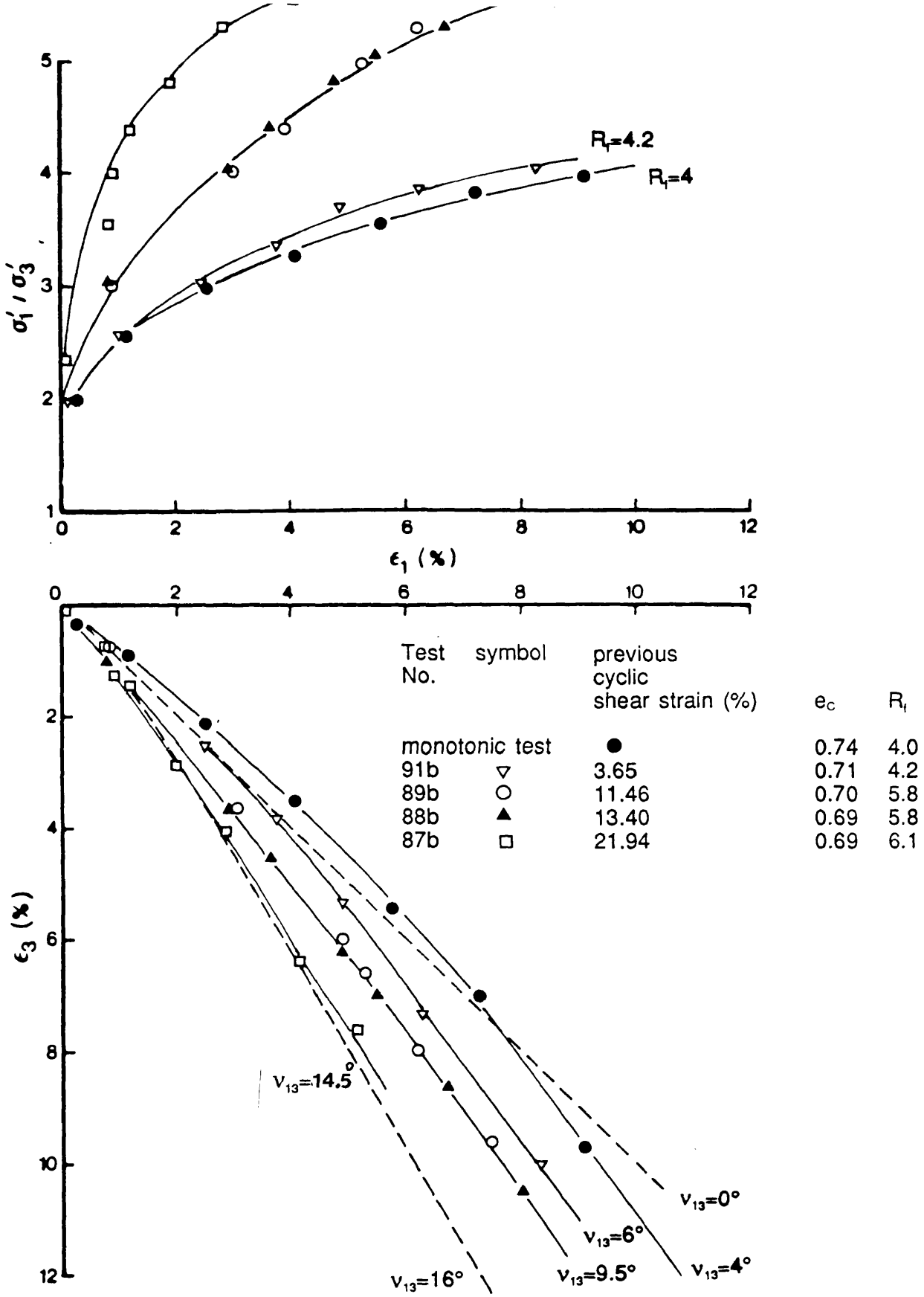

Fig. 5.29 **Stress-strain response from subsequent monotonic shear tests after continuous and cyclic rotation of principal stress directions on loose Leighton Buzzard sand samples tested in DCDSC**

CYCLIC TESTS											MONOTONIC AFTER CYCLIC								
Test No.	symbol	θ degree	ϕ_m degree	No. of cycles	ε_{1c} (%)	ε_{3c} (%)	γ_c (%)	ε_{vc} (%)	e_c	ν_{13c} degree	Test No.	symbol	ϕ_f degree	ε_{1f} (%)	ε_{3f} (%)	γ_f (%)	ε_{vf} (%)	ν_{13f} degree	Angle of Rupture
Simple monotonic (Dense)									0.52		49		49	2.74	-3.80	6.54	-1.06	16	30 ^{o}
80a	□	90	30	1000	1.00	-0.79	1.79	0.21	0.52	-5	80b	▲	49	2.32	-4.1	6.33	-1.69	18	22.5 ^{o}
85a	◇	90	32	30	2.19	-2.37	4.57	-0.18	0.52	-2.7	85b	–	51.5	3.96	-4.60	8.56	-0.64	15.3	-
84a	△	80	34	30	3.86	-5.33	9.11	-1.47	0.53	3.3	84b	●	47	0.35	-0.93	1.28	-0.57	22	23 ^{o}
86a	●	90	34	30	7.54	-9.70	17.27	-2.16	0.54	1.7	86b	□	46	0.87	-2.23	3.14	-1.41	28	21 ^{o}
72a	○	90	37	20	14.21	-17.48	32.49	-3.22		5.0			-	-	-	-	-	-	-

Table 5.1 **A summary of continuous rotation and subsequent loading tests carried out in the DCDSC on dense Leighton Buzzard sand samples at σ_3 =14 kPa.**

CYCLIC TESTS											MONOTONIC AFTER CYCLIC								
Test No.	symbol	θ degree	ϕ_m degree	No. of cycles	ε_{1c} (%)	ε_{3c} (%)	γ_c (%)	ε_{vc} (%)	e_c	ν_{13c} degree	Test No.	symbol	ϕ_f degree	ε_{1f} (%)	ε_{3f} (%)	γ_f (%)	ε_{vf} (%)	ν_{13f} degree	Angle of Rupture
Simple monotonic (Dense)									0.52		49		49	2.74	-3.80	6.54	-1.06	16	30 ^{o}
87a	□	70	24	30	12.37	-9.57	21.94	2.80	0.69	-16.6	87b	□	46	5.09	-7.58	12.63	-2.53	14.5	30 ^{o}
88a	▲	80	20	30	7.68	-5.72	13.40	2.78	0.69	-21	88b	▲	45	7.96	-10.49	18.40	-2.53	10.3	31 ^{o}
89a	○	80	15	50	7.12	-4.34	11.46	1.96	0.70	-23	89b	○	45	8.09	-10.27	18.36	-2.17	9.5	30 ^{o}
91a	▽	90	10	1000	2.47	-1.15	3.65	1.23	0.71	-36	91b	▽	38	8.026	-9.96	18.17	-1.72	6	32 ^{o}
92a		90	10	2000	1.17	-0.32	1.49	0.85	0.72	-36	92b		38	8.49	-9.12	17.61	-0.64	5	-
Simple monotonic (Loose)									0.74		79	●	37	9.10	-9.70	18.79	-0.60	4	-

Table 5.2 **A summary of continuous rotation and subsequent loading tests carried out in the DCDSC on loose Leighton Buzzard sand samples at σ_3 =14 kPa.**

CHAPTER 6 DRAINED BEHAVIOUR OF DAMP COAL UNDER CONSTANT AND CYCLIC ROTATION OF PRINCIPAL STRESS DIRECTIONS

6.1 INTRODUCTION

Chapter 5 highlighted the factors that control the initiation of flow and some of the effects of continuous cyclic rotation of principal stress direction on dry Leighton Buzzard sand using the DCDSC. The tests presented in this Chapter were performed to establish the monotonic shear strength of damp coal, and also to investigate if the effects of principal stress rotation would be similar in damp coal in which the particles were not only wet but more crushable.

This Chapter is divided into four sections. In the first section, a monotonic test was conducted on damp coal of 7% moisture content to establish the stress-strain behaviour of loose damp coal at a low stress level of σ_3 =14 kPa. The second section describes a series of simple tests, using the conventional Direct Shear Box apparatus, which were conducted to provide a quick and independent method of determining the shear strength of damp coal, and to evaluate the effect of different moisture content on the angle of friction. The third section describes the continuous cyclic rotation tests on medium loose coal samples and in the fourth section post cyclic monotonic tests are presented.

6.2 EXPERIMENTAL PROGRAMME AND TEST PROCEDURES

6.2.1 Constant direction monotonic tests

It was mentioned in Chapter 3 that, due to the damp nature of the material, loose coal samples were not prepared in the conventional method by rapidly releasing a large quantity of coal from a fixed hight above the preparation box; but samples were prepared by lightly compressing layers of the test material with a plunger. Although the prepared samples were taken to be isotropic in the plane of strain, a degree of anisotropy was introduced perpendicular to the plane of strain. The voids ratio obtained for these samples was 0.95 ± 0.01. Figure 6.1 shows the horizontal bedding created by this method of preparation. The stress-strain behaviour of the material would be affected by this method and so alternative methods of preparation should also be investigated in the future.

The sample was placed in the DCDSC and loaded monotonically using an identical procedure as for the loose sand samples (Chapter 4). Figure 6.2 shows the stress strain and volumetric behaviour of damp coal under this type of loading. In this test, like the loose sand samples, no rupture layers were found although the sample was

strained to over 10% in the major principal strain direction. The stress ratio at which the dilation rate reached zero was chosen as stress ratio at failure; the angle of friction being 32°. Figure 6.3 illustrates the strain distribution within the sample. In spite of the presence of bedding planes parallel to the plane of strain, a good degree of uniformity can be observed in this test although in the marked area in the Figure 6.3 less strain was recorded, probably due to the local over compaction during the sample preparation procedure.

6.2.2 Direct Shear Box tests

Direct Shear Box tests were carried out as a quick way of checking the plane strain shearing resistance of loose samples as well as to investigate the effect of different moisture contents in coal.

The Direct Shear Apparatus (DSA) had dimensions of 60mm x 60mm x 40 mm. To provide friction on the top and bottom platen surfaces sand particles were sprinkled uniformly on araldite coated surfaces. Figure 6.4 is a cross section of the device that was used. The loose samples were prepared by mass tipping from a small scoop as the compacting method in the shear box may induce severe anisotropy (bedding planes) on the potential failure plane. The surface was levelled using a sharp straight edge. All tests were carried out at a low stress level of σ_n=15 kPa which compares with the stress level used for coal samples tested in the DCDSC at σ_3=14 kPa.

After applying a vertical load to the loosely prepared coal sample the top rigid platen was secured to the top half of the direct shear apparatus (Figure 6.4). This was to ensure that the coal sample supports the applied vertical load when the locking screws, which held the two halves of the apparatus together during the sample preparation, were removed.

A number of tests were carried out on damp coal with different moisture contents and standard analyses was used to determine the peak internal angle of friction :

$$\tau_{yx}/\sigma_{yy} = \tan\phi$$

assuming zero cohesion due to moisture.

Table 6.1 shows the peak angles of internal friction achieved for different moisture contents; the value of ϕ_f=31.8° for the tests with 6% moisture content confirms the value of ϕ_f=32° that was obtained by monotonic shearing of the coal sample with 7% moisture content. Figures 6.5a and 6.5b illustrate the shear stress and vertical

displacements against horizontal displacements respectively for the coal with 6% moisture content.

Comparison of the results of the shear box, and the DCDSC must make allowance for the effects of inherent anisotropy. Figure 6.6 shows an element which has been prepared through vertical pouring. Any anisotropic effects will associate with the horizontal planes. In the shear box the major principal stress will be at an angle to the bedding plane whereas in the DCDSC the principal stress is parallel; which aims to eliminate the effects of inherent anisotropy. The differences in the angle of failure from this effect is greatest for dense materials and becomes small for very loose materials. If the difference in the angle of friction due to anisotropy results entirely from different dilatancy rates then for very loose materials where dilatancy rates should to be zero at failure, there would be no effect from anisotropy on the angle of friction. However, one would expect prefailure stiffness differences and consequently effects of anisotropy are ignored in these calculations.

6.2.3 Continuous cyclic rotation tests

Once the value for the angle of friction for damp coal had been established by means of monotonic tests, a series of cyclic tests were carried out to find the effect of cyclic rotation of principal stress direction on this material. The cyclic stress path and testing procedure was identical to that of sand (Chapter 5). The samples were loaded monotonically to a certain mobilised angle of friction and, after computing required boundary normal and shear stresses for a chosen amplitude of principal stress direction, the cyclic part of the test commenced. Radiographs were taken at the end of the cycles; the number of cycles and radiographs depended on the state of deformation of the sample during the cyclic process. Tests with a high mobilised angle of friction and a large amplitude of rotation underwent few cycles, whereas tests with a very low mobilised angle of friction could undergo hundreds of cycles without much of strain. In these tests adjustments of boundary normal stresses as well as alignments of shear sheets were carried out whenever necessary. At the end of the cyclic test the sample was left under low vacuum until a subsequent monotonic test began.

Figure 6.7 shows the shear strain that accumulated during cycling. There was a similar trend with that of loose sand; with larger strain associated with higher mobilised angle of friction and amplitude of rotation. The volumetric response of these tests is given in Figure 6.8 which indicates that the same trend of nonlinearity

for loose coal exists and compares with loose Leighton Buzzard sand. In loose coal tests as with loose sand the low dilatancy rate measured in the cyclic tests associate with low mobilised stress ratio. Again as with loose sand at low mobilised stress ratios a varying dilatancy rate with strain is observed with a low dilatancy rate the initial part of the cyclic coal test which, does not continue, and increases after some strain is attained. This is not so noticeable at higher mobilised stress ratios.
Figure 6.9 shows the strain distribution within a severely deformed sample after 15 cycles. Although an average value of the coefficient of variation was 2.5% in three areas of deformation within the deformed sample some degree of constraint can be observed from the boundaries towards the centre; this could be due to the limitation of manual adjustment of the normal pressure boundaries on such a soft material.

6.2.4 Post cyclic monotonic tests

The experimental procedure for post cyclic monotonic tests for damp coal was identical of that of loose sand. At the end of the cyclic process the sample was placed under approximately 10 kPa vacuum and the cyclic valves were closed and the monotonic valves were opened. The vacuum was then released and the sample was unloaded monotonically. At the end of unloading process a radiograph was taken that could be used as a reference for the initial state of deformation in the subsequent loading. The sample was reloaded monotonically and subsequent radiographs were taken at different stress ratios as required. The normal pressure backing plates and the shear sheets were adjusted and aligned whenever necessary as the sample changed shape.

Figure 6.10 illustrates the stress-strain deformation curves of two subsequent constant monotonic tests with initially loose damp coal samples which have already been subjected to continuous and cyclic rotation of principal stress direction. The volumetric changes of these tests are also included. It can be seen that after the accumulated shear strain that developed in the cyclic part, coal was initially stiffer in the subsequent monotonic loading, and that the sample in test No.4b failed at a higher stress ratios i.e. ϕ_f=41°; a difference of nearly 10° compared with that of simple monotonic test. Failure in these samples was accompanied with the presence of failure planes even in the test in which the previous cyclic shear strain was low and the subsequent monotonic angle of shearing resistance was not different from that of the simple monotonic test; around ϕ_f=32°.

The volumetric behaviour in these tests indicated an increase in the rate of dilation

as the previous cyclic strain increased. It is interesting that in test 1b, in which the previous volume change was only εv_c =2.8% at the end of the cyclic process, and the stress-strain behaviour was not significantly different from the simple monotonic test. The dilation rate increased substantially and the material was less contractive than the simple monotonic test; this is clearly illustrated in Figure 6.11. These suggest that although the material has not significantly densified, the contact normals are increased substantially during the rotation tests and these newly created particle contacts are responsible for the dilative behaviour and not the density.

6.3 DISCUSSION

The strength and deformation of particulate material has been reported by many investigators to vary with changes in surface wetness and roughness (Tschebotarioff and Welch, 1948; and Penman, 1953). Horn and Deere (1962) using a direct shear test apparatus investigated the influence of crystal structure, surface moisture, surface roughness, rate of sliding and polarity of lubricant on some minerals which are commonly found in granular materials, such as quartz, feldspar, calcite (massive structure), chlorite, serpentine, steatite and talc (layer-lattice) minerals. They concluded that the crystal structure of minerals determines the lubrication effects of moisture on the frictional resistance, i.e water acted as antilubricant when applied to crystal structures; whereas it lubricated surfaces of minerals with layer-lattice. Also quartz specimens whose surfaces had been ground with No. 240 carborundum grit, showed an increase in ϕ_f with moisture present.

In the present research all tests which were conducted in the DCDSC were carried out at 7% moisture content; but the DSA tests were carried out in a range up to 10% moisture content. The results of these tests which are given in Table 6.1 indicate a slight increase in the peak angle of shearing resistance from ϕ_f =30° to ϕ_f =32° and may be attributed to the antilubricating effect of water in coal. It would be difficult to estimate that this difference is significant.

It is interesting to note that, although the coal was damp, there was a similar stress-strain deformation behaviour when compared with loose samples of dry Leighton Buzzard sand. The angle of internal friction was 32° for both materials. The coal sample was more contractive within the range of ε_1= 2% to ε_1= 9% but dilated fairly similar to the sand at failure, this extra contraction in coal samples could be attributed to the higher voids ratio in coal i.e. 0.95 ± 0.01 when compared with that of loose sand samples of 0.74 ± 0.02 and possible particle crushing in the coal.

Figure 6.12 compares these two materials and Figure 6.13 shows three sieve analyses for the a)- damp coal prior to testing, b)- after monotonic loading and c)- after being subjected to cyclic rotation of principal stress direction. It can be seen that there is a distinct difference in particle size distribution particularly after the monotonic loading stage.

However, in spite of particle crushing and fabric changes due to the rotation of principal stress direction in the loose damp coal samples, the horizontal bedding planes that were created during the sample preparation, illustrated in Figure 6.1, survived even after the sample gained 23.51% shear strain. This can be seen in the lower half of Figure 6.14 for the same sample after being subjected to cyclic loading. The disappearance of the bedding planes in the top half of the radiograph is due to a slight error in positioning the sample in line with the X-ray focal spot of the radiography head.

Also it was noted that the angle of friction was not influenced by particle grading. The particle size used in dry loose samples was between 600 μm to 850 μm whereas in damp coal samples was between 212 μm to 2400 μm.

The post cyclic monotonic tests also show a similar behaviour to those of sands. It indicates that even in wet material the contact normals tend to concentrate in the orientation along with the major principal stress direction. This will be discussed in Chapter 8. Table 6.2 summarises results of damp loose coal.

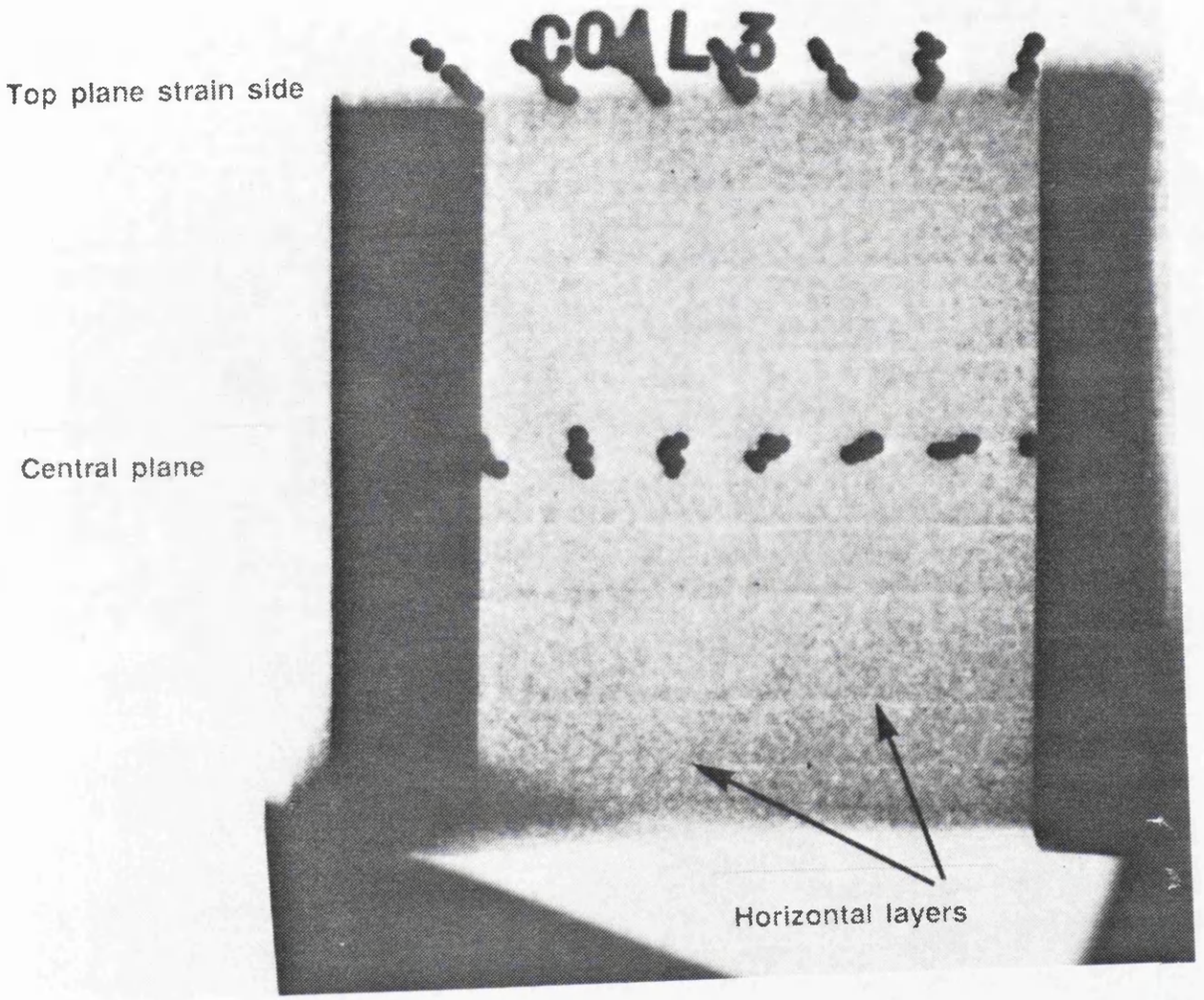

Fig. 6.1 Horizontal layers formed due to the sample preparation technique

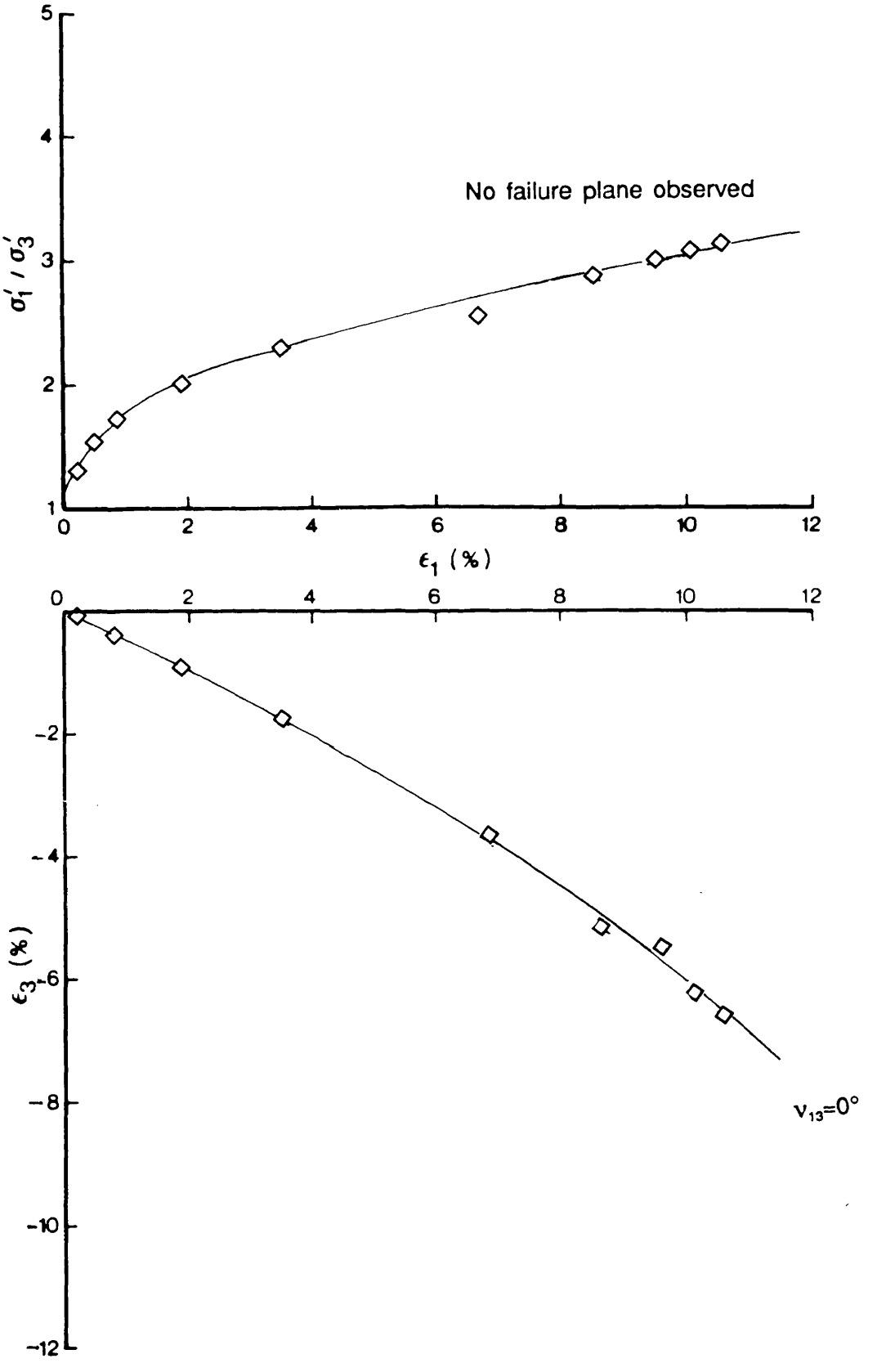

Fig. 6.2 Stress-strain and deformation response of loose damp coal sample sheared monotonically in the DCDSC at σ_3 =14 kPa

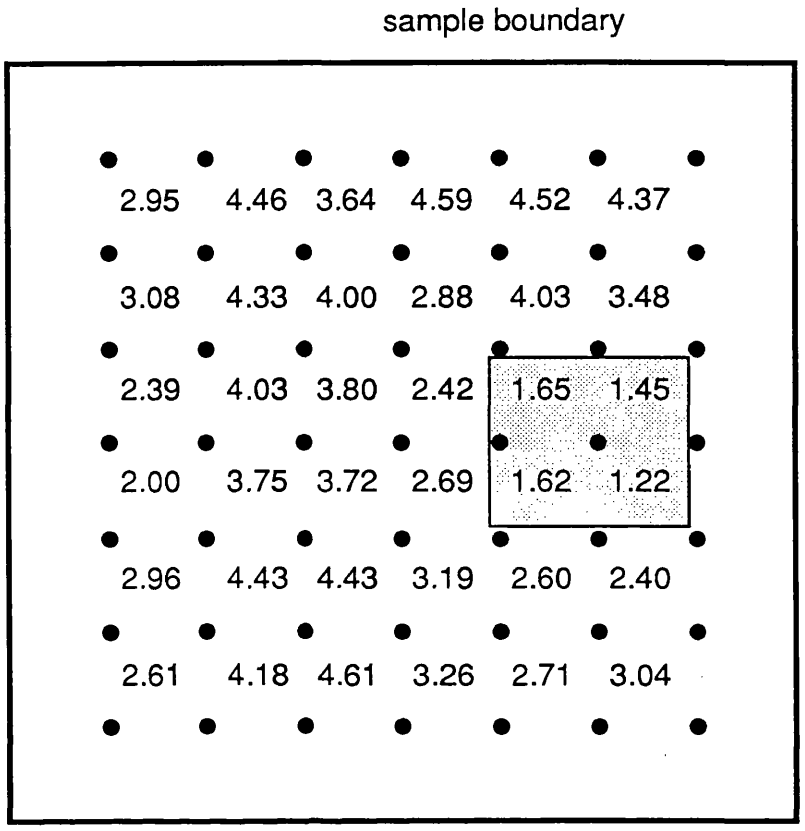

Major principal strain ε_1 (%)

Ave. in Area (1): 3.26 % with standard deviation : 0.98 %
Ave. in Area (2): 3.35 % with standard deviation : 0.96 %
Ave. in Area (3): 3.16 % with standard deviation : 0.71 %

Principal stress ratio =2.5
Principal stress direction =45°

Fig. 6.3 Example of strain distribution within a loose sample of damp coal monotonically sheared at σ_3 =14 kPa

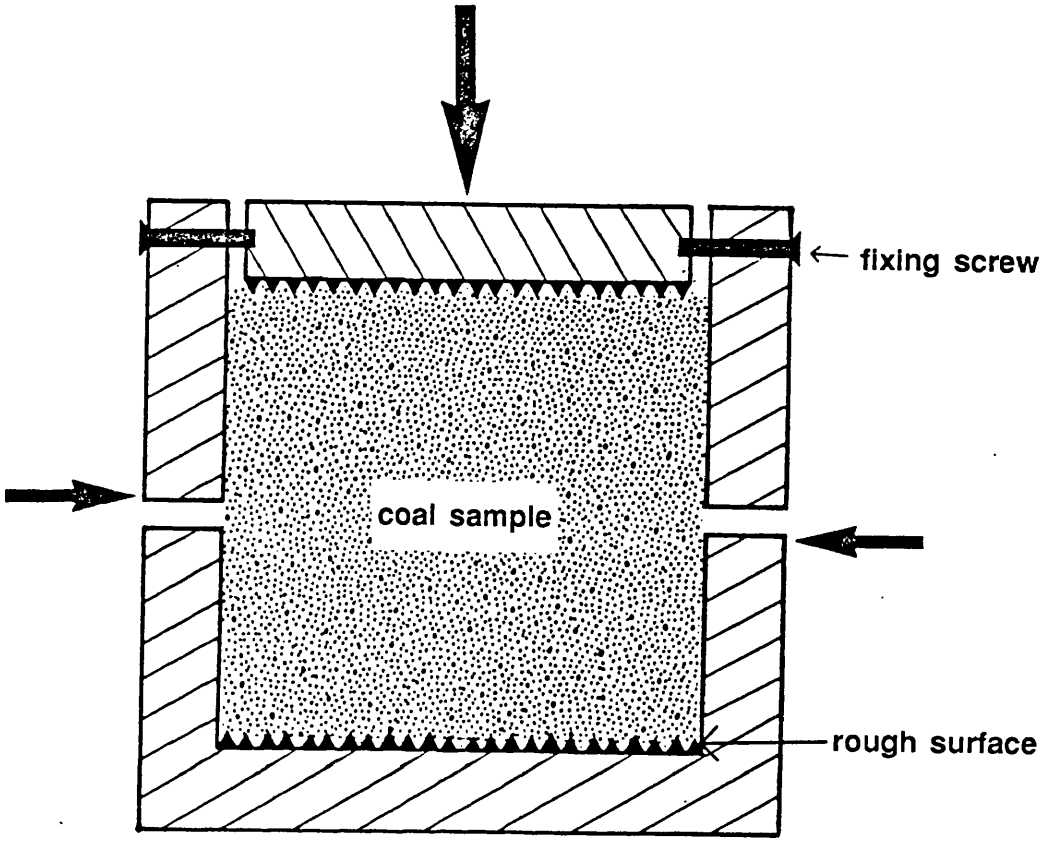

Fig. 6.4 Illustration of a cross section of the DSA device was used

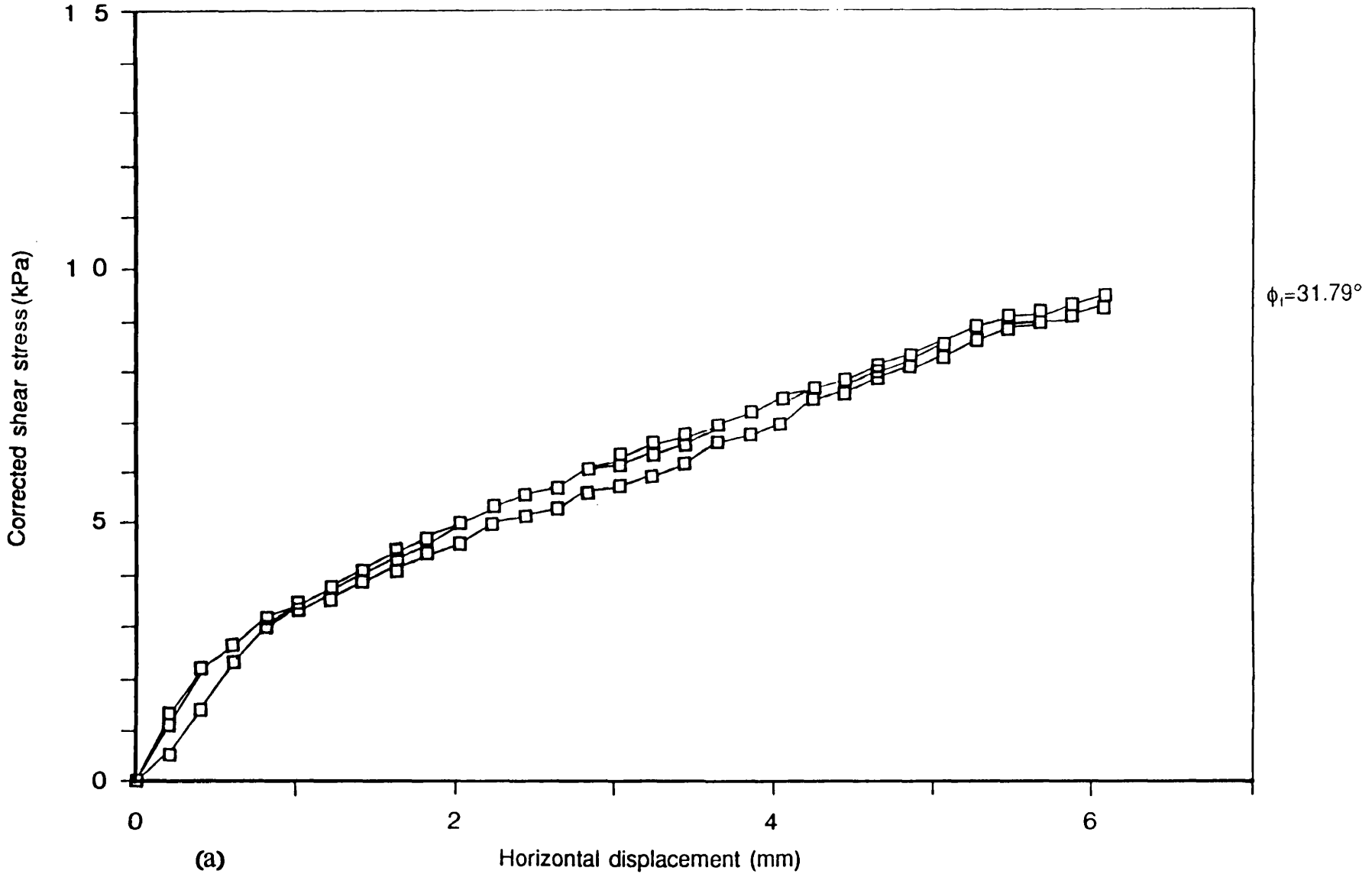

Fig. 6.5 **(a) Shear stress against horizontal displacement for loose damp coal samples tested in DSA and (b) Vertical displacement against horizontal displacement for loose damp coal samples tested in DSA**

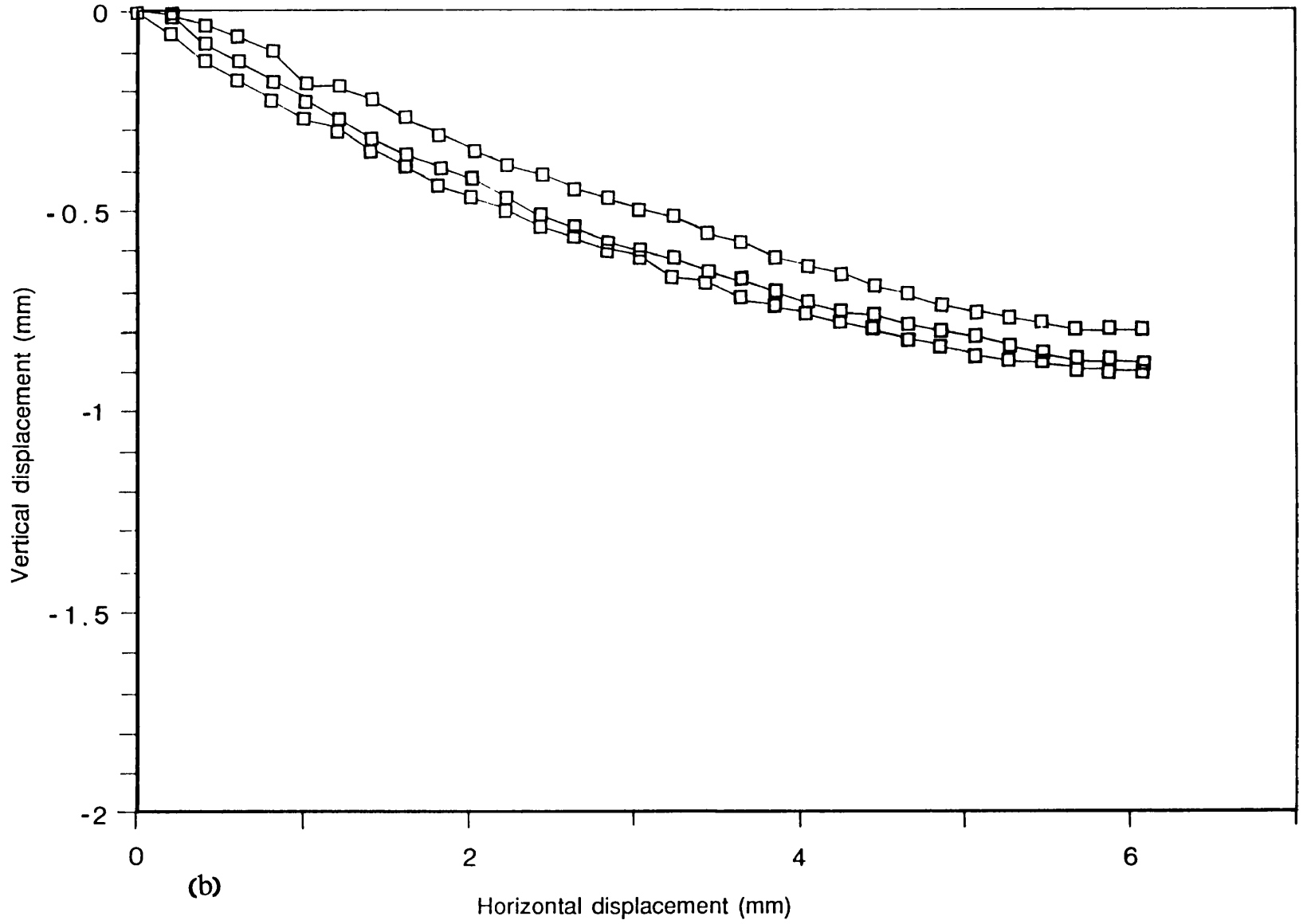
0
-0.5
-1
-1.5
-2
Vertical displacement (mm)
0
2
4
6
Horizontal displacement (mm)

(b)

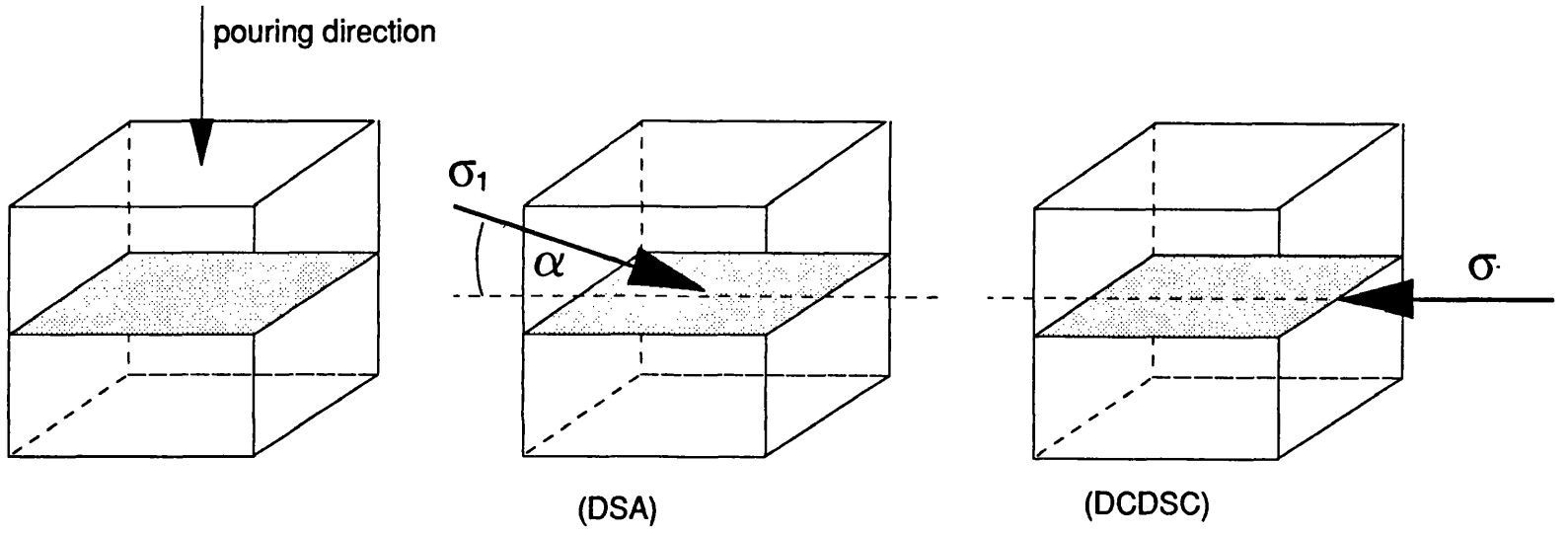

Fig. 6.6 Anisotropic effects associated with horizontal planes in the DSA

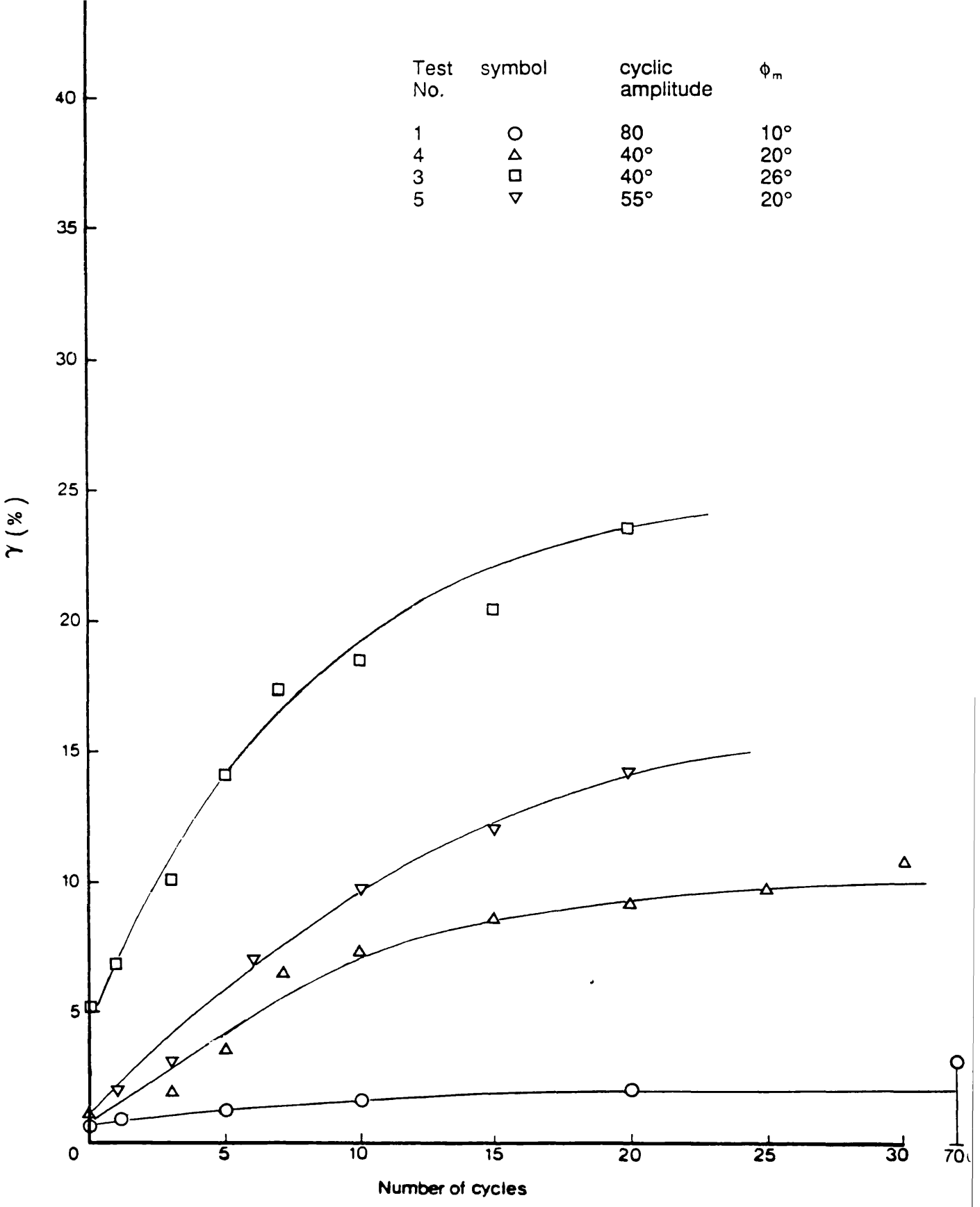

Fig. 6.7 **Development of shear strain in loose damp coal when subjected to continuous and cyclic rotation of principal stress direction in the DCDSC at σ_3 =14 kPa**

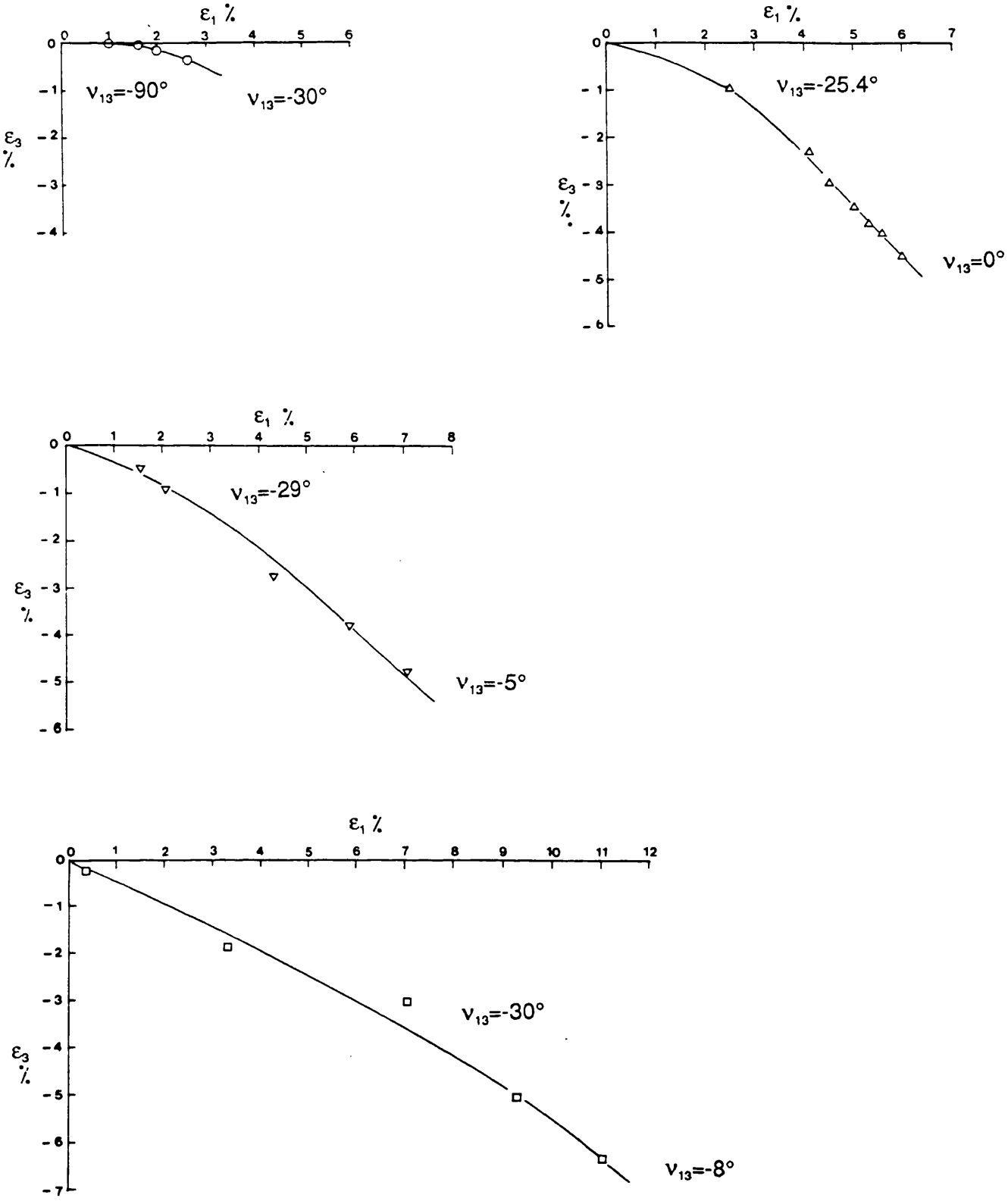

Fig. 6.8 Volumetric behaviour of loose damp coal samples tested under continuous and cyclic rotation of principal stress direction in the DCDSC at σ_3 =14 kPa

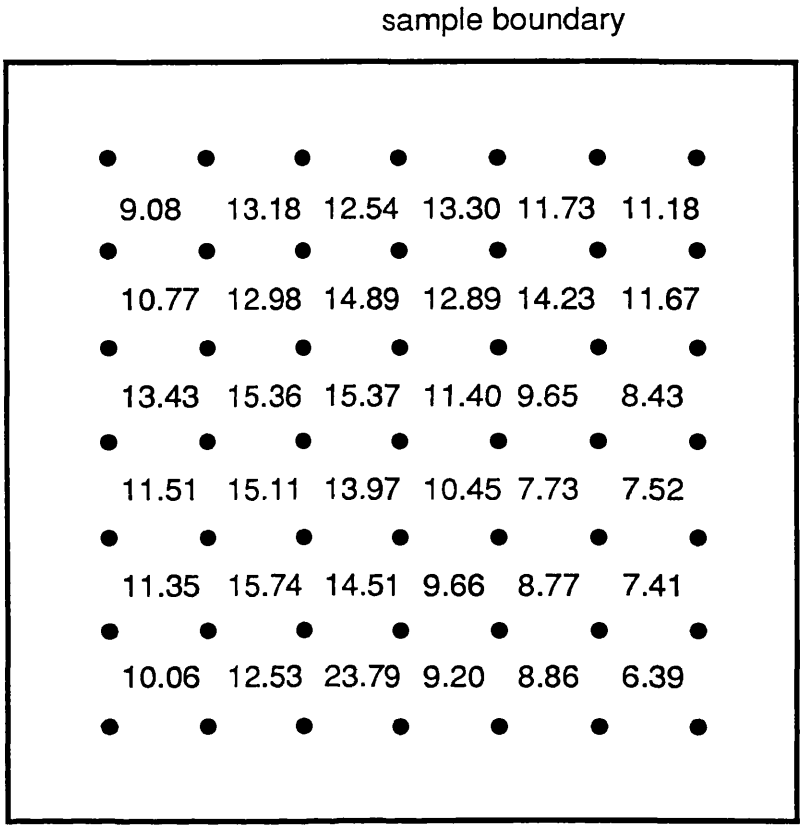

Major principal strain ε_1 (%)

Ave. in Area (1): 11.57 % with standard deviation : 2.59 %
Ave. in Area (2): 12.67 % with standard deviation : 2.67 %
Ave. in Area (3): 12.80 % with standard deviation : 2.27 %

Principal stress ratio =2.5
Principal stress direction =48.47°
after 15 cycles

Fig. 6.9 Example of strain distribution within a largely deformed cyclic sample of damp loose coal tested in the DCDSC at σ_3 =14 kPa

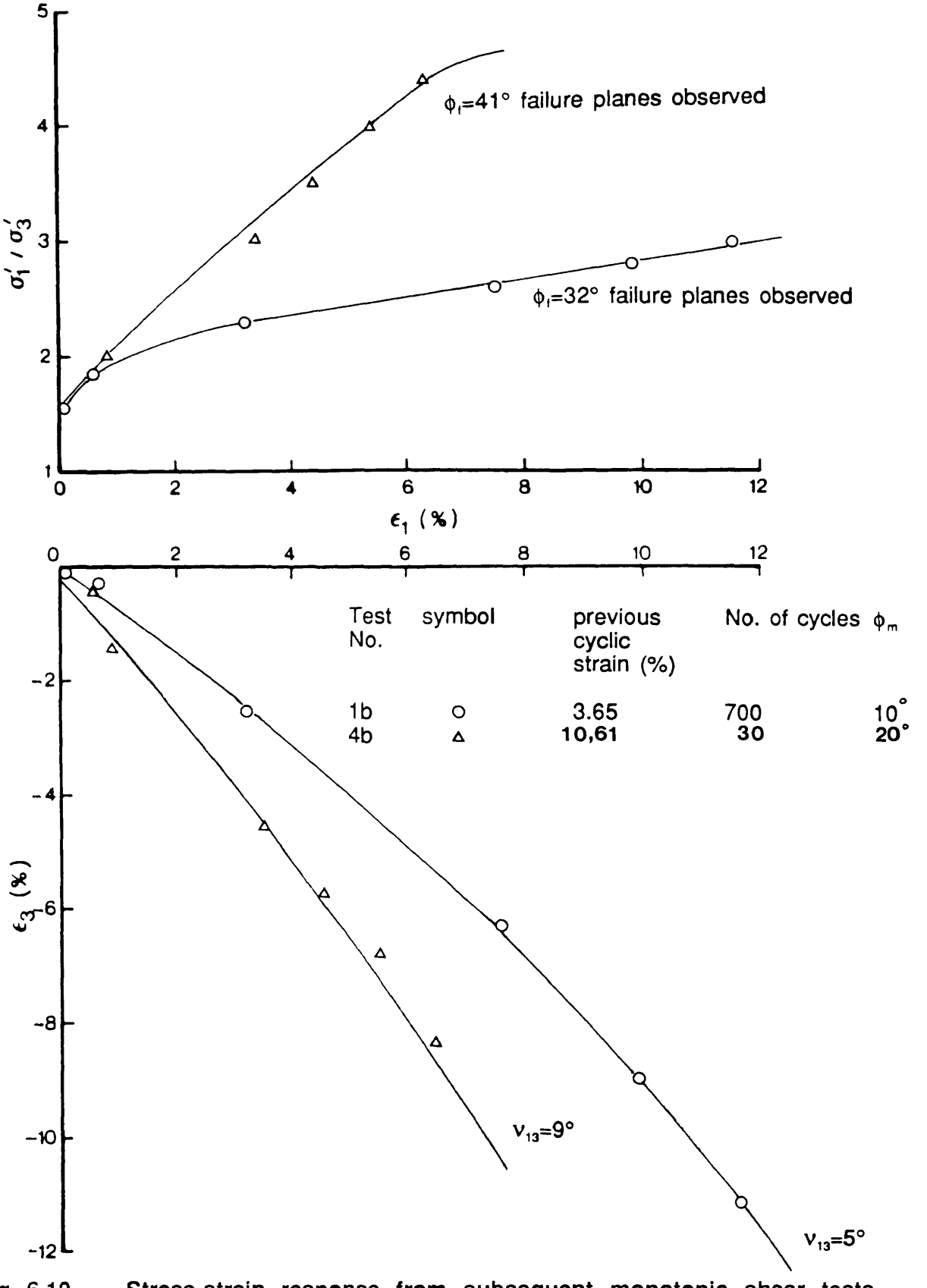

Fig. 6.10 Stress-strain response from subsequent monotonic shear tests after continuous rotation of principal stress direction on loose coal samples tested in the DCDSC at σ_3 =14 kPa

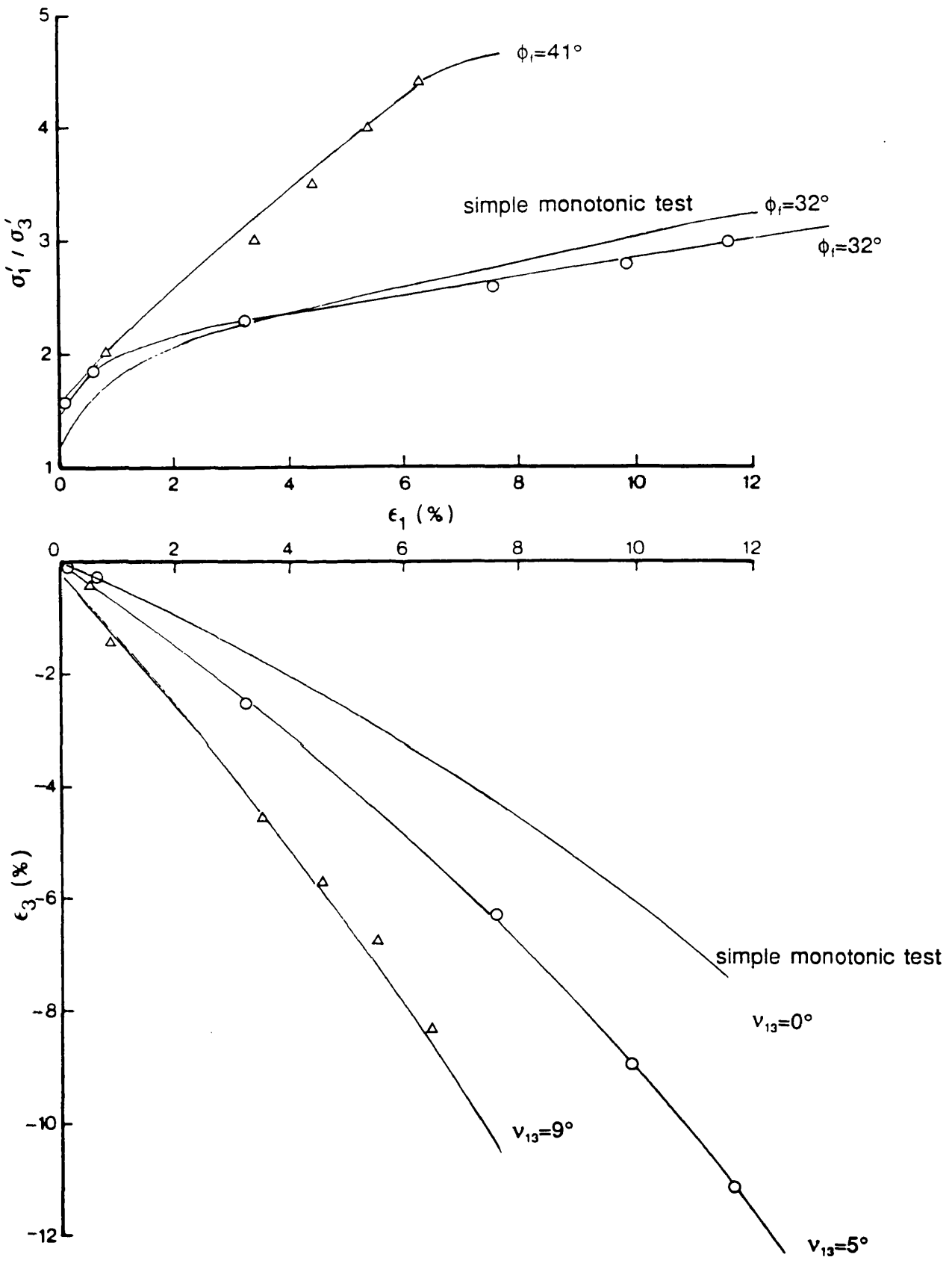

Fig. 6.11 **Comparison of stress-strain response of simple monotonic test and subsequent monotonic tests after continuous and cyclic rotation of principal stress direction in initially loose samples of damp coal**

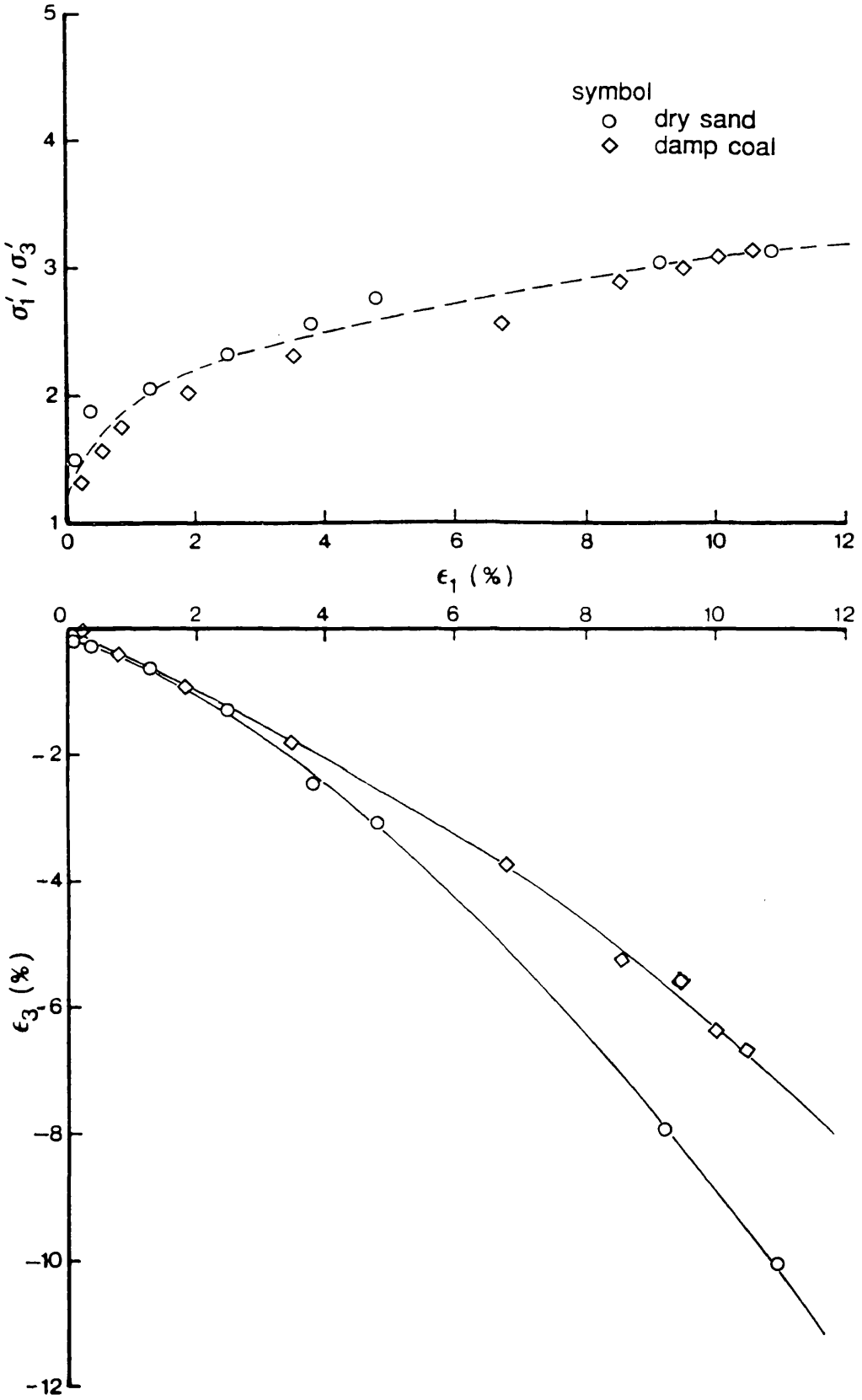

Fig. 6.12 **A comparison of two monotonic tests of dry loose sand and damp loose coal samples tested in the DCDSC at identical stress levels of σ_3 =14 kPa**

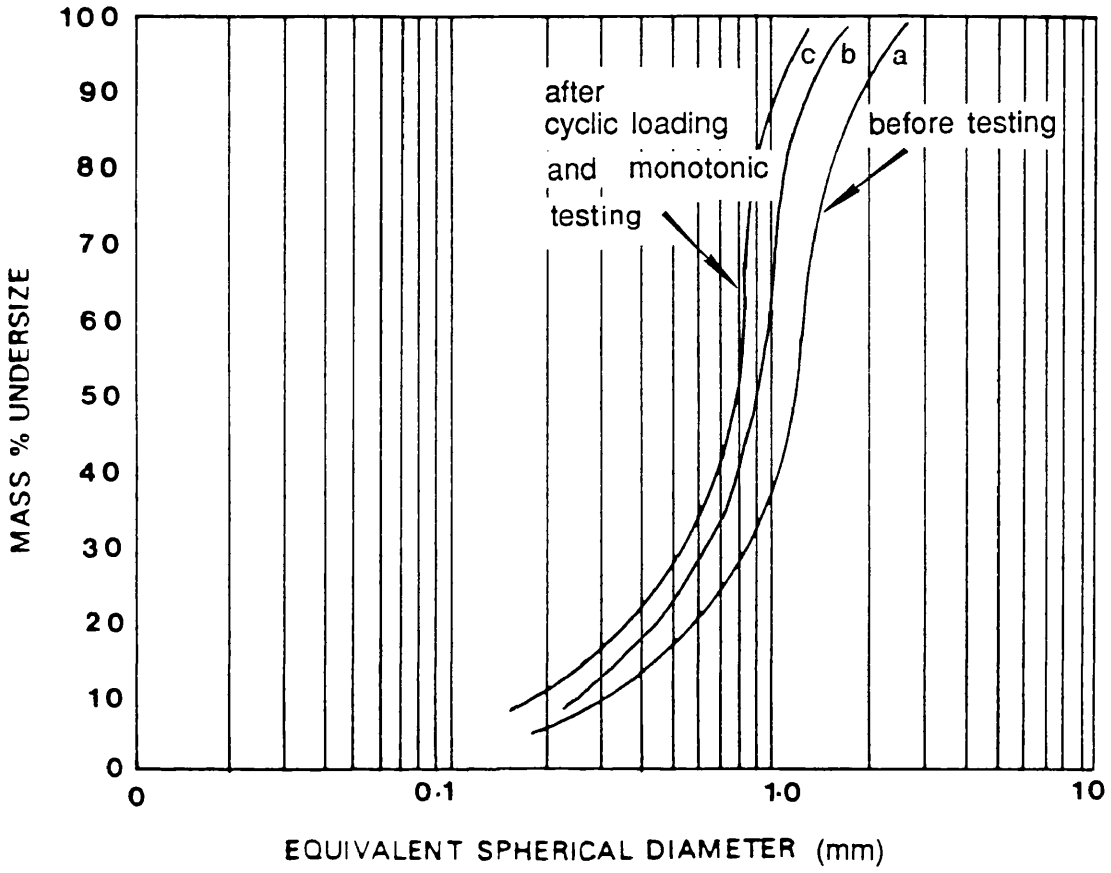

Fig. 6.13 Sieve analyses for the damp coal prior to testing, after monotonic loading and after being subjected to cyclic rotation of principal stress direction.

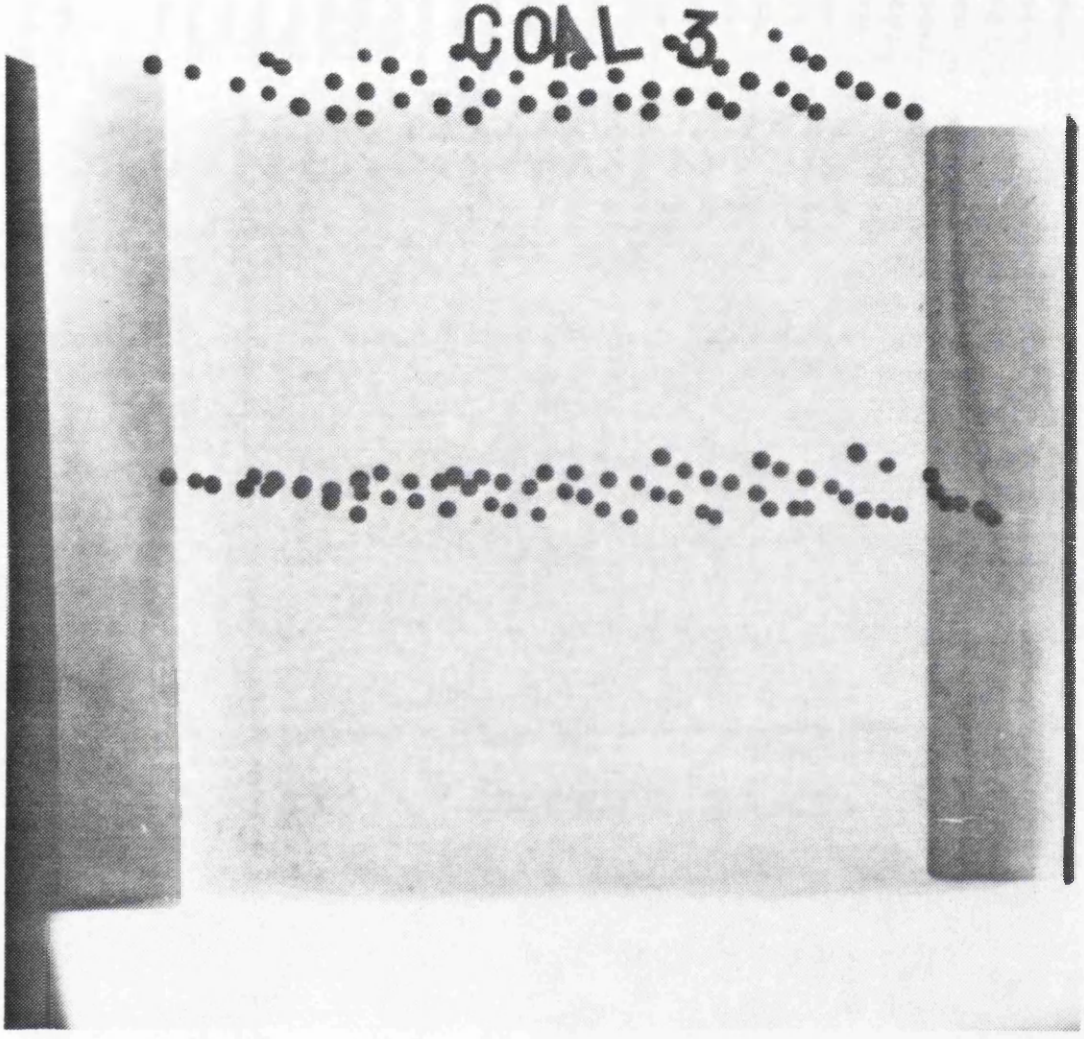

Fig. 6.14 Remaining bedding planes after cyclic rotation of principal stress direction

no. of tests	moisture content %	angle of shearing resistance
4	4	30.9°
4	6	31.8°
4	10	32.2°

Table 6.1 Possible effects of moisture content on the peak angle of shearing resistance in loose samples of damp coal tested in the DSA

CYCLIC TESTS										MONOTONIC AFTER CYCLIC								
Test No.	symbol	θ degree	ϕ_m degree	No. of cycles	ε_{1c} (%)	ε_{3c} (%)	γ_c (%)	ε_{vc} (%)	ν_{13c} degree	Test No.	symbol	ϕ_f degree	ε_{1f} (%)	ε_{3f} (%)	γ_f (%)	ε_{vf} (%)	ν_{13f} degree	Failure plane
Simple monotonic											◇	32	10.5	-6.57	17.67	4.19	-12.3	not observed
1a	○	80	10	700	3.25	-0.42	3.65	2.8	0.0	1b	○	34	14.27	-14.42	28.68	-0.15	0.3	observed
4a	△	40	20	30	6.5	-4.50	10.61	1.61	-8.72	4b	△	38	6.29	-8.42	14.71	-2.13	8.34	observed
5a	▽	55	20	20	8.31	-5.93	14.23	2.37	-9.6	5b		-	-	-	-	-	-	-
3a	□	40	26	20	14.20	-9.32	23.51	4.88	-11.98	3b		-	-	-	-	-	-	-

Table 6.2 The results of loose damp coal tested in the DCDSC at σ_3 =14 kPa

CHAPTER 7 CONSTANT VOLUME SHEARING BEHAVIOUR OF KAOLINITE UNDER MONOTONIC AND CYCLIC ROTATION OF PRINCIPAL STRESS DIRECTIONS

7.1 INTRODUCTION

7.2 EXPERIMENTAL PROGRAMMES, TEST PROCEDURES AND TECHNIQUES DEVELOPED FOR NEARLY SATURATED SAMPLES

7.2.1 Constant direction monotonic tests

7.2.1.1 Test results

7.2.1.2 Development of a technique for splitting tested samples and discovery of failure planes.

7.2.2 Continuous cyclic rotation tests

7.3 EXPERIMENTAL PROGRAMMES, TEST PROCEDURES AND TECHNIQUES DEVELOPED FOR FULLY SATURATED SAMPLES

7.3.1 Introduction

7.3.2 Constant monotonic tests of fully saturated samples without pore water pressure measurement

7.3.3 Cyclic tests on fully saturated samples without pore water pressure measurement

7.3.4 Development of a miniature probe to measure pore water pressure in the centre of the fully saturated samples

7.3.4.1 Introduction

7.3.4.2 Assembly of developed pore water pressure measuring device

7.3.4.3 Calibration of miniature pore water pressure transducer

7.3.4.4 Obtaining the response time (Skempton's B value)

7.3.4.5 Setting up procedure for measuring pore water pressure in the centre of the Kaolinite samples

7.3.5 Constant direction monotonic tests with pore water pressure measurements

7.3.6 Cyclic tests using Null method

7.4 DISCUSSION OF RESULTS OF CONSTANT VOLUME TESTS

FIGURES

TABLES

This Chapter is divided into four sections, After the introduction in the first section, the second section explains the experimental programmes and procedures as well as techniques developed to conduct tests on nearly saturated kaolinite samples. The third section outlines the test programme and techniques developed to test fully saturated samples with and without pore water pressure measurements. In the fourth section results and findings are discussed.

7.1 INTRODUCTION

The previous two Chapters illustrated the conditions that controlled the initiation and suppression of flow and the effects of continuous and cyclic rotation of principal stress direction on dry Leighton Buzzard sand and damp coal.

It was important to investigate if similar effects, such as accumulation of strain due to the rotation of principal stress direction, would be observed in clay, as it is plausible that clay is more of a continuum media than sand or coal. Here, in this chapter monotonic and cyclic tests were undertaken on samples that were prepared in two ways so that these were near to and fully saturated.

In order to obtain a comprehensive view of how kaolinite samples behave, additional parameters such as rate of loading, cyclic pulse shape, creep, etc. also need to be considered.

The effect of the rate of loading on the undrained shear strength of clay has been investigated by several researchers. It has been reported that the undrained shear strength increases with loading rate, the effect being more pronounced for higher the plasticity soil index, (Bjerrum, 1969).

Richardson and Whitman (1963), using data from undrained triaxial tests on a saturated remoulded clay in which strain rate varied from 1 to 0.002% per minute, and with pore water pressure taken at the centre of the specimen, reported that the maximum shear stress increased by about 10% from the slow to fast strain-rate. They suggested that at the faster rate of strain, soil particles find it more difficult to move relative to each other and unless restrained by increased effective stress, will tend to ride up on one another. Thus the effect can be thought of as an increased resistance to shear due to a tendency to dilate. This has also been confirmed by Nagraj (1968). He investigated the effects of strain-rate on the undrained shear strength of saturated kaolinitic clay exhibiting different initial soil structures which were obtained by electrochemical methods. He observed that the rate of decrease in strength with time

to failure was large in samples exhibiting flocculated structure compared with dispersed ones. Nagraj's hypothesis was that when saturated clays are subjected to deviatoric stress, a large number of particle contacts are disrupted, and new contacts are being simultaneously established but with the overall tendency for the particles to orientate parallel to the incipient plane of failure. For the flocculated structure, where the particles are randomly oriented, the possibility of reorientation to a parallel array is more probable, and hence the rate of decrease in strength is greater. In a dispersed structure where the orientation of the clay particles is already towards parallelism, the rate of decrease in strength with slower rates of strain is less.

Also it seems likely that the effects of frequency of loading is greater for more plastic clays, and intuitively it seems reasonable that the slower cycles give the clay more time to follow the applied load, to produce greater strain and greater pore water pressures.

Many investigators have found that the angle of internal friction in terms of effective stress decreased for slow tests (Bjerrum et al., 1958; Alberro and Santoyo, 1973). It could be concluded that the developed excess pore pressure during undrained shear is generally found to be higher the slower the rate of loading. Brewer (1975) showed that for triaxial tests on kaolinite (plasticity index ≈35) in the frequency range 0.01-4 Hz, the lower the frequency, the higher the strain. Brown, Lashine, and Hyde (1975) reported that varying the frequency in the range of 0.01-10 Hz had no significant effect for cyclic triaxial tests on Keuper marl (plasticity index ≈14). It appears that if loading rate is sufficiently slow the effects are minimal, however the effects of creep should not be neglected particularly in plastic clays.

Different pulse shapes have also been used by investigators in their cyclic tests and have included rectangular, trapezoidal, triangular and sinusoidal forms. The relative effect of different pulse shapes on strain can be expected to depend on the proportion of time that the soil spends at particular points in the cycle. For example, Seed and Chan (1966) showed that rectangular stress pulses have much more effect on strain than triangular pulses; and Murayama and Shibata (1960) reported that rectangular stress pulses are also more damaging than sinusoidal pulses. Anderson (1975) showed that, in terms of the number of cycles to reach a cyclic strain amplitude of ± 3% in stress-controlled simple shear tests on Drammen clay, rectangular and trapezoidal pulses produced the same results for normally consolidated samples, whereas the rectangular pulses were slightly more damaging for samples with an overconsolidated ratio of 4.

If the rate of loading is sufficiently slow the pulse shape was shown to have no effect,

provided there was no discontinuity in the pulse as the soil should always be in equilibrium. Here, sinusoidal stress waves were applied in the cyclic tests.

It was stated earlier that in this research, due to the limitation of the DCDSC, conducting undrained tests at fast rates was impossible and all tests were carried out at very slow rates. The duration of a monotonic test in nearly and fully saturated samples was around 90-120 minutes, except for two which were 9 hours long and most of cyclic undrained consolidated tests were performed at periods greater than 300 sec/cycle.

7.2 EXPERIMENTAL PROGRAMMES, TEST PROCEDURES AND TECHNIQUES DEVELOPED FOR NEARLY SATURATED SAMPLES

The first series of kaolinite samples tested in the DSC were prepared by the method which has already been explained in Chapter 3. It was appropriate to start with a simple method of sample preparation as these nearly saturated samples were the first series of tests carried out by the author in order to become familiar with testing soft kaolin samples in the DSC.

The behaviour of imperfect soils (e.g partially saturated or gaseous soils) is of great concern to our understanding of instability problems of the sea floor; and these tests might shed some light on the behaviour of material of this type.

The earlier version of the DSC was used for the monotonic tests to provide a direct comparison with those tests carried out by Wong, Arthur and Dunstan (1987); these tests are described in section 7.2.1. The DCDSC was used to conduct the continuous rotation tests which are explained in section 7.2.2.

All the samples tested in this series had the properties indicated in Table 7.1 and the homogeneity of the samples was assessed after tests were carried out by taking small sub-samples from various positions and measuring the moisture content. Typical moisture content for kaolinite samples after testing ranged from 48.2% to 48.6%.

Since no water pressures were measured in these tests, neither the effective stresses nor the pre-consolidation stresses can be known. These measurements were obtained subsequently in the fully saturated test series that will be described later. Nevertheless the state of consolidation for these tests could be indirectly obtained from a series of one-dimensional consolidation tests carried out on kaolinite (Figure 7.1). As all DSC samples were initially consolidated to 14 kPa and had a moisture content of about 50% Figure 7.1 implies an over consolidation ratio of approximately 7.5.

7.2.1 Constant direction monotonic tests

Shearing the kaolinite sample commenced after the sample was set up in the apparatus (Section 3.4.1.3). Initially an isotropic stress of 14 kPa was applied to the faces of the sample for 3 to 4 hours to bed the rubber sand surface into the kaolin sample and provide sufficient traction for the shear stresses to be transmitted to the sample and to allow p.w.p. to equilibrate.

After consolidation, the samples were subsequently sheared, undrained, to failure using a monotonic stress path in which the major principal stress was increased while the minor principal stress was kept constant at the consolidating stress of 14 kPa. In these tests consecutive radiographs were taken at appropriate load increments. Tests were carried out over a period of 60 to 90 minutes. This loading was sufficient for the sample to not to drain and as such could be considered as undrained loading conditions; this was confirmed by close values for moisture content before and after testing and near to constant volume behaviour (Figure 7.3). It should be noted that conducting faster tests in the present version of the DSC is very difficult, since the normal pressure backing plates and shear sheets have to be adjusted manually during the shearing process in the DSC which was used in this research. Also the time required for radiography slows down the testing process.

Most of the monotonic tests were carried out at ψ =45°, only two tests were conducted at ψ =90°. The distance between the normal pressure bags backing plates and the faces of the sample was maintained as 30mm and adjustment of the backing plates and alignment of the shear sheets were carried out from the early stages of the test.

7.2.1.1 Tests results

Figure 7.2 illustrates the stress-strain deformation behaviour. This Figure presents the deviatoric stress plotted against shear strain data of two kaolinite samples sheared in the DSC with sufficient lubrication on the plane strain platens. Undrained peak shear strengths of 10 kPa were obtained for these tests. This undrained shear strength value of 10 kPa is comparable to the value obtained by Wong et al. (1986) and Ogunbekun (1988) testing similarly prepared kaolinite samples in the DSC and the Biaxial tester with the use of conventional lubrication methods on the plane strain surfaces.

The volumetric changes of these samples are shown in Figure 7.3. in the form of ε_1 plotted against ε_3. The data indicates the occurrence of a relatively small volume

change during the deformation of the sample when compared with the line signifying constant volume deformation. Thus, these nearly saturated samples of kaolin, could be assumed to reflect undrained loading behaviour.

Figures 7.4a and 7.4b show examples of strain distribution within the kaolin sample. The degree of uniformity is comparable to the data obtained by Wong et al. (1986) and by Ogunbekun (1988) from tests performed in the DSC and the Biaxial tester on similar samples; and also with fully saturated samples of Boston Blue Clay (BBC) carried out at MIT by Germaine (1982) which were prepared from slurry in a one-dimensional consolidation cell.

Figure 7.5 shows a comparison of the stress-strain response from three different zones across the sample. A single curve can be drawn through all the data points with a little scatter. It is interesting to note that a higher degree of restraint can be observed on the plane strain boundaries compared with a central plane. However, this restraint is less at the bottom flexible plane strain boundary where the σ_2 bag is placed. Suggesting that flexible boundaries minimise boundary restraint and help achieve higher uniformity of strain throughout the sample (Figures 7.6a and 7.6b indicate the uniformity of strain distribution on the middle and near to the top planes of strain).

Figure 7.7 indicates coincidence of the directions of principal stress and strain increment within the sample. Deviation between the major principal stress and strain increment directions against shear strain are illustrated in Figure 7.8. This coincidence of axes as well as uniformity of strain within the samples ensured the correct combination of normal and shear stresses were applied and were used as a further check on the performance of the DSC on testing soft clay samples.

Figure 7.9 illustrates the stress-strain deformation behaviour of two tests in which the shear sheets were removed from the faces of the samples and the samples were monotonically sheared with ψ =90°. The material behaved differently and failed at a lower undrained shear strength of 5.2 kPa. The volumetric behaviour of these tests are demonstrated in Figure 7.10.

The lower shear strength recorded for these tests are difficult to understand but could be due to instability created by normal pressure boundaries which were not restricted by shear sheets. Ogunbekun, using the Biaxial Apparatus, measured the undrained strain of 10 kPa and it may be that his device provided more stability.

7.2.1.2 Development of a technique for splitting tested samples and discovery of failure planes.

It was mentioned in section 2.3.1.2 that the author used a precise grating on an acetate transparent film fixed to the top platen to aid the adjustment of the backing plates. The presence of this sheet allowed the top platen to be lifted up without disturbing the sample. The undisturbed surface of the sheared sample showed a number of parallel discontinuities as the cling film and the greased top rubber membranes were removed. Scientific curiosity led the author to further investigate the extent of these discontinuities within the sample. Thus, the measurement of final moisture content was sacrificed and the sample left over night in the cell. The sample lost some moisture and could be removed from the cell with minimal disturbance. The sample membrane was then peeled off from the shear sheets left for a few hours and was carefully lifted from the bottom plate and placed in a low heated oven for final drying.

When the sample was dry enough to be split in two halves where the tungsten spheres were placed, failure planes associated with Coulomb rupture were observed. Figure 7.11 illustrates these planes.

7.2.2 Continuous cyclic rotation tests

After the sample was monotonically loaded to a desired deviatoric stress, the sample was cyclically loaded as dry sand had been (section 5.3.1) at a constant mobilised deviatoric stress. However, unlike the sand or coal samples, the kaolinite samples could not be placed under vacuum and to check the pre-calculated boundary stresses four "control transducers" and a chart recorder were used. The control transducers were located before the valves which control the calculated air pressure to the normal pressure bags and the shear pistons (Figure 2.27). Once a satisfactory waveform was recorded through the motorised regulators the "cyclic valves" were opened and all "monotonic valves" were closed except the one for the σ_2 which was kept constant throughout the cyclic process. At this stage the actual cyclic process commenced. Since the cyclic period was long, adjustment and alignment of the boundary normal pressure backing plates and the shear sheets could be carried out during the cyclic process whenever required.

Figure 7.12. illustrates the accumulated shear strain for two tests which were cycled at deviatoric stresses of 8.12 kPa and 10.22 kPa. It can be seen that in the first cycle of loading showed a relatively large strain variations; developing approximately 13% and

20% shear strain respectively. These samples deformed such that the tests had to be terminated in the second cycle. A deviation of approximately 22° between the axes of stress and strain increment was observed at the end of the first cycle for the latter test.

The volumetric behaviour of these tests during the continuous rotation of principal stress direction are presented in Figure 7.13. It can be seen the material behaved at nearly constant volume form throughout the cyclic process.

Figure 7.14 demonstrates a high degree of uniformity at the end of the monotonic process in test 11. The sample was slightly restrained close to the sample boundaries i.e strain in area one was 0.4% less than the other two areas. It is thought that the sample deformed and failed in the first cycle. Figure 7.15 shows the non-uniform distribution of strain within the sample at the end of the first cycle; the sample was restrained significantly at the boundaries.

Figure 7.16 shows ruptures developed during the cycle for test 11. It can be seen that multiple parallel ruptures are in line with the mean direction of major principal stress. It appears that these planes are tension cracks which are produced perpendicular to the direction of minor principal stress. Although some shear displacements can be observed along lead dust lines especially in the central part; these displacements can be attributed to the post failure deformation. It is possible that the deformed sample had failed during the first cycle in tension and the shear displacement developed subsequently. This was seen from the first cycle radiograph which was taken at the end of the cycle; in this radiograph the shear displacements along the lead dust lines are small and were observed only in the centre of the sample. Furthermore, the photograph in Figure 7.16 demonstrates that in some parts of the sample there are no shear displacements along the lead dust lines, although the tension cracks are crossing these lines; these lines were not affected by the post failure boundary conditions, these areas are shown by arrow heads. It should also be noticed that in these tests the ruptures can not develop right up to the boundaries of the samples and some degree of boundary restraint can be observed.

Figure 7.17 illustrates the influence of the magnitude of mobilised deviatoric stress on the behaviour of nearly saturated kaolinite samples when subjected to cyclic rotation of principal stress directions. The accumulated shear strain in the sample increases with the increase in the mobilised deviatoric stress. This is similar to that of dry sand and damp coal.

7.3 EXPERIMENTAL PROGRAMMES, TEST PROCEDURES AND TECHNIQUES DEVELOPED FOR FULLY SATURATED SAMPLES

7.3.1 introduction

In this section the behaviour of fully saturated samples of kaolin are presented. Anisotropically consolidated samples with moisture content of 50% ± 2% were subsequently sheared both monotonically and cyclically with and without the pore water pressure measurement, all at a slow rate of loading.

Initially the DCDSC samples were loaded to an isotropic stress level of 14 kPa after being one dimensionally consolidated to a stress of 152 kPa. Over Consolidation Ratio is a directional measurement and was calculated to be 7.5 (k_0 =1 - sinϕ = 0.68) in the plane of strain and 10.7 perpendicular to the plane of strain. Time was allowed for swelling (24 hours) and equalisation of pore water pressure.

Once the pore water pressure had equalised, as indicated by the outputs from the miniature transducer and registered by computer and the chart recorder, shearing the sample commenced.

Most tests were carried out at ψ =45° because the constraint from the shear sheets will be less than for tests at ψ =90°. Figure 7.18 shows the deformation in an undrained test when ψ =45°. The surfaces of sample will result in little extensive strain when the shear strain is 20% the extensive strain along the face of a shear sheet is only 0.5%.

Four types of tests were carried out on the fully saturated samples and are described in the following sections.

7.3.2 Constant monotonic test of fully saturated sample without pore water pressure measurement

In order to compare the undrained behaviour of nearly saturated kaolinite samples tested monotonically in the DCDSC at stress level of σ_3= 14 kPa with the fully saturated sample a monotonic test was carried out on a sample consolidated in the Rowe cell.

Figure 7.19 illustrates the stress strain curve. A peak strength of 10 kPa was obtained and was slightly stiffer prior to failure compared with the nearly saturated samples

tested in the DSC (see Figure 7.20). This undrained shear strength value of 10 kPa is also comparable to the value obtained by Wong et al. (1986) using the DSC and Ogunbekun (1988) using the Biaxial Tester apparatus when testing nearly saturated samples.

Figure 7.21 shows a comparison of strength-deformation response of this test and the aforementioned monotonic test conducted in the Biaxial Tester. An excellent fit can be observed and a single curve can be drawn through the data points.

Figure 7.22 shows that the high degree of uniformity of the strain distribution within the sample. It is interesting that Coulomb slip planes were not observed in this sample (Figure 7.23).

7.3.3 Cyclic tests on fully saturated samples without pore water pressure measurement

Tests were carried out to compare the behaviour of the fully saturated samples with those of nearly saturated samples when subjected to continuous rotation of principal stress direction. Two fully saturated samples are consolidated in the Rowe cell and in modified oedometer were tested.

The procedure for conducting these tests was identical to the cyclic test carried out on the nearly saturated samples. The samples were monotonically loaded to a desired mobilised deviatoric stress, and subsequently cyclically loaded with a known amplitude of rotation. The boundary shear and normal stresses were adjusted and aligned within the cycle whenever necessary. After an arbitrary numbers of cycles the sheared samples were dismantled, oven dried and broken into two halves to be inspected for discontinuities.

The samples consolidated in the modified oedometer were tested at an amplitude of 55° and a mobilised deviatoric stress of 5.8 kPa. The cyclic period was 97 seconds/cycle.

The sample consolidated in the Rowe cell was tested at an amplitude of rotation of 80° at a mobilised deviatoric stress of 5.8 kPa. The cyclic period was sample was 300 sec/cycle.

Figure 7.24 shows the shear strain accumulated during the continuous rotation test with a total shear strain of approximately 17% recorded at the end of tenth cycle. This

amount of strain is comparable with the 17.8% shear strain that was gained at the end of the first cycle of the nearly saturated sample test 13 (see Figure 7.12). The larger strain accumulated in the nearly saturated sample can be attributed to the higher mobilised deviatoric stress of 8.12 at this test.

The volumetric changes are illustrated in Figure 7.25 and are very close to constant volume while Figure 7.26 relates the coefficient of variation with the accumulated shear strain. Clearly these samples deformed with a high degree of uniformity even at large deformation.

It is interesting to note that discontinuities did not develop in these fully saturated samples compared to those developed in the nearly saturated samples at the same amount of shear strain. Figures 7.27 and 7.28 show oven dried halves of the two fully saturated samples with no tension cracks.

7.3.4 Development of a miniature probe to measure pore water pressure in the centre of the fully saturated samples

7.3.4.1 Introduction

Pore water pressure measurements are essential for undrained shear testing as they provide the only means to assess effective stresses within the soil sample.

Experimentally, Richardson and Whitman (1963) show effective stress paths deduced in fast and slow undrained tests on normally consolidated clay (Figure 7.29a) with pore water pressure measured at the end of the sample. The restraint at the ends concentrates the deformation into the central part of the sample and in normally consolidated samples tested in triaxial cells pore water pressure develop at the centre, and in the slow tests pore water pressure is able to flow down the pore pressure gradient, increasing the water content at the end of the sample at the expense of the centre. An opposite effect is observed in tests on heavily overconsolidated samples where there is a tendency for negative pore pressures to develop in the central deforming region.

Wood (1980) reported data by Carter who performed finite element analyses of triaxial samples in which the effect of finite permeability of the soil was taken into account. Pore water pressure affects the results of drained tests through the applied strain rate. Fast tests produced a response similar to that in ideal undrained tests. Slow tests behaved as an ideal drained test would. Different elements of soil within the sample

follow quite different effective stress paths (Figure 7.29b). In an undrained test, although no overall change in volume may occur, individual elements of soil within the sample may expand or contract, and different stress paths are followed.

Pore water pressure measurements at the ends of a triaxial specimen are unlikely to be useful unless the test is conducted sufficiently slowly for equalisation of pore pressure to occur. Sangrey, Pollard, and Egan (1978) note that no rapid test can be meaningful when applied to in situ conditions if the non-uniformities of pore pressure within the sample are large.

Reliable pore water pressure measurements have only recently been recorded, H ight (1982). H ight developed a technique for installing a piezometer probe on samples down to 38mm in diameter, which was simple and relatively quick. The probe was based on a miniature silicone diaphragm pressure transducer which was mounted with its porous ceramic face flush with the cylindrical surface of the sample at mid height. Height found that using such a combination leads to a short response time for the piezometer soil system. In this case changes in pore pressure were also recorded at the boundary of the sample. Clearly for good quality triaxial testing measurements of pore water pressure and deformation must be made in the central deforming region of the sample.

However, the boundary conditions of the DCDSC are not compatible with the measuring devices used by H ight (1982). The four faces of the sample on which shear stresses must be applied are designed to be flexible and rough such that porous ceramic could interfere with the application of uniform shear stresses. The bottom end of the plane strain face is also made of a water-filled pressure bag and placing a porous ceramic on that location is not possible. The top plane strain side was the only surface suitable for placing the transducer. However, in comparison with the triaxial apparatus the DCDSC cannot fully maintain undrained condition and drainage could occur at all surfaces resulting in low pore water pressure values. It was decided that the only way to measure reliable pore water pressure within the sample was to use a probe that could be inserted into the kaolin sample.

Several investigators have used different kinds of probes to measure pore water pressure in the centre of the sample. As reported by Whitman (1960), Taylor carried out several triaxial tests from 1944 to 1948 in order to measure strength characteristics in terms of effective stress. He measured pore water pressure using a porous probe inserted into saturated Boston Blue clay (BBC) in the anticipated failure zone; tests had to be performed at sufficiently low rates to allow for the pore water

pressure measuring device to respond and therefore give a full value of the pore water pressure changes. To check the system reliability, Taylor increased the chamber pressure suddenly and monitored the pore water pressure.

Koutsoftas (1970) used a probe made of a fine porous ceramic stone protected by a steel tip. The probe was inserted into a preaugured hole drilled 80% of its penetration length into the sample and then pushed into position.

Germaine (1982) developed a miniature probe to measure pore water pressure in the centre of the Boston Blue Clay samples tested in the DSC (Figure 7.30). The probe he used was 2.15mm in diameter with a sharpened tip fabricated from a fine porous ceramic stone with a small bore hole penetrated through the inside of the stone to facilitate drainage and de-airing. The water pressure was measured with a Kulite miniature transducer with a 2.16 mm diameter sensing zone. The total system volume was approximately 0.11 cc or 0.01% of the sample volume. This probe was found to produce a very quick response time.

Generally, the use of penetrating probes can create problems, the greatest disadvantage being the creation of a disturbed zone around the penetrating object. The problems are reduced if the relative size of the probe to the sample is minimised.

7.3.4.2 Assembly of developed pore water pressure measuring device

Based on the aforementioned considerations, the following criteria should be adhered to in order to assist in the development of the pore water pressure probe: i) The probe should be as thin as possible to minimise local disturbance to the surrounding soil. ii) The internal volume of fluid of the device must be as small as possible. iii) De-airing the system should be quick and easy. iv) Sealing the probe soil/interface must be perfect.

Figure 7.31 is a schematic view of the probe and the miniature transducer. The pore water pressure device consists of a hypodermic needle 0.25 mm external diameter, 0.15 internal diameter and 75 mm long with a sharp tip. The needle can be fixed to a quick fit water tight connector that is welded to a brass casing. The brass casing houses the screw type miniature transducer e.g. (1 bar Druck PCDR 200 or 3bar Kulite 3M99). To prevent any leakage the quick fit connector was smeared with a viscose grease. In Figure 7.32 Germain's transducer and the nearly developed transducers are compared.

De-airing the needle was very important to obtain consistent time responses, if any air bubble was trapped in the tube it could be compressed and result in false and delayed reading. The de-airing procedure was conducted using a hypodermic syringe of 50cc in volume filled with de-aired, distilled water. The syringe was connected to the needle under water and the water was pushed through to ensure no air bubbles were trapped. The transducer and the joining parts were also put together under de-aired, distilled water. In the probe no porous ceramic or stone was used, thus the de-airing process was easy and quick.

7.3.4.3 Calibration of miniature pore water pressure transducer

To calibrate the miniature pressure transducer, the pore pressure probe was de-aired and filled with de-aired, distilled water and screwed to a water container with an air/water interface. While air pressure was increased incrementally the elevation in mercury manometer and changes on the Dvm were recorded. The calibration value for each transducer was different and had to be calculated separately; Figure 7.33 shows one such curve for a Druck transducer.

7.3.4.4 Obtaining the response time (Skempton's B value)

In order to ensure the reliability of the pore water pressure measuring device a response time analysis was necessary. To fulfil this requirement a kaolinite sample that had already been consolidated in the modified Oedometer (and was identical to those be tested in the DSC) was placed in a triaxial apparatus. The miniature probe was inserted into the centre of the sample and fixed to the bottom base of the cell (Figure, 7.34). Care was taken to minimise disturbance to the clay around the inserted probe. The sample was left for twenty four hours under a confining stress of 10 kPa for the pore water pressure to equilibrate.

After the pore water pressure had equilibrated within the kaolinite sample, the confining pressure was increased to 30 kPa and the output of the cycling pressure and pore water pressure transducers were simultaneously and continuously monitored by the computer and the Skempton's Pore Water Pressure Parameter ($B = \Delta u/\Delta\sigma_3$) was calculated. The results of response time tests and the values of B are given in Figures 7.35a and 7.35b.

It is worth noting that the response times were checked for different needles lengths (50mm to 1000mm) and diameters (0.2mm to 0.8mm) and satisfactory results were obtained for all.

7.3.4.5 Setting up procedure for measuring pore water pressure in the centre of the Kaolinite samples

Once the fully saturated sample was set up in the DCDSC in the manner explained in section 3.4.3.7, the sample was left for twenty four hours under a confining stress of 14 kPa and the pore water was allowed drain from the sample.

After the pore water pressure probe was de-aired and filled with distilled de-aired water it was taken out from the water container very carefully so that a drop of water was left on the tip of needle; this would prevent an air bubble being trapped between the needle and the needle guide passage. Just prior to insertion of the probe into the sample, a zero reading was taken on the Dvm with the probe in its testing orientation. The probe was slowly pushed into the soil and the transducer was screwed in, to squeeze a small amount of water in to avoid possible blockage of the needle that may be created by insertion. After the joining piece rested on the 'o' ring of the fixing ring (see Figure 7.36) the probe was clamped to the top plane strain platen and allowed to reach equilibrium.

7.3.5 Constant direction monotonic tests with pore water pressure measurements

Two undrained tests were carried out at ψ =45° while the pore water pressure was measured and the samples were incrementally sheared in the following sequence at a very slow rate (i.e the total tests duration was 9 and 10 hours):

1- A small incremental deviatoric stress was increased by increasing first the normal stress, then the shear stress and finally intermediate principal stress.

2- After each increment the change in pore water pressure was recorded.

3- Radiographs were taken at appropriate intervals during the shear.

4- Samples were strained up to a 10 kPa boundary shear stress, a level comparable to remoulded samples.

Figure 7.37 shows the stress-strain response of these two tests and the volumetric behaviour is illustrated in Figure 7.38; a constant volume deformation can be observed from these curves.

The effective stress paths (ESP) for the two tests sheared undrained are shown in Figure 7.39. Similar stress paths were observed for monotonic tests carried out by O'Neill (1985) on Boston Blue Clay with the OCR=4 in the DSC (Figure, 7.40).

No failure planes were observed in these samples.

An important feature of Figure 7.39 is that at failure the shear stress in very nearly equal to the mean normal stress. This implies that the effective stress Mohr Circle passes through the origin (Figure, 7.41).

It was stated that for cyclic tests on the partially saturated samples tension cracks were observed in the mean direction of the major principal stress. These occurred when a deviatoric stress of approximately 10 kPa was applied (Figure 7.12), i.e. a shear stress of 5kPa.

Figure 7.39 shows that at a shear stress of 5 and 7 kPa the effective stress paths turns abruptly to the right implying that the sample approaching a state of dilation. This form of dilation could well associate with tensile failure.

Although the findings are not conclusive, there is a possibility that tensile failure has an equal chance of occurring as Coulomb failure (Figure 7.41); both these failure mechanisms will be prevented if the soil is fully saturated.

7.3.6 Cyclic tests using Null method

Since the pore water pressure is to be detected in the centre of the sample the effects of local boundary drainage conditions on the pore water pressure measurements in the DCDSC will be greatly reduced. The Null method of testing was conducted on the fully saturated kaolinite samples. The total stress path was controlled to maintain the excess pore pressure at zero, hence minimising water migration to or from the sample boundaries where it is possible for some drainage to occur.

This method has also been used by several investigators using direct simple shear devices and triaxial cells. In their standard configurations, some of these devices are unable to perform truly undrained tests with pore water pressure measurements; instead, shear tests maintaining constant volume are performed.

The simple shear apparatus prohibits lateral deformations of the sample and only the height has to be maintained during shear to achieve constant volume conditions.

This is performed either physically by fixing the sample height (e.g. Finn and Vaid, 1977) or, as for the NGI simple shear apparatus in which an automatic loading system always maintains a constant sample height. In constant volume simple shear testing, it is assumed that the change in applied vertical stress as the sample height is maintained constant during deformation is equal to the excess pore water pressure that would have been measured in a true undrained test (Bjerrum and Landva, 1966) with constant total vertical stress.

This was verified for the NGI shear apparatus by Dyvik, Berre, Lacasse and Raadim; 1987. They conducted two series of truly undrained tests with pore water pressure measurements and constant volume tests on normally consolidated Drammen clay. The comparison showed that the test results obtained by the two methods were similar (Figures 7.42a and 7. 42b).

The Null method has been checked by Berre (1981) and Vucetic and Lacasse (1983) for triaxial tests. Berre conducted four undrained and constant volume triaxial tests on anisotropically normally consolidated Drammen clay and showed that the pore pressure-axial strain curves were identical both in compression and extension for both methods. For the constant volume tests, the change in cell pressure required to maintain the volume constant was called the pore pressure change; his data are illustrated in Figure 7.43.

In the present research the DCDSC was used to conduct a cyclic test on a fully saturated sample of anisotropically consolidated kaolinite employing the Null method. This was to compare the behaviour of fully saturated samples when subjected to the cyclic rotation of principal stress under two different conditions, i.e. one in which the pore water pressure is allowed to develop and in the other the development of pore water pressure is prevented by changing the normal stresses which is assumed to be equivalent to the excess pore water pressure.

This test was performed in two stages; first, the sample was loaded monotonically in a drained condition to a deviatoric stress of 10.2 kPa at a very slow rate. Secondly, the sample was cycled undrained with rotation angle of 85° controlled by a special computer programme using the Null method.

As the cyclic process commenced any changes in pore water pressure could be detected by the pore water pressure probe, consequently the boundary normal stresses would change automatically through motorised regulators. The boundary normal stresses were reduced substantially after one cycle which took approximately

32 minutes, due to increasing pore water pressure within the sample caused by the rotation of principal stress direction.

Figure 7.44a shows that the sample developed up to 13% shear strain within this first cycle. The volumetric deformation curve illustrates a constant volume during the cyclic loading (Figure 7.44b).

It can be seen that the trend of deformation under cyclic rotation of principal stress direction of kaolinite sample tested by the Null method was similar to those of common undrained tests. The sample developed substantial shear strain in the first cycle and no ruptures were observed.

It worth noting that there was an extreme interference between σ_2 bag and the normal pressure bags in another Null method test that was discarded. This was reduced by placing a metal plate with a square window of 102 mm x 102 mm in the centre on the σ_2 bag.

In the present research the value of the intermediate principal stress was kept constant during all cyclic tests. The boundary normal stresses are changed to keep the pore water pressure zero and the effects of σ_2 are not known. Obviously it would be better that the intermediate principal stress be controlled with the boundary normal and shear stresses during cyclic loading; this will be fulfilled in a future design.

It was encouraging that the transducer gave an excellent response when linked to the miniature probe.

7.4 DISCUSSION OF RESULTS OF CONSTANT VOLUME CHANGE TESTS

Firstly, it was found that the undrained strength of kaolinite samples is not affected by the method of sample preparation. They were all of about the same value. The results of tests on nearly saturated samples prepared without anisotropic bias and the fully saturated, and the anisotropically consolidated samples indicate that, at failure, different mechanisms are observed. The remoulded samples prepared with approximately 10% air content showed Coulomb failure planes whereas the saturated ones showed no discontinuities.

The factors causing the formation of shear planes during testing laboratory specimens are still poorly understood (Jamiolkowski et al., 1985). Failure planes are frequently associated with such phenomena as induced shear stresses, soil volume changes,

non-uniformity of laboratory specimens and consequent nonuniform strain distributions, boundary constraints, and stress concentrations imposed by the laboratory apparatus. It should be emphasised that once a failure plane has developed in a soil sample, deformations are concentrated along these slip planes. Displacements and stresses measured at the sample boundaries at this stage no longer represent the actual stress strain behaviour of the tested material. However internal strain measurements would better illustrate the deformed sample after the formation of the failure planes.

Failure planes occur in soils which are on the dry side of the critical state (e.g. heavily overconsolidated clays and dense sands) and which strain hardened, dilate, and then soften and weaken during drained monotonic shearing. Once part of the soil has dilated, soil within the dilated zone is less stiff and is weaker than the surrounding soil. Thus further straining must now take place primarily in the softer, and weaker region which will continue to dilate until it reaches the critical state.

Soils which are on the wet side of the critical state (e.g. normally consolidated and lightly over consolidated clays and very loose sands) behave differently. During drained shearing they compress, stiffen and gain strength. Once a region has sheared and compressed it becomes stiffer and stronger and further straining takes place in the surrounding soil which itself compresses. This stiffening and gaining strength continues and consequentiy in these types of soil failure planes are unlikely.

Dilation, softening and weakening appears to be the necessary conditions for the development of failure planes in soils and these conditions occur only in soils on the dry side of the critical state during deformation in which drainage occurs. Soils on the wet side of the critical state compress, stiffen and strengthen during drained shearing.

In completely undrained loading, soils neither compress nor dilate, therefore theoretically no failure plane should occur during shearing unless they are imposed by other conditions such as localised volume changes due to imperfection and non-homogeneities within the soil sample, nonuniform strain distributions, boundary constraints, and stress concentrations imposed by the apparatus.

Owing to the method of sample preparation, the samples can be regarded as nearly or partially saturated and overconsolidated. Hence it is possible that the samples are not entirely homogeneous. Although the strain distribution data of Figures 7.4a and 7.4b indicate a good level of deformation homogeneity (a level comparable with the deformation of fully saturated homogeneously prepared samples) it should be noted that the strain measurement markers were placed at 12 mm intervals and it was the

average strain over each 12 mm grid that was computed. Thus, in view of the clay particle size relative to the grid, it would be difficult to detect any inhomogeneity of strain within the 12 mm grid. Therefore formation of slip planes in the remoulded kaolinite samples in these tests can be attributed to local volume changes that have been encouraged and amplified by strain non-homogeneity within the sample.
Existence of air bubbles entrapped in the sample during preparation may not be readily identified from visual inspection when the sample is wet, however, after the sample is oven dried and broken to pieces one can easily see tiny gas pockets in the specimen. Figure 7.45 illustrate magnified sections of nearly and fully saturated samples after being oven dried.

Slip planes and discontinuities were suppressed in the fully saturated samples and none of the fully saturated samples that were tested undrained, either monotonically or cyclically, developed slip planes in spite of being largely deformed (Figures 7.23 and 7.28). Suppression of failure slips in the fully saturated samples could be attributed to the extremely uniform and homogeneous structures that these samples gained during sample preparation. This, together with suppression of local dilation, due to full saturation, maintained uniform continuous strain with no failure planes. Figure 7.20 illustrates a comparison between a fully saturated sample prepared in the Rowe cell and sheared monotonically in the DCDSC with a nearly saturated sample tested in the Biaxial tester. It can be seen although the strength-deformation response in both samples were similar, the mechanism of failure was different. Failure planes were observed in the remoulded samples in both DSC and the Biaxial Tester whereas there were no failure planes in the Rowe cell prepared samples although the final shear strength that was recorded was γ=32.44%.

The mechanism of formation of slip planes in normally consolidated clays has been proposed by Wroth (1987) on tests by Borin (1973) that were carried out in a simple shear apparatus with detailed measurements of boundary stresses. Wroth proposed that maximum shear resistance is reached as the Coulomb limiting stress obliquity is attained for the first time in the test and the planes on which it is attained are vertical. Wroth concludes that if Coulomb slips are the mechanism of failure there must be multiple slips on a single orientation (with non-coincidence axes of stress and strain rate) and material rotation according to the book shelf model of de Josselin de Jong (1972) shown in Figure 7.46. This is then the only way that the displacement boundary conditions of the apparatus can be met with uniform strain. However, this interpretation has been questioned by Airey and Wood (1987) on the grounds that radiography of similar clay samples does not show any evidence of vertical slips through the deformation of lead shot pattern.

In the present research further and stronger evidence that such multiple Coulomb slips occur in clays under certain conditions were found. Airey and Wood (1987) are correct in that these Coulomb slips cannot be seen in the deformation pattern of lead shot and displacements are very small with the sample strain remaining very uniform as can be seen from Figure 7.11.

Although it is very difficult to observe exactly when failure planes first develop in soil, particularly in undrained clay samples; it is likely that in most cases of drained shearing of dense sands or heavily overconsolidated clays the failure planes may occur at, or shortly after, the peak state and can be observed on radiographic films due to contrast in the density. However, Desrues, (1984) and Desrues et al, (1984) using a stereophotogrammetric technique, obtained quantitative results concerning strain field and showed that the rupture layer is initiated before peak, and peak appeared to be rather a consequence of the development of the localized deformation.

In this research the author was able to observe with more certainty when failure planes triggered off in the remoulded samples on radiographs. This was achieved by placing a series of parallel lead dust lines in the middle of the sample where the tungsten markers were embedded. Any relatively small displacement along these lines could be detected on radiographs. It should be noted that radiographs were taken more frequently when the development of failure planes were expected. This method also could help to observe the development of failure planes even without breaking the sample into two halves as explained earlier. Furthermore the test could be terminated when the failure planes were formed. Figures 7.11 and 7.16 illustrate these lines in a monotonic and a cyclic test respectively. Figure 7.23 demonstrates a fully saturated sample in which failure planes have not been developed even after approximately 35% shear strain and no displacement can be observed on the lead dust lines.

It was mentioned earlier that the sample was formed from sections so that the lead shot pattern could be set in planes parallel to central plane of strain. The sample could then be cleanly split apart on these planes after drying. Three splitting surfaces in a sample established the continuity of the slip planes through the depth of the sample. Figures 7.47 (a)-(c) show photographs of these surfaces after shearing and splitting. Figures 7.47 (d)-(f) show line interpretations of photographs 7.47 (a)-7(c). These slips were usually asymmetric and measurements show that the orientation to major principal stress direction corresponded to an angle of failure of 26°, the value quoted by Schofield and Wroth (1968). Only samples that were sheared to too great a strain to interpret the evolution contained symmetric slips (Figures 7.48 and 7.49).

It should be noted that these slips disappear before reaching the sample boundaries probably due to restraint imposed by the boundary rubber membrane. Figure 7.50 (after Ogunekun, 1988) illustrates a nearly saturated sample tested in the Biaxial tester in which the sample membrane was adhered to the normal pressure bag and could stretch as the sample deformed. It can be clearly seen that in this test the slip planes developed right to the sample boundaries. In some cases there was also apparent boundary strain probably caused by the contraction of the rubber during the unloading process after testing. This contraction was eliminated in later tests by cutting the sample membranes of nearly saturated samples in the direction of minor principal strain for ψ =45° tests.

The mode of operation of the shear sheets in the DSC ensures that the whole sample cannot rotate. Deformations resulting from one set of Coulomb planes alone would produce a difference in the axes of stress and strain rate. The observed incremental difference was very small so each increment of strain appeared to be made of some complex deformation combining perhaps some Coulomb slip with continuous strains.

It can be concluded that Coulomb slips may be an important mechanism of failure in a wider range of circumstances than supposed at present. However, in view of the absence of ruptures in the fully saturated samples it seems unlikely that Coulomb slips are the dominant feature creating failure but may well develop just after failure.

Secondly, behaviour of kaolinite samples, regardless of sample preparation, was characterized by:

(a) Irrespective of apparatus used i.e. the DSC, and the DCDSC, the overall behaviour of the material was not affected, and all monotonic samples (except for the two without the shear sheets which appeared instable) failed at a shear strength of about 10 kPa. This was comparable with the value obtained from the Biaxial Tester (Ogunbekun, 1988).

(b) The samples strained uniformly not only in the central plane but throughout the depth and a small deviation from coincidence of stress and strain increment axes was observed prior to failure.

(c) In both versions of the DSC some amount of boundary constraint was observed due to shear sheet stiffness and sample boundary confinement. The question of apparatus restraints remains to be resolved. Similar techniques to those employed in investigating sands will be needed (Ogunbekun, Dalili, Arthur

and Dunstan, 1988) and good quality pore water pressure measurement will be essential. For undrained tests, restraints due to the shear sheets were shown to be minimal when ψ =45° even when the sample was strained about 20% in shear.

(d) Strain in the σ_2 direction was small and was found to be 0.6% at the end of a monotonic test. This amount of strain was tolerated when the sample had strained over 15% in the other two directions.

(e) The initial stage of cyclic loading tests, showed large strain especially during the first cycle of loading. Tension cracks in the nearly saturated samples might have developed during the first cycle. No tension cracks were observed in the fully saturated samples.

(f) The cyclic test carried out with the Null method showed a similar trend in development of shear strain during the cyclic process.

Thirdly, for samples tested at very low stress levels there appears to be a chance that tensile failure could occur equally with Coulomb failure (Figure 7.41). Different elements of soil within the sample would then follow quite different stress paths.

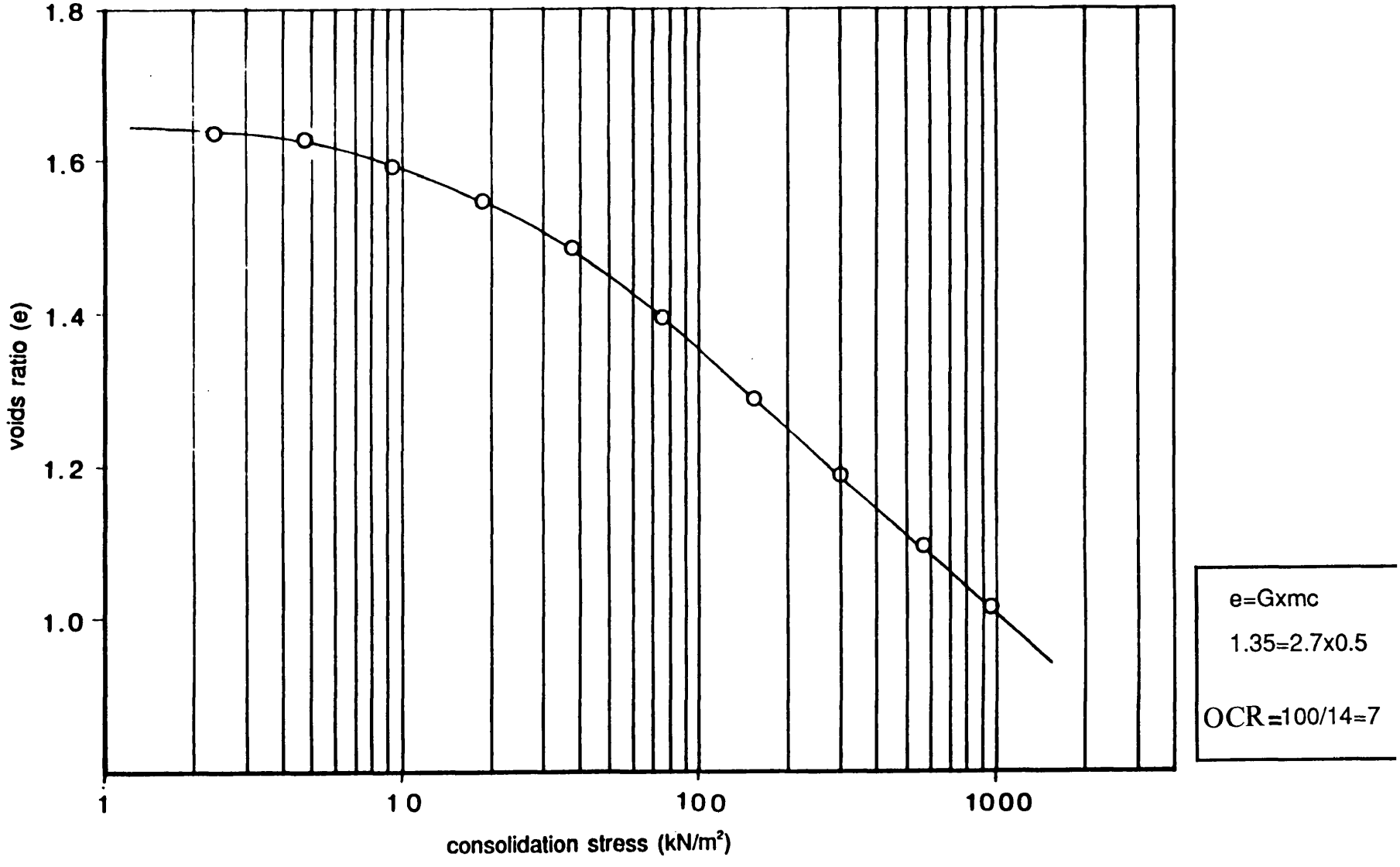

Fig. 7.1 One dimensional consolidation tests on kaolinite

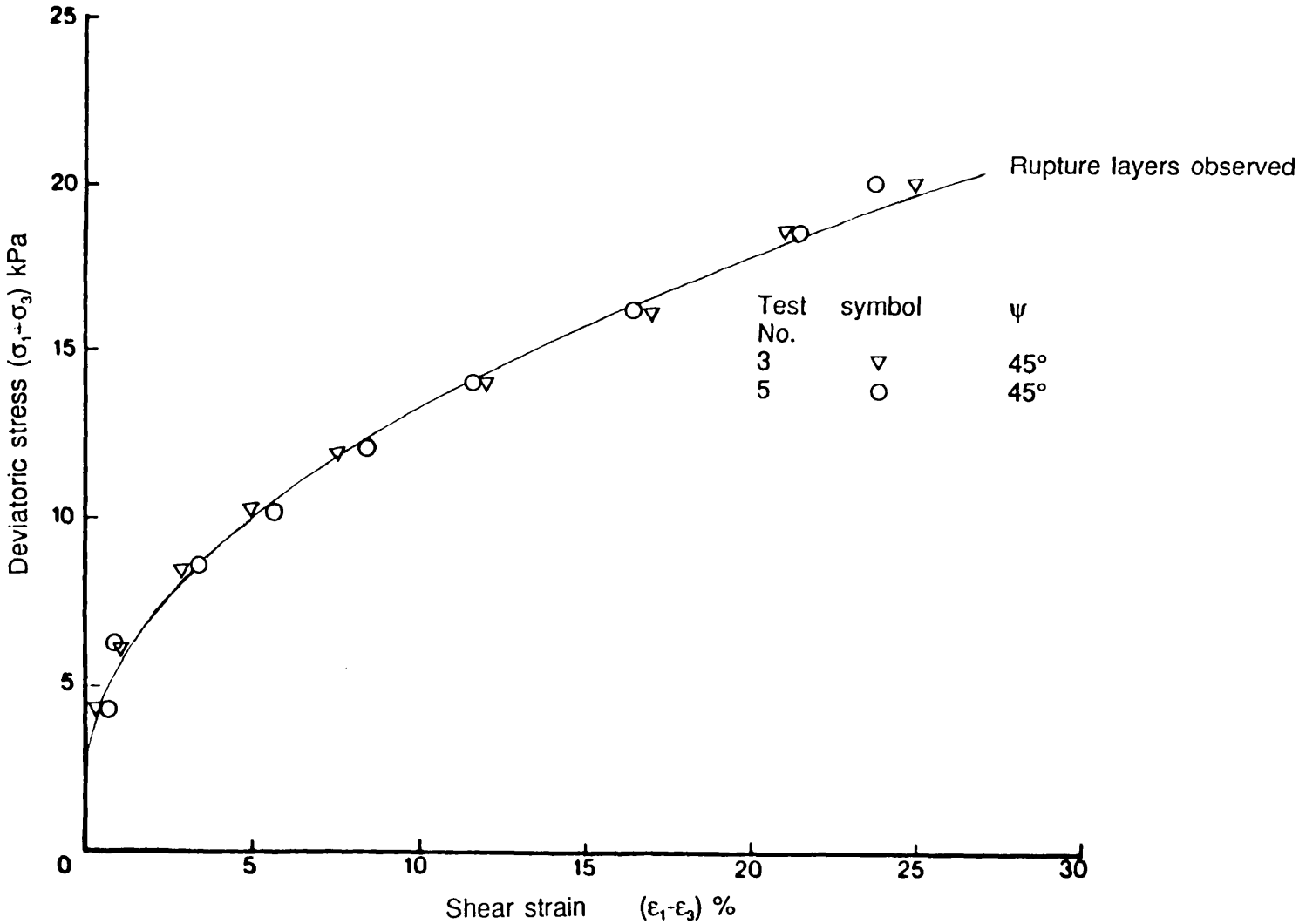

Fig. 7.2 **Stress-strain response of nearly saturated kaolinite samples sheared monotonically in the DSC at σ_3= 14kPa**

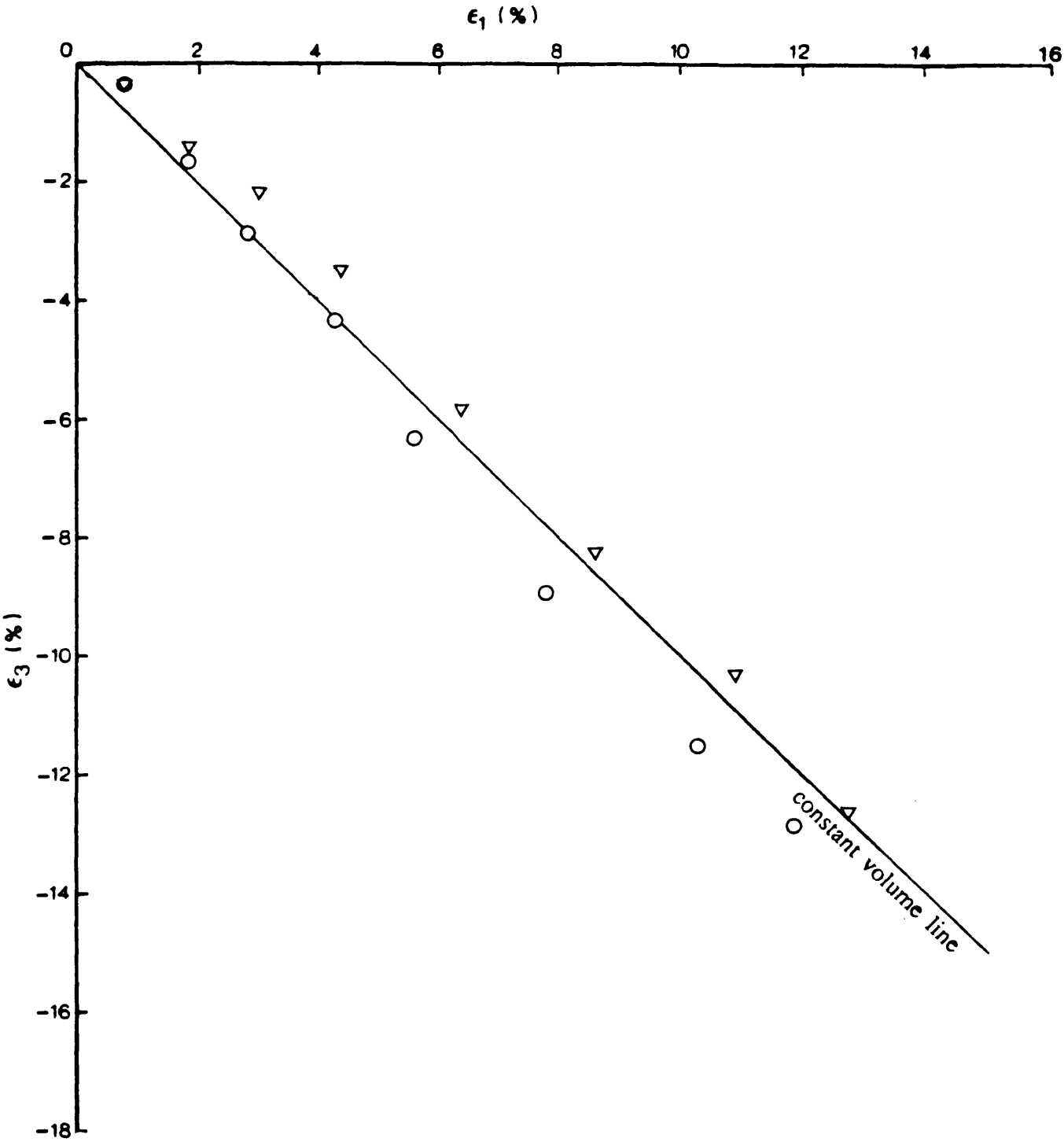

Fig. 7.3 Volumetric change behaviour of nearly saturated kaolinite samples sheared in the DSC

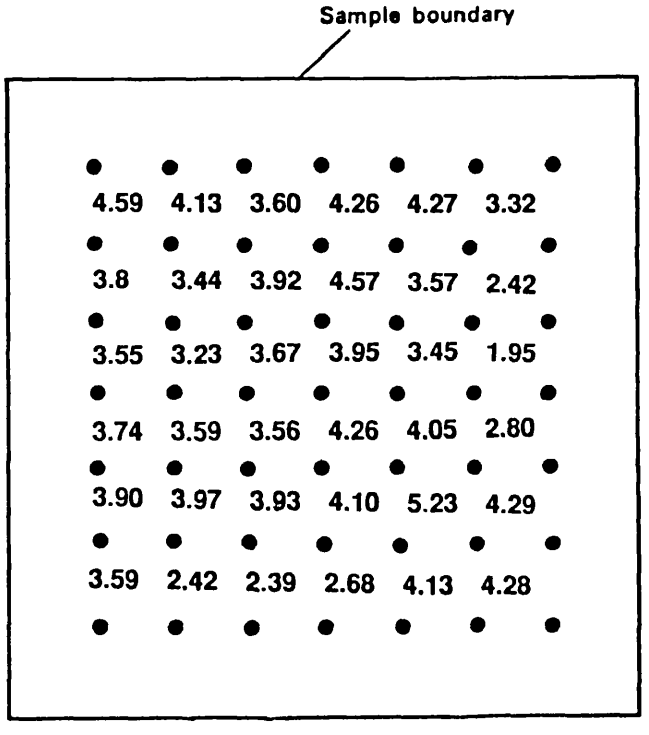

Major principal strain ε_1 (%) (a)

Ave. in Area (1): 3.68 % with standard deviation : 0.7 %
Ave. in Area (2): 3.91 % with standard deviation : 0.49 %
Ave. in Area (3): 3.86 % with standard deviation : 0.31 %

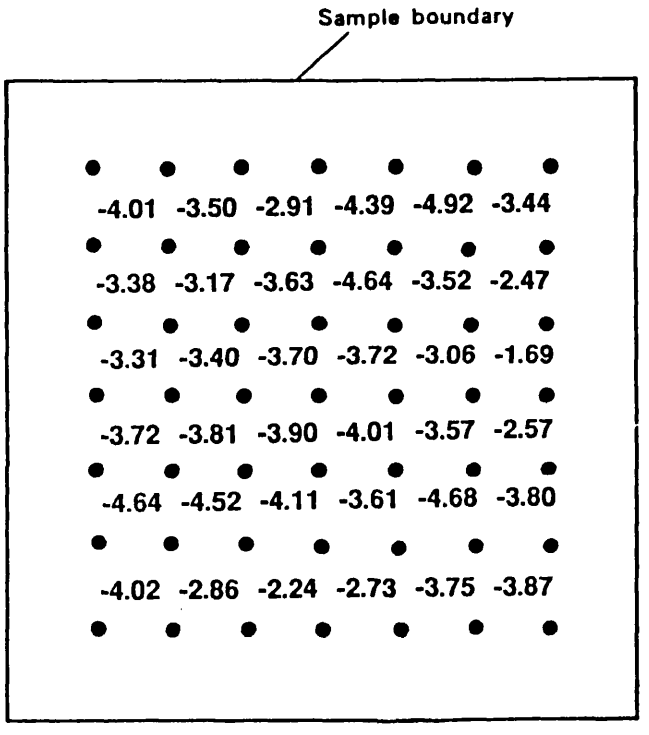

Minor principal strain ε_3 (%) (b)

Ave. in Area (1): -3.58 % with standard deviation : 0.74 %
Ave. in Area (2): -3.82 % with standard deviation : 0.48 %
Ave. in Area (3): -3.83 % with standard deviation : 0.15 %

Fig. 7.4 (a) and (b) Typical examples of strain distribution within the sample of the nearly saturated kaolinite sheared monotonically in the DSC

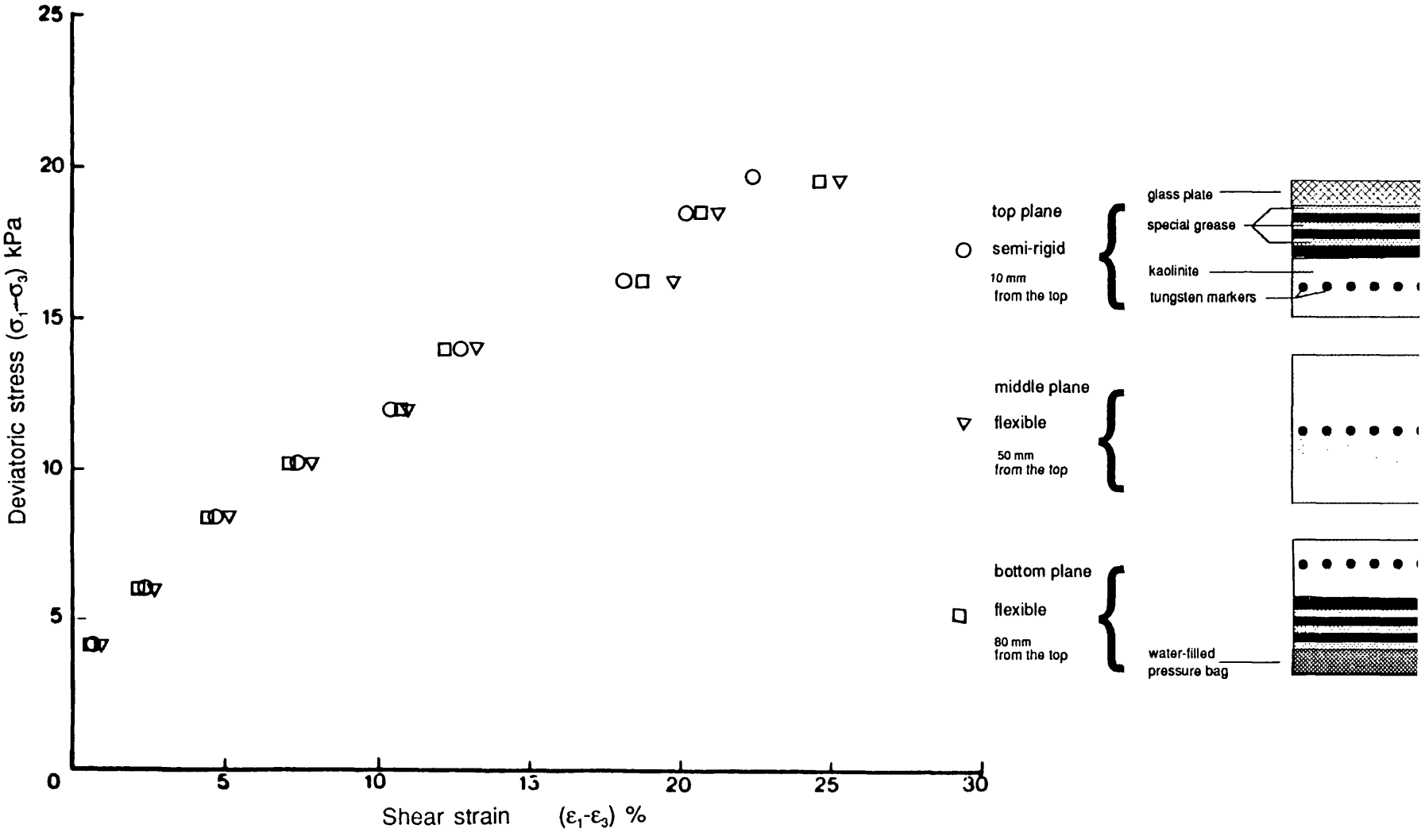

Fig. 7.5 **Comparison of strength-deformation response of nearly saturated samples measured in three different zones of deformation**

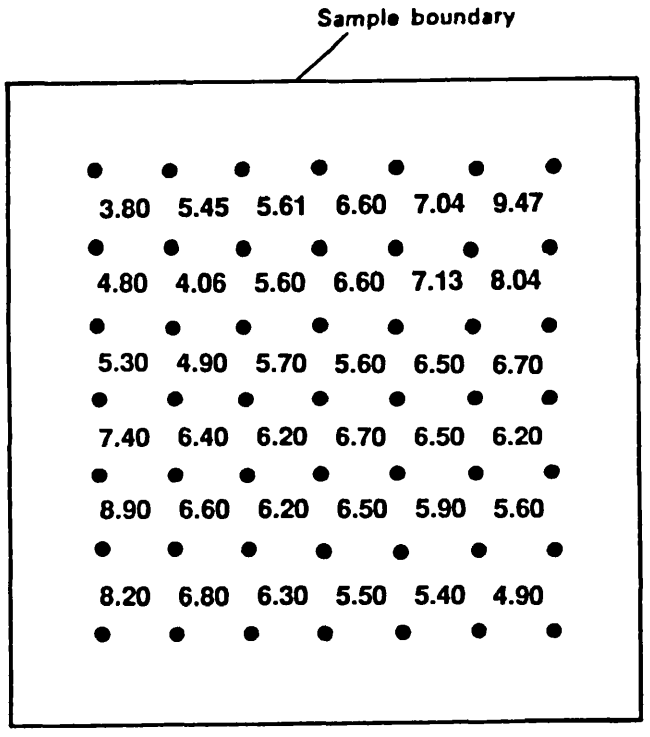

Major principal strain ε_1 (%) (a)

Ave. in Area (1): 6.26 % with standard deviation : 1.20 %
Ave. in Area (2): 6.08 % with standard deviation : 0.77 %
Ave. in Area (3): 6.08 % with standard deviation : 0.52 %

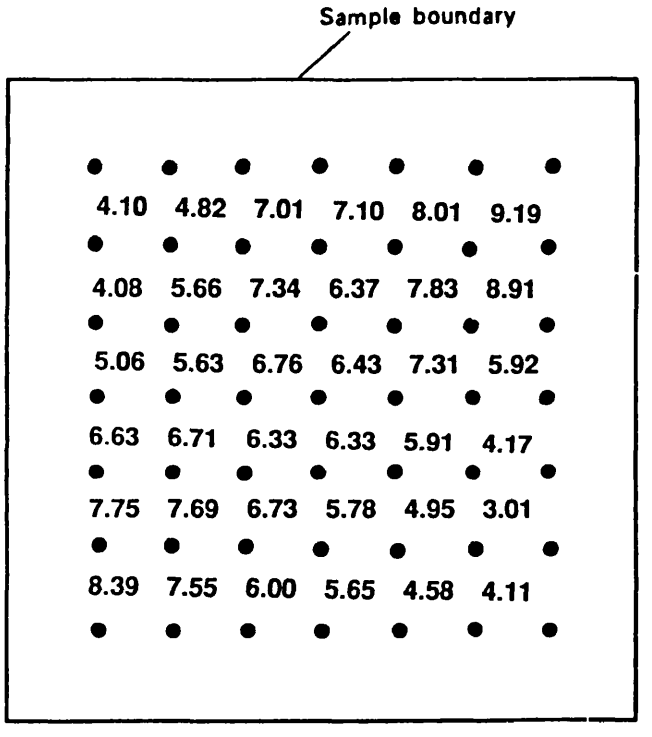

Major principal strain ε_1 (%) (b)

Ave. in Area (1): 6.28 % with standard deviation : 1.40 %
Ave. in Area (2): 6.48 % with standard deviation : 0.79 %
Ave. in Area (3): 6.46 % with standard deviation : 0.20 %

Fig. 7.6 (a) Example of strain distribution on the middle of the nearly saturated kaolinite sample sheared monotonically in the DSC and (b) example of strain distribution near the plane strain surface of the nearly saturated kaolinite sample sheared monotonically in the DSC

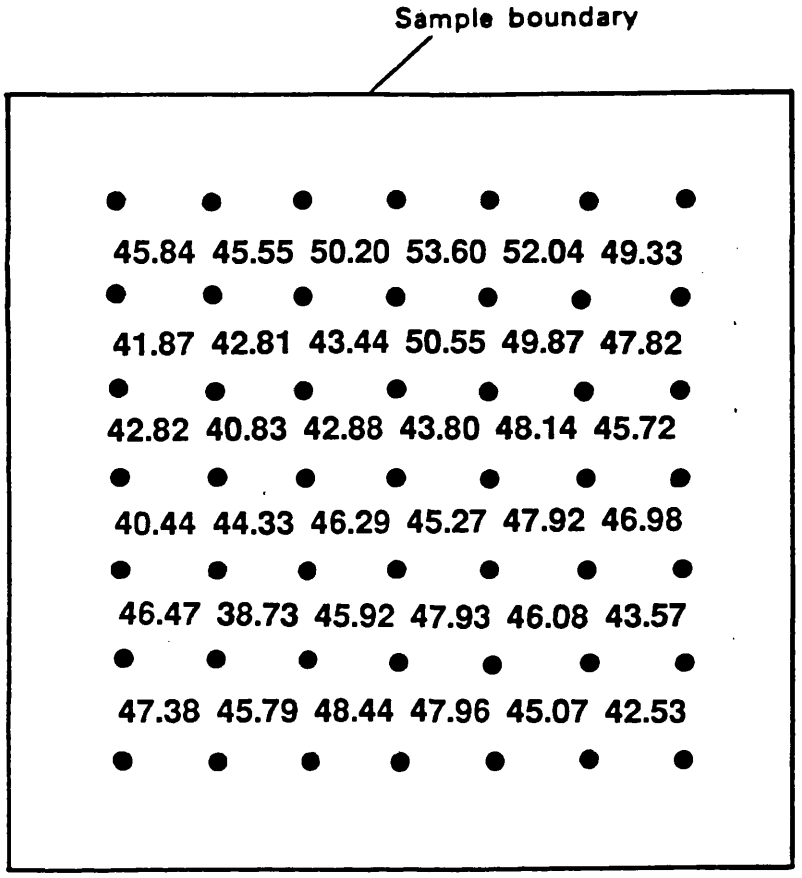

Ave. in Area (1): 45.55
Ave. in Area (2): 45.19
Ave. in Area (3): 44.36

Fig. 7.7 Coincidence of major principal stress and strain increment directions in a nearly saturated sample of kaolinite sheared monotonically in the DSC

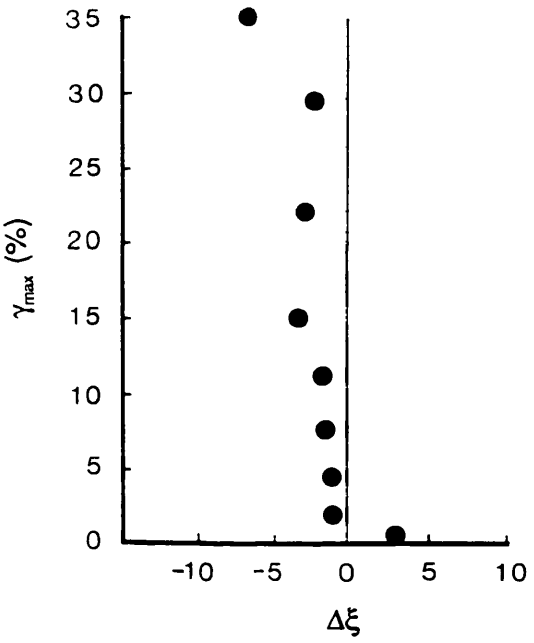

Fig. 7.8 **Deviation between axes of principal stress and strain increment in the nearly saturated samples of kaolinite sheared monotonically in the DSC**

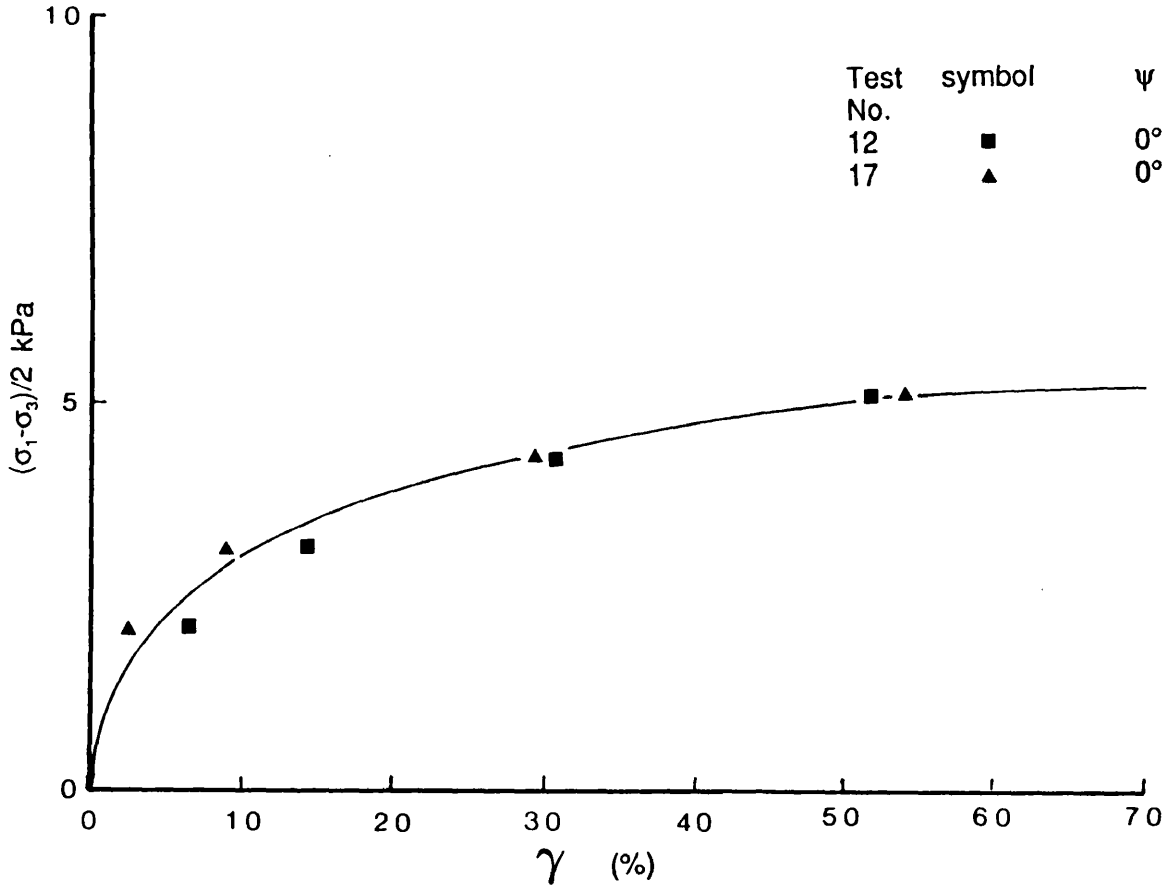

Fig. 7.9 Stress-strain response of nearly saturated kaolinite samples sheared monotonically in the DSC at σ_3= 14kPa without the shear sheets around the sample with ψ =90°.

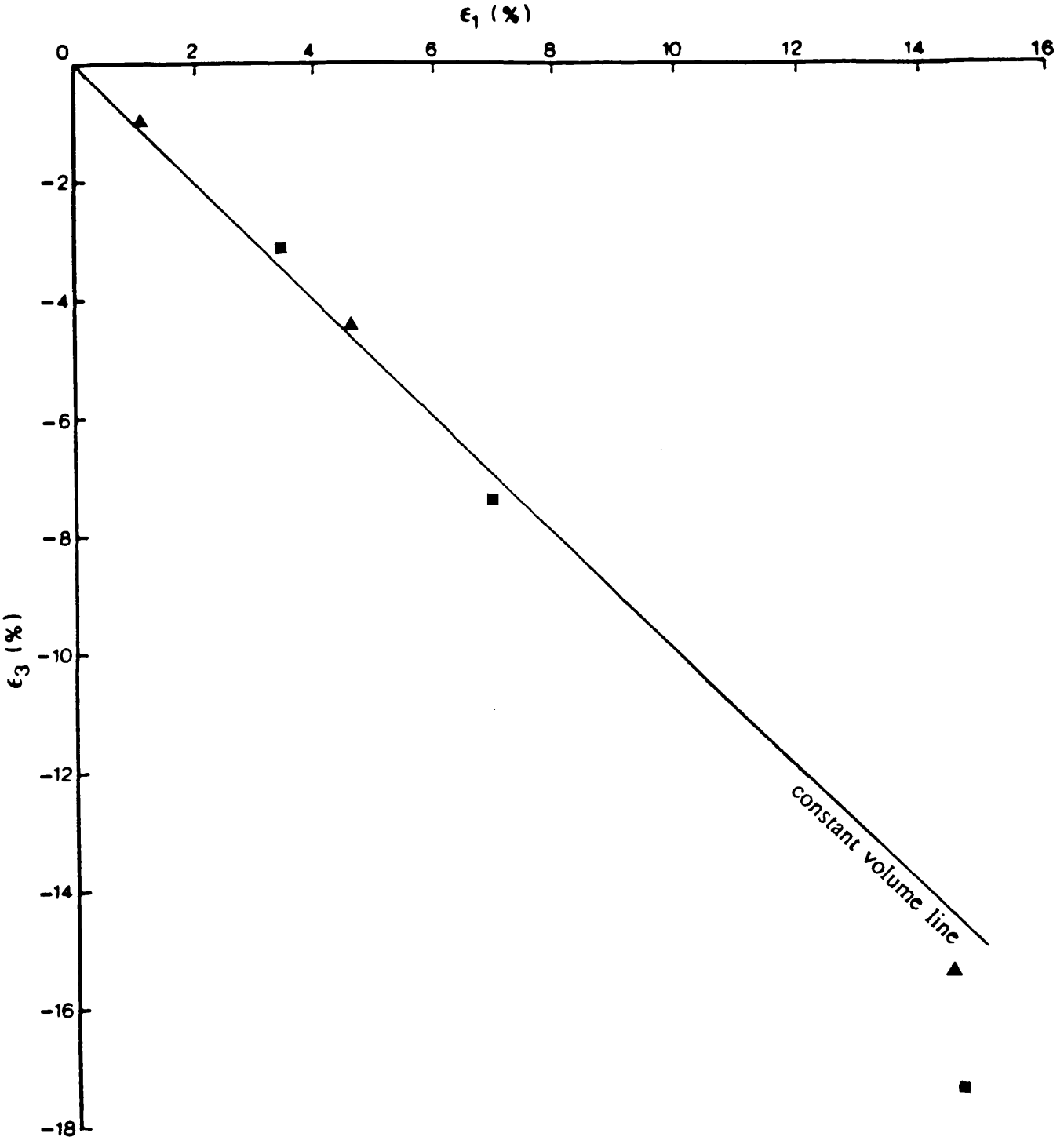

Fig. 7.10 Volumetric behaviour of two nearly saturated samples of kaolinite sheared monotonically at ψ =90° without the shear sheets.

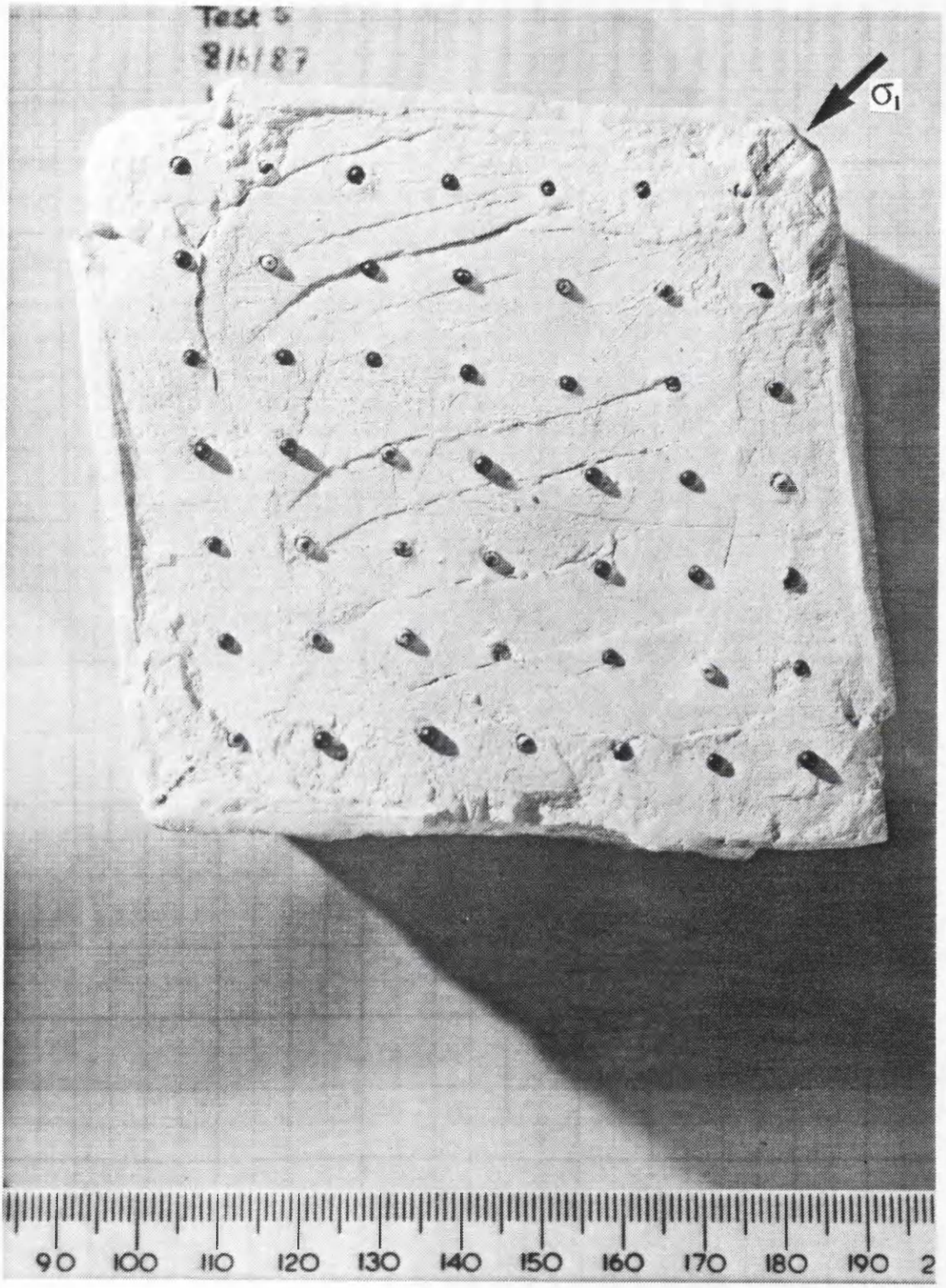

Fig. 7.11 Asymmetric Coulomb slips in nearly saturated kaolinite sample sheared in plane strain in the DSC with ψ =45°

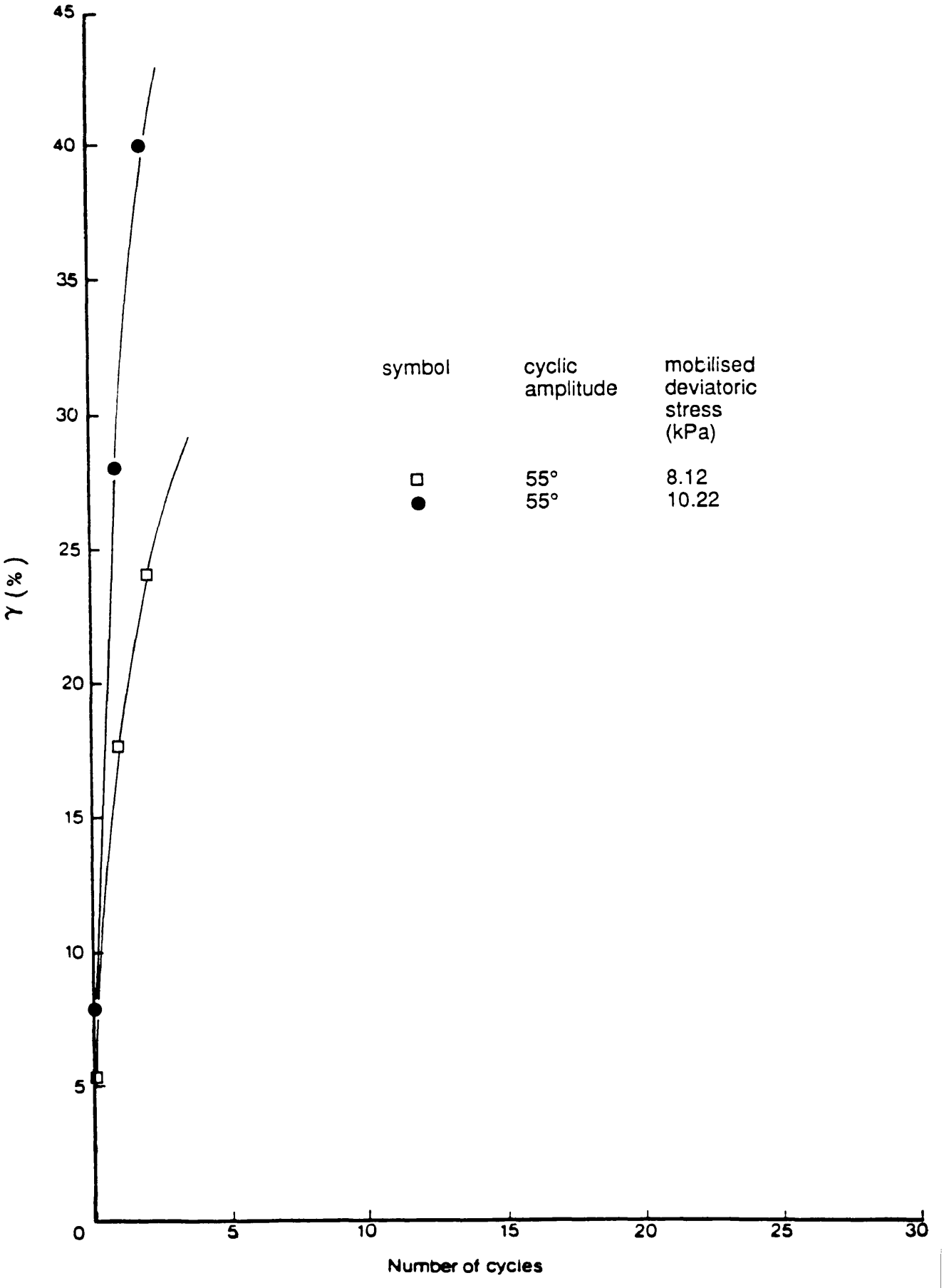

Fig. 7.12 The development of shear strain during continuous and cyclic rotation of principal stress direction on nearly saturated kaolinite sample tested in the DCDSC.

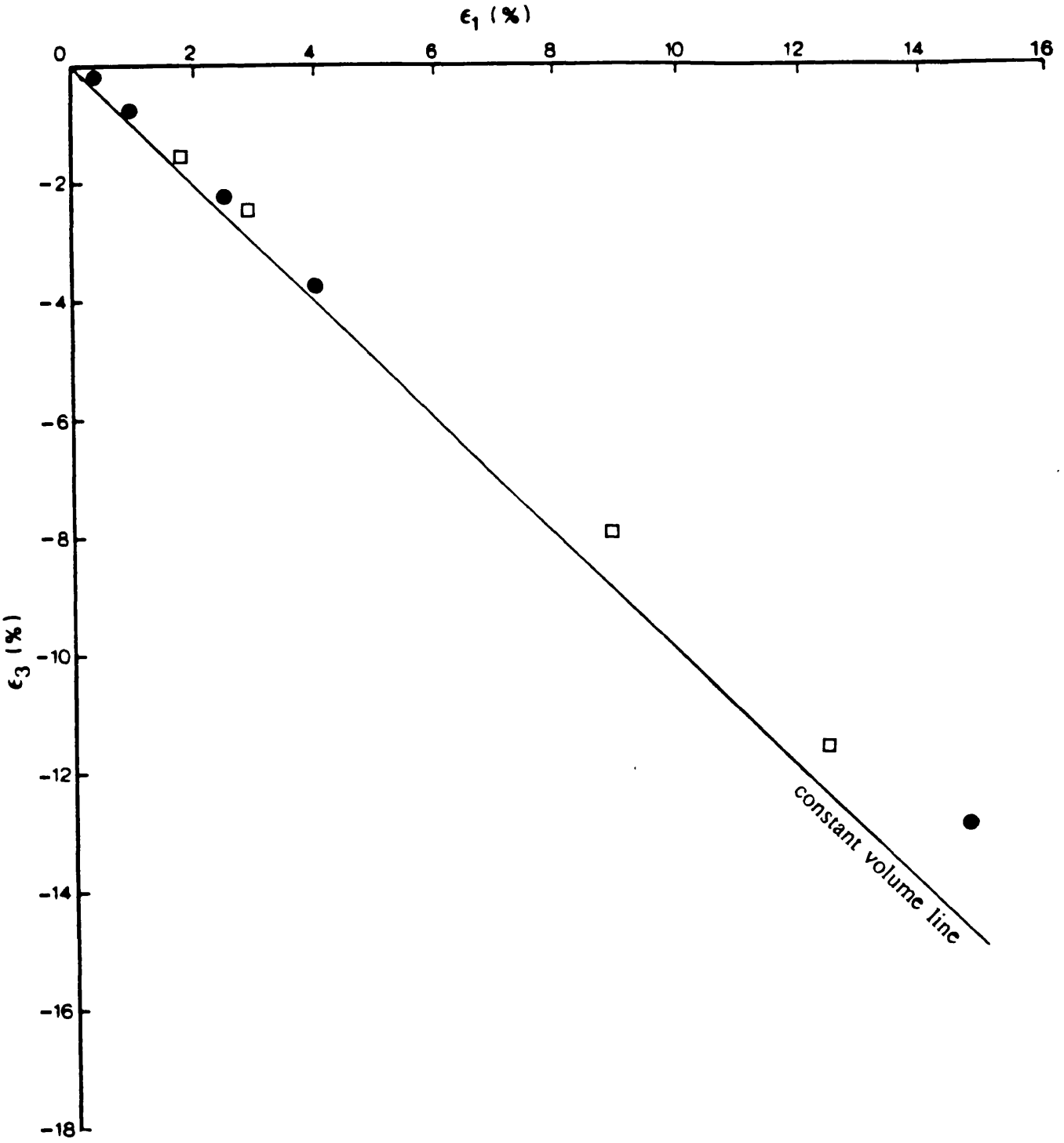

Fig. 7.13 Volumetric behaviour of nearly saturated samples of kaolinite subjected to continuous and cyclic rotation of principal stress direction in the DCDSC at σ_3 =14kPa

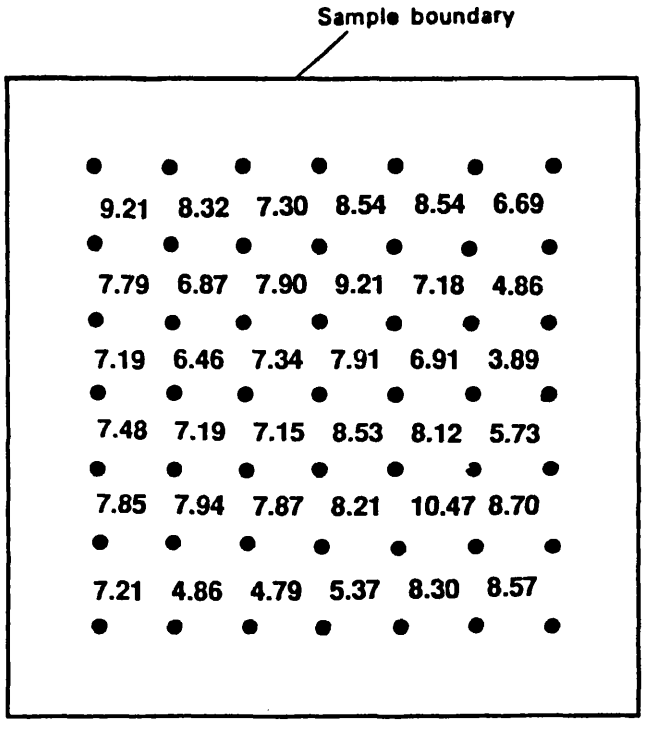

Major principal strain (%)

Ave. in Area (1): 7.40 % with standard deviation : 1.40 %
Ave. in Area (2): 7.83 % with standard deviation : 0.99 %
Ave. in Area (3): 7.73 % with standard deviation : 0.62 %

Fig. 7.14 Shear strain distribution of a nearly saturated sample of kaolinite in the monotonic part just before being subjected to principal stress rotation

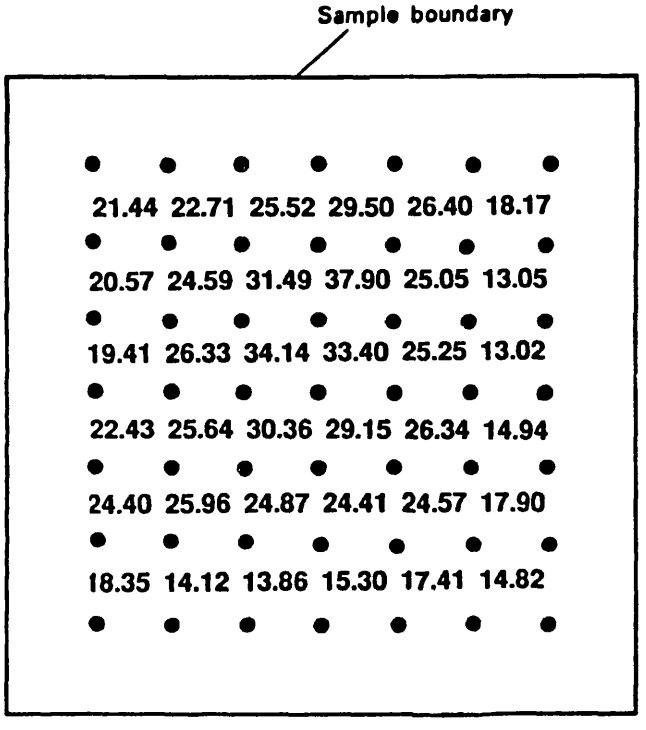

Shear strain (%)

Ave. in Area (1): 23.13 % with standard deviation : 6.35 %
Ave. in Area (2): 28.09 % with standard deviation : 4.18 %
Ave. in Area (3): 31.76 % with standard deviation : 2.39 %

Fig. 7.15 Shear strain distribution of a nearly saturated sample of kaolinite at the end of the first cycle

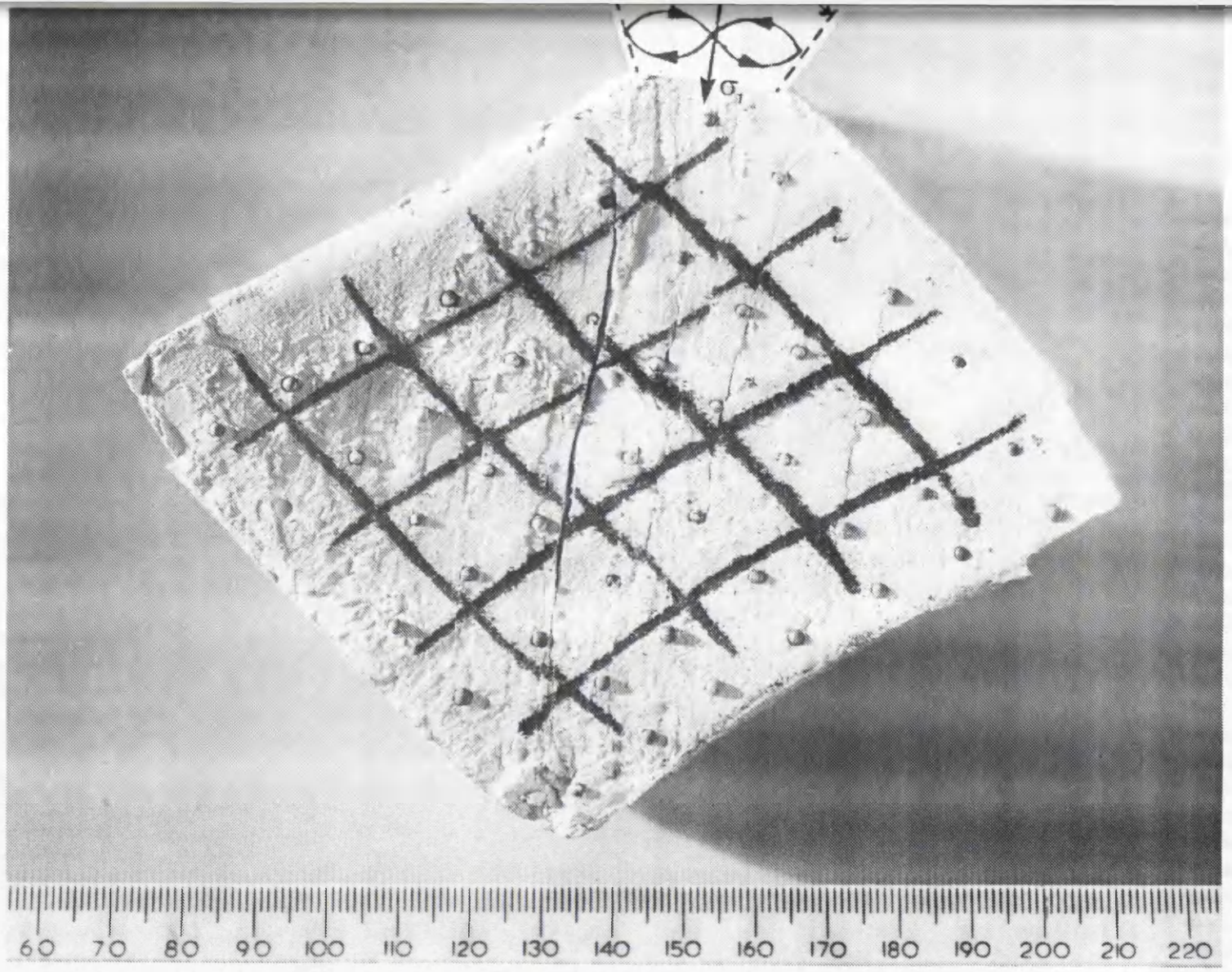

Fig. 7.16 **Development of ruptures in the nearly saturated kaolinite samples subjected to continuous and cyclic rotation of principal stress direction at σ_3 =14 kPa**

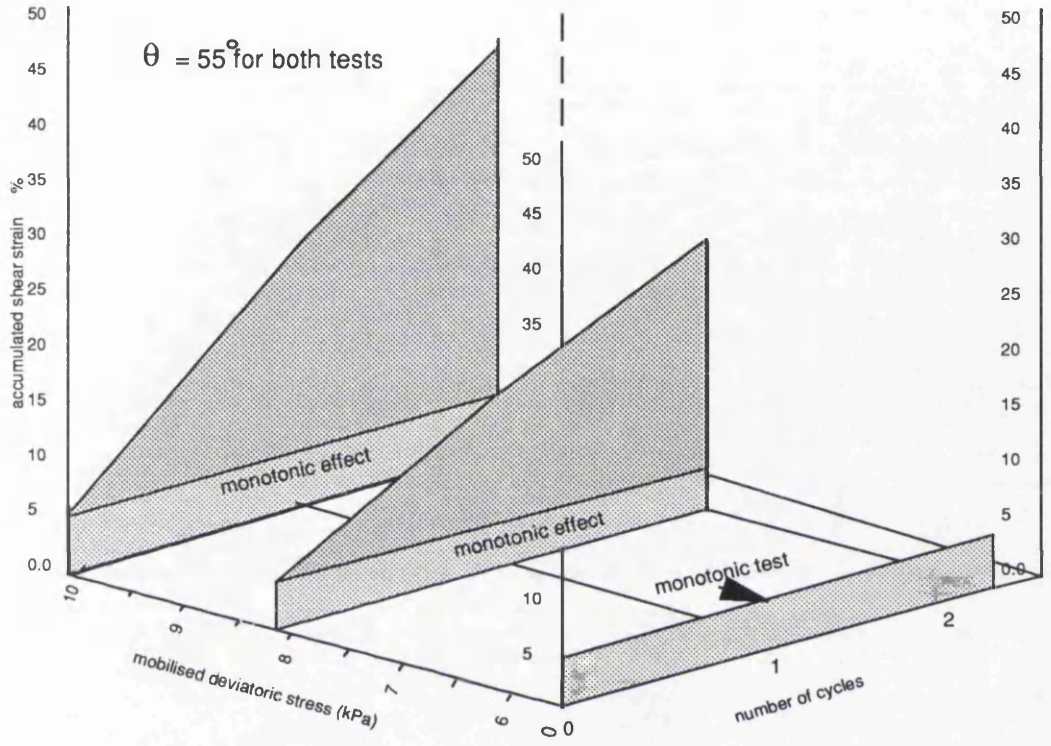

Fig. 7.17 **The influence of the magnitude of mobilised constant deviatoric stress on the development of shear strain in the nearly saturated kaolinite samples tested in the DCDSC**

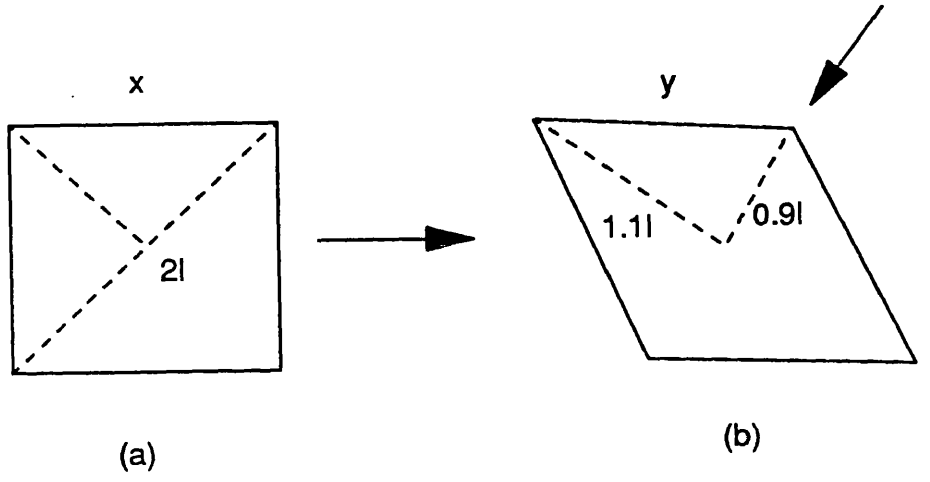

condition: $\varepsilon_1 = 10\ \%$ and $\varepsilon_3 = 10\ \%$

Fig. 7.18 Change in shape of a cubical sample in a $\psi = 45°$ test

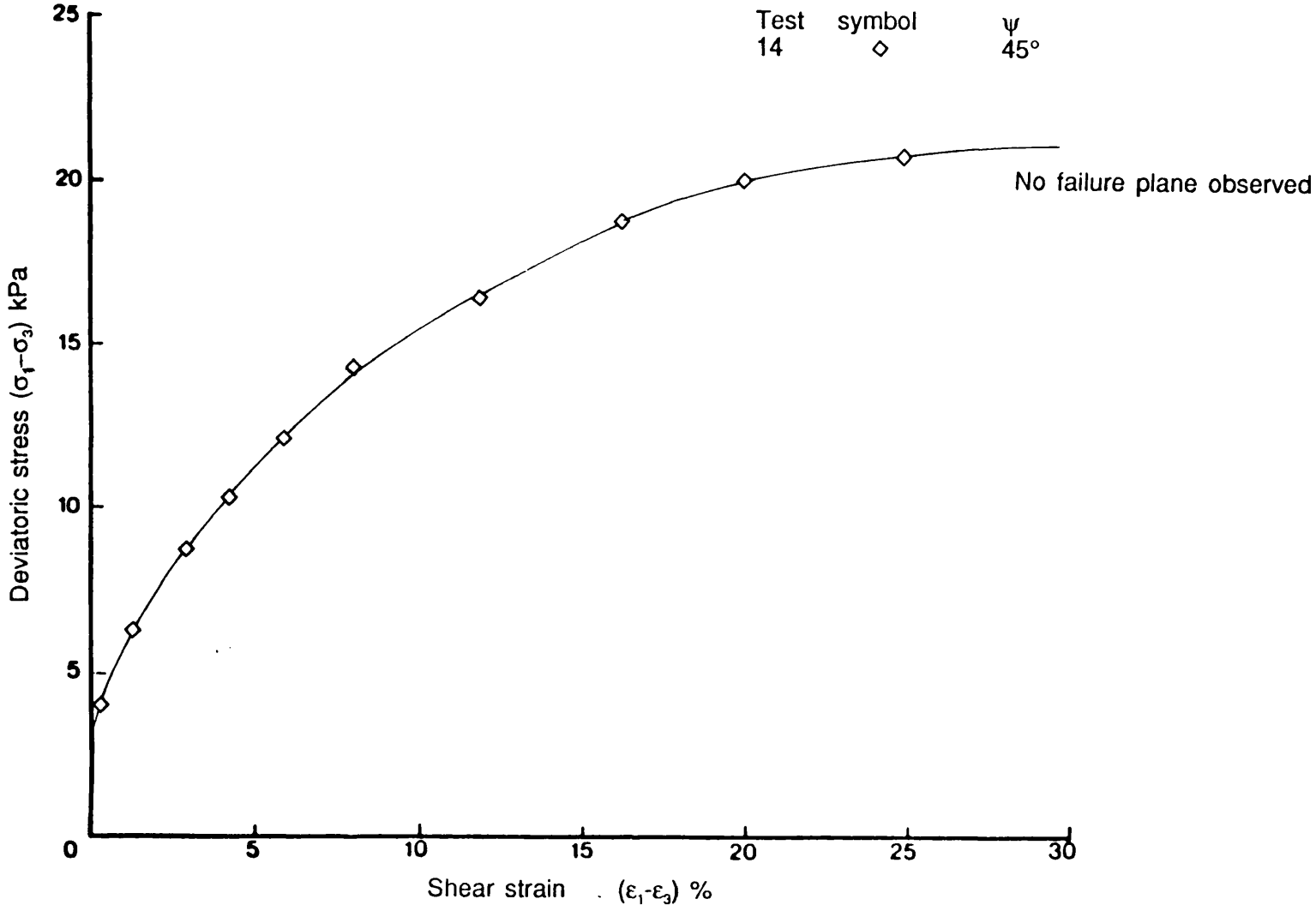

Fig. 7.19 **Stress-strain response of a fully saturated kaolinite samples sheared prepared in the Rowe cell and monotonically in the DSC at σ_3= 14kPa with ψ =45°**

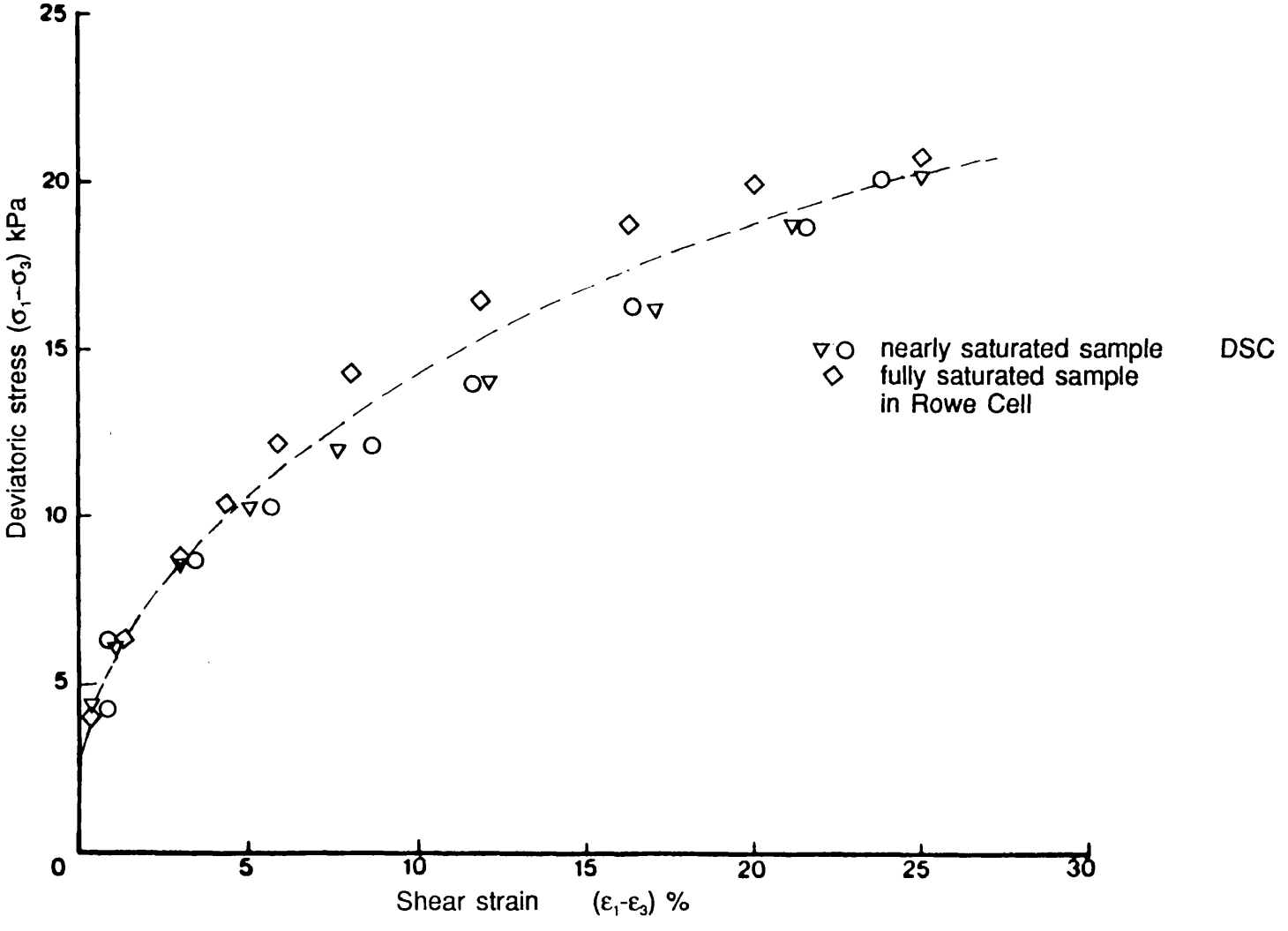

Fig. 7.20 **Comparison of stress-strain behaviour of two nearly saturated samples and a fully saturated kaolinite samples sheared monotonically in the DSC at σ_3= 14kPa with ψ =45°**

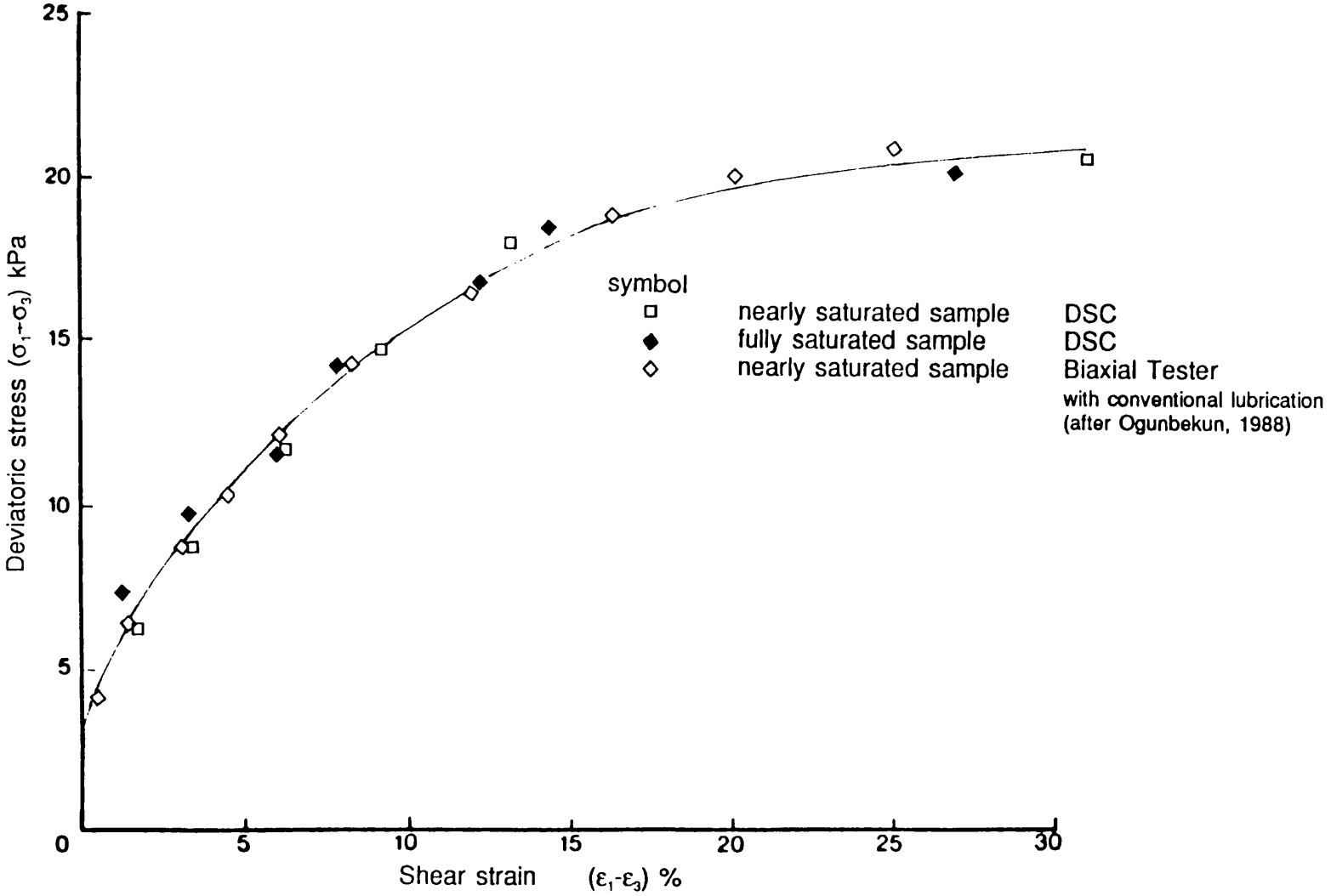

Fig. 7.21 **Comparison of stress-strain behaviour of a fully saturated kaolinite sample and a nearly saturated sample sheared monotonically in the DSC and the Biaxial tester respectively at σ_3= 14kPa**

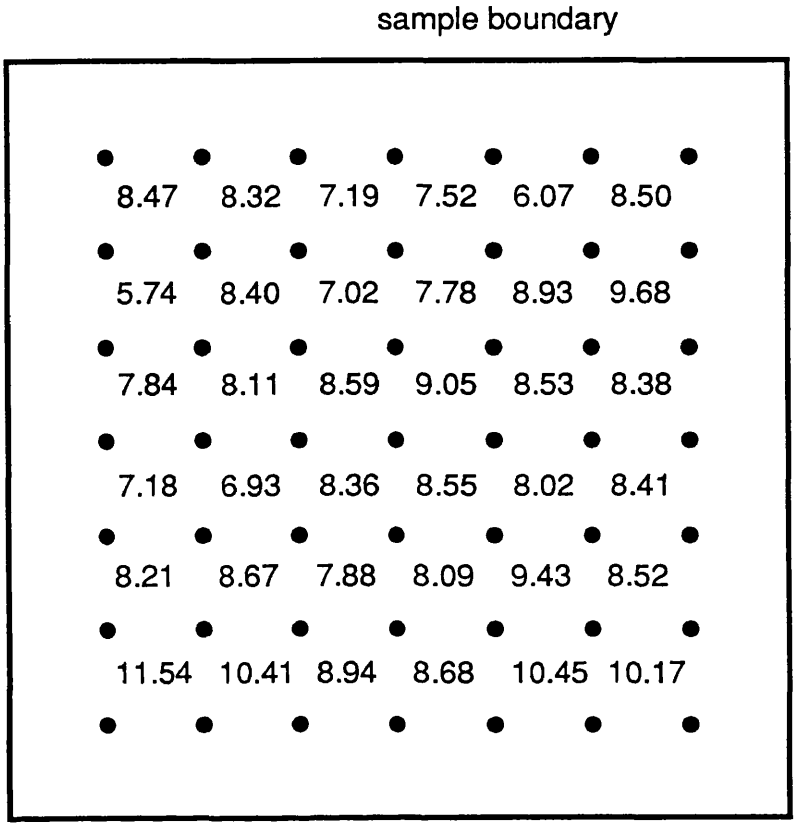

Major principal strain ε_1 (%)

Ave. in Area (1): 8.28 % with standard deviation : 1.39 %
Ave. in Area (2): 8.27 % with standard deviation : 0.67 %
Ave. in Area (3): 8.64 % with standard deviation : 0.29 %

Fig. 7.22 Example of strain distribution on the middle of a fully saturated kaolinite sample prepared in the Rowe cell and sheared monotonically in the DSC at σ_3= 14kPa with ψ =45°

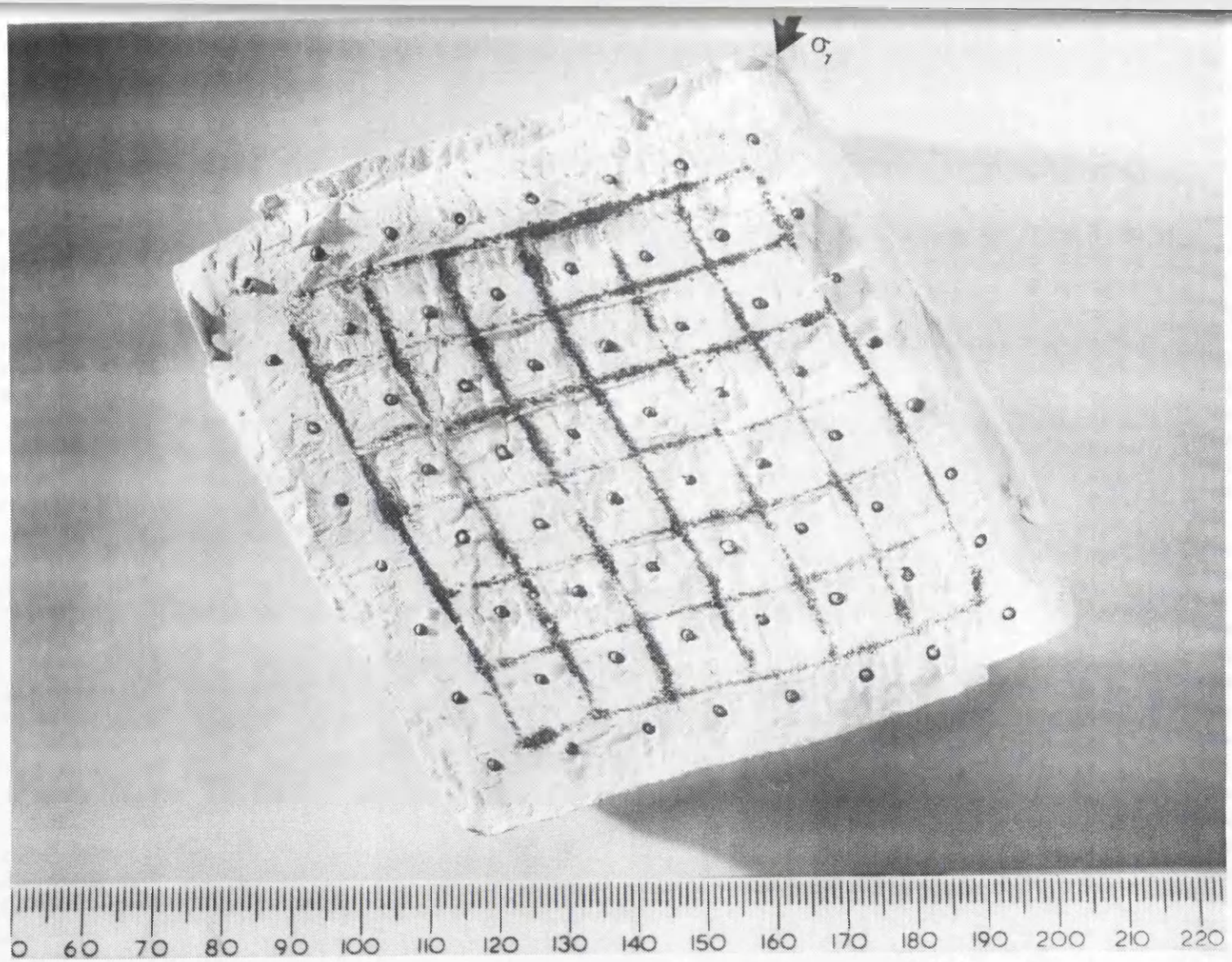

Fig. 7.23 **No Coulomb slips were observed in fully saturated kaolinite sample consolidated in the Rowe cell and sheared monotonically in plane strain in the DSC at σ_3= 14kPa with ψ =45°**

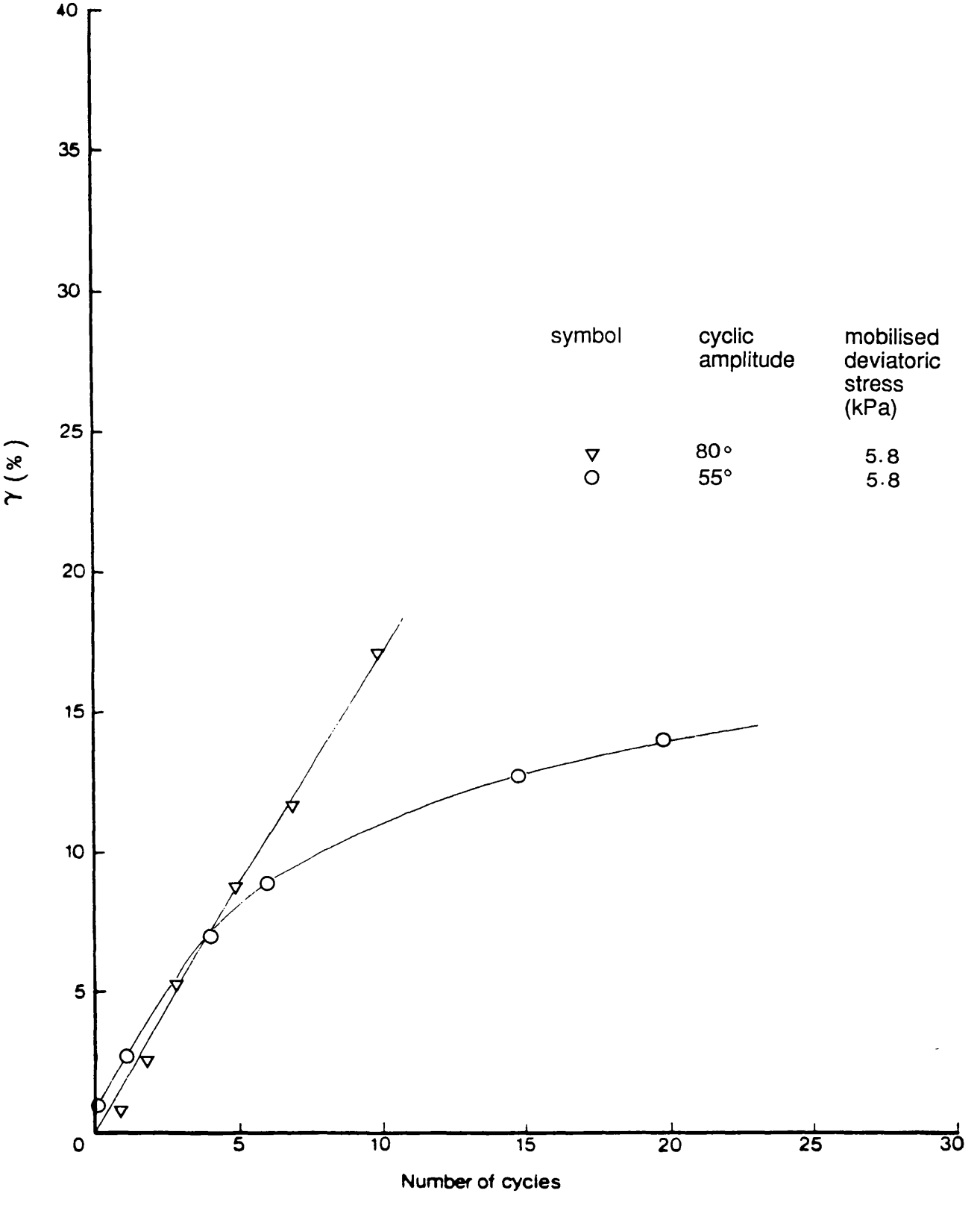

Fig. 7.24 **The development of shear strain during the continuous and cyclic rotation of principal stress direction on two fully saturated kaolinite sample consolidated in the modified oedometer and the Rowe cell tested in the DCDSC with OCR=7.5.**

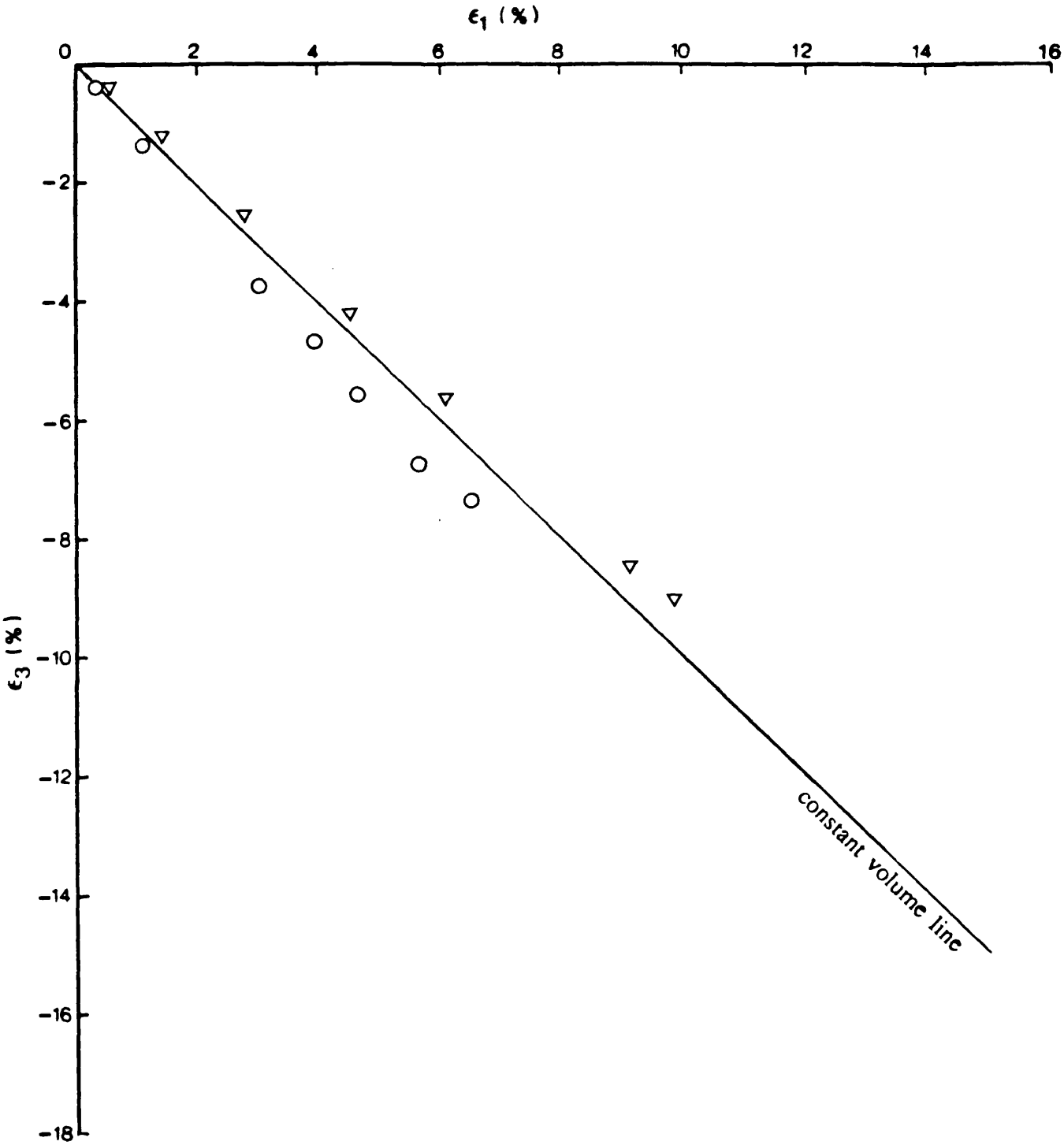

Fig. 7.25 Volumetric behaviour of two fully saturated samples of kaolinite subjected to continuous and cyclic rotation of principal stress direction in the DCDSC at σ_3 =14kPa

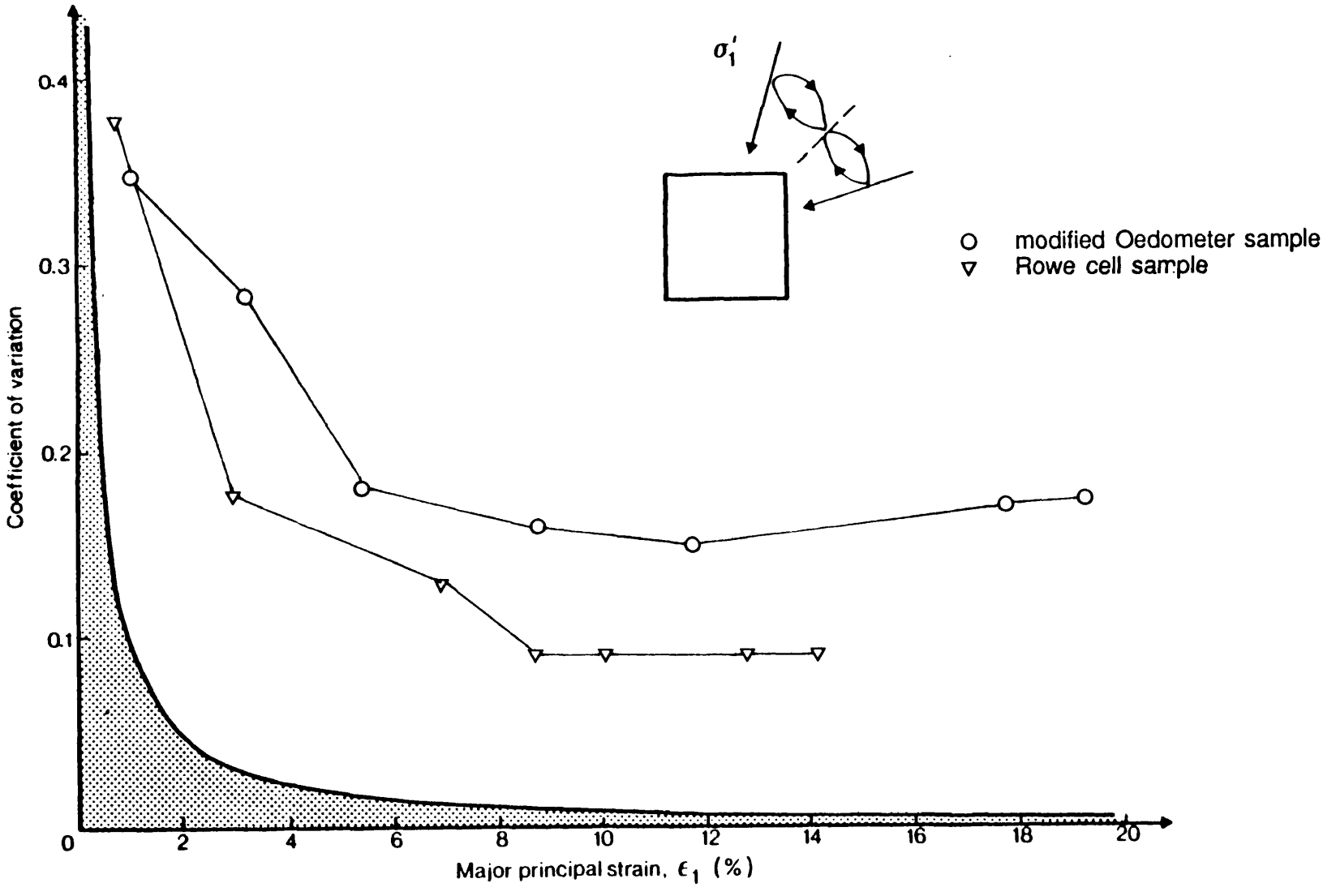

Fig. 7.26 Coefficient of variation of the maximum shear strain for two fully saturated kaolinite samples subjected to continuous and cyclic rotation of principal stress direction in the DCDSC at σ_3 =14kPa

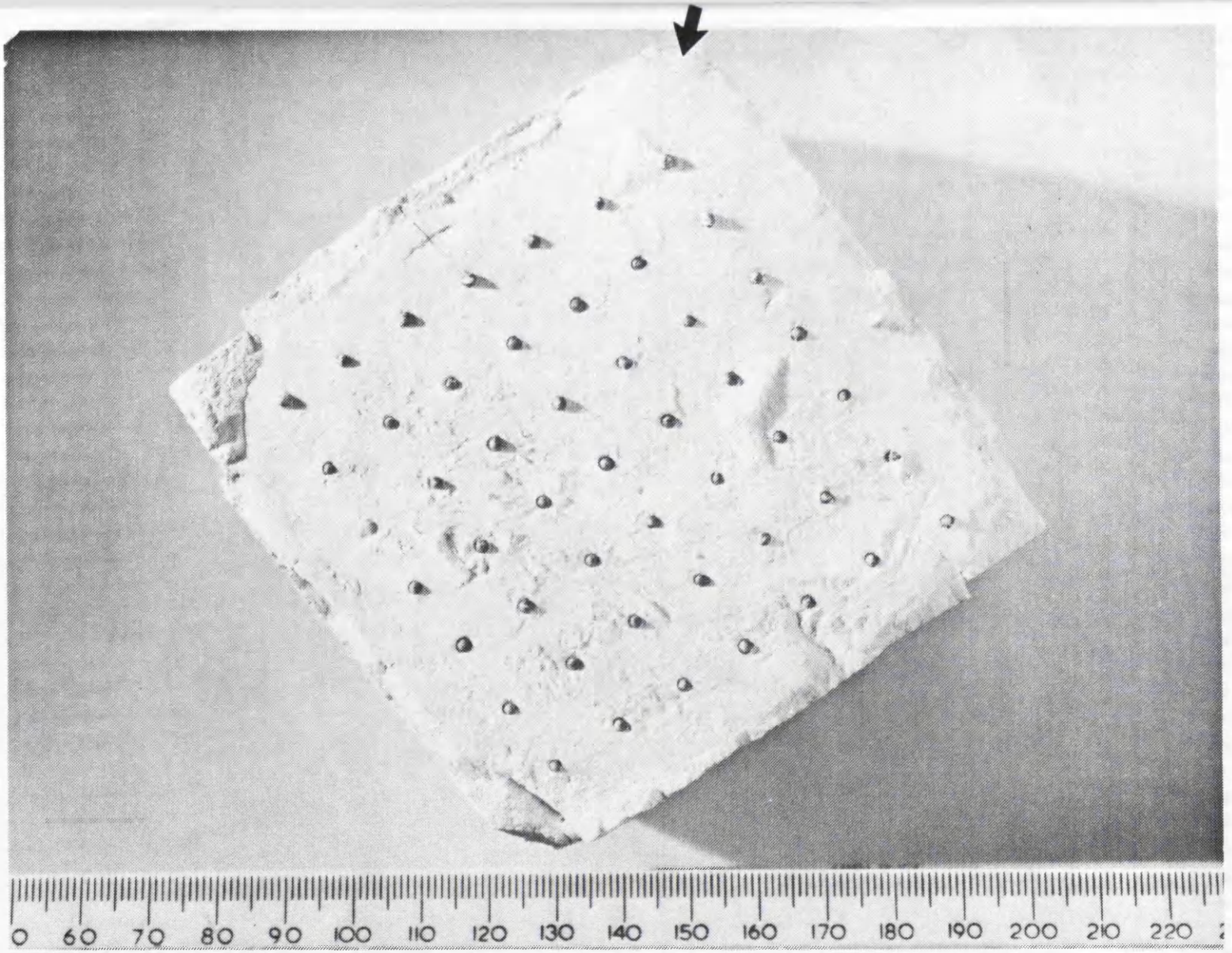

Fig. 7.27 No ruptures were observed in fully saturated kaolinite sample consolidated in the Rowe cell when subjected to continuous and cyclic rotation of principal stress direction.

Fig. 7.28 No ruptures were observed in fully saturated kaolinite sample consolidated in the modified oedometer when subjected to continuous and cyclic rotation of principal stress direction.

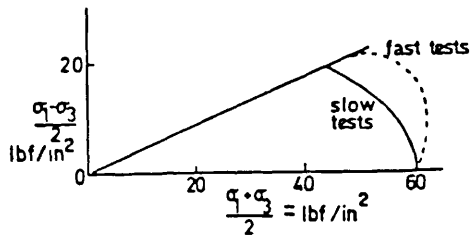

(a)

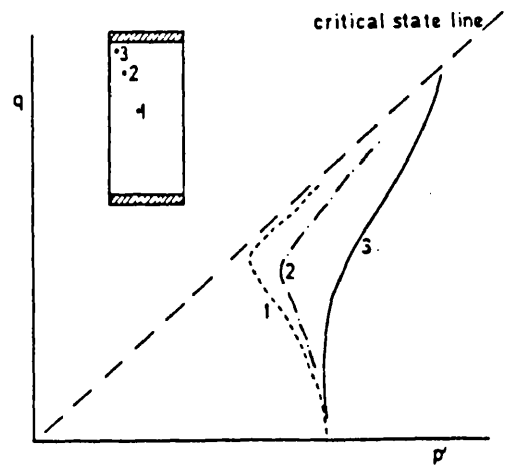

(b)

Fig. 7.29 (a) Effect of speed of testing on effective stress path observed in undrained triaxial test on normally consolidated clay (after Richardson and Whitman, 1963), (b) stress path computed by finite element analyses for three elements within a triaxial sample with smooth ends during a fast drained compression test. (after Wood, 1981)

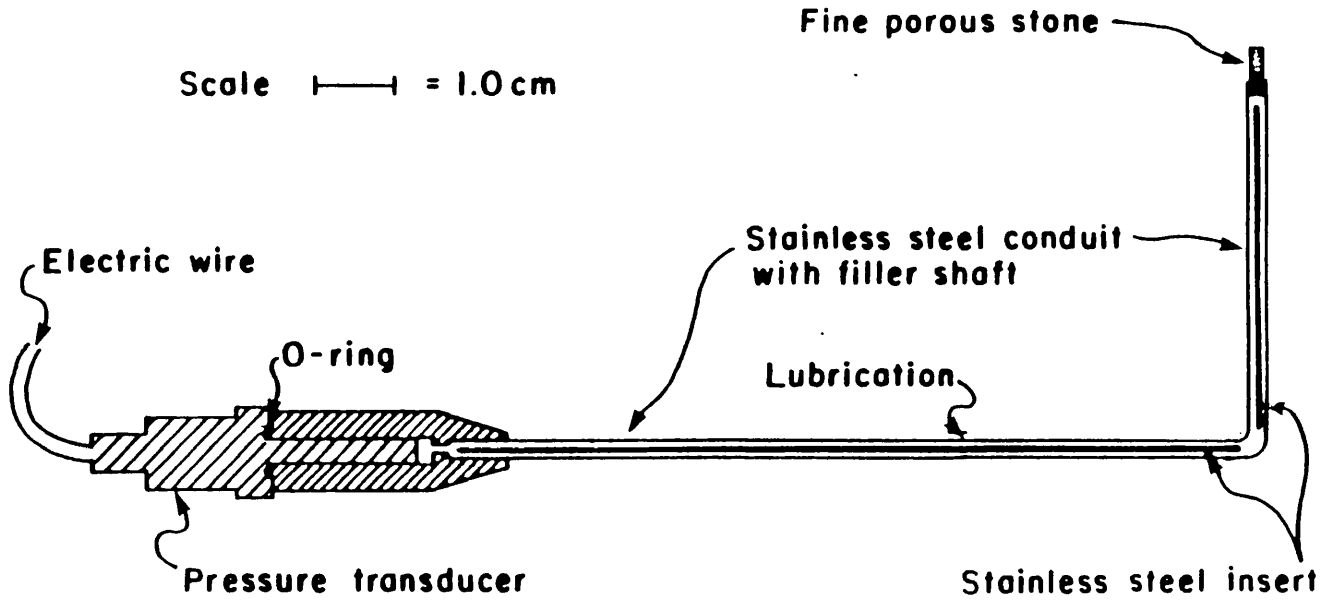

Fig. 7.30 A schematic view of probe used by Germaine to measure the pore water pressure at the centre of the DSC sample (after Germaine, 1982)

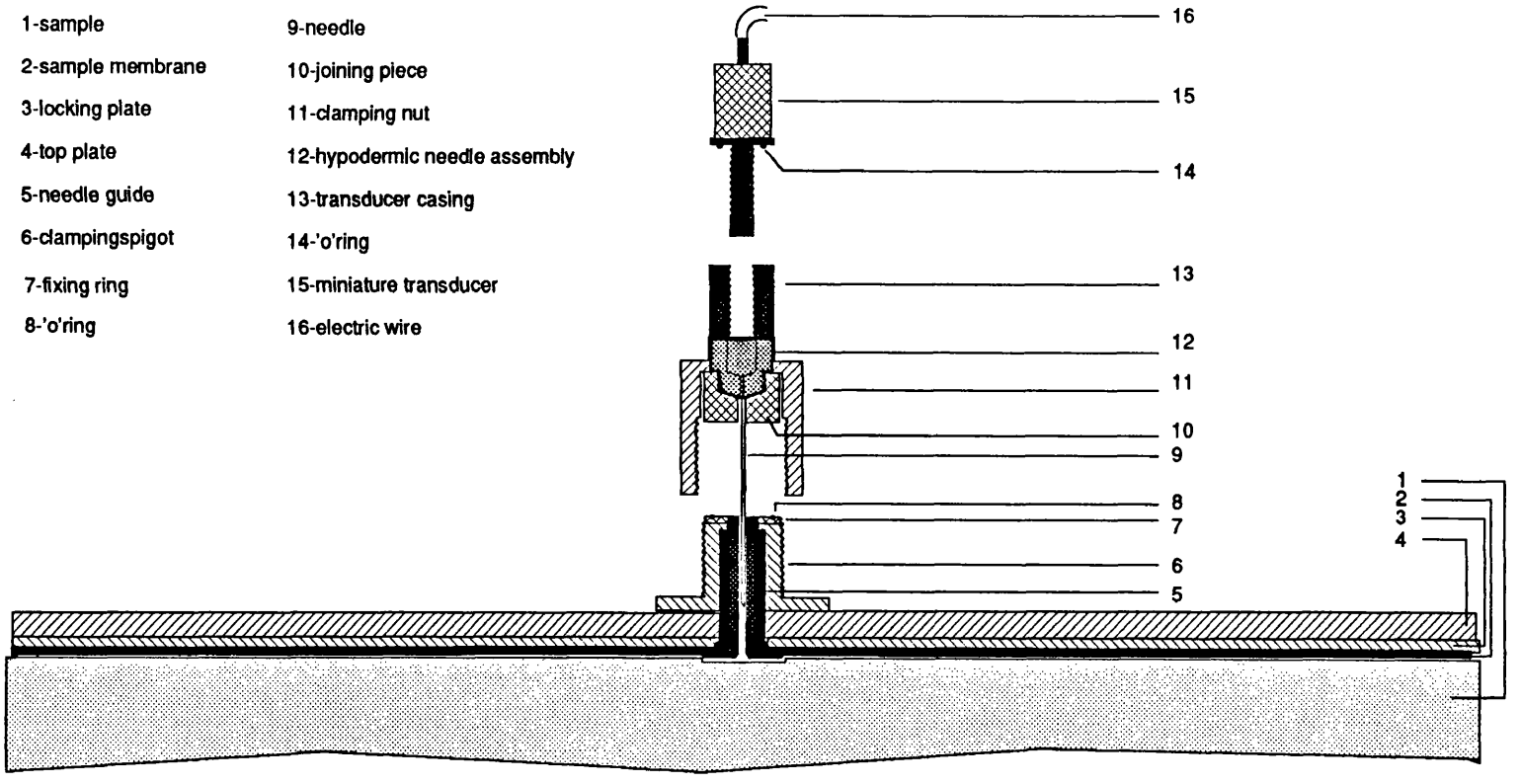

Fig. 7.31 **A schematic view of the probe and the miniature transducer developed to measure the pore water pressure in the centre of the DCDSC samples**

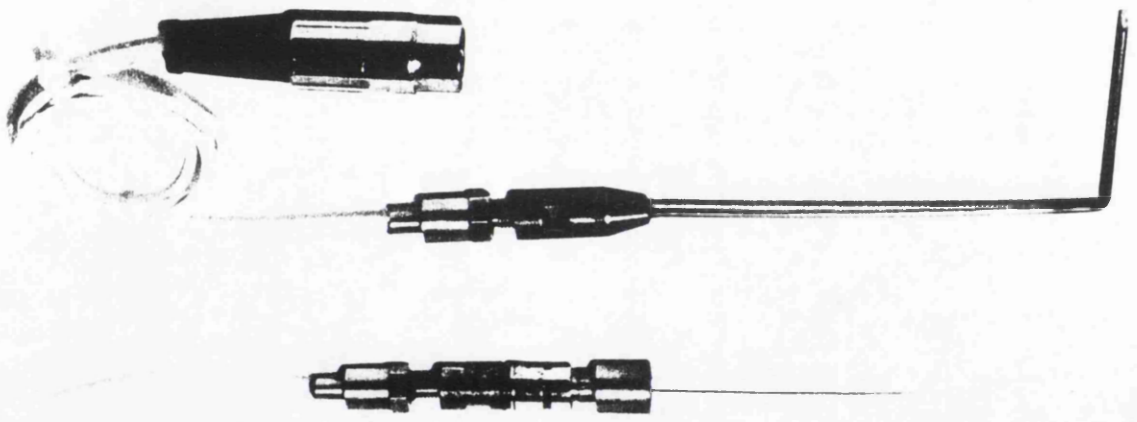

Fig. 7.32 Comparison between the existed and developed pore water pressure measuring devices

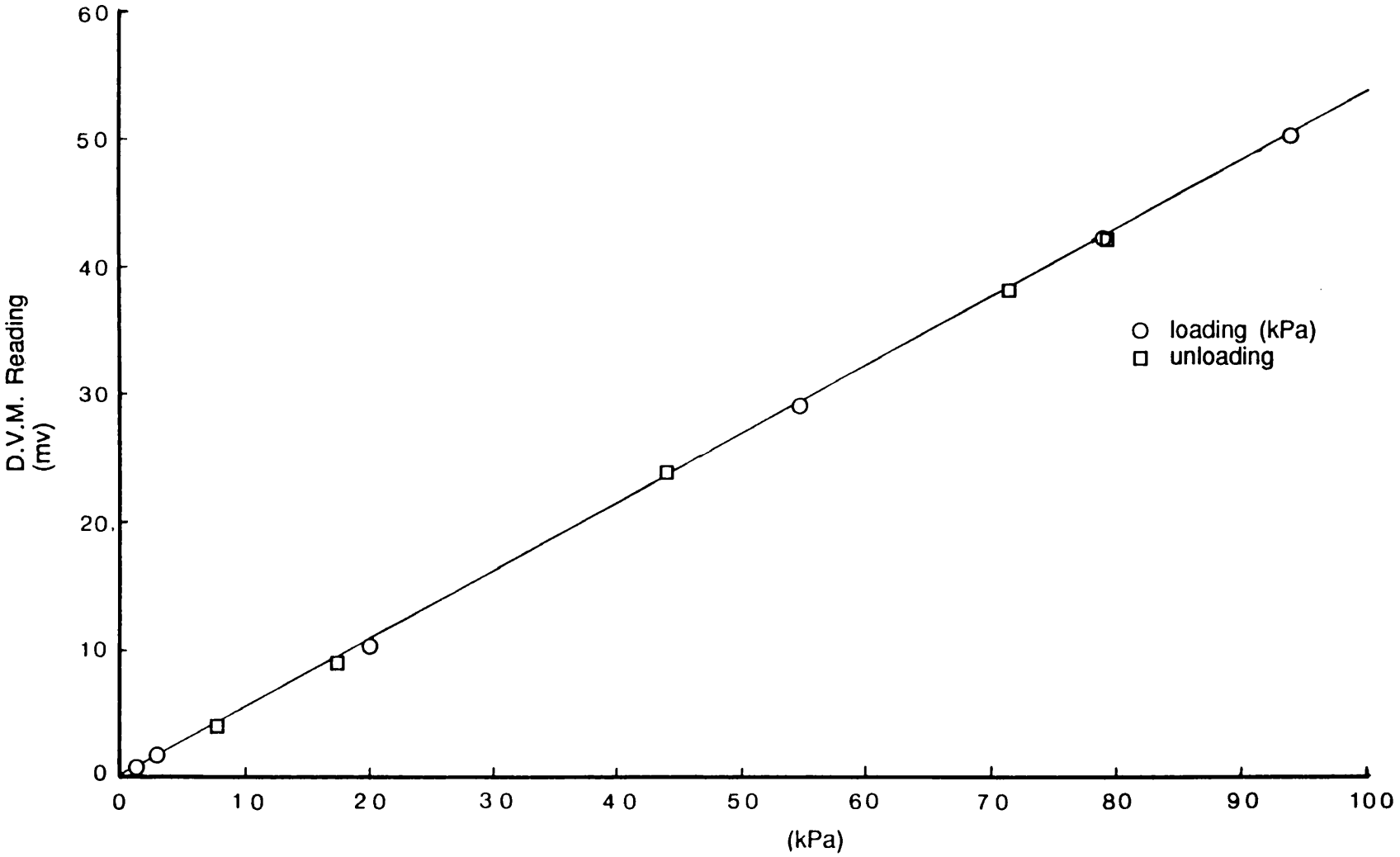

Fig. 7.33 **Calibration curve for a Druck transducer.**

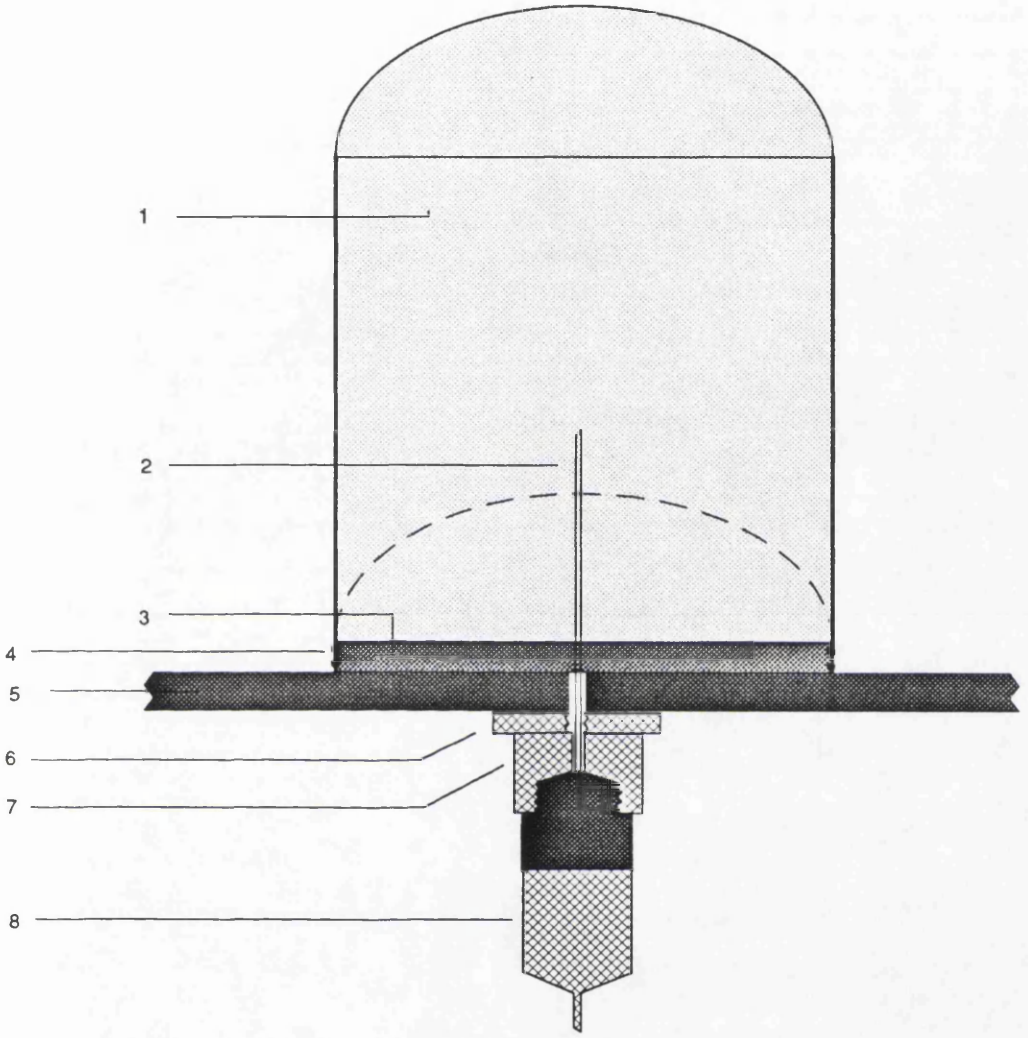

1-fully saturated kaolinite sample
2-inserted needle
3-sample base
4-'o' ring
5-bottom base
6-fixing screw
7-joining piece
8-transducer

Fig. 7.34 The miniature probe was inserted and fixed into position at the base of a triaxial chamber

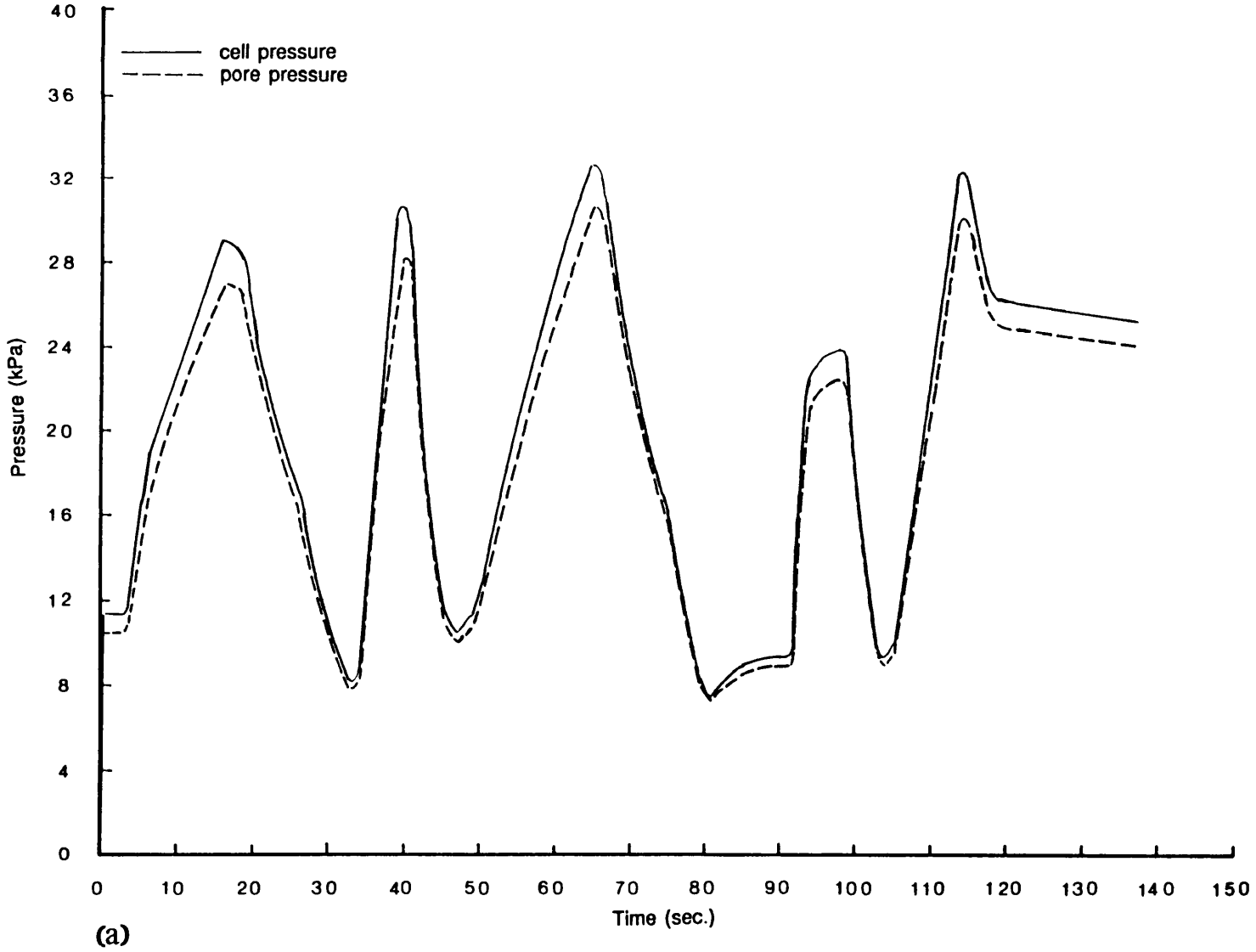

(a)

Fig. 7.35 (a) The results of response time tests using the developed miniature probe and (b) the Skempton's B values

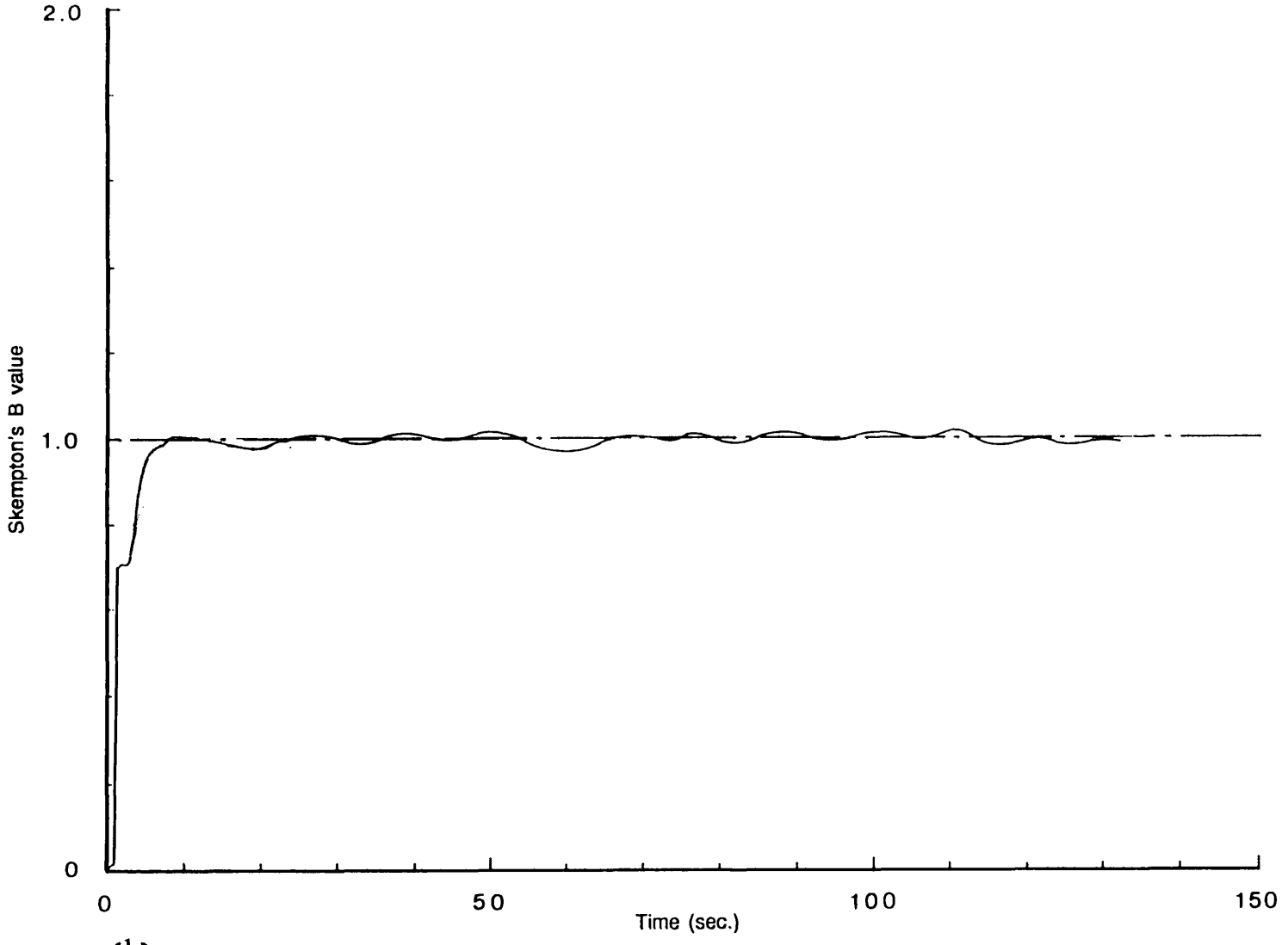

(b)

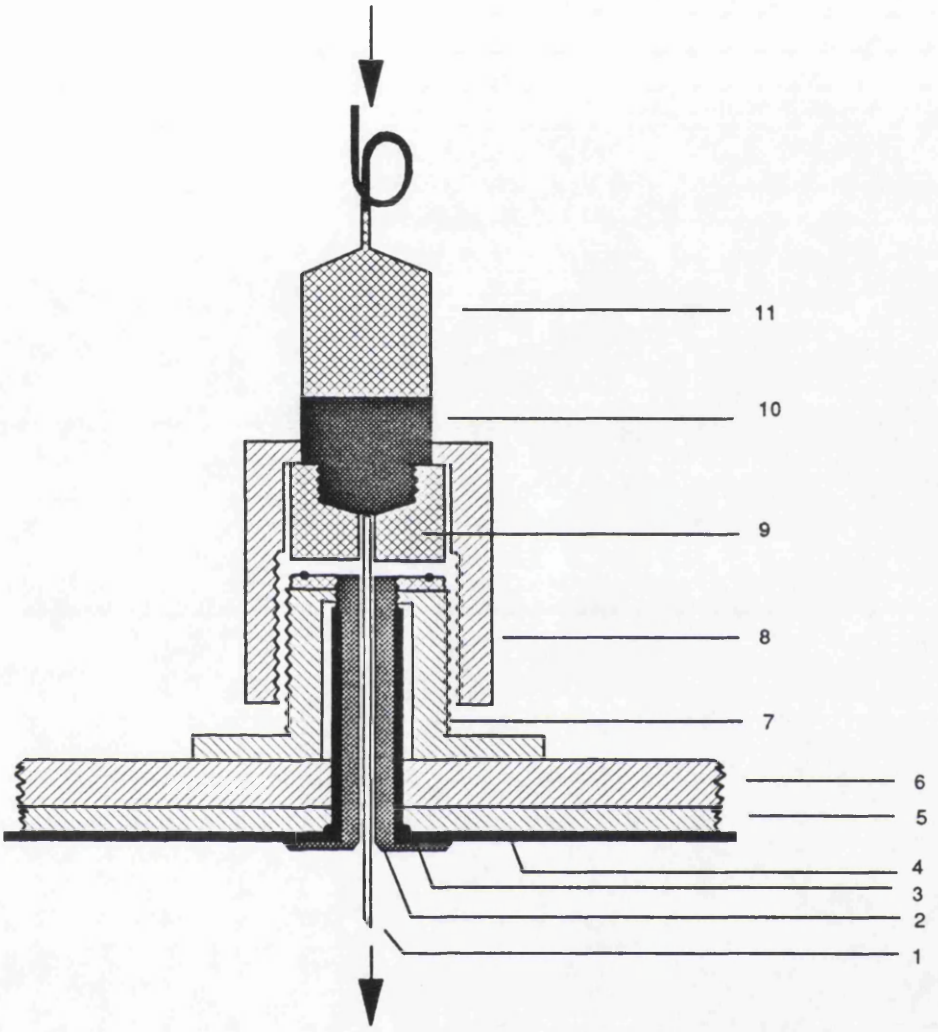

1-needle
2-needle guide
3-'o' ring
4-rubber membrane
5-locking plate
6-top plate
7-clamping spigot
8-clamping nut
9-joining piece
10-hypodermic needle assembly
11-pressure transducer

Fig. 7.36) Setting up the developed pore water pressure measuring probe on the top platen of the DCDSC

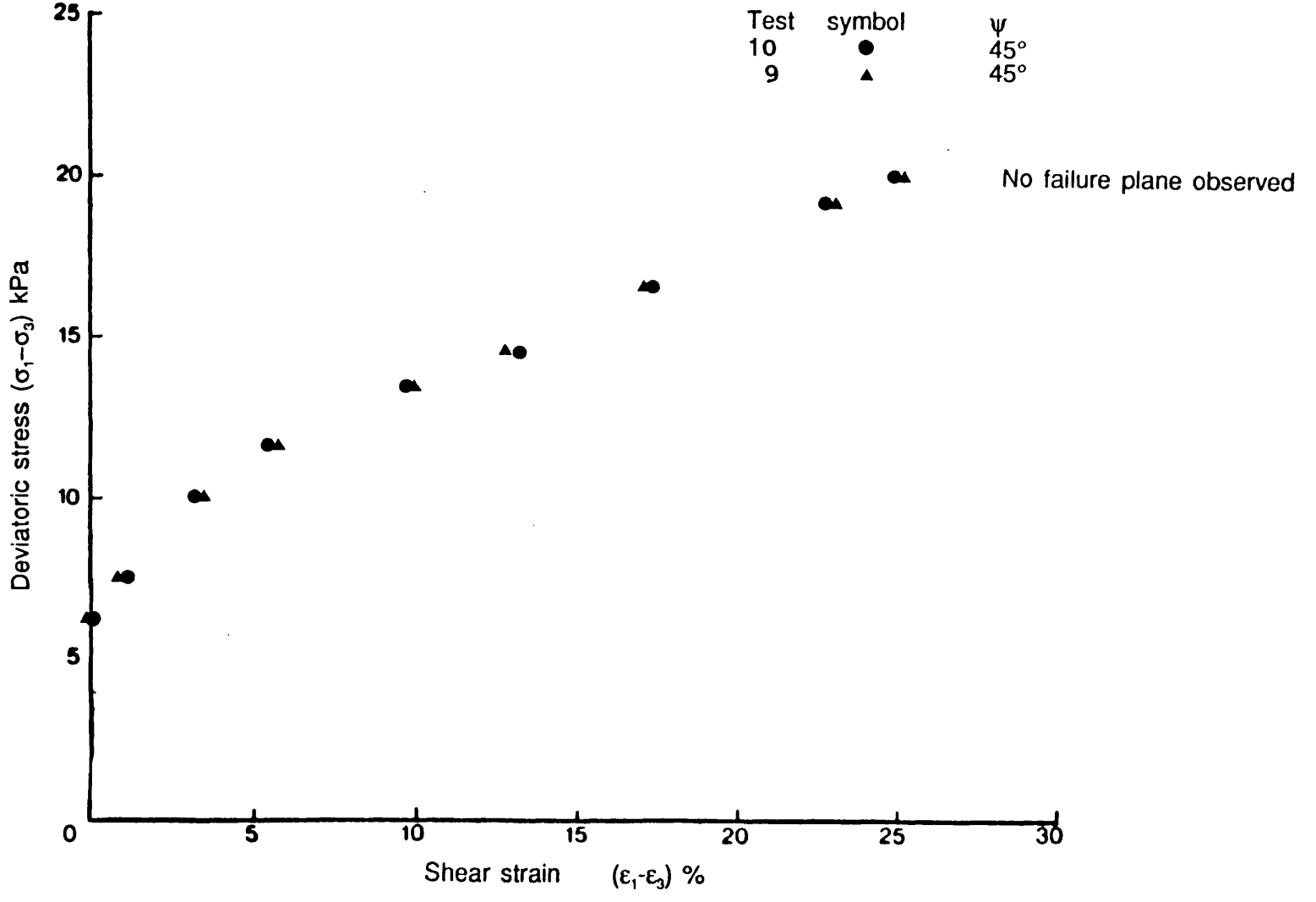

Fig. 7.37 Stress-strain response of two fully saturated kaolinite samples sheared monotonically very slowly in the DCDSC at σ_3= 14kPa

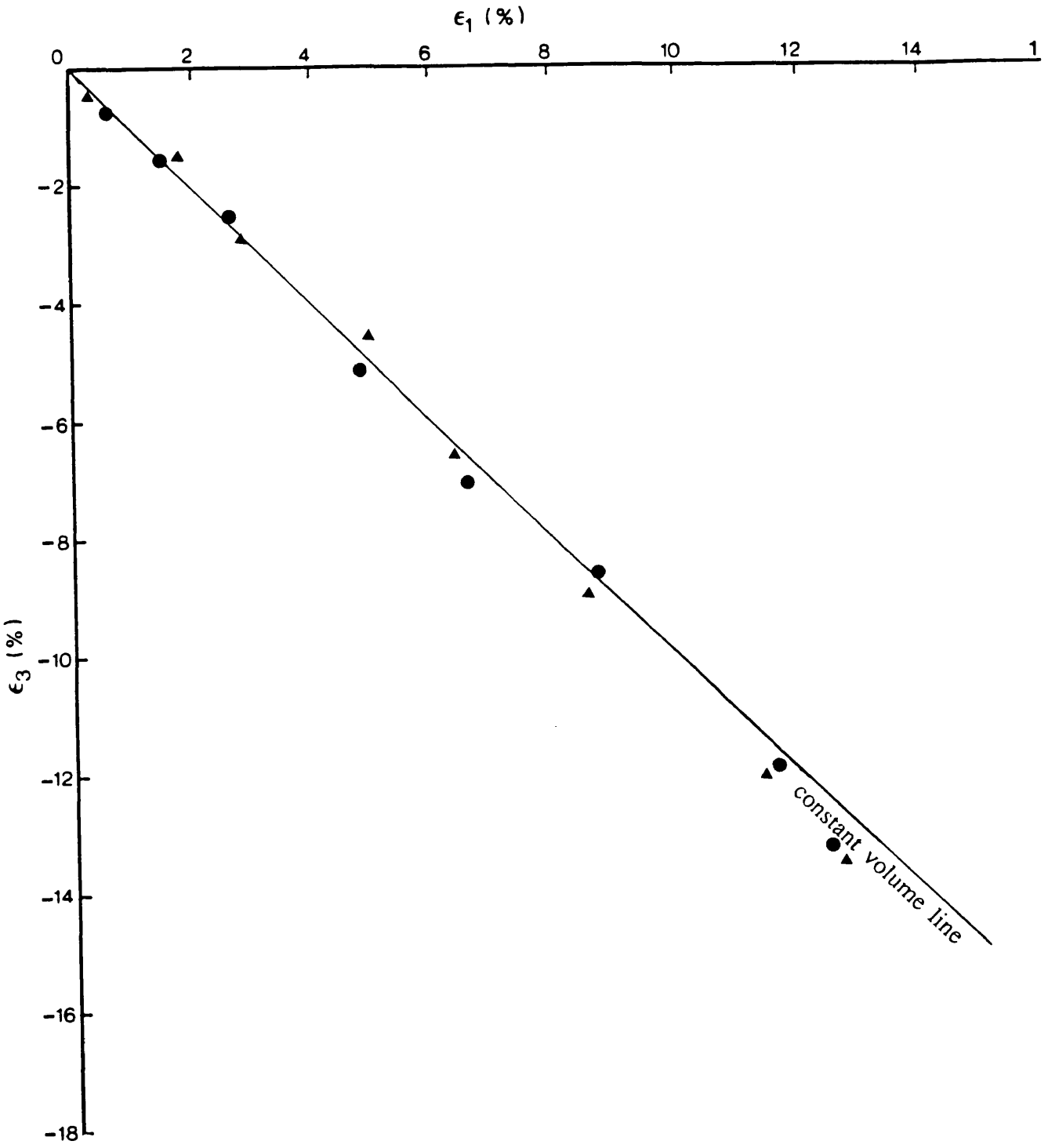

Fig. 7.38 Volumetric behaviour of two fully saturated samples of kaolinite sheared monotonically very slowly with pore water pressure measurements in the DCDSC at σ_3 =14kPa

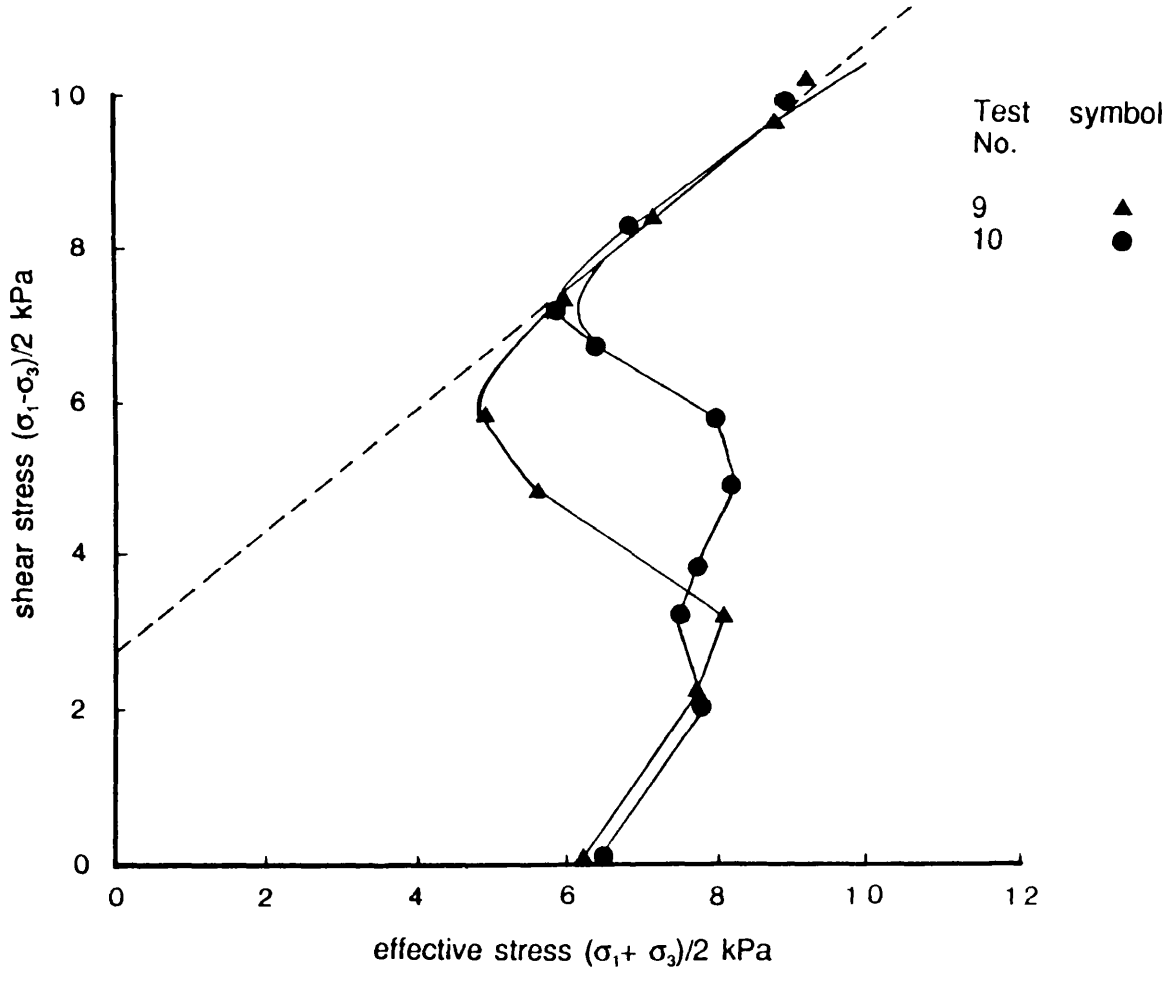

Fig. 7.39 **Effective stress paths (ESP_s) for two fully saturated samples sheared monotonically at a very slow rate in the DCDSC at σ_3 =14 kPa**

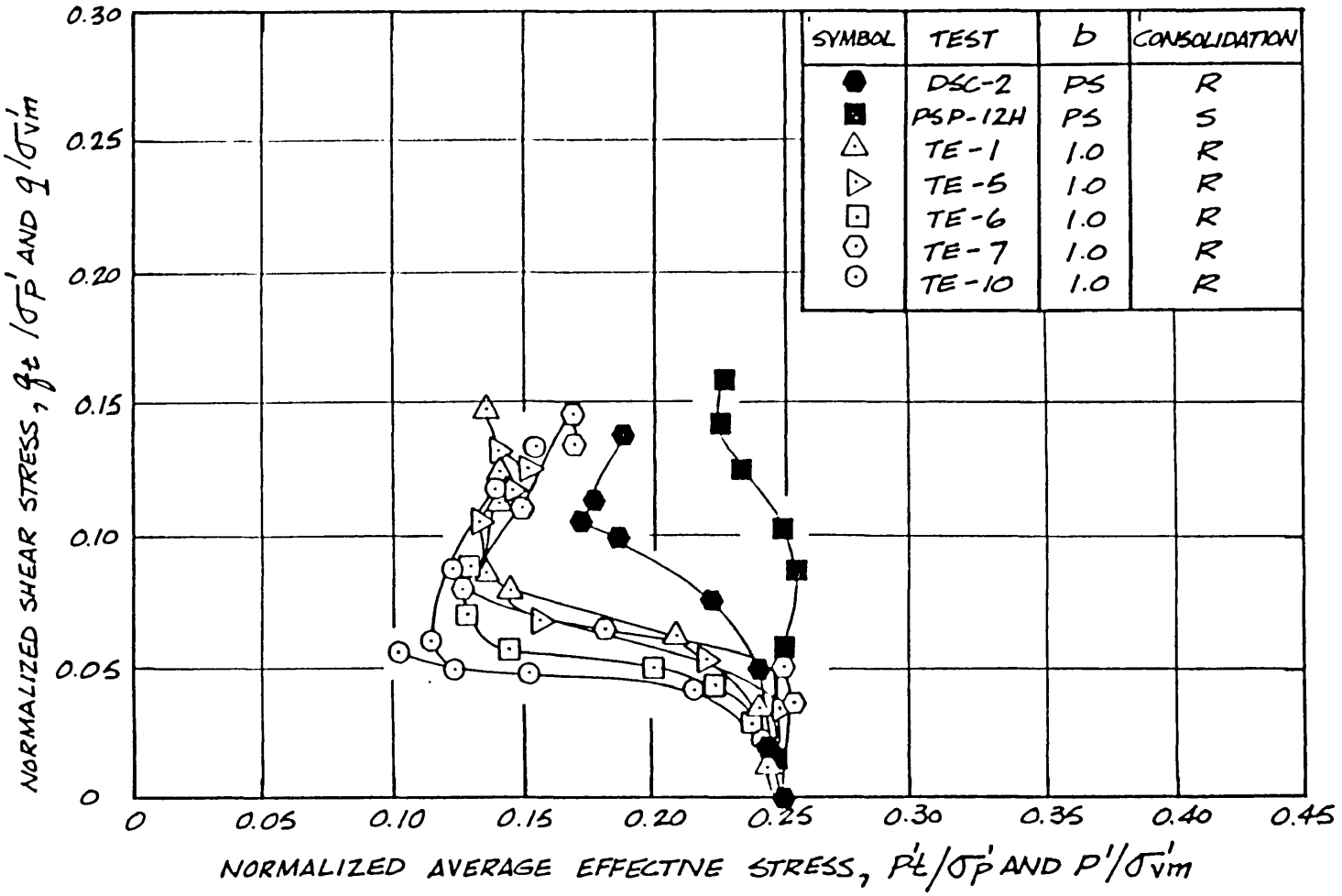

Fig. 7.40 Normalised average effective stress paths for tests on BBC (OCR=4) (after o' Neill, 1985)

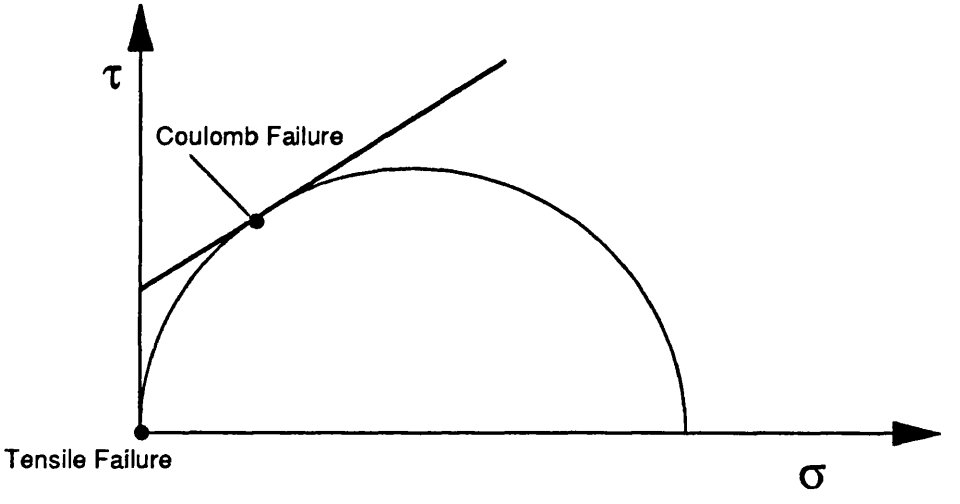

Fig. 7.41 A Mohr circle showing equal opportunity for tensile and Coulomb failure to occur

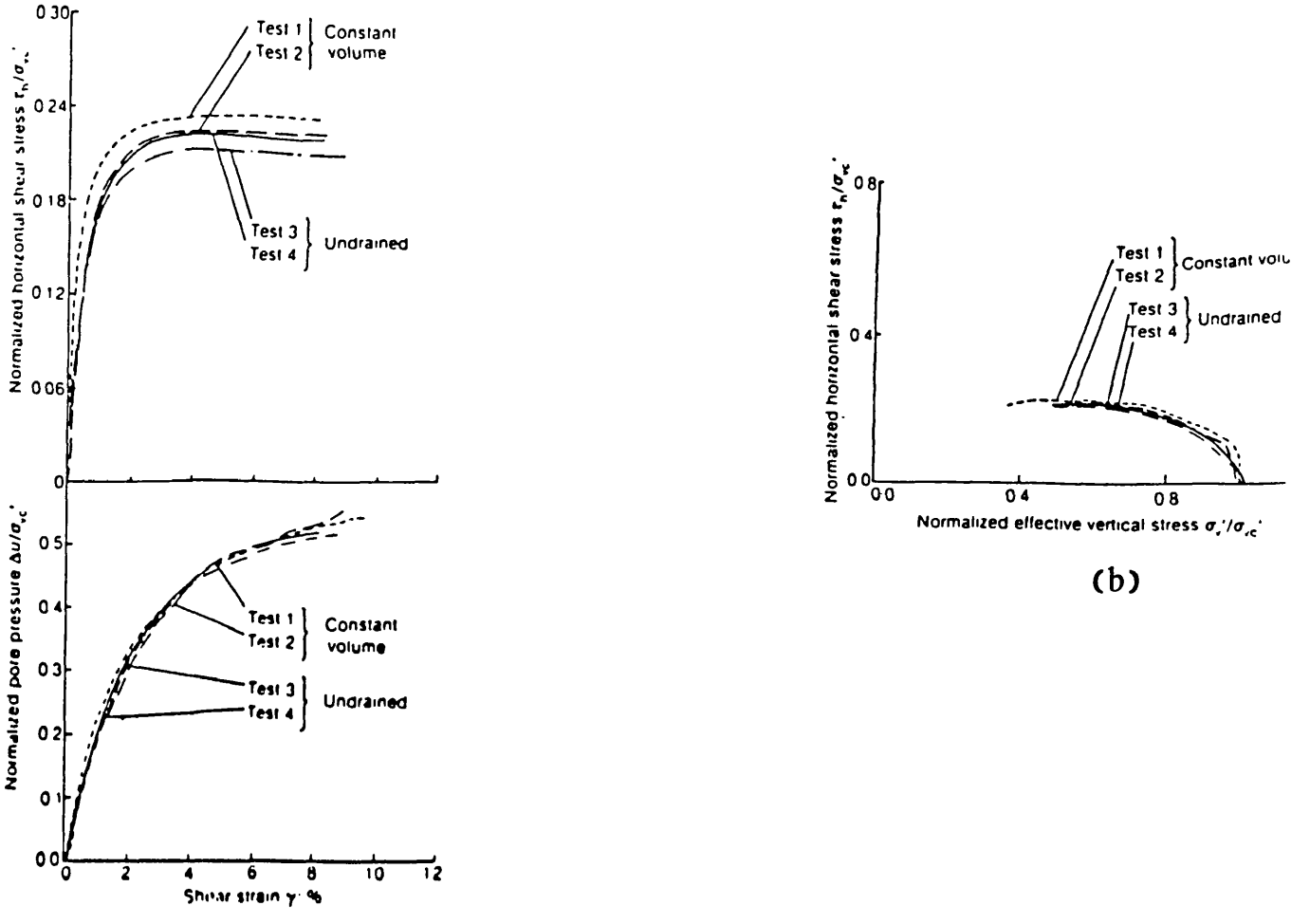

Fig. 7.42 **(a) Comparison of constant volume and undrained test results and (b) comparison of constant volume and undrained test results (after, Dyvik, Berre, Lacasse and Raadim; 1987)**

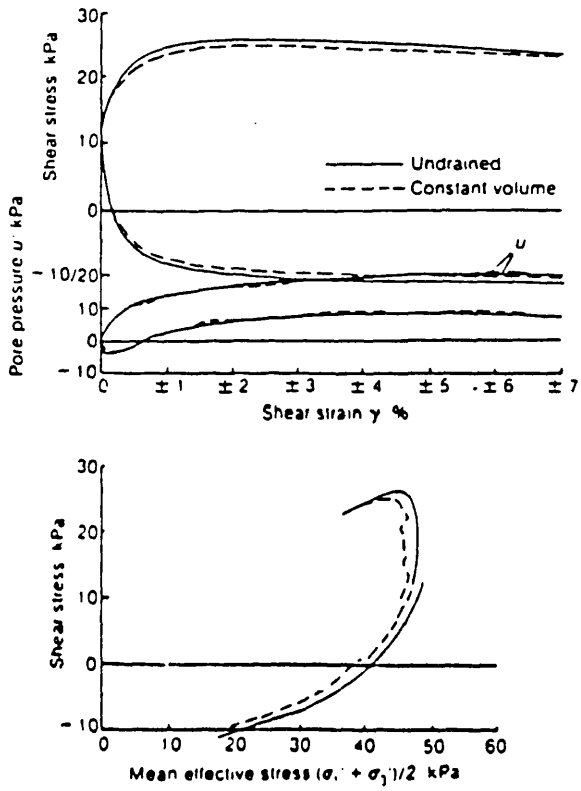

Fig. 7.43 Undrained and constant volume triaxial tests on Drammen clay (after Berre, 1981)

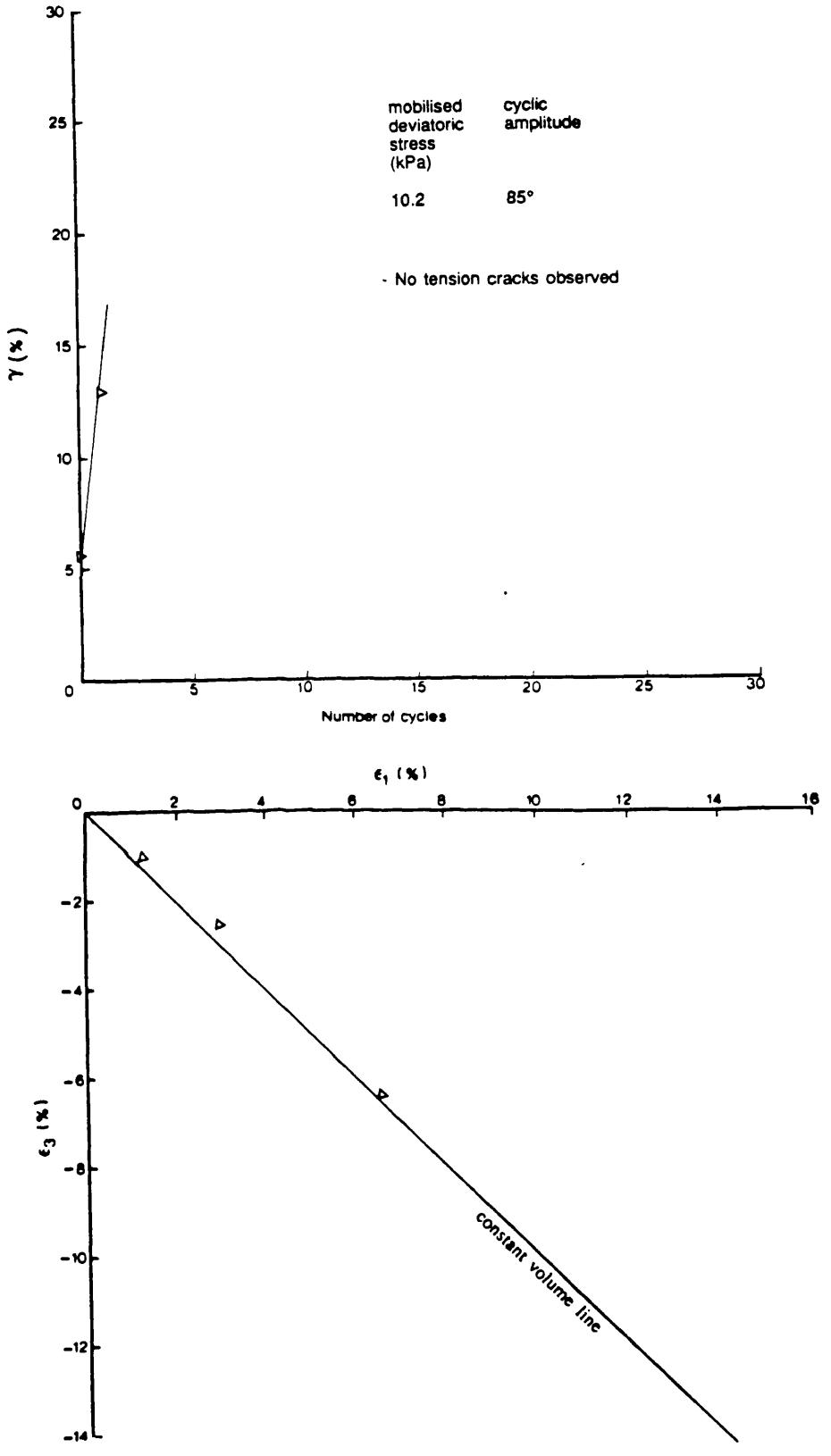

Fig. 7.44 (a) The development of shear strain during a cyclic Null method of testing on a fully saturated kaolinite sample consolidated in the modified oedometer tested in the DCDSC and (b) Volumetric behaviour of the same sample.

Fig. 7.45 Magnified sections of nearly and fully saturated samples after being oven dried.

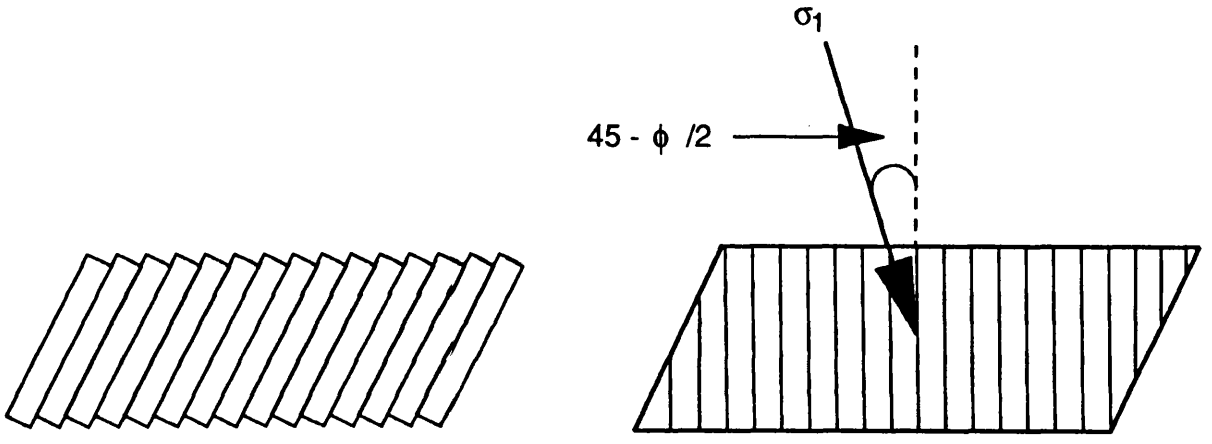

Fig. 7.46 Book shelf model of de Josselin de Jong (1972)

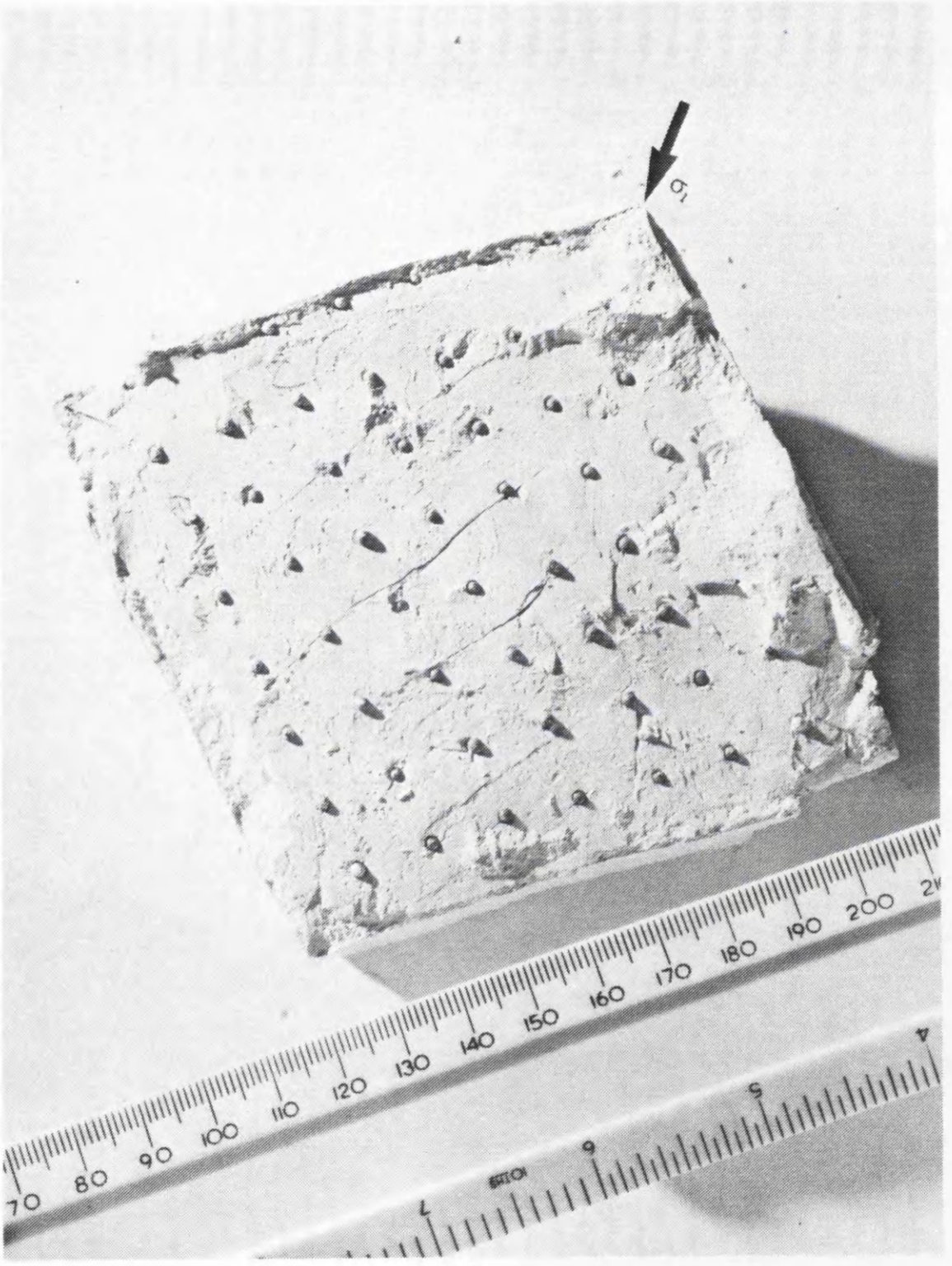

(a)

Fig. 7.47 (a)-(c) Three splitting surfaces in a nearly saturated sample indicate the continuity of the Coulomb slip planes through the depth of the sample and (d)-(f) the line interpretations of the Coulomb failure planes

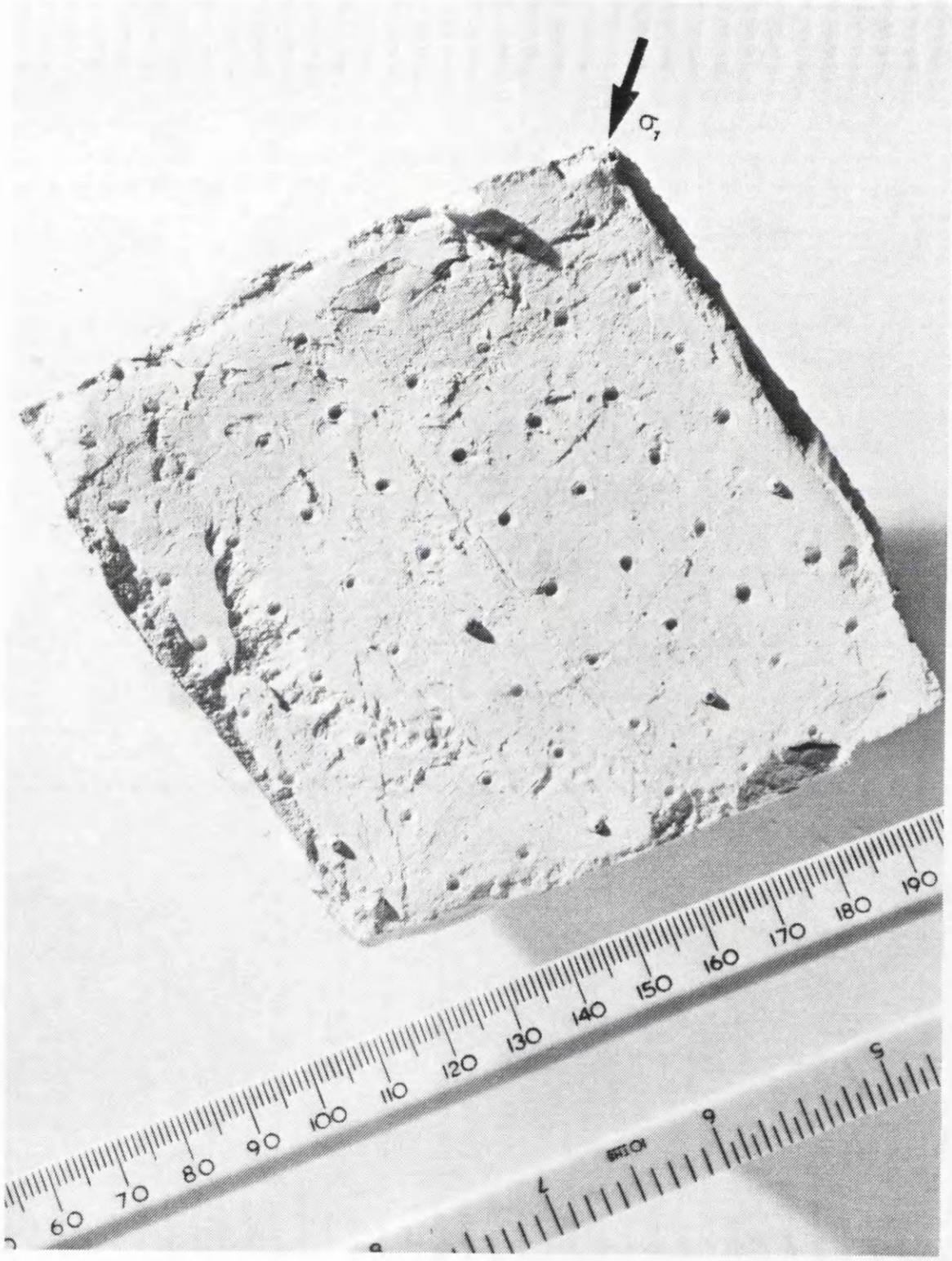

(b)

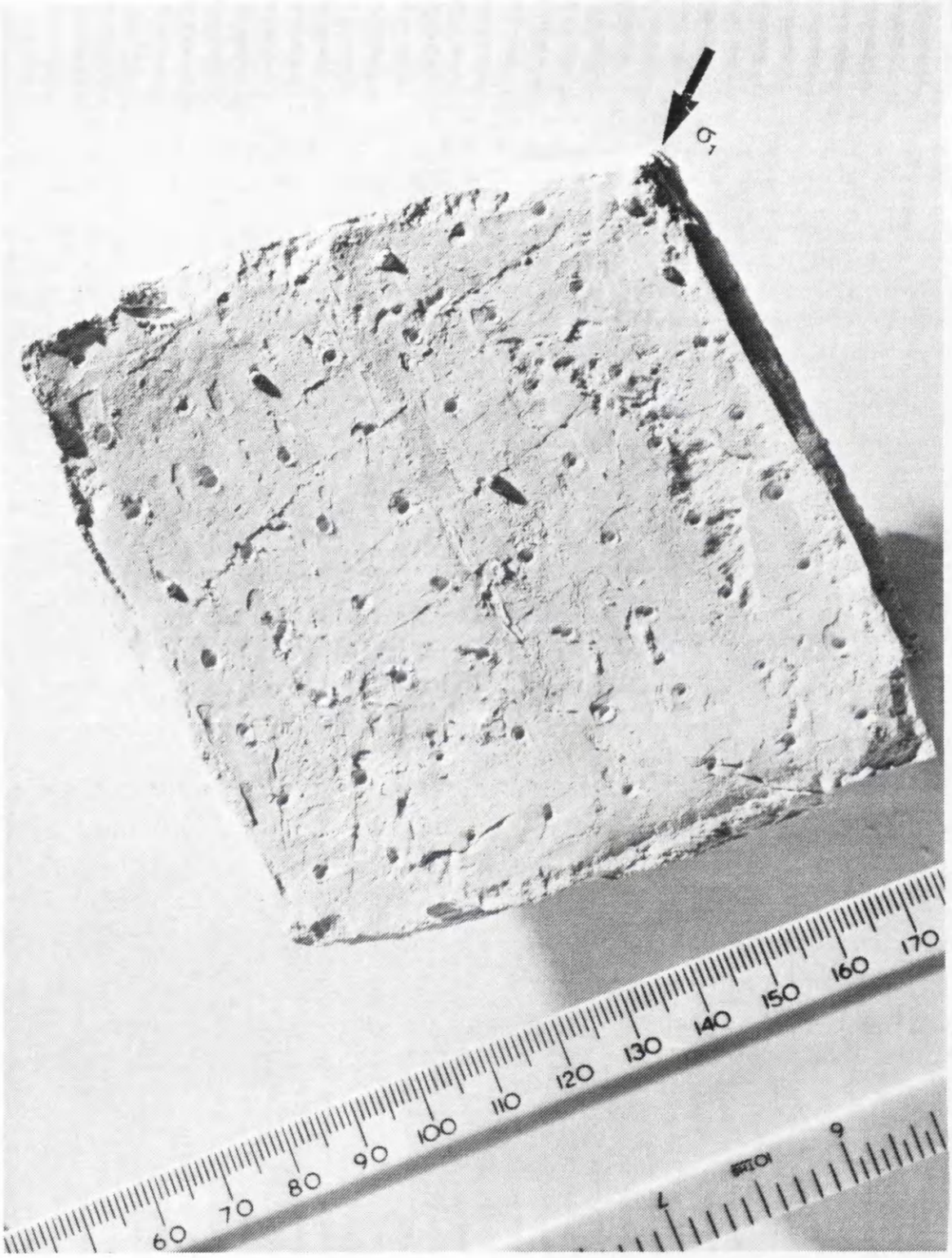

(c)

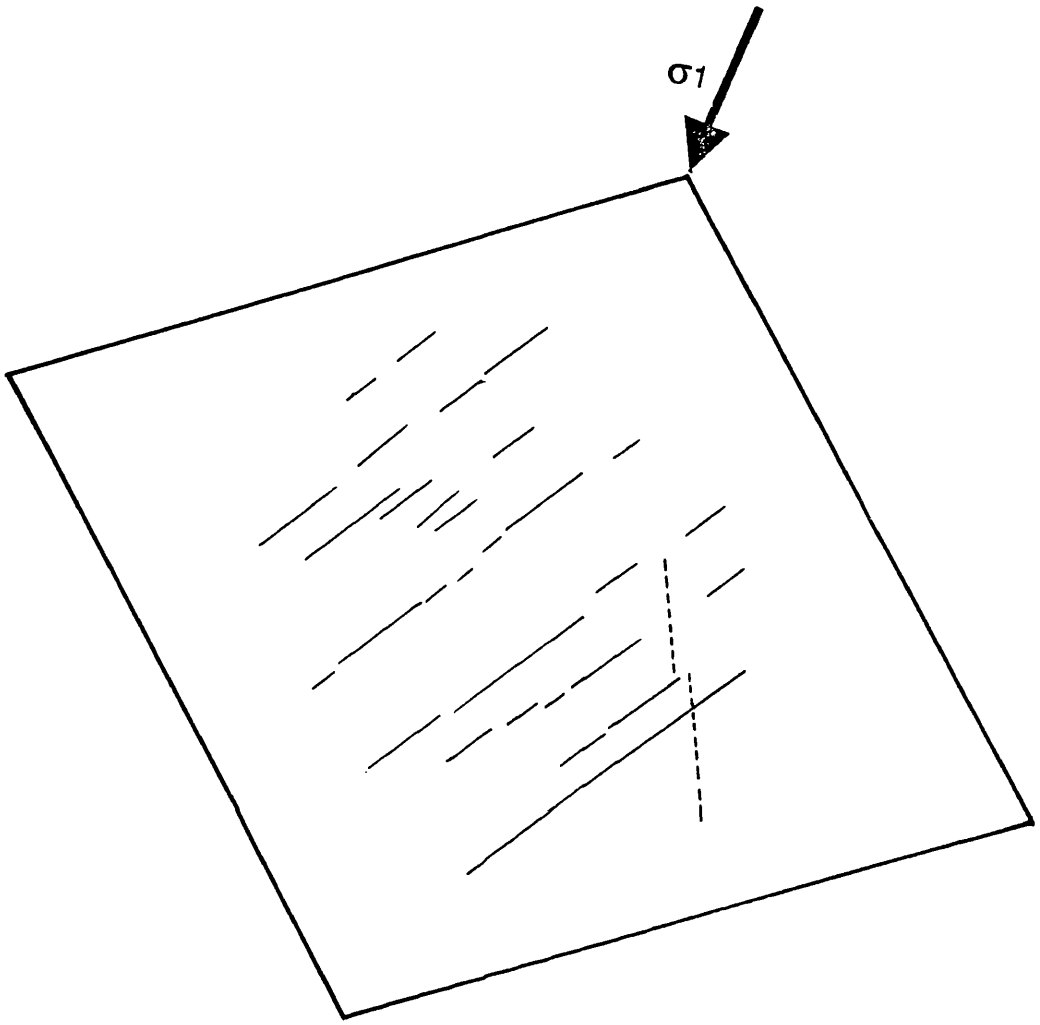

(d)

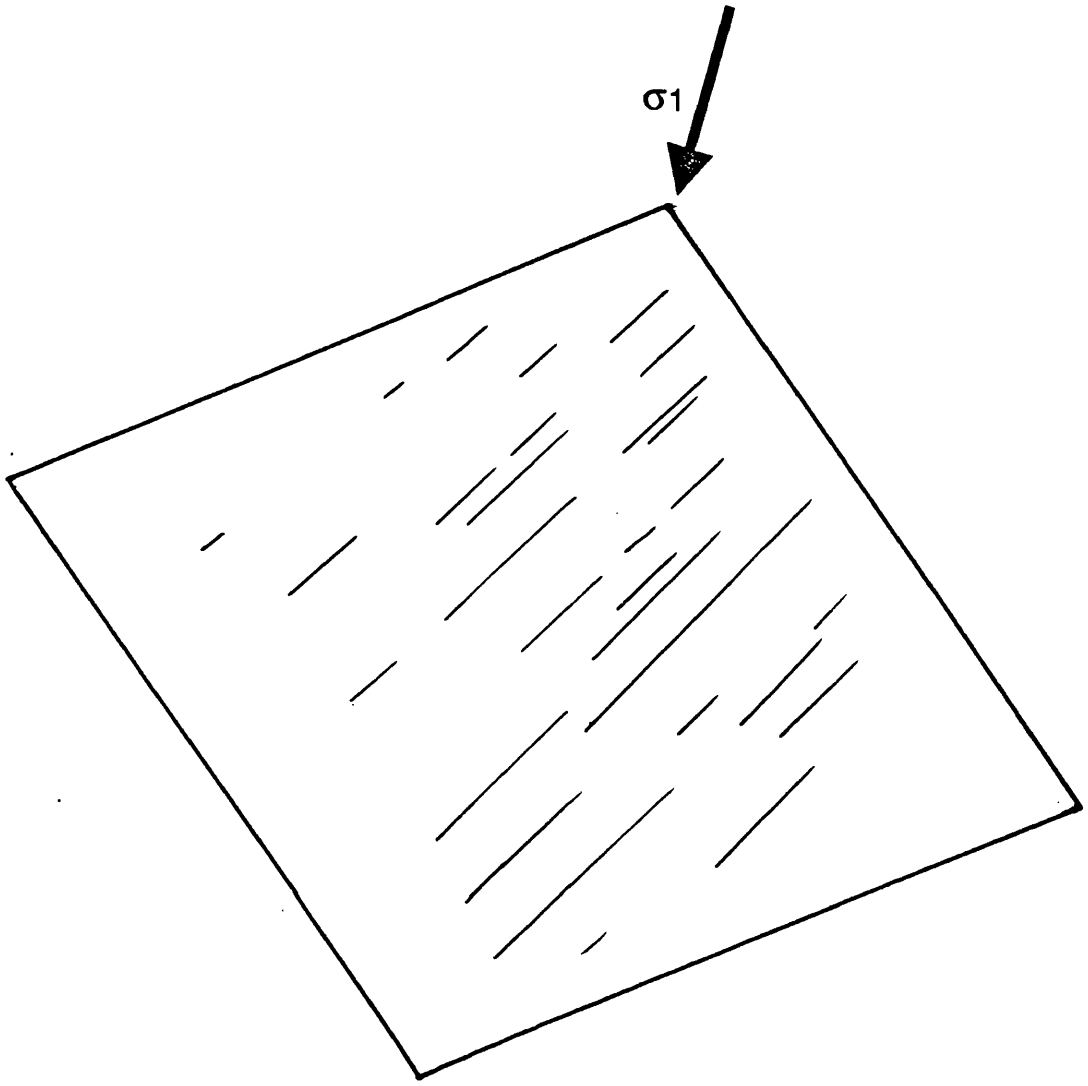

(e)

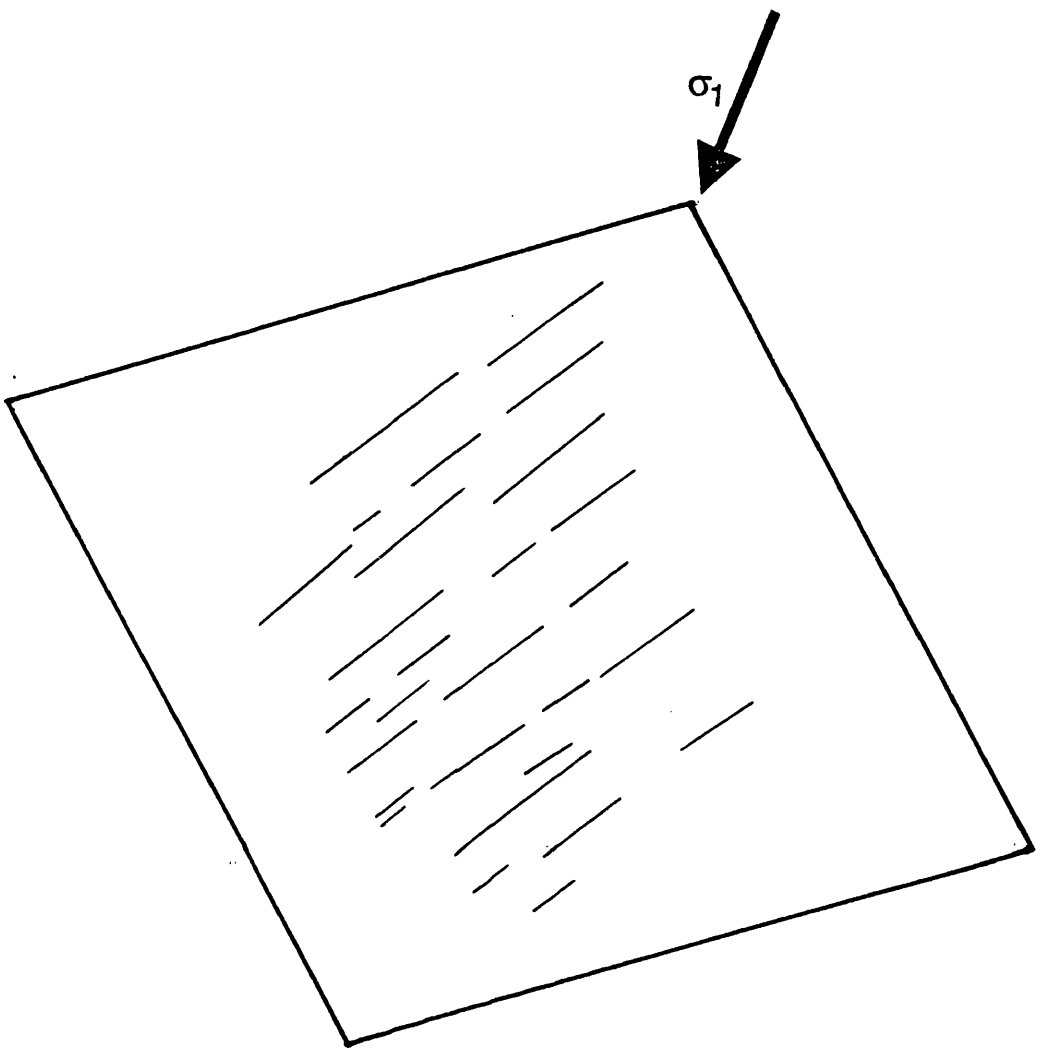

(f)

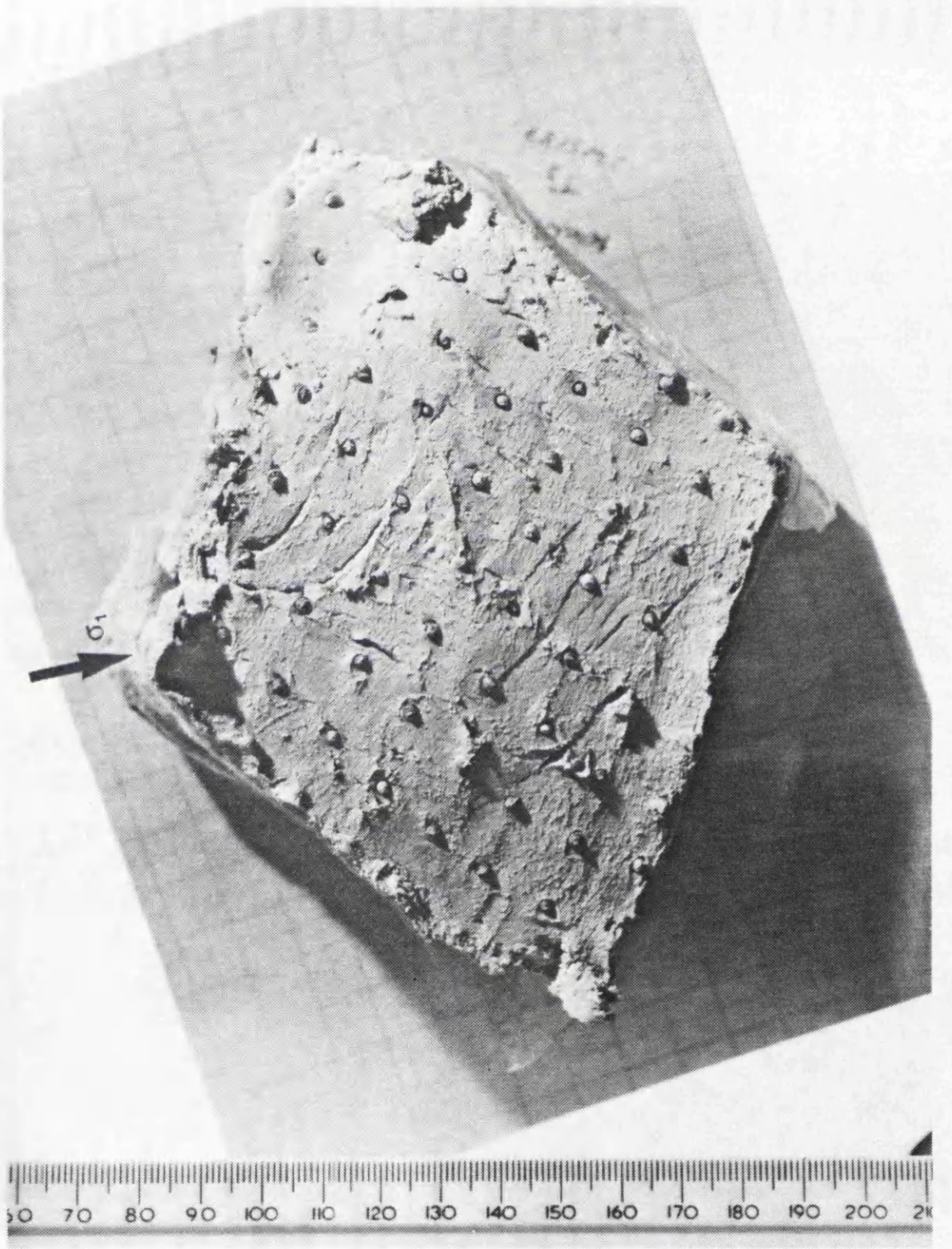

Fig. 7.48 Symmetric slip planes in a sample sheared to too great a strain

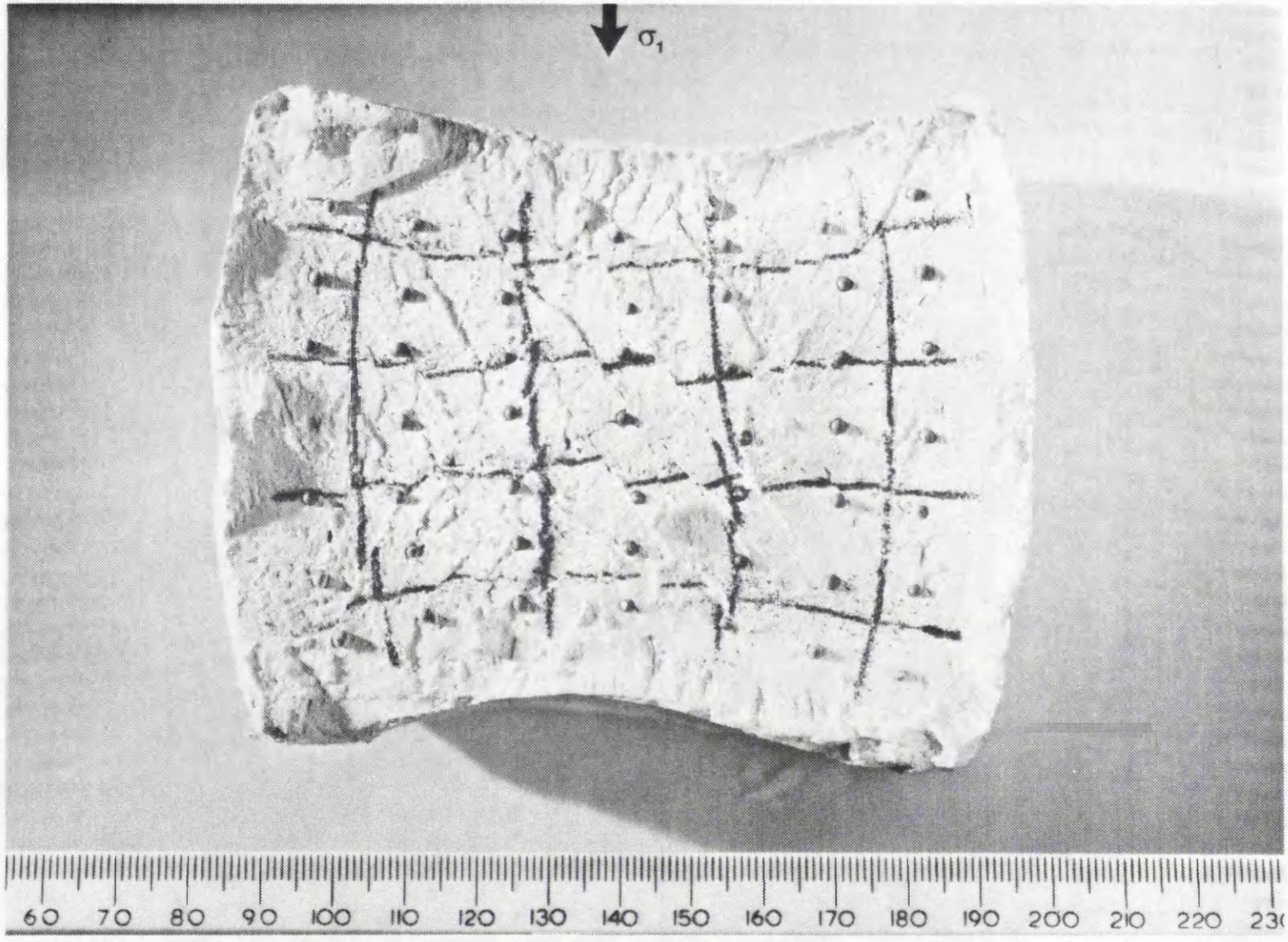

Fig. 7.49 **Coulomb slips in nearly saturated kaolinite sample sheared monotonically in plane strain in the DSC without the shear sheets around the sample with ψ =90°**

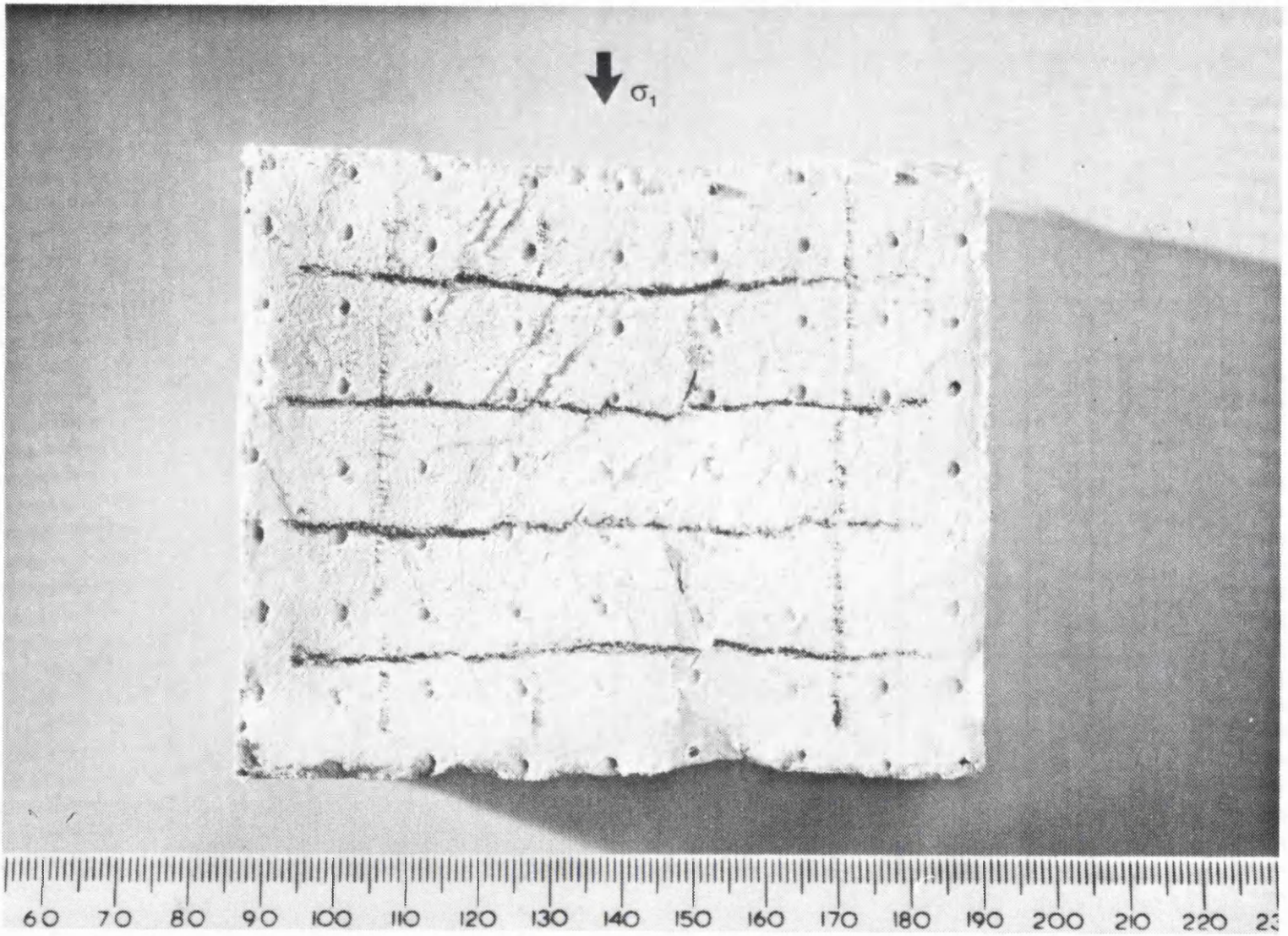

Fig. 7.50 **Coulomb slips in nearly saturated kaolinite sample sheared monotonically in plane strain in the Biaxial tester with ψ =90° (after Ogunbekun, 1988)**

porosity	o.60
water content (as % of whole by wt)	50%
% air voids	10%
liquid limit	63
plastic limit	30

Table 7.1 properties of kaolinite used

CHAPTER 8 DATA REVIEW AND ANALYSIS WITH MODEL DEVELOPMENT

8.1 INTRODUCTION

8.2 SUMMARY OF TESTING CAPABILITIES AND RESULTS

8.3 DISCUSSION ON THE INITIATION OF SHEAR AND FLOW BEHAVIOUR OF PARTICULATE MATERIALS

- 8.3.1 Inhomogeneous flow and factors controlling the intervention of rupture
- 8.3.2 Homogeneous flow in particulate materials
- 8.3.3 The effects of principal stress rotation
- 8.3.4 Stress dilatancy relationship and extension of a steady state concept
- 8.3.5 Super-homogeneity

FIGURES

8.1 INTRODUCTION

Chapter 5, 6 and 7 presented the strength deformation behaviour of dry sand, damp coal and saturated kaolin respectively. The effects of the rotation of principal stress directions on the initiation of flow of these materials was studied experimentally. The results illustrate that controlled flow associated with positive dilation is possible if principal stresses are continuously cycled rather than applied monotonically. This form of loading also encourages homogeneous strains. Continuous slow flow is maintained with specific combinations of stress ratio and cyclic amplitude, the greater the cyclic amplitude the lower the stress ratio necessary to initiate flow. This chapter offers further interpretation of the observed principal stress rotation effects and presents a novel view of particulate material behaviour.

8.2 SUMMARY OF TESTING CAPABILITIES AND RESULTS

A Flexible Boundary Directional Shear Cell was developed to investigate the stress-strain deformation of three different particulate materials such as sand, coal and kaolinite with a full range of dampness from dry to full saturation under monotonic and cyclic loading conditions. This apparatus provided for the principal stress directions to be changed by varying combinations of uniform shear and normal stress applied to the four faces of a cubical sample in the plane of strain whilst the intermediate principal stress was controlled. The change in directions of principal stress was achieved in step type increments or continuously using computer control. The investigation concentrated chiefly on the effects of continuous cyclic loading for initiating flow. Both the rotation angle and the stress ratio σ_1/σ_3 could be varied.

The DSC developed during this work had certain an advantage over the previous one in that shear stress hysteresis was eliminated and by cycling boundary shear stresses the effects of mean stress level variation was separated from the rotational effects and a larger range of rotation of principal stress direction, up to 90°, was achievable.

By improving stepper motor performance with 4:1 reduction pressure boosters cycling at very low mobilised ϕ, of down to 10°, was made possible.

A new technique of dismantling and splitting clay samples allowed visual observation of failure planes, the orientation of which could be measured.

Deformable corners were introduced for DSC sand samples that could follow the change in sample shape and, at the same time, provide enough stability where the shear sheets interleave.

Testing techniques for de-airing, mixing and consolidating kaolinite were improved and a trimmer was developed to cut 100 mm x 100 mm x 100 mm samples.

A miniature pore water pressure measuring system was developed that could provide a 100% response within 5 seconds with minimal disturbance to the sample and could be inserted to the centre of the sample for pore pressure measurements.

8.3 DISCUSSION ON THE INITIATION OF SHEAR AND FLOW BEHAVIOUR OF PARTICULATE MATERIALS

In geotechnical engineering the onset of flow is failure. The margin of safety against flow can only be estimated when the conditions for initiation are well defined. This requires a thorough understanding of the factors controlling the deformation prior to initiation and those contributing to the initiation itself. Although potential for expansion and contraction play a vital role in flow initiation, the initiation of flow is a complex process in comparison with the maintenance of steady flow (critical state) in which flow occurs at a constant volume.

In contrast, in chemical engineering, where production plants have to be operated effectively, controlled flow is required. Repeated stopping and re-initiation must be effectively carried out and very often maintenance of homogeneity of flow will be a significant factor.

Results in this research enable one to appreciate that the major subdivision of flow should be into homogeneous and inhomogeneous flow. Flow in dry or partially saturated material will frequently degenerate into an inhomogeneous form so this will be reviewed first. Subsequently, homogeneous flow will be considered and a mechanism of internal dissipation of energy has been proposed; this has lead to a new interpretation of stress dilatancy relationships which sheds light on the process of initiating and suppressing flow.

multiple Coulomb rupture layers
PD fixed
probably dilatant (no rot.)

intermediate cohes.
dense dry sand
but Coulomb after cyclic rot.

8.3.1 Inhomogeneous flow and factors controlling the intervention of rupture

Inhomogeneous flow is limited here to intense and continuing plane strain shear deformation in one or more thin layers of material set between material which is either not deforming or deforming at a considerably lower rate.

Arthur and Dunstan (1982) have explained that in situations in which the boundary conditions impose local high shear strains before failure the eventual rupture layer will follow the no extension direction of the pre-failure strain, and this direction will usually be associated with coincident axes of stress and strain increment. The Cambridge rotating plate is a typical plane strain experiment of this kind (Figure 8.1). The lines of zero extension in increments of strain prior to failure coincided with the subsequent orientation of the rupture layer (Roscoe, 1970 ; James and Bransby, 1970). Figure 8.2 defines lines of no extension, the angle of dilation υ_{13} and plane of maximum stress obliquity (the Coulomb plane), which is often considered to be the plane associated with rupture. In the rotating plate flow is initiated in a thin layer defined by pre-flow strain and there is no sudden change from continuous to discontinuous behaviour as typified by Coulomb rupture.

Three types of discontinuity were observed during the present research:
As illustrated in Figure 7.11, multiple Coulomb rupture layers were observed in samples of nearly saturated kaolin loaded with constant principal stress directions. Orientation of the rupture layer associated with the plane of maximum stress obliquity. It is thought that as the material is partly saturated the soil has the ability to deform with a positive angle of dilation. There is immediate non-coincidence of axes of stress and previous strain rate; continuous behaviour has been exchanged for discontinuous. The multiple layers indicate the approximate uniformity of the stress distribution but also show that a single rupture layer is prevented from developing fully, probably due to boundary constraint.

The DSC apparatus is designed to impose uniform stresses on a uniform sample. Under these conditions, all dense samples of Leighton Buzzard sand sheared monotonically failed with rupture layer orientations between No-Extension and Coulomb. Figure 8.3 shows an example for dry dense sand in which the rupture layer was approximately 45-1/4 ($\phi + \upsilon$). Quite possibly this is the result of a combination of the two modes of failure brought about by boundary conditions and the ratio of particle size to sample dimension. However, Coulomb rupture layers {(45- ϕ/2) = 22°} were observed in dense samples that were previously sheared under cyclic rotation of

tension cracks
sheared under cyclic reloading

if dilation → continuous cyclic ret. clutter inhom. strain

if shrinkage → no reorientation
(undrained)

principal stress and subsequently loaded monotonically (Table 5.1). Here, it is thought that a more homogeneous particulate structure is created by the rotation of principal stress direction which will prevent the formation of a rupture layer until the whole sample reaches the expansive volumetric strain to cause unlocking. In this situation rupture layers appears to align with maximum stress obliquity.

Figure 7.16 illustrated apparent tension cracks in nearly saturated kaolin samples which were sheared under cyclic rotation of principal stress direction. The crack orientation aligns with the mean direction of the major principal stress and is consistent with the proposition that tensile strength reduces with extensive strain. The tensile condition would then be reached first on this orientation. As radiographs were only taken after one complete cycle, these may be Coulomb planes initiated during one part of the cycle. There is insufficient information to be sure whether these are tension cracks or Coulomb ruptures.

8.3.2 Homogeneous flow in particulate materials

All four listed inhomogenieties require positive dilation to occur; this condition will frequently be met and here it was found that then only continuous cyclic rotation of principal stress directions will deter inhomogeneous strain (with the possible exception of nearly saturated kaolin samples). There may be no sure way of preventing inhomogeneous flow entirely but its development will be significantly reduced if forced to flow at constant volume. Figures 7.27 and 7.28 show oven dried samples of kaolin which have been sheared in a fully saturated condition. The constant volume is maintained by complete saturation of pores, low permeability of the material and the rate of boundary loading which is "fast" in relation to this permeability and the sample dimensions.

Figure 8.4 represents the stress-strain relationships for all stages of slow deformation in plane strain. Point A represents the state at the initiation of flow and is preceded by a strain hardening phase and followed by a transient flow phase which leads to steady flow in the critical state; that is at constant volume and under constant stress. Materials are thought to be entirely unstable in the transient stage and unless the special conditions already referred to are imposed it is inevitable that some degree of inhomogeneous deformation will occur. It is possible to study homogeneous deformation at large strains by imposing cyclic rotation of principal stress directions and this was an enormous advantage, the dilatant transient phase is not reached yet large strains can be measured. These measurements revealed that within this phase there was an imp important limited steady state of stress dilatancy.

Les colonnes ne peuvent pas se former
→ le seuil de τ pour déclencher l'instabilité

8.3.3 The effects of principal stress rotation

The effects of jump rotation of principal stress on the stress-strain deformation of particulate material has been clearly illustrated by Arthur et al., 1977; 1986, and Wong et al., 1987. These show a strong anisotropic stiffness in the pre-flow strains. Large variations in magnitude of pre-flow strains are illustrated for sand in Figure 8.5. These variations can be important for flow initiation, but also emphasise the fundamental anisotropic behaviour of frictional particulate materials.

The discrete nature of particulate materials was visualised in Chapter 1 and it was demonstrated that the way in which particulate materials support externally applied load is dependent on distribution of particle contact normals and contact forces (e.g. Biarez and Wiendieck 1963, Oda, 1972; Drescher and de Josselin de Jong, 1972; Oda and Konishi, 1974; Cundall and Strack, 1983). These authors demonstrated that strain under fixed principal directions set up a strongly anisotropic distribution of particle contact normals. These normals were most frequently in alignment with the major principal stress direction and least frequently in alignment with the minor principal stress direction. The particles in contact with each other can be visualised as forming paths through which applied loads are conveyed to opposite boundaries. The main load paths will form along lines in the major principal stress direction and these can be seen as stable crooked columns, whilst secondary load paths, formed by particles in contact in the intermediate and minor principal stress directions, provide lateral support to the particles along the main load path (Figure 8.6). As particles and the corresponding interparticle contacts re-arrange during deformation, the main load paths become more aligned with the major principal stress direction. These columns are transient; and an increment of strain will cause several to become unstable and the associated column loads to be distributed amongst the remaining columns and the creation of new ones. The birth and death of columns will be at the same rate when steady state conditions are reached during continuous deformation as proposed by Cundal and Strack (1983). However, the steady state referred to is one in which constant principal stress directions are applied. It should be noted that the underlying mechanism of deformation in this material is associated with local instability and the elastic loading of transient columns rather than a homogeneous interparticle sliding which is the traditional interpretation.

The effects of continuous rotation of principal stress directions on the particulate material behaving in this way are clear; the column structure cannot be fully developed in the changing direction of the major principal stress and the shear stress or principal stress ratio σ_1 / σ_3 necessary to initiate flow will fall. This interpretation is confirmed by

several series of cyclic continuous rotation tests carried out in this research using the DCDSC. The results of such cyclic tests for dense and loose Leighton Buzzard sand and loose coal are presented in Figures 5.18, 5.21 and 6.7. As the threshold stress ratio for the initiation of flow (Figure 8.4) for these materials were $R_{f.\ (dense\ sand)}$= 7.15, $R_{f.\ (loose\ sand)}$ =4 and $R_{f.\ (loose\ coal)}$= 3.2 respectively for monotonic loading, the effects of continuous rotation of principal stress directions are clear. Figures 8.7, 8.8 and 8.9 illustrate relationships between the critical mobilised principal stress ratio and the amplitude of principal stress rotations. The lines represent the state of flow in materials when subjected to continuous and cyclic principal stress rotation. It can be seen that as the rotation increases the stress ratio required to initiate flow falls. Correlation between dry sand and damp coal can be seen with the exception of the pronounced curvature for damp coal at low mobilised principal stress ratios. Although these relationships can be taken to be linear in the range of cyclic rotation between 0° and 80° (except for coal), they will not be linear at larger magnitudes of rotation as the mobilised principal stress ratio approaches unity. Limitation of the present shear sheets design of the DCDSC does not allow for larger magnitudes of rotation greater than 90° to be investigated. Nevertheless, these Figures may be useful guides in assessing the maximum strength that can be mobilised with limited deformation for a given amplitude of cyclic rotation.

8.3.4 Stress dilatancy relationships and extension of a steady state concept

Dilation in granular media during shear was discussed first by Osborne Reynolds in 1886 and its importance in geotechnics has been acknowledged since the pioneering work of Taylor (1948). Rowe's stress dilatancy theory (1962) which is based on particles sliding has influenced many geotechnical modellers. There has been an abundance of flow rules to approximate the stress dilatancy relationships of granular materials. Stress dilatancy relationships are derived from an equation describing the incremental work and internal energy dissipation balance for material. However, all these balances have assumed that the main control on the internal dissipation of energy was some frictional property of the material. The significance of interparticle friction in this regard has been questioned by Skinner (1969) and Bishop (1972). The transient column concept which was introduced earlier can be used to propose an entirely different control for the internal dissipation. It has been proposed that this dissipation can be controlled by the release of elastic energy stored in the transient columns as these fail. This new mechanism does not eliminate the frictional dissipation mechanism.

It is a cherished wish of the soil mechanics community that there should be a unique relationship between principal stress ratio $(\sigma_1 - \sigma_3)/(\sigma_1 + \sigma_3)$ and rate of dilation - $(\delta\varepsilon_1 + \delta\varepsilon_3)/(\delta\varepsilon_1 - \delta\varepsilon_3)$. However, measurements of rate of dilation are always difficult to make in tests in which the stress ratio is increasing.

Wong and Arthur (1986) presented totally new steady state measurements from their cyclic tests on dense Leighton Buzzard sand with cyclic rotation of principal stress directions. Their tests gave large strains in which the dilation rate could be measured more precisely (Figure 8.10). They also provided steady state measurements from cyclic tests in which only the mean stress level was cycled and the principal stress directions were constant. Deformation was large but there was no tendency to inhomogeneous flow. They showed that limited steady states exist in dilating particulate media in that when the material is cycled under constant principal stress ratio a constant angle of dilation can be maintained through a finite strain increment. In such a limited steady state, that slow change in volume which is inevitably occurring is having a negligible effect on the stress dilatancy. Two experimental stress dilatancy relationships were plotted by these authors which is illustrated in Figure 8.11. However, this work was limited to dense Leighton buzzard sand but shows that possibly a unique stress dilatancy relationship does not exist. Rowe's data (1962) also casts doubt on a unique line.

As a consequence two simplified stress dilatancy models are proposed (Figure 8.12). One model, in a manner similar to Cundall and Strack's computer simulation, pictures the deformation of particulate material as a mechanism consisting of a series of collapsing and regenerating columns. The second contains no dissipation of energy. The relationships are strongly confirmed in a wide range of experimental conditions. These stress dilatancy relationships could be of practical value in describing particulate behaviour during the complex phase of initiating flow.

It was suggested earlier that particulate materials can be modelled as changing collections of spatially dispersed crooked columns which are supported by distributed lateral forces arising from the minor principal stress and which transmit all the major principal stress through the material. During the very momentary existence of each of these transient columns in a minute strain increment, the column stores elastic energy, just as would a continuous column, and on collapse the stored energy is released and dissipated. The internal dissipation of energy from the columns occurs entirely through a frequently repeated process of one dimensional storage and release of elastic energy.

Figure 8.13 illustrates dissipation of energy (i.e, deformation at constant stress) when a collapsing of the columns is the only mechanism of deformation. The quantity of energy, E, that is momentarily stored and then dissipated is the same as that which would have been stored in a continuous compressive linear elastic spring which had been initially loaded to the σ_1 level and then reduced back to the σ_3 level.

$$E= 0.5\ (\sigma_1 - \sigma_3)\delta\varepsilon_1 + \sigma_3\delta\varepsilon_1$$

which gives

$$E=(\sigma_1 + \sigma_3)/2\ \delta\varepsilon_1$$

The model estimates that there will be a sequence of about 1000 multiple column failures per unit volume in a 1% major principal strain increment for a quartz sand.

The energy is dissipated from a pure loading and unloading column mechanism of deformation in which the released elastic energy is dissipated internally. This occurs when columns in the major principal stress direction collapse to a level sufficient to support the minor principal stress. Equilibrium at the minor principal stress level in the columns is brought about by a local 90° jump in the major principal stress direction which would occur if the load remaining in the columns fell below this level. This would produce a strong wedging action on the collapsing column and would be likely to hold the force level at the level equivalent to σ_3. In the steady state σ_1 represents the summation of the contact forces in that direction and is constant; the contact forces unloaded from columns that fail are redistributed to all existing and new columns. This redistribution causes elastic compression in these columns and this compression is the whole major principal strain increment. The process is continually repeated in this limited steady state.

The energy dissipated is represented by the upper line in Figure 8.12 which is a straight line intersecting the $(\sigma_1 - \sigma_3)/(\sigma_1 + \sigma_3)$ axis at 0.5, and corresponds to a ϕ value of 30°. The intersection of the $-(\delta\varepsilon_1 + \delta\varepsilon_3)/(\delta\varepsilon_1 - \delta\varepsilon_3)$ at -1 comes from visualising very loose sand, in which the possibility exists for vertical strain to take place with no horizontal strain.

The incremental work equation in Figure 8.13 for plane strain is:

$$\sigma_1\delta\varepsilon_1 + \sigma_3\delta\varepsilon_3 = 0.5\ (\sigma_1 - \sigma_3)\ \delta\varepsilon_1 + \sigma_3\delta\varepsilon_1$$

which rearranges to

$$(\sigma_1 - \sigma_3)/(\sigma_1 + \sigma_3) = 0.5\ (1 - [\delta\varepsilon_1 + \delta\varepsilon_3/\delta\varepsilon_1 - \delta\varepsilon_3])$$

The lower line represents a deformation process of column branching by sliding and rolling of particles which, for an ideal frictionless material. No energy is dissipated internally and the system acts as a 100% efficient machine; the work put into the system ($\sigma_1\delta\varepsilon_1$) equals the work extracted ($\sigma_3\delta\varepsilon_3$) from the system. The equation of this line for plane strain conditions is:

$$\sigma_1\delta\varepsilon_1 = -\sigma_3\delta\varepsilon_3$$

This may be re-arranged in the form:

$$(\sigma_1 - \sigma_3)/(\sigma_1 + \sigma_3) = -(\delta\varepsilon_1 + \delta\varepsilon_3)/(\delta\varepsilon_1 - \delta\varepsilon_3)$$

Thus if no energy is dissipated by the system, plotting $(\sigma_1 - \sigma_3)/(\sigma_1 + \sigma_3)$ against $(\delta\varepsilon_1 + \delta\varepsilon_3)/(\delta\varepsilon_1 - \delta\varepsilon_3)$ will produce a straight line starting at the origin with unit gradient (Figure 8.12). This stress dilatancy relationship corresponds to Cole's relationship (Cole, 1967) when the shear resistance at constant volume is set to zero to allow for perfectly smooth grains. The two limiting steady state strength dilation relationships are represented as two lines in Figure 8.12.

The two stress dilatancy relationships cover the complete range of stress ratios (0 to 1) and strain ratios (+1 to -1), one is pure dilation and the other is the release of elastic energy. Any constant upward displacement of real data points from the theoretical lines could be attributed to the dissipation of energy through friction; such displacement is to be expected.

In order to ascertain if the models are satisfactory, data must cover the complete stress/ratio - strain/ratio limits. Regions that are not commonly observed are those associated with large compressive strain at low stress ratio.

Triaxial compression data, extracted from the work of Lee and Seed (1968) on both dense and loose sand at a wide range of stress levels are illustrated in Figures 8.14a and 8.14b. Here particle crushing was observed which can be interpreted as loss of stored elastic energy. It can be seen that the data is approximately parallel to the upper line. The incremental work equations were adjusted for axisymmetric stress condition to give:

$$(\sigma_1 - \sigma_3)/(\sigma_1 + \sigma_3) = 0.5\ (1 - [(\delta\varepsilon_1 + 2\delta\varepsilon_3)/(\delta\varepsilon_1 - 2\delta\varepsilon_3)])$$

The small offset of the upper line indicates close compliance with the simple column model and very little frictional dissipation. This is a strong confirmation of the

Il n'y a pas de cas présenté

essentially one dimensional model and in addition the data includes crushing particles at high stress levels.

Wong and Arthur (1986) presented data that does not fit the upper line (elastic energy dissipation). However when plotted on the proposed model it can be seen that it is displaced but parallel to the lower line (frictional line). Figure 8.15 shows experimental results from monotonic plane strain tests. In these tests the magnitude of strain was small which could have led to large error in prediction of dilation rate. They overcame this by conducting cyclic tests in which the stress ratio was held constant while the mean stress level was cycled. The data from these experiments are also included on Figure 8.15. This indicates that two stress dilatancy relationships may exist. Although the upper line is covered completely there is a lack of information to cover the lower line. All the data described involved a fixed direction of the major principal stress and are shown on Figure 8.16. It now is necessary to consider if a rotation of principal stress direction has an effect on the these relationships.

Data from the SSA in which the principal stress has to rotate are presented in Figure 8.17. Although it was discussed earlier that the angle of rotation is not great in the plastic range (Chapter 1), it can be seen that the results fit the upper line well over a limited range of dilatancy.

A test of the strength of the model can be to investigate if soil, subjected to continuous rotational cyclic loading, also plot on the two lines.

Cyclic rotation tests by Wong (1986) on dense sand which deform at a constant dilation rate will be plotted as a single point on Figure 8.18. A series of tests at different cyclic stress ratio and amplitudes give a series of points which plot parallel to the upper line. As strain is large the calculated strain ratios are precise (Figure 8.10). The author using a different apparatus working at higher stress levels found similar results for dense sand and these are superimposed on Figure 8.18.

In order to investigate cyclic loading data associated with a lower dilatancy rate the author conducted a series of tests on loose and dense sand cycled at low stress ratio and high amplitude of rotation. It was found that at a lower mobilized stress ratio the soil no longer dilated at a constant rate but changed from being very contractant to less contractant (Figure 5.22). Figure 8.19 shows the data for these series of tests. It is interesting to note that for tests cycled at low stress ratios there is a movement from the upper line to the lower line. The arrow heads are data points showing the end of this movement. On reaching the lower line strain eventually ceases even

though the soil is still subjected to cyclic loading. It appears that the frictional nature of the soil suppresses further strain.

For samples that are cycled at higher mobilized stress ratios migration to the bottom line was not detected but strain actually developed until the deformation limit of the apparatus was reached. It is not certain if migration to the lower line occurred. However for tests involving positive dilatancy no migration occurred and it is thought that here that as the soil is dilating elastic release of energy will continue.

The limited data available for the damp coal is plotted in Figure 8.20 and shows reasonable conformity but more data is needed. It can be seen that the dampness and particle crushing has no effect on the model lines and the behaviour is similar to loose sand.

Low elastic modulus materials such as clays are unlikely to achieve full release of elastic energy by column collapse and would therefore plot below the 0.5 point on the vertical axis at zero dilatation. This is confirmed by many reports of constant volume tests on clays when the angle of failure is less than 30°.

Tests imposing cyclic principal stress rotation confirm the predictions of the model for complete cycle data equally as well as monotonic tests. However, within individual cycles variations in principal stress and strain increment directions have been reported by Wong and Arthur (1986) and were produced in Figure 5.26. There are two occasions in each cycle when these principal axes are coincident and it seems likely that the dilation on these occasions controls the residual angle of dilation for the cycle. This residual strain is that which is found by measurements made at the end of one or more cycles.
Figure 8.21 summarises all the data that has been used to check the validity of the model. The plots includes data from both triaxial, plane strain, tests simple shear tests, and plane strain tests involving rotation of principal stress direction.

Figure 8.22 shows two examples:

1, A dense material with a monotonic failure strength at P is cyclically loaded at a constant stress state at Q. Flow is initiated on the upper line representing the column instability mechanism at the lower stress ratio Q and the material slowly expands. This limited steady state continues until the effect of the cumulative expansion dominates and the strength under monotonic shear drops to Q and then inhomogeneous flow starts. Note that the initiation of flow on the upper line must be determined by reference to a threshold relationship such as

that in Figure 8.7.

2, A loose material with a monotonic failure state at A is cyclically loaded at a constant stress state B. Briefly the stress dilatancy state is at C but the concentration of material is initially high and the material moves rapidly to D on the lower limited steady state relationship associated with frictional dissipation. Here the frictional dissipation slows the flow until it stops. Data showing such a migration from the upper line to the lower one have been noted during expansive dilation; in these cases the cyclic component of loading was the mean stress and there was no rotation of principal stress directions. Again the flow gradually ceased.

Additional monotonic data from shear tests performed in the Biaxial Tester (Figure, 4.33) where a variety of plane strain boundary conditions were applied are presented in Figure 8.23. The various boundary constraints produce data points parallel to the upper theoretical line but displaced by different amounts from it. This parallelism can be interpreted as implying that the degree of constraint results in varying offsets from the ideal line illustrating the effects of plane strain boundary constraints on the deformation mechanism. So, the deformation mechanism is dominated by the collapsing of loaded columns, which are readily susceptible to the constraining effects of the plane strain boundaries. Pre-failure stress-dilatancy data points from the DSC tests in which thick plane strain membranes were used also lie parallel to the upper line. This also provides additional information of deformation dominated by collapsing columns with extra stability afforded to the secondary columns by the thick plane strain membranes.

The stress dilatancy graphs presented indicate modes of behaviour during the initiation of flow; Figure 8.24 is a first attempt at this type of interpretation. The onset of inhomogeneous flow can be predicted and the changes in stress dilatancy associated with change from full flow to the gradual arrest of flow are depicted. A possible range of steady critical state flow is also indicated; the exact value attained in a real material depends on the proportion of the deformation achieved by the frictional and collapsing columns mechanisms.

Although the model has been used to interpret only drained tests on granular media it can also suggest the shape of stress paths associated with undrained behaviour from soils of different initial voids ratio.
At the critical state the model suggests that sand will be expected to deform at a mobilised angle of friction of 30°. Soils that would dilate under drained conditions will

be restricted to constant volume deformation and will then rapidly gain strength with an eventual stress path reaching 30° as illustrated by path (1) in Figure 8.25.

A sand which is extremely loose would tend to contract under drained loading and, with this contraction, would gain in strength. Prevention by loading undrained may result in a stress path which terminates at the origin (stress path (2)) and associate with liquefaction.

Path (3) is a typical undrained stress path for medium loose sand. The initial path indicates instability of the soil but with column development the eventual stress path will again be at 30°.

8.3.5 Super-homogeneity

Present work illustrates that induced anisotropy, developed during cyclic rotation of principal stress directions, strongly increased stiffness, strength and the angle of dilation in the subsequent monotonic loading even though the change in voids ratio after the cyclic loading was small.

Wong (1986) subjected DSC samples, initially isotropic in the plane of strain, to continuously cycling principal stress direction with an arbitrary amplitude at a constant principal stress ratio for a number of cycles, (stress path (A) Figure 8.26a). Thereafter a stress path (B) with constant principal stress directions was followed in which $\Delta\psi$ was coincident with the mean direction of major principal stress of the cyclic loading and equal to zero.

The author did similar tests on dense and loose sands and loose damp coal, Figures 8.26b and 8.26c. It can be seen that the effects are related to the magnitude of residual shear strain occurring under cyclic loading.

In the case of dense sand the material becomes brittle with quite a remarkably high angle of dilation, from v_m=16° for a simple monotonic to v_{sm} =22° and even 28° (see Figure 5.28) in brief pre-rupture strain, after cycling. These tests did not strain more than 0.5% in the subsequent loading and failed at a sudden brittle type of failure. The rupture planes formed on planes of maximum stress obliquity ($\pi/4 - \phi/2$) = 21° ± 1°, Coulomb failure, in forms of narrow shear bands. This was a different orientation to that of 30° ± 2° typically observed for medium size Leighton Buzzard sand (0.65 mm - 0.80 mm) in simple monotonic tests by the author and other investigators (e.g. Arthur et al., 1977; Wong, 1986; Ogunbekun 1988).

This dramatic change in the fabric of material can tentatively be attributed to improved homogeneity of particle contact distribution in the mean direction of principal stress. Such uniformity or super homogeneity would make for effective load carrying columns through the material and associated sudden failure.

There seem to be implications for many aspects of the handling granular materials in the processing industries. Super homogeneity is clearly unhelpful when flow has to be restarted. On the other hand when strength is a requirement for some particulate agglomeration or sintering this effect may be extremely desirable.

It is interesting to note that for dense sand although cyclic loading has changed the fabric and initial stiffness and provided a more brittle material, the failure strength is the same but the failure mechanism is different as Coulomb ruptures were observed.

In the case of loose sand and loose coal the effects of continuous rotation of principal stress is so strong that not only the failure mechanism is changed through presence of rupture layers, but the failure strength is increased towards dense material.

It can be concluded that previous loading history exists in the "memory" of the material and voids ratio alone cannot account for the material's behaviour. It is therefore essential to add parameters derived from a particulate approach to the study of granular material. Number and orientation of contacts, orientation of particle axes, and distribution of contact normals, would be fundamental additional parameters needed to describe the state of the material.

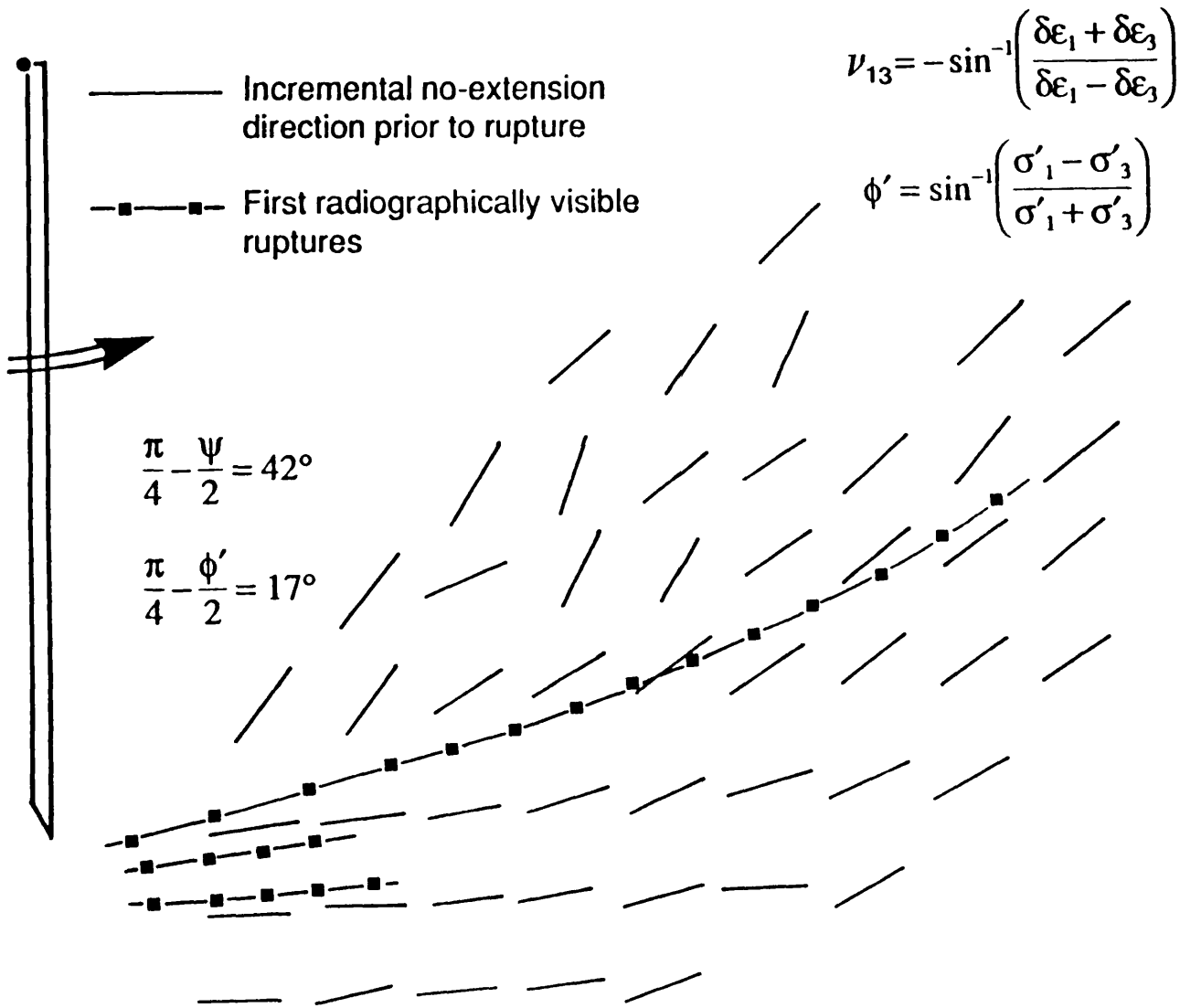

Fig. 8.1 **Cambridge Rotating Plate (after Roscoe, 1970). Incremental no-extension directions prior to failure compared to subsequent initial rupture layers in sand.**

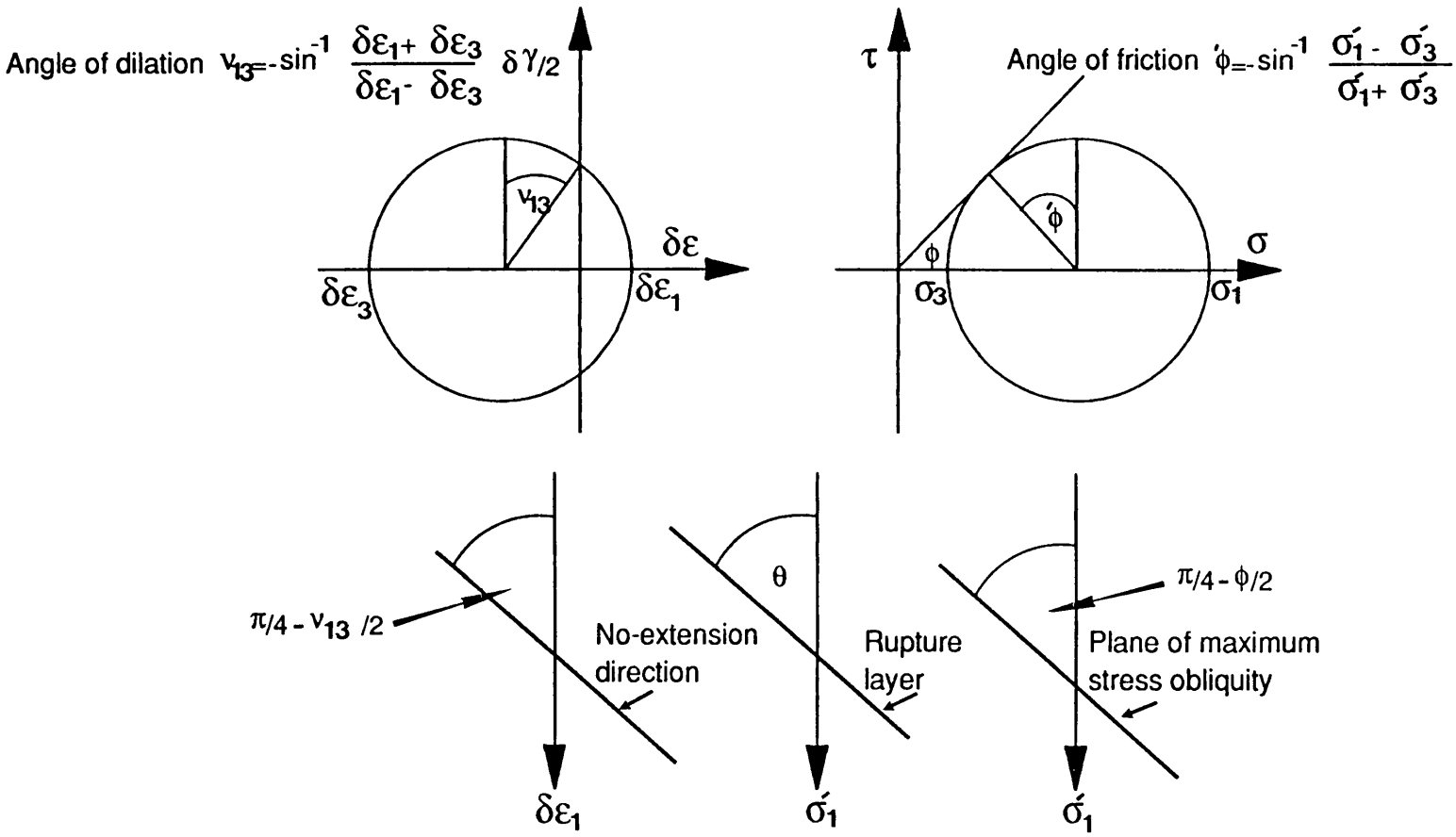

Fig. 8.2 **Definitions of orientations and angles used**

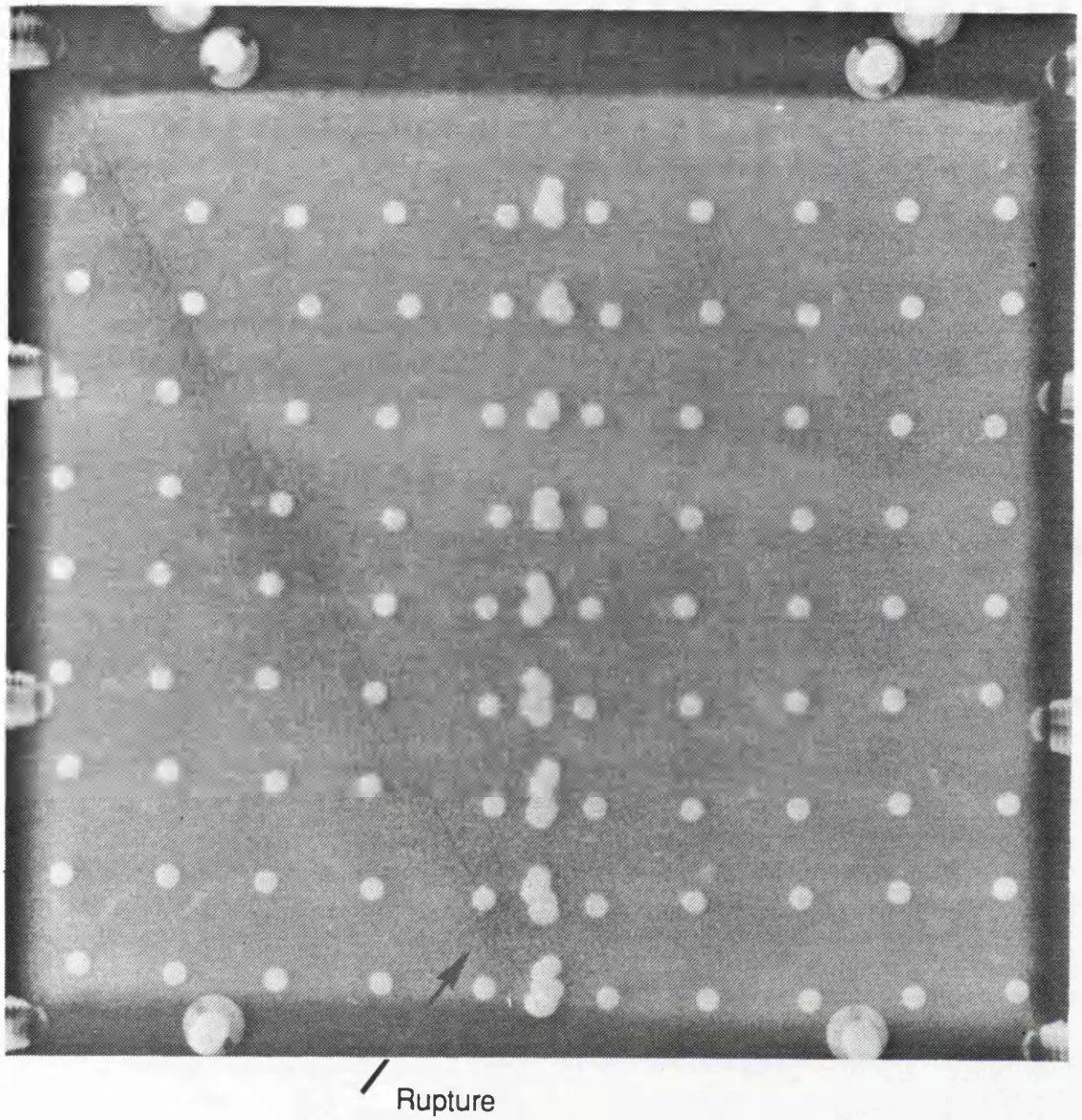

Fig. 8.3 Rupture layer initiated in dense dry sand

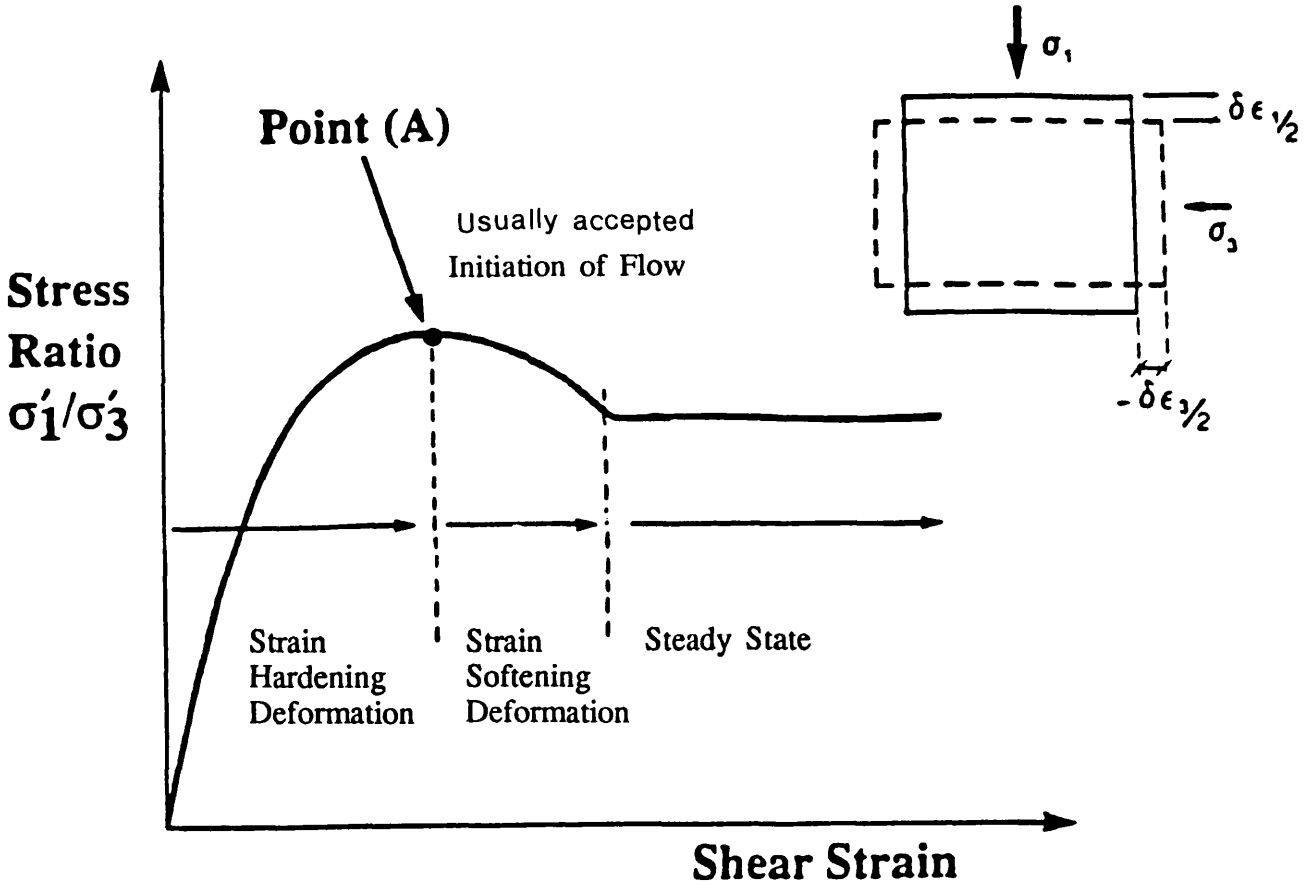

Fig. 8.4 **Simple representation of the development of flow in granular material when under monotonic loading**

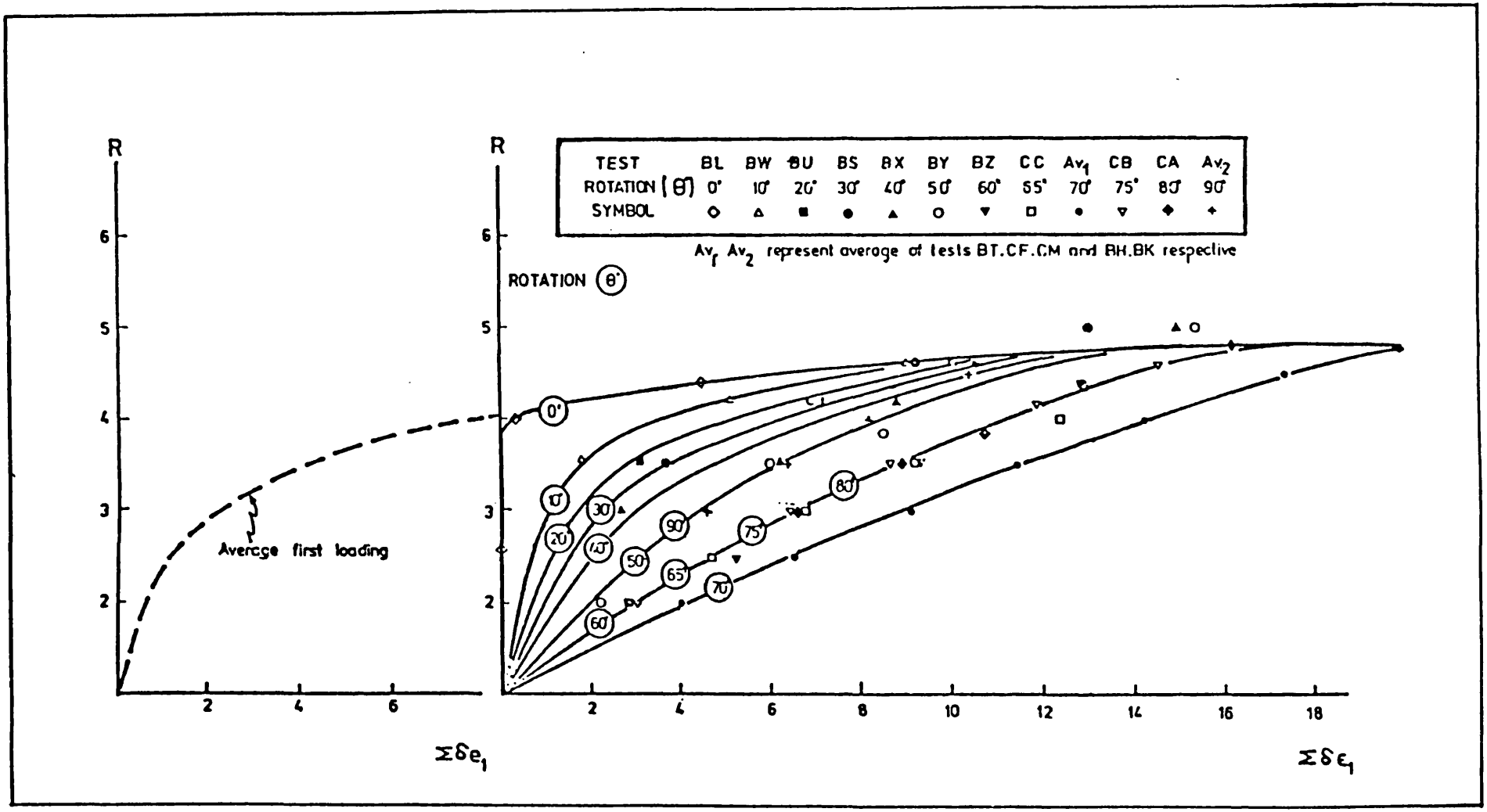

Fig. 8.5 Stiffness variations of sand that had previously been monotonically loaded and subsequently loaded in different directions (after Rodriguez del C., 1977)

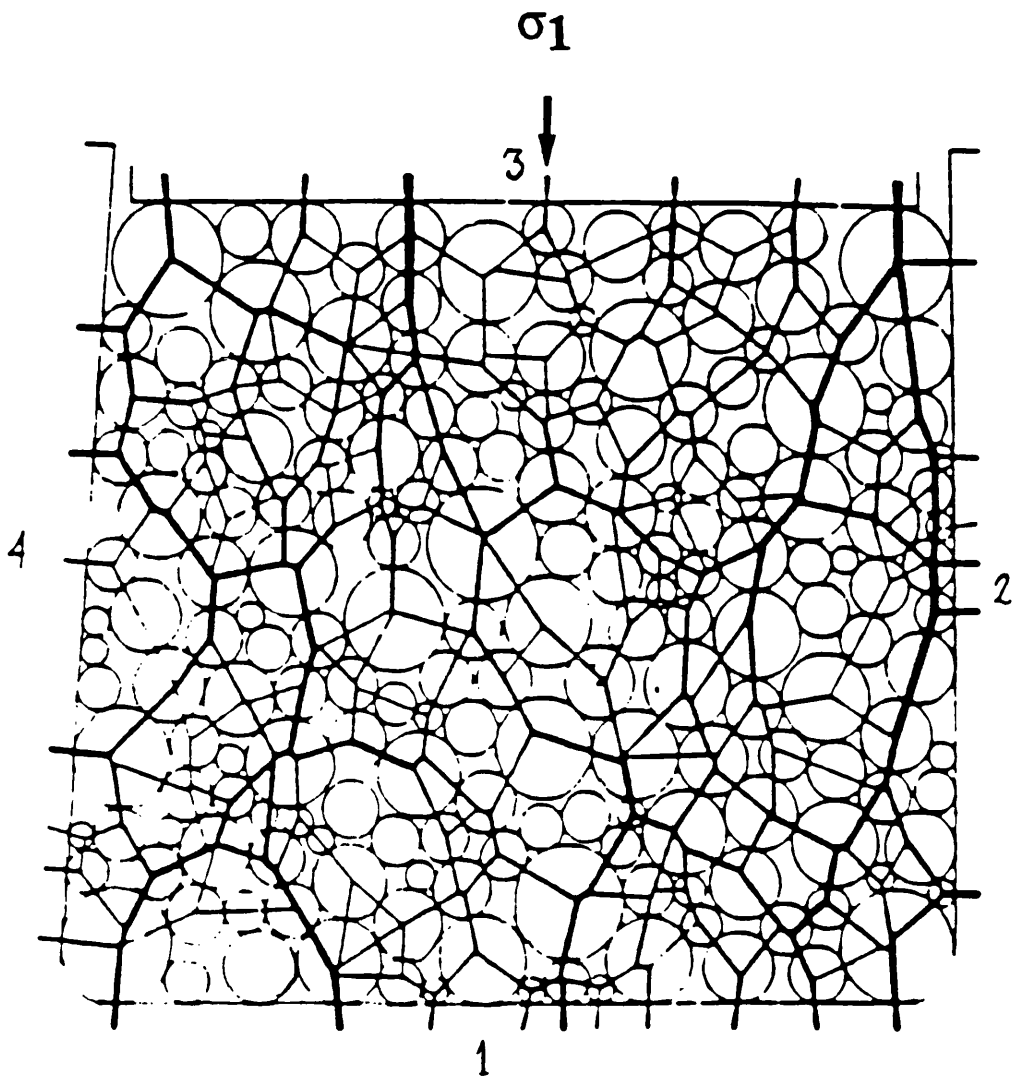

Fig. 8.6 Transient columns related to major principal stress direction in particulate materials (after De Josselin de Jong and Verruijt, 1969)

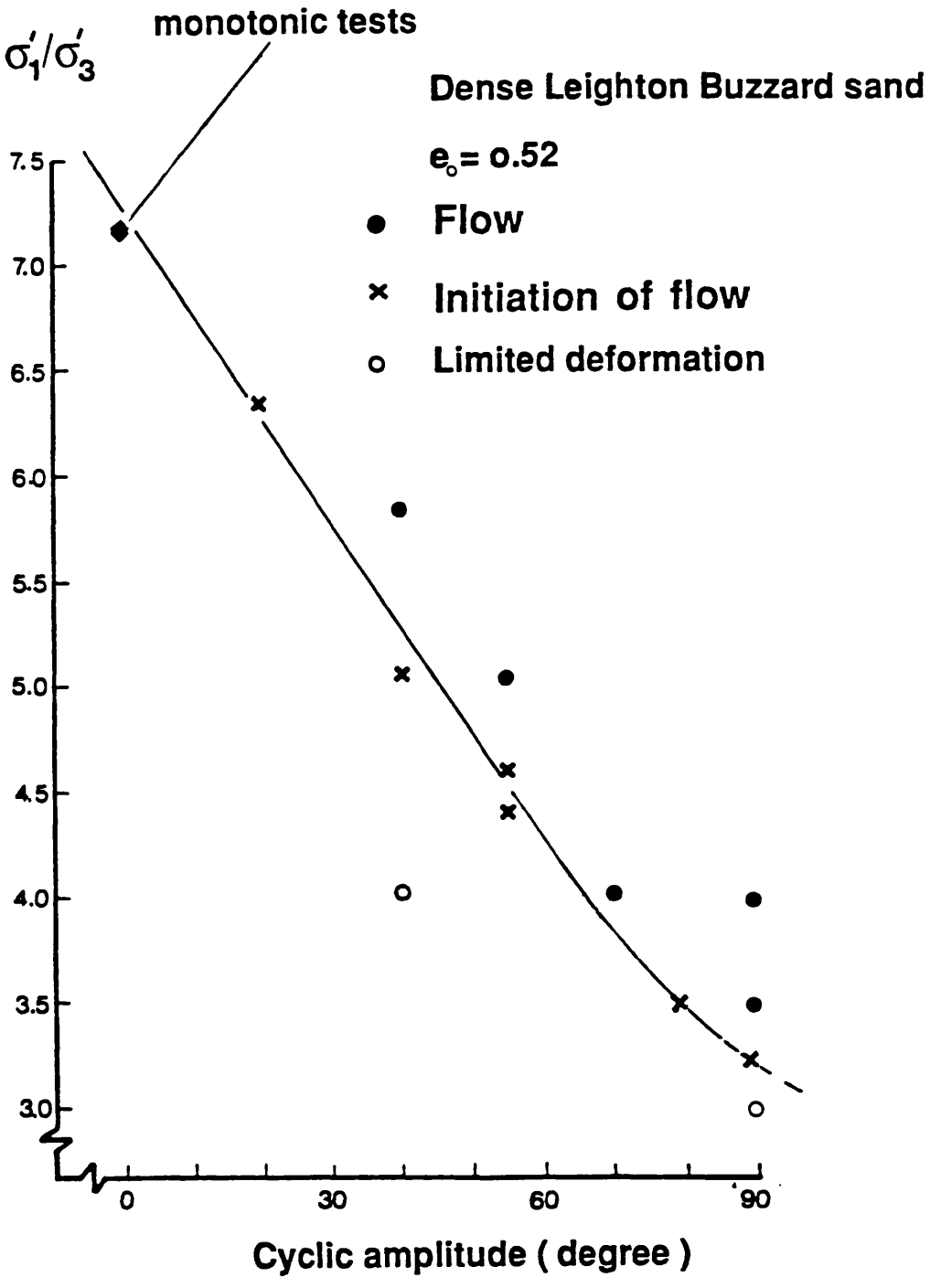

Fig. 8.7 Relationship between stress ratio and cyclic amplitude necessary to initiate flow in dense sand

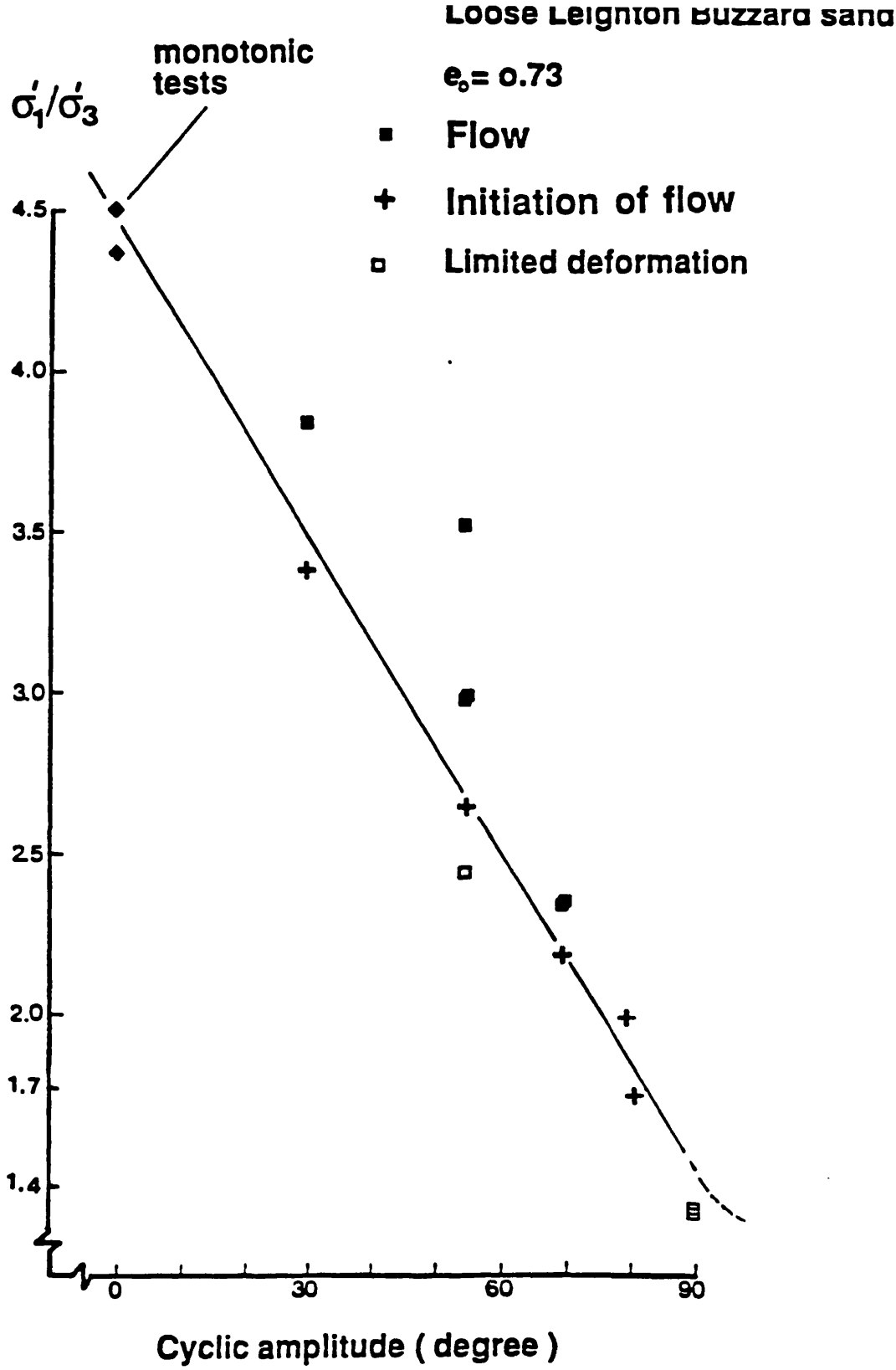

Fig. 8.8 Relationship between stress ratio and cyclic amplitude necessary to initiate flow in loose sand

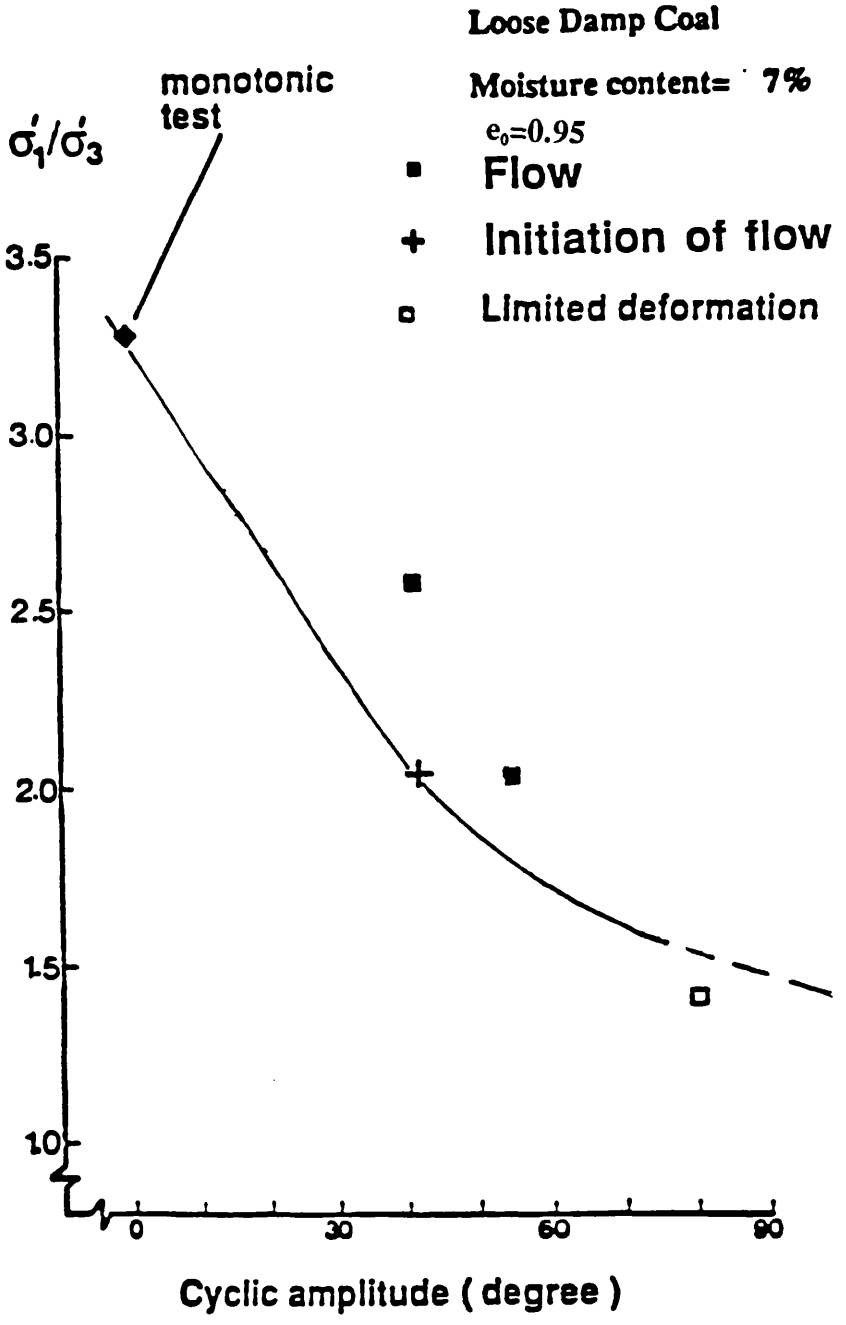

Fig. 8.9 Relationship between stress ratio and cyclic amplitude necessary to initiate flow in loose damp coal

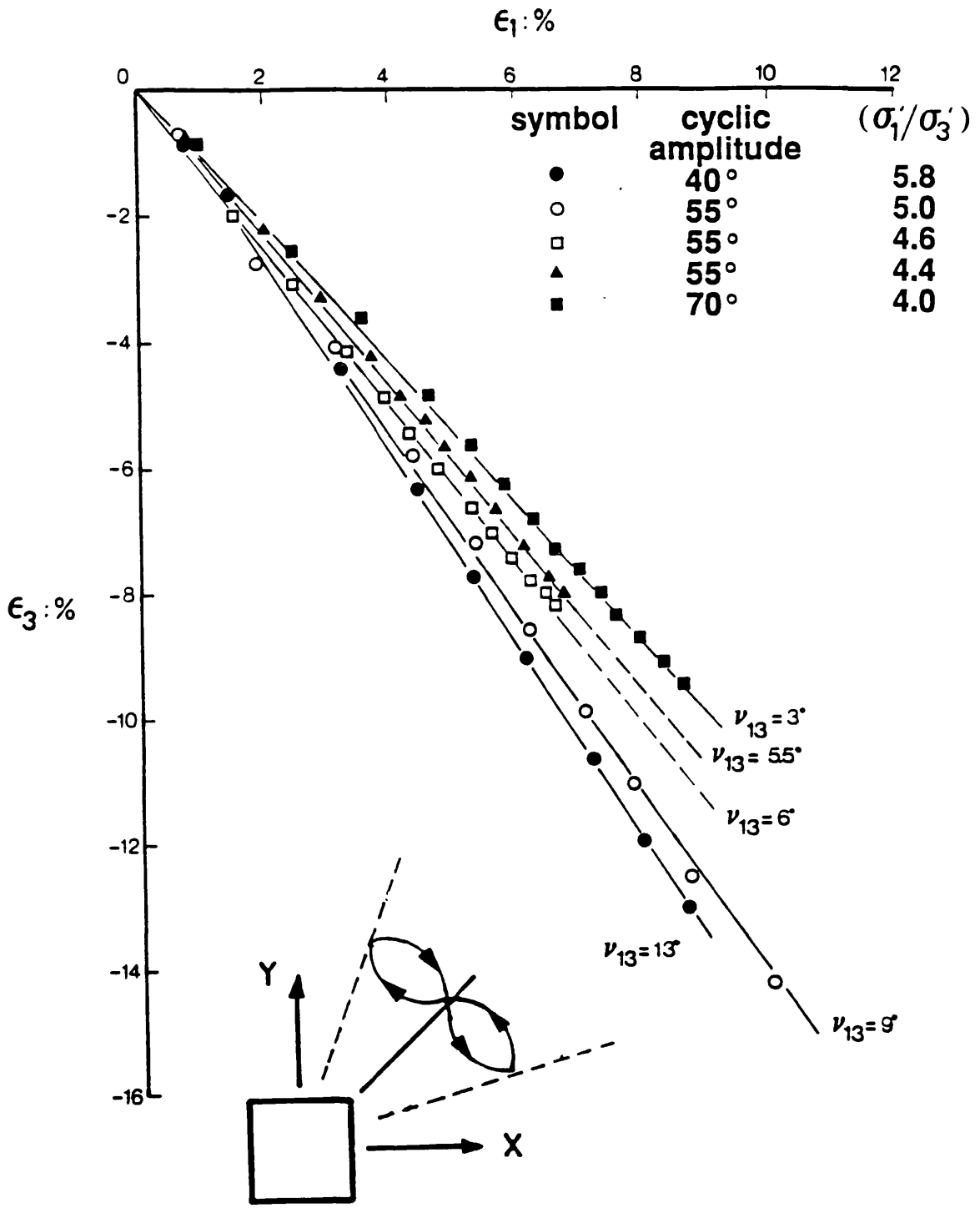

Fig. 8.10 Variation in the angle of dilation with amplitude of principal stress rotation and mobilised angle of friction on dense samples (after Wong , 1986)

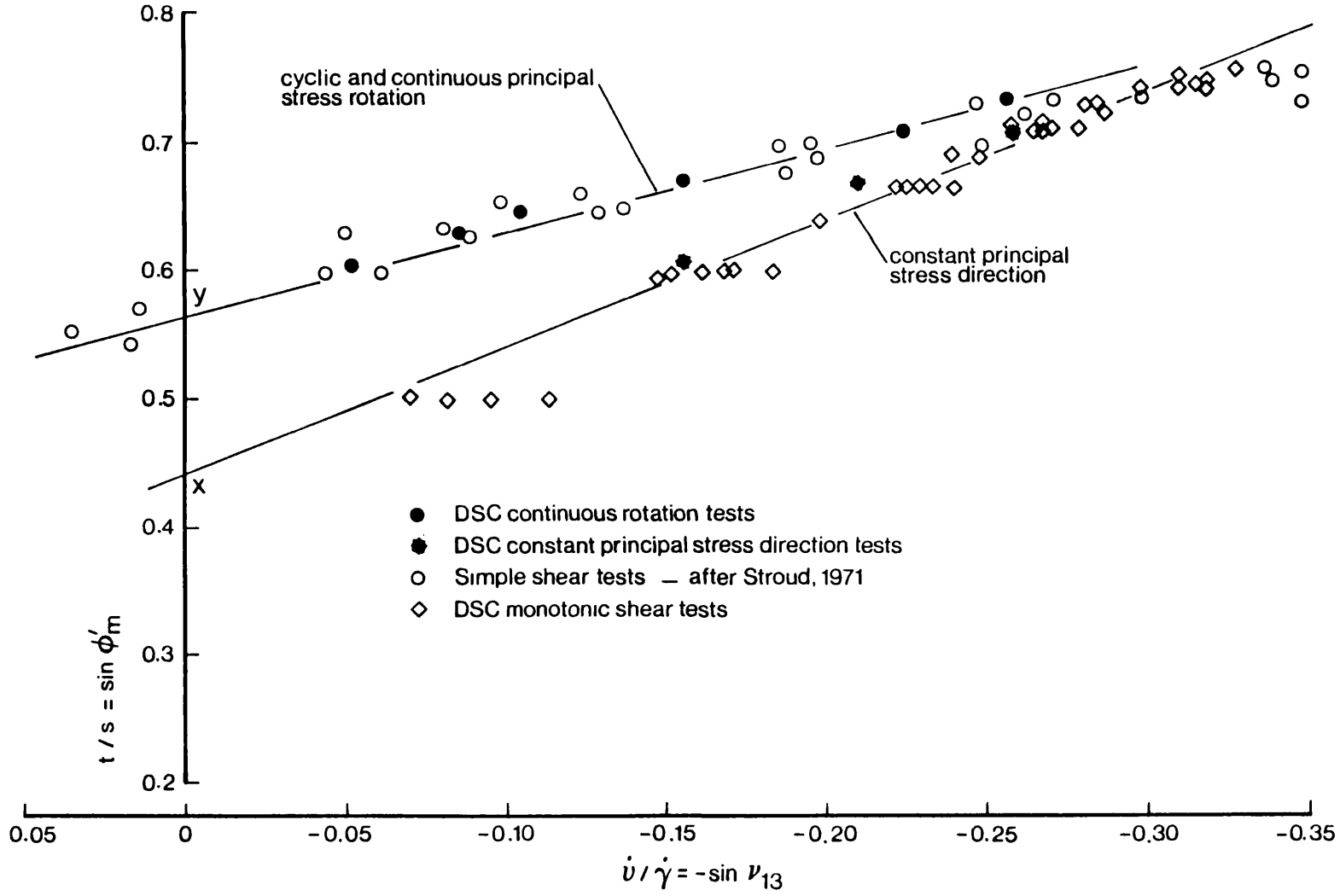

Fig. 8.11 **Stress-dilatancy measurements for dense sand (after Wong and Arthur, 1986)**

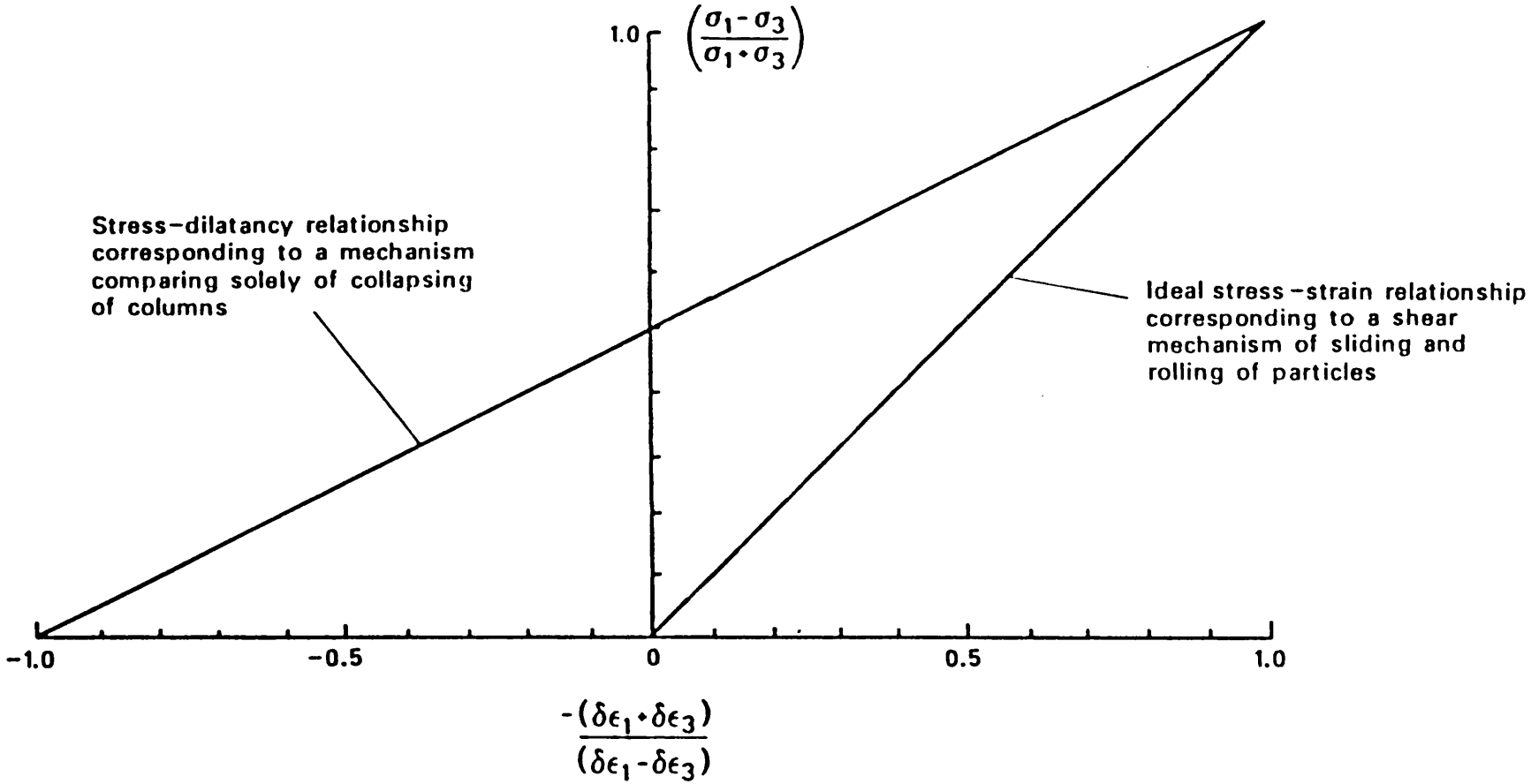

Fig. 8.12 Two proposed stress dilatancy relationships for particulate materials

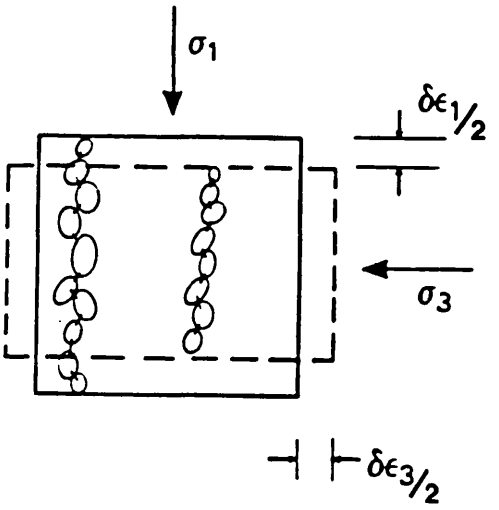

Regeneration of load paths due to collapse of columns during strain movement $\delta\epsilon_1$

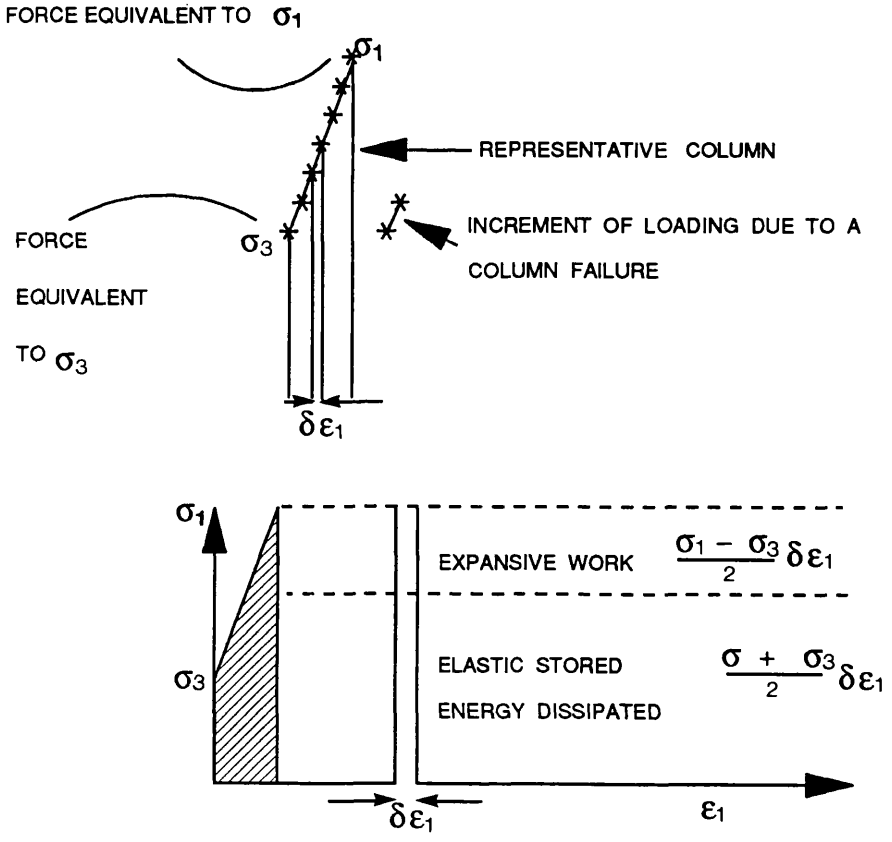

Fig. 8.13 **A conceptual representation of energy dissipated from collapsing columns during a strain increment $\delta\varepsilon_1$ whilst supporting a major principal stress σ_1**

(a)

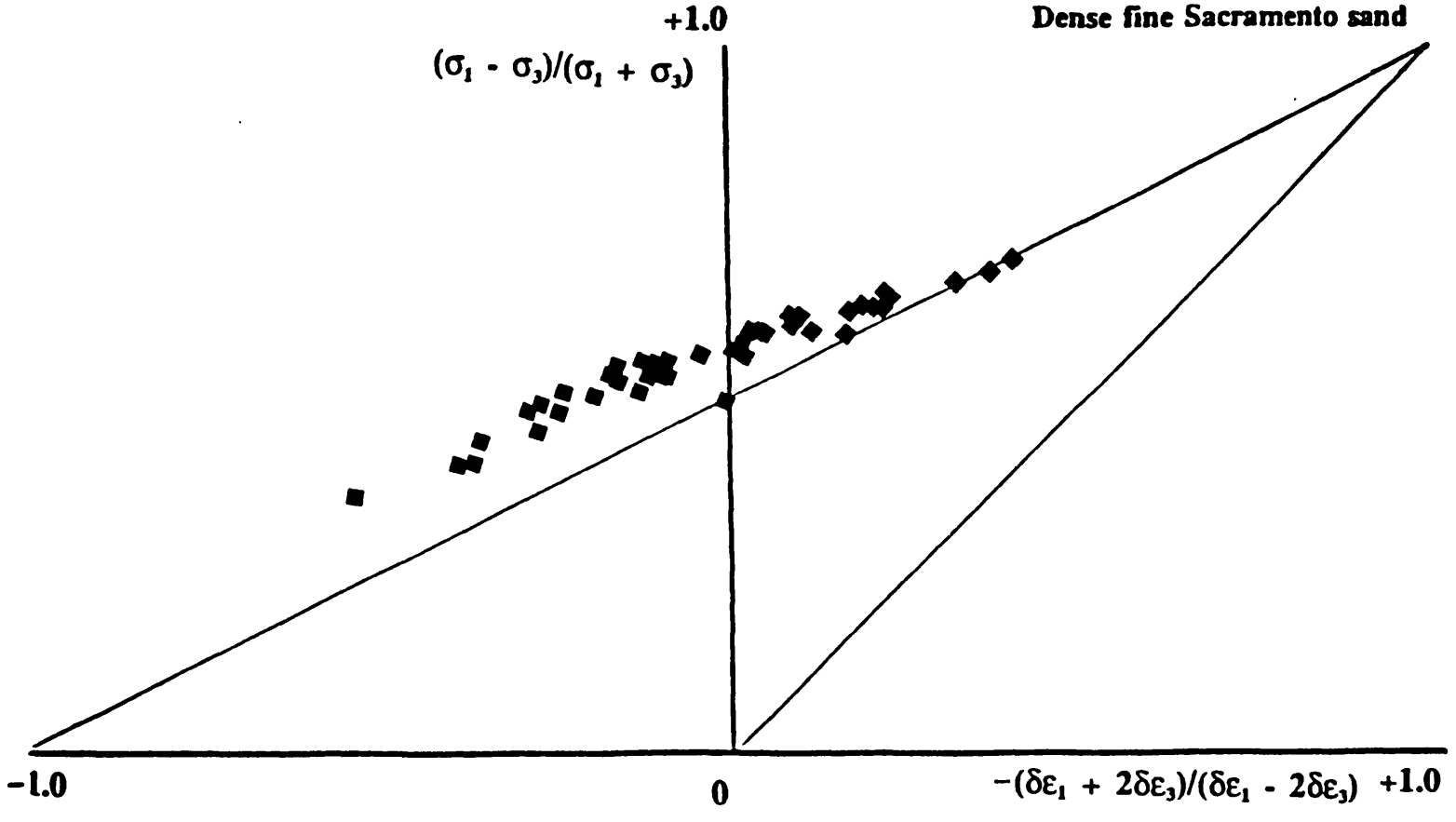

Fig. 8.14 (a) Axisymmetric triaxial compression experimental data for dense fine Sacramento sand superimposed on the ideal stress dilatancy relationships and (b) axisymmetric triaxial compression experimental data for loose fine Sacramento sand superimposed on the ideal stress dilatancy relationships.

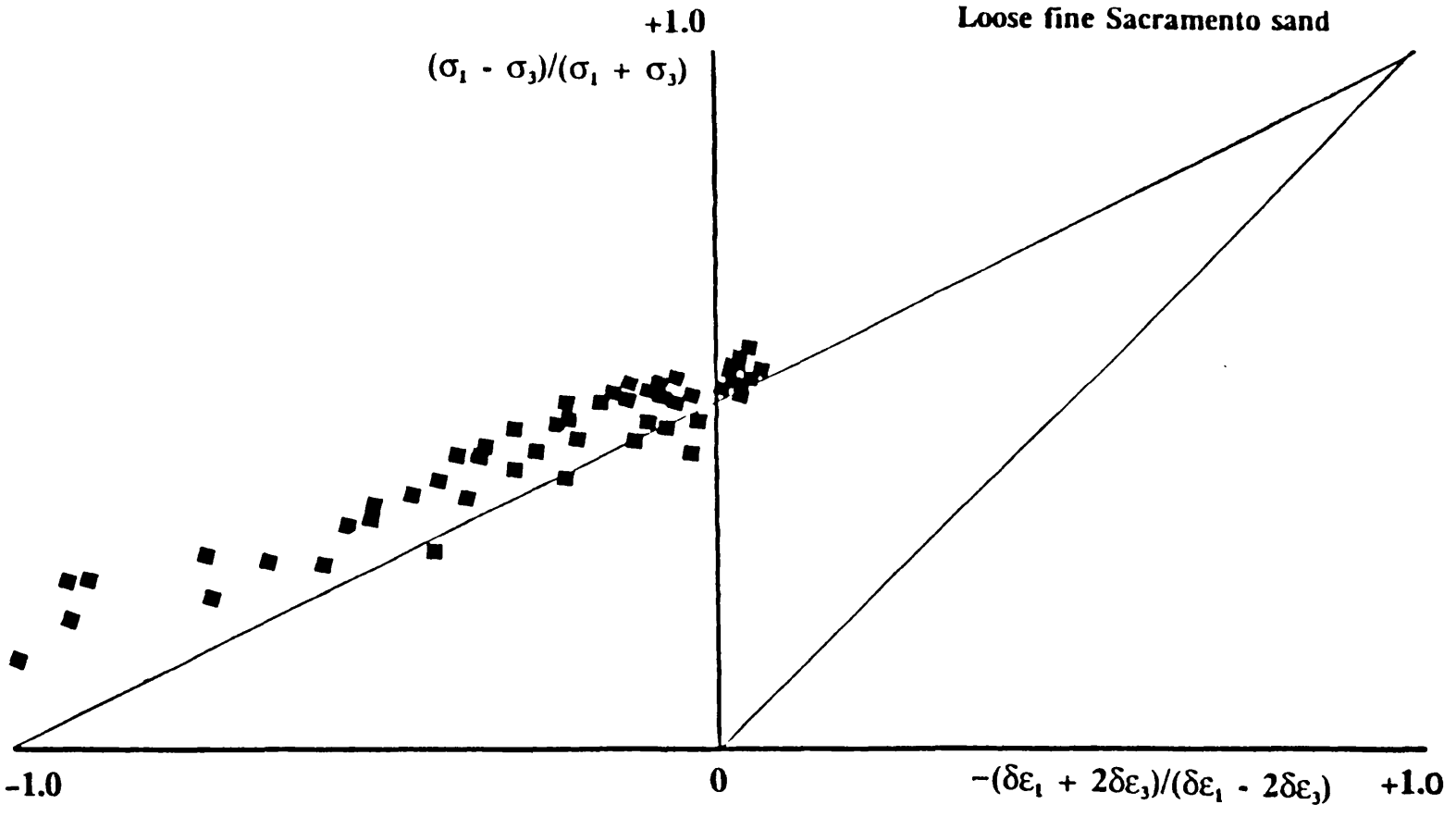
Loose fine Sacramento sand
+1.0
$(\sigma_1 - \sigma_3)/(\sigma_1 + \sigma_3)$
-1.0
0
$-(\delta\varepsilon_1 + 2\delta\varepsilon_3)/(\delta\varepsilon_1 - 2\delta\varepsilon_3)$
+1.0

(b)

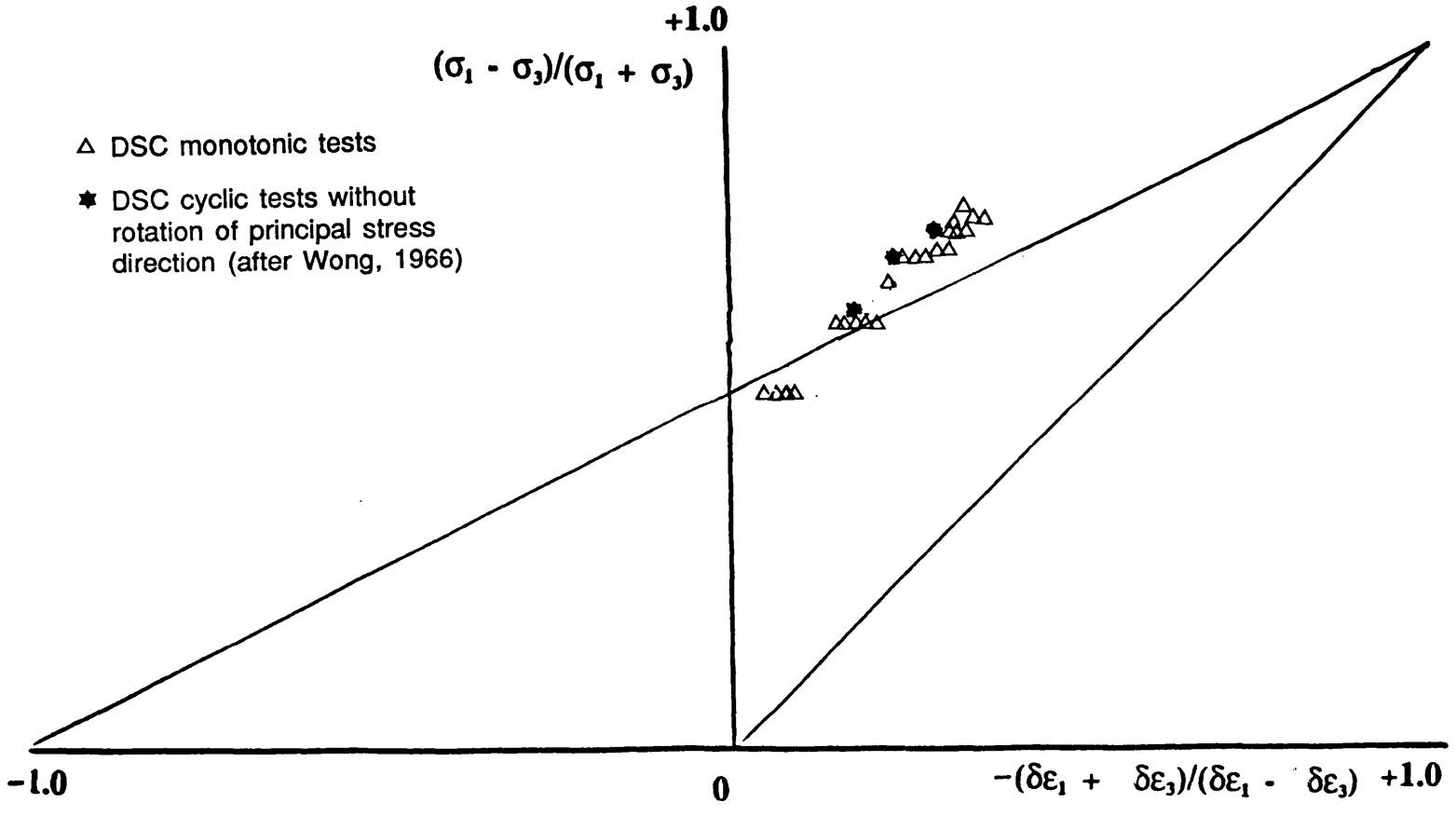

Fig. 8.15 Plane strain tests data with fixed direction of principal stress for Leighton Buzzard sand superimposed on the ideal stress dilatancy relationships.(after Wong, 1986)

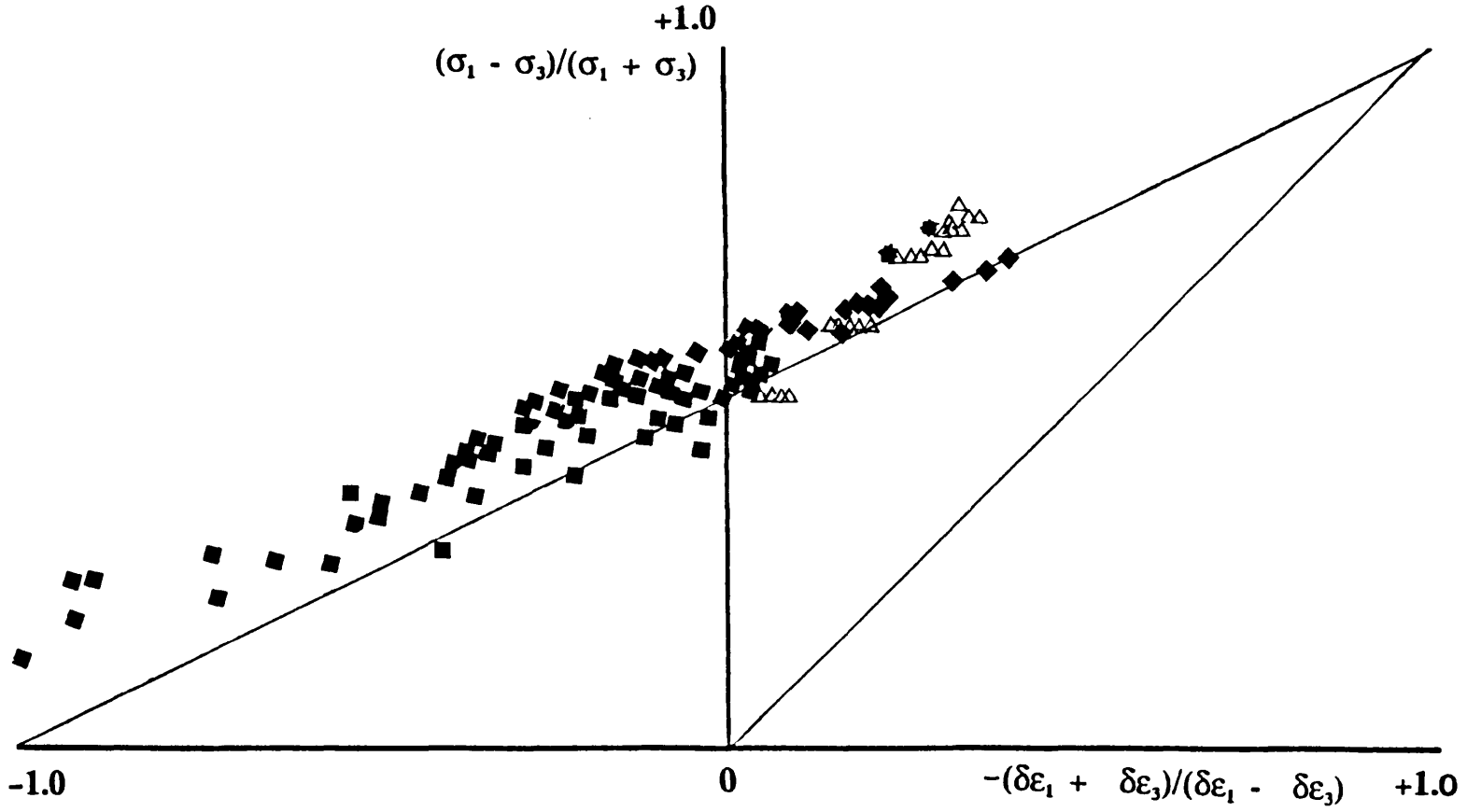

Fig. 8.16 Experimental data from different apparatuses involving fixed direction of principal stress superimposed on the ideal stress dilatancy relationships.

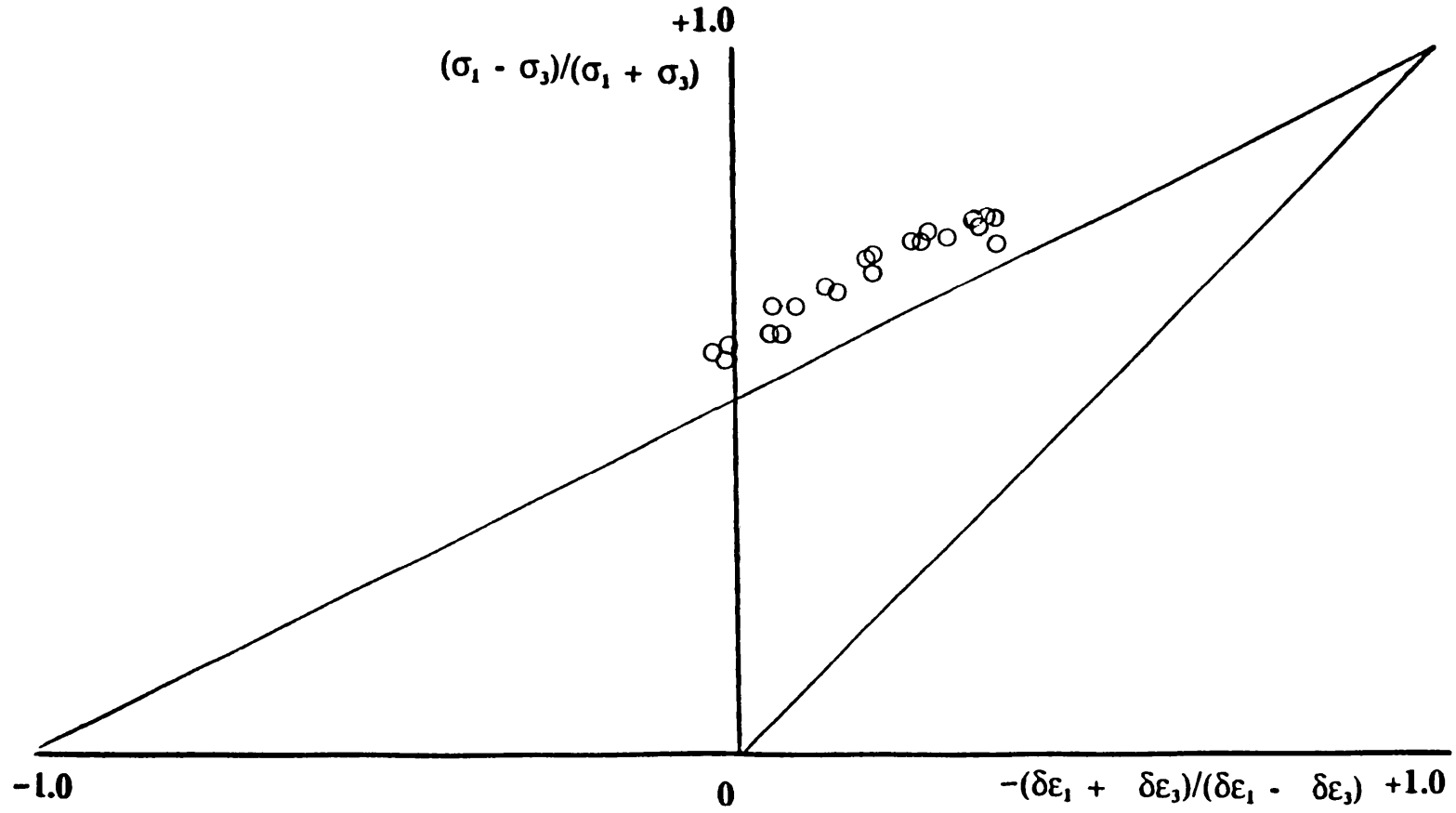

Fig. 8.17 Simple shear experimental data for dense Leighton Buzzard sand superimposed on the ideal stress dilatancy relationships. (after Stroud, 1971)

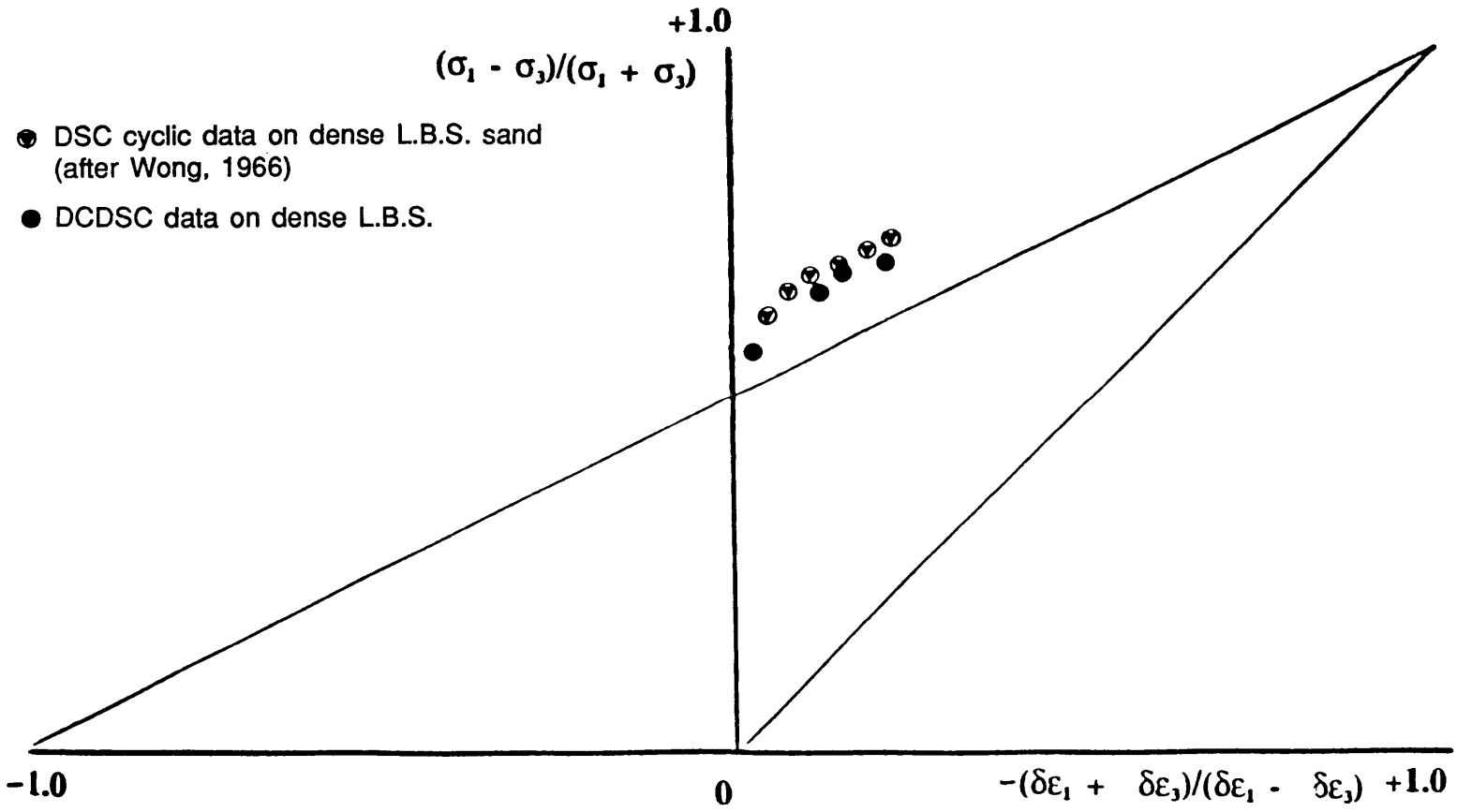

Fig. 8.18 Cyclic data involving continuous rotation of principal stress directions for dense sand tested in the DSC and the DCDSC superimposed on the ideal stress dilatancy relationships.

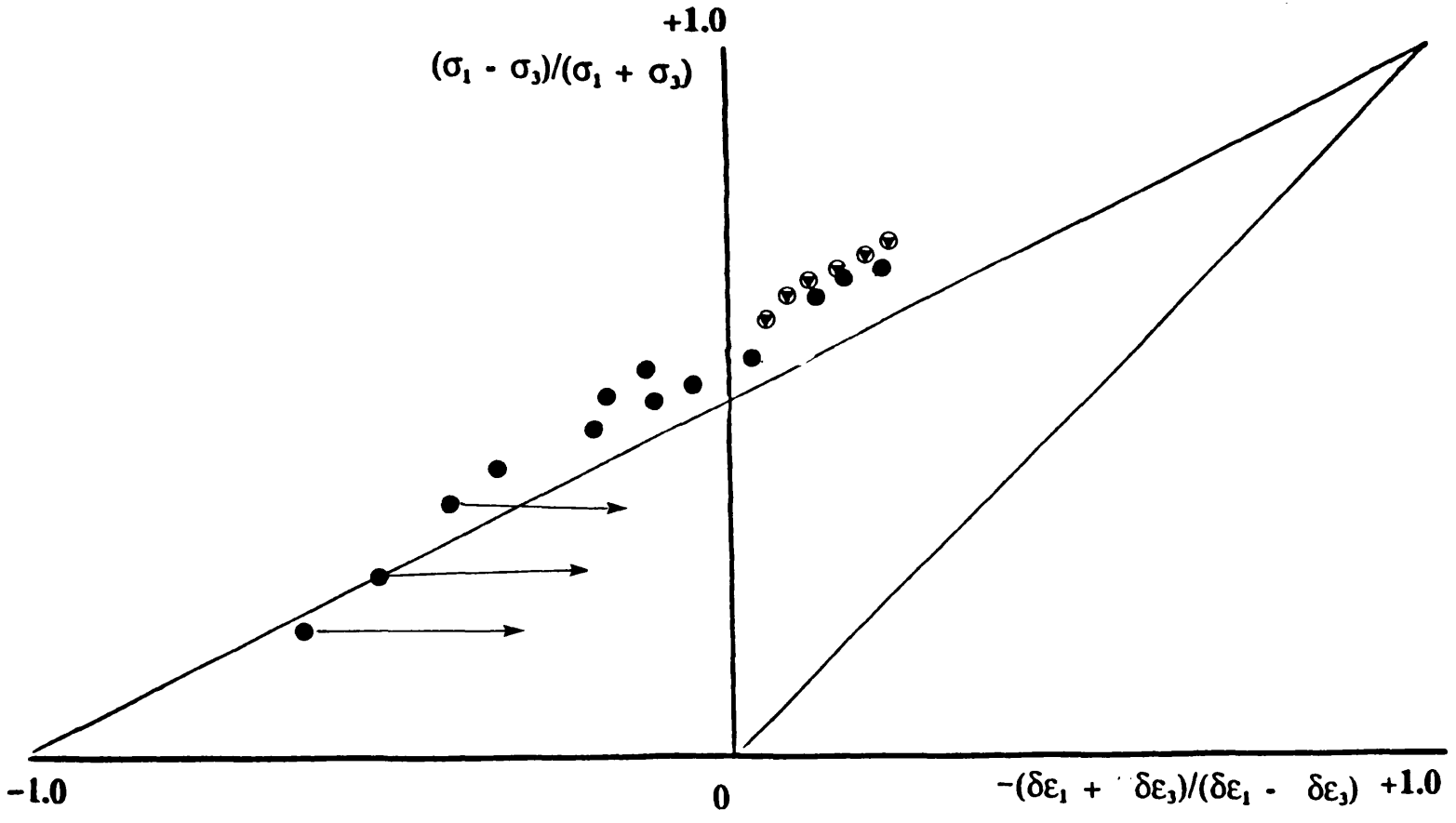

Fig. 8.19 Cyclic data involving continuous rotation of principal stress directions for dense and loose sand tested in the DCDSC superimposed on the ideal stress dilatancy relationships.

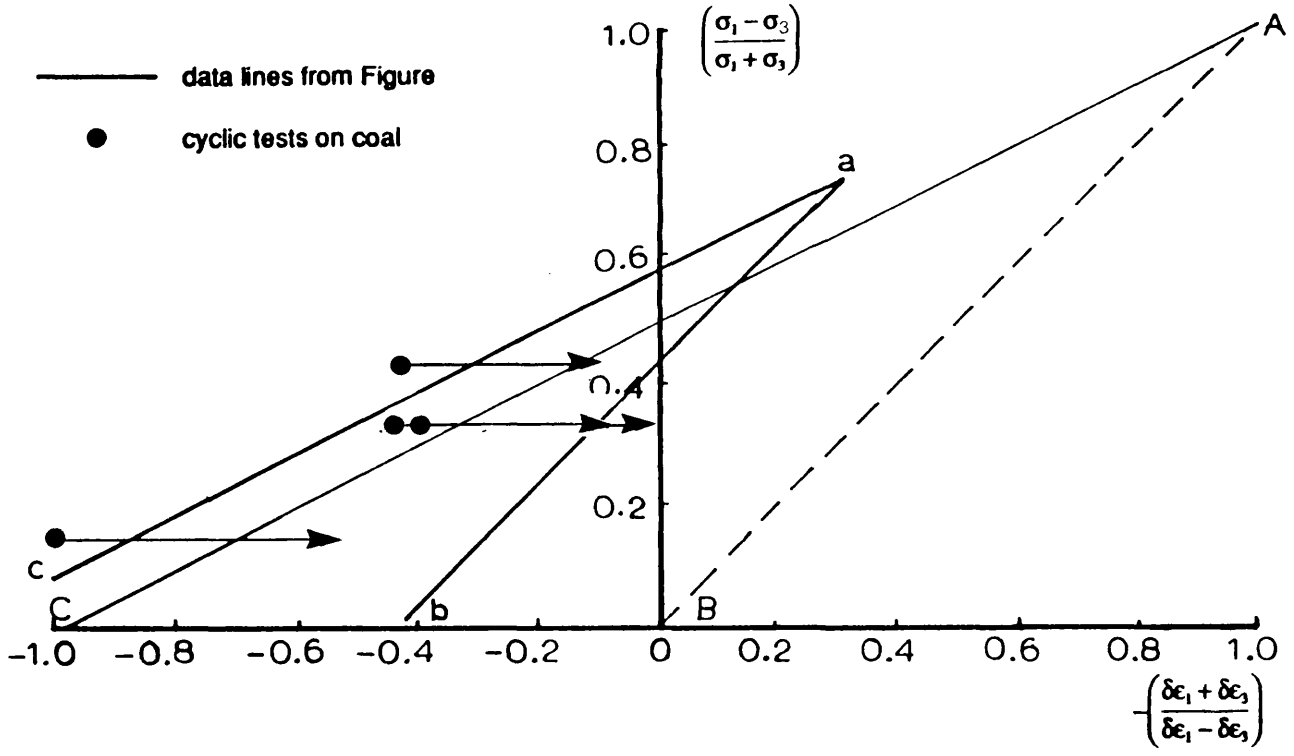

Fig. 8.20 **Cyclic data for damp loose coal superimposed on the ideal stress dilatancy relationships.**

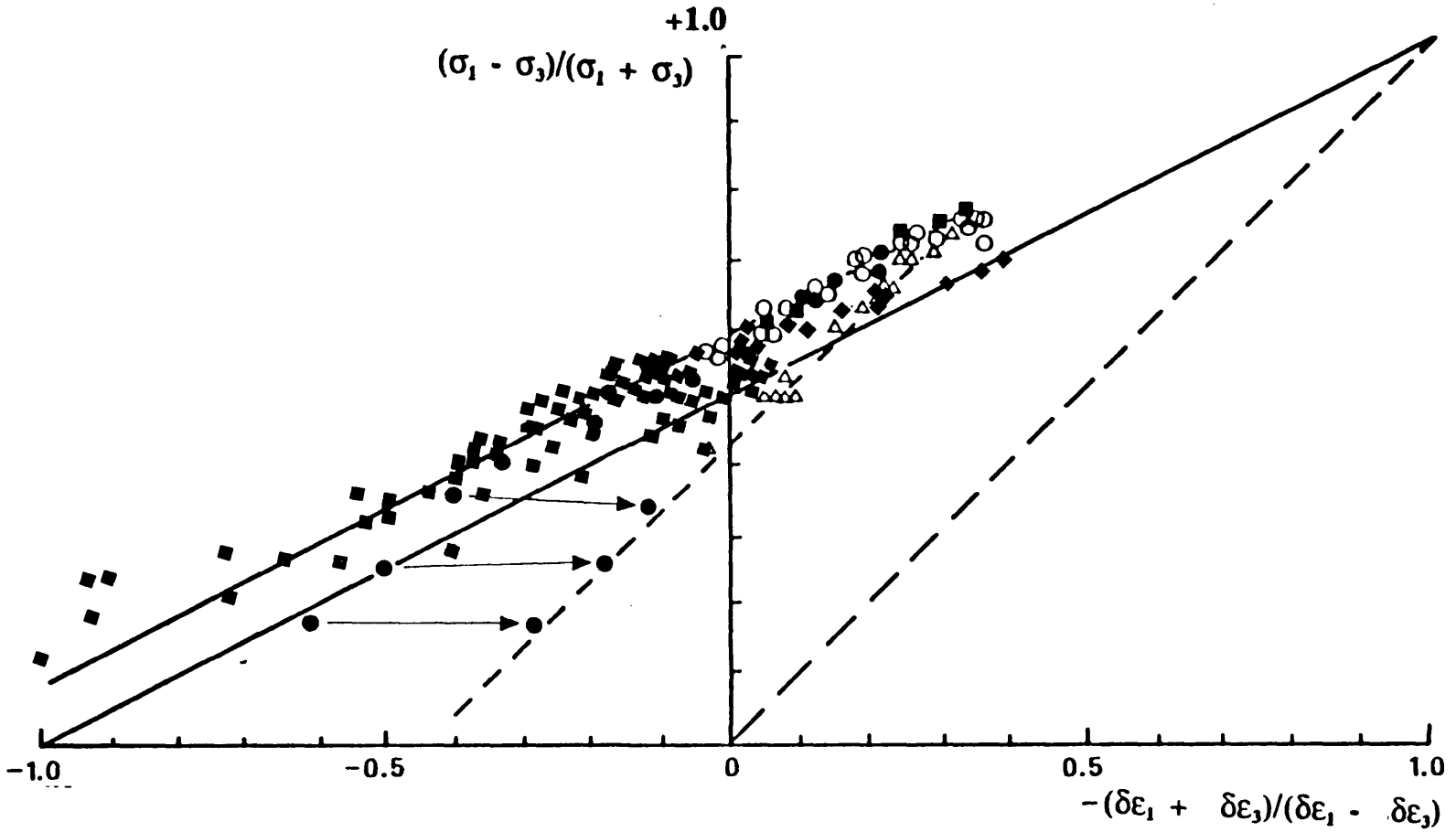

Fig. 8.21 Experimental data from several apparatuses involving fixed and continuous rotation of principal stress directions superimposed on the ideal stress dilatancy relationships.

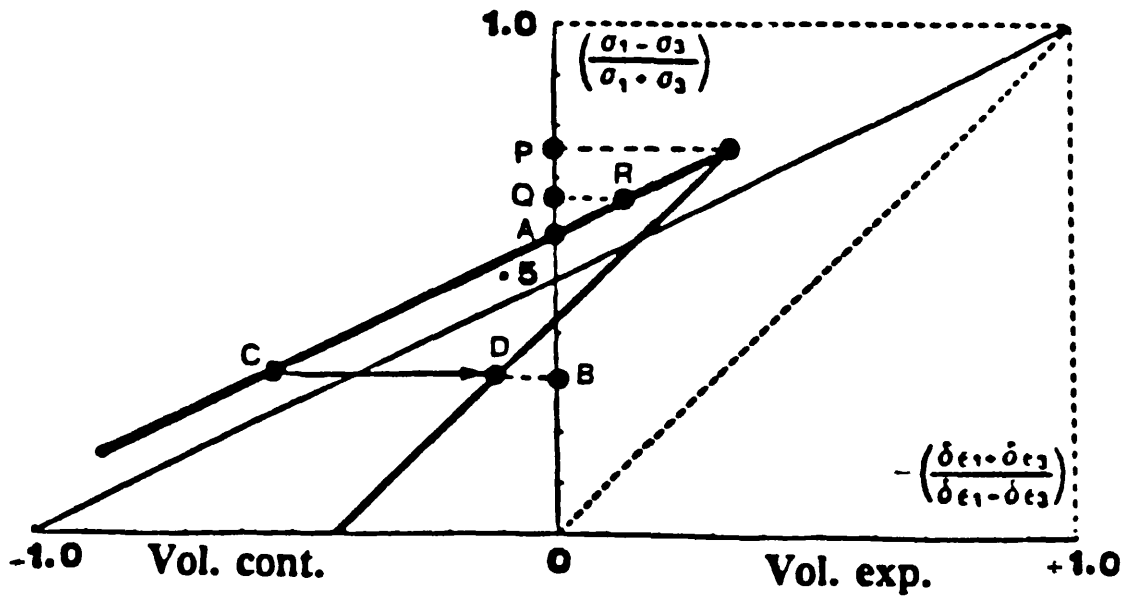

Fig. 8.22 Example of initiation of flow in particulate materials subjected to cyclic loading at different stress ratios.

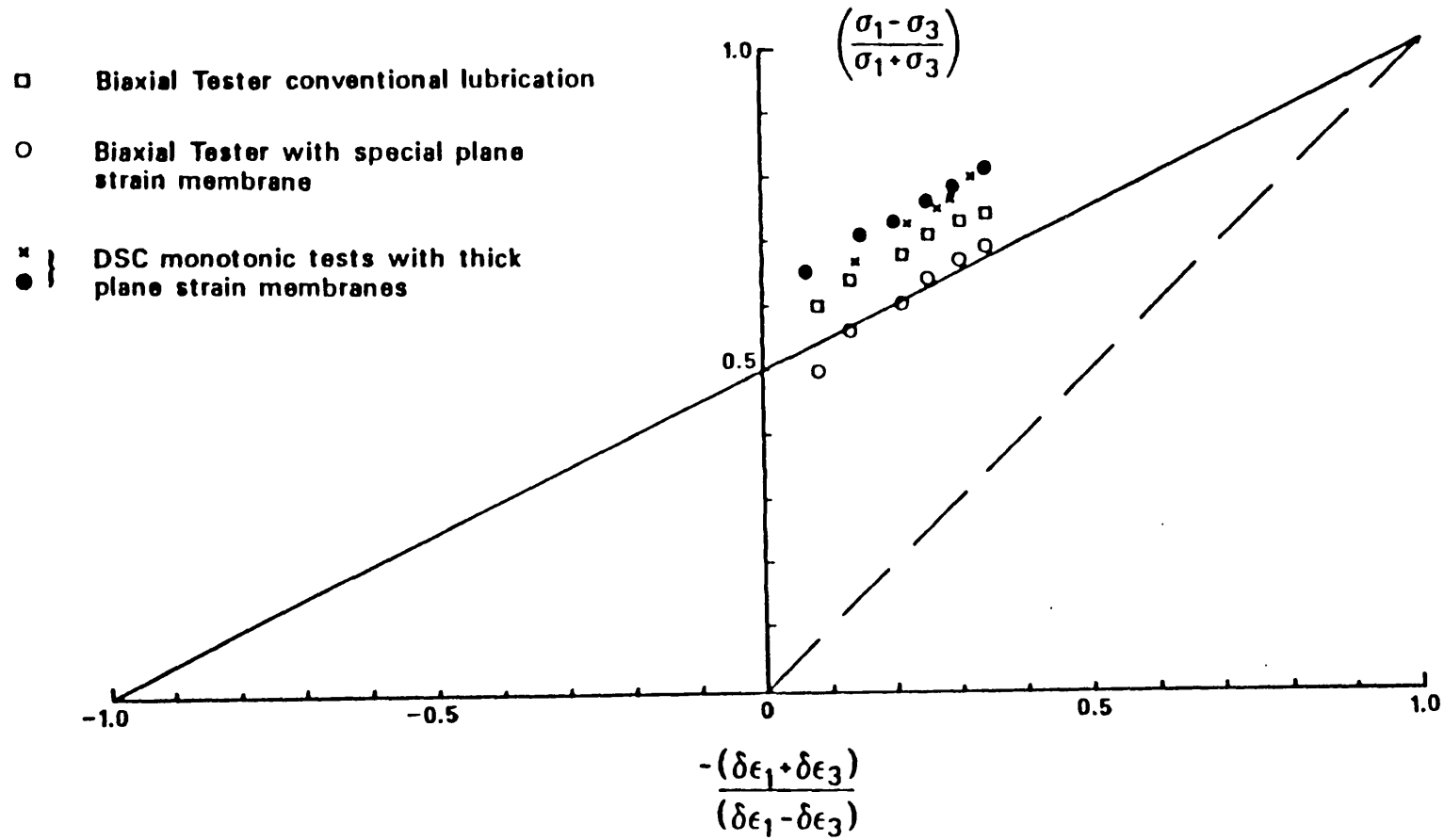

Fig. 8.23 Data from Biaxial Tester tests and the DCDSC with thick membrane Leighton Buzzard sand superimposed on theoretical stress-dilatancy relationships. (after Ogunbekun, 1988)

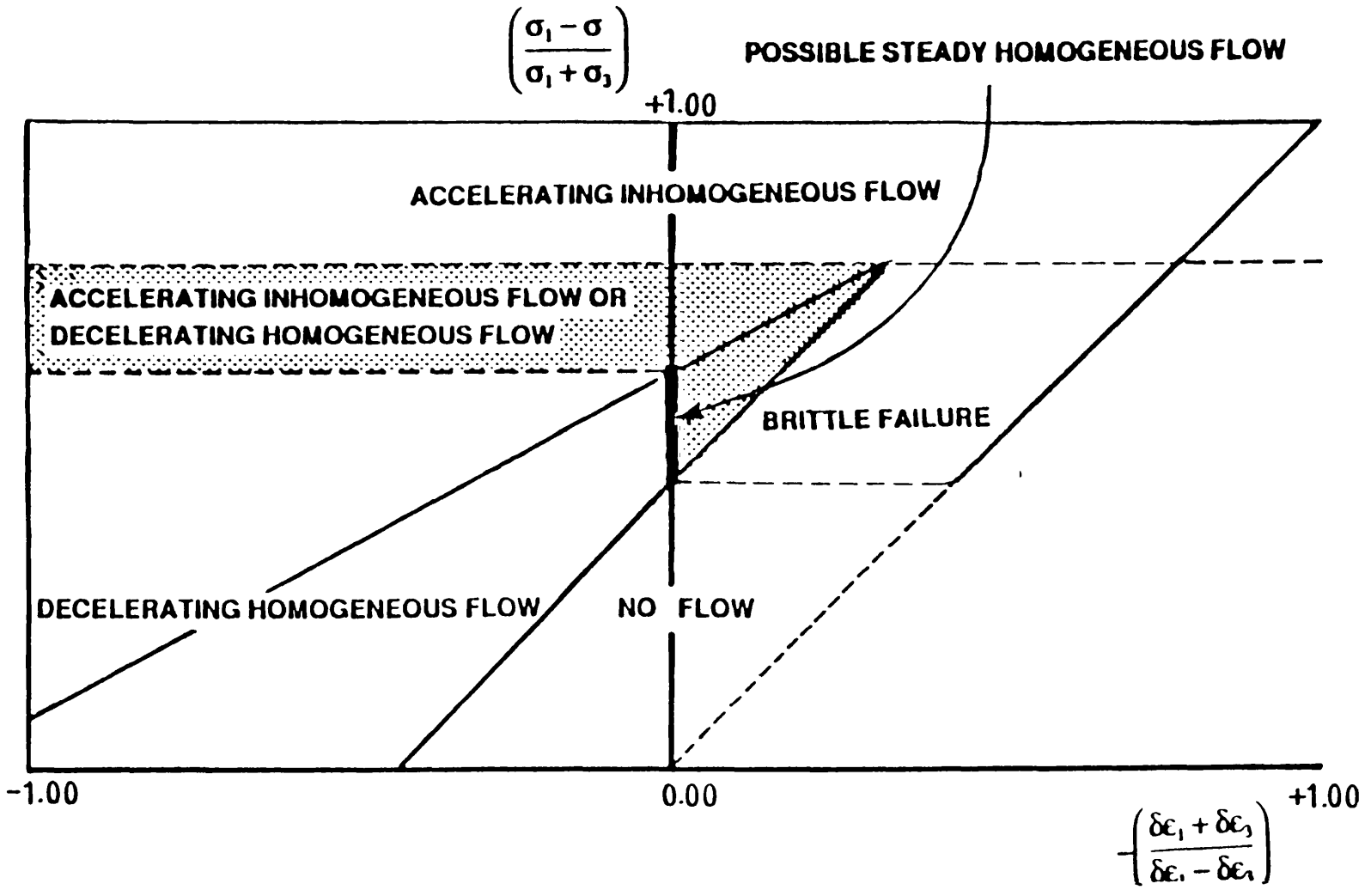

Fig. 8.24 Possible forms of flow associated with stress ratio and dilation rate in particulate materials

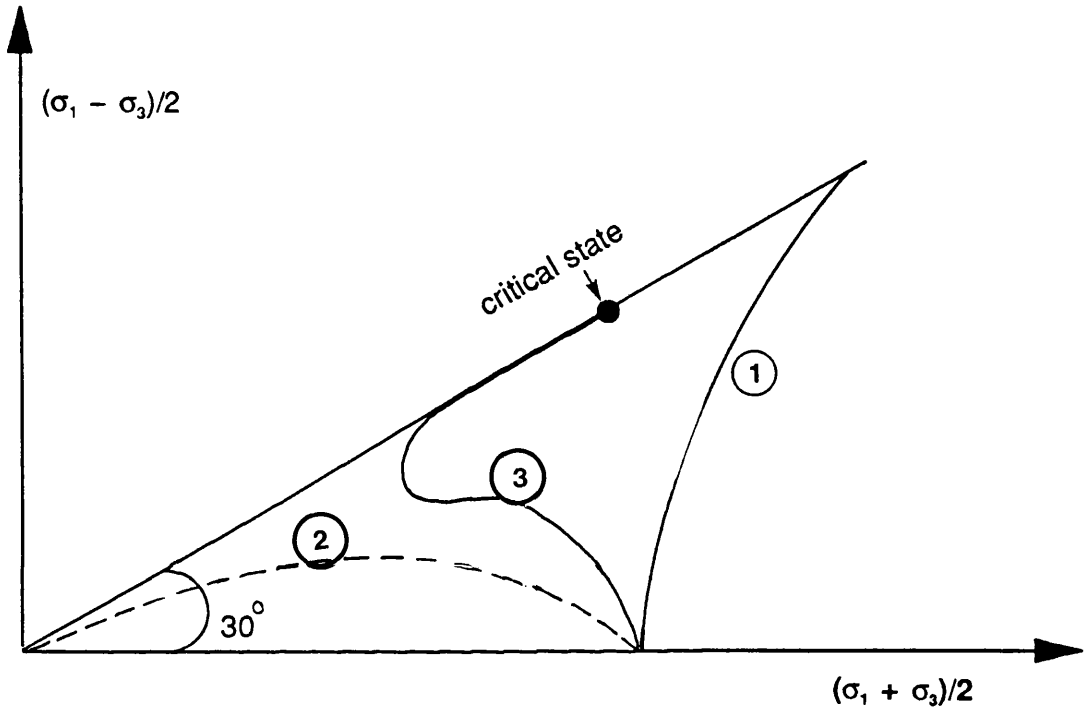

Figure 8.25 Stress paths for sand under drained and undrained conditions

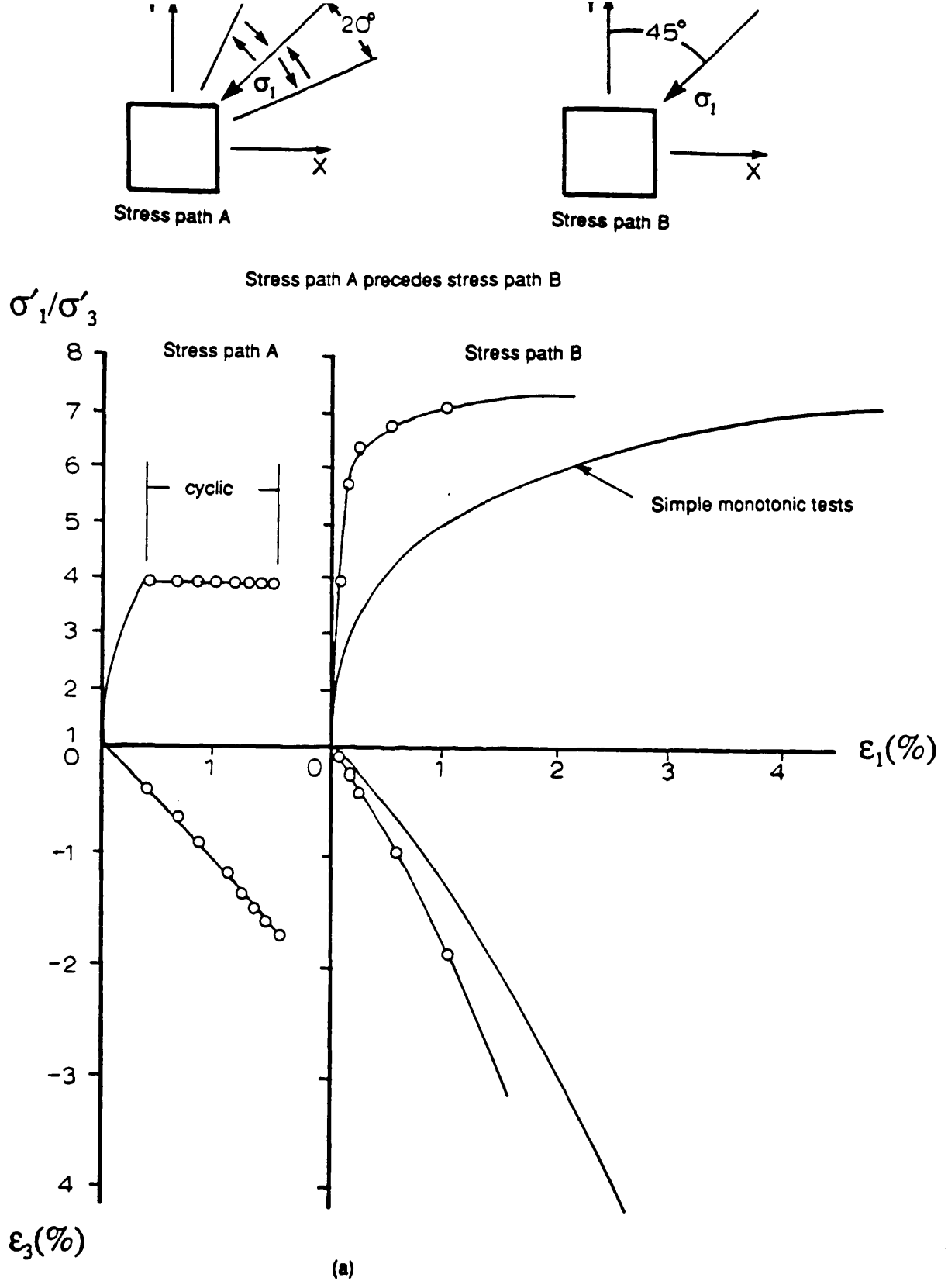

Fig. 8.26 Monotonic stiffness of different materials induced after previous cyclic rotation of principal stress direction, (a) Dense Leighton Buzzard sand, (b) loose Leighton Buzzard sand and (c) loose damp coal.

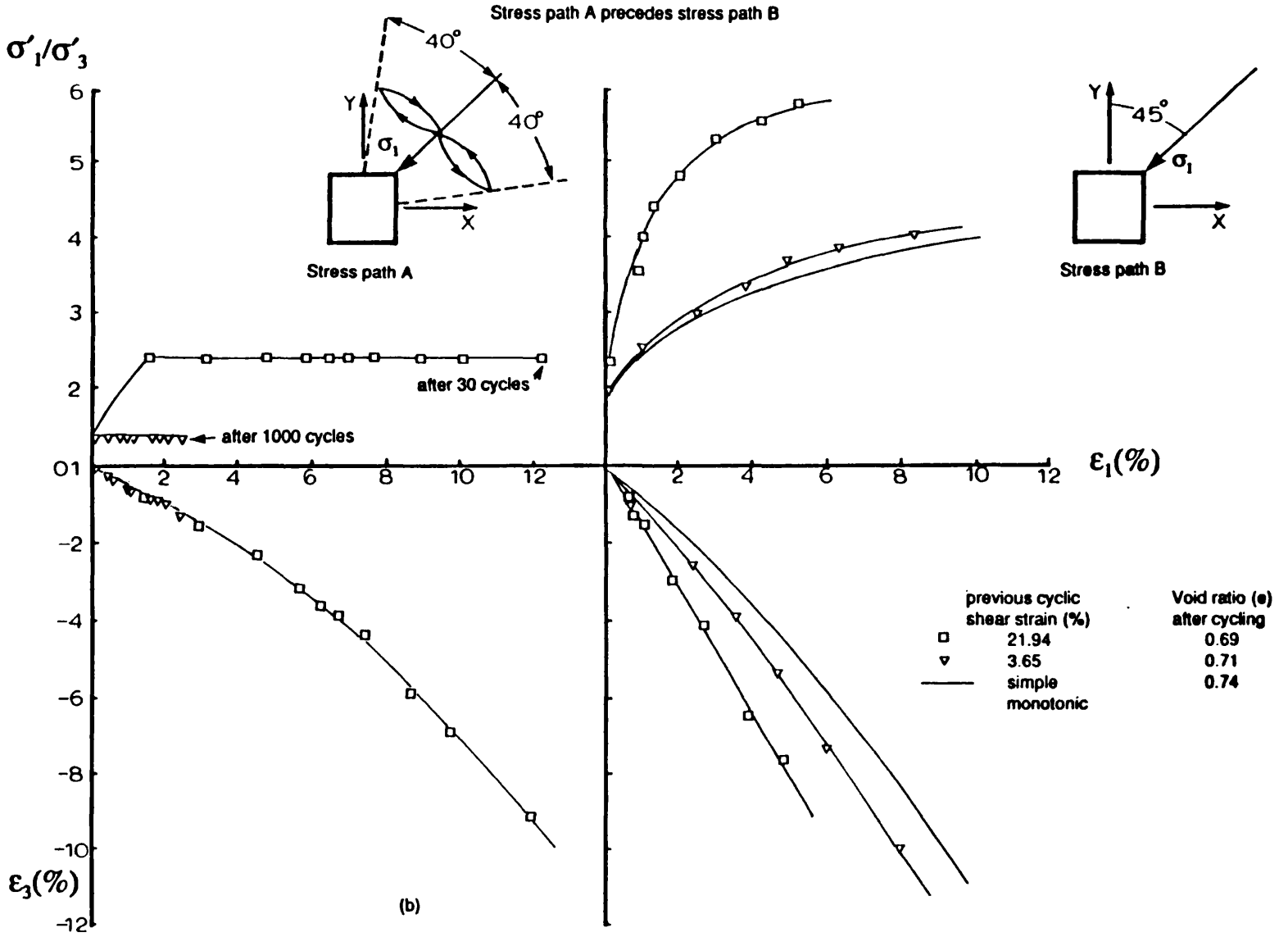
Stress path A precedes stress path B
σ'_1/σ'_3
40°
40°
Y
σ_1
X
Stress path A
Y
45°
σ_1
X
Stress path B
after 30 cycles
after 1000 cycles
ε_1(%)
ε_3(%)
(b)
previous cyclic shear strain (%)
Void ratio (e) after cycling
21.94
0.69
3.65
0.71
simple monotonic
0.74

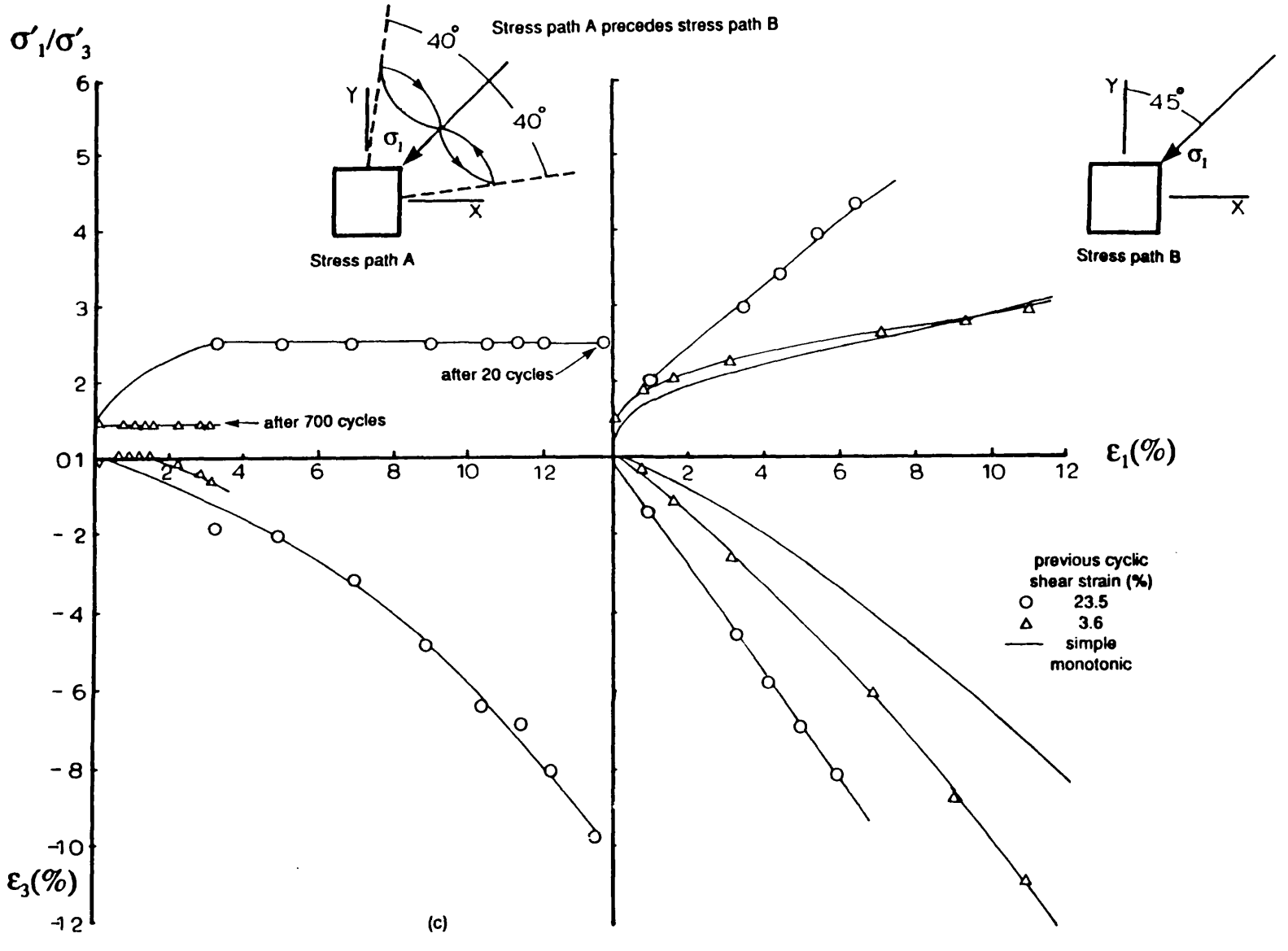
σ'1/σ'3
Stress path A precedes stress path B
40°
40°
Y
σ1
X
Stress path A
Y
45°
σ1
X
Stress path B
after 20 cycles
after 700 cycles
ε1(%)
ε3(%)
previous cyclic shear strain (%)
23.5
3.6
simple monotonic
(c)

CHAPTER 9 CONCLUDING REMARKS

9.1 SUMMARY

9.2 SUGGESTIONS FOR FURTHER RESEARCH

9.2.1 Further Improvement to the DCDSC

9.2.2 Additional work using DCDSC

9.1 SUMMARY

A major factor in geotechnical engineering design concerns the effect of cyclic loading on the foundation material which commonly occurs in nature as a result of the action of wind, waves and earthquakes. This type of loading causes a principal stress rotation of the subsoil structure, with significant influence on the stress-strain properties and induced pore water pressure.

A Directional Shear Cell can achieve simulations of these in-situ stress paths and is capable of controlling both magnitude and direction of principal stresses.

A new type of Directional Shear Cell with an entirely different shear sheet design was developed which avoids hysteresis particularly under cyclic loading and allows tests to be carried out at a constant mean stress level. Higher stress levels could also be achieved. Sample preparation techniques have been improved to provide fully saturated clay samples, and a trimmer device has been constructed to minimize the sample disturbance. A new technique has been developed to measure pore water pressure accurately in the centre of the sample.

The experimental work investigated the stress-strain behaviour of dry Leighton Buzzard sand, damp coal and saturated and nearly kaolinite at low stress levels when subjected to continuous and cyclic rotation of principal stress directions.

The results of monotonic tests on dense Leighton Buzzard sand at σ_3=30 kPa compared with that of σ_3 =14 kPa show that there was no change in soil behaviour.

The angle of friction for damp coal was found to be similar to that of loose Leighton Buzzard sand, i.e ϕ_f =32°, in spite of dampness and different grading and particle shape and strength.

When testing nearly saturated kaolin multiple small Coulomb slips were observed at failure.

The results of cyclic principal stress rotation tests on damp coal and saturated kaolinite show parallels with dry sand results in that large strains occur at low applied stress ratios with no rupture layers, but the underlying mechanism is different for nearly saturated Kaolin as the failure mechanism may be a tension crack.

Comparing the results of two different cyclic stress paths, i.e. constant mean stress level while cycling the boundary shear stresses and varying mean stress level while the boundary shear stress is constant indicates that the principal stress rotation is the governing factor and the stress level variation effect is secondary.

It has been found that shear under cyclic rotation of principal stress directions has a profound effect on subsequent shear behaviour under monotonic loading. Large increases in stiffness, dilation rate and strength/brittleness are achieved by strain under cyclic principal stress rotation without significant changes in voids ratio; loose sand becomes nearly as strong as dense sand and dense sand becomes brittle. The behaviour of fully saturated kaolin has yet to be investigated.

Data from radiographs for the central plane of strain of three types of tests under different boundary plane strain constraints indicated that there were three differentiated groups of results and three different peak shear strengths depending on the level of restraint on the plane strain surfaces. A low value, an intermediate value and an upper value, all for samples with the same initial voids ratio even though the measured strains were unchanged (Figure 4.31). However, the angle of friction associated with the intermediate level of constraint (ϕ_f =48.7°) corresponded to an angle of friction from independent results from active wall and infinite slope stability experiments. It appears that there exists a natural level of lateral restraint in the material itself as a result of inherent inhomogeneities in deformation and contact distribution forces.

A new mechanism has been proposed for the stress-dilatancy behaviour of slowly and steadily flowing particles. It is suggested that internal dissipation of energy is controlled by frequently repeated releases of elastic energy. This energy is stored in transient columns formed from particles with contact normals aligned close to the major principal stress direction. This simple proposition fits data from a surprising range of imposed flow conditions. It includes both dry and damp materials of relatively high permeability. In addition, if a material of this type has a sufficiently high density to be potentially dilatant, inhomogeneous unsteady deformation and rupture layers are likely. This tendency can be suppressed by continuous rotation of principal stress. Comparison of experimental data with the two limiting stress-dilatancy relationships, show parallelness but with some offset.

The results of nearly saturated Kaolinite (around 10% air voids) suggested that flow in this nearly saturated material is likely to lead to discontinuities. These may be

tension cracks as well as the more readily anticipated shear rupture layers. This tendency to inhomogeneous deformation cannot be suppressed by the rotation of principal stress direction on partially saturated soil. When materials of similar low permeability are fully saturated with a pore liquid, the requirement of constant volume will maintain homogeneous deformation through large changes in pore liquid pressure provided no gas is generated during the shearing process.

Sand and coal that have been subject to cyclic loading involving principal stress rotation show increased stiffness on subsequent monotonic loading and an eventual failure plane associated with Coulomb.

9.2 SUGGESTIONS FOR FURTHER RESEARCH

The present work has attempted to investigate experimentally the behaviour of three particulate materials; sand, coal and kaolinite. A full range of dampness from dry to full saturation was considered subject to a wide range of monotonic and cyclic loading conditions.

9.2.1 Further Improvement to the DCDSC

Further improvement to the DCDSC could include:

(a) Higher stress level capability.
(b) No limitation on the amplitude of rotation.
(c) Automatic alignment and adjustment of boundary shear and normal stresses in the new design.
(d) Automatic control of intermediate principal stress
(e) The ability to impose different boundary constraints.

9.2.2 Additional work using the DCDSC

Only three materials were tested; sand coal and kaolinite with emphasises being placed on sand. Both coal and kaolinite require more research.

A miniature pore water pressure cell has been developed for fully saturated samples tested undrained. This will be of value for further work in this direction.

The effects of boundary constraints on the behaviour of Leighton Buzzard sand was investigated, these effects could be studied with finer particulate materials such as

clay and the effects of principal stress rotation on mixture of clay and sand could be investigated.

In this investigation only isotropic and homogeneous samples were studied. The significance of inhomogeneity and inherent anisotropy of natural soils has long been recognised and should be investigated.

Without accurate strain measurement within the sample, it is impossible to verify model predictions with sufficient precision. The existing X-ray techniques provide for principal strain measurements above 0.1%, and photography is sufficient for second-grade research purposes. At present, there are no satisfactory techniques to cover strains less than 0.1%, although good techniques do exist using mechanical/electrical devices for other apparatuses (Burland and Symes 1982) such as the Hollow Cylinder and the Triaxial apparatuses. As the measurement of the shear modulus at low strain is extremely important to engineers, it is essential to develop a small strain measurement technique suitable for the DSC.

APPENDIX 1

3.12 Thin metal corner in place

3.13 A micrograph of kaolinite

3.14 Preparation box used to form kaolin into a cubical shape

3.15 Former used to make rubber membrane for remoulded kaolin samples

3.16 (a) Stretching box used to expand the rubber membrane and (b) fine sand glued to the inner surface of the rubber membrane

3.17 Rowe cell in full assembly

3.18 The sequence in which the consolidated cake in the Rowe cell was cut

3.19 The consolidation stress versus moisture content for speswhite kaolin using conventional Oedometer

3.20 Mixing and de-airing procedure for speswhite kaolinite; (a) assembly of the equipment to be used to mix and de-air the slurry, (b) a schematic view of the rotary bearing used for vacuum sealing the centre shaft of the mixing chamber, (c) spraying the kaolin slurry into a thick glass container and (d) the glass container placed on the shaking table for de-airing

3.21 (a) Arrangement of modified oedometers and (b) a schematic view of modified oedometer

3.22 The principal features of a consolidation cell

3.23 Part of the sample pushed out of the cell

3.24 The trimming device used for fully saturated samples

3.25 Trimming procedure to provide a 100 x 100 x 100mm fully saturated kaolin sample; (a) the kaolin cake is placed on the trimming device, (b) method to prevent the cut slice from resticking, (c) lead shot placed onto the x-y plane, (d) positioning the second slice on the first cut, (e) four faces of the sample is cut, (f) second rotating base used to rotate the sample vertically, (g) placing the sample on the second rotating base and (h) a fully cut sample of kaolin

3.26 Former for making rubber membrane used to conduct fully saturated samples

3.27 (a) Needle guide prior to being pushed into the tube located in the central part of membrane and (b) needle guide in place

3.28 (a) Stretching box with lining porous material in place and (b) uniformly expanded membrane in the stretching box

3.29 Drainage system for fully saturated kaolinite samples

3.30 Stretching box guiding device

3.31 Placing the sample into the rubber membrane and sealing procedure; (a)

encasing the sample into the rubber membrane, (b) pulling the guiding device out, (c) coating the edges with adhesive and (d) sealing the fully saturated sample

3.32 A completed sample in rubber membrane

3.33 Setting up procedure for fully saturated kaolin sample in the DCDSC; (a) bottom plane strain platen, (b) sample placed on the σ_2 bag, (c) and (d) centralising the sample using the split perspex plate, (e) placing the shear sheets around the sample, (f) normal pressure bags and shear sheets in place, (g) split platen locked in position and (h) complete set up with the centrally inserted probe in position

4.1 The experimental arrangement for shear sheet calibration

4.2 The effects of different volumes of water in a normal pressure bag used to calibrate the shear sheets

4.3 The method used to calibrate the shear piston transducers

4.4 The theoretical and experimental results of calibration of the shear sheets

4.5 The major principal stress direction and stress path in monotonic shear tests

4.6 Correction for angular distortion of a deformed sample during directional shear testing

4.7 Surface failure in the boundaries of dense samples of Leighton Buzzard sand sheared monotonically at σ_3= 60 kPa.

4.8 Stress-strain and deformation response of dense samples of Leighton Buzzard sand monotonically sheared in the DCDSC with sufficient lubrication on plane strain surfaces at σ_3=14 kPa

4.9 Stress-strain and deformation response of loose sample of Leighton Buzzard sand monotonically in the DCDSC with sufficient lubrication on the plane strain surface at σ_3=14 kPa

4.10 Effects of unstressed shear sheets surrounding the sample on stress-strain behaviour of dense sand in the DCDSC at σ_3=14 kPa and ψ=90

4.11 Example of strain distribution within the dense sample of Leighton Buzzard sand sheared monotonically in the DCDSC which was confined with unstressed shear sheets at σ_3= 14 kPa

4.12 Comparison of stress-strain deformation behaviour of dense sand samples monotonically loaded in the DCDSC and the earlier version of DSC at σ_3=14kPa

4.13 Comparison of stress-strain deformation behaviour of loose sand samples monotonically loaded in the DCDSC and the earlier version of DSC at σ_3=14kPa

4.14 Stress-strain and deformation response of dense sample of Leighton Buzzard

at σ_3 =14 kPa

6.11 Comparison of stress-strain response of simple monotonic test and subsequent monotonic tests after continuous and cyclic rotation of principal stress direction in initially loose samples of damp coal

6.12 A comparison of two monotonic tests of loose dry sand and loose damp coal samples tested in the DCDSC at identical stress levels of σ_3 =14 kPa

6.13 Sieve analyses for the damp coal prior to testing, after monotonic loading and after being subjected to cyclic rotation of principal stress direction.

6.14 Remaining bedding planes after cyclic rotation of principal stress direction

7.1 One dimensional consolidation tests on kaolinite

7.2 Stress-strain response of nearly saturated kaolinite samples sheared monotonically in the DSC at σ_3= 14kPa

7.3 Volumetric change behaviour of nearly saturated kaolinite sampls sheared in the DSC

7.4 (a) and (b) Typical examples of strain distribution within the sample of the nearly saturated kaolinite sheared monotonically in the DSC

7.5 Comparison of strength-deformation response of nearly saturated samples measured in three different zones of deformation

7.6 (a) Example of strain distribution on the middle of the nearly saturated kaolinite sample sheared monotonically in the DSC and (b) example of strain distribution near the plane strain surface of the nearly saturated kaolinite sample sheared monotonically in the DSC

7.7 Coincidence of major principal stress and strain increment directions in a nearly saturated sample of kaolinite sheared monotonically in the DSC

7.8 Deviation between axes of principal stress and strain increment in the nearly saturated samples of kaolinite sheared monotonically in the DSC

7.9 Stress-strain response of nearly saturated kaolinite samples sheared monotonically in the DSC at σ_3= 14kPa without the shear sheets around the sample with ψ =90°.

7.10 Volumetric behaviour of two nearly saturated samples of kaolinite sheared monotonically at ψ =90° without the shear sheets.

7.11 Asymmetric Coulomb slips in nearly saturated kaolinite sample sheared in plane strain in the DSC with ψ =45°

7.12 The development of shear strain during continuous and cyclic rotation of principal stress direction on nearly saturated kaolinite sample tested in the DCDSC.

stress direction.

7.28 No ruptures were observed in fully saturated kaolinite sample consolidated in the modified oedometer when subjected to continuous and cyclic rotation of principal stress direction.

7.29 (a) Effect of speed of testing on effective stress path observed in undrained triaxial test on normally consolidated clay (after Richardson and Whitman, 1963), (b) stress path computed by finite element analyses for three elements within a triaxial sample with smooth ends during a fast drained compression test. (after Wood, 1981)

7.30 A schematic view of probe used by Germaine to measure the pore water pressure at the centre of the DSC sample (after Germaine, 1982)

7.31 A schematic view of the probe and the miniature transducer developed to measure the pore water pressure in the centre of the DCDSC samples

7.32 Comparison between the existed and developed pore water pressure measuring devices

7.33 Calibration curve for a Druck transducer.

7.34 The miniature probe was inserted and fixed into position at the base of a triaxial chamber

7.35 (a) The results of response time tests using the developed miniature probe and (b) the Skempton's B values

7.36 Setting up the developed pore water pressure measuring probe on the top platen of the DCDSC

7.37 Stress-strain response of two fully saturated kaolinite samples sheared monotonically very slowly in the DCDSC at σ_3= 14kPa

7.38 Volumetric behaviour of two fully saturated samples of kaolinite sheared monotonically very slowly with pore water pressure measurements in the DCDSC at σ_3 =14kPa

7.39 Effective stress paths (ESP_s) for two fully saturated samples sheared monotonically at a very slow rate in the DCDSC at σ_3 =14 kPa

7.40 Normalised average effective stress paths for tests on BBC (OCR=4) (after o' Neill, 1985)

7.41 A Mohr circle showing equal opportunity for tensile and Coulomb failure to occur

7.42 (a) Comparison of constant volume and undrained test results and (b) comparison of constant volume and undrained test results (after, Dyvik, Berre, Lacasse and Raadim; 1987)

7.43 Undrained and constant volume triaxial tests on Drammen clay (after Berre,

APPENDIX 2

LIST OF TABLES

APPENDIX III

LIST OF SYMBOLS

R	Principal stress ratio (σ_1/σ_3)
R_f	Principal stress ratio at failure
b	Intermediate principal stress ratio $[(\sigma_2 - \sigma_3)/(\sigma_1 - \sigma_3)]$
e	Voids ratio
e_c	Voids ratio at the end of cyclic loading
K_o	Ratio between horizontal and vertical stresses in a 1-Dimensional consolidation situation
s	$(\sigma_1 + \sigma_3)/2$
t	$(\sigma_1 - \sigma_3)/2$
x,y,z	Orthogonal cartesian axes
$'$	Effective stress
σ	Normal stress
σ_a,σ_b	Applied boundary normal stresses
σ_x,σ_y	Normal stresses in x and y direction
$\sigma_1,\sigma_2,\sigma_3$	Major, intermediate and minor principal stresses
τ	Shear stress
τ_a,τ_b	Applied boundary shear stresses
τ_{xy},τ_{yx}	Shear stress in x and y direction
Δ	Deviation between axes of principal stress and strain increment
α,β	Angle of distortion
δ	Small increment of ...
$\varepsilon_x,\varepsilon_y$	Normal strains in x and y direction
ε_{xy}	Shear strain
$\varepsilon_1,\varepsilon_2,\varepsilon_3$	Major, intermediate and minor principal strains
$\varepsilon_{1c},\varepsilon_{3c}$	Major and minor principal strains at the end of cyclic loading
$\varepsilon_{1f},\varepsilon_{3f}$	Major and minor principal strains at failure
γ	Shear strain $(\varepsilon_1 - \varepsilon_3)$

γ_{max}	Maximum shear strain (ε1 - ε3)
γ_c	Shear strain at the end of cyclic loading
ε_v	Volumetric strain ($\varepsilon_1 + \varepsilon_2 + \varepsilon_3$) ($\varepsilon_2$=0 for p.strain)
ε_{vc}	Volumetric strain at the end of cyclic loading
ε_{vf}	Volumetric strain at failure
θ	Amplitude of cyclic rotation
ξ	Direction of major principal strain increment
ϕ'	Angle of friction [Sin^{-1} $\{(\sigma_1 - \sigma_3)/(\sigma_1 + \sigma_3)\}$]
ϕ'_m	Mobilised angle of friction
ϕ'_f	Angle of friction at failure
ϕ_μ	Effective interparticle angle of friction
ν_{13}	Angle of dilation in plane strain [= Sin^{-1} $\{(\delta\varepsilon_1 + \delta\varepsilon_3)/(\delta\varepsilon_1 - \delta\varepsilon_3)\}$]
ν_{13c}	Angle of dilation at the end of cyclic loading
ν_{13f}	Angle of dilation just before failure
θ	Amplitude of cyclic rotation
ψ	Direction of major principal stress
ψ_a	Direction of major principal stress; first shear
ψ_b	Direction of major principal stress; second shear
OCR	Over consolidation ratio
p	$(\sigma_1+\sigma_2+\sigma_3)/3$
q	Deviatoric stress $(\sigma_1-\sigma_3)$
B	Skempton's pore pressure parameter

REFERENCES

Airey, D.W. (1987), "Some observations on the interpretation of shear box results", Report No. CUED/D-SOILS/TR 196, University of Cambridge.

Alberro, J.A. and Santoyo, E.Y. (1973), "Long term behaviour of Mexico clay", Proc. 8th Int. Conf. on Soil Mechanic. Found. Eng., Moscow, Vol.1, pp.1-9.

Andersen, K.H., (1975), "Research project repeated loading on clay", Progress Report 4, Report 74037-1, Norwegian Geotechnical Institute, Oslo.

Andersen, K.H., Brown, S.F., Foss, I. Pool, J.H. and Rosenbrand, W.F. (1976), "Effect of cyclic loading on clay behaviour", Design and Construction of Off-shore structures, Institute of Civil Engineers, London, pp.75-79.

Arthur, J.R.F., Koenders, M.A. and Wong, R.K.S. (1986), 'Anisotropy in particle contacts associated with shearing in granular media', Acta Mechanica 64, pp. 19-29.

Arthur, J.R.F. and Menzies, B. (1972), "Inherent anisotropy in sand", Geotechnique, Vol.22, No.1, pp.115-128.

Arthur, J.R.F., Dunstan, T. and Enstad, G.G. (1985), "Determination of the flow function by means of a cubic plane strain tester", Int. Jour. Bulk Storage in Silos, Vol.1, No.2, pp.7--10.

Arthur, J.R.F. and Phillips, A.B. (1975), " Homogeneous and layered sand in triaxial compression", Geotechnique, Vol.25, No.4, pp.799-815.

Arthur, J.R.F. (1977), "Industrial radiography in soil mechanics research", British Journal of Non-Destructive Testing, Vol.19, No.1, pp.9-13.

Arthur, J.R.F., Dunstan, T. and Enstad, G.G. (1985), "Determination of the flow function by means of a cubic plane strain tester", Int. Jour. Bulk Storage in Silos, Vol.1, No.2, pp.7-10.

Arthur, J.R.F. (1988), "Cubical devices, versatility and constraint", Proc. Sym. on Advanced Triaxial Testing of Soil and Rock, ASTM, STP 977, pp. 743-765.

Arthur, J.R.F. (1988), "Effective development of the advanced directional shear cell at Waterways Experimental Station", U.S. Army European Res.Off., Contract DAJA-87-C-0030, Final Report, unlimited release.

Arthur, J.R.F. and Assadi, A. (1977), "Ruptured sand sheared in plane strain", Proc. 9th Int. Conf. SMFE, Tokyo, Vol.1, pp.19-22

Arthur, J.R.F., Chua, K.S. and Dunstan, T. (1977), "Induced anisotropy in sand", Geotechnique, Vol.27, No.1, pp.13-30.

Arthur, J.R.F., Dunstan, T., Dalili, A., Ogunbekun, O. and Pulsford, J. (1987), "The strength of dense sand sheared in plane strain at low stress level", Draft of Int. Rpt., Civ. Eng. Dept., University College, London.

Arthur, J.R.F., Cutler, F., Dunstan, T., Ford, J., Leavell, D.A., Peters, J.F., and Pulsford, J.R., (1988), "Design, Development and Operation of a Directional Shear Cell", Dept. of the Army, Waterways Experiment Station, Corps of Engineers, Vicksburg Mississippi.

Arthur, J.R.F., Bekenstein, S., Germaine, J.T. and Ladd, C.C. (1981), "Stress path tests with controlled rotation of principal stress directions", Laboratory shear strength of soil, ASTM, STP 740, pp.516-540.

Arthur, J.R.F. and Dalili, A. (1979), "On the lubrication of rubber surfaces", Geotechnique, Vol.29, No.1, pp.96-98.

Arthur, J.R.F., Dalili, A. and Dunstan T., (1988), "Coulomb ruptures in soils", Contribution to Discussion of sixth Symposium in print, Geotechnique, 38,No. 1, pp.146-148.

Arthur, J.R.F., Dunstan, T. (1969), "Radiographical measurements of particle packing", Nature, Vol.223, No.5205, pp.464-468.

Assadi, A. (1975), "Rupture layers in granular materials" Ph.D. thesis, University of London.

Bekenstein, S. (1980), "Directional shear tests on Leighton Buzzard sand", M.S. thesis, Department of Civil Engineering, Massachusetts Institute of Technology.

Berre, T., (1981), "Triaxial testing at the Norwegian Geotechnical Institute", N.G.I. Publication 134, pp. 1-17.

Biarez, J. and Wiendieck, K. (1963), La comparaison qualitative entre l'anisotropie mecanique et l' de structure des milieux pulverulents, Comptes Rendus Hebdomadaries des Seances de l'Academie des Sciences, Paris, Vol.256, pp.1217-2220.

Bishop, A.W. and Henkel, D.J. (1962), The measurement of soil properties in the triaxial test, 2nd ed., Edward Arnorld (Publishers) Ltd., London.

Bishop, A.W. (1972), "Shear strength parameters for undisturbed and remoulded soil specimens", Proc. Roscoe Memmorial Symp., G.T. Foulis and Co., Henley on Thames, England, pp.3-58.

Bishop, A.W. (1966), "The strength of soils as engineering materials", Geotechnique, Vol.16, No.2, pp.91-130.

Bishop, A.W. and Green, G.E. (1965), "The influence of end restriant on the compression strength of a cohesionless soil", Geotechnique, Vol.15, No.3, pp.243-266.

Bjerrum, L. (1969), "Effect of strain on undisturbed shear strength of soft clays", Proc. 7th Int. Conf. on Soil Mech. Found. Eng., Mexico, Vol3, pp.412-414.

Bjerrum, L. and Landva, A.(1966), "Direct simple-shear tests on a Norwegian quick clay", Geotechnique, Vol.16, No.1, pp.1-20.

Bjerrum, L., Simons, N. and Torblaa, I., (1958), "The effect of time on the shear strength of a soft Marine clay.", Proc. Brussels Conf. on Earth Pressure Problems, Vol.1, pp.148-158.

Borin, D.L. (1973), "The behaviour of saturated sand in the simple shear apparatus", Ph.D. thesis, University of Cambridge.

Bransby, P. L. (1968), "Stress and strain in sand caused by rotation of a model wall", PhD. Thesis University of Cambridge.

Brewer, R. (1964), "Fabric and Mineral Analysis of Soils", Edition John Wiley and Sons, pp.129-158.

Brewer, J.H. (1972), "The Response of Cyclic Stress in Normally Consolidated Saturated Clay",PhD thesis, North Carolina State University, Raleigh.

Brown, S.F., Lashine, A.K.F., and Hyde, A.F.L., (1975), "Repeated load triaxial testing of a silty clay", Geotechnique, 25(1), pp.95-114.

Cassagrande, A. (1975). "Liquifaction and cyclic deformation of sands: a critical review", Proc. 5th Pan American Conf. SMFE, Buenos Aires, Vol.5, pp.80-133.

Cassagrande, A. and Carrillo, N. (1944), "Shear failure of anisotropic materials", J. Boston Society Civil Engineers, Vol.31, No.4, pp.74-87.

Castro, G. (1969), "Liquefaction of Sands", Ph.D. Thesis, Harvard University, Massachusetts, U.S.A.

Cole, E. R. (1967), "The behaviour of soils in the Simple Shear apparatus", Ph.D. thesis, University of Cambridge.

Cundall, P.A. (1971), "A Computer Model for Simulating Progressive, Large-Scale movements in Blocky Rock Systems", Proceedings, Symposium of International Society of Rock Echanics, Nancy 2, art.8.

Cundall, P.A., Drescher, A. and Strack, O.D.L. (1982), "Numerical Experiments on Granular assemblies; Measurements and Observations", IUTAM Conference on Deformation and Failure of Granular Materials, Delft.

Cundall, P.A. and Strack, O.D.L. (1979), "A discrete numerical model for granular assemblies", Geotechnique, Vol.29. No.1, pp.47-65.

Cundall, P.A. and Strack, O.D.L. (1983), "Modelling of microscopic mechanisms in granular material", Mechanics of Granular Materials: New Models and Constitutive Relations, Edited by Jenkins, A.T. and Satake, M., Elsevier Science Publishers, Amsterdam, pp.137-149.

Dantu, P. (1957), "Contribution a l'etude mechanique et geometrique des milieux pulverulents", Proceedings, 4th International Conference on soil Mechanics and foundation Engineering, London, Vol.1, pp.144-148.

Davoudzadeh, F. (1982), "Response of sand to three independently controlled principal stresses", Ph.D. thesis, University of London.

Dayer, M.R., (1985), "Observation of the stress distribution in crushed glass with applications to soil reinforcement" Dhil thesis, University of Oxford.

Desrues, J. et al. (1984), "La localisation de la deformation dans les materiaux granulaires ", These de doctorat d'etat, USMG, Grenoble.

Desrues, J. et al. (1984), "Localization of the deformation in tests on sand samples", Engineering Fracture Mechanics.

Drescher, A and De Josselin De Jong, G (1972), "Photoelastic verification of a mechanical model for the flow of a granular material", J.Mech.Phys.Solids. Vol.20. pp.337-351.

Dunstan, T. (1968), "Anisotropy in homogenous granular soils", Ph.D. thesis, University of London.

Dunstan, T., Arthur, J.R.F., Dalili, A., Ogunbekun, O. and Wong, R.K.S. (1988), "Limiting mechanisms of slow dilatant plastic shear deformation of granular media", Nature, Vol. 336, No. 6194, pp.52-54.

Dunstan, T. (1971), "The influence of grading on the anisotropic strength of sand", Geotehnique, Vol.22, no.2, pp.529-532.

Dyvik, R., Berre, T., Lacasse, S. and Raadim, B., (1987), "Comparison of truly undrained and constant volume direct simple shear tests", Geotechnique, Vol. 32, No.1, pp.3-10.

Finn, W.D.L., Pickering, D.J. and Bransby, P.L. (1971), "Sand liquefaction in triaxial and simple shear tests", ASCE, Journal of Soil Mechanics and Foundations Division, Vol.96, No.SM4, pp.639-659.

Finn, W.D.L., and Vaid, Y.P., (1977), "Liquefactin potential from drained constant volume cyclic simple shear tests", Proc. 6th WCEE, New Delhi6, pp.7-12.

Fukushima, S. and Tatsuoka, F. (1984), "Strength and deformation characteristics of saturated sand at extremely low pressures", Soils and Foundations, Vol 24, No.4, pp.30-48.

Germaine, J.T. (1982), "Development of the Directional Shear Cell for measuring cross anisotropic clay properties", Sc.D thesis, Massachusetts Institute of Technology.

Green, G.E. (1971), "Strength and deformation of sand measured in an independent stress control cell", Proc. Roscoe Memmorial Symp., G.T. Foulis and Co., Henley on Thames, England, pp.285-323.

Habib, P. (1986), "Effet d'echelle et surfaces de glissement", Revue Fançaise de Geotechnique, No.31, pp.6-10.

Hadjieuthymiou, D. (1979) "Particle structure of a deforming sample" , Ph.D. thesis, University of London.

Hambly, E.C. and Roscoe, K.H. (1969), "Observation and predictions of stresses and strains during plane strain of 'wet' clays", Proc. of 7th Int. Conf. SMFE., Vol.1, pp.173-181.

Hansen, J., Brinch and Gibson, R. E. (1949), "Undrained shear strengths of anisotropically consolidated clays", Geotechnique No.3.

Henkel,D.J. (1970), "The role of waves in causing submarine landslides", Geotechnique, 20, 1, pp.75-80.

Hettler, A., (1985), "setzugen von einzelfundamenten auf sand", bautechnik, 6, 189-197.

Hight, D.W. (1983), "Laboratory investigations on sea-bed clays", Ph.D. thesis, University of London.

Hight, D.W., Gens, A and Symes, M.J. (1982), "The development of a new Hollow Cylinder Apparatus for investigating the effects of principal stress rotations in soils",

Geotechnique, Vol. 33, no.4, pp.355-383.

Horn, H.M. and Deere, D.V., (1962), "Frictional characteristics of minerals", Geotechnique 12 4, 319-335.

Horne, M.R., (1969), "The behaviour of an assembly of rotund, rigid, cohsionless particles", parts III, Proceedings of the Royal Society, A 310 21-34.

Horne, M.R., (1965), "The behaviour of an assembly of rotund, rigid, cohsionless particles", parts I and II, Proceedings of the Royal Society, a 286 62-97.

Ishihara, K. and Momenzadeh, M., (1986), "Influence of rotation of principal stress directions on the cyclic behaviour of sand", "nd International Symposium on Numerical Models in Geomechanics, pp.827-835.

Ishihara, K. and Towhata, I. (1983), "Sand response to cyclic rotation of principal stress directions as induced by wave loads", Soils and Foundations, Vol.23, No.4, pp.11-26.

James, R.G. and Bransby, P.L. (1970), "Experimental and theoretical investigation of a passive earth pressureb problem", Geotechnique 20 1, 17-37.

James, R.G. (1973), "Determination of strains in soft soils by radiography", Internal report, CUED/C-Soils/LN(1a). Cambridge University Engineering Department.

Jamiolkowski, M., Ladd, C.C., Gremaine, J.T., and Lancellota, A., (1985), "New developments in field and laboratory testing of soils", Theme Lecture, Proceedings of Eleventh International Conference on Soil Mechanics and Foundation Engineering, Vol.1, pp.57-153.

Jewell, R.A. (1988), "Unreinforced direct shear tests" Report No. OUEL 1719/4/88, University of Oxford.

Jewell, R.A. and Wroth, C.P. (1988), Discussion on "The engineering application of direct and simple shear testing", Geotechnique, Vol.38, No.1, pp.146-148.

Jewell, R.A. and Wroth, C.P. (1987), "Direct shear tests on reinforced sand", Geotechnique, Vol.37, No.1, pp.53-68.

Johansson, G., (1965), "Structural studies of sedimentary deposits", Geol. for. i.Stockh, Forh. 87, part 1, No.520, 3-61.

Kjellman, W. (1951),"Testing the shear strength of clay in sweden", Geotechnique, Vol.2, No.3, pp.225-235.

Ko, H.Y., and Scott, R.F. (1967), "A new soil testing apparatus", Geotechnique 17, No.1., pp.40-57.

Koenders, M.A. (1984), "A two dimentional non-homogeneous deformation model for sand", Ph.D. thesis, University of London.

Kolbuszewski, J.J. (1948), "An experimental stydy of the maximum and minimum porosities of sand", Proc. 2nd Int. Conf. SMFE, Rotterdam, Vol.1, pp.158-165.

Konishi, J., Oda, M. and Nemat-Nasser, S. (1982), "Inherent anisotropy and shear strength of assembly of oval cross-sectional rods", Proc. IUTAM symp. on Deformation and failure of granular Materials, Delft, pp.403-412.

Koutsoftas, D.C. (1978), "Effect of cyclic loads on undrained strengths of two Marine clays", Proc. ASCE, Vol.104, No.GT5.

Ladd, C.C., Foott, R. Ishihara, K., Schlosser, F., and Poulos, H.G., (1977), "State of the art", 9th Int. Conf. on Soil Mechanics and Foundation Engineering, Tokyo, pp.421-433.

Lade, P.V. and Duncan, J.M. (1973), "Cubical triaxial tests on cohesionless soil", JSMD, Proc.ASCE, Vol.99, SM10, pp.793-812.

Lambe, T.W. and Marr, W.A. (1979), "Stress path method: second edition", JGED, PROC.ASCE, Vol.105, GT6, pp.727-738.

Lambe, T.W. (1967), "Stress path method", JSMFD, Proc.ASCE, Vol.93, SM6,pp.309-331.

Lambe, T. W. and Marr, W. A. (1980), Closure to "Stress path method: second edition". Jnl. of Geotech. Eng. Div., ASCE, 106, GT9, 1074-1077.

Lee, K.L. (1978), "End restriant effects on undrained static triaxial strength of sand", Proc.ASCE Vol.104, No.GT.6. pp.687-704.

Lee, K.L. and Seed H.B. (1967), "Cyclic stress conditions causing liquefaction of sand", JSMFD, Proc.ASCE, Vol.93, SM1, pp.47-70.

Lee, K.L. and Focht, J.A. (1975), "Liquefaction potential at Ekofisk tank in North Sea", JGED, Proc.ASCE, Vol.101,GTl, pp.1-18.

Lee, K.L., and Seed, H.B. (1967), "Dynamic strenrth of anisotropically consolidated sand", J.Soil Mechanics and Foundation Div., ASCE, 93 (SM5), Proc.paper 5451, pp.169-90.

Lo, H.Y. (1965), "Stability of slopes in anisotropic soils", Jnl Soil Mech.Fnds Div. Am.Soc. Civ.Engrs 91, SM4, 85-106.

Lord, J.A. (1968), "stresses and strains in an earth pressure problem" PhD. Thesis University of Cambridge.

Luong, M.P. (1980), "Stress-strain aspects of cohesionless soils under cyclic and transient loading", Proc. Int. Symp. on Soils under Cyclic and Transient Loading, Swansea, Vol.1.pp.315-324.

Mahmood, A. and Mitchell, J.K., (1974), "Fabric-property relationship in fine granular materials", Clay and clay minerals, Vol.22, No.516, pp.397-408.

Marachi, N.D., Duncan, J.M., Chan, C.K. and Seed, H.B. (1981), "Plane strain testing of sand", Laboratory shear strength of soil, ASTM, STP 740, pp.294-302.

Matchett, (1988), Department of Chemical Engineering, Teeside Polytechnic, Private communication, Teeside Polytechnic. UK.

Matsuoka, H. (1974), "A microscopic study on shear mechanism of granular materials", Soils and Foundations, Vol.14, No.1 pp.29-43.
Matsuoka,H. (1973), "Deformation characteristics of soil", Doctor thesis of Kyoto University.

Menzies, B.K. and Phillips, A.B. (1972), "On the making of rubber membranes",

Geotechnique, Vol.22, No.1, pp.153-155.

Mitchell, J. K. (1976), Fundamentals of soil behaviour, John Wiley and Sons, Inc. New York, pp.315.

Mitchell, J.K., Chatoian, J.M., and Carpenter, G.C. (1976), "The influences of sand fabric on Liquefaction behaviour", Report No.TE76-1, Cpllege of Engineering, Office of research services, University of California, Berkeley, California.

Miura, S. and Toki, S. (1984), "Anisotropy in mechanical properties and its simulation of sand sampled from natural deposits", Soils and Foundations, Vol.24, No.3, pp.69-84.

Mogami, T., (1965), "A statical approach to the mechanics of granular materials", Soils and Foundations, 5, No.2, pp.26-36.

Molyneux, B. (1987), "A method of assesment of the shear strength of particulate materials", 3rd yr project rpt. Dept. of Civ. Eng., University College London.

Mulilis, J.P., Chan, C.K. and Seed, H.B. (1975), "The effects of method of sample preparation on the cyclic stress-strain behaviour of sands", Report No. EERC 75-18, University of California, Berkeley.

Murayama, S., and Shibata, T. (1960), "On the dynamic properties of clay" Proc. 2nd WCEE, Tokyo,1 297-310.

Nagraj, T.S. (1968), "Strain-Rate influence on shear strength characteristics of a saturated kaolinite clay", J. of Materials Vol.3, No.1, pp.210-235.

Nemat-Nasser, S. (1979) "On behaviour of granular materials in simple shear", Earthquake Research and engineering laboratoriTech. Report No. 79-6-19, Dept. of Civil Engineering ,Northampton University, Evanston.

Nemat-Nasser, S. and Tobita, Y., (1981), "Influence of fabric on liquefactin and densification potential of cohesionless sand", Earthquake Research and Engineering Laboratory, Tech.Report. No.81-2-40, Dept of Civil Engineering,North western University, Evanston, IL; (1982), Mechanics of Materials,1,43.

Newland, P.I. and Allely, B.H. (1957), "Volume changes in drained triaxial tests on granular materials", Geotechnique, 7, pp.17-34.

Norris, G.M. (1981), "Effects of end membrane thickness on the strength of 'friction-less' cap and base tests", Laboratory shear strength of soil, ASTM, STP 740, pp.303-314.

O'Neill, D.A., (1985), "Undrained strength anisotropy of an overconsolidated thixotropic clay", S.M. thesis, Department of Civil Engineering, MIT, 359 p.

Oda, M., Nemat-Nasser, S. and Konishi, J. (1985), "Stress-induced anisotropy in granular masses", Soils and Foundations, Vol.25, No.3, pp.85-97.

Oda, M., Konishi, J. and Nemat-Nasser, S. (1983), "Experimental micro-mechanical evaluation of strength of granular material; effects of particle rolling", Mechanics of Granular Materials: New Models and Constitutive Relations, Edited by Jenkins, A.T. and Satake, M., Elsevier Science Publishers, Amsterdam, pp.21-30.

Oda, M. (1972a), "Initial fabrics and their relations to the mechanical properties of

granular material.", Soils and Foundations, Vol.12, No.1, pp.17-36.

Oda, M. (1972b), "The mechanism of fabric changes during compressional deformation of sand", Soils and Foundations, Vol.12, No.2, pp.1-18.

Oda, M. (1974), "A mechanical and statical model of granular material", Soils and Foundations, Vol. 12, No.2, pp.13-27.

Oda, M. Konishi, J. and Nemat-Nasser, S., (1982),"Experimental micromechanical evaluation of strength of granular materials: Effects of particle rolling", Mechanics of Materials Vol.1, No.4, pp.269-283.

Oda, M. (1976), "Fabrics and their effects on the deformation behaviours of sand", Report of Dept. of Fdn. Engng., Saitama University, Japan.

Oda, M. (1972c), "Deformation mechanism of sand in triaxial compression tests", Soils and Foundations, Vol.12, No.4, pp.45-63.

Oda, M. and Konishi, J. (1974), "Microscopic deformation of granular material in simple shear", Soils and Foundations, Vol.14, No.4, pp.25-38.

Ogunbekun O., Dalili A., Arthur J.R.F. and Dunstan T., (1988), "Distributed Disturbance and Constraint in Soils", Micromechanics of Granular Materials, Elsevier, Tokyo, pp.235-244.

Ogunbekun, O.O.O. (1988) "The influence of boundary constraints on the shearing characteristics of particulate solids at extremely low stress levels",Ph.D. thesis, University of London.

Öner, M., (1984), "Analysis of fabric changes during cyclic loading of granular soils", 8th W.C.E.E, Sanfrancisco, Vol.3, pp.55-61.

Palmeira, E.M. (1988), Discussion on "The engineering application of direct and simple shear testing", Geotechnique, Vol.38, No.1, pp.146-148.

Palmira, E.M., (1987), "The study of soil-reinforcement interaction by means of large scale laboratory tests", DPhil thesis, University of Oxford.

Peacock, W.H. and Seed, H.B. (1968), "Sand liquefaction under cyclic loading simple shear conditions", JSMFE, Proc.ASCE, Vol.94, SM3, pp.689-708.

Pearce, J.A. (1971), "A new true triaxial apparatus", Proc. Roscoe Memmorial Symp., G.T. Foulis and Co., Henley on Thames, England, pp.330-339.

Penman, A.D.M. (1953), "Shear characteristics of saturated silt measured in triaxial compression"Geotechnique 3 4, 312-328.

Phillips, A.B. and May, P.H., (1967), "A form of anisotropy in granular media", Special Task Report, Dept. of Civ. and Munic. Engng., University College, London.

Reynolds, O., (1885) "On dilatancy of media composed of rigid particlesin contact" with experimental illustrations, Phil. Mag. Vol. 11, pp.469-481.

Richardson, A.M. and Whitman, R.V. (1963), "Effect of Strain-Rate upon undrained resistance of saturated remoulded fat clay", Geotechnique, Vol.13, No.4, pp.310-324.

Rodriguez del Camino, J.I. (1977), "Induced anisotropy in a loose sand", Ph.D.

thesis, University of London.

Rodriguez del Camino, J.I., and Dunstan, T. (1981), "The directional shear cell", Proc. 10th Int. Cof. SMFE, Stockholm, Vol.1, pp.765-770.

Roscoe, K.H., and Schofield, A.N. (1964), Discussion of "Stress-dilatancy, earth pressures and slopes", JSMD, Proc.ASCE, Vol.90, SM1, pp.136-150.

Roscoe, K.H., Basset, R.H. and Cole, E.R.L. (1967), "Principal axes observed during simple shear of a sand", Proc. Geotechnical Conf., Oslo, Vol.1, pp.231-237.

Roscoe, K.H., Arthur, J.R.F. and James, R.G. (1963b), "The determination of strains in soils by X-ray method", Civ. Eng. and Public works review, July & Aug, pp.873-876 & pp.1009-1112.

Roscoe, K.H. (1953), "An apparatus for the application of simple shear to soil samples", Proc. of 3rd Int. Conf. SMFE, Zurich, Vol.1,pp.186-191.

Roscoe,K.H., (1970), "The influence of strains in soil mechanics", Geotechnique, Vol.20, No.2 pp.129-170.

Rothenburg, L. and Buthurst, R.J. (1989), "Analytical study of induced anisotropy in idealized granular materials", Geotechnique 39, No.4, Pp.601-614.

Rowe, P.W. (1962), "The stress dilatancy relation for an assembly of particles in contact", Proc. Royal Society, Series A. Vol. 269, pp.500-527.

Rowe, P.W. and Barden, L. (1964), "Importance of free ends in triaxial testing", JSMFD, Proc.ASCE, Vol.90, SM1, pp.1-27.

Saada, A.S. and Townsend, F.C. (1981), "State-of-the-art: laboratory strength testing of soils", Laboratory shear strength of soil, ASTM, STP 740, pp.7-77.

Sangrey, D.A., Pollard, W.S., and Egan, J.A., (1978), "Erroes associated with rate of undrained cyclic testing of clay soils", Dynamic Geotechnical Testing, ASTM: STP 654, pp.280-94.

Scarpelli, G. and Wood, D.M., (1982), "Experimental observations of shear band patterns in direct shear tests", Proc.IUTAM Symposium, Balkema, pp.473-484.

Seed, H.B. (1976), "Liquefaction problems in geotechnical engineering", ASCE, Annual Convention and Exposition, pp.1-105.

Seed, H.B. and Chan, C.K., (1966), "Clay strength under earthquake loading condition", Proc. ASCE, Vol.92, No.SM2, pp.53-78.

Seed, H.B. and Lee, K.L. (1966), "Liquefaction of saturated sands during cyclic loading", ASCE, Journal of the Soil Mechanics and Foundations Division, Vol.92, No.SM3, pp.105-134.

Shibata, T. and Karube, D. (1965), "Influence of the variation of the intermediate principal stress on the mechanical properties of normally consolidated clays", Proc. 6th Int. Conf. SMFE, Montreal, Vol.1, pp.359-363.
Shibuya, S. (1985), "Undrained behaviour of granular materials under principal stress rotation", Ph.D. thesis University of London.

Simons, N.E., (1971), "The stress path method of settlement analysis applied to

London Clay", Stress-strain behaviour of soils. Proc. Roscoe Memorial Symposium, Camb. G.T. Foulis, Henley-on-Thames.

Skinner, A.E. (1969), "A note on the influence of interparticle friction on the shearing strength of a random assembly of spherical particles", Geotechnique, Vol.19, No.1, pp.150-157.

Stroud, M.A. (1971), "The behaviour of sand at low stress levels in the simple shear apparatus", Ph.D. thesis, University of cambridge.

Sture, S., Budiman, J.S., Ontuna, A.K., and Ko, H.Y., (1987), "Directional Shear Cell experiments on a dry cohesionless soil", Geotechnical Testing Journal, GTJODJ, Vol.10, No.2, pp.71-79.

Sture, S. and Desai, C.S. (1979), "Fluid cushion truly triaxial or multiaxial testing device", Geotechnical testing journal, Vol.2, No.1, pp.20-33.

Sture, S., Ko, H.Y.Budiman, J.S., and Ontuna, A.K., (1985), "Development and application of a Directional Shear Cell", Proceedings of the 11th International Conference on Soil Mechanics and Foundation Engineering, Vol.2, Sanfrancisco, CA, pp.1061-1064.

Symes, M.J.P.R. (1983), "Rotation of principal stresses in sand", Ph.D. thesis, University of London.

Symes, M.J.P.R., Gens, A. and Hight, D.W. (1984), "Undrained anisotropy and principal stress rotation in saturated sand", Geotechnique, Vol.34, No.1, pp.11-28.

Tatsuoka, F. and Haibara, O. (1985), "Shear resistance between sand and smooth or lubricated surfaces", Soils and Foundations, Vol.25, No.1, pp.89-98.

Tatsuoka, F., Sakamoto, M., Kawamura, T. and Fukushima, S. (1986), "Strength and deformation characteristics of sand in plane strain compression at extremely low pressures", Soils and Foundations, Vol 26, No.1, pp.65-84.

Taylor, D.W. (1948), Fundamentals of Soil Mechanics, John Wiley.

Terzaghi, K.V., (1955), "Evaluation of cefficient of subgrade reaction", Geotechnique, 5, No.4, 297-329.

Tschebotarioff, G.P. and Welch, J.D. (1948), "Lateral earth pressures and friction between soil minerals", Proc.2nd Int. Conf. Soil Mech. Rotterdam VII 135-138.

Vaid, Y.P. and Chern, J.C. (1983), "Mechanism of deformation during cyclic undrained loading of saturated sands", Soil Dynamics and arthquake Engineering, Vol.2, No.3, pp.171-177.

Vaid Y.P. and Chern J.C., (1982) "Mechanism of deformation during cyclic undrained loading of saturated sands", Soil Dynamics and Earthquake Engineering Conference, Southampton.07.13-15, pp.101-115.

Vucetic, M. and Lacasse, S. (1983), "Specimen size effect in simple shear test", Closure. J. Geotech. Engng Div. Am. Soc. Civ. Engrs 110, Gt4, 447-453.
Wakabayashi, T. (957), "Photoelastic method for determination of stress in powdered mass", Proceedings, 7th Japan Nat. Congr. Appl. Mech., pp.153-158.

Ward, W.H., Marsland, A. and Samuels, S.G. (1965), "Properties of the London clay

at the Ashford Common shaft, in situ and undrained strength tests", Geotechnique 15, No. 4, 321-344.

Weindieck, K. (1967), "Zur Struktur Korniger Medien", Die Bautechnik, Berlin, Vol.44, No.6, pp.196-199.

Whitman, R.V. (1960), "Some considerations and data regarding the shear strength of clays", Proc. conf. on shear strength of cohesive soils, Boulder, Clorado, pp.581-614.

Wong, R.K.S. (1986), "Sand subjected to cyclic principal stress rotations", Ph.D. thesis, University of London.

Wong, R.K.S., Arthur, J.R.F. and Dunstan, T. (1987), "Induced anisotropy in wet remoulded Kaolinite and Bentonite model materials", Chem. Engng. Sci., Vol.42, No.4, pp.745-751.

Wood, D.M. and Budhu, M. (1980), "The behaviour of Leigthon Buzzard sand in cyclic simple shear tests", Proc. Int. Symp. on soils under Cyclic and Transient Loading, Swansea, Vol.1, pp.9-21.

Wong, R.K.S. and Arthur, J.R.F. (1985a), "Induced and inherent anisotropy in sand", Geotechnique, Vol.35, No.4, pp.471-481.

Wong, R.K.S. and Arthur, J.R.F. (1985b), "Determination and uses of strain distributions in sand samples", Geotechnical testing journal, Vol.8, No.3, pp.101-110.

Wong, R.K.S. and Arthur, J.R.F (1986), "Sand sheared by stresses with cyclic variations in direction", Geotechnique, Vol.36, No.2, pp.215-226.

Wroth, C.P. (1987), "The behaviour of normally consolidated clay as observed in undrained shear tests", Geotechnique 37, No.1, 37-43.

Youd, T.L. (1977), "Packing changes and liquefaction susceptibility", JGED, Proc.ASCE, Vol.103, GT8, pp.918-922.

ABBREVIATIONS

ASCE = American Society of Civil Engineers
ASME = American Society of Mechanical Engineers
ASTM = American Society of Testing Materials
EERC = Earthquake Engineering Research Centre
IUTAM = International Union Of Theoretical and AppliedMechanics
JSCE = Japanese Society of Civil Engineers
WCEE = Wold.Conference on Earthquake Engineering